doi: 10.3289/geomar_rep_062_1997

FS SONNE

FAHRTBERICHT SO 123
CRUISE REPORT SO 123

MAMUT

MAKRAN MURRAY TRAVERSE -
GEOPHYSIK PLATTENTEKTONISCHER EXTREMFÄLLE

Maskat - Maskat
07.09 - 03.10.1997

Edited by
Ernst R. Flueh, Nina Kukowski, and Christian Reichert
with contributions of cruise participants

GEOMAR
Forschungszentrum
für marine Geowissenschaften
der Christian-Albrechts-Universität
zu Kiel

Kiel 1997

GEOMAR REPORT 62

GEOMAR
Research Center
for Marine Geosciences
Christian Albrechts University
in Kiel

Redaktion der Serie: Gerhard Haass
Redaktion dieses Reports: Ernst R. Flueh, Nina Kukowski, and Christian Reichert
Umschlag: Kerstin Kreis, Harald Gross, GEOMAR Technologie GmbH

Managing Editor: Gerhard Haass
Editors of this issue: Ernst R. Flueh, Nina Kukowski, and Christian Reichert
Cover: Kerstin Kreis, Harald Gross, GEOMAR Technologie GmbH

GEOMAR REPORT
ISSN 0936 - 5788

GEOMAR REPORT
ISSN 0936 - 5788

GEOMAR
Forschungszentrum
für marine Geowissenschaften
D-24148 Kiel
Wischhofstr. 1-3
Telefon (0431) 600-2555, 600-2505

GEOMAR
Research Center
for Marine Geosciences
D-24148 Kiel / Germany
Wischhofstr. 1-3
Telephone (49) 431 / 600-2555, 600-2505

Table of contents

1.1 Zusammenfassung

Das Hauptziel der FS SONNE Ausfahrt SO123 - MAMUT (Makran Murray Traverse) vom 7. September bis 3. Oktober 1997 war es, die seewärtigen Untergrundstrukturen des Makran Akkretionskeils und des Murray Rückens/Dalrymple Trogs zu untersuchen. Entlang von 10 Profilen mit einer Gesamtlänge von 1220 km wurden Ozeanboden Hydrophone (OBH) an insgesamt 92 Lokationen und Ozeanboden Seismometer (OBS) an insgesamt 5 Lokationen abgesetzt und erfolgreich wieder geborgen. Das neu entwickelte OBS arbeitete zuverlässig und registrierte verwertbare Daten. Gleichzeitig wurde Einkanalseismik aufgenommen. Um die Qualität der gewonnenen Daten zu kontrollieren sowie erste wissenschaftliche Interpretationen zu ermöglichen, wurden die gesamten seismischen Daten während der Ausfahrt bearbeitet, dargestellt, analysiert und archiviert. Eine kontinuierliche Datenerfassung der Hydroakustik und Gravimetrie wurde innerhalb der pakistanischen EEZ durchgeführt. Magnetische Messungen mit Hilfe eines empfindlichen Gradientenmagnetometers wurden auf einer Gesamtstrecke von 2700 km vorgenommen. In Ergänzung zu den auf der vorangegangenen Ausfahrt SO122 gewonnenen Daten wurde eine gute Überdeckung von bathymetrischen, gravimetrischen und magnetischen Daten entlang eines Korridors um 63° E erhalten. Im Bereich des Makran Akkretionskeils konnte eine Fläche von ca. 10000 km^2 detalliert kartiert werden; für den Dalrymple Trog konnte ebenfalls eine bathymetrische Karte erstellt werden.

Eine erste Auswertung der seismischen Daten über den Murray Rücken/Dalrymple Trog deutet auf eine ungestörte ozeanische Krustenstruktur nördlich des Dalrymple Trog bei einer Mächtigkeit der Sedimentbedeckung von 3-5 km hin. Die ozeanische Kruste wird als 2 Schichten Modell intepretiert. Sie besitzt eine Mächtigkeit von 5-7 km, wobei die Schicht 'layer 3' etwas mächtiger als die Schicht 'layer 2' erscheint. Eine ungewöhnlich starke Reflexion von der Grenze zwischen layer 2 und layer 3 wird bis in den Steilwinkelbereich der seismischen Daten beobachtet. Innerhalb des Vermessungsgebietes enthält der Dalrymple Trog drei Beckenstrukturen, jede mit einer Tiefe von 4200 m. Die Flanke im Südosten ist extrem steil und bis zu 2000m hoch, während im Nordwesten diese aus mehreren kleineren Terassen besteht. Innerhalb des Dalrymple Trogs wurden Sedimente mit einer Mächtigkeit von 5 bis 7 km abgelagert. Die Kruste ist ungewöhnlich mächtig (10 km) und zeigt geringe Geschwindigkeiten, welche 6.4 kms^{-1} nicht übersteigen. Diese Beobachtungen widersprechen der üblichen Vorstellung über den Aufbau der ozeanische Kruste und können zur Zeit nicht erklärt werden.

Auf dem Profil über den Murray Rücken war die Eindringtiefe des seismischen Signals gering, es wurde jedoch deutlich, daß auf der Indischen Platte aus dem Indus Fächer stammende Sedimente von bis zu 7 km Mächtigkeit abgelagert wurden. Die ozeanische Kruste scheint hier besonders dünn, nur 4 km mächtig zu sein und weist sehr hohe seismische Geschwindigkeiten auf. Dieses stimmt mit den Ergebnissen aus der Gravimetrie überein, welche eine positive Freiluftanomalie in der Arabischen See südlich des Murray Rückens und eine negative Freiluftanomalie nördlich des Rückens zeigen. Der erhebliche Unterschied in der Krustenstruktur muß mit dem Murray Rücken zusammenhängen, da hier eine Krustenverdickung stattfindet und die größten Krustenmächtigkeiten unterhalb des Dalrymple Trogs beobachtet wurden.

Im Oman Becken liegt der sogenannte 'Little Murray Ridge', welcher mehrfach mit gravimetrischen und magnetischen Profilen vermessen wurde. Markante Anomalien deuten auf eine lineare Struktur hin, welche im östlichen Bereich des Beckens die Subduktionszone erreicht.

Die Morphologie des Makran Akkretionskeiles ist nicht so gleichförmig wie zuvor angenommen. Die sogenannte 'Protothrust' ist in unterschiedlichen Entwicklungsphasen, aber der erste Akkretionsrücken mit einem Steilhang von über 1200m ist ein markantes und kontinuierliches Gebilde entlang des gesamten

Untersuchungsgebietes. Weiter landeinwärts werden mehrere kleinere Rücken mit zwischengelagerten Sedimenten und von geringerer lateraler Ausdehnung beobachtet. Es wurden vier seismische Profile in Streichrichtung und ein seismisches Profil senkrecht dazu vermessen. Alle Profile zeigen das gleiche Erscheinungsbild, wobei die Profile in Streichrichtung eine auffällige laterale Homogenität aufweisen. Im allgemeinen konnten 5 verschiedene Sedimentschichten unterschieden werden. Ein BSR (Bottom Simulating Reflector) wurde häufig beobachtet. In den ersten drei Schichten steigt die Geschwindigkeit von 1.8 auf 4.0 km/s an. Die darunter liegende Schicht ist eine Zone verminderter Geschwindigkeit (low velocity zone LVZ), an welche eine Schicht mit Geschwindigkeiten von 4.3 bis 5.3 kms^{-1} anschliesst. Die Geschwindigkeiten nehmen landeinwärts zu. Unterhalb dieser Sedimentschichten wurde die ozeanische Kruste mit einer Mächtigkeit von 6 km modelliert. Da die Intervallgeschwindigkeiten innerhalb einer LVZ schwierig zu bestimmen sind, konnte die Tiefe und Neigung der subduzierten Platte nur unzureichend bestimmt werden. Unsere vorläufige Interpretation beruht auf einem Neigungswinkel von 2° bis 3°, welche jedoch durch weitere sorgfältige Analysen quantifiziert werden muss. Die LVZ wird als Zone überhöhten Porendrucks in der Umgebung des Décollements interpretiert. Das darunter liegende Sediment wird subduziert.

Ein weiterer Schwerpunkt der Forschungsfahrt bestand in der Beobachtung der natürlichen Seismizität innerhalb des Makran Akkretionskeiles. Während einer Beobachtungsdauer von 14 Tagen wurden 10 Instrumente eingesetzt, die eine Fläche von 100 * 100 km abdeckten. Es konnte bisher nur ein Ereignis detektiert werden. Dieses lag vermutlich außerhalb des seismologischen Netzes und wurde an nur vier Stationen beobachtet, was die Genauigkeit der Lokalisierung des Bebens erschwert und verschlechtert. Damit wird die geringe natürliche Seismizität des Gebietes dokumentiert, die vermutlich mit einer extrem niedrigen basalen Reibung am Décollement zusammenhängt.

Die weitere Datenbearbeitung, Modellierung und Integration von Erkenntnissen anderer Ausfahrten in dieses Gebiet sollte es dann ermöglichen, detaillierte und zuverlässige Modelle zu erstellen. Damit wird eine Beschreibung der Struktur und Evolutionsgeschichte in diesem Untersuchungsgebiet möglich sein.

1.2 SUMMARY

The main goal of RV SONNE cruise SO123 - MAMUT (MAkran-MUrray Ridge Traverse) was to investigate the large scale structure of the offshore parts of the Makran accretionary wedge and the Murray Ridge/Dalrymple Trough. The cruise was carried out from 07. September to 03. October 1997. Along 10 profiles with a total length of about 1220 km, multiple deployments of Ocean Bottom Hydrophones (OBH) at 92 locations and of Ocean Bottom Seismometers (OBS) at 5 locations were made and successfully recovered. The newly developed OBS worked properly and returned valuable data. Single channel reflection data were simultaneously acquired along the same profiles. All seismic data have been processed, plotted, archived and analyzed during the cruise for quality control and initial scientific interpretations. Hydroacoustic and gravity data were continuously recorded while within the Pakistan EEZ. Magnetic measurement using a sensitive gradient magnetometer was done along about 2700 km. Along the seismic profiles a single channel streamer was deployed. After combining with data from a previous cruise (SO122), a good coverage of bathymetric, gravity and magnetic data along a corridor centered at 63° E is obtained. On the Makran accretionary wedge, an area of about 10.000 km^2 was mapped in detail, in addition to the Dalrymple Trough, for which also the first detailed bathymetric map was created.

Initial evaluation of the seismic data for the Murray Ridge-Dalrymple Trough area suggests an undisturbed oceanic crust north of Dalrymple Trough with a sediment cover of about 3 to 5 km and a two layer oceanic crust of 5 to 7 km

thickness, with layer three each being slightly thicker than layer 2. A strong reflection is often observed at near zero offsets between layers 2 and 3, which is a notable and unusual feature. Within the surveyed area, Dalrymple Trough consists of three bull's-eye shaped basins, each with a depth of 4200 m. The flank to the southeast is rather steep and up to 2000 m high, while to the northwest it consists of several smaller terraces. Within Dalrymple Trough, between 5 and 7 km of sediment is deposited. The crust is unusually thick (10 km) and shows low velocities not exceeding 6.4 km/s. This does not correspond to oceanic crust in general, and a good explanation for this crustal type is still lacking. On a profile across Murray Ridge signal penetration was not at optimum, but it can be seen that on the Indian Plate up to 7 km sediment of the Indus Fan are deposited. The crust here seems to be rather thin, only 4 km, and displays high velocities. This is in close agreement with the observed gravity field, which shows a positive free air anomaly in the Arabian Sea south of Murray Ridge and a negative free air anomaly north of the ridge, despite a thicker sediment cover south of Murray Ridge. A dramatic change of crustal structure seems to be associated with Murray Ridge, where the crust starts to thicken to its maximum value observed beneath the Dalrymple Trough.

In the Oman Basin lies the so called Little Murray Ridge, that was traversed by several gravimetric and magnetic profiles. Pronounced anomalies suggest that this is a linear feature, which may have already entered the subduction zone further to the east.

The morphology of the Makran accretionary wedge is much less uniform than previously assumed. The protothrust is at different stages of development, but the first ridge with a steep cliff of about 1200 m is a remarkably stable feature observed throughout the mapped area. Landward of that ridge, several smaller ridges are seen, separated by ponded sediment, but these never extend for a long distance. Several deep canyons cut through these ridges, and older canyons, no longer active, are easily distinguished. One dip and four strike lines with seismic wide-angle data were observed on the wedge. They all show a similar pattern, and some of the strike lines suggest a pronounced lateral homogeniety. Generally, five sedimentary layers can be distinguished, and a BSR is often very clear. In the first three layers seismic velocities increase from about 1.8 to more than 4.0 km/s. The next layer is a low velocity zone, which again is underlain by a layer with velocities of 4.3 to 5.3 km/s, increasing landwards. Below, the oceanic crust is imaged and modelled as a 6 km thick layer. As the interval velocity of a low velocity zone is notoriously difficult to establish, the depth of the plate and thus ist dip are difficult to define define with confidence. Our preliminary interpretations suggest a dip angle between 2 and 3°, which needs to be better defined by more careful analysis of the data. The low velocity zone is interpreted to be an overpressured zone around the décollement, and the sediment layer below represents sediment that is currently subducted.

We also attempted to monitor the local seismicity in the Makran accretionary wedge. Despite an observation period of up to 14 days and the use of up to 10 instruments distributed over an area of nearly 100 by 100 km, we found only one event so far, which unfortunately is located outside the net and therefore difficult to locate. This again documents the low seismicity, suggesting extremely low basal friction at the décollement.

Further processing, modelling and integration of the data collected on this cruise with those from other cruises in this region will enable us to derive more detailed and better constrained models, from which the structure and evolution of the surveyed area can be deduced with more confidence.

2. INTRODUCTION
2.1 AIMS OF THE PROJECT

(E. Flueh, T. Minshull, C. Reichert, N. Kukowski, R. Edwards)

The main objective of SO 123 is to study the Murray Ridge and Makran accretionary wedge, both of which are rather unique regarding the plate tectonic framework. The tectonic development, the quantification of material and energy fluxes as well as the seismicity of the area are among the specific issues, to which cruise SO 123 shall contribute. In the MAMUT (**MA**kran-**MU**rray Ridge **T**raverse) project, seismic wide-angle measurements, bathymetric mapping, monitoring of the natural seismicity and observation of magnetic and gravimetric data are performed and shall contribute to the above mentioned aims. In addition, cruises SO 122, SO 124, and SO 130 are also devoted to this area, and will apply additional geoscientific methods. This integrated approach will create a good database that shall lead to a much better understanding of the processes that are currently active in this region and also to a deeper insight into the evolution of the complex plate tectonic situation.

The Makran accretionary wedge and Murray Ridge are both end members of plate boundaries, and their immediate neighborhood enables us to study both of them during one cruise. Murray Ridge is believed to be an active rift zone. However, the extension rate is extremely small (0.2 cm/a, DeMets et al., 1990), and the extension is highly oblique. It separates the Arabian from the Indian plate. The Arabian plate, of probably Cretaceous age, is covered by up to 7 km sediment, one of the largest sediment covers in the oceans. This thick pile of mainly sandy material is brought into the Arabian-Eurasian plates collision zone, where the convergence rate is about 4.5 cm/a. As a result of this collision, the Makran accretionary complex has been built up. This complex stretches from the strait of Hormuz in the west to the Indus Fan in the east and is about 300 km wide on average, the largest active accretionary complex on Earth. The recent active volcanic belt is at a distance of 500-600 km from the accretionary front.

Along a traverse, centered around 63° E longitude, numerous closely spaced seismic wide-angle profiles will define the structure of the crust and upper mantle. Most profiles are coincident with near vertical MCS lines collected earlier (Minshull et al., 1992; Roeser et al., 1997), and thus allow the crustal structure to be determined in great detail. These data will provide insight to how the oceanic plate is modified by rifting on Murray Ridge and upon subduction underneath the Makran accretionary wedge. On the Makran accretionary wedge detailed seismic velocity fields can be analysed to determine the amount and location of the dewatering of the incoming sediment cover and also possibly the oceanic plate, and can be used to constrain the depth of the oceanic plate beneath the wedge.

The multibeam bathymetric data, when combined with data from the preceeding leg of SONNE (Roeser et al, 1997) and other existing data, will provide the first detailed bathymetric map of this area, which can be used for morphotectonic investigations. Magnetic and gravity field data can be used to define lineaments of the oceanic crust and put further constraints on the lithologic interpretation of the seismic velocity fields.

The monitoring of the natural micro-seismicity with offshore instrumentation will provide valuable information regarding the state of stress and stress release in the Makran region. Together with the detailed velocity field obtained from the wide-angle profiles, earthquakes can be located with high precision and thus be indicative for the location of active faults.

2.2 REGIONAL BACKGROUND MAJOR TECTONIC ELEMENTS

The Gulf of Oman is part of the Arabian plate, and is bordered by three different plate boundaries (Figure 2.1). The Murray Ridge in the south is thought to be an active rift zone. In the north, the Arabian plate is subducted beneath the Eurasian plate. Resulting from this convergence is the Makran accretionary wedge. The eastern boundary to the Indian plate is a strike slip boundary, that extends into the Pamir and is commonly known as the Ornach-Nal Fault Zone. The oceanic crust in the Gulf of Oman is probably 70 to 100 Ma old (Hutchinson et al., 1981), and was formed at the Proto Carlsberg Ridge that became inactive at about chron 20 time in Lower to Middle Eocene. The modern Carlsberg Ridge became active in Miocene (Chron 6). An alternative plate reconstruction (Mountain and Prell, 1990), which better fits basement depth and geological observations on the east Oman margin, has a fragment of Eocene to Miocene age crust in the Gulf of Oman. These two models are shown in Figure 2.2 (after Minshull et al., 1992).

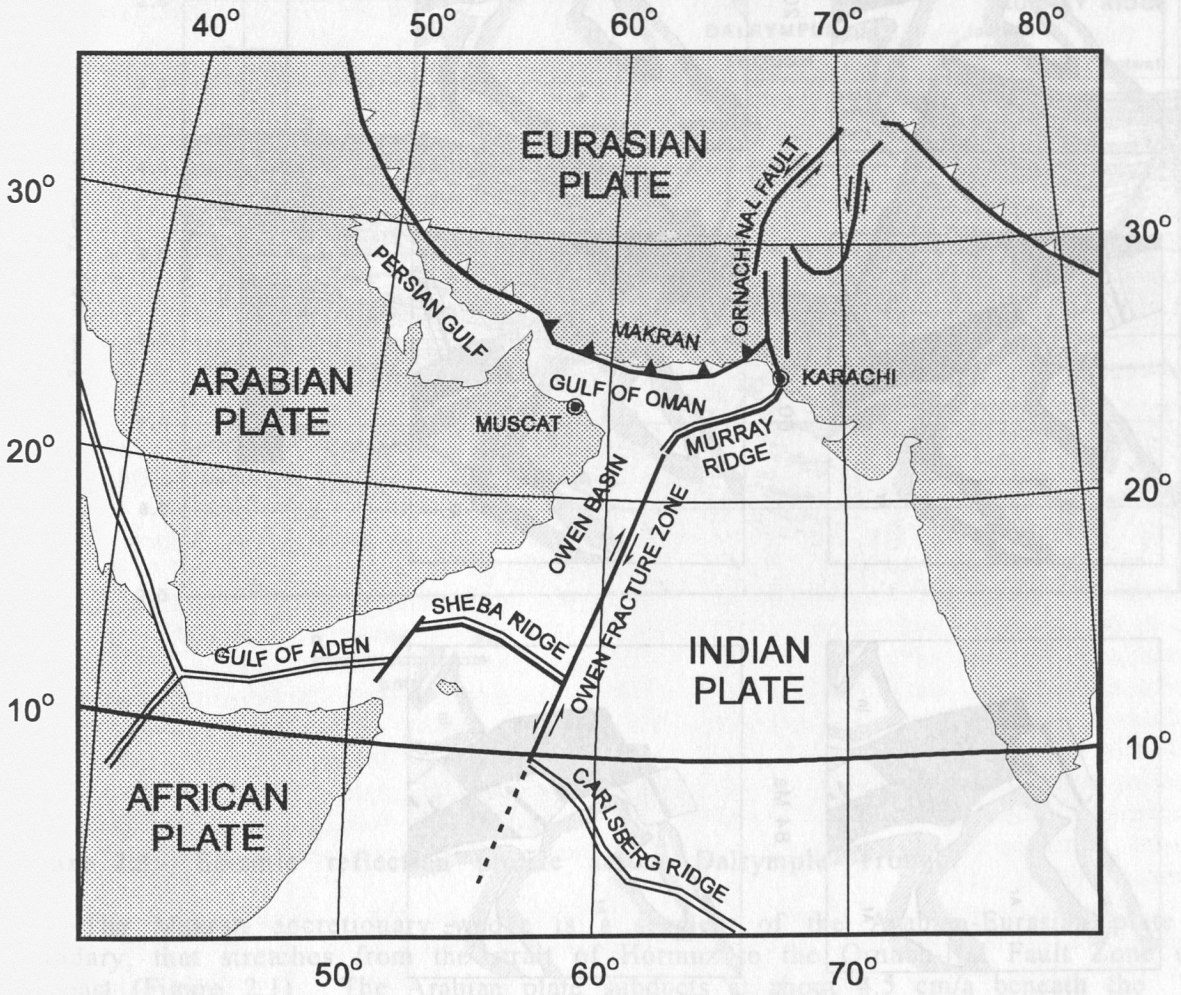

Figure 2.1: Plate tectonic setting around the Gulf of Oman.

The Murray Ridge, discovered by S. Seymour on the 1933 John Murray cruise, is the northeastern prolongation of the Owen Fracture Zone, along which right lateral strike slip motion occurs (Gordon and DeMets, 1989). Volcanism and compression probably both contributed to the build-up of Murray Ridge, even before extension occured in modern times (Minshull et al, 1992). Along Murray Ridge, several segments are evident from the bathymetry (Figure 2.6), and extension is indicated by deep troughs, such as the Dalrymple Trough, named by Barker, 1966, on his HMS Dalrymple cruise. The average extension rate is believed

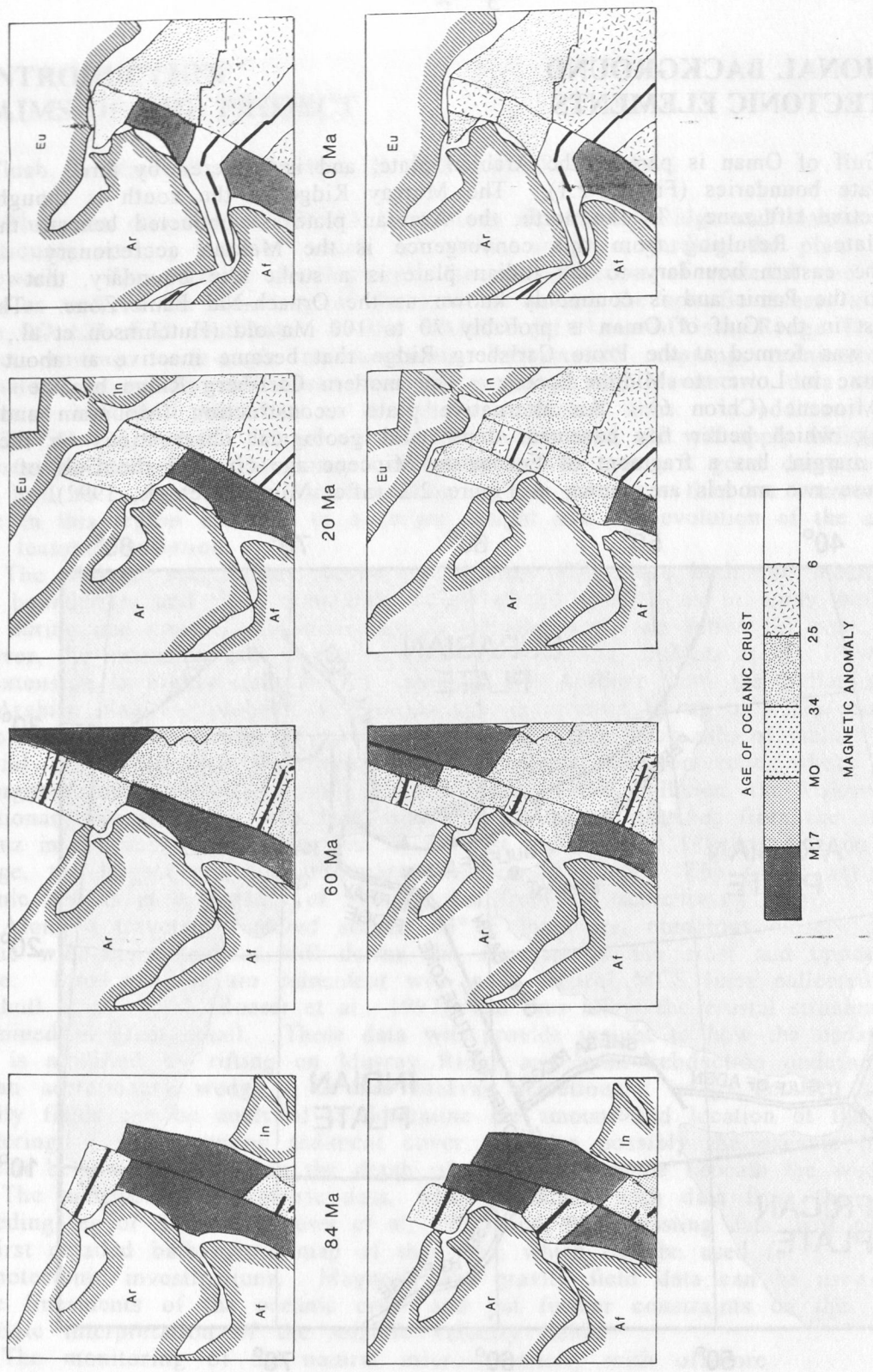

Figure 2.2: Two alternative plate reconstructions for the Gulf of Oman region. The upper sequence assumes that the transform offset of the proto-Carlsberg Ridge was entirely along the Owen Fracture Zone and predicts Jurassic-aged crust in the Owen Basin; the lower sequence assumes that there was a second transform further west, along the east Oman continental margin and predicts a late Cretaceous age for the Owen Basin, which is more consistent with observed basement depth (Mountain and Prell, 1990; Minshull et al., 1992).

to be 2 mm/a, the smallest spreading rate of any active ridge on Earth (Gordon and DeMets, 1989). A reflection seismic profile across Dalrymple Trough is shown in Figure 2.3 (Minshull et al, 1992). Further multichannel-reflection data were collected on the preceeding leg of SONNE, and can be found in the cruise report (Roeser et al., 1997) The main fault lies on the southern shoulder, and antithetic faults are seen on the northern flank. Within the trough about 2.5 km of sediment is deposited, and preliminary analysis of two seismic wide-angle recordings from OBS indicates a crustal thickness of 10 to 12 km (Edwards et al, in prep.), rather unusual for rift zones and oceanic crust.

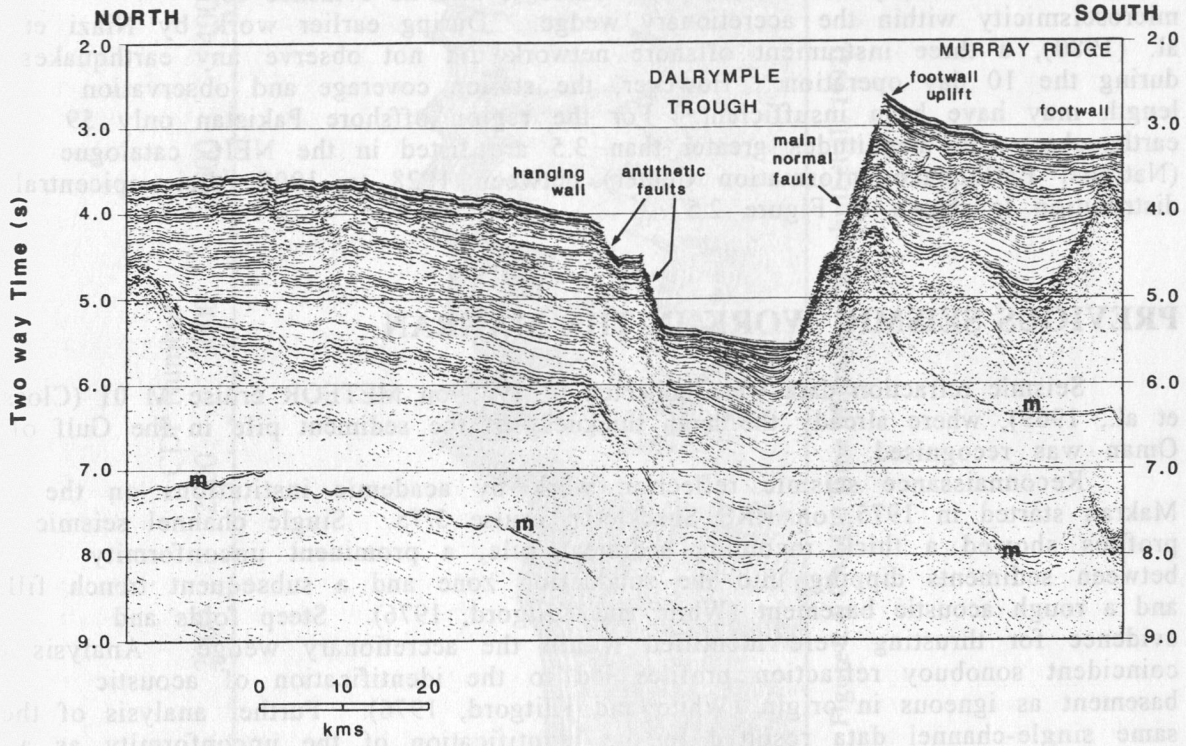

Figure 2.3: Seismic reflection profile across Dalrymple Trough.

The Makran accretionary wedge is a segment of the Arabian-Eurasian plate boundary, that stretches from the strait of Hormuz to the Ornach-Nal Fault Zone in the east (Figure 2.1). The Arabian plate subducts at about 4.5 cm/a beneath the Eurasian plate (DeMets, 1990), and up to 7 km thick sedimentary sequences on the Arabian plate are fed into the subduction zone. Within the sedimentary cover, a prominent unconformity marks the boundary between pelagic sediment below and turbidites above. As a consequence of sediment accretion and underplating, the hugh Makran accretionary wedge has been built up; its submarine width is about 150 km and it stretches further onto the continent for 200 to 300 km. The coastline is assumed to migrate at about 1 cm/a to the south (Page et al., 1979). As such, it is the largest accretionary wedge on Earth. In Figure 2.4, a MCS profile across the Makran accretionary wedge is shown (Minshull et al., 1992). In the Oman Basin, the undeformed sediment layers and the basement of the oceanic

crust are clearly recognized. Along the wedge, several imbricated slices are seen, the most seaward thrust reaches an elevation of 1200 m. The duplexing of the accreted sediment points towards a low basal friction décollement (Kukowski et al., 1994, Gutscher et al., in press). However, multiples mask the décollement and the plate boundary, and thus the depth of the plate boundary is not known in detail. Further east, on near-trace monitor records from profiles collected during SONNE cruise SO 122, this boundary can be traced up to 40 km landward of the trench (Roeser et al., 1977). It is one of the goals of project MAMUT to image and map the plate boundary across the submarine part of the wedge, which is an important constraint on the structural and also the hydrological investigations of this margin. Bottom simulating reflections (BSRs) are commonly observed in the seismic data, and extend also seaward of the steep frontal fold as far as the protothrust.

Seismicity is rather low in general, however, large earthquakes with magnitudes up to 8.1 are known to have occurred here (Page et al., 1979), the last major one in 1945 (Byrne et al., 1992). There is also no evidence for microseismicity within the accretionary wedge. During earlier work by Niazi et al. (1980), a three instrument offshore network did not observe any earthquakes during the 10 day operation. However, the station coverage and observation length may have been insufficient. For the region offshore Pakistan only 59 earthquakes with magnitudes greater than 3.5 are listed in the NEIC catalogue (National Earthquake Information Center) between 1928 to 1997, their epicentral distribution is shown in Figure 2.5.

PREVIOUS SEISMIC WORK IN THE MAKRAN

Seismic refraction data were collected in 1965 on METEOR cruise M 01 (Closs et al., 1969), where already the hugh thickness of the sediment pile in the Gulf of Oman was recognised.

Reconnaissance seismic reflection work by academic institutions on the Makran started in 1975, on RRS Shackleton cruise 3/75. Single channel seismic profiles showed a thick incoming sediment pile, a prominent unconformity between sediments dipping into the subduction zone and a subsequent trench fill, and a rough acoustic basement (White and Klitgord, 1976). Steep folds and evidence for thrusting were identified within the accretionary wedge. Analysis of coincident sonobuoy refraction profiles led to the identification of acoustic basement as igneous in origin (White and Klitgord, 1976). Further analysis of the same single-channel data resulted in the identification of the unconformity as a decollement surface between sediments which were folded at the deformation front and undeformed sediments beneath (White, 1977a). Seismic "bright spots", indicating the presence of gas, were found in the abyssal plain (White, 1977b) and a "bottom simulating reflector" (BSR) in the accretionary wedge which marks the contrast between hydrate-bearing sediment and underlying free gas-bearing sediment (White, 1979).

This reconnaissance seismic work was followed by the acquisition of some multichannel seismic profiles in the western Gulf of Oman from the R/V Atlantis II in 1979, which imaged thrust faults more clearly and allowed the development of an imbricate thrust slice model for the Makran (White and Ross, 1979), and a detailed grid of single-channel profiles collected in 1980 between 62°E and 63°E, with a ~10 km line spacing, which allowed a more three-dimensional view (White, 1982). During the same cruise, long range refraction work was also done, using explosive shots along two 180 km lines, a prototype Cambridge OBH, and five internally recording sonobuoys (White and Louden, 1983). Slope-intercept solutions indicated a crustal thickness of 6-9 km in the Gulf of Oman, and that the downgoing plate dipped at an angle of less than 2° into the accretionary wedge. Fowler et al. (1985) conducted a more detailed analysis of the sonobuoy data collected in 1975 and 1980 and showed that rapid velocity changes occurred in the sediment at the toe of the wedge, indicating rapid dewatering. Behind the first

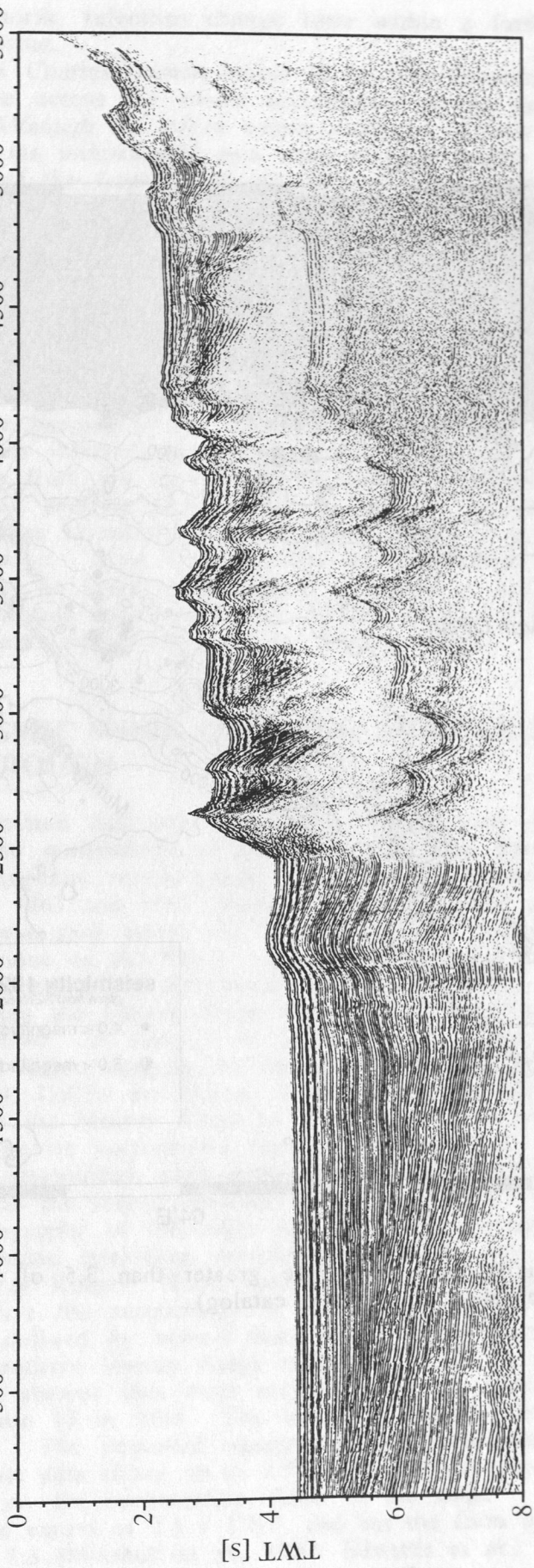

Figure 2.4: CAM30 Time Migration (Minshull et al., 1992).

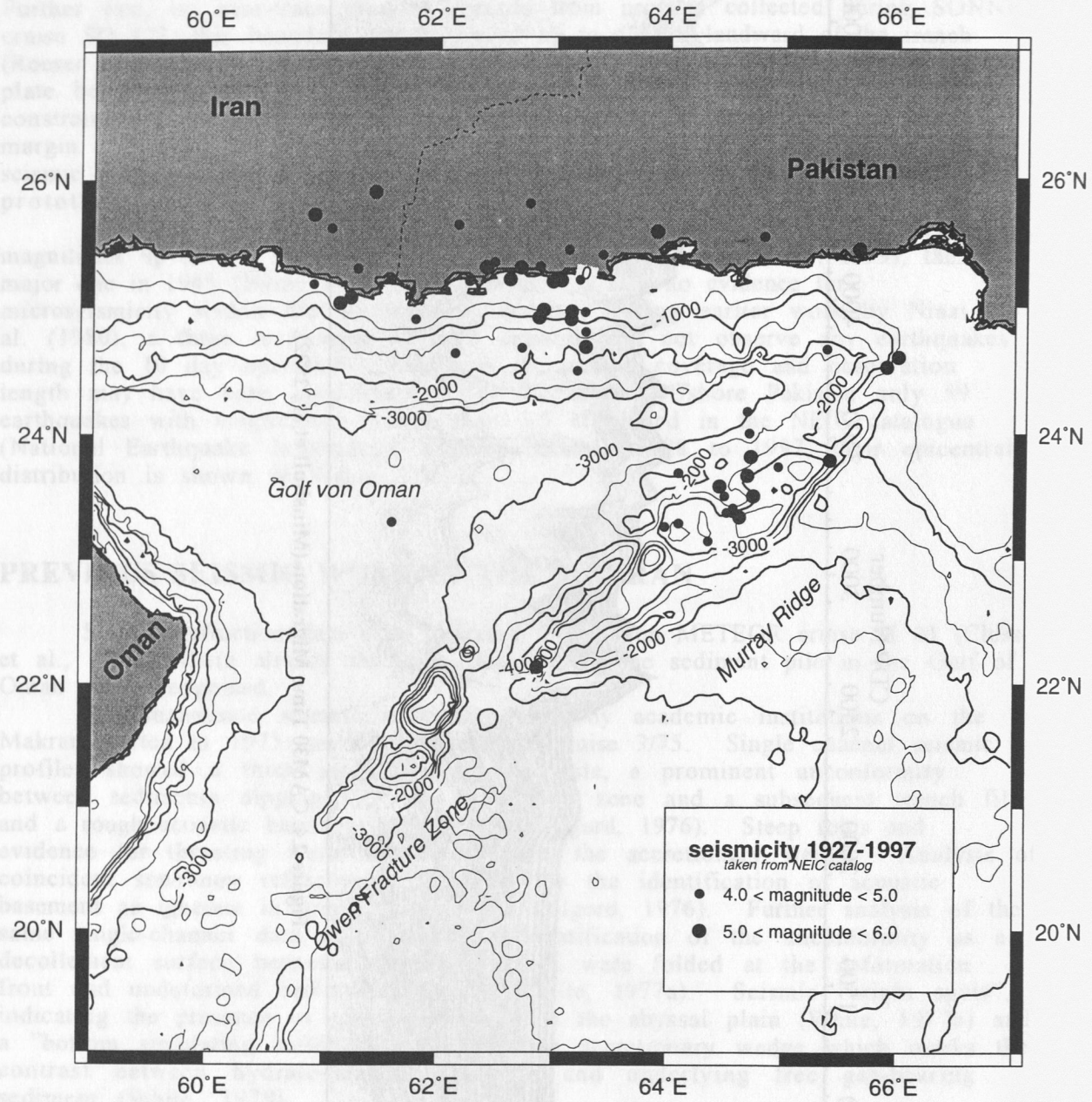

Figure 2.5: Natural seismicity with magnitude greater than 3.5 of the studied area (data are taken from NEIC catalog).

ridge toward the north, velocities change little within a further 75 km landward of the deformation front.

Finally, RRS Charles Darwin cruise 18 in 1986 recorded a single long multichannel profile across the whole accretionary wedge near 63° (Profile CAM 30, Figure 2.4). Although the airgun source consisted of only six guns of a total capacity of 25 l, the multichannel data were of good quality and imaged a proto-thrust zone ahead of the frontal fold, a series of thrust faults within the accretionary wedge, and a BSR which can be followed almost continuously for about 100 km from the abyssal plain seaward of the proto-thrust into the shallower part of the accretionary wedge (Minshull and White, 1989; Minshull et al., 1992). Examination of multichannel stacking velocities allowed further quantification of the dewatering process, and the BSR was used for a preliminary analysis of the thermal regime in the wedge. Local shallowing of the BSR in the vicinity of thrust faults indicated possible focussed expulsion of warm pore fluids along these faults. Prestack depth migration of part of the same profile (Fruehn et al., 1997) led to more precise imaging of the faults and folds, and to tighter constraints on velocities and hence inferred porosities of the dewatering sediment.

Seismic data from the above research efforts is supplemented by 1970s multichannel seismic profiles acquired in the Makran by Marathon and Shell. Some of these profiles extended into deep water, though none as far as the toe of the accretionary wedge. Most of these data are unpublished, but an indication of the data quality may be found in the papers of Harms et al.(1983) and Lehner et al.(1983). The latest data were collected on SONNE cruise SO 122 (Roeser et al., 1997) and cover the Makran wedge and also the Murray Ridge.

PREVIOUS SEISMIC WORK OVER THE MURRAY RIDGE AND DALRYMPLE TROUGH

Seismic reflection data over the Murray Ridge were very scarce until the 1980's, although the morphology of the ridge had been previously mapped from bathymetric and magnetic measurements from cruises aboard the H.M.S. Dalrymple between 1961 and 1963 (Barker, 1966). In 1975 a single channel seismic reflection profile was shot across the southern Murray Ridge and the Dalrymple Trough during a cruise on the R.R.S. Shackleton (Whitmarsh, 1979). The main part of this cruise focussed on the Owen Basin to the south. The first significant seismic dataset across the Murray Ridge was acquired in 1980 during R.R.S. Shackleton cruise 1/80. A suite of 8 single-channel seismic reflection profiles was acquired across the ridge, imaging the structure of the ridge along most of its length (White, 1984; Collier and White, 1990). The reflection profiles show the southern portion of the Murray Ridge to be a highly asymmetric feature, with a broad, low uplift on its northeastern flank, the steep-sided Dalrymple Trough in the centre, and a steep-sided, high ridge on its southeastern flank where acoustic basement outcrops at the seabed (Edwards et al., in prep.). The profiles clearly show that the topography of the ridge and Dalrymple Trough is largely controlled by deep normal faults, providing unequivocal evidence for extension along the length of the Murray Ridge. These lines also crossed the northern portion of the Murray Ridge. Here the morphology is characterised by more gentle troughs and uplifts which are defined by normal faults with smaller surface throws than those observed on the southern Murray Ridge (Edwards et al., in prep.).

Multichannel seismic data were acquired over the Murray Ridge on R.R.S. Charles Darwin cruise 18 in 1986. The lines are located over the southern end of the Murray Ridge. The improved imaging of the multichannel seismics compared to the single channel data shows up to 2.5 s TWT of sediments overlying the acoustic basement on the northwestern flank of the ridge. The Dalrymple Trough contains sediment in excess of 2.5 s TWT, and has the form of a classic rift half-graben, see Figure 2.3 (Minshull et al., 1992: Edwards et al., in prep).

In addition to the multichannel seismic reflection profiles, a wide-angle seismic line, recorded with two ocean bottom seismometers, was shot along the axis

of the Dalrymple Trough during the 1986 cruise. Preliminary modelling of these data suggests that the crust under the Dalrymple Trough may be as thick as 10-12 km, and therefore much thicker than would normally be expected for oceanic crust (Edwards et al., in prep.)

Besides a series of east-west single-channel lines shot by the U.S. Navy ship Wilkes in 1981, the latest multichannel reflection profiles were acquired on SONNE cruise SO 122 (Roeser et al., 1997). They mainly investigate a segment boundary of the Murray Ridge in the central part. One profile was surveyed in the southwestern part and a couple of subparrallel profiles were acquired in the northeastern part (for location see Figure 2.7). Along ist axis Murray Ridge shows a highly variable shape. Contrasting the steep symmetric antiformal structures in the southwest are the smooth morphology in the central part and the asymetric steep faults in the northeast.

MAGNETIC AND BATHYMETRIC SURVEYS IN THE STUDY AREA

Echosoundings and magnetic measurements in the Gulf of Oman were made on various cruises, and the data quality depends much on the navigation systems available during these cruises. The best evaluation of bathymetric data is in the GEBCO digital dataset of 1997 (Figure 2.6). Additional swathmapping data are available to us from previous SONNE cruises SO 90 (von Rad et al., 1997) and SO 122 (Roeser et al., 1997). Magnetic measurements are generally even more sparse. The age of the oceanic crust subducting beneath the Makran continental margin is still disputed (see Figure 2.2). In the area bounded by the Owen Fracture Zone and the Murray Ridge in the south and by the Arabian Peninsula and the Makran in the west and in the north we are probably dealing, at least partly, with crust of the old Tethys ocean (Stein & Cochran, 1985). So far, there are no reliable ages available. South of the Murray Ridge in the Arabian Basin Miles & Roest (1993) identified anomaly 28 (i.e. about 65 Ma) as the oldest anomaly located west of the border between oceanic crust to the southwest and thinned continental crust to the northeast. This age coincides with the emplacement of the Deccan flood basalts.

In the study area or portions thereof several magnetic surveys were conducted. The data of Barker (1966a,b) along the Murray Ridge acquired with H.M.S. Dalrymple show small-scale anomalies correlating with bathymetric highs that probably indicate volcanic-magmatic origin. However, the observed anomalies are very untypical for active spreading mid-oceanic ridges. Thus, the nature of this tectonic feature is still an open question. The positioning errors lie within 1 - 5 nm.

The entire study area was covered by an aeromagnetic survey in 300 m altitude (Taylor, 1968). Here, the positioning error is around 10 nm. North of the Murray Ridge the data show no significant magnetic anomalies neither along the Makran shelf nor in the Oman Abyssal Plain. Analogously to observations off NW-Africa (Wefer et al., 1993) crustal accretion during periods of very frequent magnetic reversals can be represented by very faint small-scale anomalies that might be hidden in the magnetic field offshore Makran, but have not been detected, so far, due to lack of required resolution.

One exception, however, is represented by a linear chain of small-scale anomalies trending sub-parallel to the Murray Ridge some 130 km NW of it. At the SW edge of that chain one circular anomaly coincides with a bathymetric high which is obviously formed by volcanic/magmatic processes according to MCS results of SO 122 (Roeser et al., 1997). So far, however, it is not proven wether we are actually dealing with a continuous feature (named 'Little or Lesser Murray Ridge') as the geometrical arrangement might suggest. Shipboard magnetic data are also available from cruises R.R.S. Shackleton 3/75 and 1/80, R.R.S. Charles Darwin 18 and U.S.Navy ship Wilkes (Edwards et al., in prep.).

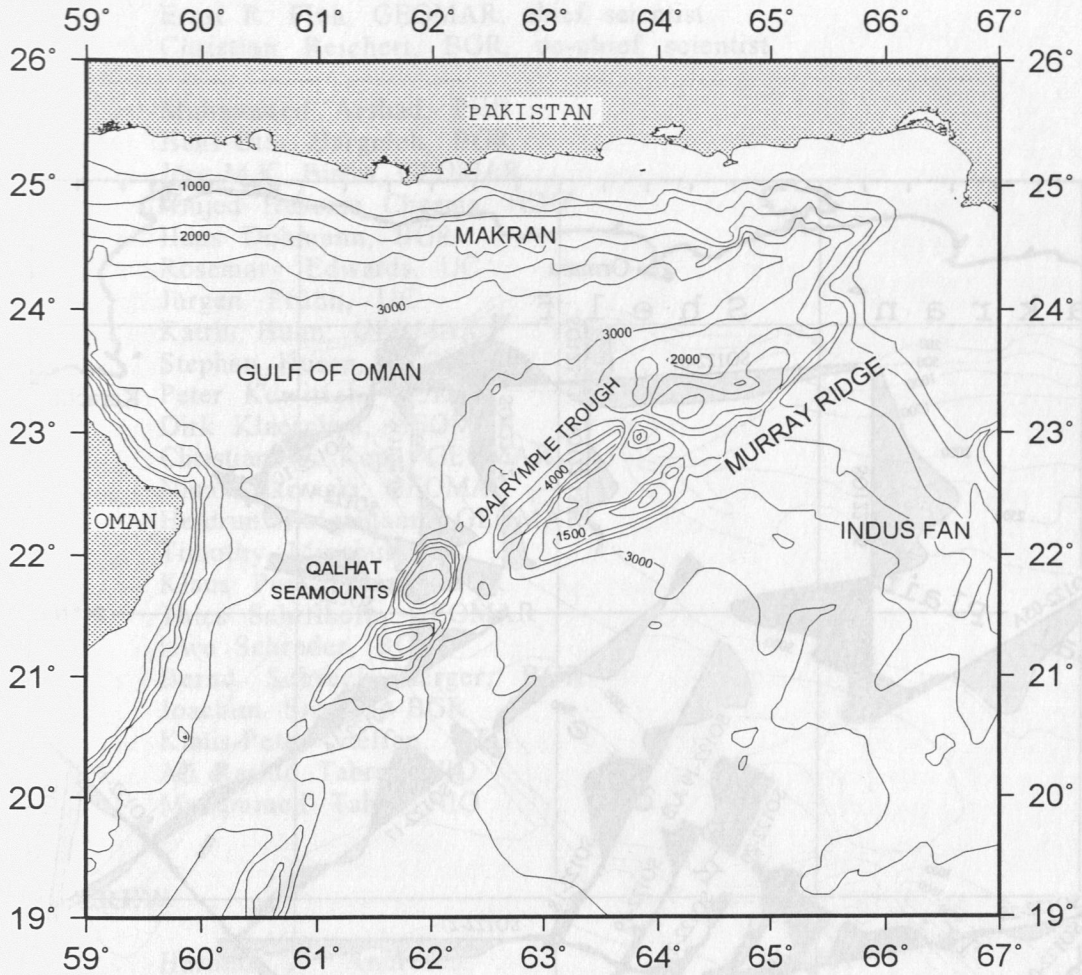

Figure 2.6: Bathymetry of the Gulf of Oman (contours are taken from the GEBCO (General Bathymetric Chart of the Oceans) digital dataset (1997). Contour interval 500 m.

According to Donovan et al.(1979) oil seeps can induce weak magnetization of their close surroundings. So far, it is not known whether fluid vents in accretionary wedges can produce similar effects. The quiet magnetic field of the Makran area with its large number of sub-marine vents provides a good opportunity to test this hypothesis.

All the properties of the magnetic field and the aims mentioned before require a high-resolution tool for detection of weak magnetic anomalies. The BGR gradiometer consisting of two proton magnetometers 150 m apart and towed in a distance of 600 m from the ship's stern fulfils this requirement because the gradiometer cancels the diurnal variations of the magnetic field. It was used along almost all tracks during the cruises SO 122 (Roeser et al., 1997). The observed magnetic anomalies are displayed along the respective tracks in Figure 2.7.

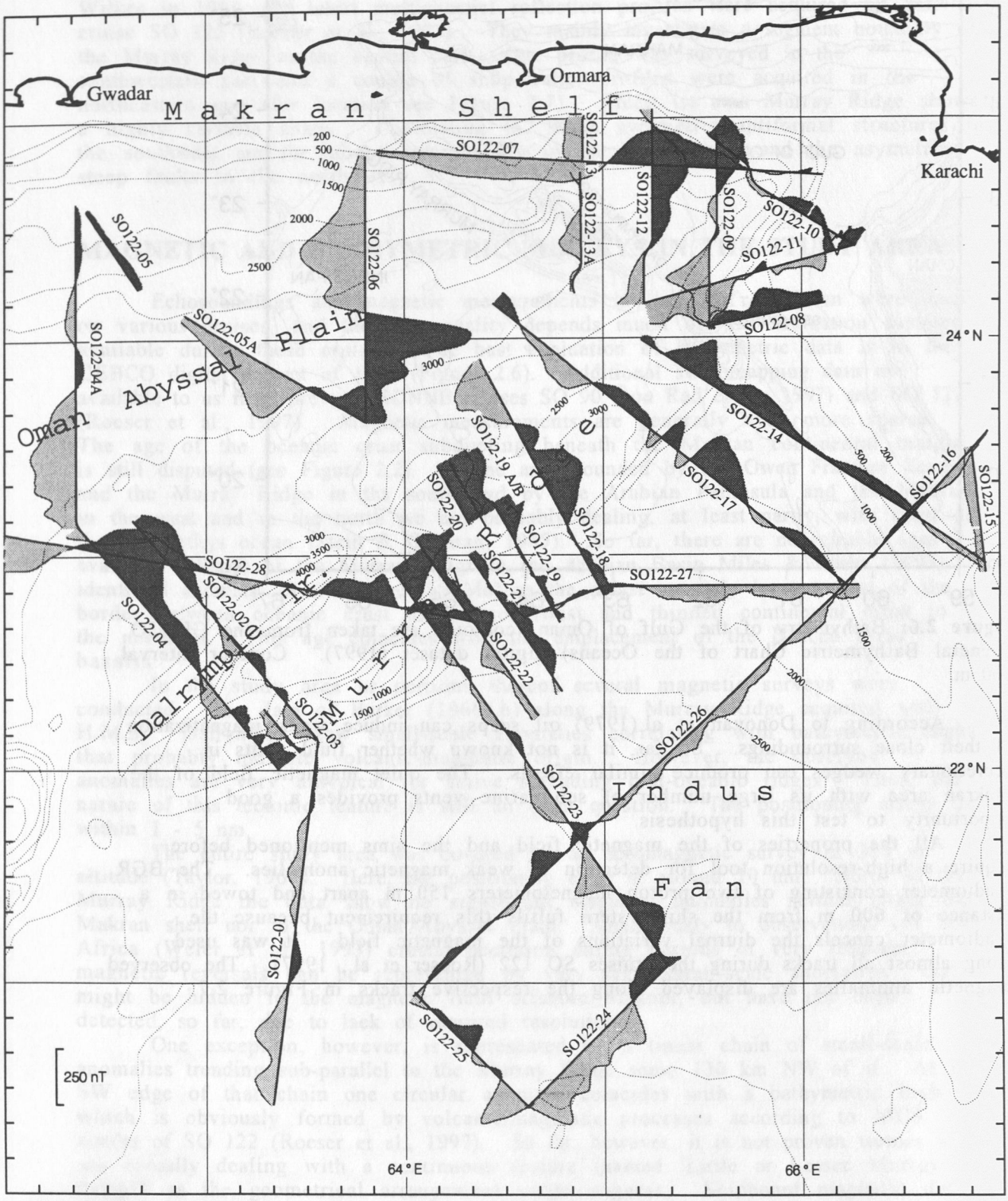

Figure 2.7: SONNE cruise SO 122: tracks and total magnetic field observed (after Roeser et al., 1997). Gray: negative amplitudes; black: positive amplitudes.

3. PARTICIPANTS

3.1. SCIENTISTS

Ernst R. Flüh, GEOMAR, chief scientist
Christian Reichert, BGR, co-chief scientist

Muhammed Arshad, PHD
Hans-Otto Bargeloh, BGR
Jörg M.K. Bialas, GEOMAR
Amjed Hussain Cheema, HDIP
Hans Dohmann, BGR
Rosemary Edwards, UC
Jürgen Frühn, UC
Katrin Huhn, GEOMAR
Stephan Husen, GEOMAR
Peter Kewitsch, BGR
Dirk Klaeschen, GEOMAR
Christian W. Kopp, GEOMAR
Nina Kukowski, GEOMAR
Heidrun Lelgemann, GEOMAR
Timothy Minshull, UC
Klaus Puskeppeleit, BGR
Thies Schillhorn, GEOMAR
Uwe Schrader, BGR
Bernd Schreckenberger, BGR
Joachim Sievers, BGR
Klaus-Peter Steffen, GTG
Ali Rashid Tabrez, NIO
Muhammed Tahir, NIO

3.2. CREW

Hartmut A. Andresen	Master
Leszek T. Szymanski	Chief-Officer
Detlef Korte	1st Officer
Wolfgang Sturm	Radio-Officer
Ingo F. Naeve	Surgeon
Volker Hartig	Chief-Engineer
Peter Uwe Schade	2nd Engineer
Eberhard Bochnik	2nd Engineer
Uwe Rieper	Electrician
Hilmar Hoffmann	Electrician Engineer
Rainer Duthel	Electronic Engineer
Jens Grigel	System-Operator
Andreas Klein	System-Operator
Rudolf Tscharnke	Fitter
Gerhard Paul	Motorman
Hans G. Bethge gen.Becher	Motorman
Helmut Meyer	Motorman
Johannes G. Arronet	Motorman
Wolfgang Evers	Chief-Cook
Lazaros Drakopoulos	2nd Cook
Johann Bronn	Chief-Steward
Heinrich Schramme	2nd Steward
Hans-Jürgen Prechtl	2nd Steward
Hans-Jürgen Vor	Boatswain
Günther Lude	Able Bodied Seaman
Günther Staengl	Able Bodied Seaman
Andreas Schrapel	Able Bodied Seaman
Herman Röpti	Able Bodied Seaman
Ingo Wittkowski	Able Bodied Seaman
Jürgen Kraft	Able Bodied Seaman

3.3. ADDRESSES OF PARTICIPATING INSTITUTIONS

GEOMAR: GEOMAR
Forschungszentrum für
marine Geowissenschaften der
Christian-Albrechts-Universität zu Kiel
Wischhofstraße 1-3
24148 Kiel
Germany
Tel. 0049 - 431 - 600 - 2972
Fax. 0049 - 431 - 600 - 2922
e-mail: nn@geomar.de

BGR: Bundesanstalt für Geowissenschaften und Rohstoffe
Stilleweg 2
Postfach 510153
30631 Hannover
Germany
Tel. 0511/643-0
Fax. 0511/643-3663
e-mail: creichert@bgr.de

UC: University of Cambridge
Department of Earth Sciences
Bullard Laboratories
Madingley Road
Cambridge
CB3 OEZ
United Kingdom
e-mail: minshull@esc.cam.ac.uk

GTG: Geomar Technologie GmbH
Wischhofstraße 1-3
24148 Kiel
Germany
Tel. 0049- 431 - 7209610
Fax 0049- 431 - 7209699
e-mail: gtg@geomar-gtg.de

NIO: National Institute of Oceanography
St. 47, Block-1
Clifton, Karachi
Pakistan
Tel. (092)-21- 5860028
- 5860029
- 5860128
Fax. (092)-21-5860129
e-mail: nodc@niopk.khi.sdnpk.undp.org

HDIP: Hydrocarbonal Development Institute of Pakistan
18-H/9 Islamabad
Pakistan
Tel. (092)-51-853964
Fax. (092)-51-9204902
-9208897

PHD: Pakistan Hydrographic Department
DY Hydrographer of Pakistan Navy
11-Liaquat Barracks
Karachi
Pakistan
Tel. (092)-21-56636151-4
Telex: 20774 HYDRO PK

4. AGENDA OF THE SONNE CRUISE SO 123

(E. Flueh)

SONNE cruise SO 123 started on 07. September in Muscat, Oman and lasted until 03. October 1997, again being Muscat being the port. After loading and installing equipment, SONNE left the pier at 10:15 08.09. and reached the Pakistan economic zone at 02:00 09.09. Continuous recording of hydroacoustics and gravity started here and ended when leaving the economic zone at 23:00 on 02.10. A complete trackchart of cruise SO 123 is shown in Figure 4.1.

After two runs for testing releasers of the OBH using W6 winch to 3100 m, a CTD-measurement was made in the Oman Basin in front of the Makran accretionary wedge to waterdepth of 3250 m.

The deployment of 22 OBH, during which two short magnetic profiles were also recorded, was finished 13:30 10.09. Ten instruments were widely distributed (20 mile grid) and should monitor the microseismicity. The remaining instruments were closely spaced along two E-W oriented lines (SO123-01, SO123-02). Shooting along profile SO123-01 started at 15:42 and ended 03:00 11.09. During transit to the next line shooting continued, and profile SO123-02 was started 05:00 11.09. It had to be interrupted at 07:00, due to a fleet of fishing boats on course. After giving way, shooting was resumed at 09:00 about 4.6 nm south of the profile while on transit back to the line heading. The profile was finished at 19:15 11.09 and subsequently those OBH, that were not intended to be part of the network, were recovered. At 21:45 the first OBH (20) was onboard. OBH19 was surrounded by fishing vessels, and could only be retrieved after some detours. OBH17 did not respond immediately to the release commands, but after the active transponder had been deployed to a depth of 150 m, it popped up. At 09:30 12.09 ten instruments were recovered and a search for a suitable waterdepth to test the OBS and several new hydrophones was started. Three OBH (23 to 25) and the OBS were deployed by 15:00. A swimming line with a small surface buoy was attached to the OBS for safety. Shooting was made along the 17 nm long line (profile SO 123-03) twice, using different airgun arrays, and was terminated by 23:00. Two OBH (23 and 24) were recovered by 01:00 13.09, while the OBS and OBH26 were picked up in daylight.

Closely spaced lines to swathmap the complete accretionary complex between 62°15´and 63°15´were run until 23:00 14.09, with the magnetometer also being deployed.

14.09. 23:30: An attempt to release OBH16 failed, despite trying from different azimuths. OBH09 was recovered at 03:00 15.09. and three more Hydrosweep lines were added before trying another release of OBH16 during daylight. This failed again and at 10:30 15.09. SONNE headed south (with magnetics) towards Dalrymple Trough, were deployment of eight OBH (26-33) and the OBS (OBS02) along Profile SO 123-04 was terminated at 03:00, 16.09. Shooting started at 7:00, 16.09. and ended at 22:00. Magnetic and hydroacustic data were subsequently collected along a parallel track to increase the width of the swath, and recovery of the instruments started at 04:00 17.09. with OBH33. OBH28 was picked up at 11:30, and deployment for Profile 05 was finished at 20.00 17.09. OBH27 at the crosspoint of profiles 4 and 5 was left. Approaching the intended start of the shooting line fishing vessels were observed and the startpoint had to be moved to the north. Shooting lasted from 23:30 17.09. to 12:30 18.09. Recovery of the instruments and subsequent deployment along profile 6, with OBH35 at the intersection being left in the water, was finished at 06:00 19.09. Shooting along line 6 was done from 10:00 to 21:30 19.09. The planned recovery of all instruments deployed along line 6 could not be done immediately, because fishing vessels were active in the area. Therefore some more Hydrosweep lines including magnetics on the Dalrymple Trough were made. During this survey for the first itme the sea got a little rough (6 Beaufort). The ship had to deviate from the planned tracks due to another fleet of fishing vessels.

Instrument recovery along SO123-06 was done between 11:00 and 16:00 20.09., and subsequent deployment of 10 instruments across the Murray Ridge on SO123-07 was completed between 20:00 20.09. and 01:30 21:09. Shooting along this line was performed between 05:00 and 22:00 21.09., and recovery lasted from 02:00 to 10:00 22.09. Several profiles with hydroacoustics and magnetics were run to

increase the swathwidth on Murray Ridge and the Dalrymple Graben, before SONNE left the Murray Ridge area on 23.09. and headed north to Makran in perfectly calm seas. Two more fishing fleets prohibited to fill some of the gaps in the swathmapping survey, but the main elements can be recognized. Along the four lines in this area in total 32 OBH and 3 OBS positions had been successfully deployed and recovered, each of them recording the airgunshot without any loss of data.

Recovery of the instruments deployed in the Makran seismological network started 08:00 23.09. with OBH01. Near to the coast again fishing vessels prohibited a straightforward operation, but by 09:00 24.09 all instruments were recovered, including OBH16, which did not release when visited beore on 14./15.09.

Deployment of 19 instruments (OBH58 to 75, OBS05) along profile SO123-08, coincident with the MCS line CAM30, started at 05:00 24.09. and was completed by 17:00. Shooting started on Little Murray Ridge at 4 kn and lasted from 21:00 24.09. to 17:00 25.09.; the magnetometer was not deployed during this line. Subsequent pickup was made until 9:00 26.09., with OBH64 left due to fishing vessels.

The last two profiles (SO123-09 and SO123-10) were covered with nine OBH each, deployment started after a safety exercise at 13:00 26.09. and was finished at 22:30. Shooting along Profile SO123-09 was done at 4 knots between 01:00 and 17:00 27.09., with the magnetometer being deployed again. The shots were also recorded by the nine instruments along SO123-10. Recovery of the OBH from the profile SO123-10 was done between 20:00 27.09. and 02:00 28.09. After transit, shooting along SO123-10 started at 05:00 and was completed at 21:30, at a ship speed of 4 knots. Soon after the start SONNE had to deviate from the planned course to bypass some fishing vessels. The magnetometer was not deployed. Subsequent pickup of the instruments was made between 01:00 and 06:00 on 29.10., which ended the seismic programme after 92 OBH and 5 OBS deployments, all of which were safely recovered.

Swathmapping of the Makran slope between 63°15' and 63°40' was made along 11 tracks and was terminated at 4:00 on 30.09. Then the magnetometer was taken in to be prepared for packing. Further swathmapping between 62°10' and 62°20' and filling gaps in the central part continued until 20:00 01.10., when SONNE headed towards Muscat. Recording of Hydrosweep data ended at 23:00 on 01.10., when the Pakistan EEZ was left. The Muscat pilot met SONNE at 15:00 and she finally docked after 25 days at sea at the pier at 16:00 on 02.10. During the very successful cruise SONNE travelled a total distance of 4800 nm, in always almost perfect weather conditions and without any noticeable delay.

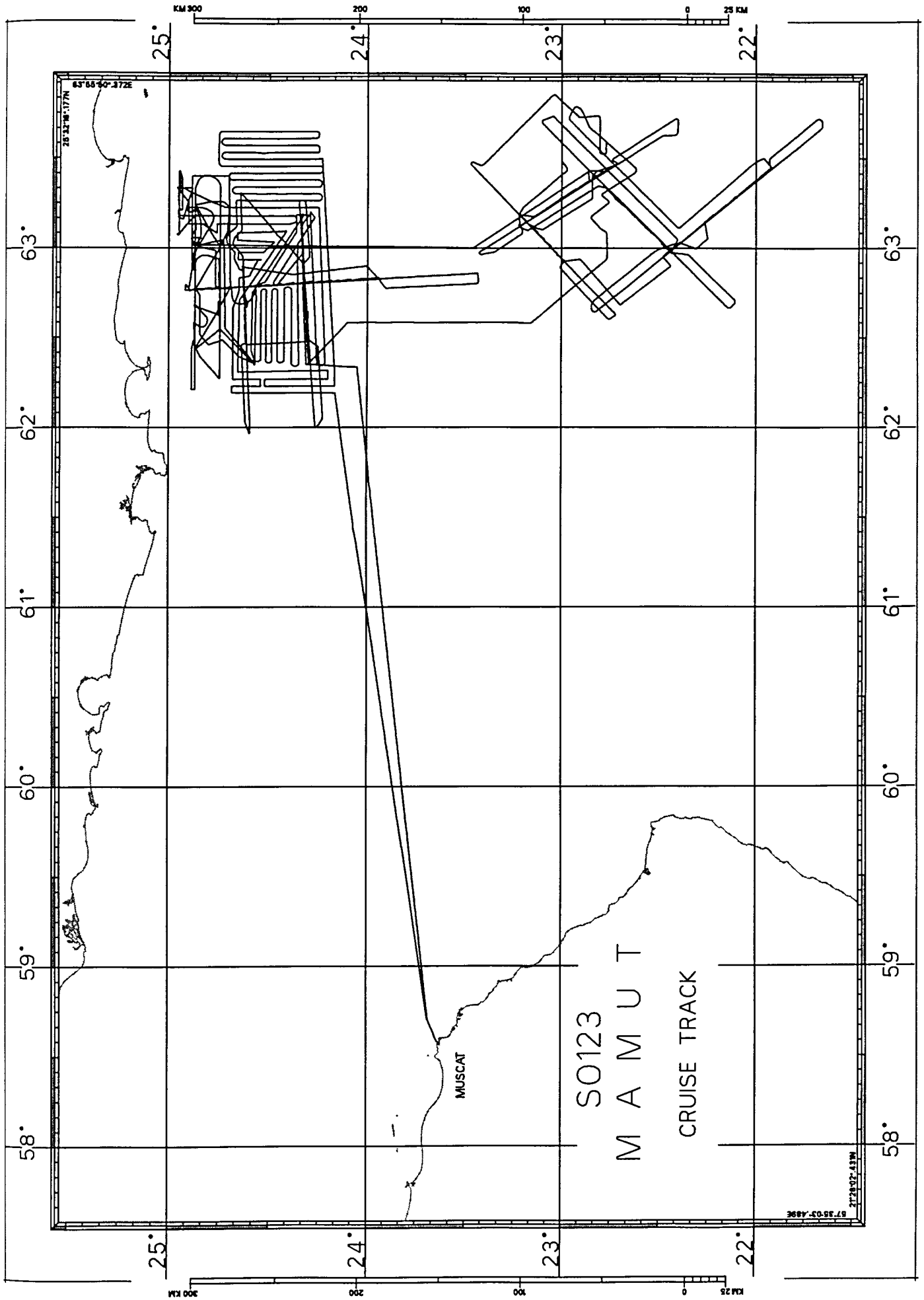

Figure 4.1: Trackchart of SO 123-MAMUT.

5. SCIENTIFIC EQUIPMENT
5.1 COMPUTER FACILTIES
5.1.1 COMPUTER SYSTEMS FOR SEISMIC WORK

(J. Bialas)

For data analysis and processing purposes GEOMAR installed the following hardware configuration into the SONNE's scientific computer network:

a) Sun-IPC:
24 MB RAM, 4.5 GB disk, 17" color monitor
HP-DAT drive, CD ROM
1/2" Storage Tek tape drive with long record driver

b) Sun-Lx:
32 MB RAM, 9.5 GB disk, 17" color monitor
Methusalem SCSI (OBH playback)
HP-DAT drive
OYO G612 thermal plotter

c) Sun-Ultra 1:
32 MB RAM, 19 GB disk, 17" color monitor

d) HP 5900:
32 MB RAM, 6 GB disk, 19" color monitor
HP-DAT drive
CD-ROM

e) Macintosh PowerPC:
16 MB RAM, 500 MB disk, 17" color monitor

f) Macintosh PowerPC:
16 MB RAM, 500 MB disk, 17" color monitor

g) HP LaserJet 4MV:
1 MB RAM, MIO (Ethernet, Local Talk), Paper Size A3

h) 1 X-Terminal:
14" color monitor

i) 1Pentium PC:
32 MB RAM, 1 GB disk, Windows 95 & Linux operating system
17" color monitor, HP-DAT drive, CD-ROM

In addition several portable labtops and PC were installed for word processing and dedicated tasks. The BGR group continued with their set of Vax workstations and PC's which were already installed for cruise SO 122 and are described in chapter 5.1.2. The Cambridge group installed a Sun Sparc 10 with a 2 GB disk and an Exabyte drive.

The dry and wet chemistry laboratories were choosen for the set up of the GEOMAR and Cambridge units while one Macintosh was placed into the Reinlabor. All components were connected to the ship's thinwire ethernet. Easy access could be provided as only one network wide home account per user was established. Data access was simplified by remote mounting of data disks across the network. Using ftp and telnet the Sun workstations and the ship's Vax computer could be contacted.

The rather old Sun-IPC workstation was dedicated to serve as terminal and data storage. The Sun Lx system and the Sun Ultra were used for the seismic processing of the OBH data. Using the software packages GEOSYS (Schlumberger, formerly Prakla-Seismos, restricted to the LX) and Seismic Unix (Colorado School of Mines) first processing steps and section display were done. First raytracing models could be done using Rayinvr on the Sun workstations and MacRay on the Macintosh computers. A two dimensional FD inversion code of Ammon and Vidale (1993) was provided on the Sun Ultra. Hydrosweep data processing was done on the GEOMAR HP 5900 using the MB software package with data display through the GMT plotting system. Printing of PostScript Files was mainly done through the GEOMAR HP-4MV printer on size A3 and A4 paper. As the shipboard printers do not have a Postscript

module only the HP workstation was able to print out plots on those printers due to HP internal applications.

With increasing network activities the connections became instable and forced to reconfigure the additional ethernet rings 14 days after start of the cruise. The GEOMAR and Cambridge workstations were disconnected from the VAX network and included into the ship's PC network ring in order to stabelize the remaining ethernet again. This was necessary to ensure the navigation processing by the BGR computer systems. Since 24. Sept. the GEOMAR Power Macintosh computer in the Reinlabor seemed to cause sever network collisions and was switched off the network. Network connections became more stable untill the end of the cruise although the repeaters were still reporting much more network data collisions than expected during „normal" traffic. The heavy data load caused by the cross mounted data disks and home accounts slowed down the network remarkably. Several times network hung ups on one or the other sun workstation interrupted data processing and backup operations. A separation of such a heavy duty set up of processing computers should be choosen next time. Setting up a local network ring which is connected to the shipboard ethernet via a bridge or repeater is adviced for the next cruise.

5.1.2 COMPUTER SYSTEMS FOR NAVIGATION, GRAVITY, AND MAGNETICS

(B. Schreckenberger, H.-O. Bargeloh)

The BGR's marine gravity/magnetics group operates two VAXstation computers that run under the operating system VMS. On board of R.V. SONNE they are connected with the ship's computers and terminal servers via thinwire Ethernet. One of the computers (VAXstation 3200) is equipped with 32 serial interface connectors and is used for data acquisition and realtime data display. Data processing, interpretation, and text processing is done on a VAXstation 3100/M76.

The following list contains the hardware used for data acquisition and data processing:

- Workstation for data acquisition: VAXstation 3200, 32 MB memory, 32 serial lines, 2 GB hard disk, MO optical drive
- Workstation for data processing and interpretation: VAXstation 3100/M76, 32 MB memory, 3 GB hard disk, MO optical drive, DAT tape drive
- 2 PC systems
- 3 Plotters (1 drum plotter Hewlett-Packard Draftmaster II, 1 desk-top plotter Mutoh iP 220, 1 ink-jet printer/plotter DEC LJ250)
- 3 printers (1 laser printer DEClaser 3500, 1 dot-matrix printer Fujitsu DL-2400, 1 dot-matrix-printer DEC LA50)
- 3 graphic terminals, 1 alphanumeric terminal
- 1 precision digitizer Kontron Summagraphics (DIN A1)
- 1 scanner Hewlett-Packard ScanJet 4c
- 1 satellite controlled clock Meinberg GPS 166

All computers were integrated into the LAN of the ship. The VAXstation 3100 also worked as a network server (file and print services using Digital PCSA) for the PC systems.

EQUIPMENT OF THE SHIP USED DURING THE SURVEY

The list contains only the most important systems:

- 2 GPS receivers Ashtec LD-XII
- 1 GPS receiver Trimble 4000 DS
- 1 DGPS system Racal Skyfix incl. MultiFix 2 software
- 1 interface processor belonging to the ANP2000 navigation system
- 1 general purpose minicomputer MicroVax 3100 (‚WISVAX')
- 4 Digital terminal servers
- 1 plotter Graphtec MP 4300 (DIN A3)
- 1 ink-jet plotter Hewlett-Packard DesignJet 650C
- 1 precision digitizer Kontron Summagraphics (DIN A0)
- Alphanumeric terminals
- PC systems (text processing and graphic data processing)

DATA ACQUISITION

All data are read into the computer via serial interfaces or over the Ethernet network. There is a number of real time programs that write the data into the memory as soon as they are available. The main data acquisition program checks, reformats, and collects the data items to one data set each 20 seconds and writes it to direct access files on magnetic disk.

The navigation data come via the ship's WISVAX computer over an ethernet link once per second. On this cruise the following data were received from the ship's navigation system:

- Position from Differential GPS
- Heading from the gyro
- Speed from the doppler-sonar (DO-Log)
- Waterdepth values from HYDROSWEEP (the central beam only) and PARASOUND
- Weather data, water temperature, and salinity.

The following data are read over serial lines:

- Precice time marks (UTC) from a GPS controlled clock once per second
- Shot point numbers and shot point times from the seismic system
- Magnetic total intensity and depth below the sea surface for both sensors from the gradient magnetometer
- Heading of the magnetometer array from the compass between the sensors
- Raw gravity values from the marine gravimeter

The data acquisition program provides online navigation data for the following systems:

- Once per second to the marine Gravity meter where they are used to support the gyro system
- For every shotpoint to the seismic system

Analog recordings are written for the magnetic total intensity, the gradient, and the gravity. Moreover, we use a small navigation program (Roeser et al., 1992) for plotting the planned profile lines and a continuous online track plot on a DIN A3 plotter.

5.2 SEISMIC DATA AQUISITION

5.2.1 THE CAMBRIDGE MINISTREAMER (SINGLE CHANNEL SEISMIC ACQUISITION SYSTEM)

(T. Minshull, R. Edwards, J. Fruehn)

Single channel seismic reflection data were obtained using a Geomechanique 30 m active section with a 100 m tow cable, about 70 m of which was outboard of the stern of the ship. A test deployment suggested that the streamer was towing too shallow, so a 5 kg weight was added to the tow cable just ahead of the active section for the first shooting (lines 1, the turn, and part of line 2). Data were recorded on the Bullard Laboratories PC-based SAQ acquisition system, with a record length of 12 s and a sample interval of 4 ms, in SEGY format 3, i.e. 2-byte integers. The hydrophone signal was passed through a pre-amplifier and two different analogue filters for recording on two different channels. Gains were set so that the direct water wave was just clipping. Channel 1 was filtered 3-80 Hz, and channel 2 was filtered 6-50 Hz, while the anti-alias filter of the acquisition system is active above 64 Hz. Channel 2 was used for real-time display, while channel 1 was used for subsequent processing. The data from the first shooting suffered from strong low-frequency noise (10-20 Hz), presumably caused by the close proximity of the streamer to the airgun array and ship, so a further 5 kg depressor weight was added for the remainder of line 2. The noise persisted in line 2, so weights were removed for line 3, then replaced by 9 kg of scrap cable taped around the tow cable, for a more streamlined configuration, during line 4. For line 5 onwards, the tow cable was extended a further ~10 m, to place the streamer ~80 m astern of the ship. For line 6 the extra cable weight was removed, but there was no improvement in the data, so the cable weight was added for the rest of the cruise.

The acquisition system was triggered directly from the airgun firing system, i.e. 30 ms before the shot instant. Examination of the data showed that the trigger time was varying by ~10 ms with respect to the shot instant, presumably because the trigger signal shape varied slightly from shot to shot. The resulting "jitter" was removed by automatic picking of the direct arrival and application of a corresponding static correction to each trace. The strong low-frequency noise and the large (150 m) shot interval meant that data quality was poor, but application of a low cut filter, set typically to 15-20 Hz, allowed good imaging of the top 1-2 s of the sediment, particularly in flatter areas where spatial aliasing was less severe.

5.2.2 THE GEOMAR OCEAN BOTTOM HYDROPHONE (OBH)

(E. Flueh and J. Bialas)

THE INSTRUMENT

The first GEOMAR Ocean Bottom Hydrophone was built in 1991 and tested at sea in January 1992. A total of 22 instruments were available for SO123. This type of instrument has proved to have a high reliability; in fact during this cruise, the 700th successful deployment was made. Altogether 97 locations were occupied during the MAMUT cruise.

The principle design of the instrument is shown in Figure 5.2.2.1, and a photograph showing the instrument upon recovery is seen in Figure 5.2.2.2. The design is described in detail by Flueh and Bialas (1996).

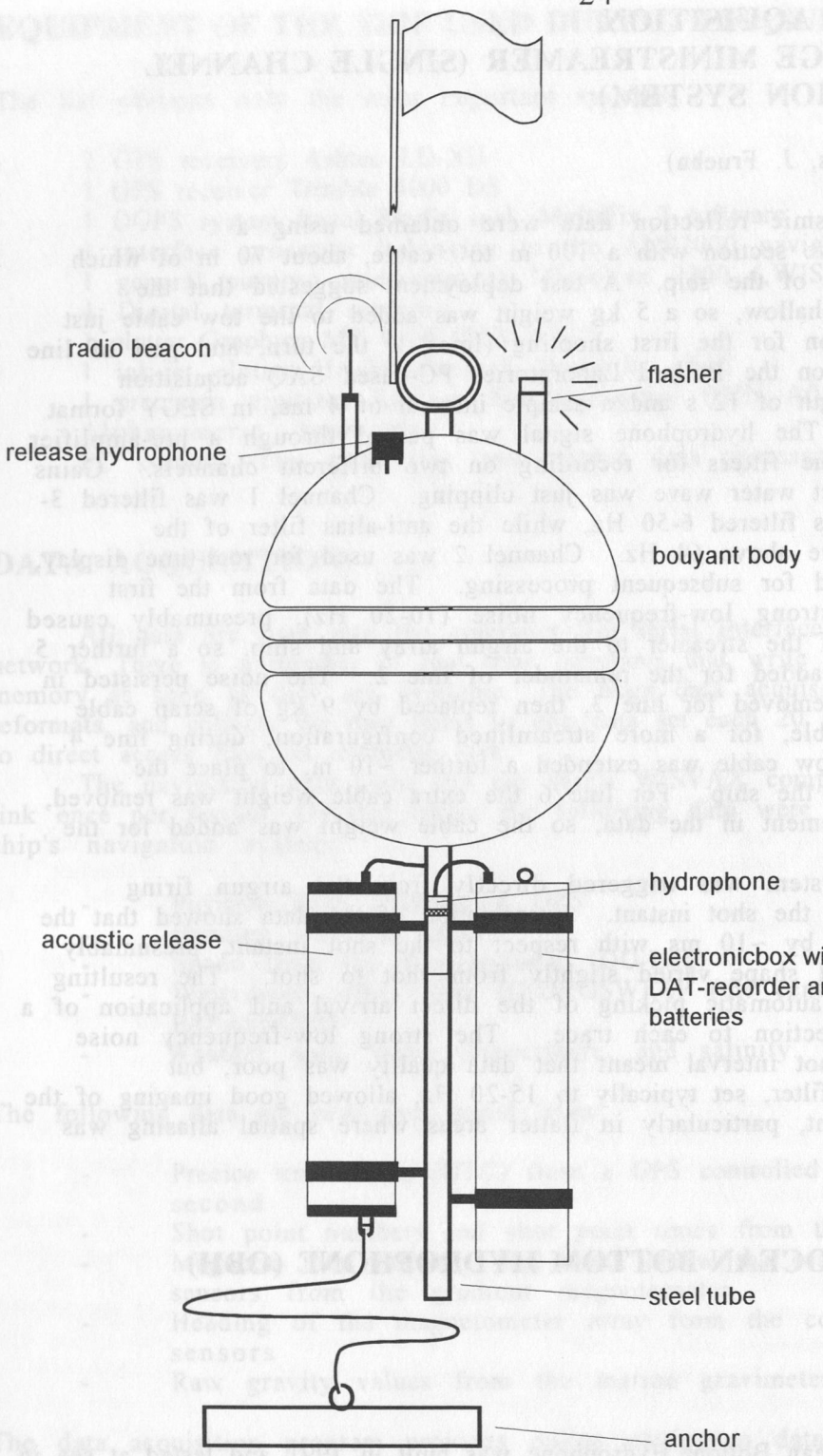

Figure 5.2.2.1: Principle design of the GEOMAR OBH

The systems components are mounted on a steel pipe, which holds the buoyancy body on its top. The buoyancy is made of syntactic foam and is rated, as are all other components of the system, for a waterdepth of 6000 m, except for the pressure cylinders, holding the recording electronics. Here various models for variable depth (2500 m, 3000 m, and 6000 m) are available. Attached to the buoyant body are a radio beacon, a flash light, a flag and a swimming line for retrieving from aboard the vessel. The hydrophone for the acoustic release is also mounted here. The release transponder is a model *RT661CE* made by *MORS Technology*. Communication with the instrument can be made through the ships transducer system, and even at maximum speed and ranges of 4 to 5 miles release and range commands are successful. For anchors, we used pieces of railway tracks that

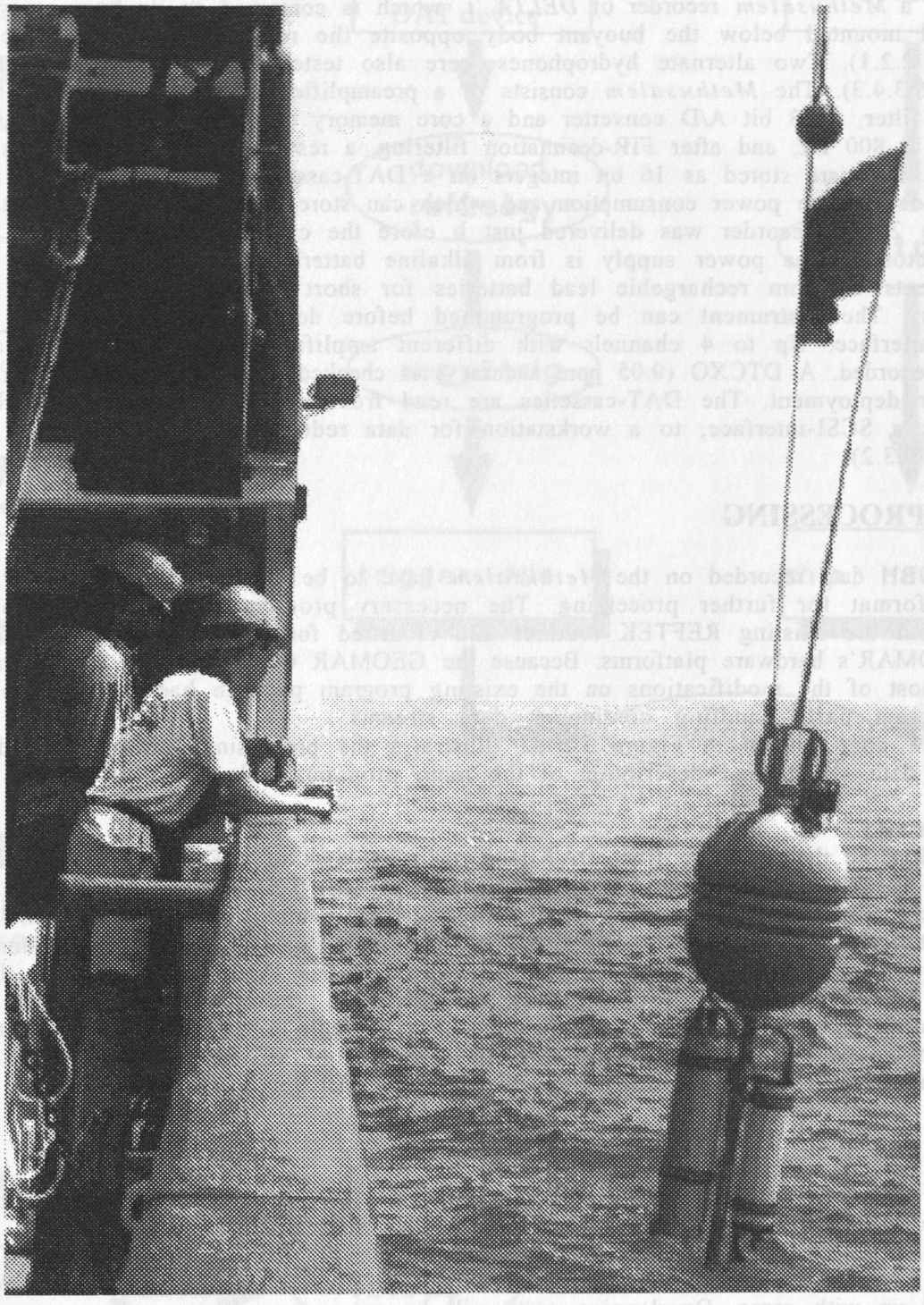

Figure 5.2.3.2: The GEOMAR OBH upon recovery.

weighed about 40 kg each. The anchors are suspended 2 to 3 m below the instrument. The sensor is an *E-2PD* hydrophone from *OAS Inc.*, and the recording device is a *Methusalem* recorder of *DELTA t*, which is contained in its own pressure tube and mounted below the buoyant body opposite the release transponder (see Figure 5.2.2.1). Two alternate hydrophones were also tested during this cruise (see chapter 6.3.4.3). The *Methusalem* consists of a preamplifier (26 dB), a highpass and antialias filter, a 13 bit A/D converter and a core memory of 0.768 MB. Signals are sampled at 800 Hz, and after FIR-decimation filtering, a resolution of 14 to 15 bits is achieved. Data are stored as 16 bit integers on a DAT-cassette, which is run in audio-mode to save power consumption and which can store about 1.1 GB of data. A prototype 24 bit recorder was delivered just b efore the cruise, but tests were unsatisfactory. The power supply is from alkaline batteries for long term deployments or from rechargeble lead batteries for short term deployments (up to 3.5 days). The instrument can be programmed before deployment through an RS232 interface. Up to 4 channels with different amplifications and sampling rates can be recorded. A DTCXO (0.05 ppm accuracy) is checked against GPS time before and after deployment. The DAT-cassettes are read from a playback system, which simulates a SCSI-interface, to a workstation for data reduction and analysis (see Chapter 6.3.2).

DATA PROCESSING

The OBH data recorded on the *Methusalem* have to be converted into standard SEG-Y format for further processing. The necessary program structure was mainly taken from the existing REFTEK routines and modified for the OBH requirements and GEOMAR's hardware platforms. Because the GEOMAR OBH works in a continous mode, most of the modifications on the existing program package had to be done in the program parts handling continuous data streams.

A flow chart shown in Figure 5.2.2.3 illustrates the processing scheme applied to the raw data. A detailed description of the main programs follows below:

- **ref2segy**

Downloading the raw data from DAT tape on a harddisk of a SUN workstation is done by the program ref2segy. It will produce a pseudo SEG-Y trace consisting of one header and a continous data trace containing all samples. For each channel (different amplifications) one file will be created. The name of this file contains the start time, the serial number of the *Methusalem* and the channel number. In addition a log and an error file will track the download process. The file size of the data is directly related to the recording time. For example a recording time of one hour sampled with 200 Hz will produce a file size of 1.44 MB per channel. A record with two channels and a recording time of two days will get a total data volume of 70 MB.

- **merge**

If a tape error occured during the download process, the ref2segy program has to be restarted. This will lead to several data files with different starting times. Merging these files into a single file is done by the program merge. The gap between the last the sample and the first sample of the consecutive data trace will be filled up with zeros. Overlapping parts will be cut out.

- **segy2trig**

The trigger signal, which is provided by the airgun controll system, is recorded simultaneously on an additional *Methusalem* during the shoting period. This tape is treated as a regular data tape and downloaded to the harddisk via the ref2segy program. The segy2trig program detects the shot times in the data stream. It determines the shot times by detecting the trigger signal through a given slope steepness, duration and threshold of the trigger impulse. The output is an ASCII table consisting of the shot number and the shot time. The accuracy of the shot time is one of the most crucial matters in seismic wide-angle work. It has to be reproduced with a precision of 5 ms. Due to this demand the shot times have to be corrected with the shift of the internal recorder clock. As additional information the trigger file contains the profil number and the start/end time of the profil and

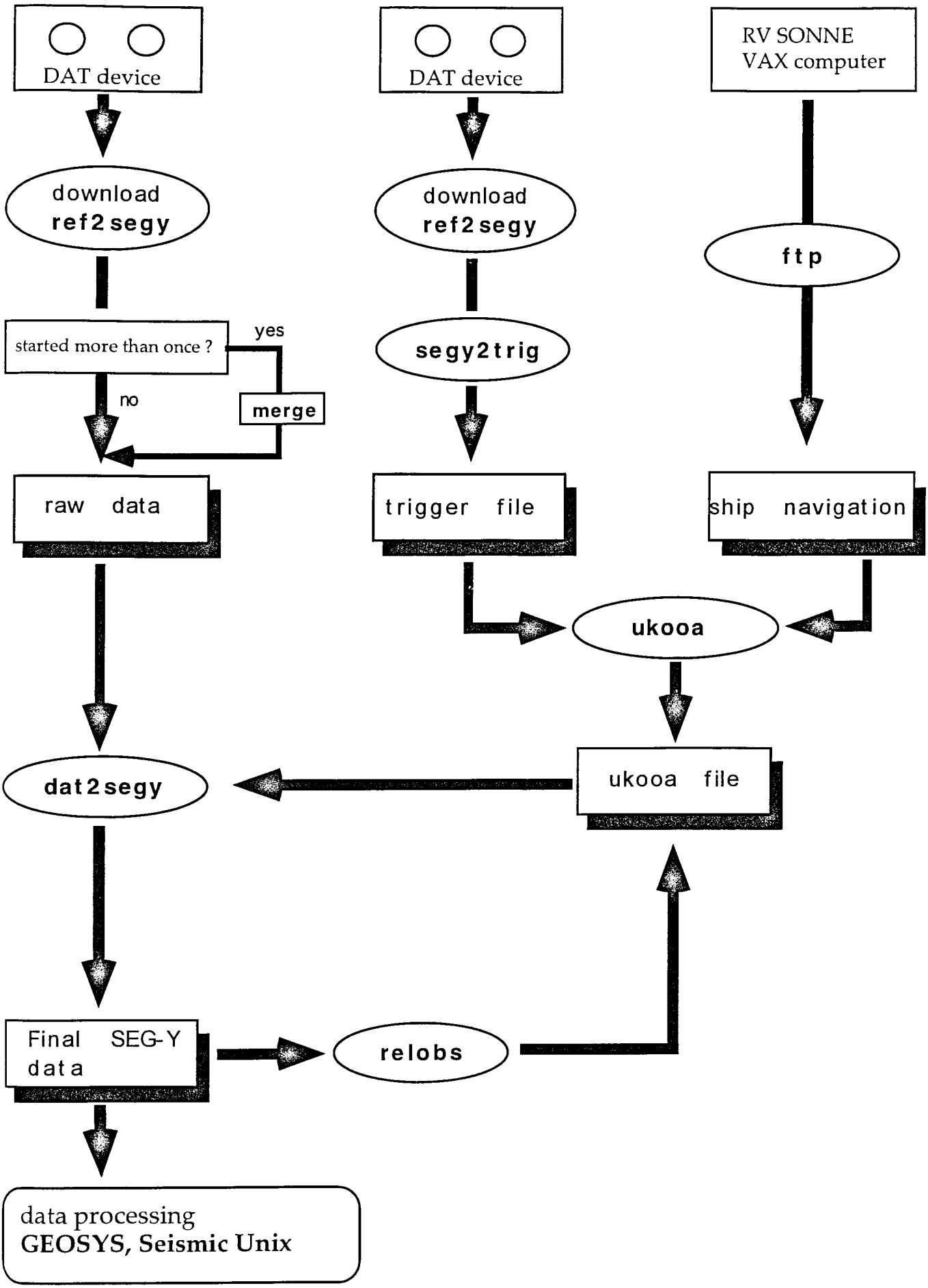

Figure 5.2.3.3: processing flow from raw data to SEG-Y records.

the trigger recording. The shot times are part of the UKOOA file which links the coordinates of the source and the hydrophones with the shot times.

- **ukooa**

The ukooa program is used to establish the geometric data base. It requires the trigger file containing the shot times, the ships navigation and the position of each OBH for input. The ship navigation is stored in a database about every 30s (see Chapter 5.4.3). The program calculates the coordinates of each shot and creates a file in the UKOOA-P84/1 format as output. This file will be used when creating a SEG-Y section via the dat2segy program.

- **dat2segy**

The dat2segy program produces standard SEG-Y records in a 16 bit integer format by cutting the single SEG-Y trace (from the merged ref2segy file) into traces with a certain time length. It reads both the ukooa file with the geometry informations and the downloaded raw data as produced with the ref2segy program. In addition the user can use several parameters for controlling the output. These parameters are informations about the profile and the receiver station, number of shots to be used, trace length, time offset of the trace and reduction velocity (to determine the time of the first sample within a record (see Chapter 6.3.2)). Also the clocks drift of the recorder is taken into account and corrected for. The final SEG-Y format consists of the file header followed by the traces. Each trace is built up by a trace header followed by the data samples. The output of the dat2segy program can be used as input for further processing with GEOSYS or Seismic Unix (SU).

Beside these main programs for the regular processing sometimes additional features are needed for special handling of the raw data:

- **divide**

The program divide cuts the raw data stream in traces with a given length without offset and time informations. The output is stored as SEG-Y format. The routine is useful for a quick scan at the raw data or if a timing error has occured.

- **segyhdr**

The routine segyhdr prints all the header values of the raw data on the screen.

- **segyshift**

The program segyshift modifies the time of the first sample, which means that the whole raw data trace can shifted by a given value. This is very useful when shifting the time base from Middle European Time to Greenwich Mean Time or any local time. Because of recording problems, the data sometimes shows a constant time shift, which can be corrected as well with segyshift.

- **castout**

The program castout allows you to cut out a specified time window of the raw data stream. When the shoting window is much smaller than the recording time, one can reduce the data volume by cutting out only the useful informations. This will reduce the demand on diskspace.

- **relobs**

Due to a drift of the OBH during deployment and errors of the ship's GPS-navigation system the OBH-positioning may have a mislocation of up to several 100 m. As this error leads to an asymmetry and wrong traveltime information in the record section it has to be corrected, which is done with the program relobs.
As input the assumed OBH-location, shot-locations and the picked traveltimes of the direct wave near to its apex are needed. By shifting the OBH-position relobs minimizes the deviation between computed and real traveltimes using a least mean square fitting algorithm assuming a constant water velocity.

5.2.3 THE GEOMAR OCEAN BOTTOM SEISMOMETER

(J. Bialas, K.-P. Steffen, E. Flueh)

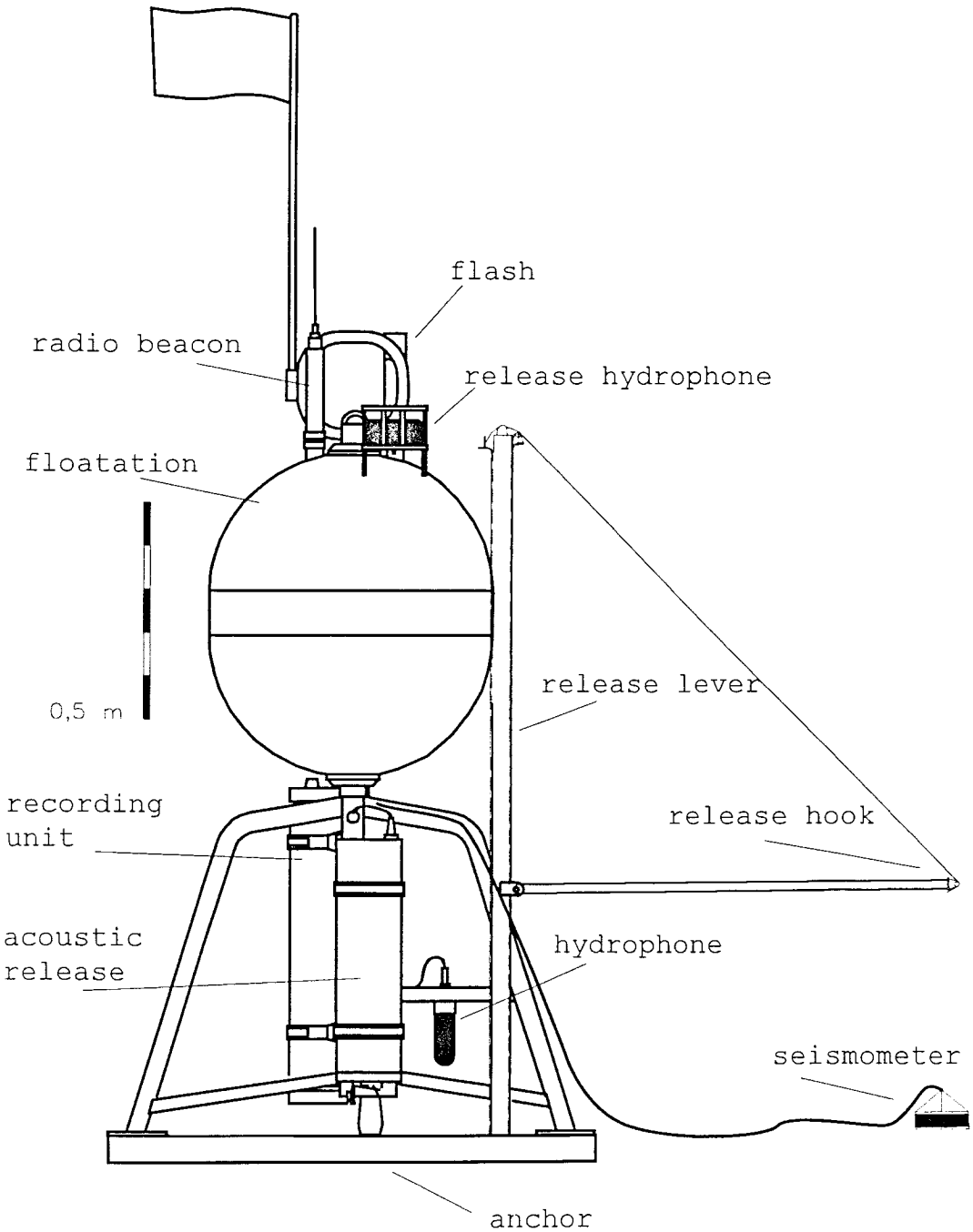

Figure 5.2.3.1: The GEOMAR Ocean Bottom Seismometer.

The prototype Ocean Bottom seismometer construction (Fig. 5.2.3.1) is based on the experiences with the GEOMAR OBH. It was built by GTG, Kiel, Germany. For system compatibility acoustic release, pressure tubes, and the hydrophone are identical to those used for the OBH. Syntactic foam was used as floatation again but of larger diameter due to the increased payload. Other than the OBH the OBS has three legs around its center post to which the anchor weight is attached. While the OBH is floating about 1 m above the sea bottom, the OBS touches the sea bottom to avoid collision of the the seismometer cable with the anchor. The sensible seismometer is deployed about 1 m to the side of the system once the sea floor is touched. During diving of the system the footplate of this seismometer release lever is about one meter below the base of the anchor and will therefore hit the

seafloor at first. During touch down the baseplate forces an upward movement of the lever which will lay out the seismometer hook until the seismometer anchor is about 0.5 m above the seafloor. At about 45 degrees to the vertical the seismometer is released from its hook and falls to the sea floor from about 1 m height. This should ensure the coupling of the seismometer to the sea floor. At this time the only connection from the seismometer to the instrument is a cable and an attached wire which will take the pull load while rising to the sea surface later. A movement or current on the instrument is thus not transmitted mechanically to the seismometer. All three channels are preamplified within the seismometer housing and recorded by the standard Methusalem recorder as used in the OBH units. Parallel to these three channels the standard hydrophone is recorded on the fourth channel.

5.2.4 THE METHUSALEM MARINE BROADBAND SEISMOGRAPH MBS

(J. Bialas)

Besides the OBS another prototype system, the Methusalem Marine Broadband Seismograph (MBS), was brought to the MAMUT cruise.

Experience from the last years showed that the 16 bit Methusalem DAT recorders are no longer sufficient to satisfy the increased needs of data quality and operating times. During airgun profiling amplitude variations are rather strong. To avoid dipping the direct arrivals and reflections at short offset, a low amplification is needed, but the 16 bit data have a too narrow dynamic range. Modern seismic systems use 24 bit technology. Use of the DAT tapes suffers time by time from tape read. Power consumption of the DAT drives is much lower than standard disk drives but needs to be reduced further to enable long term observations longer than 20 days.

These requests lead to the development of the next generation for OBH recorders. Due to rapidly decreased costs of flash memory cards known from PCMCIA slots of portable computers a new storage media is available. The new MBS comprises these advantages together with 32 bit data storage and data reduction techniques. The system design was changed to enable the change of the analog front end with the corresponding A/D converters just by a simple switch. This will enable an easy exchange of recording units between different recording purposes just by exchanging the front end module. Power consumption is also reduced remarkably to 25% of the existing Methusalem version (20 mA sleep, 120 mA wake up).

Unfortunately the prototype version arrived at GEOMAR just one day before departure and could therefore not be checked prior to the cruise. Testing on board RV SONNE was not successful, despite the fact that several error descriptions and diagnoses were exchanged with the producer by e-mail. It turned out that the MBS could not be used due to an internal hardware problem which could not be fixed on board.

5.3 SEISMIC SOURCES
5.3.1 THE AIRGUN ARRAY

(C. Reichert, J. Adam, and U. Schrader)

The seismic signals were generated by a tuned set of 20 airguns (VLF, Prakla-Seismos) grouped in two identical linear sub-arrays 10 m apart on starboard and port side, respectively (Figure 5.3.1). The total volume of the BGR airgun array is 51.2 litres (3,124 cu.in.) filled by pressured air of 135 bar (1,920 psi). Each sub-array consists of 3 groups from stern to tail:

- 4 x 3.0 L + 2.5 L
- 2.5 L + 2.3 L + 2.0 L
- 2.3 L + 2.0 L

The total length of each sub-array is 19.6 m starting at 40 m behind the stern. The geometrical airgun centre is 50 m behind the stern and 110 m behind the positioning reference point (satellite antenna on the main mast). Three buoys per sub-array keep the airguns at 7 m water depth.

Exact shot timing of the particular airguns is ensured by a microprocessor-controlled airgun-synchronisation unit type Prakla VZAD and VZAC2 with storage oscilloscope. The system start is externally triggered by a Meinberg clock GPS 166 during SONNE cruise SO-123.

The pressured air was provided by SONNE's LMF compressor, manufactured by Leobersdorfer, Austria, with a capacity of 25 cbm/minute. In case of malfunction an identical LMF alternate compressor is available.

Quality control during airgun operation consisted of:

- continuous control of the airgun pressure;
- control of the airgun operation (autopops, misfires, delays);
- duly maintenance of particular airgun assembly parts during off-times (e.g. gaskets, valves etc.).

Throughout the survey all 20 airguns were properly working, the air pressure was always in the range 134-135 bar (1,900 psi).

TIME REFERENCE

The Meinberg clock GPS 166 provides the absolute universal time corrected (UTC) from the GPS system. The minute and second pulses bear an accuracy of < 1 ms. 21 GPS satellites and 3 additional spare satellites are on orbit in 20,000 km altitude with a period of ca 12 h per cycle. This ensures that at least 4 satellites can be received at any time at any location in the world. By positioning with 4 satellites an automatic position dependent traveltime compensation is applied.

This time reference was fed into the shooting PC, into the mini-streamer recording system and into the PC that was used for calibration of the internal quartz clocks installed in the respective OBH systems. Thus, an identical time base was provided for all seismic systems.

VZAD AND VZAC

The VZAD unit controls synchronisation and triggering of up to 20 airguns. According to external trigger pulses a 20 ms TTL pulse is generated and sent to the VZAC unit. Here, it is transformed to 60 V and sent to the magnetic airgun valves. The valves do open and in the same instant a sensor sends the time break signal to the VZAD. The deviation between this response pulse and target value (offset) is determined and used for correction of the trigger pulse sent to the airguns providing optimum synchronisation. This procedure automatically compensates

for time delay produced by worn-out assembly parts of particular airguns in the course of operation.

SHOOTING PC AND PROGRAMME CODE

The so-called shooting PC keeps control on all systems. It is connected to the VZAD, to the positioning system and - in case of multi-channel seismics - to the recording system. The programme code TIMER21 used to run this PC is an upgrade of an earlier version TIMERSYN by J. Adam (Hinz et al., 1995). The programme internally generates a series of suitable trigger signals for the VZAD with selectable intervals between 10,000 and 65,535 ms on the PC quartz clock time base. Simultaneously, a random function is superposed varying the interval between ± 300 ms. In combination with multiple coverage seismics and related stacking this is used to suppress the direct waves from previous shots that disturb the current seismic reflection signals.

Alternatively, an external input (e.g. the Meinberg clock GPS 166) can be used. In this mode, TIMER21 generates a series of trigger signals on an absolute time base with selectable intervals between 10 and 65,535 seconds. The random function superposition option is inactive in this case. This mode was used for the operation during SO-123.

The trigger signals are sent to the VZAD that fires the airguns and returns a time break pulse to the shooting PC with a delay of 63,8 ms. This delay is considered when the trigger signals are generated by TIMER21 so that the time break will be exactly at the selected absolute time if the external time base is used.

Simultaneously, via 9 serial RS232 interfaces different data are read and compiled. An 'external header' is generated and saved in a protocol file. The external header comprises the following information:

- shot no, status, GPS time, GPS date, PC date, PC time, actual time, nominal time, half random width
- error, GPS latitude, GPS longitude, course, speed, shot interval
- error, shot no, trigger mode, gun dalay average interval, gun offset
- gun no, status, offset, delay, error
- streamer data (n.a. on SO-123)
- error code, sign, starboard air pressure, label
- error code, sign, port air pressure, label
- error code, latitude, longitude, altitude (position corrected by BGR nav system)
- extension
- software version no

SHOT TRIGGERING DURING SO 123

Generally, the shots were triggered in time intervals of 60 seconds on full minute UTC. Thus, the ship's speed of 5 knots over ground yields a shot distance of 154 m. One exception was made during the first run on the SO123-03 profile that served as a test for a maiden deployment of an Ocean Bottom Seismometer (OBS). Here, a shot interval of 30 s was used with alternating airgun arrangements of the starboard linear sub-array (see also chapter 6.3.4.3). This yielded a shot distance of 77 m at a ship's speed of 5 knots over ground. The shot sequence consisted of three different airgun arrangements fired four times each in a row with the said shot interval:

1. airguns 11 and 12 (= 4.3 L);
2. airguns 16 through 20 (= 14.5 L);
3. airguns 11 through 20 (= 25.6 L).

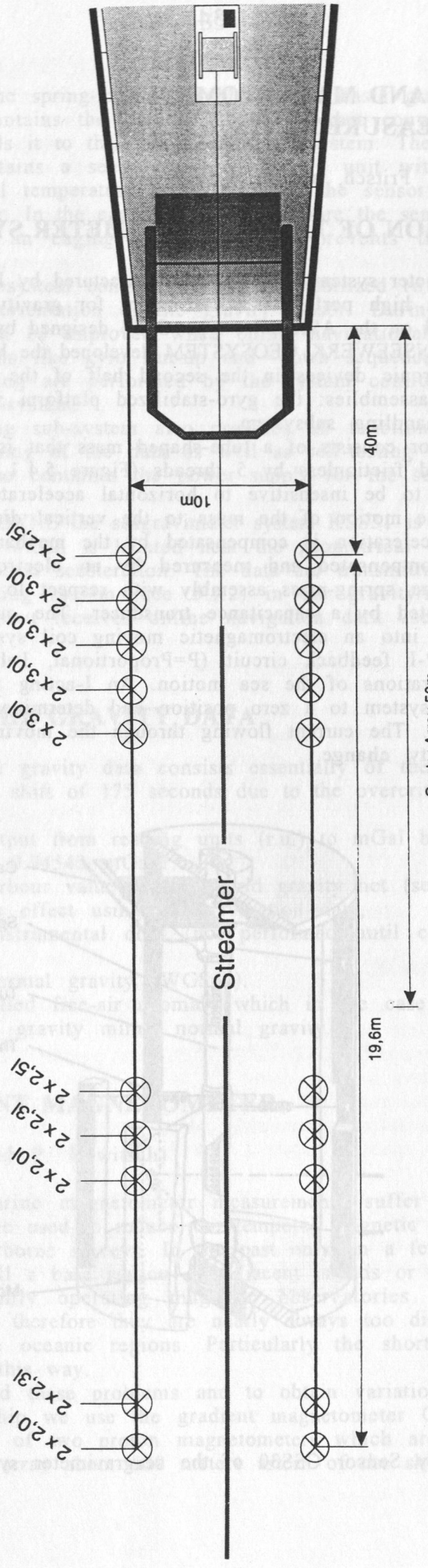

Figure 5.3.1: Geometry of the BGR airgun array.

5.4 GRAVIMETER AND MAGNETOMETER
5.4.1 GRAVITY MEASUREMENTS AT SEA

(B. Schreckenberger, J. Fritsch, and P. Kewitsch)

SHORT DESCRIPTION OF THE SEAGRAVIMETER SYSTEM

The BGR owned gravimeter system KSS31 was manufactured by BODENSEEWERK GEOSYSTEM and is a high performance instrument for gravity measurements at sea. The sensor is based on the ASKANIA type GSS3 designed by Prof. Graf in the 60ties, while the BODENSEEWERK GEOSYSTEM developed the horizontal platform and the corresponding electronic devices in the second half of the 70ties. The system consists of two main assemblies: the gyro-stabilized platform with the gravity sensor and the data handling subsystem.

The gravity sensor consists of a tube-shaped mass that is suspended on a metal spring and guided frictionless by 5 threads (Figure 5.4.1.1). It is non-astatized and designed to be insensitive to horizontal accelerations which is achieved by limiting the motion of the mass to the vertical direction. The main part of the gravity acceleration is compensated by the mechanical spring, but the gravity changes are compensated and measured by an electromagnetic system. Any displacement of the spring-mass assembly with respect to the outer casing of the instrument is detected by a capacitance transducer. The output from the transducer is fed back into an electromagnetic moving coil system used for feedback control. A P-I feedback circuit (P=Proportional, I=Integration) compensates the accelerations of the sea motion. An I-acting feedback provides a signal that drives the system to a zero position and determines an overcritical damping of the system. The current flowing through the moving coil is the measure for the gravity change.

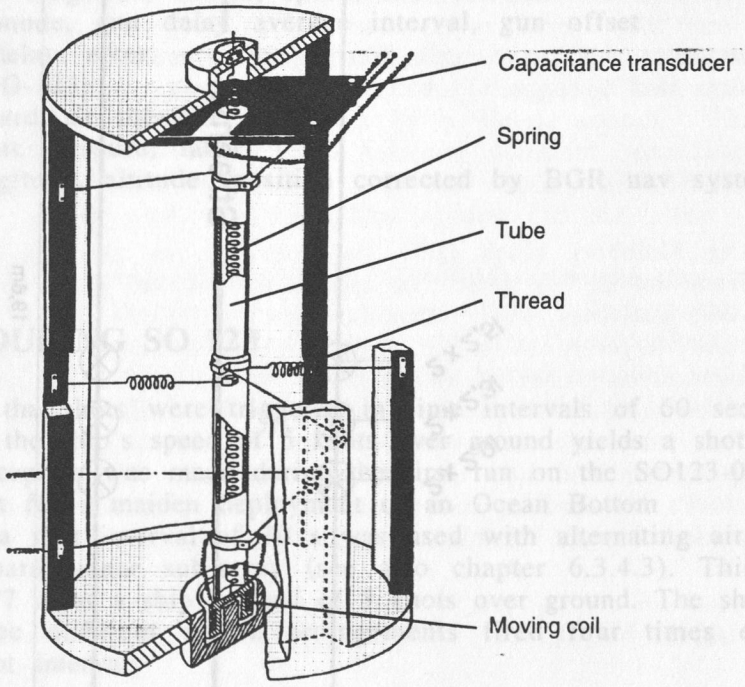

Figure 5.4.1.1: Gravity Sensor GSS30 of the seagravimeter system KSS31.

In addition to the spring-mass assembly as the basic gravity detector the sensor housing also contains the control electronics that converts the current to voltage output and sends it to the data handling subsystem. The power supply of the gravity sensor contains a sealed buffered battery unit with sufficient capacity to maintain the internal temperature stabilization of the sensor for 24 hours in case of a loss of power. In the case of a system failure the sensor electronics automatically activates an caging mechanism that prevents the spring-mass assembly from demage.

The levelling subsystem consists of a gyro stabilized two-axes platform that maintains the vertical orientation of the gravity sensor. During changes of the course this function can be improved when online navigational data are sent to the gravimeter. Functions like gyro run-up and -down sequences as well as automatic platform caging are performed by the system controller unit located in the data handling sub-system.

The data handling sub-system also provides all functions like filtering, logging, and pre-processing of the data as well as self-testing of the instrument and the platform. It also containes the power supply for the sensor and the platform.

On board R.V. SONNE the seagravimeter system KSS31 is installed in the so-called gravimeter room which is located near the geometrical center of the ship, thus minimizing the motion acceleration. The data are transmitted to the BGR data acquisition and processing system (see 5.1.2) in the gravity/magnetic laboratory from where the instrument receives online navigation data used to support the stable platform.

PROCESSING OF THE GRAVITY DATA

Processing of the gravity data consists essentially of the following steps:

- application of a time shift of 175 seconds due to the overcritical damping of the sensor,
- conversion of the output from reading units (r.u.) to mGal by applying a conversion factor of 0.94542 mGal/r.u.,
- connection of the harbour value to the world gravity net (see 6.4.1)
- correction for Eötvös effect using the navigation data,
- correction for the instrumental drift (not performed until completion of the cruise)
- subtraction of the normal gravity (WGS67).

The result is the so-called free-air anomaly which in the case of seagravimetry simply is the observed gravity minus normal gravity.

5.4.2 THE GRADIENT MAGNETOMETER

(B. Schreckenberger and P. Kewitsch)

Generally all marine magnetometer measurements suffer from the lack of base stations that can be used to reduce the temporal magnetic variations as it is routine for land and airborne surveys. In the past only on a few cruises we had the opportunity to install a base station on adjacent islands or coasts. Unfortunately, permanently operating magnetic observatories are rare in many areas of the world and therefore they are nearly always too distant from our survey areas in remote oceanic regions. Particularly the short period variations can not be reduced in this way.

In order to avoid these problems and to obtain variation-free magnetic measurements on the ship we use the gradient magnetometer Geometrics G-811G. The instrument consists of two proton magnetometers which are towed 150 meters apart as a longitudinal array about 600 meters astern of the ship (Figure 5.4.2.1).

Many parts of the instrument have been modified, especially the towing system including all connections of the sensors and the splitter box to the cables. We use plugs from seismic streamer technology instead of the original fixed connectors at all these connections in order to enable fast replacement of defective cables and sensors and easy handling.

Both sensors measure the total intensity of the magnetic field simultaneously. The difference between the two measurements is an approximation for the longitudinal gradient of the field in profile direction. It is free from temporal variations and its integration restores the variation-free total intensity or magnetic anomaly (apart from a constant value). The practical procedure that reconstructs the anomaly from the gradient is by no means trivial because several kinds of measuring errors have severe effects during the integration.

The remanent, viscous, and induced magnetizations of the ship are much more critical for gradiometer than for normal marine magnetic measurements. Because the two sensors have different distances to the ship a systematic error is generated in the gradient depending on the course and even on the time due to the viscous part of the ship's magnetization. This long-period errors can have a disastrous effect during the reconstruction of the magnetic field from the gradient. Because mathematical models for the magnetic effect of the ship are by far not precise enough, we are towing the sensors at a greater distance behind the ship than it is standard for normal marine magnetic surveys (Figure 5.4.2.1).

Another source of error is the deviation of the magnetometer array from the profile line and its unknown azimuth as well as the different depth of the sensors. In order to obtain information about the location and orientation of the array behind the ship we installed a fluxgate compass in the middle of the cable between the two sensors. Furthermore, both magnetometers contain pressure sensors that provide continuous values for the depth of the sensors.

A more detailed discussion of errors can be found in Eilers et al. (1994). For example, magnetic fields are induced by the movement of sea water within the earth's magnetic field. This results in a distinctively raised noise level of the records during times of rough seas. However, due to the statistical character of the disturbing fields and the smoothing effect of the integration this hardly reduces the quality of the reconstructed anomaly.

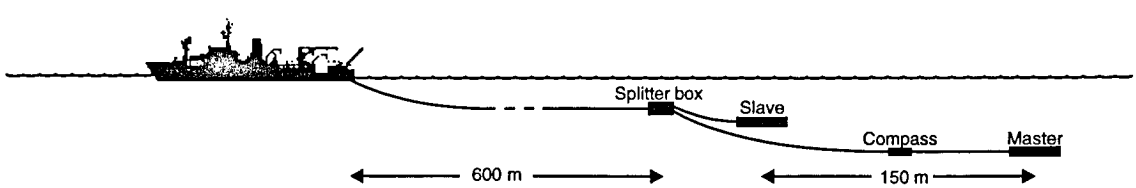

Figure 5.4.2.1: Gradient magnetometer configuration.

5.5 SHIPBOARD EQUIPMENT
5.5.1 HYDROSWEEP

(N. Kukowski, T. Schillhorn)

On board RV Sonne, the swathmapping system HYDROSWEEP ("HYDROgraphic multi-beam SWEEPing survey echosounder", Atlas Elektronik GmbH, Bremen) is available for continuous recording of bathymetric data.

The instrument works with a frequency of 15.5 kHz. The input amplifier is situated perpendicular to the longitudinal axis of the ship. With 59 acustic beams and an opening angle of 90°, a swath about twice as wide as the water depth is surveyed. Precision is about 1% if rolling is less than 10° and heaving less than about 5°. The central beam has a range of up to 10000 m, the outermost ones of at least 7000 m. There are three methods to deal with water sound velocity and its variation with depth: i) it can be calculated during data acquisition by means of a mechanism of optimal selfcalibration (Grant and Schreiber, 1990), or, ii), a constant average velocity can be assumed, or, iii), a water sound velocity depth profile as obtained e.g. from a CTD (Conductivity-Depth-Temperature) tool can be transferred to a step function with up to 20 discrete values and given to the system. Data (location, time, and water depth) are continously written to magnetic tapes and magneto-optical discs and can also be plotted as isoline charts during acquisition.

Postprocessing (bathymetric maps, couloured 3D perspektive views) is done onboard with the Hydromap 300 system (Atlas Elektronik GmbH, Bremen). Hydrosweep data can also be read, edited and processed with the free software *mbsystem* developed at Lamont Doherty Earth Observatory by D. Caress and D. Chayes.

5.5.2 PARASOUND

(N. Kukowski, T. Schillhorn)

By means of the parametric sediment-echosounder PARASOUND (PARAmetric sediment survey echoSOUNDer, Atlas Elektronik GmbH, Bremen), shallow sediment structures down to a depth of about 100mbsf can be imaged.

Parasound works differently from traditional 3.5 kHz echosounders and uses a sound beam resulting from the interference of two high frequency narrow waves of similar frequency (18 - 23 kHz) which leads to the formation of a low frequency part of the signal. The depth of penetration of the parametric 2.5 to 5.5 kHz echo is as great as that of 3.5 kHz systems, but due to the narrower beam width, a clearer and more differentiated image of multi-layer structures is obtained. The opening angle of the sound wave is about 4°, which gives a swath of 7% of the water depth. Therefore, data quality depends to a large amount on the morphology of the ocean bottom, in case of steep slopes, data quality often is quite poor. Slopes steeper than 4° cannot be imaged, areas with a slope of more than 2° normally are only poorly imaged.

Raw analogue data are written to a black and white as well as a coulour printer. With the program PARADIGMA (PARAsound DIGitalisierungs- und Mehrkanal Auswertesystem, V. Spieß (1993), U Bremen), data can also be written digitally to magnetic tape in a special SEG-Y format and then may be processed like seismic data.

5.5.3 NAVIGATION

(B. Schreckenberger and H.-O. Bargeloh)

THE NEW DGPS NAVIGATION OF R.V. SONNE

Since 1996 R.V. SONNE uses the differential GPS (DGPS) system SkyFix by Racal Survey. Data from different reference stations are processed at a land-based station and a correction message is broadcasted via INMARSAT satellites to the users. On board of R.V. SONNE the software package MultiFix 2 uses the signals from a special decoder and from the new GPS receiver Trimble 4000 DS in order to calculate the DGPS positions. The reference stations Bahrein, Baku, Bombay, and Abu Dhabi were used by MultiFix on this cruise. In general, the system calculated a mean RMS error between 5 and 10 meters for the final position solution.

Navigation by SkyFix solves the problems that we used to have with Selective Availability (S/A) and gives positions that are even better than GPS without S/A. Therefore, for the first time on geophysical cruises, it was possible to use the GPS position without further postprocessing. That was necessary because the original GPS positions used to be very noisy and the filtered data from the ship's navigation system ANP2000 sometimes yielded deviations from true positions of up to several 100 meters depending on unknown conditions. This problem is not existing when DGPS is working since filtering of the DGPS positions is not necessary.

The only problem, already observed on cruise SO-122, were short times of one or two minutes duration where the positions became zero in the navigation message. This problem is well known to the ship's officers and it is caused by technical limitations of the turnable INMARSAT antenna. Unfortunately, when the SkyFix system is not able to calculate a differential GPS position due to loss of the satellite connection it does not use the uncorrected GPS position but simply stops the data output. By a hardware switch, the ship's officers can shift to the Ashtec receivers as navigation input for the ANP2000 but that procedure is not very useful for short gaps.

In the evening of September 23, when the ship headed with 356° to the North, the problem described above occurred many times during two or three hours on a seismic profile.

The problem seems to be that the new DGPS system is not really integrated into the ANP2000 and that the interface to the old GPS system was used. It would be necessary to have a second navigation input that records the simple GPS position either from the Ashtec receivers or from Skyfix. Additionally, the position filter of the ANP2000 should try to bridge gaps in the navigation input. Likewise, it is not satisfactory that the INMARSAT antenna sometimes has problems either with adjustment of the satellite bearing or with shielding effects by the superstructure or the mast.

SHOTPOINT LISTS

Shooting was done in one minute intervals on most of the lines (exception one run along line SO123-03). In general, the speed was approximately 5 knots over ground or (on some lines) 4 knots through the water. Using the BGR computer system for data acquisition and data processing and the procedures described in 5.1.2, shotpoint lists have been prepared for every seismic line. The lists contain the profile name, shotpoint number, date, time, position (DGPS antenna), and waterdepth for every shot. In general it was not necessary to make a postprocessing of the positions. In case of the position gaps described above a linear interpolation algorithm turned out to be satisfactory.

6.1 HYDROSWEEP
6.1.1 WORK PERFORMED, DATA QUALITY

(N. Kukowski, T. Schillhorn and watches)

Hydrosweep multibeam data were acquired continuously during the whole cruise. The instrument worked nearly all time without problems. Two minor crash-downs were repaired after a few minutes. For water sound velocity, values obtained from a CTD tool (see 6.1.2) were used. Data quality was generally good, the weather was mostly calm and not too much heave and pitch occurred. Lesser data quality was only obtained on the upper slope where topography is very rough.

After aquisition, the raw data were transferred by the onboard computer network to a HP Apollo work station (see 5.1) each day, edited and carefully cleaned with *mbsystem*. Then the data sets were gridded to produce maps and perspective plots which was done using GMT software. Data from cruise SO122 (Roeser et al., 1997) were also processed and included in this data set.

mbsystem is a package of programmes and macros for processing multibeam data on UNIX systems. Relevant information (longitude, latitude, time, course, speed, water sound velocity etc.) can be extracted from the stored records. With a given water sound velocity profile, depth is recalculated by ray-tracing. By editing every single swath and eliminating erroneous beams, much better data quality can be achieved which justifies this time-consuming procedure. Data then are gridded and visualized with the GMT (generic mapping tool) software package (Wessel and Smith, 1991). There is no limitation on grid size and spacing. Gridding the MAMUT data sets needed between one and several hours depending on spacing of discretization.

6.1.2 SOUND VELOCITY PROFILES OBTAINED WITH THE CTD TOOL

For calibration of sound velocity for the determination of water depth with the Hydrosweep instrument, a CTD tool was run in deep water just south of the deformation front at 24:03.01N, 62:20.02E.

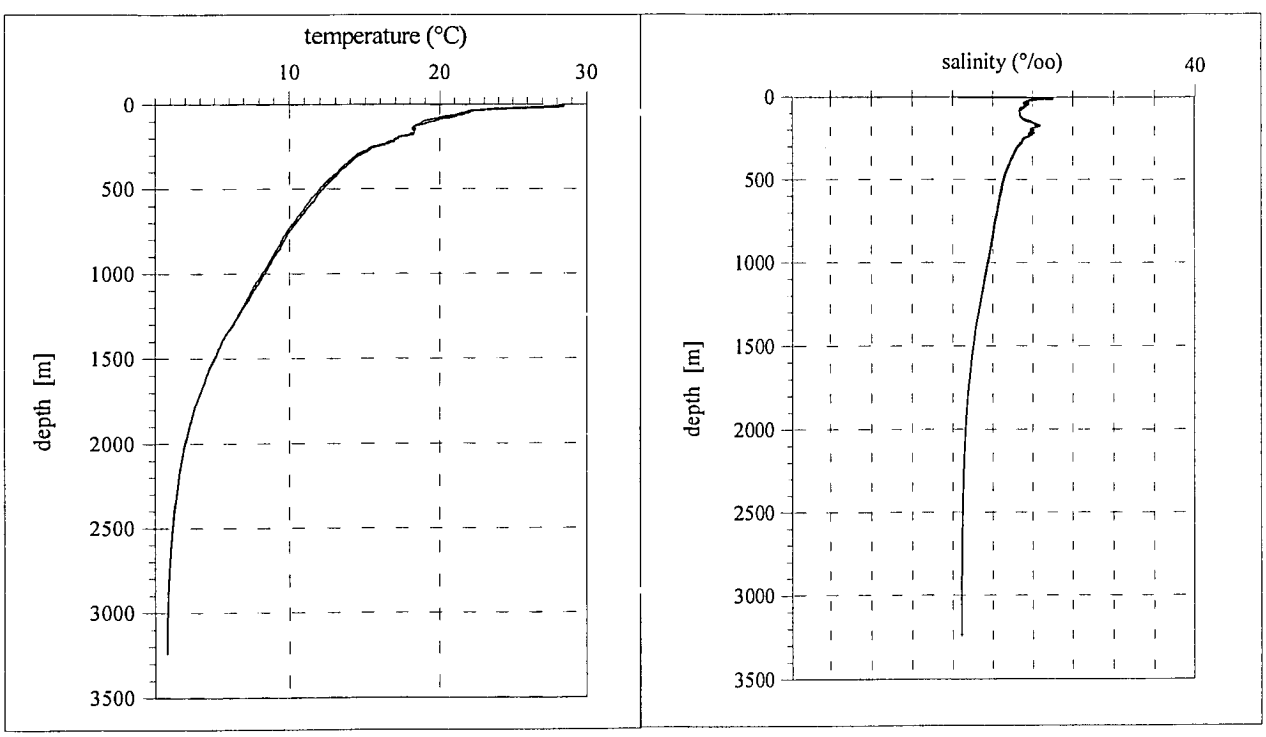

Figure 6.1.2.2: Temperature and salinity depth profiles from the CTD tool.

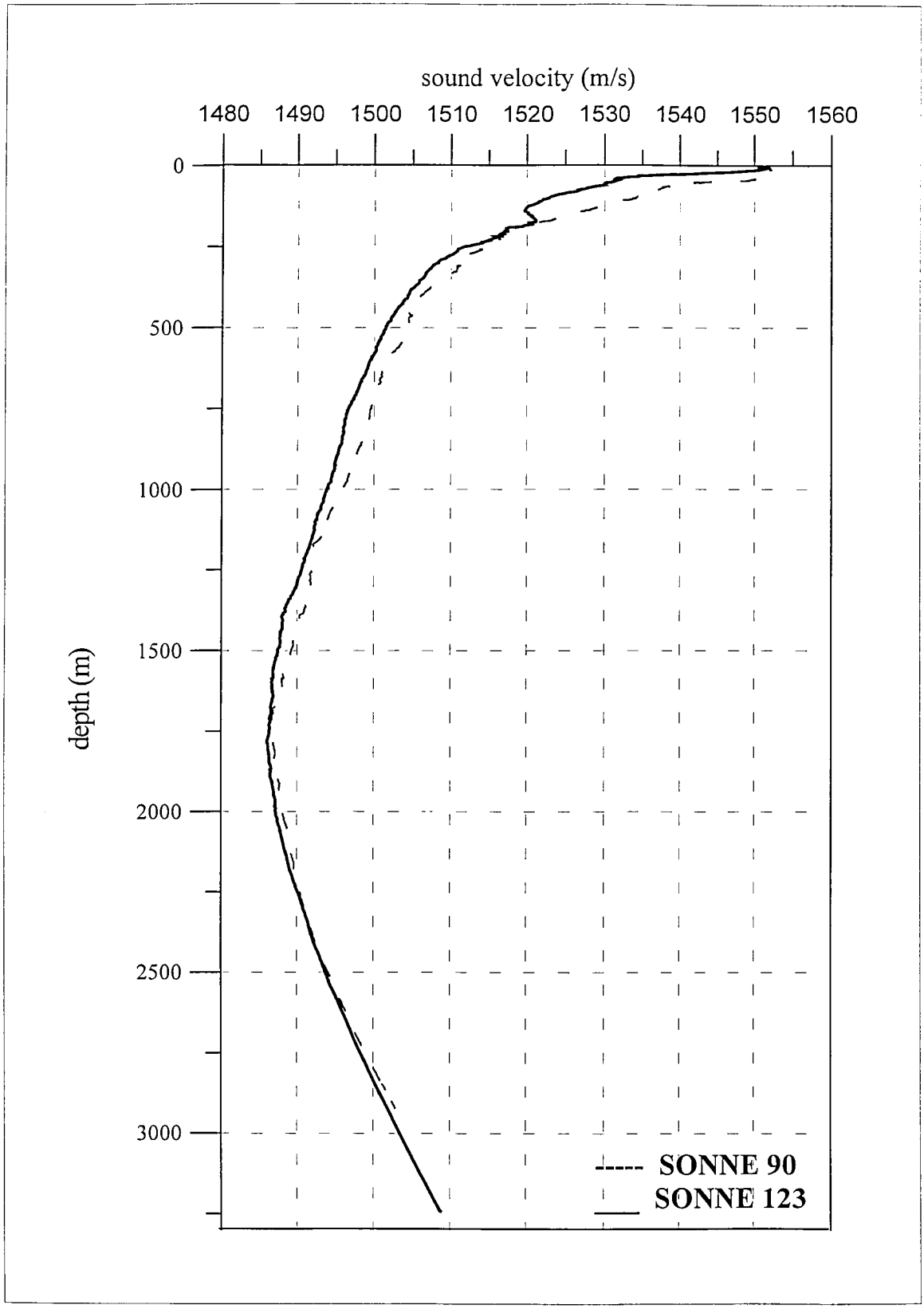

Figure 6.1.2.1: Water sound velocity obtained south of the Makran accretionary wedge from the CTD tool during SO123 and for comparison as obtained on SO90.

The sound velocity depth profile shows several striking features (Figure 6.1.2.1). Sound velocity in shallow water is remarkably high and decreases first very fast and then slowlier until the minimum of water sound velocity (1487 ms^{-1}) is reached in a depth of 1750 m. Then sound velocity increases again nearly linear. A CTD run on SO90 PAKOMIN at 23:26.4 N, 64:16.2 E (von Rad, 1993) showed the same characteristics with overall velocity about 1 to 4 ms^{-1} higher in equivalent depths. These profiles differ significantly from sound velocity profiles obtained in the Aleutian and Japan trenches, where minimum velocity was obtained in about 100 m water depth and velocity increased nearly linearly beneath 500 m water depth (Flueh and von Huene, 1994; Suess, 1994). Temperature and salinity show largest variation in shallow water down to about 300 m and then decrease continuously. Below 2500 m water depth, temperature is less than 2°C (Figure 6.1.2.2).

6.1.3 MAKRAN ACCRETIONARY WEDGE

The actual deformation front is located seaward of the first ridge and identified in the bathymetric data (Figure 6.1.3.1) as a smooth but not continuous bulge. The first ridge is very pronounced, and remarkably steep with a throw of about 600m. It runs continuously nearly W-E from the western edge of the surveyed area to about 63°06'E where it is cut by a deep canyon and retreats in a gentle bow. Here, south of it, a new accretionary ridge is in an early stage of evolution. This new ridge may be correlated with the bulge further to the west, which then is inferred to be a new accretionary ridge in a nascent stage. At the western edge, the remnant of a large slump are clearly recognized (Figure 6.1.3.2). Some parts of the ridge show deep notches but mainly it appears intact and massive. After the first ridge, two complex ridge systems, named second and third ridge, follow arcward.

Besides the first ridge, the most arcward ridge (fourth ridge) is also continuous. It is also the border towards a significant change in morphological style further landward. Here, many steep N-S running canyons cut the wedge. Some of the most pronounced canyons cut the whole wedge in the central (Figure 6.1.3.3) and eastern part (Figure 6.1.3.4) of the investigated area crossing the wedge in complex zick-zack patterns. While most canyons seem to be recently actively eroding, some dead arms are also found in the landward portion.

The second and third ridge comprise of several sub-parallel short ridges beginning, ending, and beginning again. The western and eastern toes of these ridges are buried beneath a sediment coverage. Spacing of the ridges is varying indicating that either the thickness of the accreted sediment pile is changing laterally or physical properties vary regionally. Sediments ponds inbetween the ridges are remarkably flat. Only the seaward flanks of the accretionary ridges contribute to the rise of the slope. In the central portion of the mapped area, the second and third ridge systems are cut and east of this, new ridges rise only at a significant distance again. Number and spacing of ridges is different west and east of this region which is characterized by a rough topography with numerous hill-shaped highs and evidence for erosion.

Summarizing, the structure of the wedge is that of a classical wedge on a large scale, however, quite complicated because of the complex ridge systems and canyons cutting the wedge perpendicular to strike. Large portions of the ridges are remarkably stable.

6.1.4 DALRYMPLE TROUGH AND ADJACENT AREAS

Areal mapping was not planned for the Dalrymple area, however, in addition to the data obtained during shooting and transits, several Hydrosweep profiles were recorded to cover the whole trough and especially its southern flank. Due to intensive fishing activities, some profiles unfortunately could not be

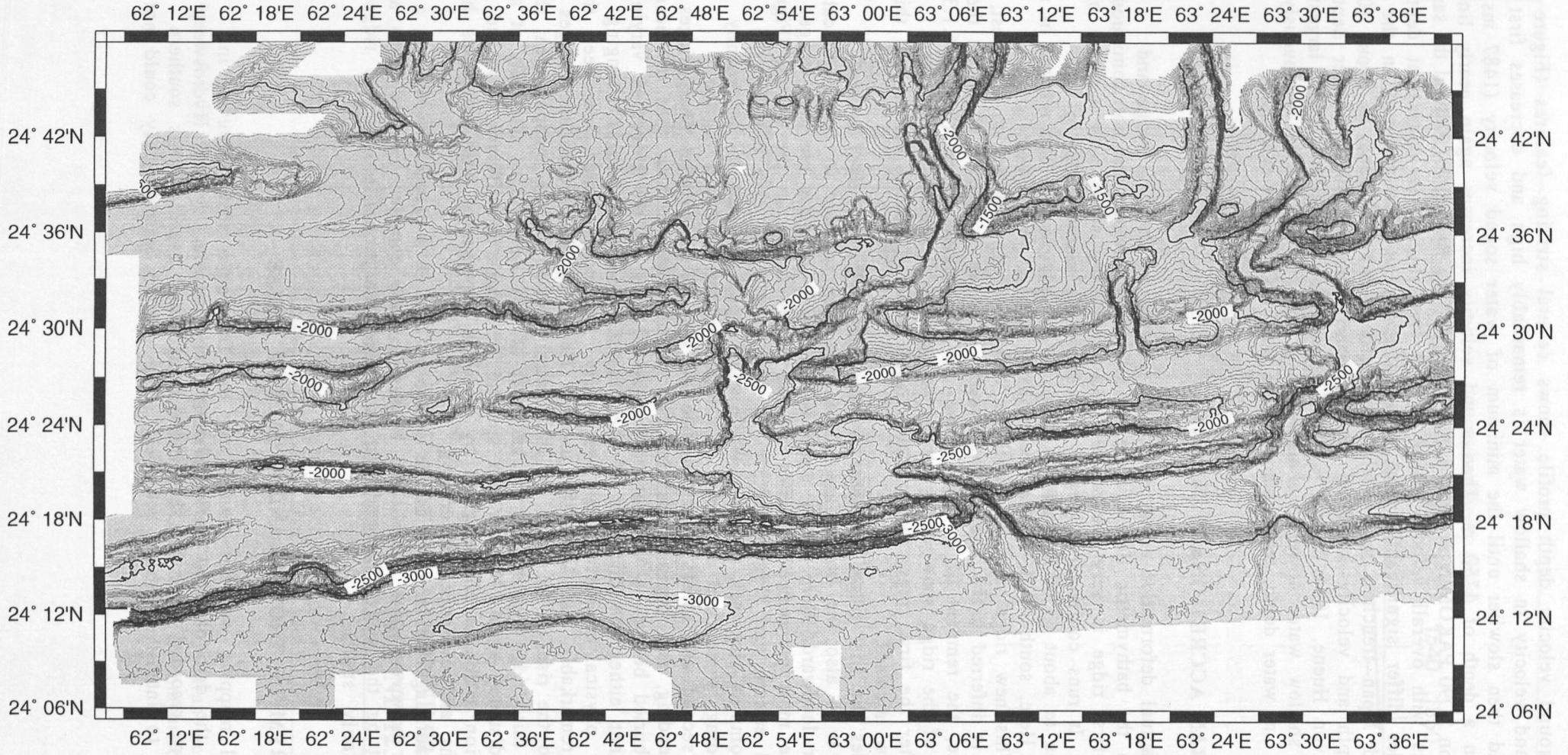

Figure 6.1.3.1a: Bathymetric contour plot of the whole portion of the Makran accretionary wedge surveyed during cruise SO-123. Contour spacing 25m. Grid size 0.002°.

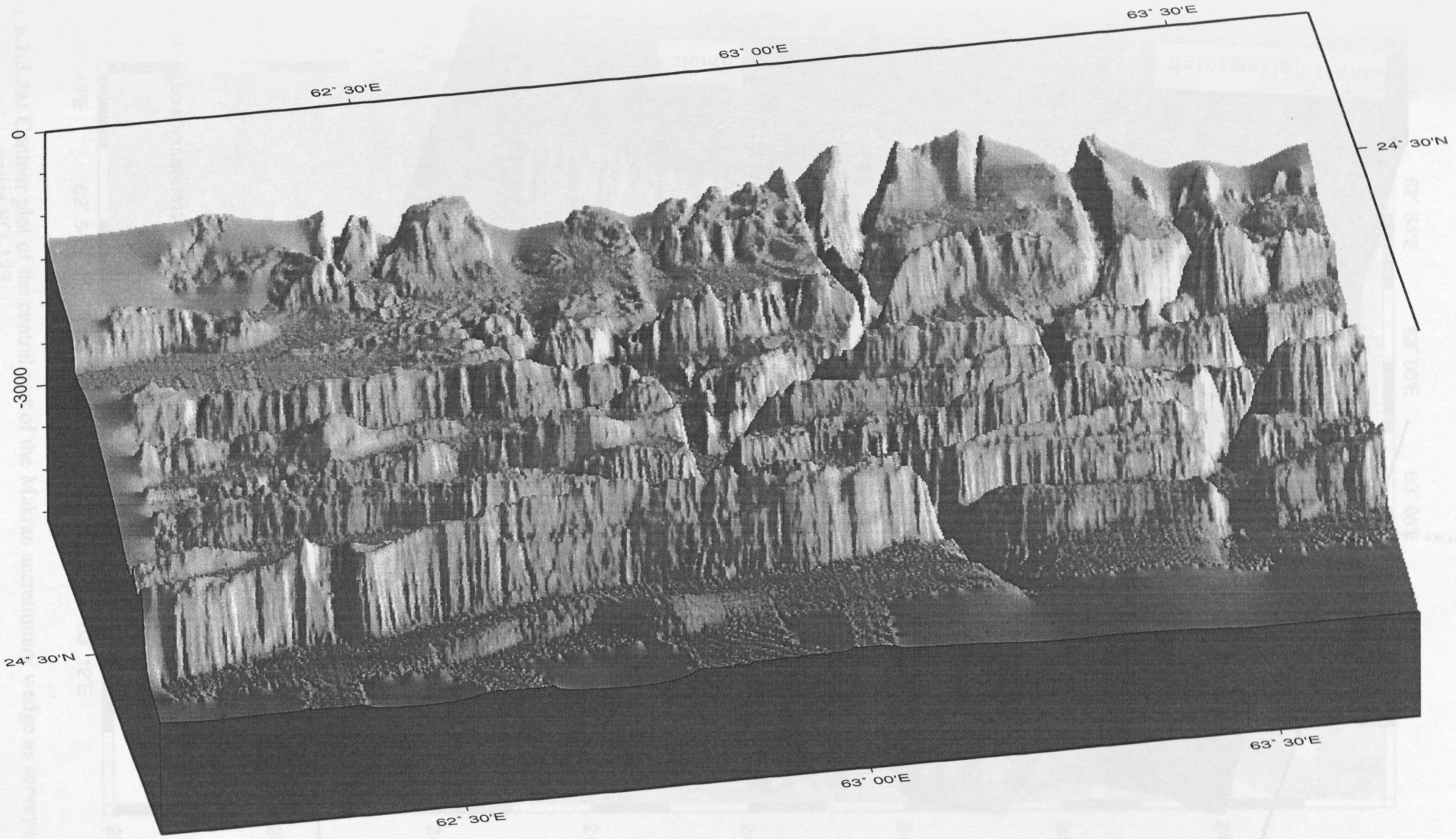

Figure 6.1.3.1b: 3D perspective view of the whole surveyed area of the Makran accretionary wedge.

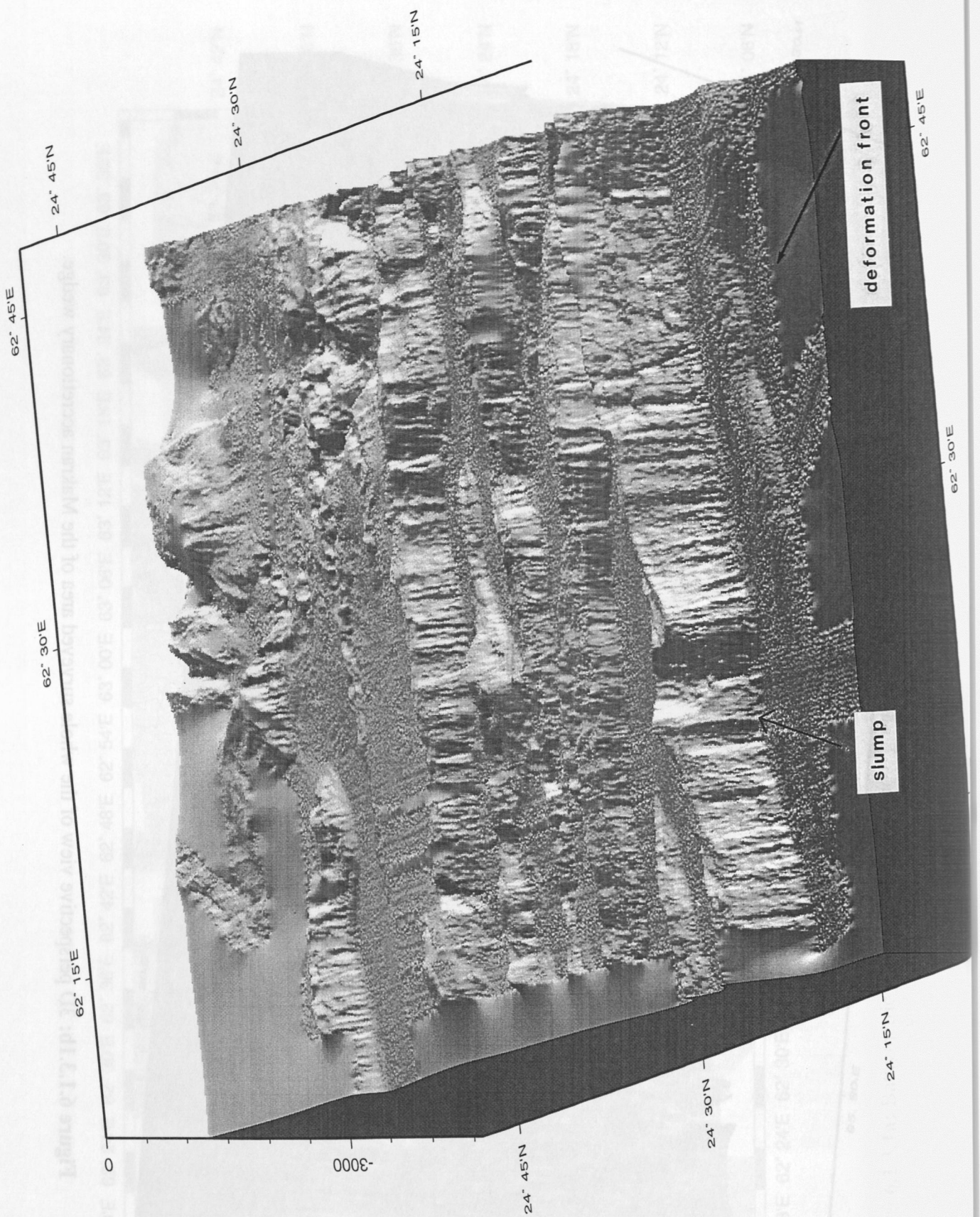

Figure 6.1.3.2: 3D perspective plot of the western part of the Makran accretionary wedge. Grid spacing is 0.001°.

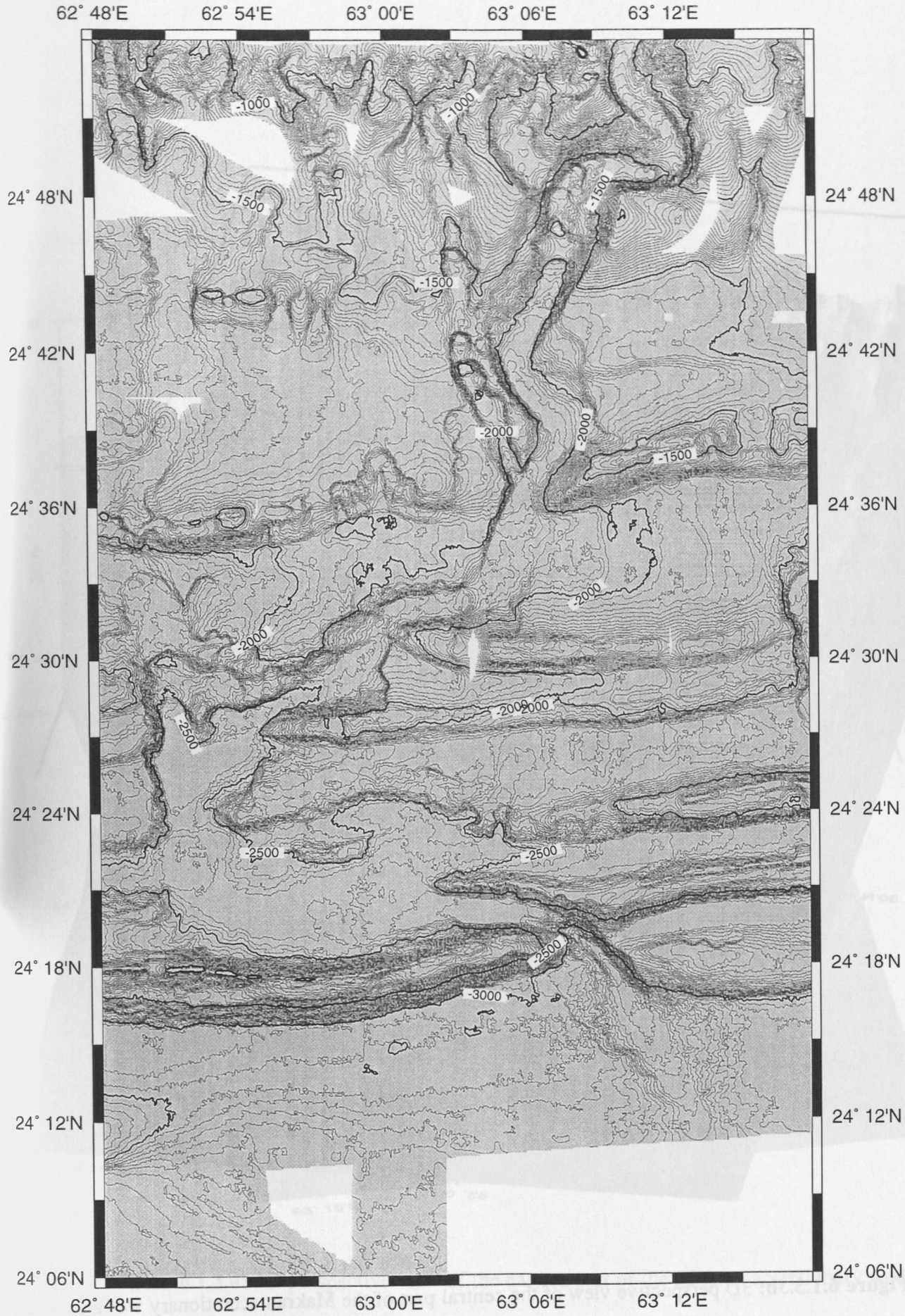

Figure 6.1.3.3a: Contour plot of the central part of the Makran accretionary wedge as surveyed on cruise SO-123.

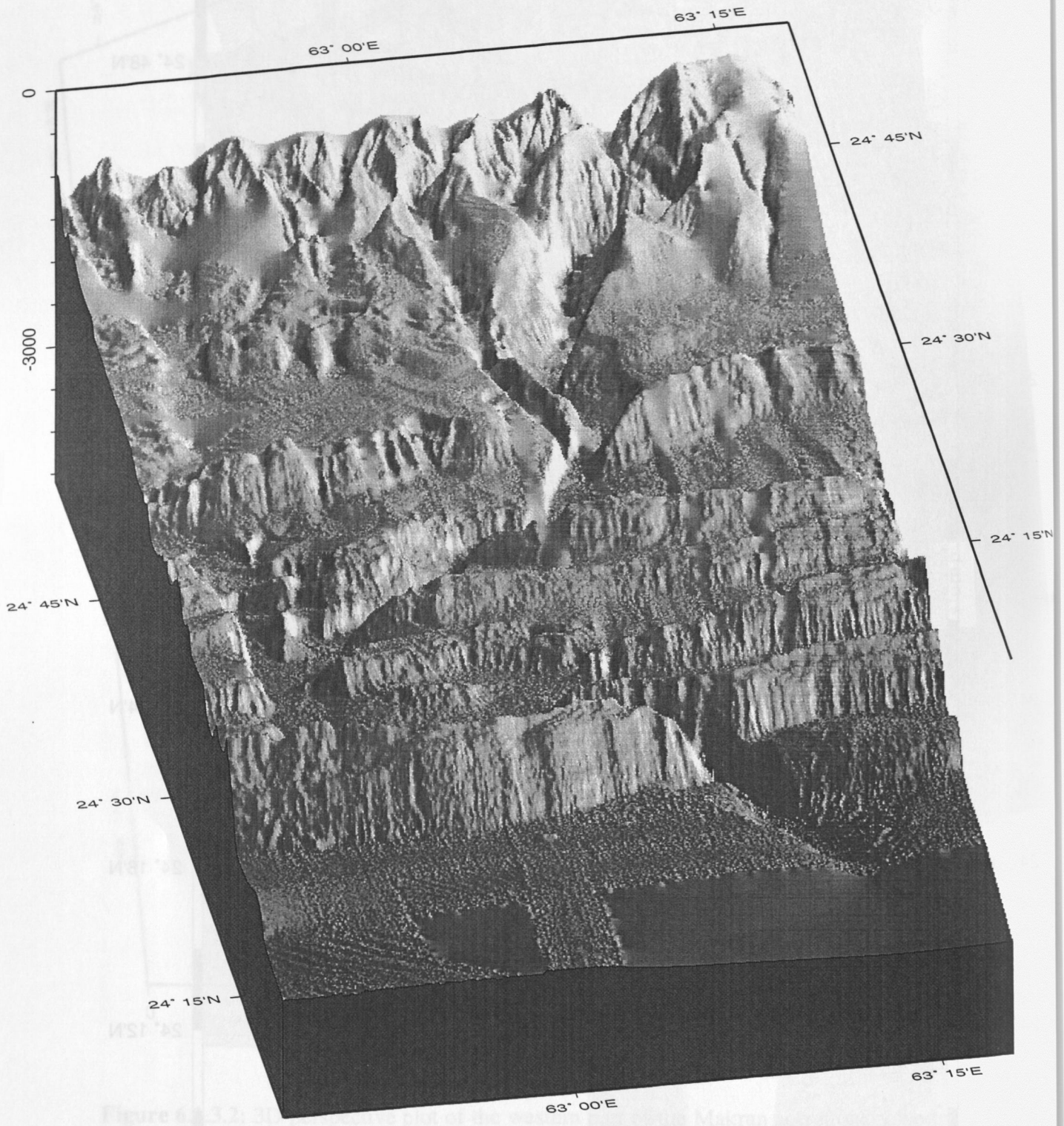

Figure 6.1.3.3b: 3D perspective view of the central part of the Makran accretionary wedge.

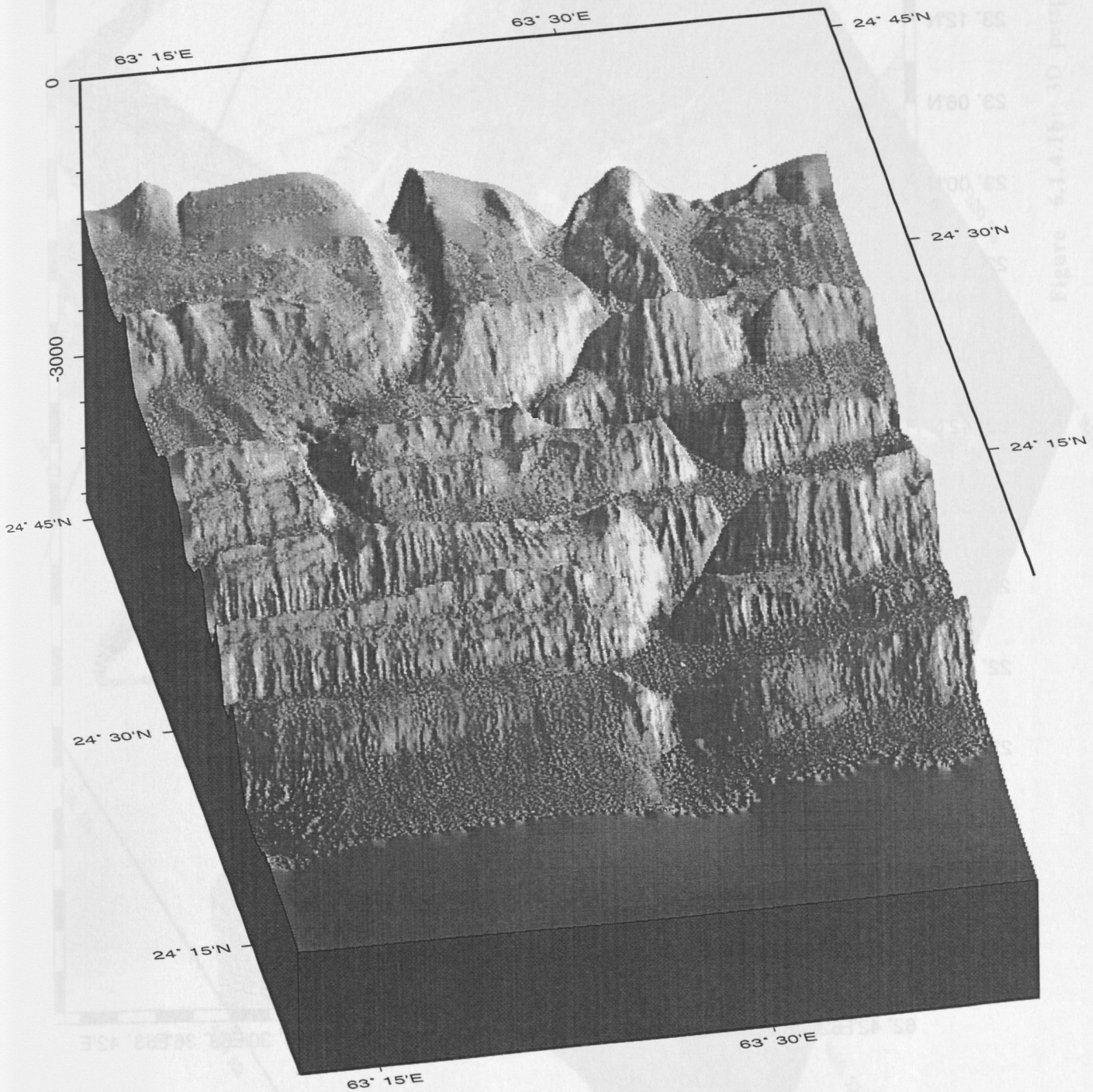

Figure 6.1.3.4: 3D perspective view of the eastern part of the Makran accretionary wedge.

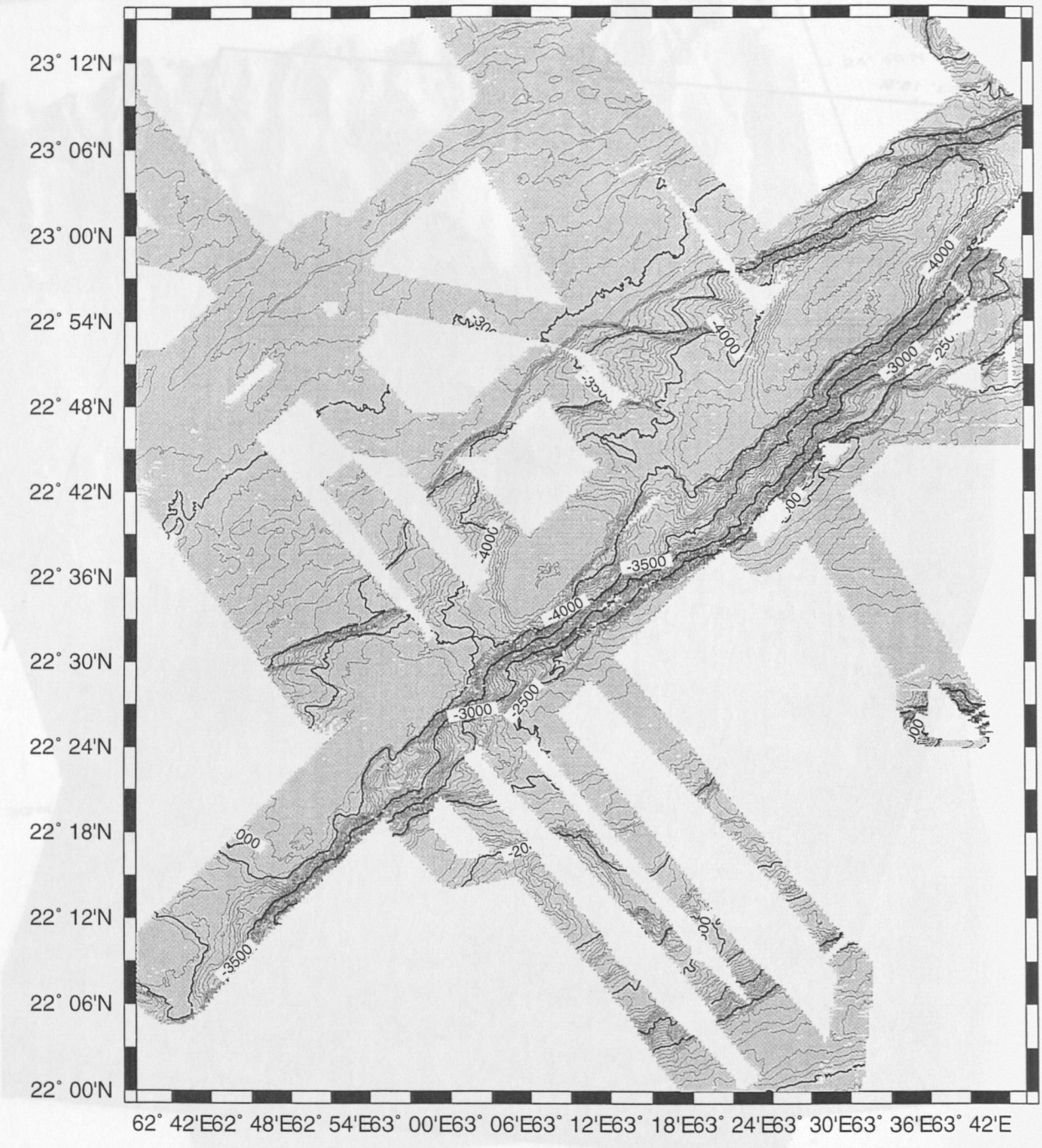

Figure 6.1.4.1a: Bathymetric map of the surveyed area in the Dalrymple region. Contours are not smoothed. Grid spacing is 0.00225°. Contour spacing is 50m.

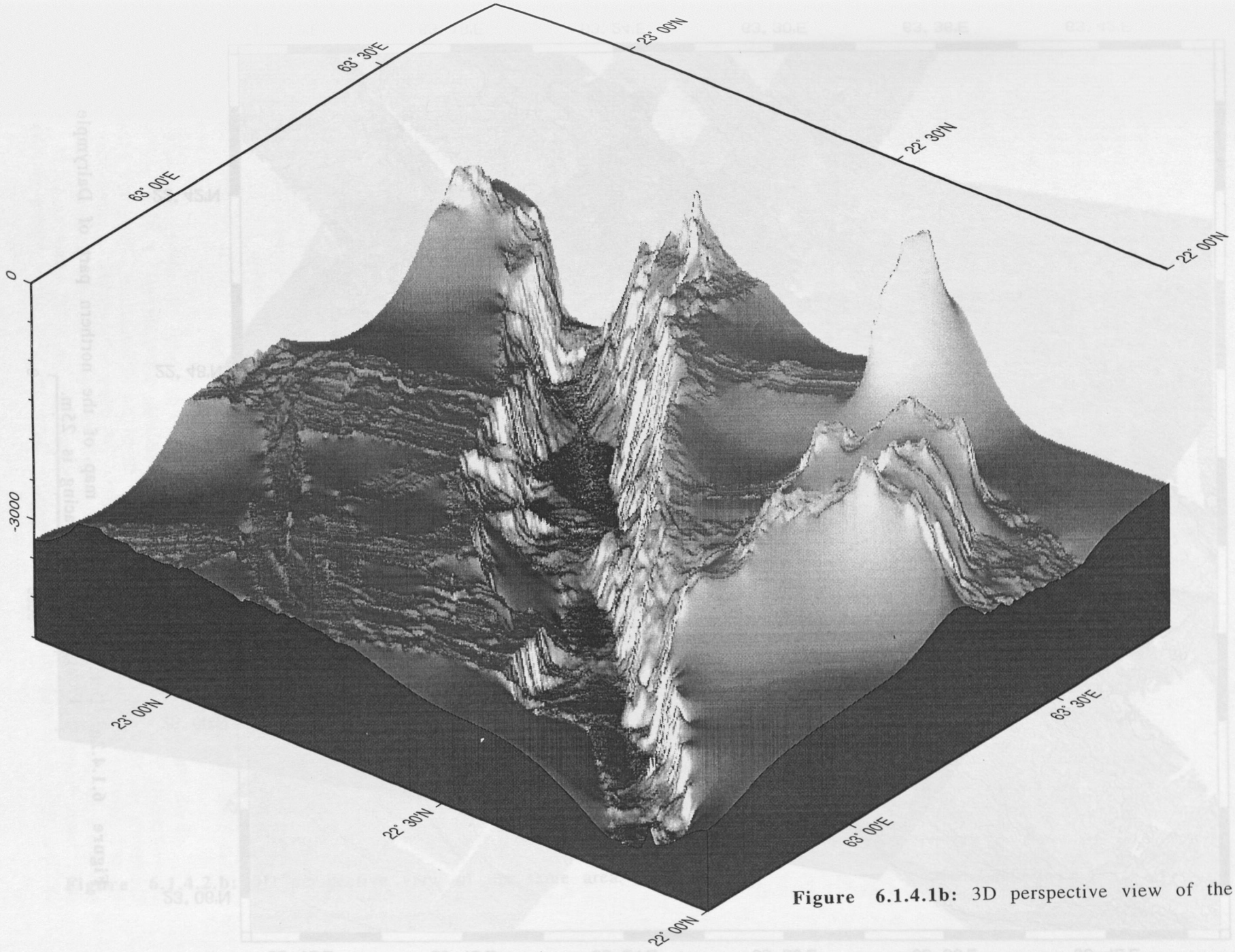

Figure 6.1.4.1b: 3D perspective view of the same area.

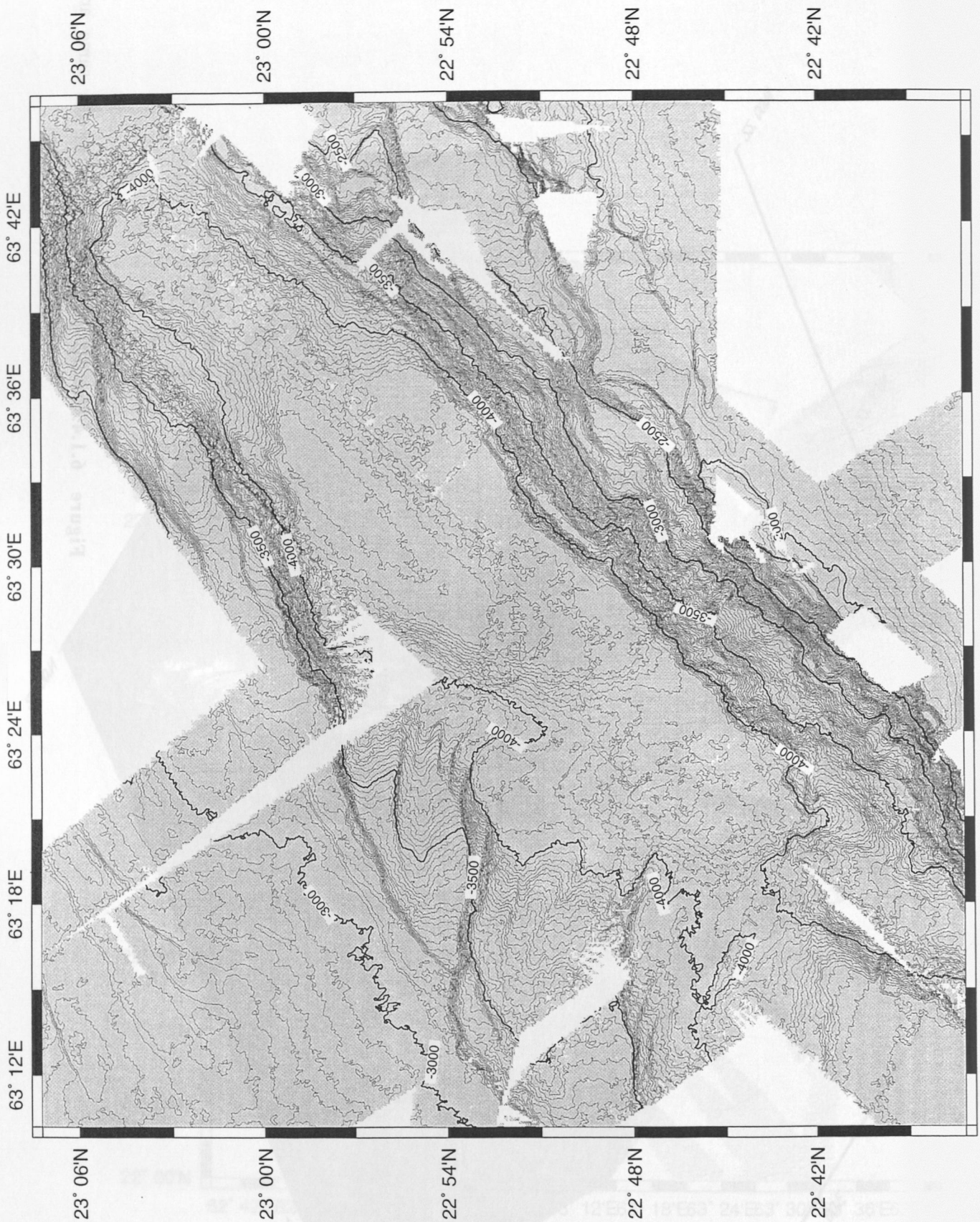

Figure 6.1.4.2a: Detailed bathymetric map of the northern part of Dalrymple Trough. Contour spacing is 25m.

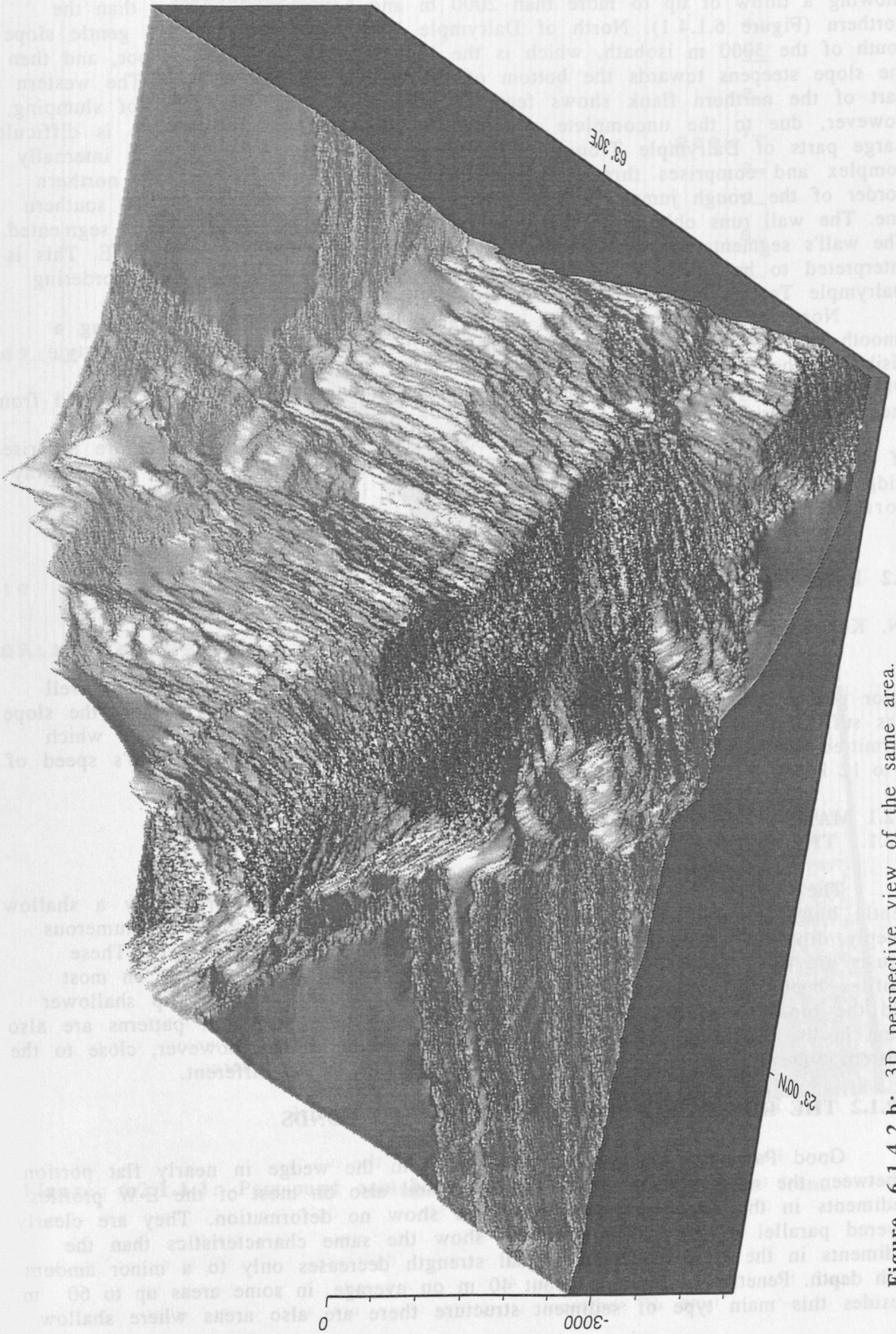

Figure 6.1.4.2.b: 3D perspective view of the same area.

run, which left coverage incomplete. The resulting data set (Figure 6.1.4.1), however, reveals all main features of the trough and its side walls.

Dalrymple Trough, the floor of which is characterized by water depths greater than 4000m, is bordered by steep walls on both sides, the southern flank showing a throw of up to more than 2000 m and being much steeper than the northern (Figure 6.1.4.1). North of Dalrymple Trough, there is first a gentle slope south of the 3000 m isobath, which is the regional depth of the seafloor, and then the slope steepens towards the bottom of the trough (Figure 6.1.4.2). The western part of the northern flank shows features which could be the result of slumping, however, due to the uncomplete coverage, a unequivocal identification is difficult. Large parts of Dalrymple Trough's bottom are quite flat, however it is internally complex and comprises three ellipse-shaped basins (bull's eyes). The northern border of the trough jumps forth and back and is not as regular as the southern one. The wall runs oblique to the long axis of Dalrymple Trough and is segmented. The wall's segments strike is about 70°E (southern part) to more than 80°E. This is interpreted to be a result of strike slip movement. The southern wall bordering Dalrymple Trough is not affected by strike slip.

North of Dalrymple Trough, topography is not very marked, showing a smooth swell with highest elevations just south of Profile 6. Deformation style visible in the shallow sediment layers (see 6.2.2) is similar on both sides of Dalrymple Trough. The folds imaged in the Parasound data cannot be detected from the bathymetric map alone.

South of Dalrymple Trough, the ocean floor is quite flat first before the rise of the northern flank of Murray Ridge begins. As Dalrymple Trough and Murray Ridge are oblique to each other, the flat region inbetween them widens toward northeast.

6.2 PARASOUND

(N. Kukowski, T. Schillhorn & watches)

Parasound was recorded continuously analog on black and white as well color plotter and data were also written largely to magnetic tapes. Where the slope was sufficient shallow, data quality was good. The maximum slope angle which permitted successful recording was about 1.8° during this cruise at ship's speed of 4 to 12 knots.

6.2.1 MAKRAN ACCRETIONARY WEDGE

6.2.1.1 THE DEFORMATION FRONT

The deformation front which is morphologically characterized by a shallow gentle bulge seaward of the first ridge regionally is chracterized by numerous steeply dipping thrusts in the Parasound recordings (Figure 6.2.1.1.1). These thrusts are not imaged in the seismic data. The spacing of the thrusts on most profiles becomes more narrow arcward. Seaward, thrusts seem to dip shallower and the blocks separated by them slightly titled. These structural patterns are also seem in the Parasound data where there is no distinct bulge, however, close to the western edge of the bulge, deformation style seems to be different.

6.2.1.2 THE RIDGES SYSTEMS AND SEDIMENT PONDS

Good Parasound images are obtained from the wedge in nearly flat portion inbetween the ridge systems on N-S profiles and also on most of the E-W profiles. Sediments in the flat areas between ridges show no deformation. They are clearly layered parallel to the sea bottom and show the same characteristics than the sediments in the Gulf of Oman. Signal strength decreases only to a minor amount with depth. Penetration depth is about 40 m on average, in some areas up to 60 m. Besides this main type of sediment structure there are also areas where shallow

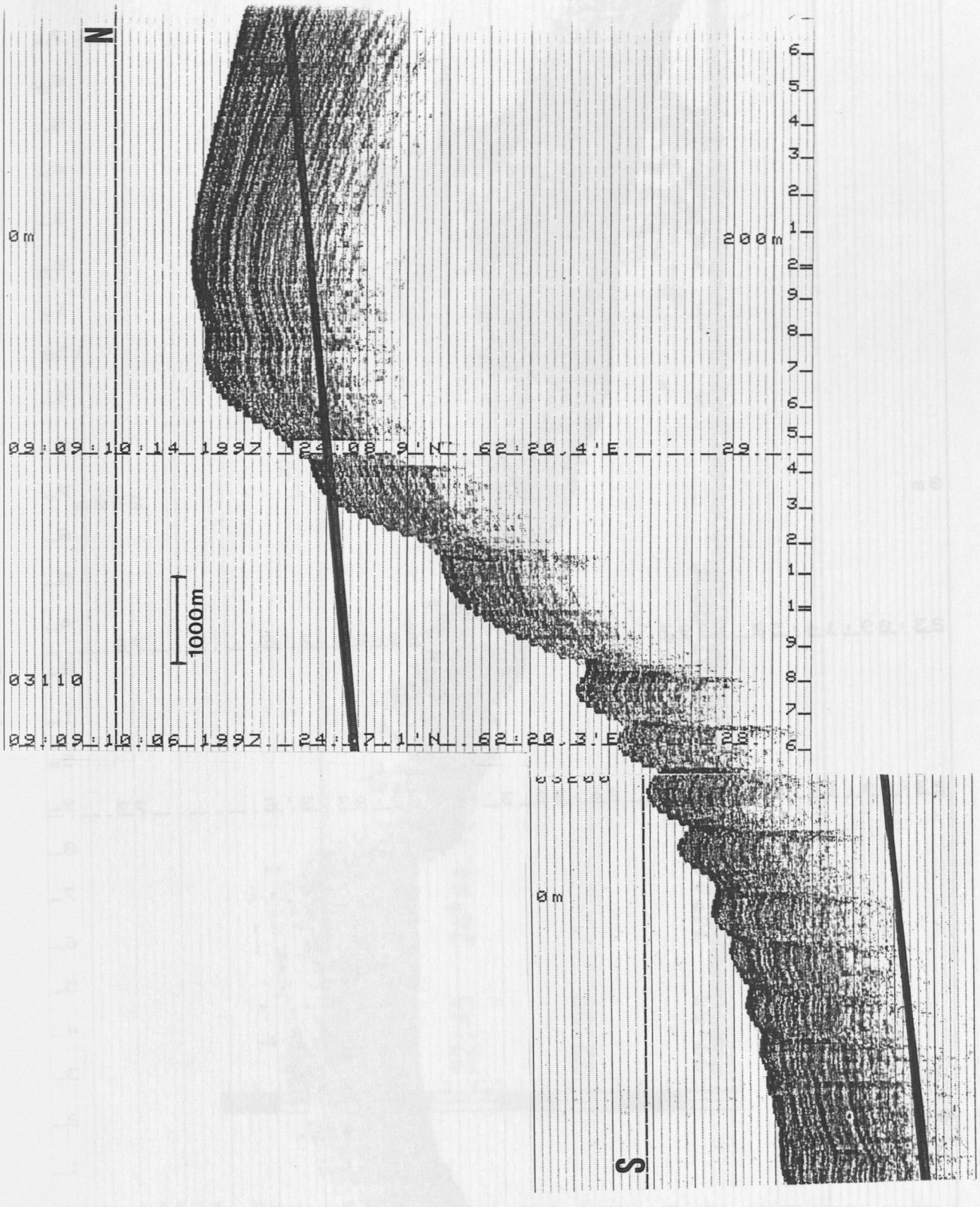

Figure 6.2.1.1.1: Parasound analog recording of the deformation front.

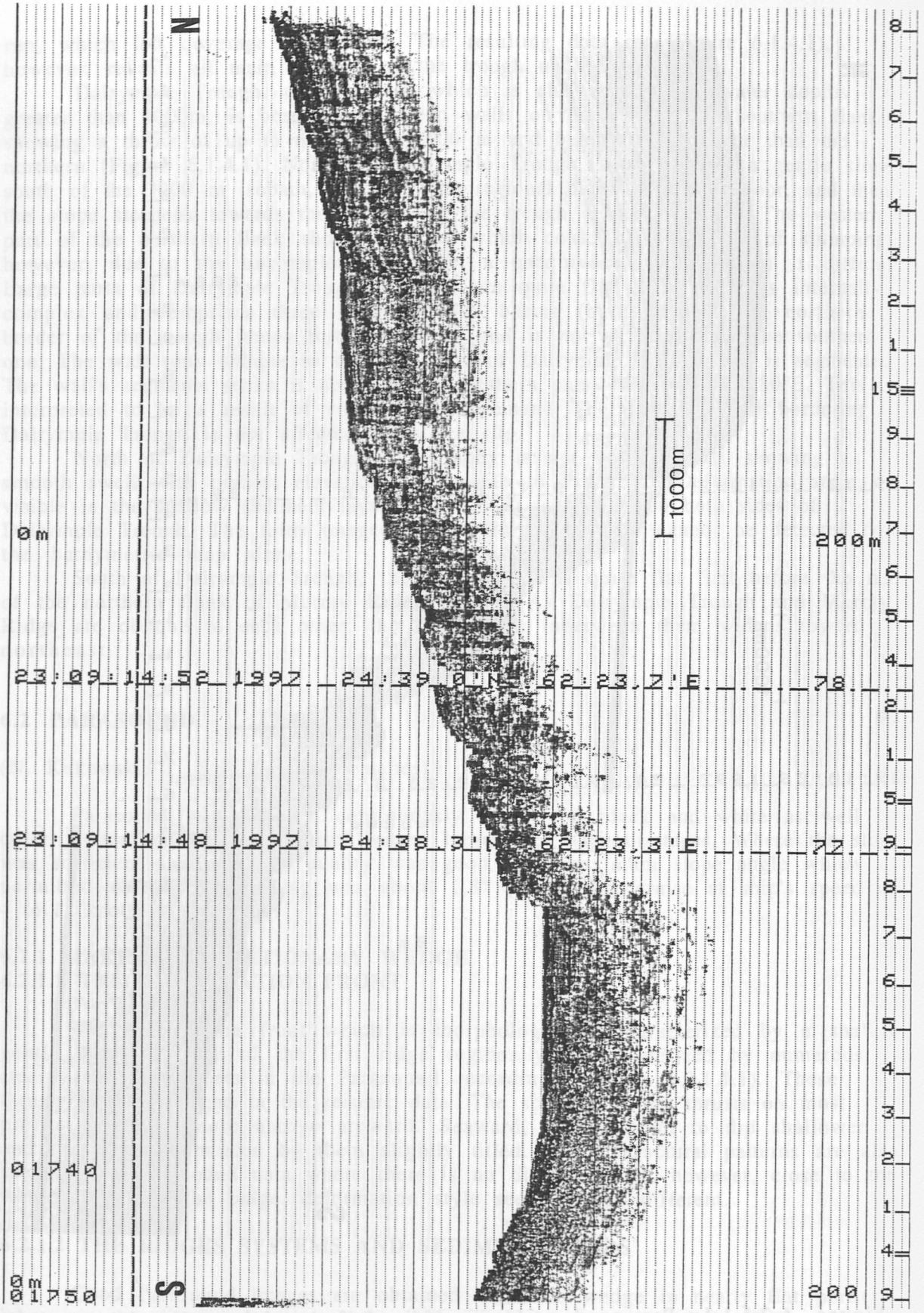

Figure 6.2.2.2.1: Parasound recordings of a faulted zone at the rise to the fourth ridge.

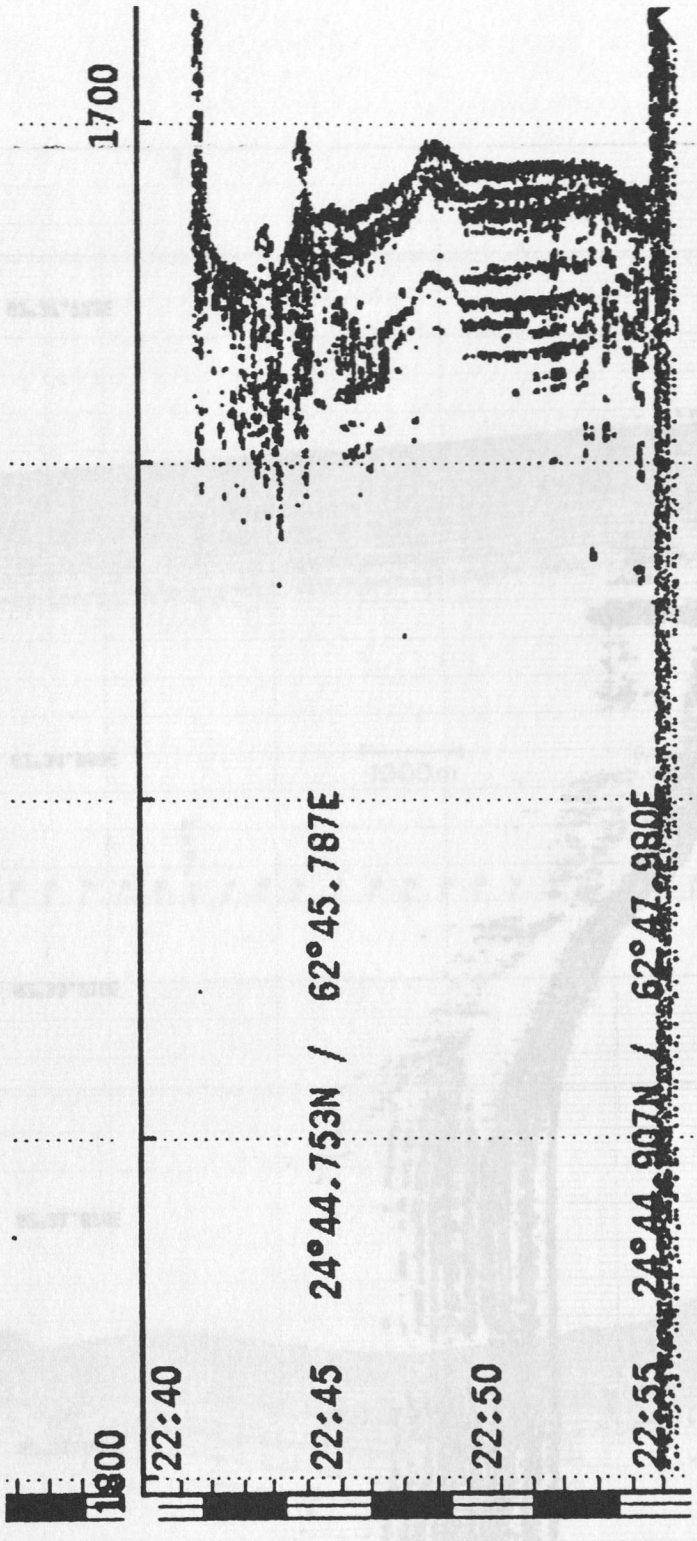

Figure 6.2.1.3.1: Parasound recording of mud diapirs in the accretionary wedge.

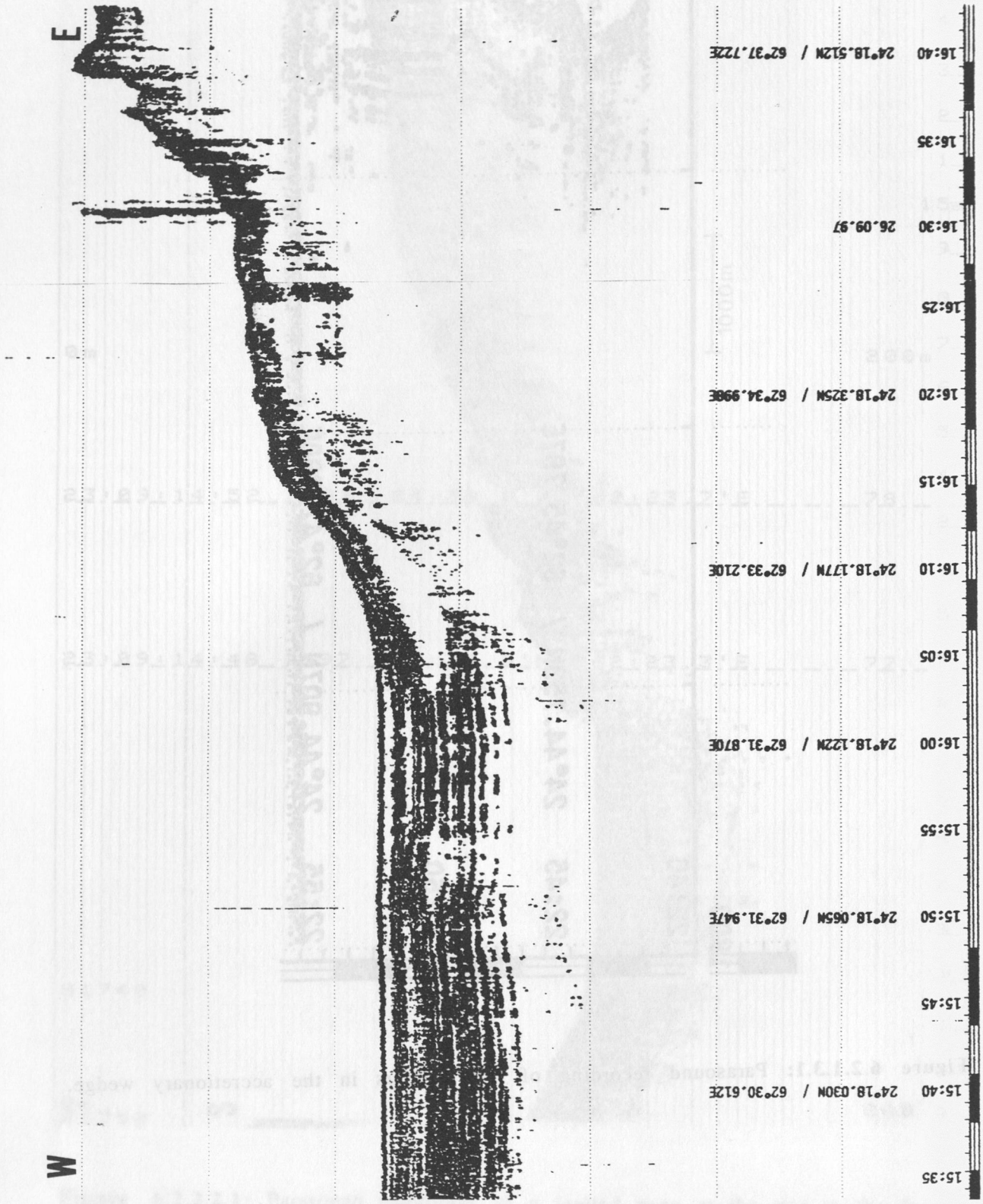

Figure 6.2.1.3.2: Parasound recording of blank zone in a W-E striking ridge on the Makran accretionary wedge. Echos visible in the eastern portion are interpreted as diapirs or outbursts of gas.

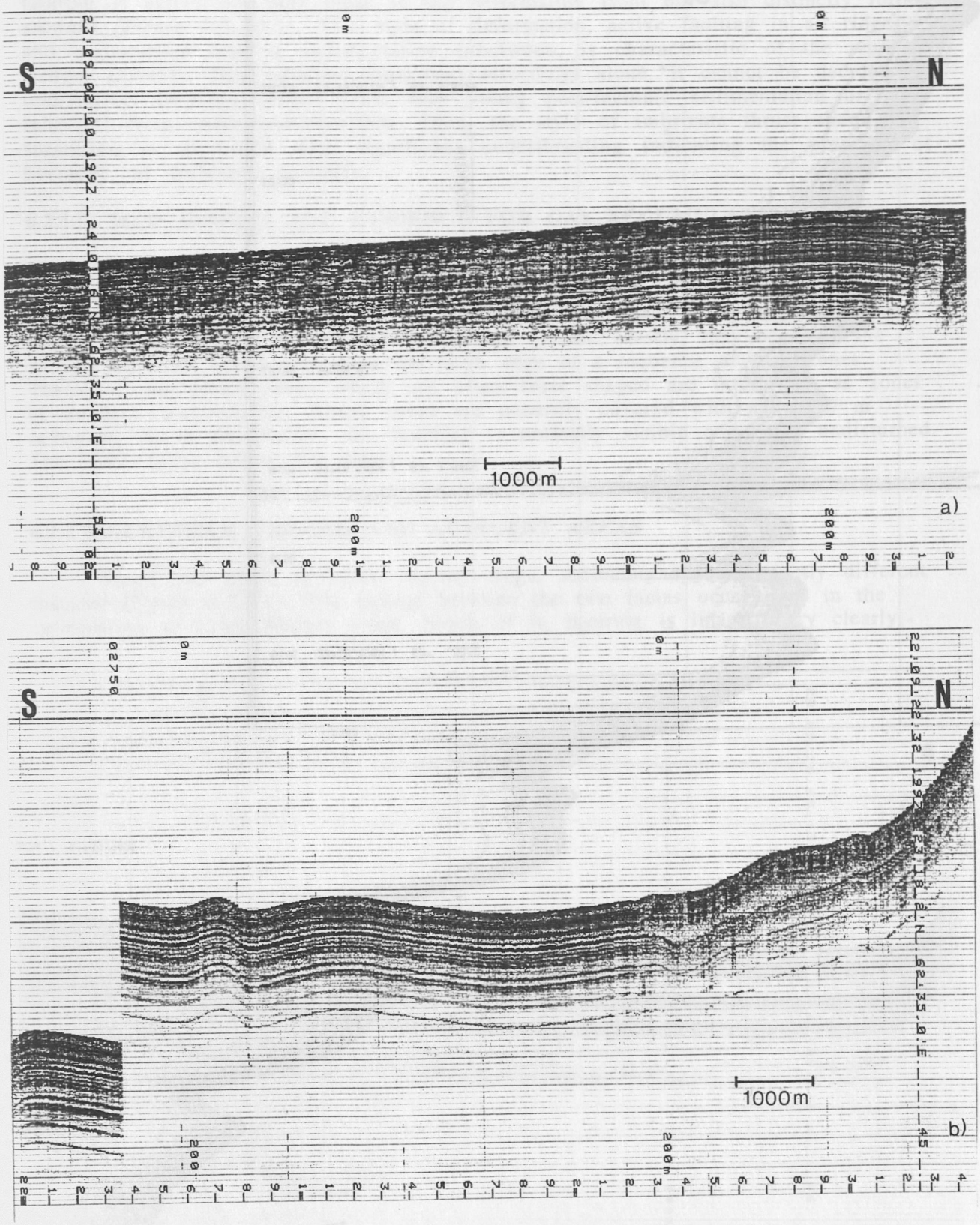

Figure 6.2.2.1: Parasound record of sediment structures north (a) and south (b) of Little Murray Ridge. The section shown in (a) is close to the deformation front, the first evidence of which is seen at the right edge if this figure (beneath 'N').

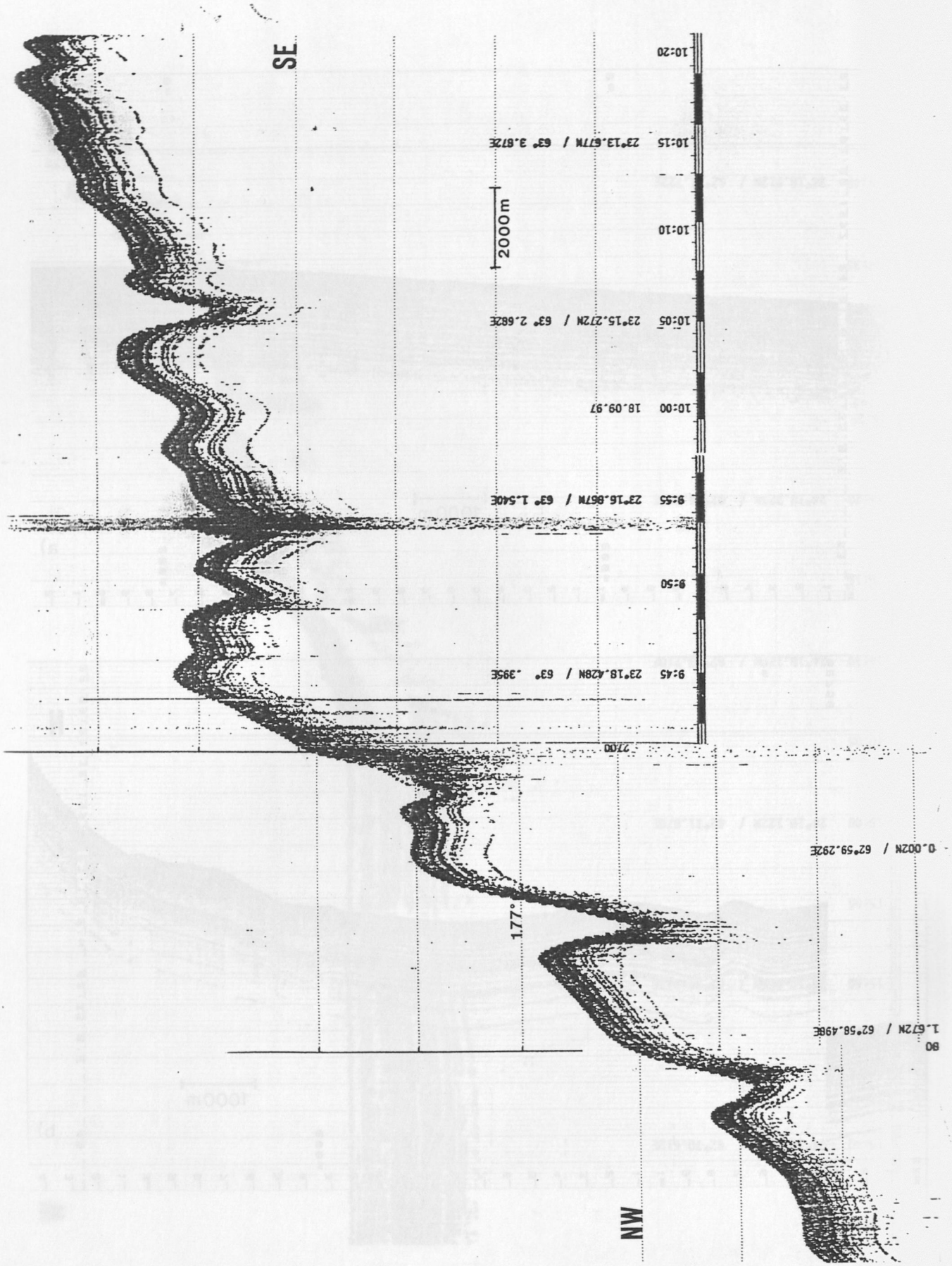

Figure 6.2.2.2: Parasound recording of gently folded sediments northwest of Dalrymple Trough. Note that the steepest slope recorded is about 1.8°.

sediments are highly reflective and massive, but layering is not identified and penetration depth is significantly lower, often less than 20 m. The southern flanks of the ridges show narrowly spaced thrusts indicating that shortening and faulting is active not only close to the deformation front but also distinctly further arcward (Figure 6.2.1.2.1). This style of deformation, active faulting in all ridges and undisturbed layered sedimentation inbetween, is characteristic of the whole wedge. Hovever, from shallow Parasound recordings alone, it cannot be decided if undisturbed layering results from very young post-tectonic sedimentation or is inherited from older sedimentation. Then, the style of imbricate thrust slice formation is combined with significant underthrusting indicating the presence of horizons of different strength.

6.2.1.3. MUD DIAPIRS AND EVIDENCE FOR GAS ACCUMULATION

At several localities within the wedge, mud diapirs have been identified in the Parasound recordings (Figures 6.2.1.3.1 and 6.2.1.3.2). Often, these structures are found on the flanks of the ridges and also at the edges of the not continuous ridges of the complex second and third ridge system. Mostly, they occur in the vicinity of blank zones and mark the slope edge of a sequence of such zones. Therefore, the blank zones which are often lense shaped are interpreted as zones of methane accumulation. These zones are normally covered with about 10 m sediment, above and below, the layering is normally visible and quite undisturbed. The blank zones follow the slope.

6.2.2 DALRYMPLE TROUGH AND ADJACENT AREAS

South and north of Little Murray ridge, sediments show distinctly different features (Figure 6.2.2.1). The change between the two facies occurs just in the culmination of Little Murray ridge. South of it, layering is imaged very clearly,

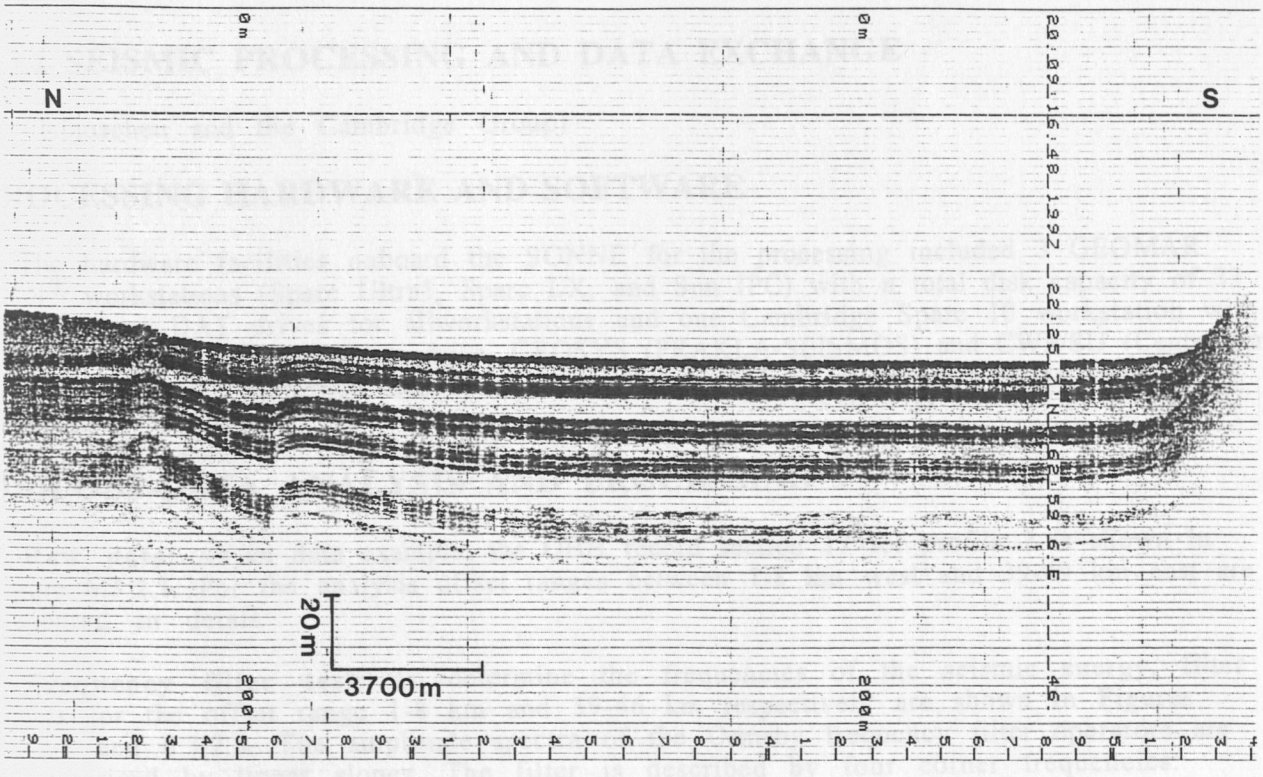

Figure 6.2.2.3: Parasound recording of the bottom sediments of Dalrymple Trough.

the strength of reflections is decreasing significantly with depth. Penetration depth is about 40 m. Gentle folds indicate a compressional tectonic regime. North of Little Murray ridge, reflections remain nearly at the same strength with increasing depth. Penetration depth is about the same as south of Little Murray ridge. However, layer spacing is smaller, and often, the upper part of the imaged portion to about 20 m depth does not show clear layering. This facies is also found largely in the flat portion of the Makran accretionary wedge.

North and south of Dalrymple Trough, Parasound data revealed both, compressional and extensional structures, in the shallow subsurface sediments. Compression is indicated by folding with long wavelengths. Shape and wavelength of the folds vary significantly. While some are close to perfectly round, others comprise a more angular shape (Figure 6.2.2.2). Superposed on the folded surface is a smooth rise and slope between Little Murray ridge and the shoulder of Dalrymple Trough. South of Dalrymple Trough, the same style of superposition of smaller wavelength folds on the here more pronounced topography is observed. The folded slopes comprise numerous steeply dipping faults which lead to the formation of graben like structures with nearly vertical walls.

While the walls of Dalrymple Trough are too steep to allow Parasound recordings, the bottom of the trough is nicely imaged (Figure 6.2.2.3). It is nearly flat, penetration depth is often more than 50 m, several strong subparallel reflectors with non-reflective layers inbetween are visible.

6.3 SEISMIC WIDE-ANGLE WORK

6.3.1 INTRODUCTION

(E. Flüh)

The major work during SO123-Mamut was devoted for the collection of seismic wide-angle data. A total of 92 OBH and 5 OBS deployments were made along 10 lines, with one of the lines being a short test line for new instrumentation. All instruments were safely recovered, only one of them causing some delay and problems. In Figure 6.3.1.1 a summary of all deployment sites and profiles is shown. The data quality is generally very good. However, on Murray Ridge and in some sites near to the coast the seismic energy could only be observed to rather short distances.

Shooting was made using the well tuned BGR airgun array, and caused no problems or delays. No malfunctioning of the guns was ever observed. However, when reducing the towing speed from 5 to 4 knots for the last three profiles, the load on the guns increased considerably and was short before failure. Details on the profiles with a total number of nearly 8600 shots along the profiles with a total length of 1220 km are given in Appendix 9.2.

The single channel streamer was deployed along all profiles, and after some initial reconfiguration provided good data, expecially when shooting at lower speed.

All seismic data collected were played out, processed and plotted during the cruise. They are stored in standard SEG-Y format and copies could be made for all participating institutions. This created a heavy load on workstation space and time. The excellent cooperation between the scientific parties onboard and the ship's crew enabled to very smooth operation. Preliminary interpretations were made for some of the profiles, especially those collected early during the cruise. In the following chapters the processing (chapter 6.3.2) and modelling techniques (chapter 6.3.3) applied are described first. This is followed by a description of each profile, which includes the chronology of the experiment (all times given correspond to local times), the most important data and some first initial results.

6.3.2 SEISMIC PROCESSING AND DATA EXCHANGE

(D. Klaeschen and the Cambridge Group)

PROCESSING HARDWARE AND SOFTWARE

The hardware facilities onboard the SONNE for the processing included 3 GEOMAR SUN® workstations (Sparc Ultra1, Sparc LX, and Sun IPC) with a total disk capacity of 33 GB and two DAT drives for allworkstations and one Cambridge Sparc 10 workstation with 2GB disk space and an Exabyte drive. GEOSYS (PRAKLA-SEISMOS) and CWP/SU (Center for Wave Phenomena, Colorado School of Mines/Seismic Unix) were used as seismic processing software.

OBH/OBS-DATA ANALYSIS AND PROCESSING

Raw data: As an data example, the OBH record section 17 for profile 2 is shown in Figure 6.3.2.1. For the analysis offset ranges between 1-8 km west and 39-49 km east are presented in detail.

Frequency filter test: To determine the frequencies of the seismic energy, filter panels for the offset range 1-8 km and 39-46 km respectively are shown in Figures 6.3.2.2 and 6.3.2.3. The amplitude spectra of the Ormsby frequency filter operators are characterised by linear slopes. The filter is described by four corner frequencies:

Lower stop/pass band boundary and upper pass/stop band boundary. The frequencies on the filter panels correspond to the lower and upper pass frequencies. The main energy for the phase between 2.0 and 2.7 s in the offset range from 1-4 km is between 5-33 Hz and for the direct wave up to 60 Hz. The main energy of the phase between 5.0

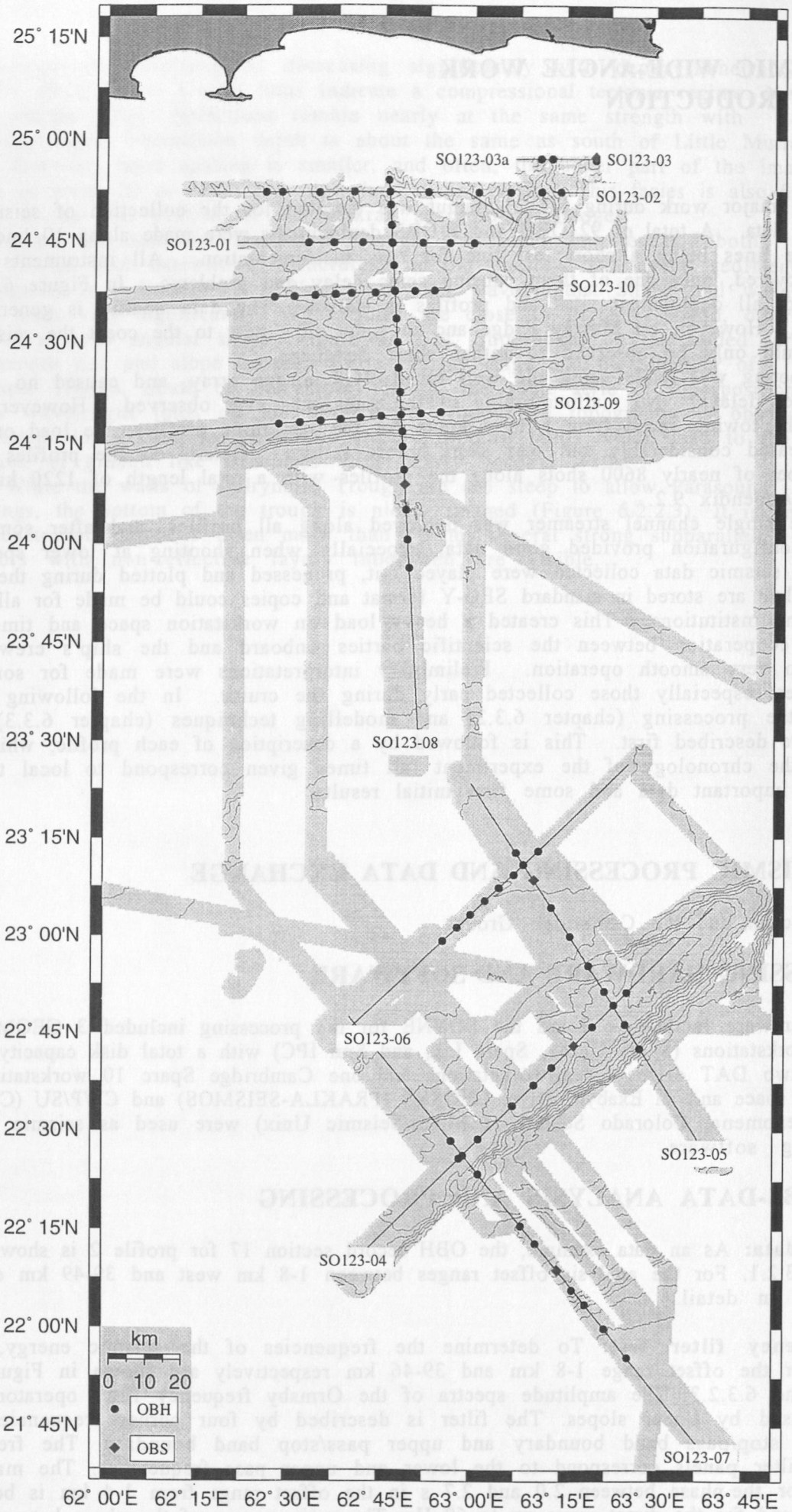

Figure 6.3.1.1: Location map of seismic profiles and OBH/OBS positions during cruise SO-123.

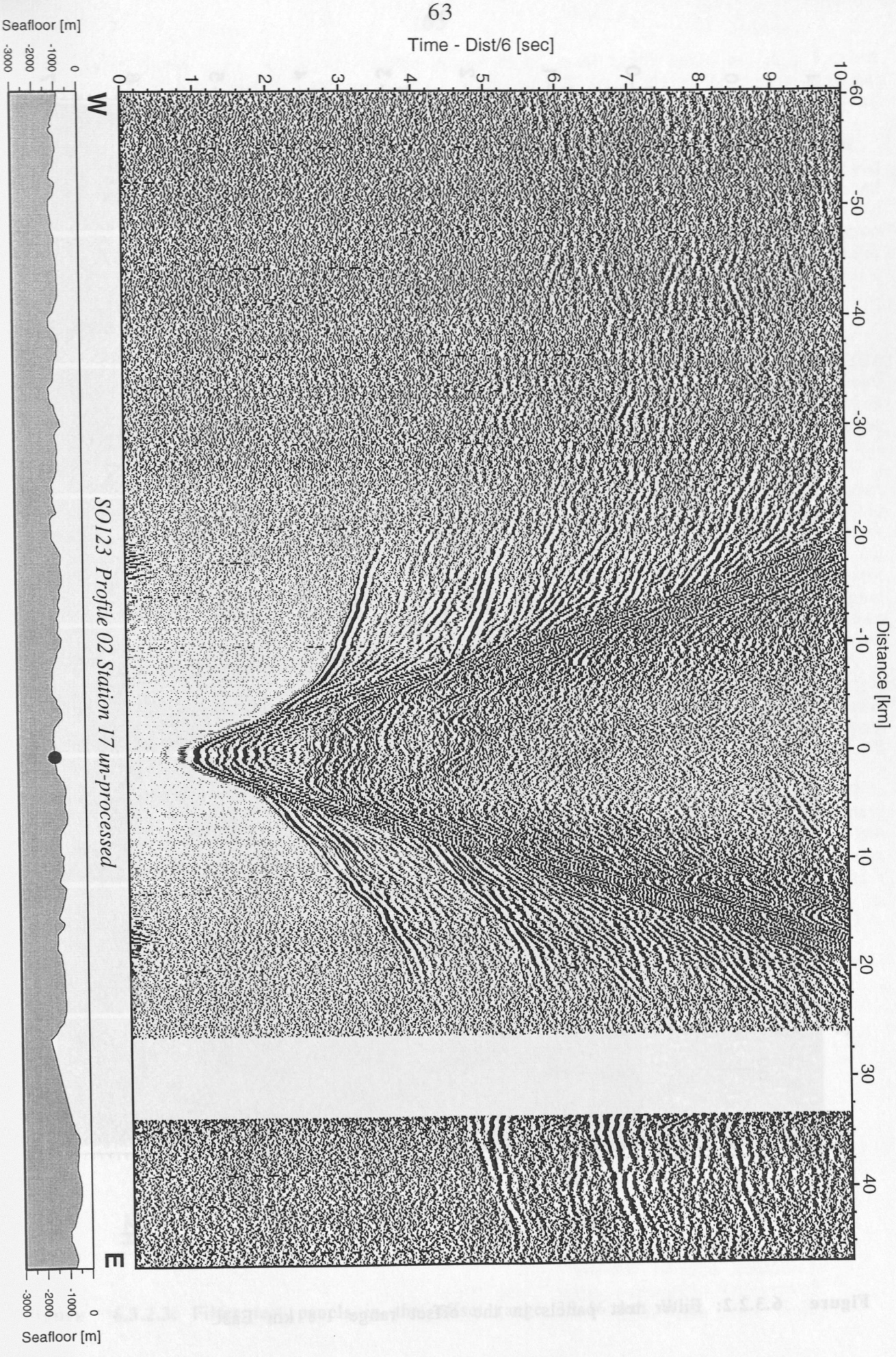

Figure 6.3.2.1: Record section from OBH 17, Profile 02 un-processed.

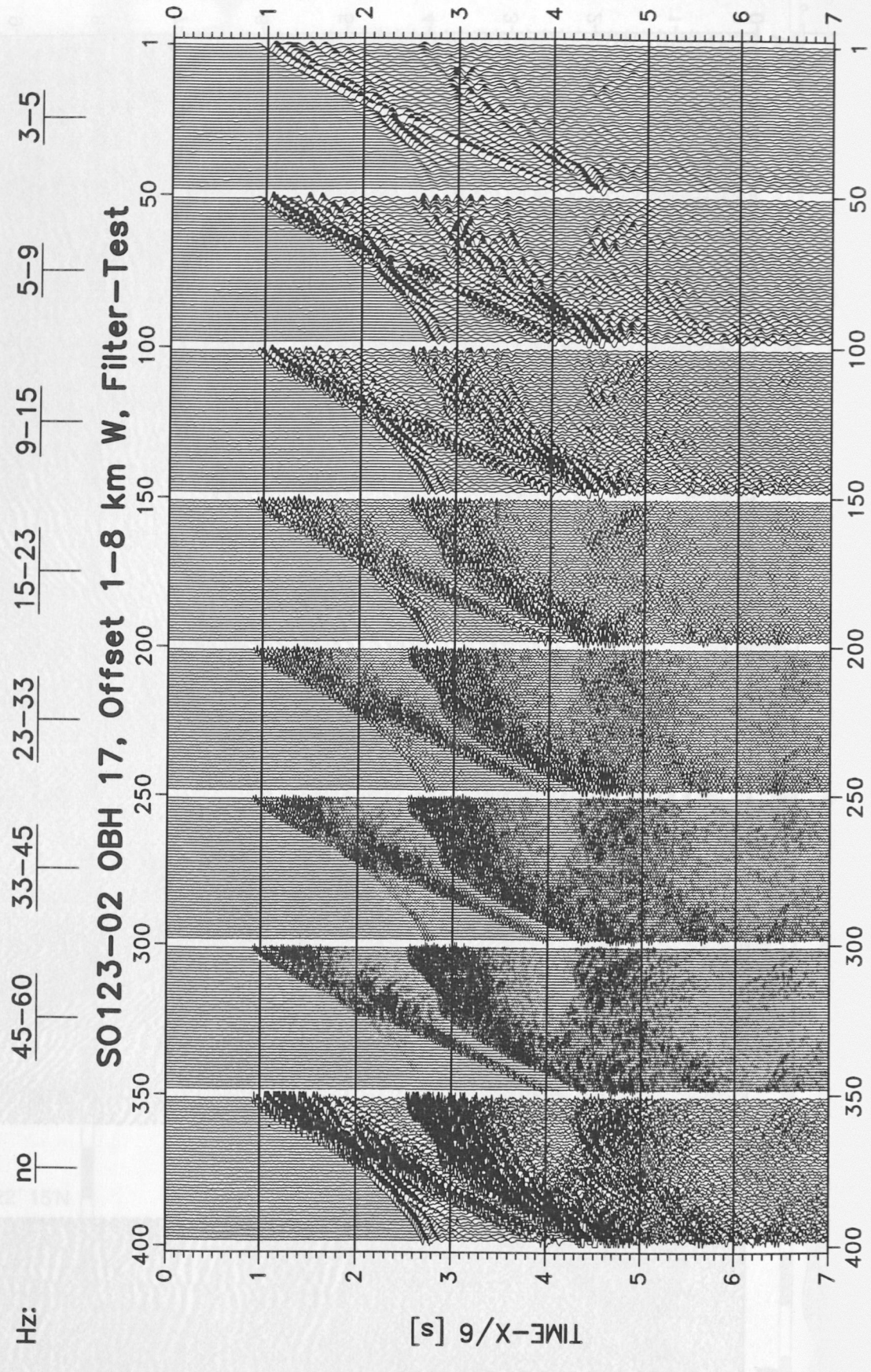

Figure 6.3.2.2: Filter test panels in the offset range 1-8 km East.

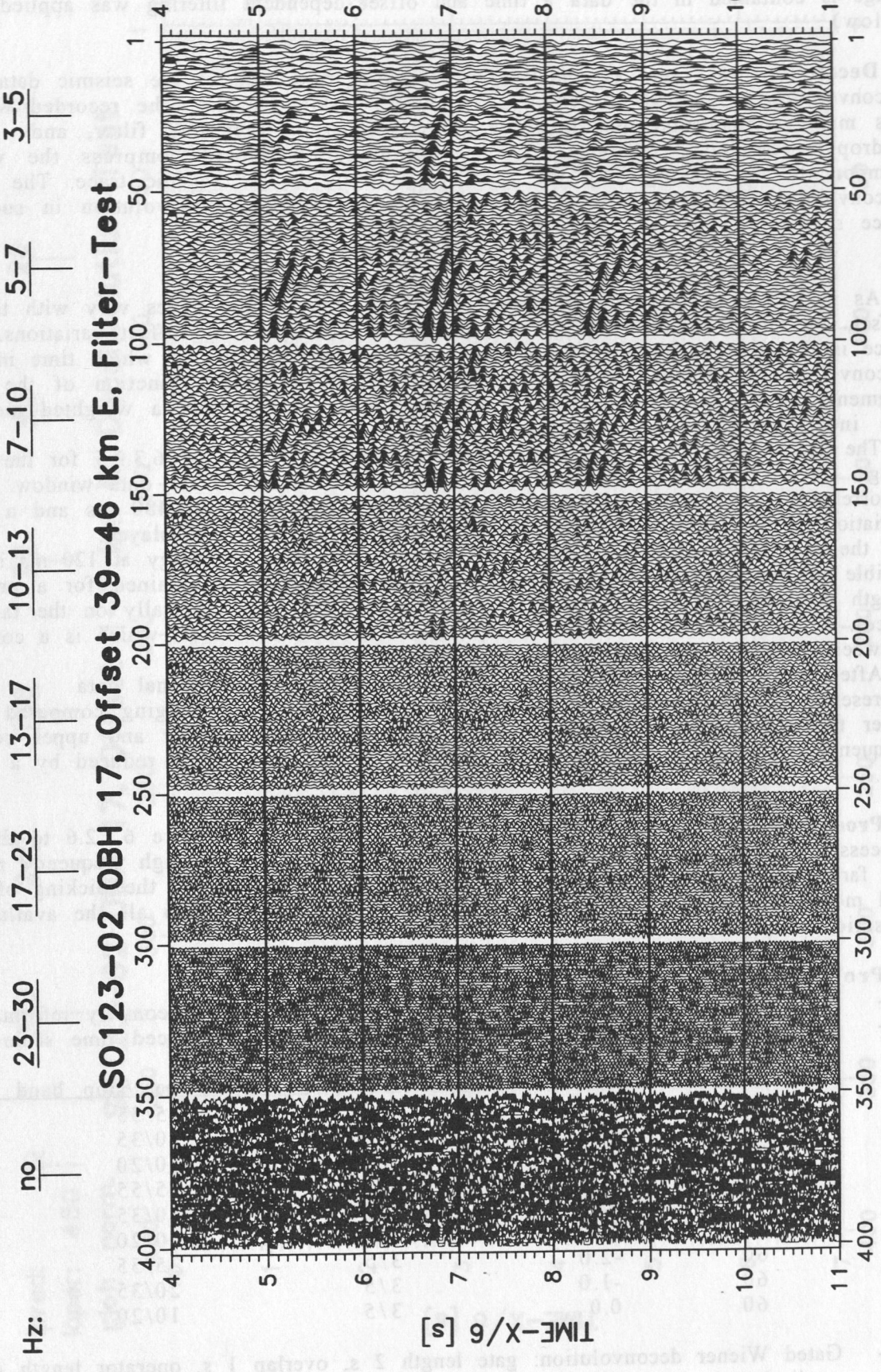

Figure 6.3.2.3: Filter test panels in the offset range 39-46 km West.

and 5.4 s in the offset range from 39-46 km is between 5-10 Hz. As a broad frequency range is contained in the data a time and offset dependent filtering was applied (see below).

Deconvolution test: To improve the temporal resolution of the seismic data a deconvolution is applied to compress the basic seismic wavelet. The recorded wavelet has many components, including the source signature, recording filter, and hydrophone/geophone response. Ideally, deconvolution should compress the wavelet components and leaving only the earth's reflectivity in the seismic trace. The deconvolution algorithm which was applied is the Wiener deconvolution in sucessive trace segments which is based on the following assumptions:

1. The earth's reflectivity is 'white'.
2. The wavelet shows the minimum-delay phase behavior.

As in wide-angle data the amplitude spectra of the seismic traces vary with time and offset, the deconvolution must be able to follow these time and offset variations. Each trace is therefore devided into 2 s data gates with 1 s overlap, in which time invariant deconvolution operators are computed from the autocorrelation function of the data segment and applied. The overall deconvolved trace results from a weighted merging of the independently deconvolved gates.

The deconvolution test panels are shown in Figures 6.3.2.4 and 6.3.2.5 for the offset range 1-8 km and 39-46 km respectively. In the last second of the data window the autorrelation function is appended. A constant operator length of 480 ms and a variation of the predictive length from 0 (spike) to 320 ms is displayed.
On the undeconvolved data in Figure 6.3.2.4 a second peak of energy at 120 ms is clearly visible in the autocorrelation function. The best resolution is obtained for a predictive length of 0 ms but with a reduction of signal-to-noise ratio especially on the far offset traces. A predictive length of 80 ms was choosen for this data set which is a compromise between temporal resolution and signal-to-noise ratio.

After deconvolution a Butterworth filter was applied for the final data representation. This filter is showing only a small amount of ringing compared to other filter technics. The Butterworth filter is characterised by a lower and upper corner frequency of 4 and 30 Hz. At these frequencies the amplitudes are reduced by a factor of 0.5.

Processed data: Comparison of the pre-processed data in Figure 6.3.2.6 to the un-processed data in Figure 6.3.2.1 shows a clear reduction of the high frequency noise on the far offset traces and a compression of the wavelet signal. For the picking of events and model building by raytracing both sections were used to keep all the available seismic information.

Processing sequence:

- Input: SEGY-data, 5 or 10 ms sample rate with complete geometry information
- time and offset dependent Ormsby frequency filter (on reduced time scale with 6 km/s):

offset (km)	100%-time (s)	lower stop/pass	upper pass/stop band (Hz)
0	4.0	3/5	35/55
0	6.0	3/5	20/35
0	8.0	3/5	10/20
40	-2.0	3/5	35/55
40	-0.5	3/5	20/35
40	1.0	3/5	10/20
60	-2.0	3/5	35/55
60	-1.0	3/5	20/35
60	0.0	3/5	10/20

- Gated Wiener deconvolution: gate length 2 s, overlap 1 s, operator length 480 ms, prediction interval 80 ms
- Butterworth frequency filter: 4-30 Hz
- linear time and offset scaling (on unreduced time scale).

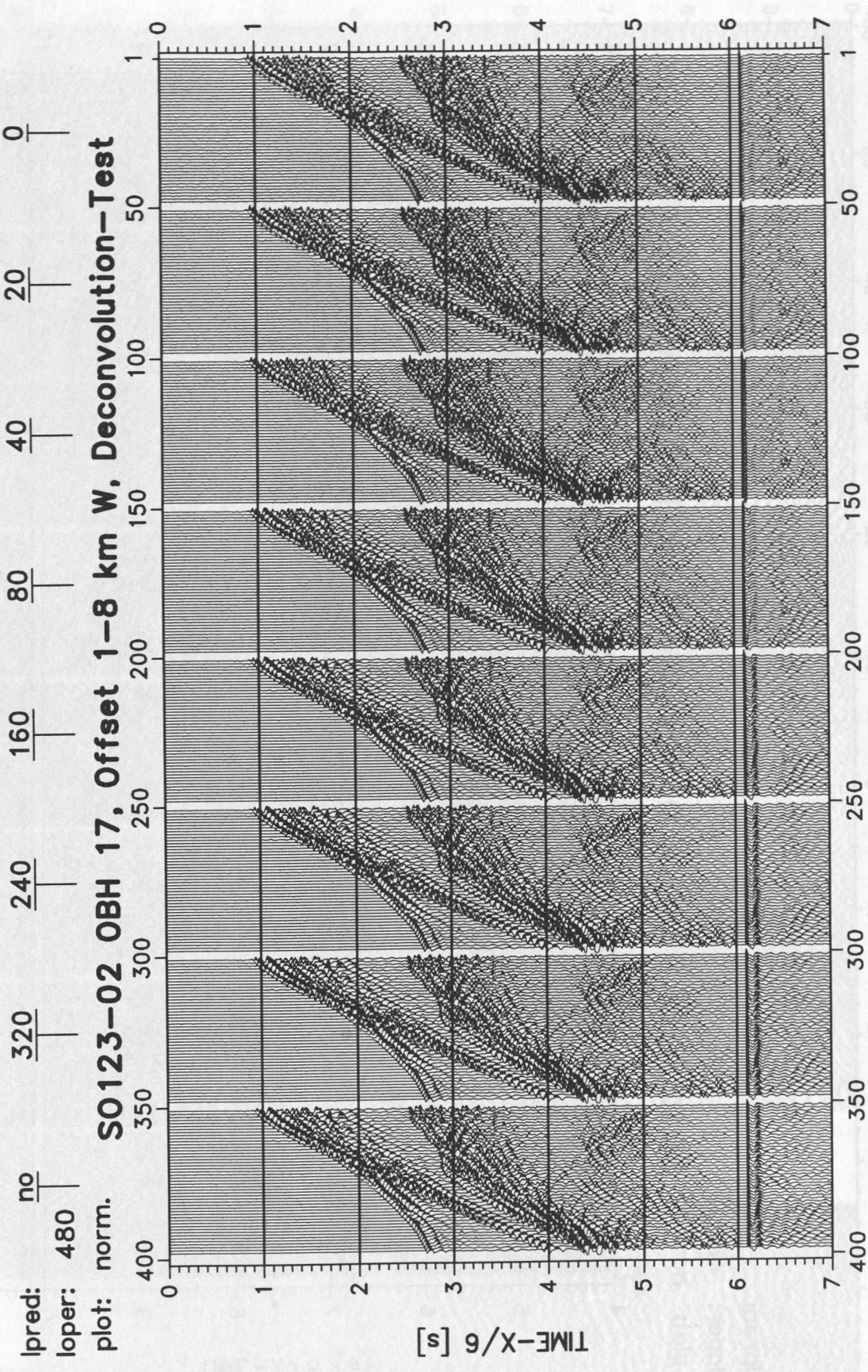

Figure 6.3.2.4: Deconvolution test in the offset range 1-8 km East.

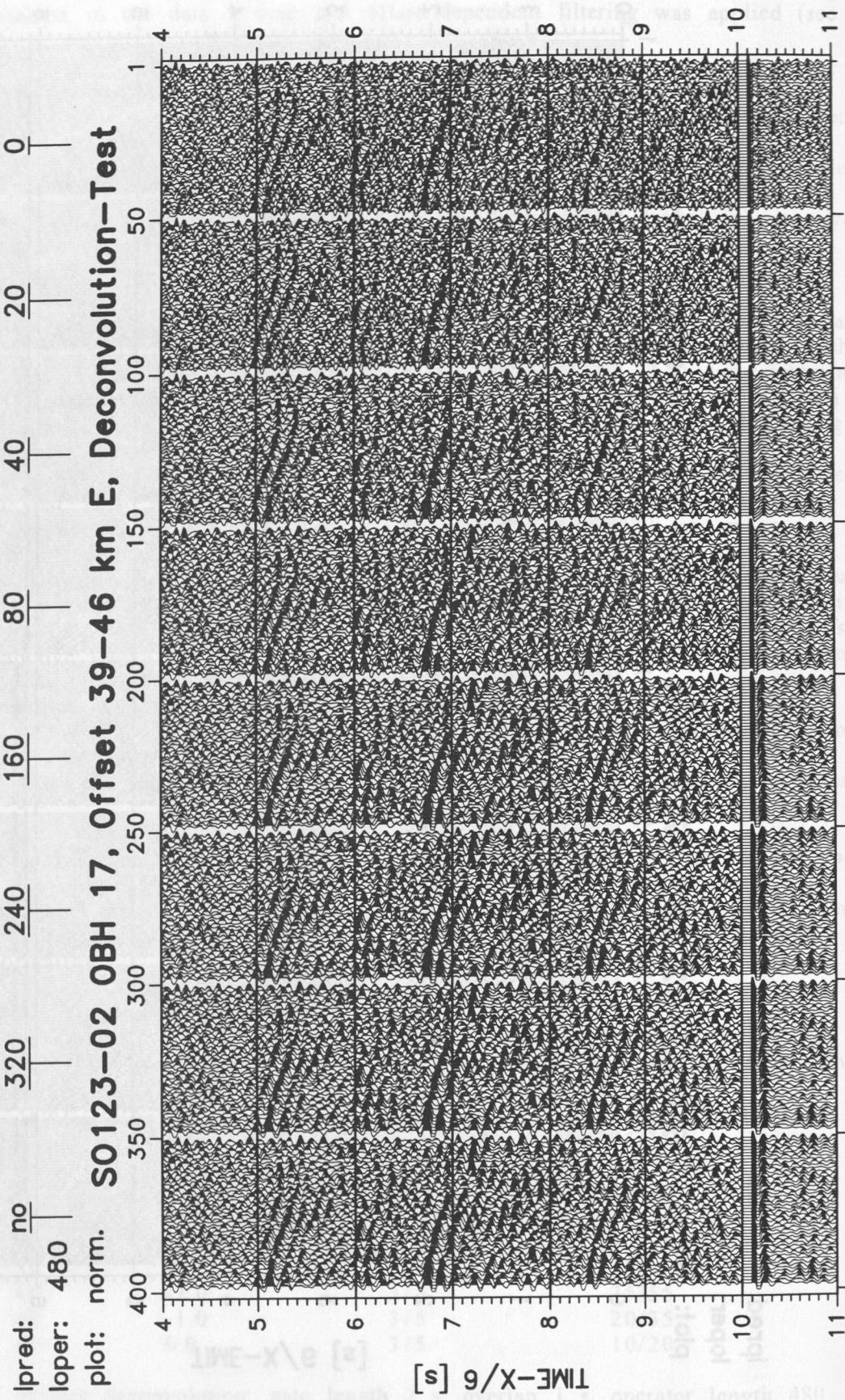

Figure 6.3.2.5: Deconvolution test in the offset range 39-46 km West.

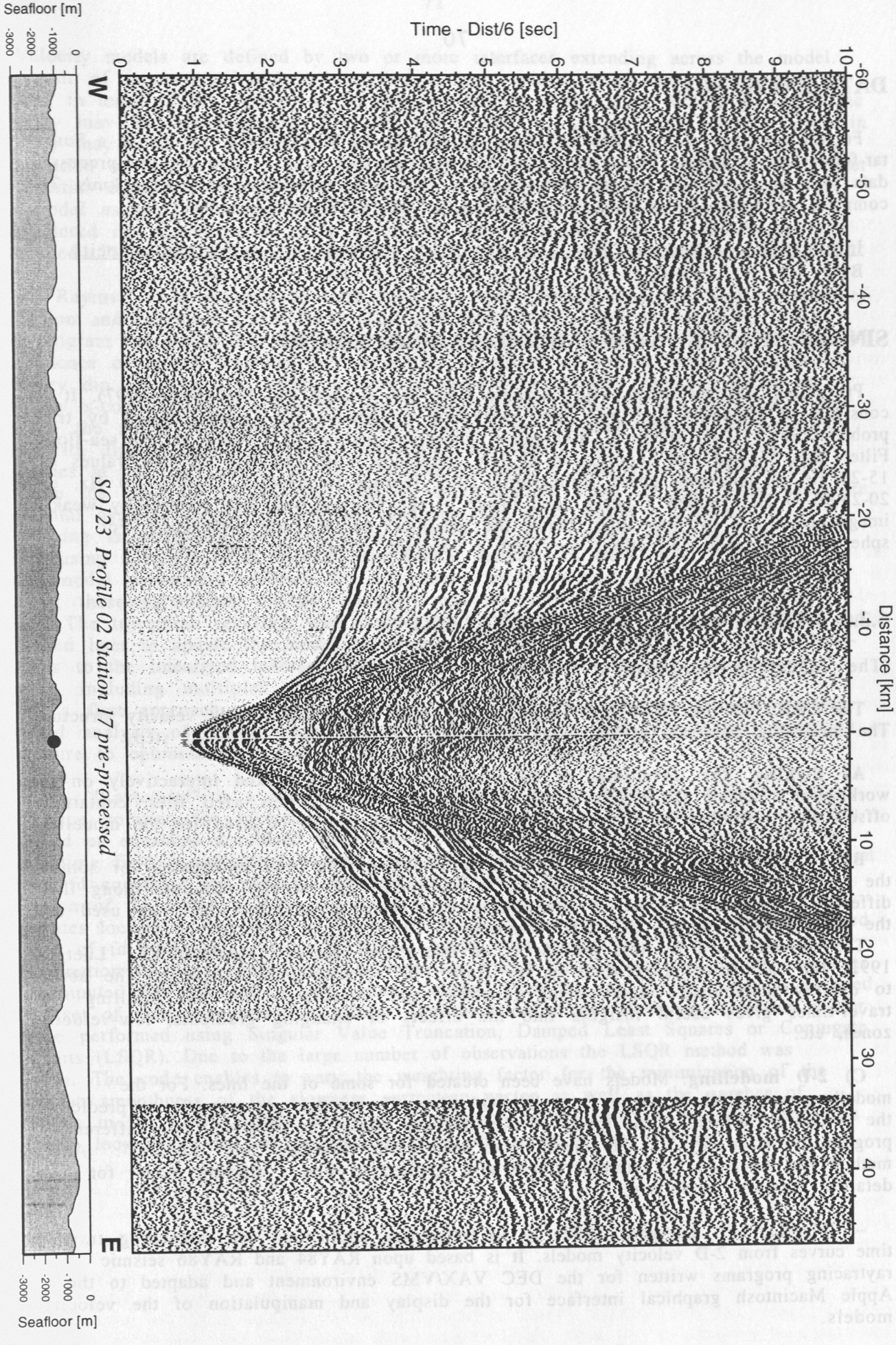

Figure 6.3.2.6: Record section from OBH 17, Profile 02 pre-processed.

DATA EXCHANGE

For the exchange of the OBH/OBS data (GEOMAR) the SEGY-format on disk in a Sun tar-format was choosen. The trace length for the raw data is 15 s and for the processed data 14 s where the time of the first sample is -2 s at a reduction velocity of 6 km/s. The complete geometry information is positioned in the SEGY-trace header:

Information	Receiver No.	Shot No	Offset	reduction velocity
Byte:	13-16	21-24	37-40	93-94

SINGLE CHANNEL STREAMER DATA PROCESSING

Processing was performed with "Seismic Unix 30" (Cohen and Stockwell, 1997). It consisted of bandpass filtering, static correction to remove the "jitter" caused by trigger problems (cf. 5.2.1), spherical divergence correction and a trace mute to the sea-floor. Filter tests showed that suppression of low frequency noise required low cut values of 15-20 Hz. A minimum phase Butterworth filter (corner frequencies 15-20-60-70 Hz, or 20-25-60-70 Hz) yielded a fairly good image of the shallow part, but a generally weak image below 2 s two-way time (below the sea-floor) due to little penetration. For spherical divergence corrections we used a constant velocity of 1500 m/s.

6.3.3 WIDE-ANGLE DATA MODELLING

(The Modelling/Interpretation Group)

The OBH/OBS data have been analyzed for crust and upper mantle velocity structure. The modelling sequence of the wide-angle data involves three different steps:

A) Picking: The traveltimes of the observed phases are picked interactively on the workstation's screen using Seismic Unix Software. This provides ascii files, containing offsets and traveltimes of phases for each record, which will be used for the modelling.

B) 1-D modelling: A 1-D velocity-depth modelling has been undertaken for some of the record sections. This first approach to determine the velocity structure along the different lines allows to define preliminary velocity-depth models, which are used as the starting point during the 2-D modelling.
The software used for this porpuse is an interactive program "MacR1D" (J. Luetgert, 1992) for calculating travel-time curves from 1-D velocity-depth functions. The ability to quickly manipulate velocity-depth functions and inmediately see the resulting travel-times gives useful insights into the effects of changing gradients, low-velocity zones, etc.

C) 2-D modelling: Models have been created for some of the lines. For the modelling waterdepth is taken from UKOOA-files. The models are capable of predicting the correct offset/time of as many of the observed phases as possible. Two different programs to trace rays in 2-D media have been used: "MacRay" and "Rayinvr". Another method for inversion („Raytomorf") was also applied to find a starting model for detailed forward modelling.

-- "MacRay" (J. Luetgert, 1992) is an interactive application for calculating travel-time curves from 2-D velocity models. It is based upon RAY84 and RAY86 seismic raytracing programs written for the DEC VAX/VMS environment and adapted to the Apple Macintosh graphical interface for the display and manipulation of the velocity models.

Velocity models are defined by two or more interfaces extending across the model. Any pair of successive interfaces describes a layer, within which the velocity may be defined in terms of the velocity at the top and bottom of the layer. Within any layer the velocity may be inhomogeneous but continuous. First or second order discontinuities in velocity may occur at interfaces. The ray tracing algorithm that is used calculates the propagation of rays within a layer by the stepwise integration of a system of first order differential equations (Cerveny et al., 1977). Lithologic interfaces are represented in the model as first or second order velocity discontinuities. When an interface is encountered in the calculation of a ray, Snell's law is applied and the calculation is continued. "MacRay" is very usefull for quickly manipulating velocity models.

-- "Rayinvr" is a program to trace rays for rapid forward modelling and inversion of refraction and reflection travel times (Zelt and Smith, 1992; Zelt and Forsyth, 1994). The program assumes a 2-D (x,z) isotropic medium and the velocity model is composed of a sequence of layers separated by boundaries consisting of linked linear segments of arbitrary dip. The velocity within a layer is defined by velocity values specified at arbitrary x-coordinates along the top and bottom of the layer. For the purposes of ray tracing, the model is automatically broken up into an irregular network of trapezoids, each with dipping upper and lower boundaries and vertical left and right sides. The velocities at the four corners of the trapezoid are used to interpolate a velocity field between the trapezoid so that the velocity varies linearly along its four sides. Therefore, horizontal as well as vertical velocity gradients may exist within a trapezoid. Raytracing is performed by numerically solving the ray tracing equations for 2-D media using a Runge Kutta method. The partial derivates of travel time with respect to those model parameters selected for adjustment are calculated analytically during ray tracing; these parameters include velocities and the vertical position of boundary nodes. The traveltime residuals with respect to the observed data are also calculated and are used later to update the model parameters by applying the method of damped least-squares to the linearized inverse problem. The algorithm can include any type of arrival, including multiples and/or converted shear waves.
As a first approach, we have performed velocity-depth modelling through classical forward analysis of arrival times. Finally, an iterative damped least-squares inversion procedure to optimize the velocity and depth values is applied.

-- "Raytomorf" is a two dimensional inversion routine based on a finite-difference solution for inversion of the velocity field. The finite-difference algorithm is based on equations developed by Vidale (1988). Based on a gridded velocity field the travel time field is calculated with the use of an expanding square. Starting from a point source fd equations are used to calculate travel times to the neighbouring grid nodes. Selection of the nodes is done according to the scheme of an expanding square where the nodes located on the sides of the square are used. Ammon and Vidale (1993) modified the set of fd equations in order to handle media with strong velocity variations. After determination of the travel time field rays are traced through and ray length segments are computed for each cell of the velocity model. Then the ray length matrix is inverted for a set of slowness correction values. The inversion of the slowness correction vector can be performed using Singular Value Truncation, Damped Least Squares or Conjugate Gradients (LSQR). Due to the large number of observations the LSQR method was choosen. The code enables to vary the weighting factor for the minimization of the Laplacian smoothness of the slowness correction vector as well as the number of iterations in the LSQR matrix inversion. Application of the program was done within a recursive loop using the last inverted model as the input to the next run.

6.3.4 SEISMIC WIDE-ANGLE PROFILES
6.3.4.1 PROFILE SO123-01

(C. Kopp, C. Reichert, E. Flueh, J. Fruehn)

Profile 1 is located about 25 nm off the coast of Pakistan in an average waterdepth of 1500-1700 m and extends for 55 nm in an E-W direction. It is centered on the reflection profile CAM30 (Minshull et al., 1992), the location of the OBH and the extent of shooting is shown in Figure 6.3.4.1.1. In total seven OBH (OBH06 to OBH12) were deployed at 4 nm spacing between 01:00 and 06:00 10.09. with OBH09 on line CAM30. The outermost instruments (OBH06 and 12) form part of the network to monitor the seismicity (see chapter 6.5). These instruments recorded at 10 msec sampling interval, while the other instruments recorded with 5 msec sampling interval. Exact locations and instrument numbers are summarized in the Appendix 9.1.1. Shooting started at 15:42 10.09. and ended at 03:00 11.09. Shooting then continued during the transit to Profile SO123-2 and along that line, so fan observations are also available but were not analysed onboard. Four instruments (OBH07, 08, 10, and 11) were recovered between 01:30 and 04:30 12.09., OBH09 at 03:00 15.09., OBH06 at 08:00 24.09. and OBH12 at 23:30 23:09. During shooting the single channel streamer was also deployed, and the section is shown in Figure 6.3.4.1.2. The OBH data were processed as described in chapter 6.3.2, the record sections for the inline data are shown in Figures 6.3.4.1.3 to 6.3.4.1.8. The data are of excellent quality, clear sedimentary arrivals and reflections as well as a prominent reflection interpreted to be the decollement reflection (or plate boundary) are recognised, as well as a Moho reflection on some sections. The BSR is also clearly recognised at near vertical offset at about 05. s TWT below sea bed, especially at OBH08 and 09.

The single channel data show structures in the top 1 s of the sediment (Figure 6.3.4.1.2). The line strikes normal to the direction of deformation (accretion), which explains the discontinuous aspect of the reflections. Clearly imaged reflections might arise from sediment ponded between two ridges (such as the section around OBH08), or from little deformed parts of the folds (shots 1-75). The areas with poor seismic imaging in the upper second two-way time have either rough bathymetry (shots 450-550) or they probably image the more deformed parts of the folds adjacent to the fold axis. A more detailed analysis of bathymetry (HYDROSWEEP) and the high resolution seismic profile (PARASOUND) will help to constrain the type of structures imaged in this line.

The BSR (Bottom Simulating Reflector) appears at ~0.5 s below the seabed at several places along the profile, and is particularly prominent near the crossing point with the profile CAM30 (shots 280-400). Here, there appears to be a band of high-amplitude reflectors at or beneath the BSR over a distance of about 50 shots (7.5 km). A more detailed image of this area from both lines is shown in Figure 6.3.4.1.9. The point of intersection of SO123-01 and CAM30 is marked by a small triangle. CAM30 is shown here as a stacked section. On this line three folds are clearly imaged with axes at cdp 4150, 4450, and 4800. The BSR is a strong reflection between cdp 4200 and 4400, clearly cutting the dipping reflections of the first fold. Near the second fold it appears deformed and it dies out at cdp 4600. Line SO123-01 images the strongly deformed sediment of the fold axis between shot number 500 and 700 as a band of discontinuous high-amplitude reflectors. The deformation of the BSR suggests a thermal anomaly in this area possibly due to recent reactivation of the thrust fault at cdp 4400.

Preliminary modelling using trial and error raytracing resulted in the velocity model shown in Figure 6.3.4.1.10. Five of the seven OBH on this line were taken into account for the modelling. They show clear sediment reflections and refractions revealing velocities from 1.8 km/s (uppermost seafloor sediment) up to 5.3 km/s at about 16 km depth. On most of the stations the 4 km/s refraction events diminish after 10-15 km to be continued at later traveltimes with the same velocity. Such a shingling is not uncommon in accretionary wedges. Figure 6.3.4.1.10 (a) indicates the picked traveltimes (crosses) with the computed arivals (solid lines) for OBH08. To the east the 4.3 km/s phase is interrupted 3 times. Generally it is possible to model those phase shifts with low velocity zones, but this solution seems unreasonable: At least three LVZ are needed (the lowermost at a depth of 10 km), interchanging with higher velocity layers. In contrast we believe that these events are produced by interbed- or peg-leg multiples in

combination with a low velocity zone at a depth of about 8 to 10 km (Figure 6.3.4.1.10 b). There is very little information about sediment velocities from 10 to 16 km depth. The best fit with most of the OBH stations can be achieved with velocities around 5 km/s. On the western part of the record section of OBH09, OBH11 and OBH12 a reflection at 16 km depth can be seen, which is interpreted as the basement reflection.

The next clear event on stations 08, 09, 11 and 12 is a distinct Moho reflection (PmP). The layer above this discontinuity is about 6 km thick with velocities between 6 and 7.2 km, hence it rpresents the oceanc crust. The only station showing a mantle refraction is OBH12. This Pn phase could be fitted with upper mantle velocities of about 8.2 km/s. These results are in good agreement with the interpretation of line SO123-02, -10, and -09 (Figures 6.3.4.2.10, 6.3.4.10.11, and 6.3.4.9.12) revealing a similar low velocity zone within the sediment, and similar velocities for both the sediment and the oceanic crust.

Stratigraphic identification of reflectors and velocity layers is only feasible in the extreme north of the study area on the Makran shelf. Even there it is difficult due to the intense faulting and folding. Stratigraphic cross-sections along selected N-S-profiles are published by Raza et al. (1990) and by Harms et al. (1982 and 1985) basing on exploration data of the oil industry (seismics and well data). General descriptions of the Makran geology are given by Hiller (1994), Farah et al. (1984), Bannert (1992) and Raza and Alam (1983). Accessible information reaches as far to the south as 24° 40' between Gwadar Peninsula and the Ornach-Nal Fault. However, in the southernmost area the published data are lacking a differentiated stratigraphy due to the complicated tectonic structures. The Makran sedimentary sequences encountered on the uppermost shelf are subdivided into five stratigraphic units (Raza and Alam, 1985):

1. Early Miocene rocks deposited in an oceanic basin and consisting of abyssal muds (Hoshab-Siahan shales) and turbidites (Panjgur formation).
2. Late Miocene sediment of the accretionary forearc basin deposited in shallow marine environment (Parkini formation) comprising a monotonous sequence of mud and sandstone beds.
3. Late Miocene - Pliocene cyclic sediment east and west of the Pasni anticlinorium (Hinglaj formation / Talar) consisting of alternating sandstones and shales.
4. Pliocene - Pleistocene neritic, massive and monotonous sequence of calcareous mudstones (Chatti formation).
5. Early to late Pleistocene marine shore-line deposits (Ormara and Jiwani formations).

Direct correlation with the wide-angle/refraction seismic data acquired on SO-123 is hampered due to the narrow tectonic structures and due to the distances of more than 20 km requiring unreliable interpolation. The small-scale intercalations and alternating beds are not obvious in the wide-angle data. A more extended velocity inversion was derived from stacking velocities of industrial MCS data in the region just southwest of Pasni and about 13 nm north of the SO123-02 profile (pers. comm. HDIP) that reaches from 500 m depth to about 2,500 m with velocities of less than 2,700 m/s. The top of that structure is overlain by velocities higher than 3,000 m/s which is very unusual in that shallow depth. Since such a structure does not exist on the nearest OBH profile SO123-02 we are obviously dealing with a regionally limited feature. On the other hand, thickness and depth beneath seafloor are comparable to an LVZ on the SO123-01 profile in 1 to 2 km below seafloor. This demonstrates that despite regional pecularities similar features exist probably due to the same depositional and tectonic setting, and might be an indication for mighty overpressured domains.

Regarding the general velocity field, the comparison shows, however, that the velocities modeled for the OBH profiles SO123-01 and -02 are in good accordance with those from the industrial survey: close to the seafloor low velocities of some 1,700 m/s were calculated gently increasing to values of somewhat more than 4,000 m/s at 9 km depth.

Necessarily, the analyses on board FS SONNE remain uncompleted. More detailed modeling and in-depth studies still have to be done.

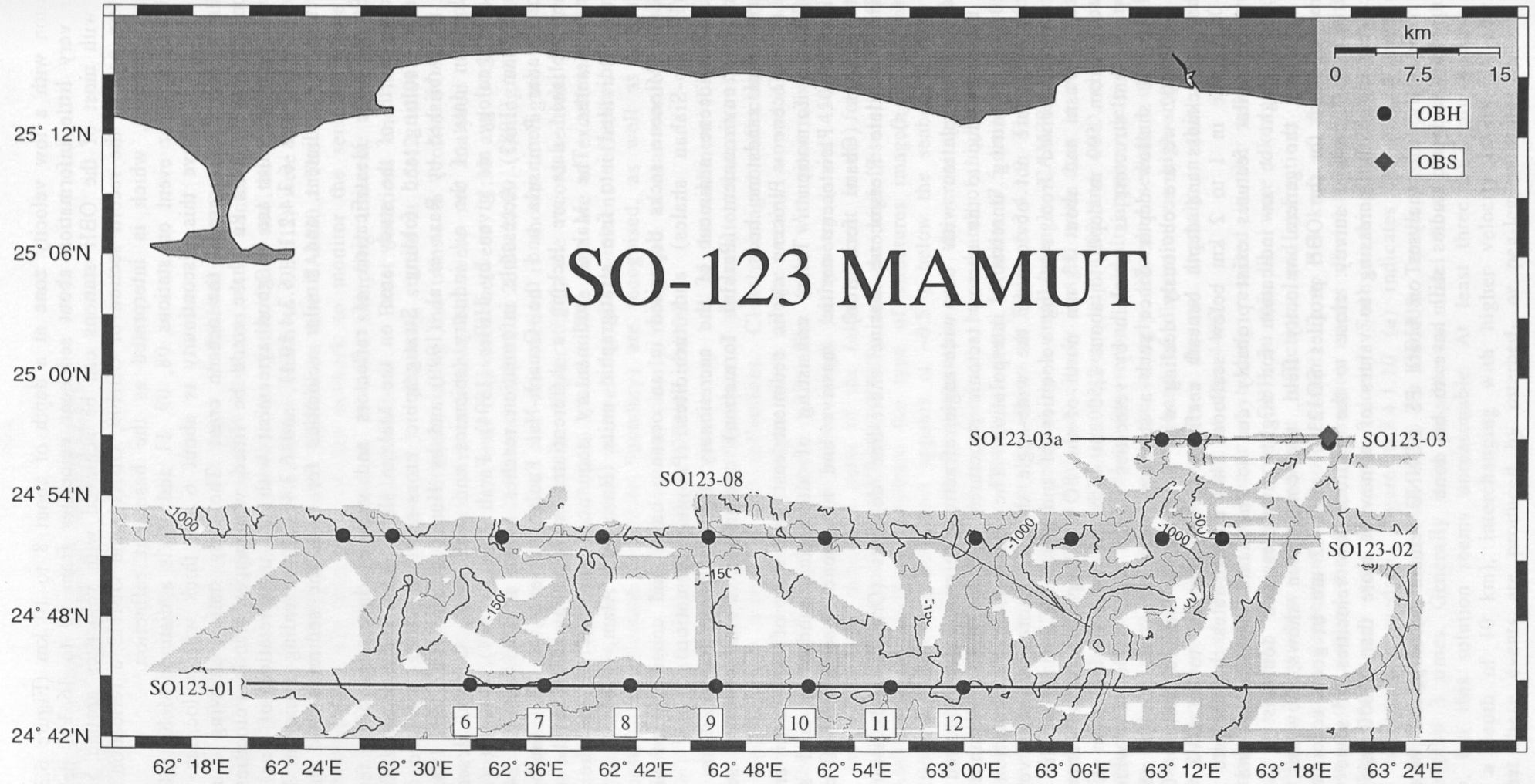

Figure 6.3.4.1.1: Location map of profile SO123-01.

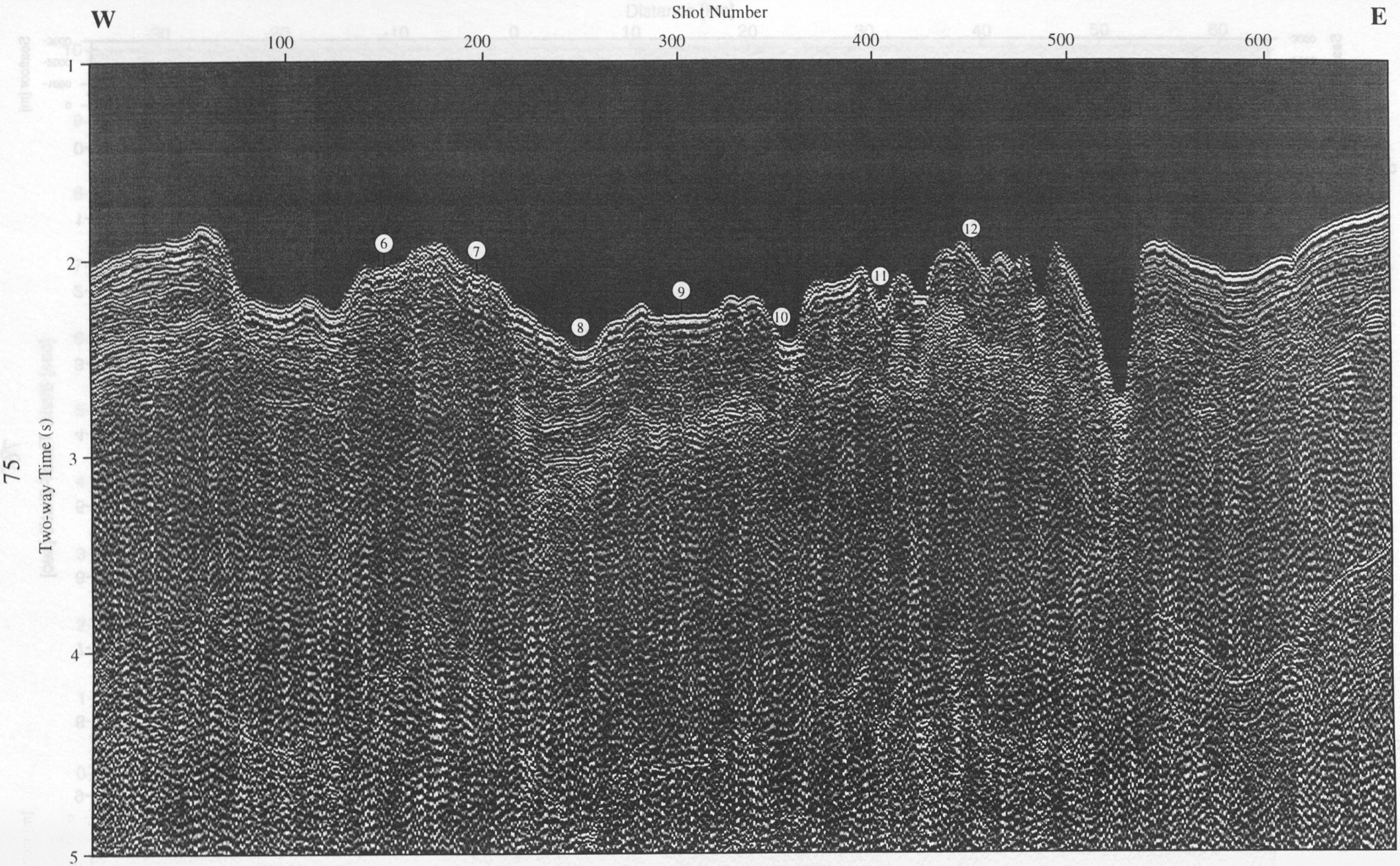

Figure 6.3.4.1.2: Single channel seismic profile SO123-01 (VE=20:1 at the sea-floor). Numbers at the sea-floor mark OBH positions.

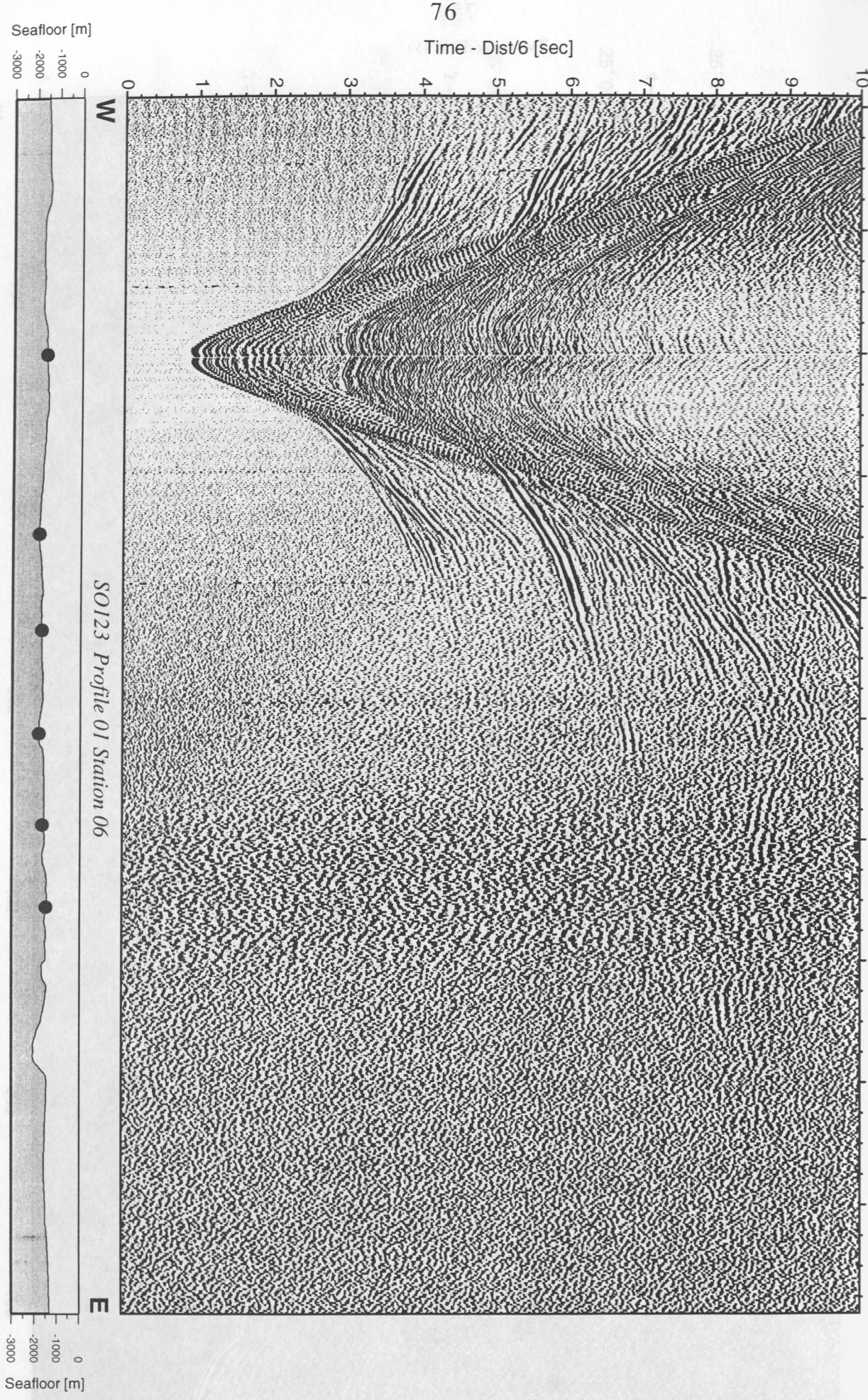

Figure 6.3.4.1.3: Record section from OBH 06, Profile 01.

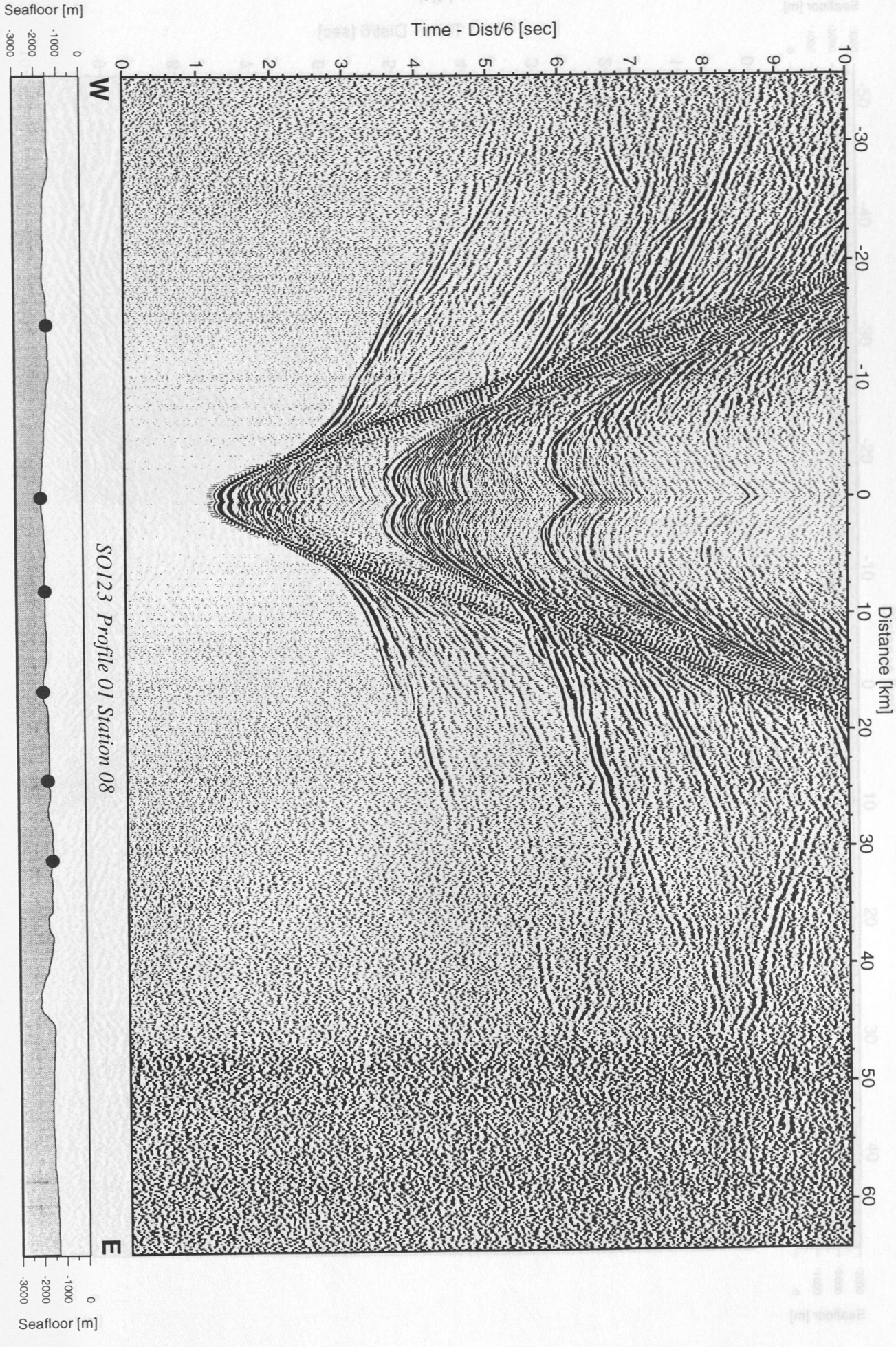

Figure 6.3.4.1.4: Record section from OBH 08, Profile 01.

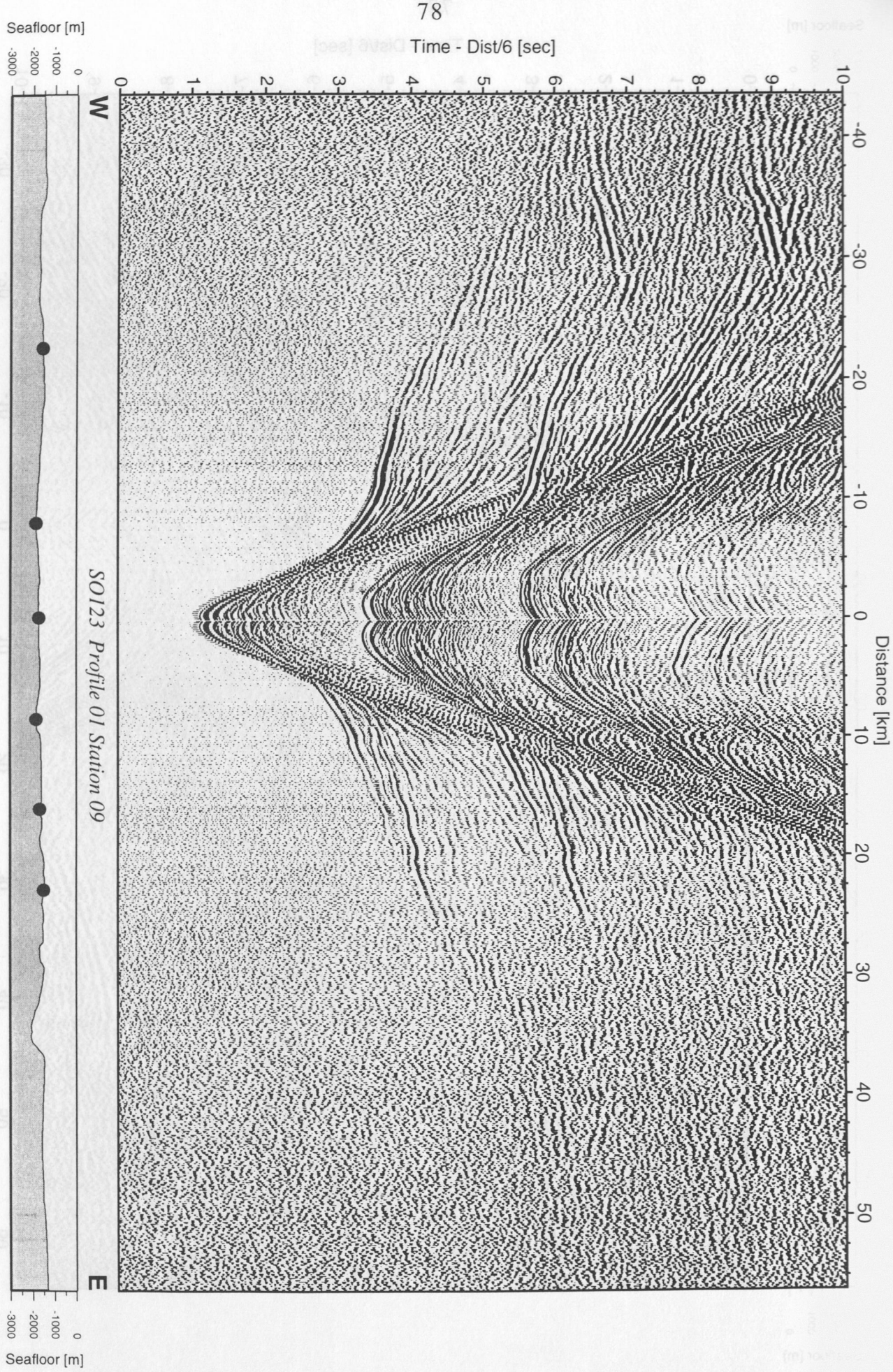

Figure 6.3.4.1.5: Record section from OBH 09, Profile 01.

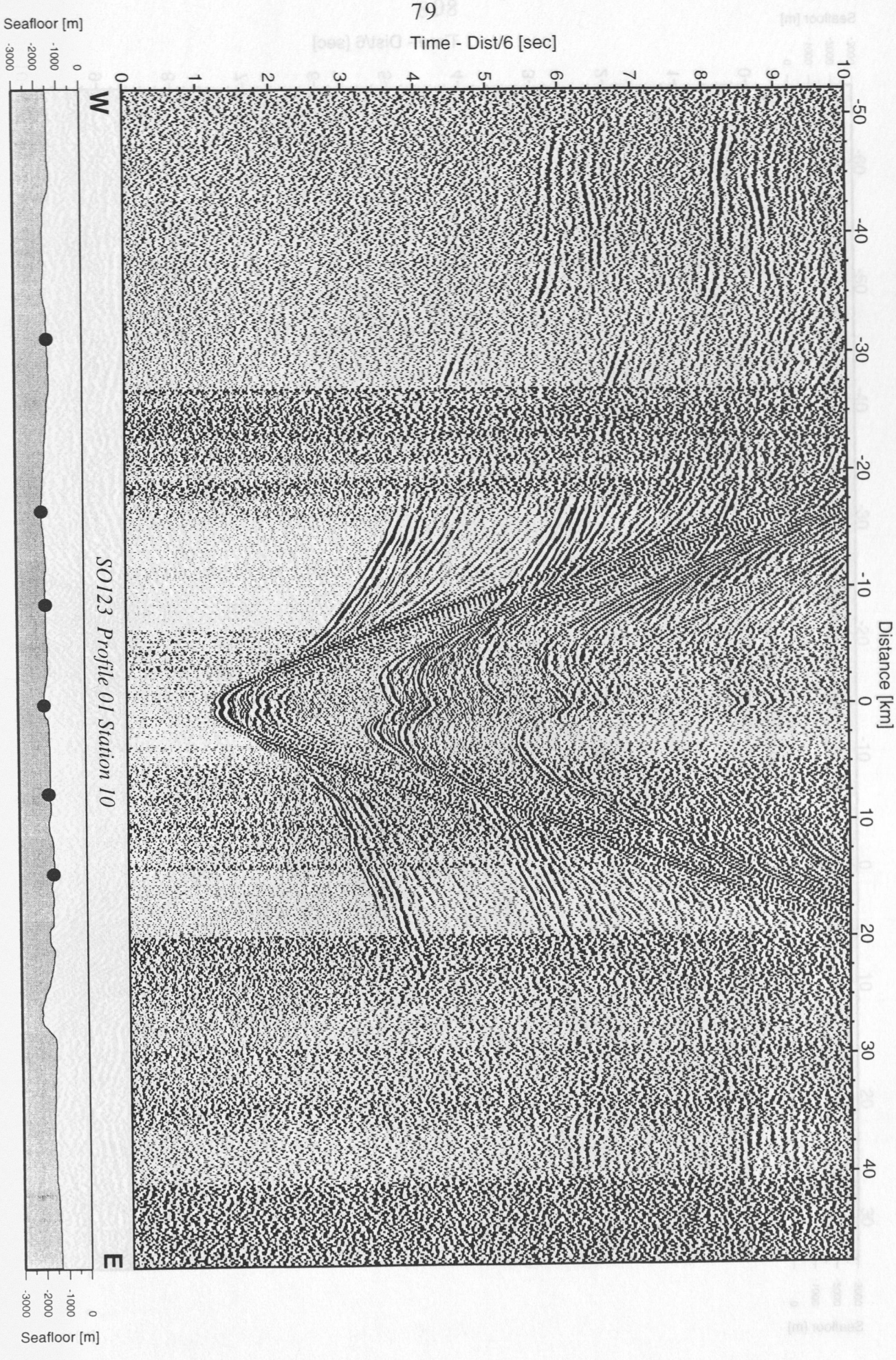

Figure 6.3.4.1.6: Record section from OBH 10, Profile 01.

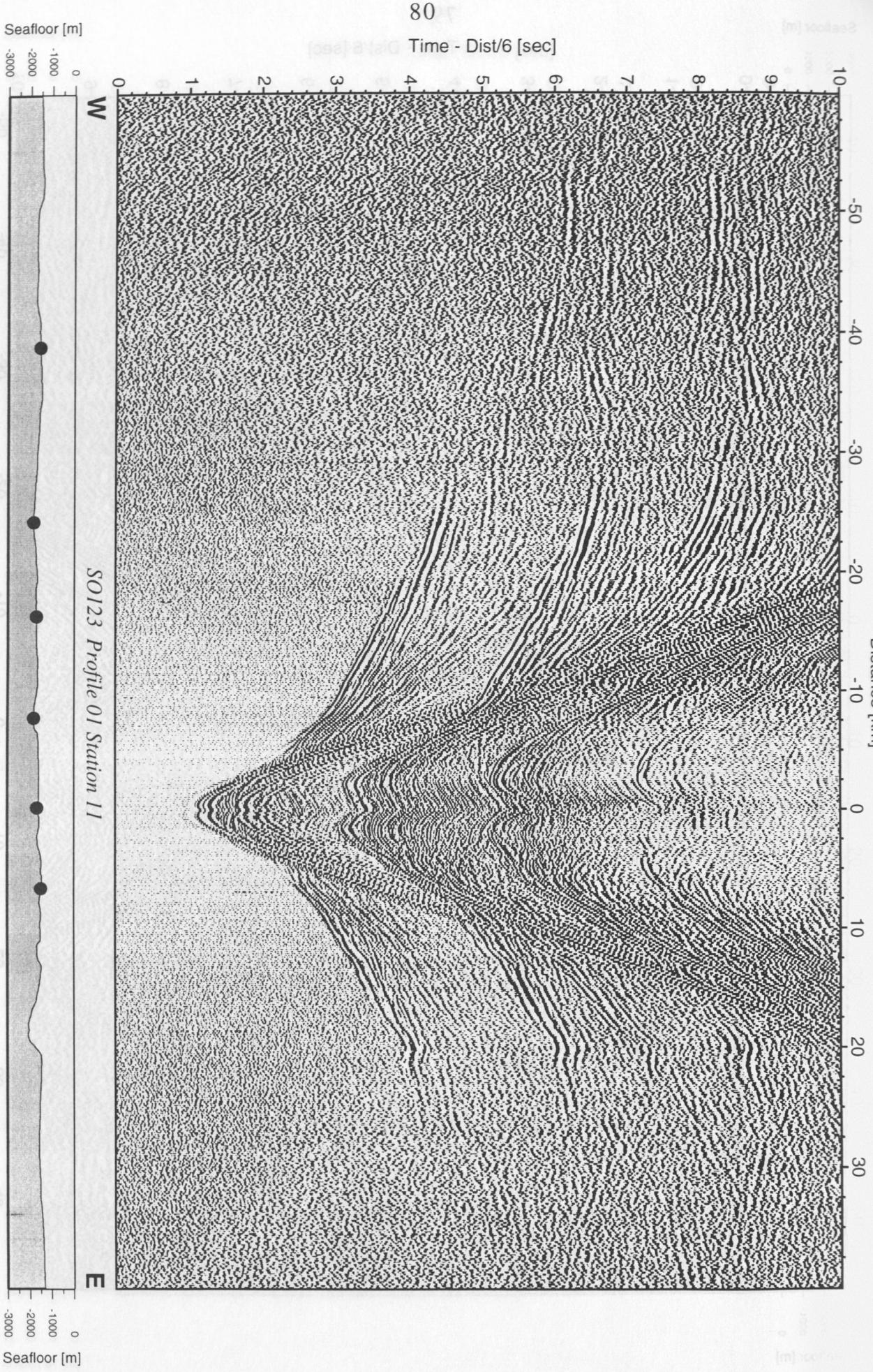

Figure 6.3.4.1.7: Record section from OBH 11, Profile 01.

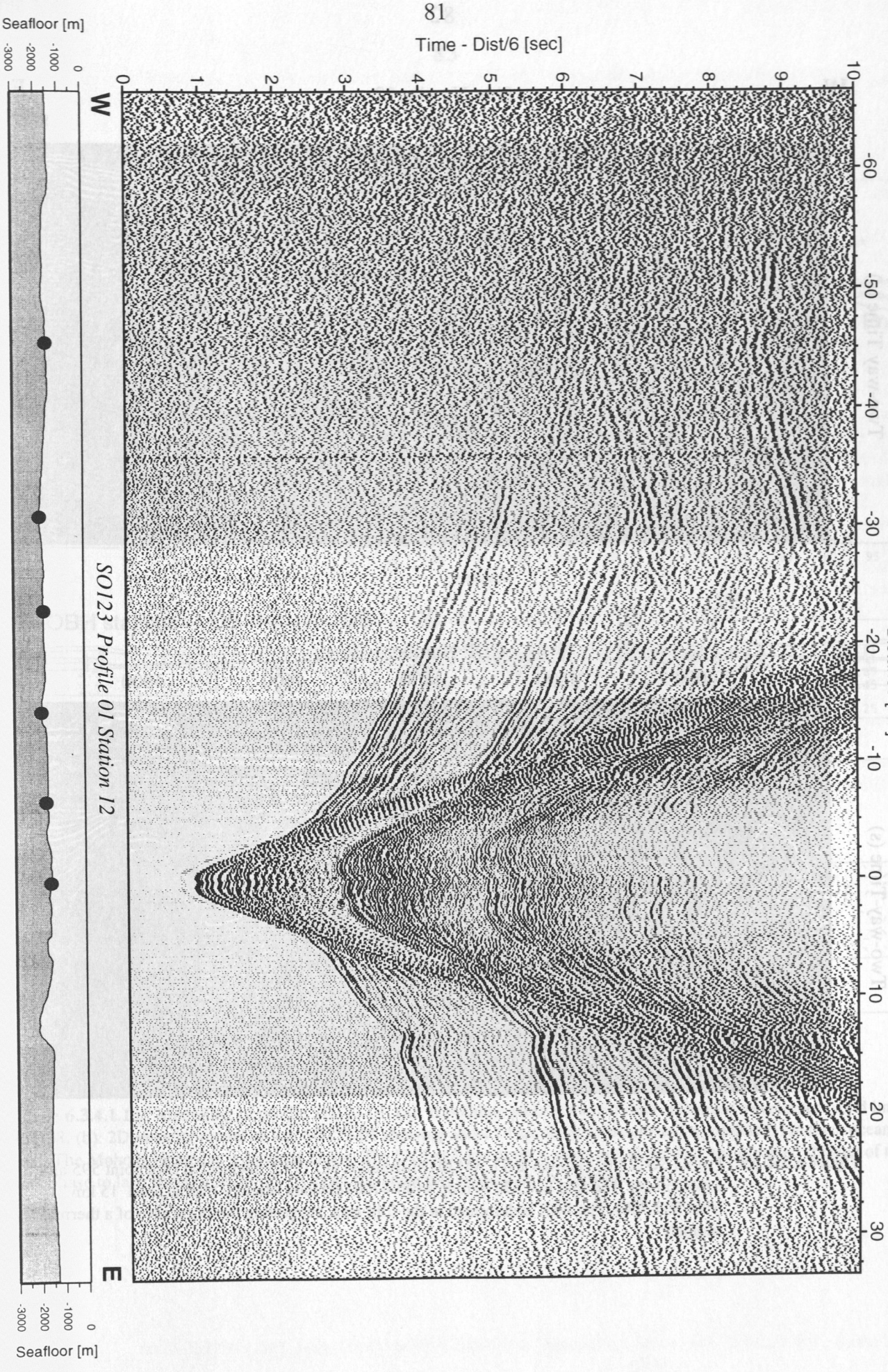

Figure 6.3.4.1.8: Record section from OBH 12, Profile 01.

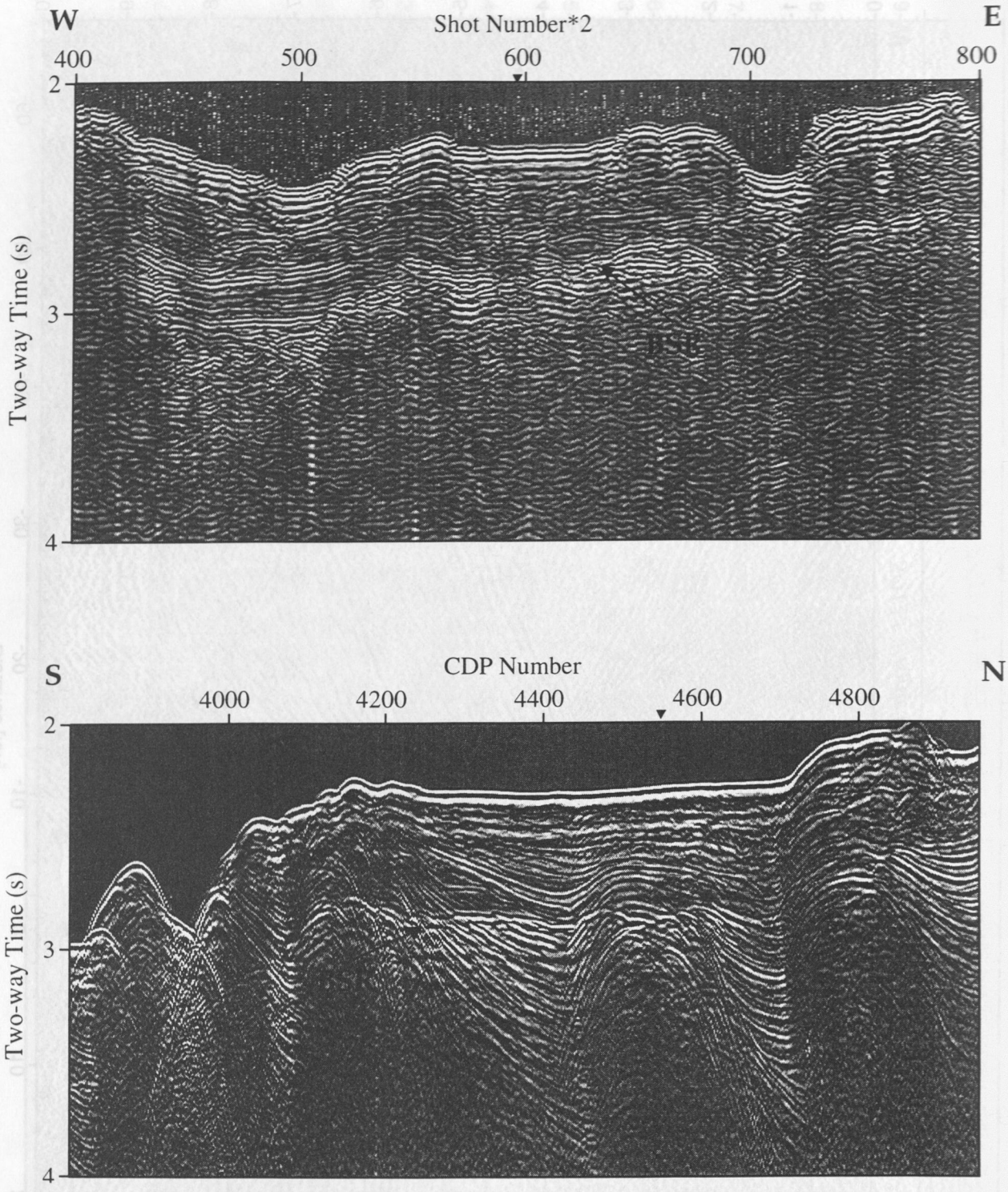

Figure 6.3.4.1.9: Profile SO123-01 (above) and CAM30 (Minshull et al., 1992) intersect at shot point 595 and cdp 4550 (▾). The fold in CAM30 (cdp 4400-4700) extends laterally over at least 15 km (shot 500-700). The BSR is deformed in the fold area, suggesting the occurance of a thermal anomaly.

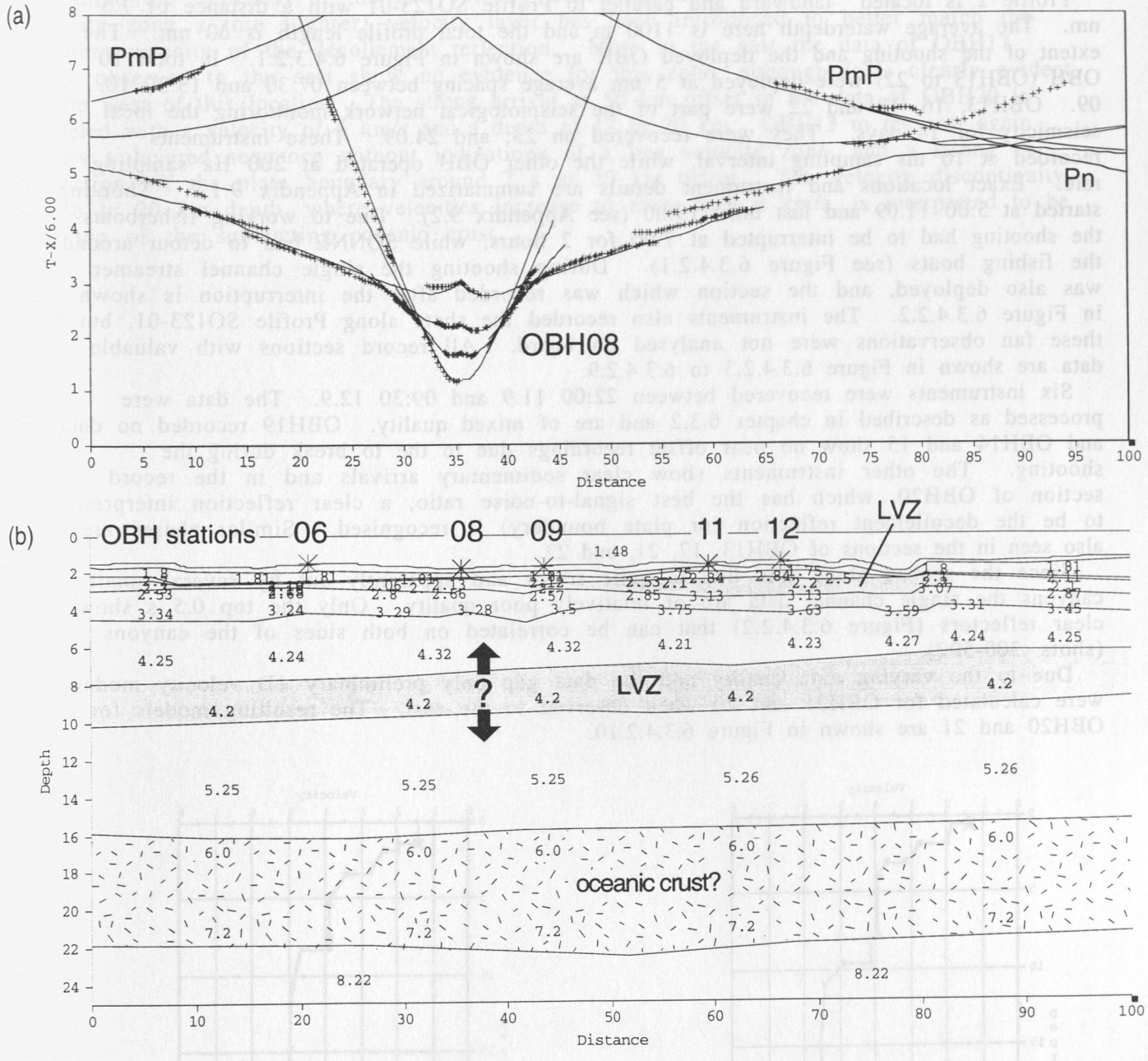

Figure 6.3.4.1.10: Modelling of profile SO123-01. (a): Traveltime picks (crosses) with calculated traveltimes (solid lines) of OBH08. (b): 2D-velocity model of line SO123-01 showing about 14 km thick sediment and a possible 6 km thick oceanic crust. The Moho is located at a depth of 22 km. The LVZ at 8 km depth is supposed to produce the repeated shifting of the 4 km/s phase to later traveltimes in (a). Its exact thickness and position is not yet clear.

6.3.4.2 PROFILE SO123-02

(S. Husen, D. Klaeschen, K. Huhn, E. Flueh)

Profile 2 is located landward and parallel to Profile SO123-01 with a distance of 7.5 nm. The average waterdepth here is 1100 m and the total profile length is 60 nm. The extent of the shooting and the deployed OBH are shown in Figure 6.4.3.2.1. In total 10 OBH (OBH13 to 22) were deployed at 5 nm average spacing between 07:30 and 13:30 10. 09. OBH13, 16, 18 and 22 were part of the seismological network monitoring the local seismicity for 14 days. They were recovered on 23. and 24.09. These instruments recorded at 10 ms sampling interval, while the other OBH operated at 200 Hz sampling rate. Exact locations and instrument details are summarized in Appendix 9.1.2. Shooting started at 5:00 11.09 and last until 19:00 (see Appendix 9.2). Due to working fisherboats the shooting had to be interrupted at 7:00 for 2 hours, while SONNE had to detour around the fishing boats (see Figure 6.3.4.2.1). During shooting the single channel streamer was also deployed, and the section which was recorded after the interruption is shown in Figure 6.3.4.2.2. The instruments also recorded the shots along Profile SO123-01, but these fan observations were not analysed on board. All record sections with valuable data are shown in Figure 6.3.4.2.3 to 6.3.4.2.9.

Six instruments were recovered between 22:00 11.9 and 09:30 12.9. The data were processed as described in chapter 6.3.2 and are of mixed quality. OBH19 recorded no data and OBH14 and 15 show no near offset recordings due to the to break during the shooting. The other instruments show clear sedimentary arrivals and in the record section of OBH20, which has the best signal-to-noise ratio, a clear reflection interpreted to be the decollement reflection (or plate boundary) is recognised. Similar phases are also seen in the sections of OBH13, 17, 21, and 22.

Since the seabed along this line is quite rough and apparently cut by several small canyons the single channel data are of relatively poor quality. Only the top 0.5 s show clear reflectors (Figure 6.3.4.2.2) that can be correlated on both sides of the canyons (shots 300-500).

Due to the varying data quality and the data gap only preliminary 1D velocity models were calculated for OBH21 and 20 when observed to the east. The resulting models for OBH20 and 21 are shown in Figure 6.3.4.2.10.

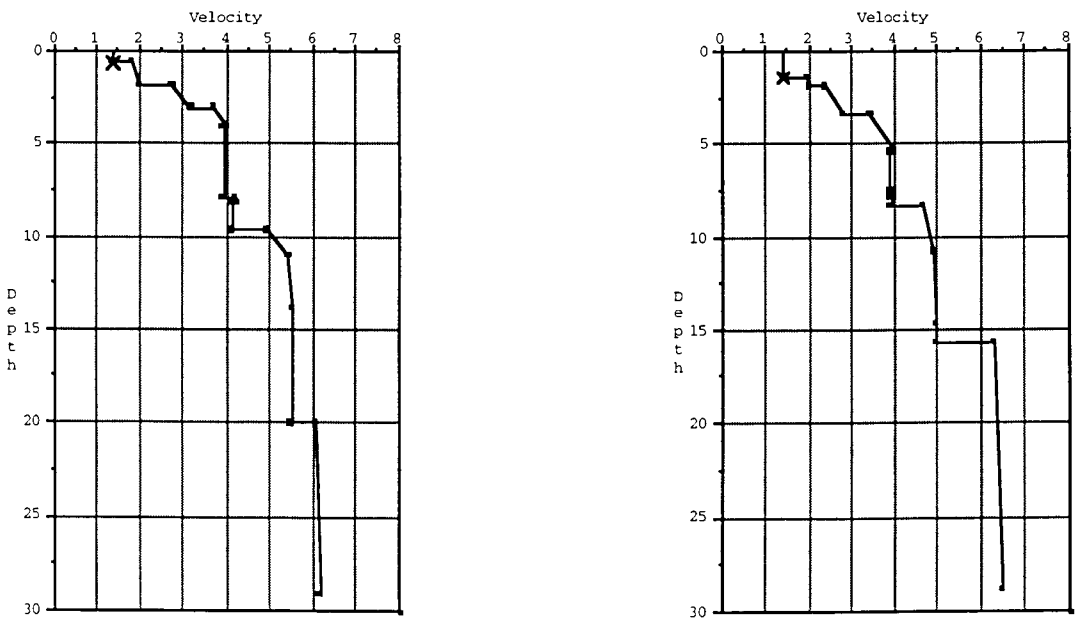

Figure 6.3.4.2.10: 1D velocity model of OBH21-East (left) and for OBH20-East (right).

In the first kilometers of the sections sediment layers with velocities from 1.8 km to 4.0 km can be distinguished. A prominent feature is a low velocity zone modeled at both stations. It starts at a depth of 4 to 5 km. At OBH21 the thickness of this layer is 5 km, decreasing to 3 km at OBH20. However, only later amplitude modelling will enable us to determine the thickness of the low velocity zone with more confidence. Within the low velocity zone a thin high(er) velocity layer has been introduced to better match the apparent velocity of the décollement reflection. More to the east the data of OBH17 when observed to the east show no evidence for this zone, although it is clearly evident to the west of this location. The strong arrival at 50 km offset in the data of OBH20 is modeled with a velocity of 6 km/s and a depth of 17 to 20 km. OBH13 to the east again shows a layered sequence without indications of a low velocity zone, and a strong reflection off the plate boundary around 7 s at 20 km offset. The velocity discontinuity at 16 to 20 km depth, where velocities increase to more than 6 km/s, is interpreted to be the top of the subducting oceanic crust.

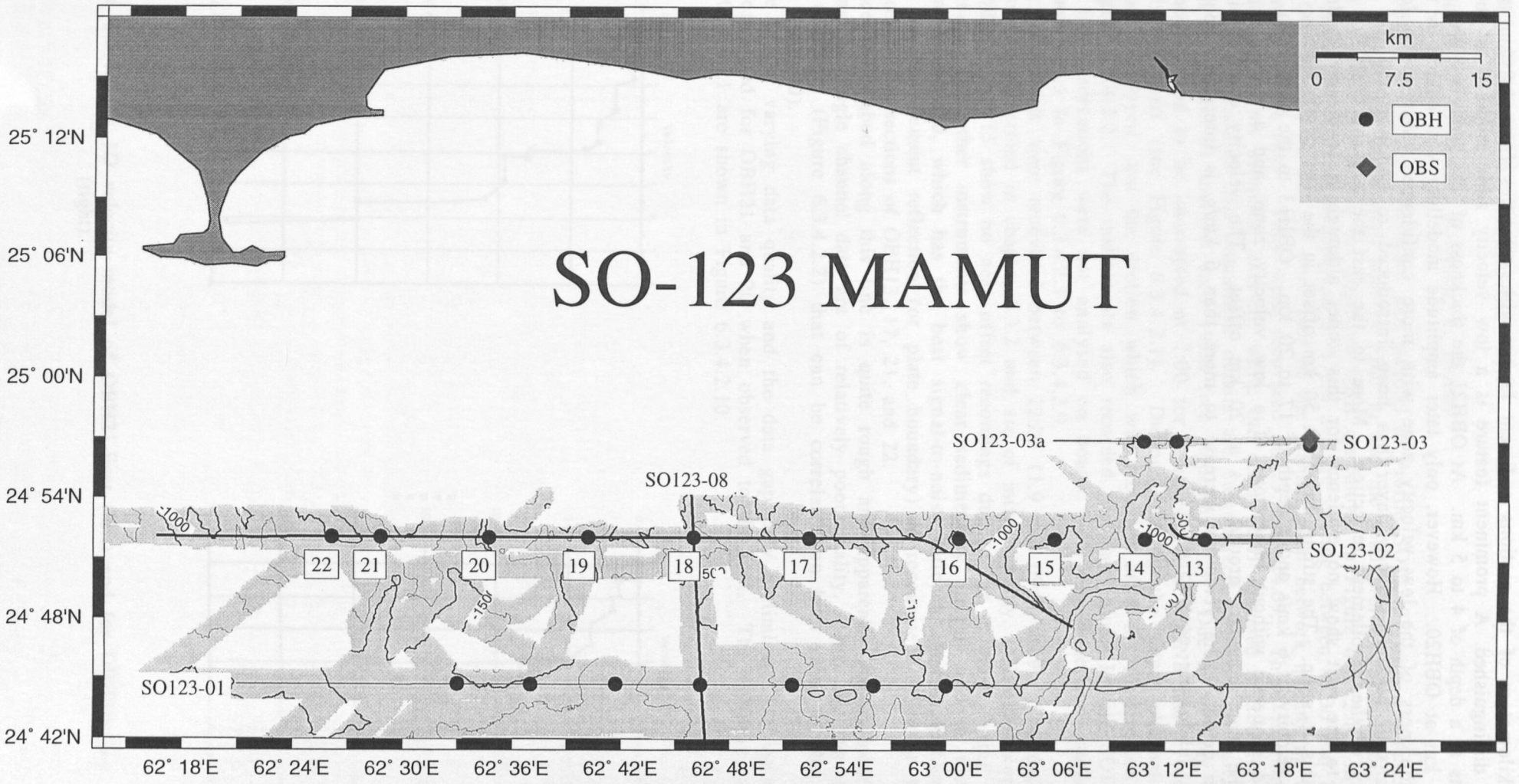

Figure 6.3.4.2.1: Location map of profile SO123-02.

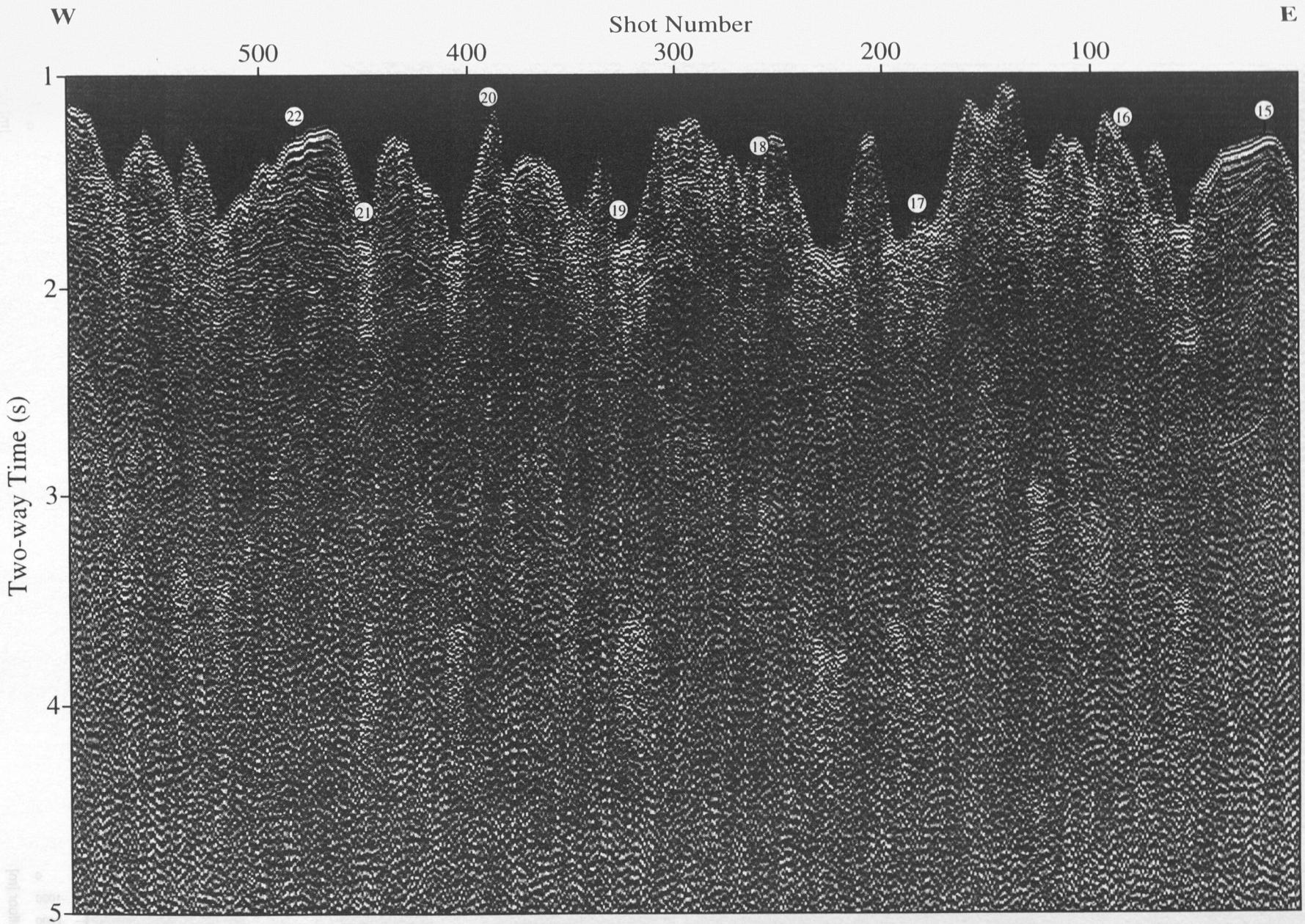

Figure 6.3.4.2.2: Single channel seismic profile SO123-02 (VE=20:1 at the sea-floor). Numbers at the sea-floor mark OBH positions; OBH 15 and OBH 16 projected. Only line segment after interruption is shown.

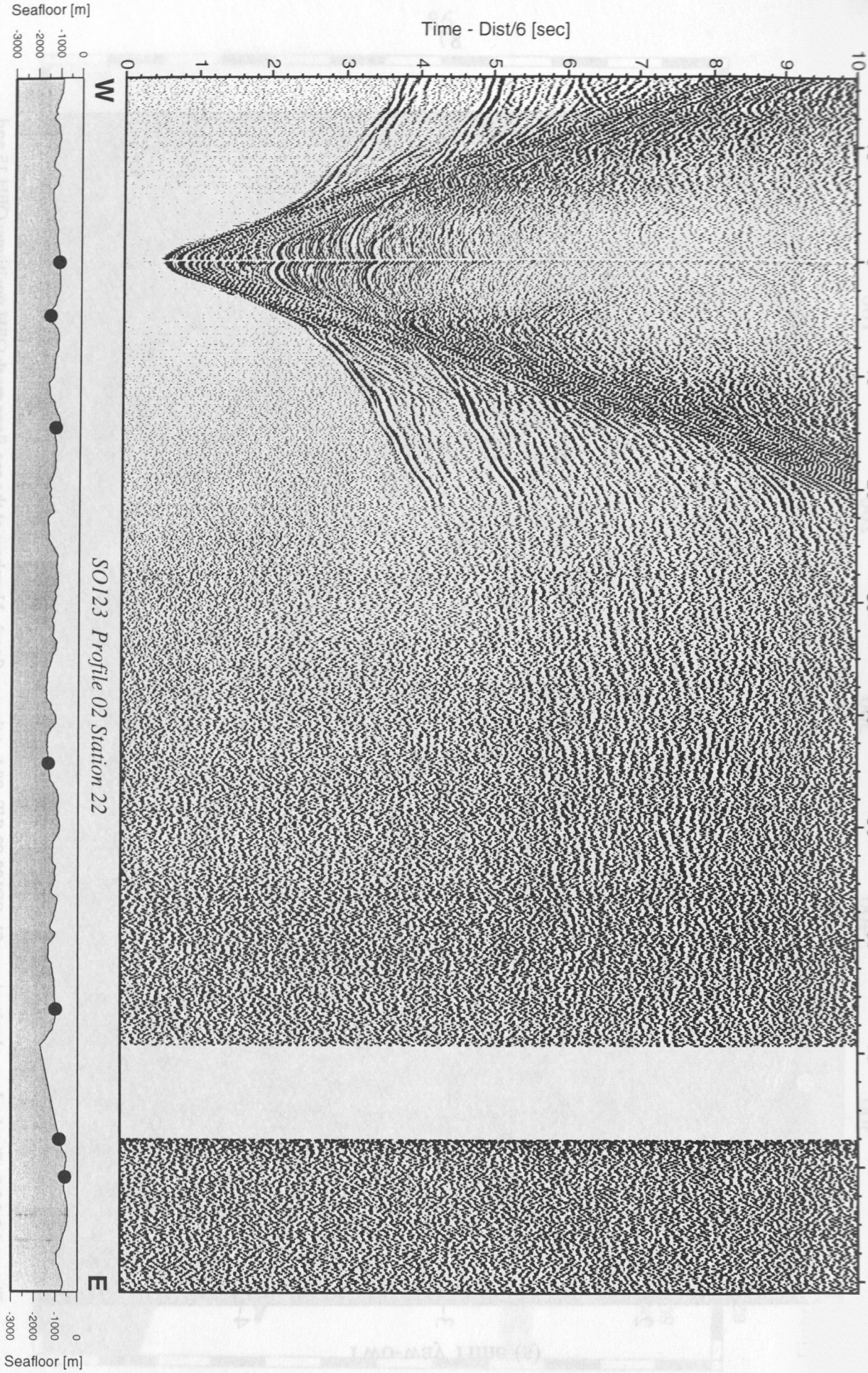

Figure 6.3.4.2.3: Record section from OBH 22, Profile 02.

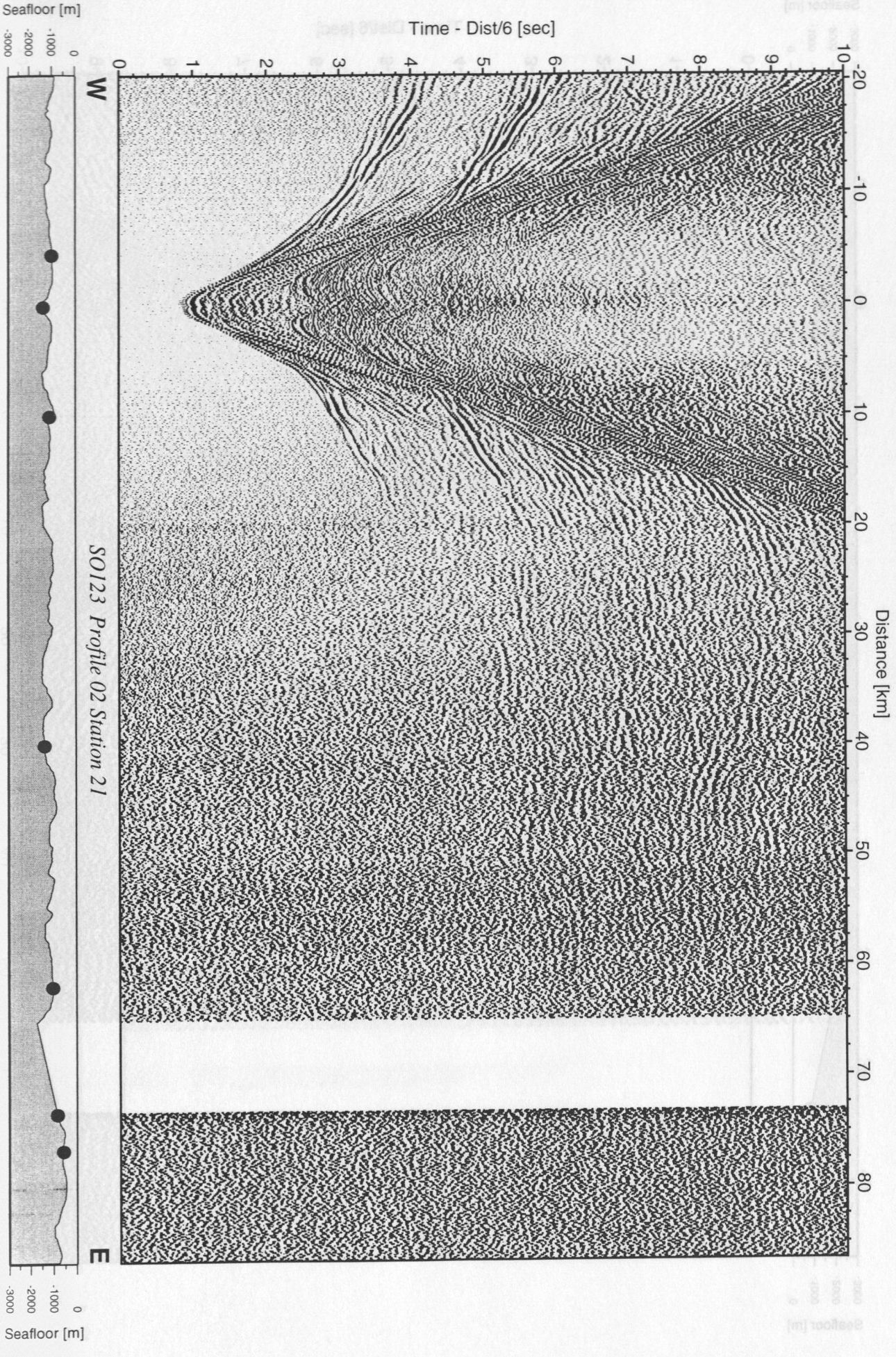

Figure 6.3.4.2.4: Record section from OBH 21, Profile 02.

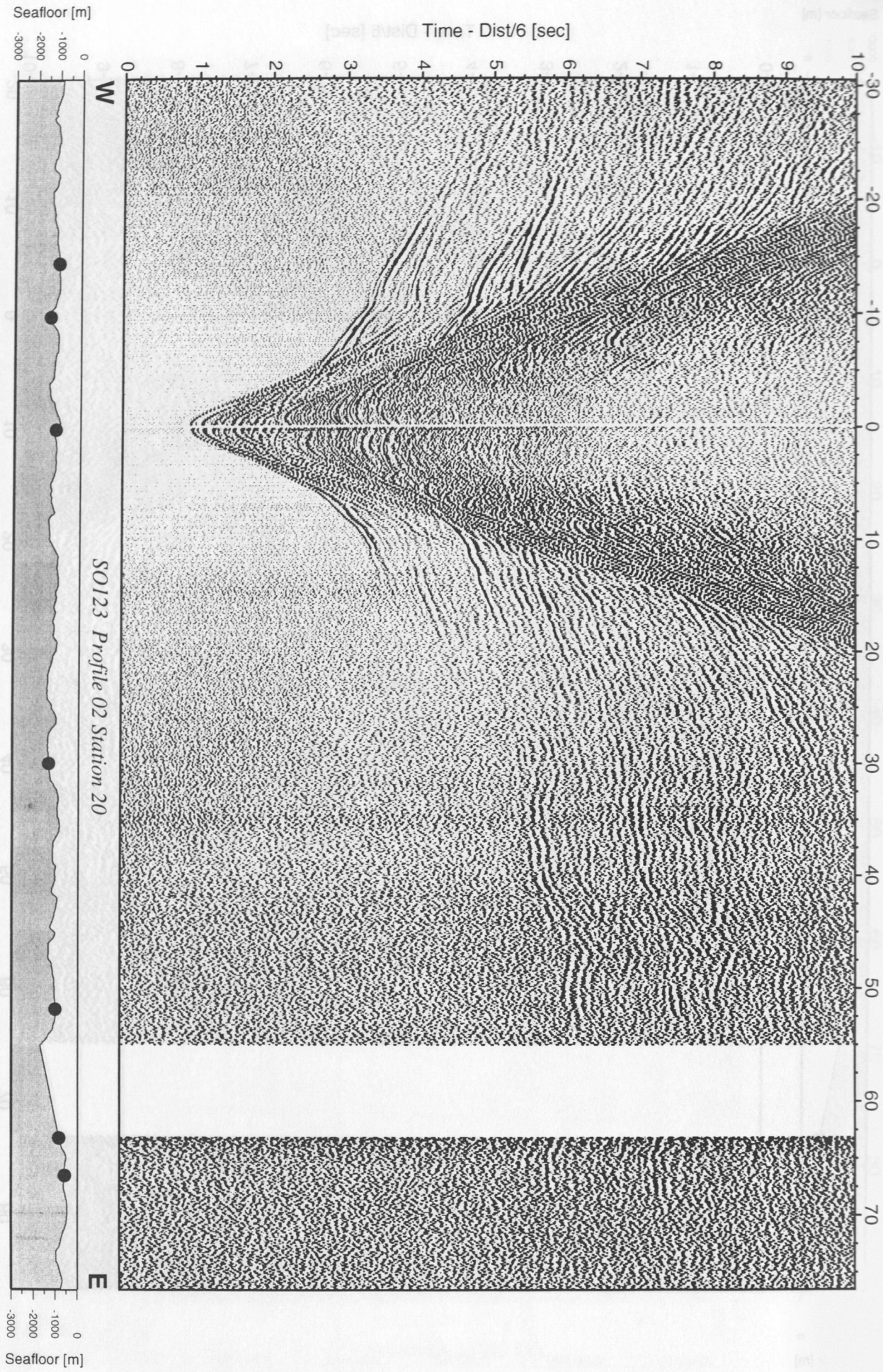

Figure 6.3.4.2.5: Record section from OBH 20, Profile 02.

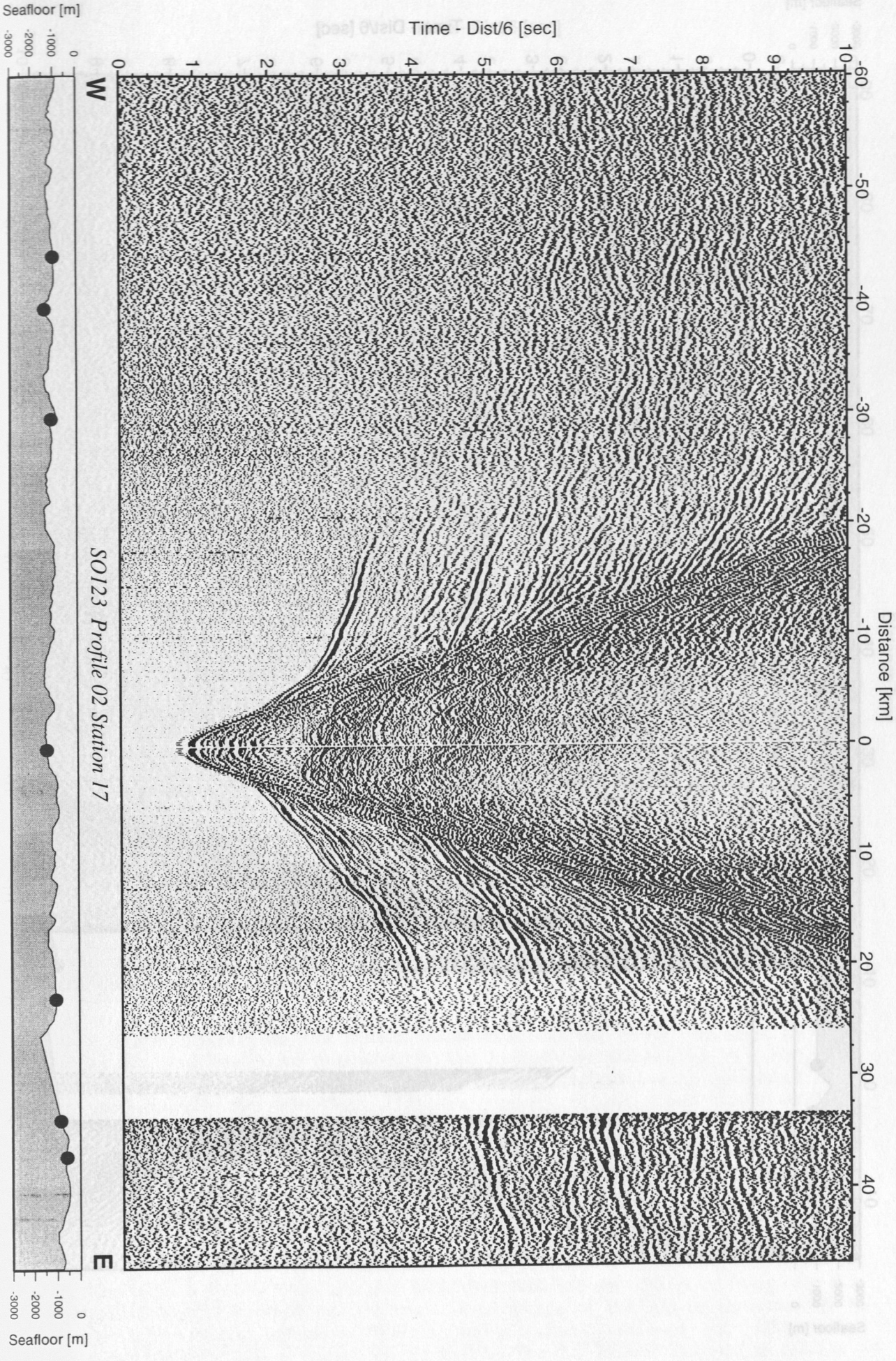

Figure 6.3.4.2.6: Record section from OBH 17, Profile 02.

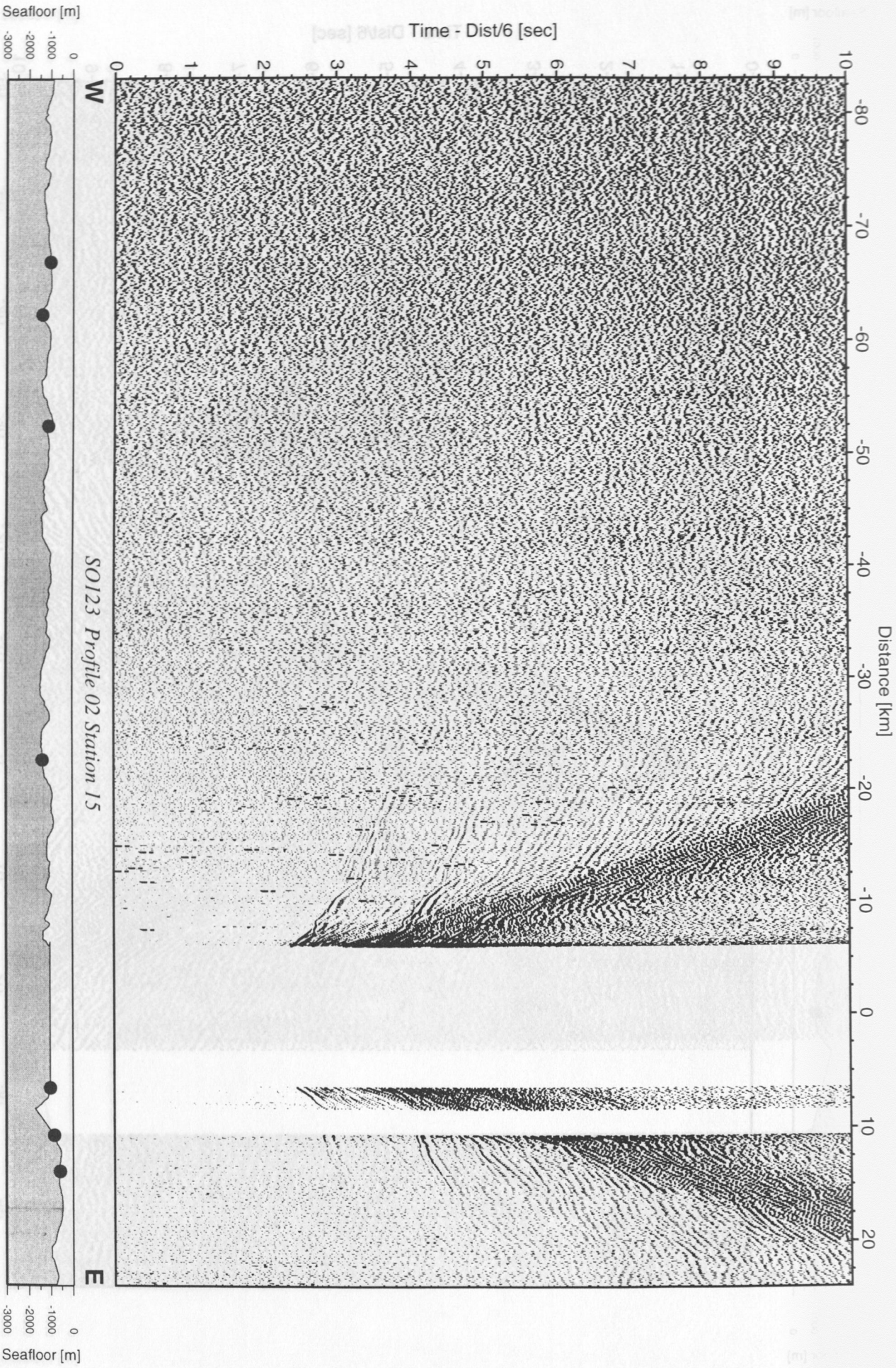

Figure 6.3.4.2.7: Record section from OBH 15, Profile 02.

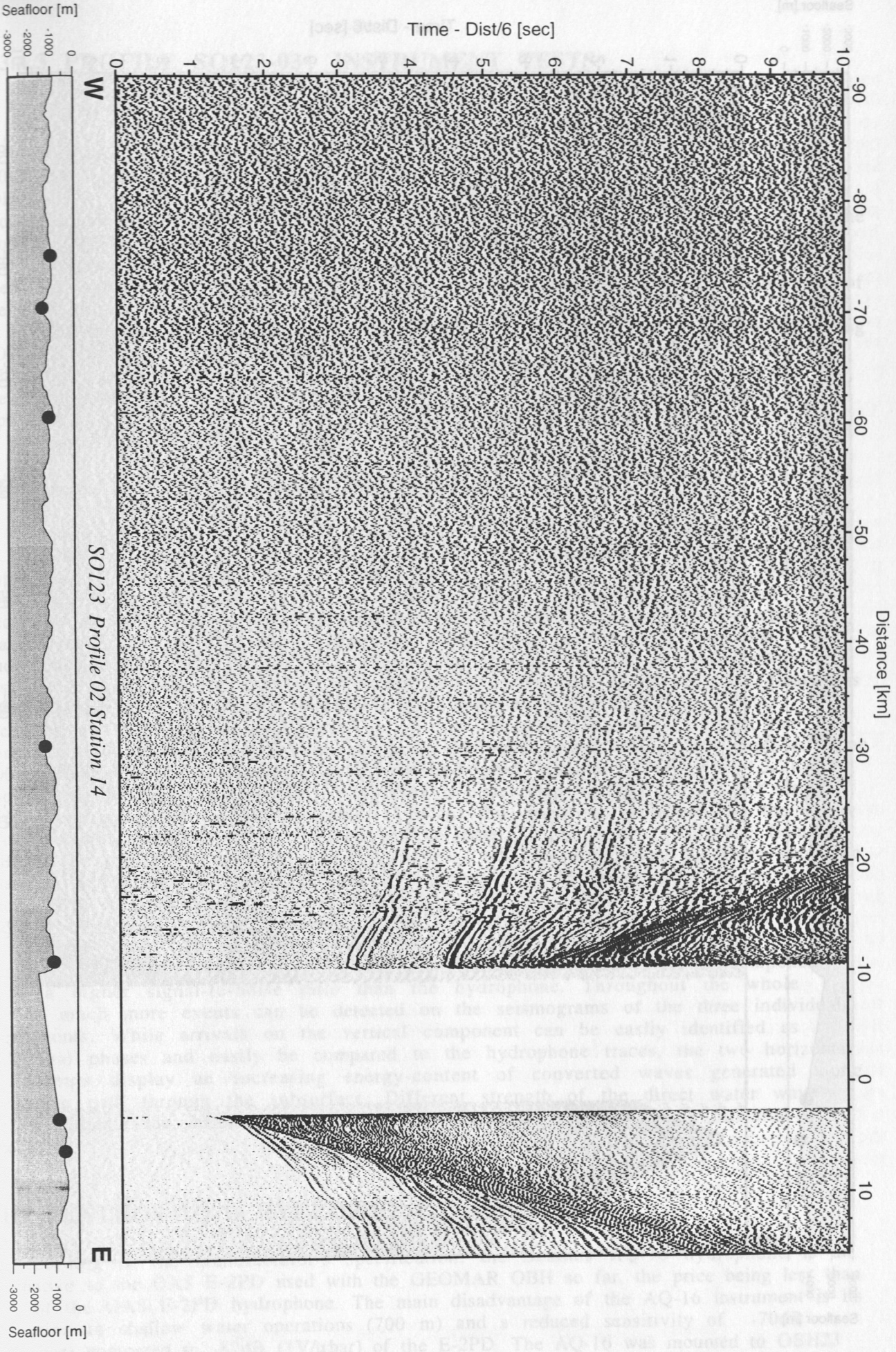

Figure 6.3.4.2.8: Record section from OBH 14, Profile 02.

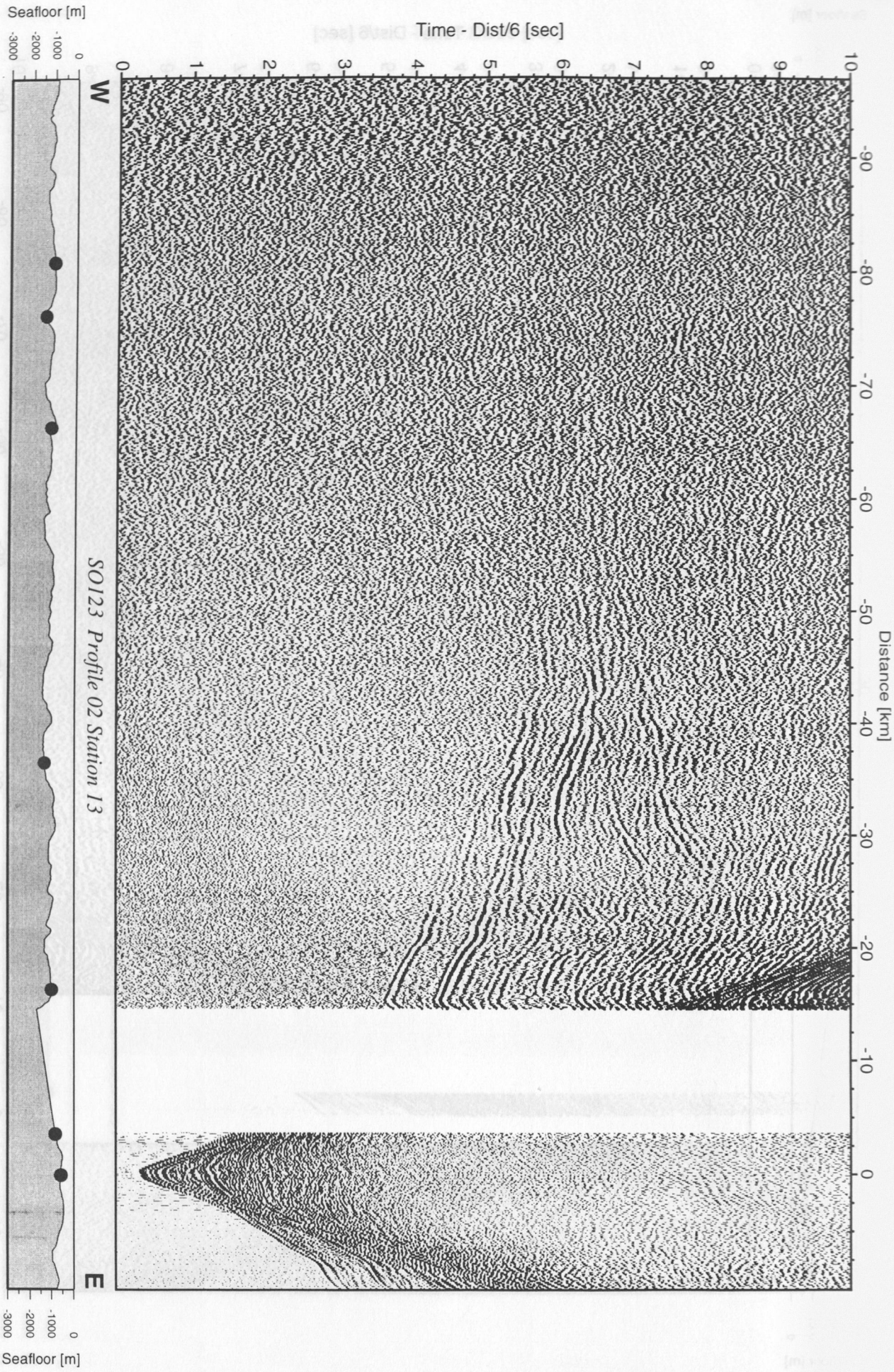

Figure 6.3.4.2.9: Record section from OBH 13, Profile 02.

6.3.4.3 PROFILE SO123-03 INSTRUMENT TESTS

(J. Bialas, E. Flueh)

Profile 3 was shot parallel to the Makran coast (Fig. 6.3.4.3.1) in shallow waters (80-200 m), but crossing two canyons of 800 m depth. This time only four instruments (OBH23, 24, and 25; OBS01) were deployed to do some tests of new equipment which should be compared with the standard GEOMAR OBH (Flueh & Bialas, 1996). First of all the prototype GEOMAR OBS was used for the first time in open waters. OBH23 and 24 carried new hydrophones which can be compared to the long used OAS hydrophone. We also used this opportunity to test the energy and spectral contents of individual subarrays of the BGR airgun array (Chapter 5. 3).

The instruments were deployed between 13:00 and 15:00 12.09., and shooting along SO123-03 from east to west using individual subarrays and from west to east using the full array was completed between 16:00 and 23:00. All instruments were recovered in the morning of 13.09. Details regarding location and instruments can be found in Appendix 9.1.3.

THE OCEAN BOTTOM SEISMOMETER (OBS)

This new instrument is described in detail in chapter 5.2.3. Although the capability of the OBS to float at the sea surface was tested before deployment, a 200 m long rope with a tail floatation was attached to the system on ist maiden trip for safety reasons, since the release had never been tested in deep water. Fortunately this was not necessary and the OBS returned to the surface and on board following the routine manoeuvres of the OBH recovery. However, ascent speed seemed to be slow and buoyancy appeared to be at its limit. Therefore and to account for a minor but possible loss of buoyancy during the first dive into deep waters four additional small floatations were attached to the OBS prior to its next deployment on profile SO123-04. Data recording on SO123-03 was successful on all four channels. To make sure that the construction of the OBS carrier does not cause additional noise, OBH25 was deployed some 100 m beside the OBS. Comparison of both hydrophone channels (Figure 6.3.4.3.2) showed that the signal-to-noise ratio on OBS01 is better than on OBH25. As the test deployment was done in shallow waters (120 m) this might be influenced by the strong water currents measured at the surface with a speed of one knot causing the floating OBH to be unstable. A much higher noise level was encountered on the three geophone channels which were probably influenced by wave induced noise and may have additionally suffered from the saftey line. It is also well known that geophone recordings in shallow water generally suffer from a high noise level (see also Flueh and Fisher, 1996). Better results were obtained on the following deep water deployments on SO123-04 (Fig. 6.3.4.3.3). Here, recordings of the vertical component show a higher signal-to-noise ratio than the hydrophone. Throughout the whole section much more events can be detected on the seismograms of the three individual components. While arrivals on the vertical component can be easliy identified as individual phases and easily be compared to the hydrophone traces, the two horizontal components display an increasing energy-content of converted waves generated along the wave path through the subsurface. Different strength of the direct water wave arrival indicate the orientation of the three components relative to the direction of shooting.

THE BENTHOS AQ-16 HYDROPHONE

According to the manufacturer`s specification, the Benthos AQ-16 hydrophone is an alternative to the OAS E-2PD used with the GEOMAR OBH so far, the price being less than 50% of the OAS E-2PD hydrophone. The main disadvantage of the AQ-16 instrument is its restriction to shallow water operations (700 m) and a reduced sensitivity of -70dB (1V/µbar) compared to -82dB (1V/µbar) of the E-2PD. The AQ-16 was mounted to OBH23

together with an E-2PD hydrophone. Signals from both were recorded with the same amplification on two different channels. The two record sections (Fig. 6.3.4.3.4) are displayed using a moderate filter (3 - 30 Hz). It is obvious from this Figure that the AQ-16 produces a better section than E-2PD. Randomly distributed large amplitude noise bursts of about 1 sec are evident on the E-2PD section, but missing on the AQ-16 section, although the two instruments were only about 15 cm apart. Unfortunately the channel recording the E-2PD hydrophone is deteriated by mono frequent noise that probably is generated within the recording electronics. This has been effectively cancelled by the frequency filter applied. Nevertheless it must be stated that the amplitudes of the seimsic events appear stronger in the AQ-16 section. In the range of near vertical incidence the direct water wave is less clipped than on the E-2PD recordings, which is expected because of the reduced sensitivity. This evaluates the Benthos AQ-16 as an possible alternate for shallow water deployment. The source for the noise on the E-2PD needs to be further examined.

THE ITI-BC6 HYDROPHONE

On OBH24 another type of hydrophone could be tested. It is a type BC-6 hydrophone from Innovative Transducer Inc. which has a sensitivity of -140 dB(1V/ubar) compared to -82 dB (1V/ubar) for the E-2PD hydrophone. Again the E-2PD recorded much more noise than the test candidate (Fig. 6.3.4.3.5). This time the noise appears to vary with time in amplitude as it is known from a lot of sections from previous cruises. Until now, it has been explained with ship noise. The ITI hydrophone does not show such a noise level and no time variation. Therefore first arrival events can be traced much better. Near vertical reflections can be identified more easily even at larger travel times. Due to the fact that in both hydrophone comparisons the OAS hydrophone showed a higher noise level than the test candidates more test deployments with two OAS hydrophones mounted in different ways were made during later deployments.

TEST SHOTS OF THE AIRGUN ARRAY

We also took the opportunity of the test line to check out various airgun configurations and determine signal strength and required amplification for the geophone of the OBS for later deployments. On the first run of line 3 only one string with 10 guns was used and following every forth shot a different set of guns was choosen. In Fig. 6.3.4.3.6 a short part of these tests with two (top), five (middle) and ten guns (bottom) is displayed together with the corresponding frequency spectra which is restricted to 50 Hz due to the aliasing filter of the OBH recorder. All spectra display a first maxima at 7 - 9 Hz which increases in energy with the volume of the gun. An additional overall maxima of the sections can be identified at higher frequencies again depending on the total volume of the guns. As expected the smalles energy was released from the two small airguns. Their maximum energy is concentrated at 20 Hz. With the five guns enough energy was released to identify the first arrival at 3.0 seconds. The main frequency is found at about 15 Hz due to the larger volume of the array. The strongest signals are observed when using all 10 guns. The 8 Hz maxima carries more energy than on the previous trials. The second maxima is found at 15 Hz again but with a broader spread than the five guns. This indicates that in the case of larger defects on the gun strings a suitable signal could still be achieved with a remaining smaller number of guns.

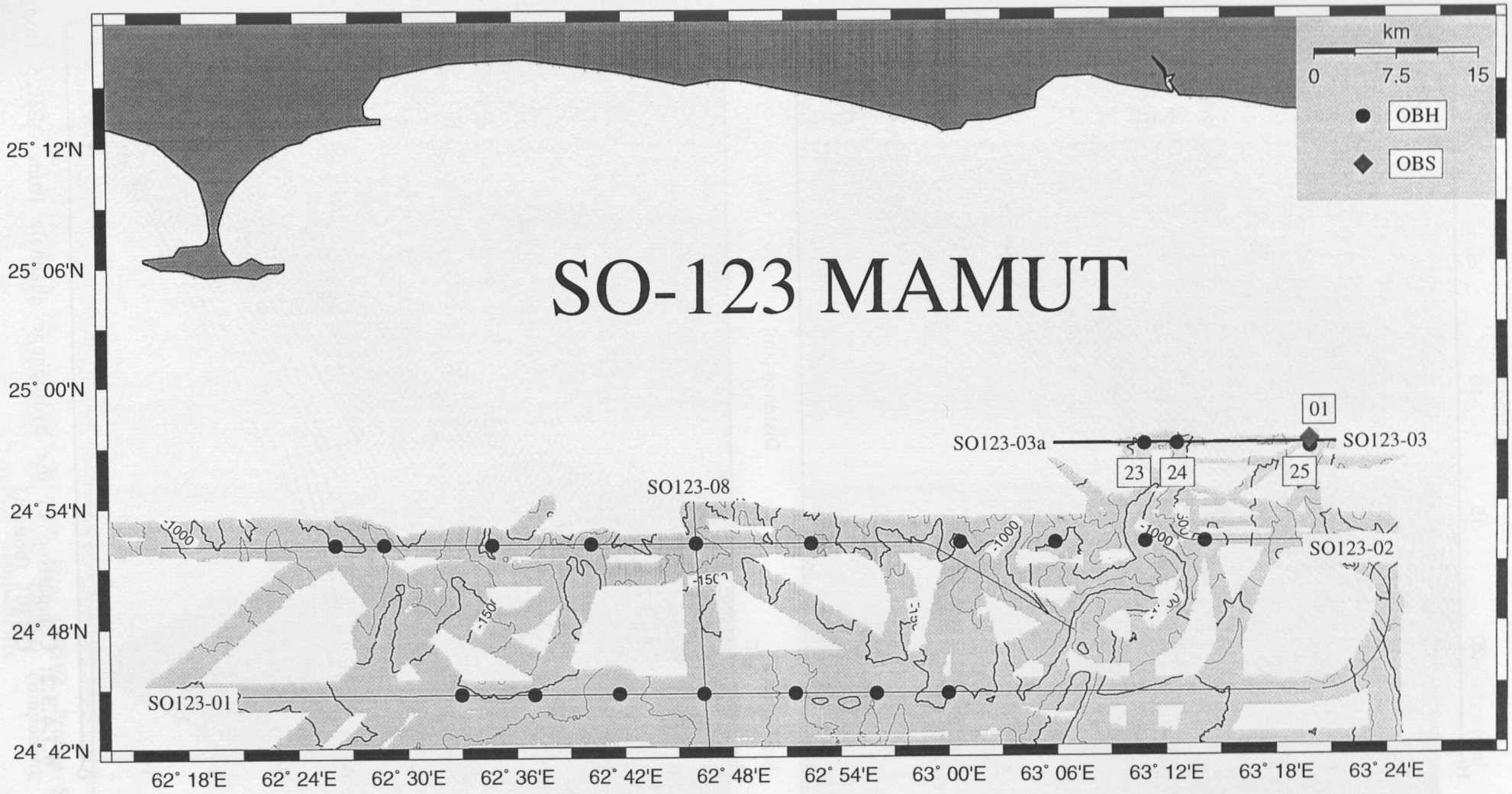

Figure 6.3.4.3.1: Location map of profile SO123-03 / SO123-03a.

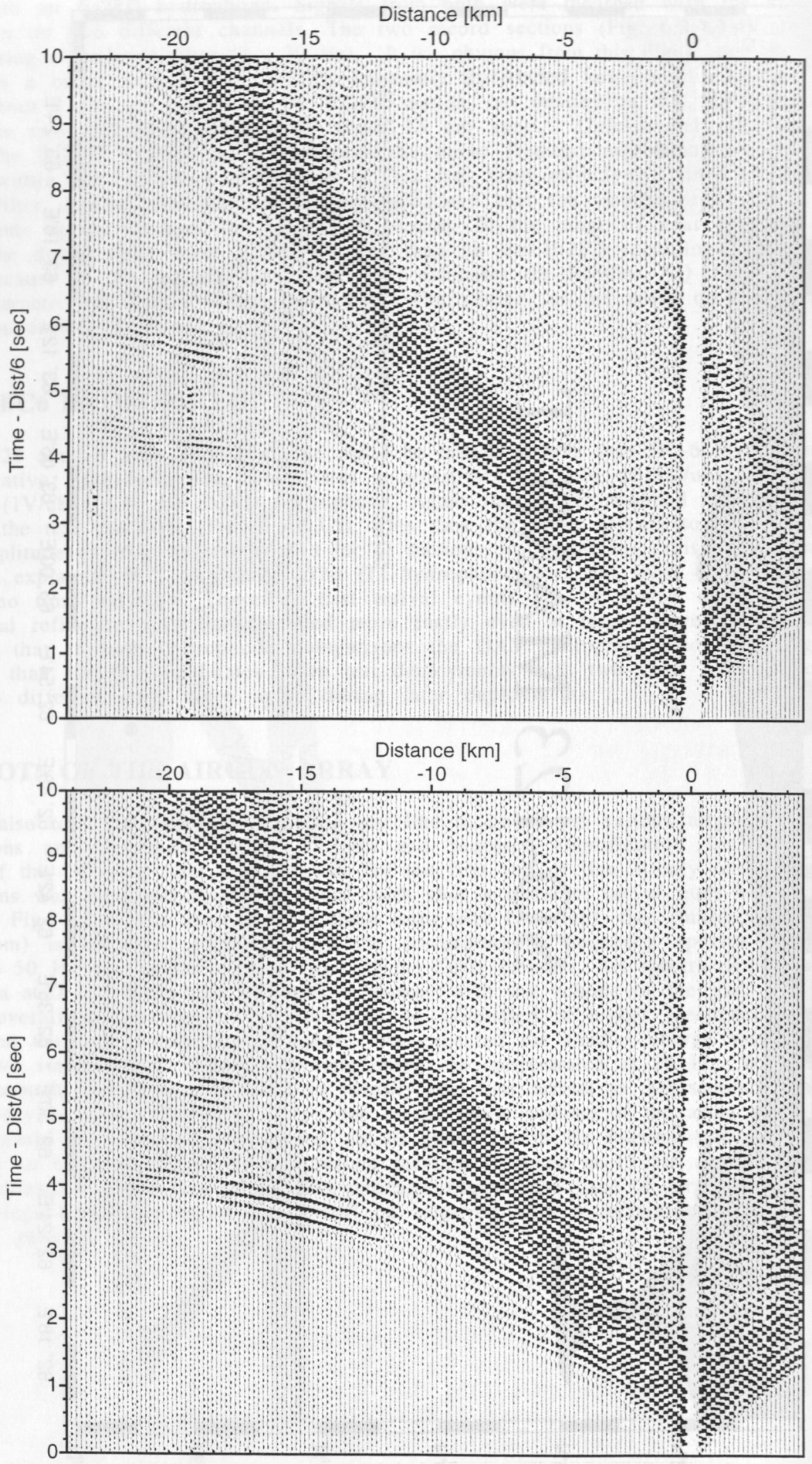

Figure 6.3.4.3.2: Comparison of the hydrophone channels from OBH25 (top) and OBS01 (bottom).

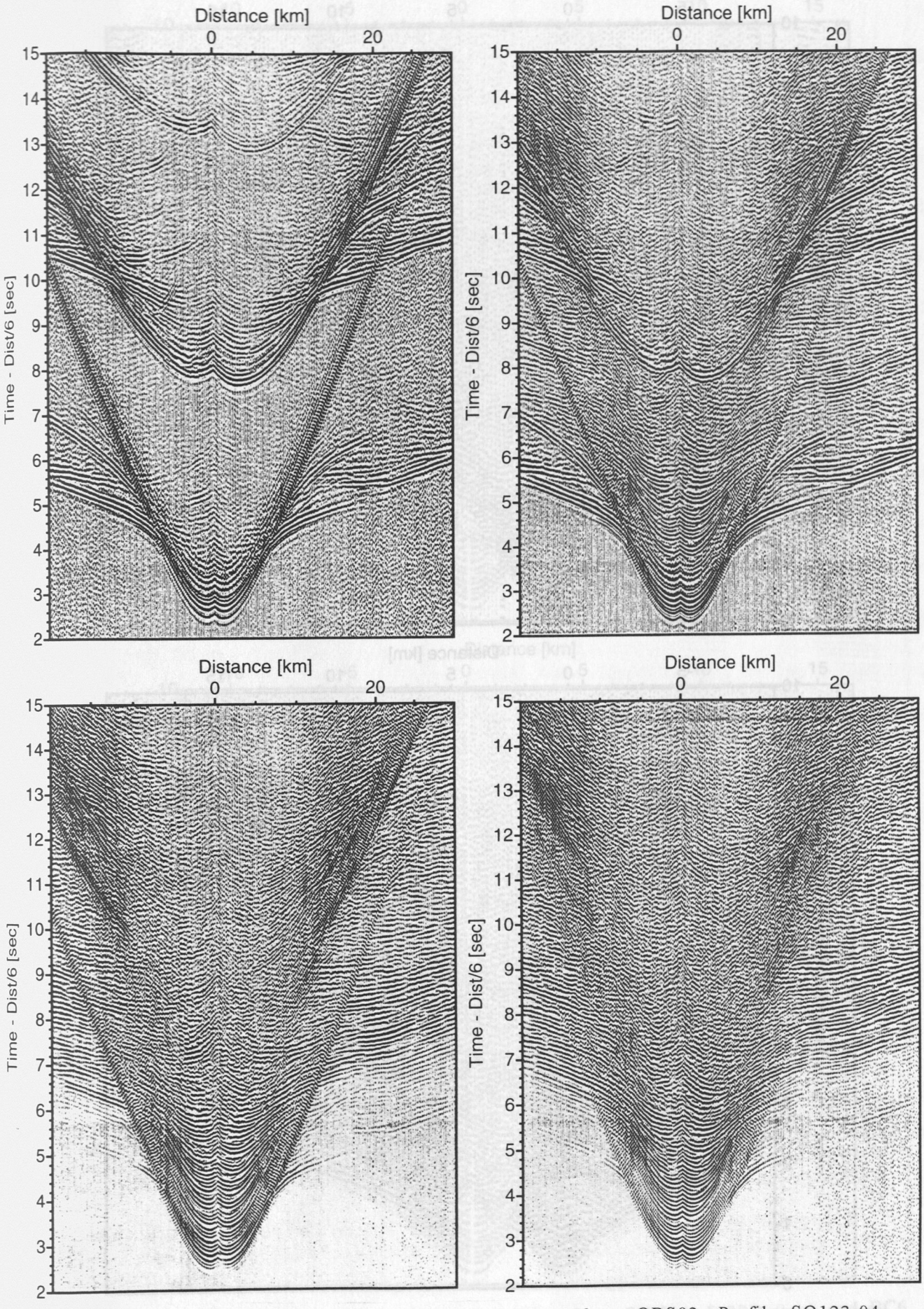

Figure 6.3.4.3.3: Enlargement of record sections from OBS02, Profile SO123-04. top left: hydrophone; top right: vertical component; lower left and lower right: horizontal components.

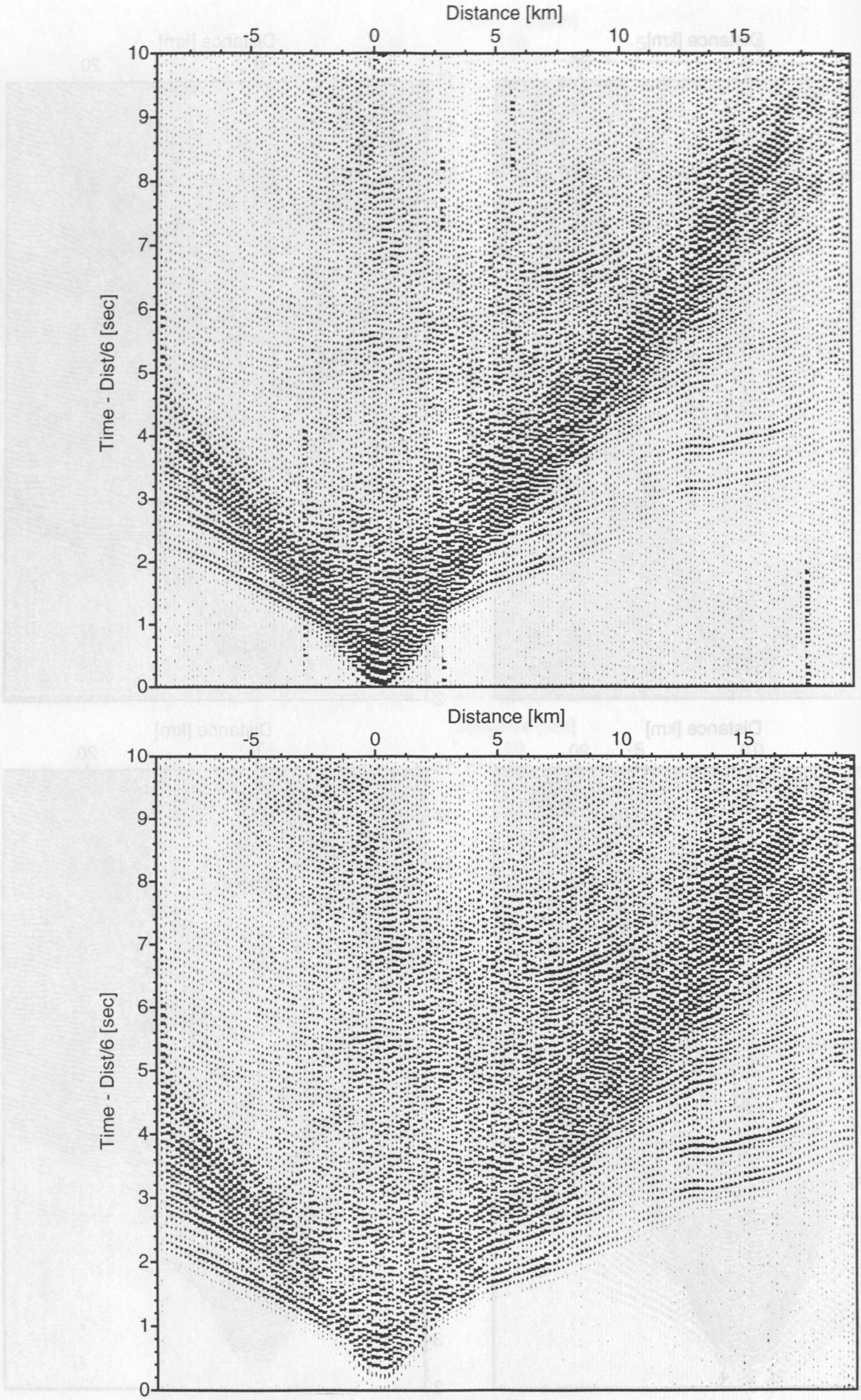

Figure 6.3.4.3.4: Comparison of record sections from OBH23: E-2PD (top) and AQ-16 hydrophone (bottom).

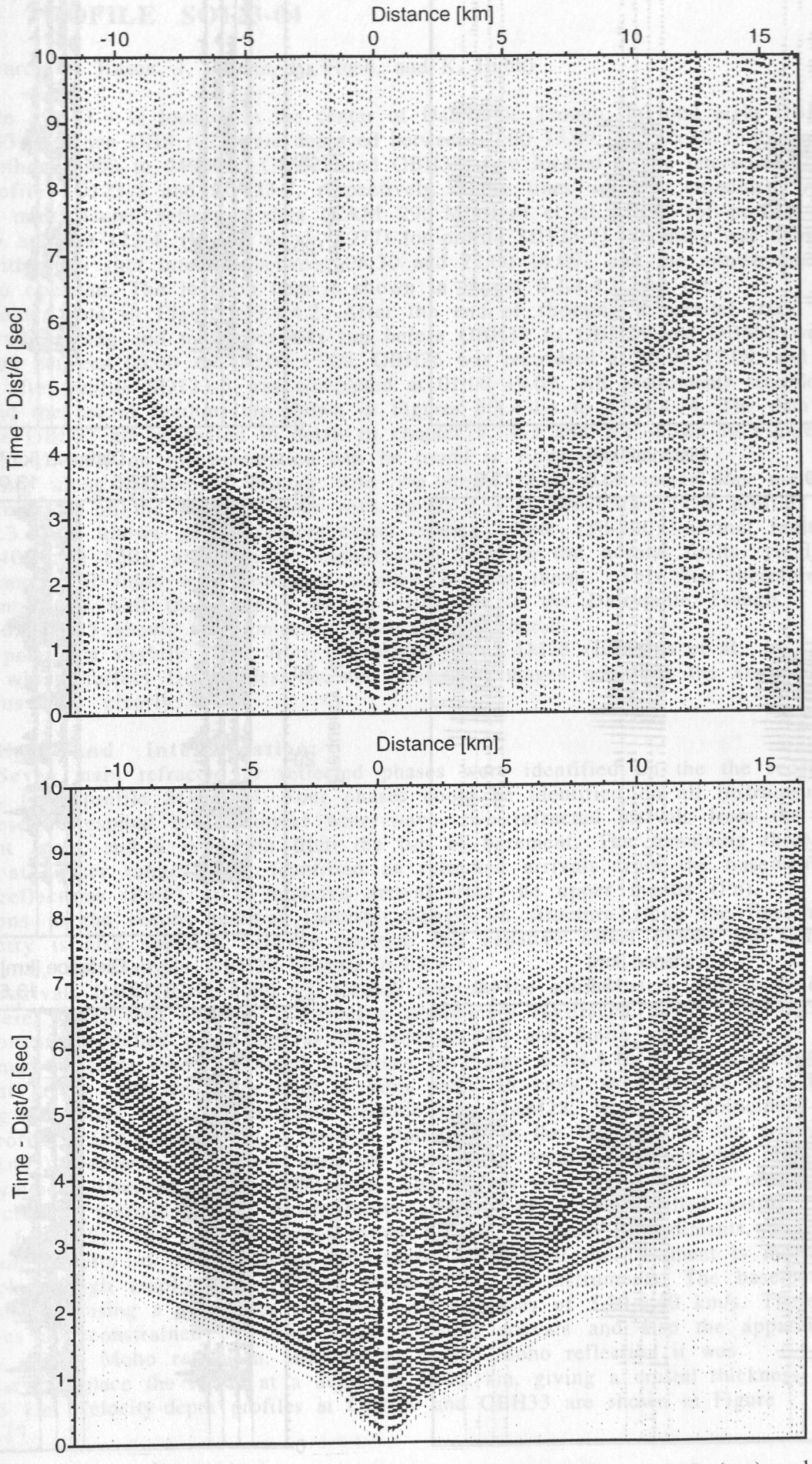

Figure 6.3.4.3.5: Comparison of record sections from OBH24: E-2PD (top) and BC6 hydrophone (bottom).

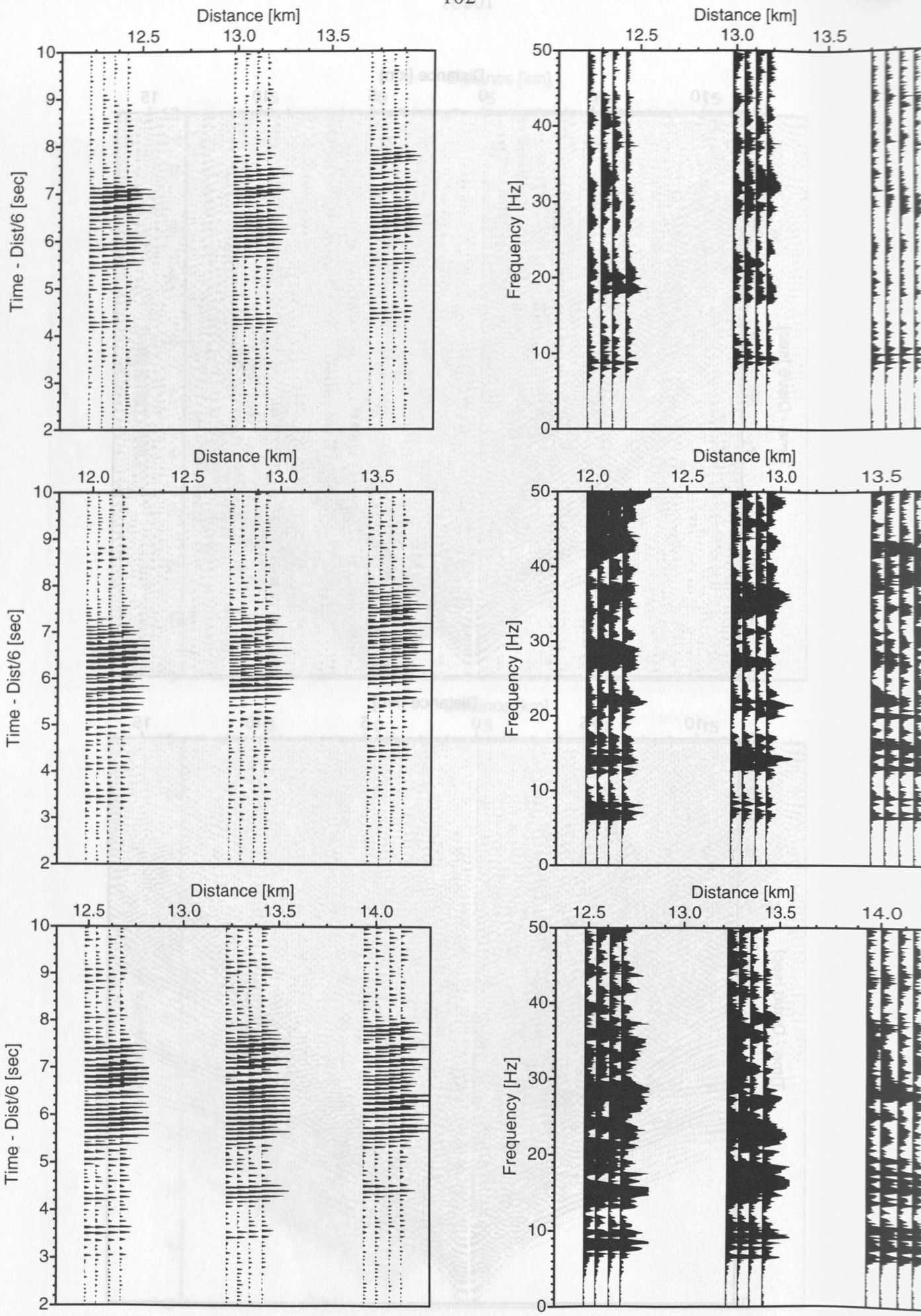

Figure 6.3.4.3.6: Comparison of selected airguns, BC6 hydrophone of OBH24: top: 2 guns; middle: 5 guns; bottom: 10 guns; corresponding frequency spectra to the right.

6.3.4.4 PROFILE SO123-04

(R. Edwards, S. Husen, J. Fruehn, E. Flueh, and K. Huhn)

Profile SO123-4 is located in the center of Dalrymple Trough. In total eight OBH (26 to 33) and one OBS (02) were deployed between 22:00 15.09. and 03:30 16.09. in waterdepth of 4000 to 4400 m. OBH27 and OBH33 were located at the intersections with profile SO123-5 and SO123-7, respectively. Those lines are also coincident with existing multichannel reflection data (CAM 29; Minshull et al., 1992 for profile SO123-5 and SO 122-4, (Roeser et al., 1977) for profile SO123-7). Shooting was done at 5 kn with 60 s shot intervall between 06:30 and 22:00 16.09., and the ministreamer was also operated. The location map is shown in Figure 6.3.4.4.1 and the ministreamer data in Figure 6.3.4.4.2. After the end of shooting a parallel track with swathmapping and magnetics was run before OBH33 to OBH28 and OBS02 were picked up between 05:00 and 12:00 17.09. OBH26 was recovered at 18:00 17.09. and OBH27 after profile SO123-5 was completed at 01:00 19.09. All instruments recorded well, and the record sections are shown in Figures 6.3.4.4.3 to 6.3.4.4.14. The data from the OBS02 are discussed in detail in chapter 6.3.4.3 and are shown in Figure 6.3.4.3.3. Details on instrumentation can be found in Appendix 9.1.4.

Imaging along Dalrymple Trough with the single channel streamer was more successful than on the previous lines with up to 2 s of penetration. The profile (Fig. 6.3.4.4.2) shows gentle compressional folding (shots 150-300), normal faulting (shots 400 and 850), and stronger compression between the normal faults, yielding two symmetrical folds with sediments ponded between them. This line therefore documents very well the complex tectonic situation in the Dalrymple Trough. Figure 6.3.4.4.15 shows the symmetric folds in more detail.

The profile is slightly offset from Cambridge line CAM28 (Edwards et al., in prep.), which suffers from sideswipe and therefore images some of the shallower structures less clearly.

Modelling and interpretation:

Seven main refracted or reflected phases were identified on the the record sections from profile SO123-04. Four phases could be identified on all instruments and these correspond to the direct water-wave, two refracted arrivals from the sediment layer, and a reflection from the top of basement. The remaining three phases at longer ranges were identified as refracted arrivals from the basement, Moho reflections (PmP) or a refracted arrival from the upper mantle (Pn). Variations in the record sections indicate changes in structure along the line, and asymmetry is also apparent between positive and negative offset phases for some instruments, for example OBH29 (Figure 6.3.4.4.7).

Arrivals from OBH29 and 33, located towards the southwestern end of the line, were picked and used to construct a preliminary ray-traced model. The data were forward modelled using the rayinvr code of Zelt and Smith (1992). The preliminary velocity model obtained is shown in Figure 6.3.4.4.16. The upper two sediment layers, with velocities of 1.75 km/s and 2.15 km/s, were derived from the stacking velocities from multichannel seismic line CAM28, which is coincident with profile 4 (Edwards et al., in prep.). Variations in the thickness of the second (2.15 km/s) sediment layer were used to account for localised topographic effects and asymmetry oberved on the OBH data. This agrees very well with the coincident single channel seismic profile which shows a series of sediment filled basins (Figure 6.3.4.4.2). The velocity model shows 5-7 km thickness of sediments, the maximum velocity of which reaches 4.90 km/s. The top of the basement is marked by a clear, high amplitude, reflection observed on all instruments. The basement was modelled using a two layer structure with velocities of 5.20-6.40 km/s. These velocities are constrained by some weak refracted arrivals and also the apparent velocity of the Moho reflection. In order to fit the Moho reflection it was neccessary to place the Moho at a depth of 20-22 km, giving a crustal thickness of 9.5-10.5 km. Velocity-depth profiles at OBH29 and OBH33 are shown in Figure 6.3.4.4.17.

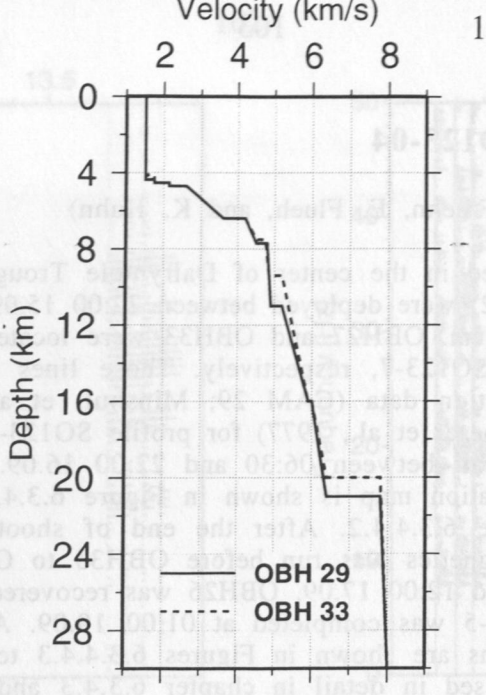

Figure 6.3.4.4.16: Preliminary velocity model along profile 4 based on ray-tracing arrivals from OBH29 and 33. Near surface structure at the northeast end of the profile has not been modelled. Layer velocities are shown in km/s.

From the preliminary ray-tracing it would appear that the Murray Ridge and Dalrymple Trough are not underlain by typical oceanic crust. The crust modelled is too thick to be normal oceanic crust and velocities indicative of oceanic layer 3 are absent. This absence of layer 3 velocities (6.6-7.2 km/s) is often considered a useful criteria to distinguish between oceanic crust and thinned continental crust. However, from the limited modelling preformed so far it is not possible to confidently identify the true nature of the crust. Although the Dalrymple Trough is currently experiencing extension it does not appear that the crust has been significantly thinned beneath the trough.

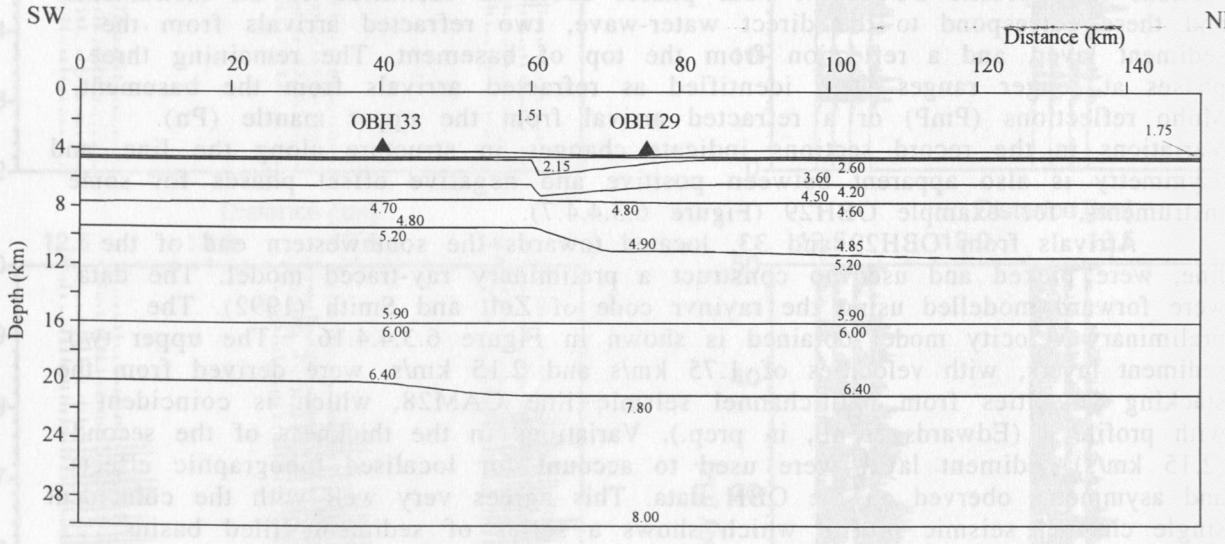

Figure 6.3.4.4.17: Velocity-depth profiles beneath OBH29 (solid line) and OBH33 (dashed line) along profile 4.

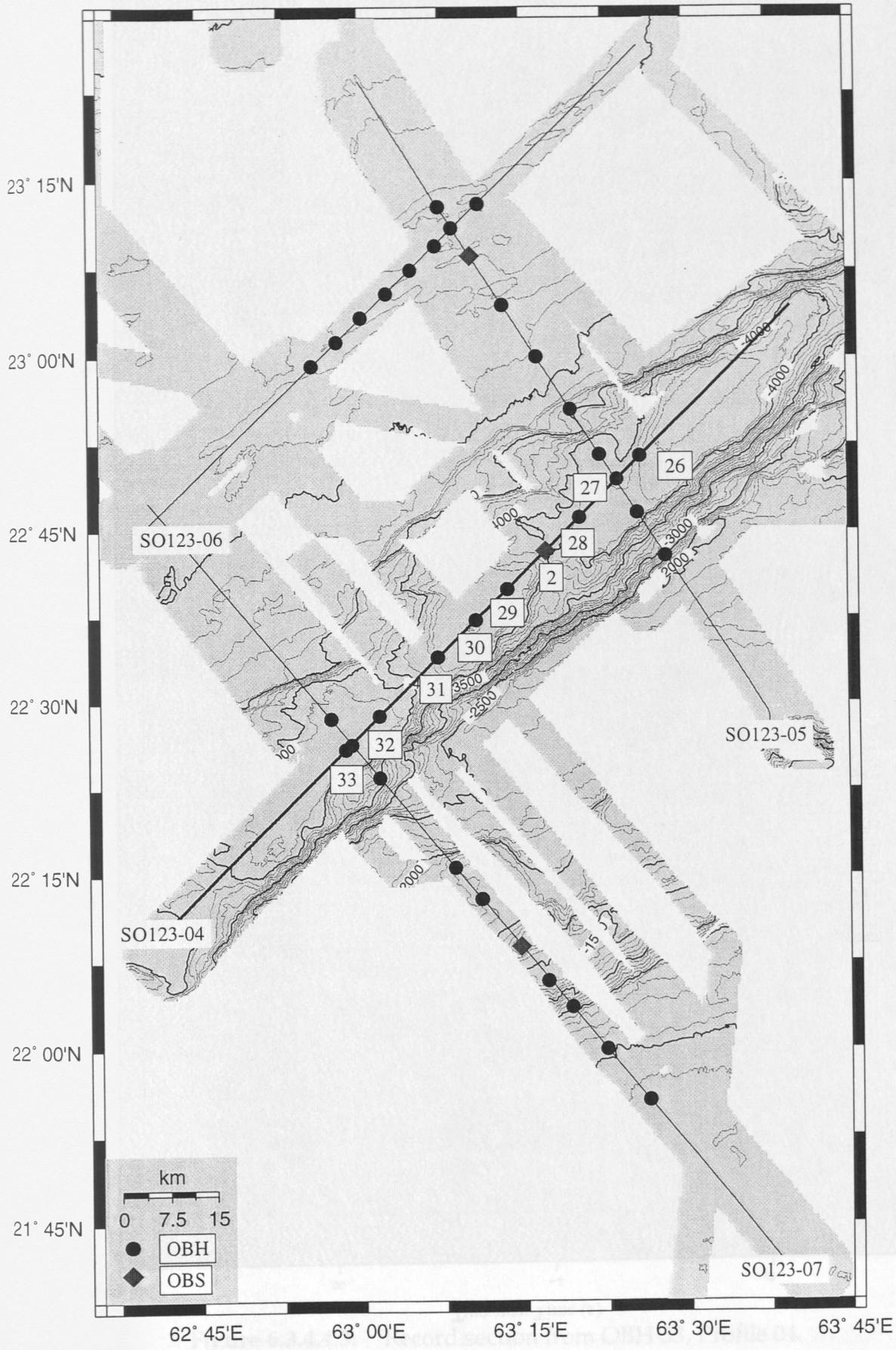

Figure 6.3.4.4.1: Location map of profile SO123-04.

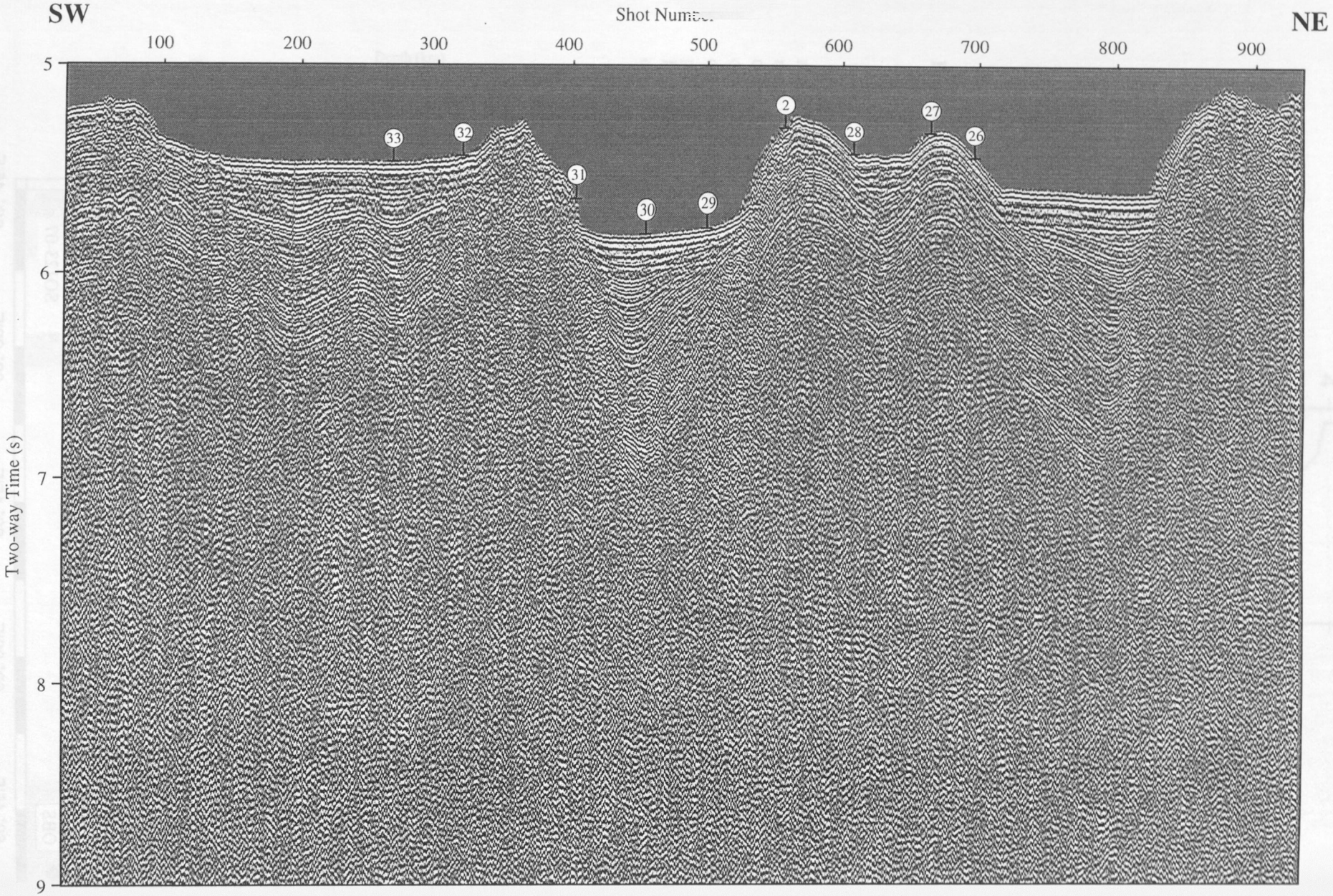

Figure 6.3.4.4.2: Single channel seismic profile SO123-04 (VE=30:1 at the sea-floor). Numbers at the sea-floor mark OBH positions.

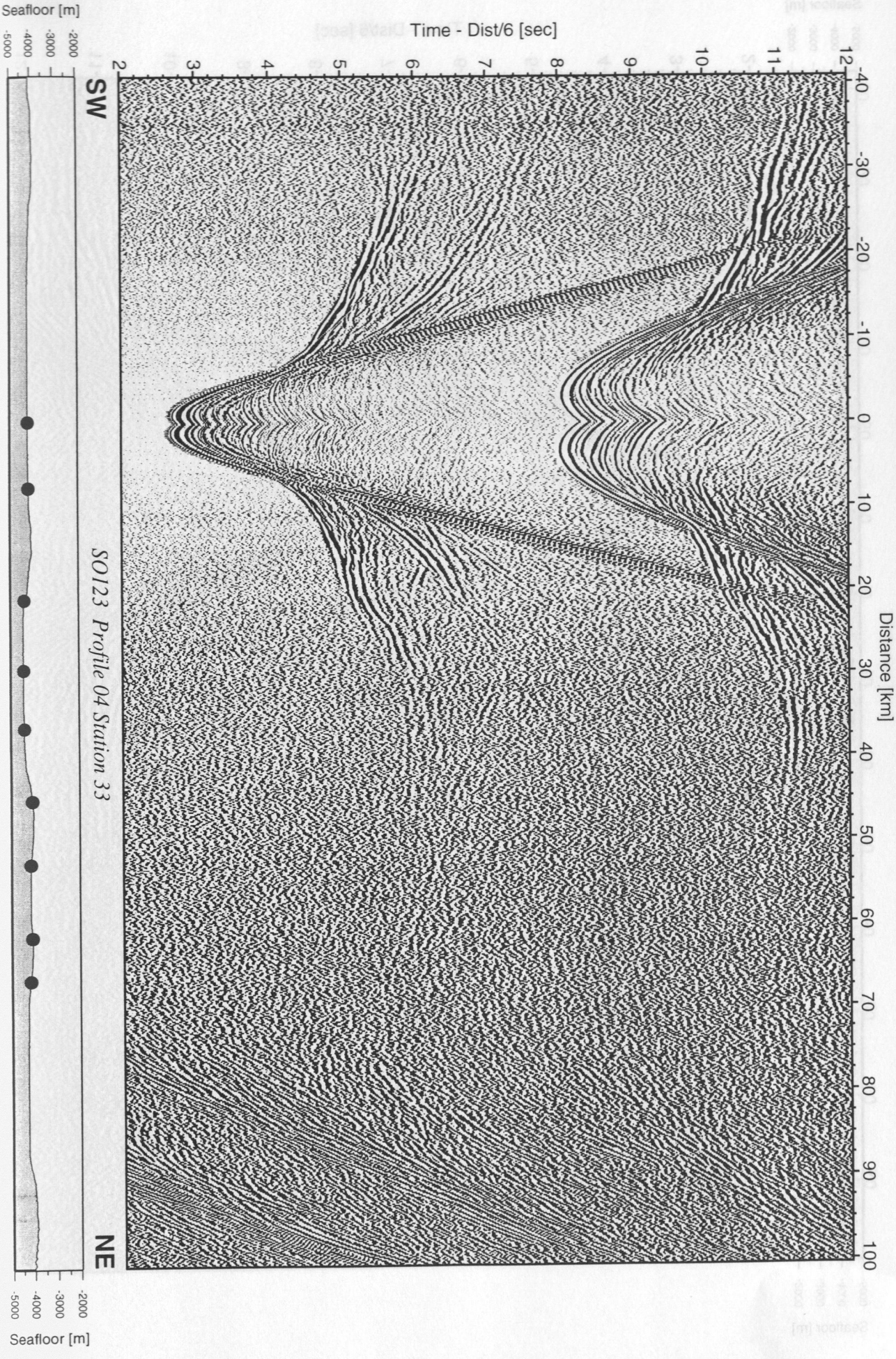

Figure 6.3.4.4.3: Record section from OBH 33, Profile 04.

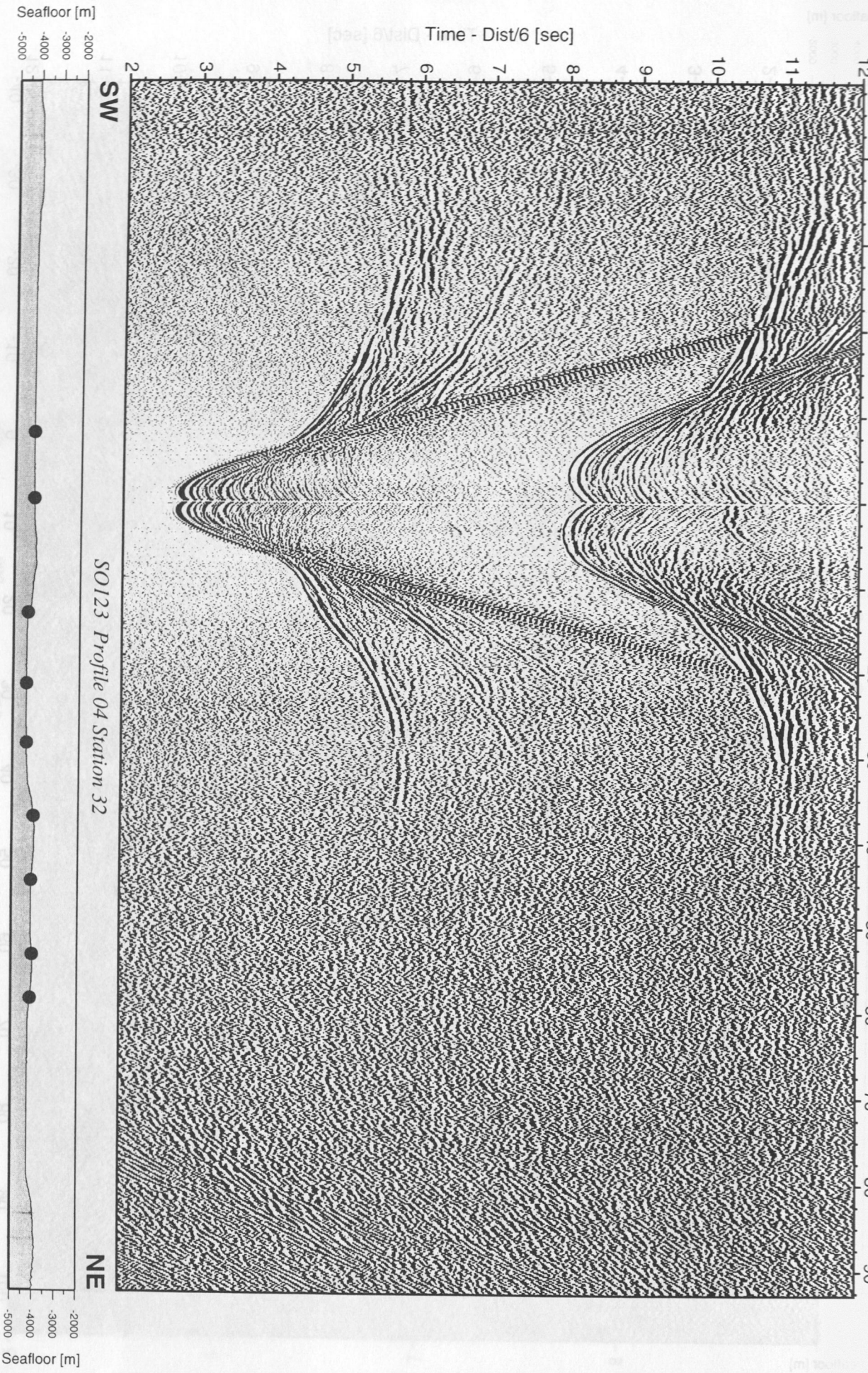

Figure 6.3.4.4.4: Record section from OBH 32, Profile 04.

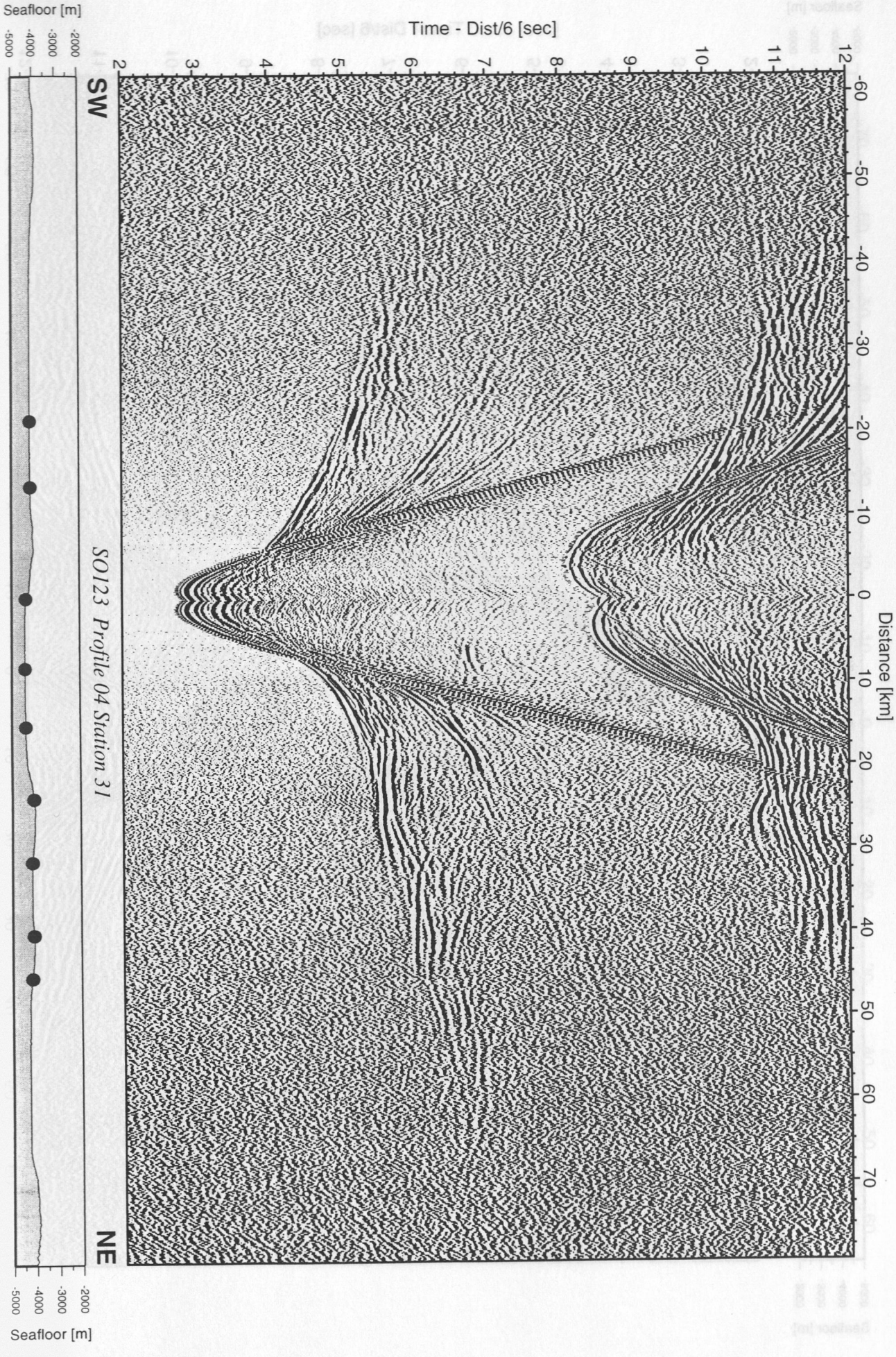

Figure 6.3.4.4.5: Record section from OBH 31, Profile 04.

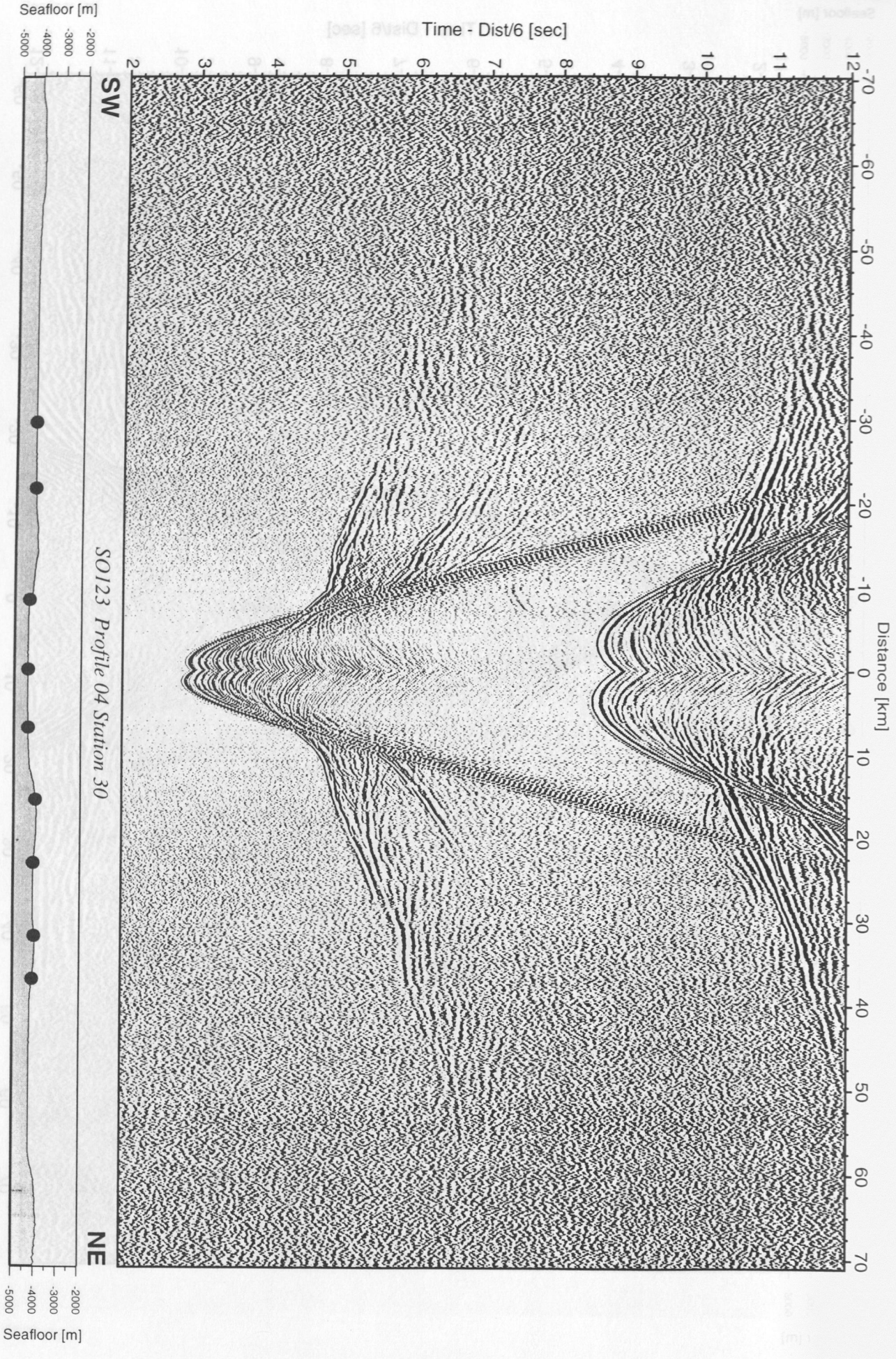

Figure 6.3.4.4.6: Record section from OBH 30, Profile 04.

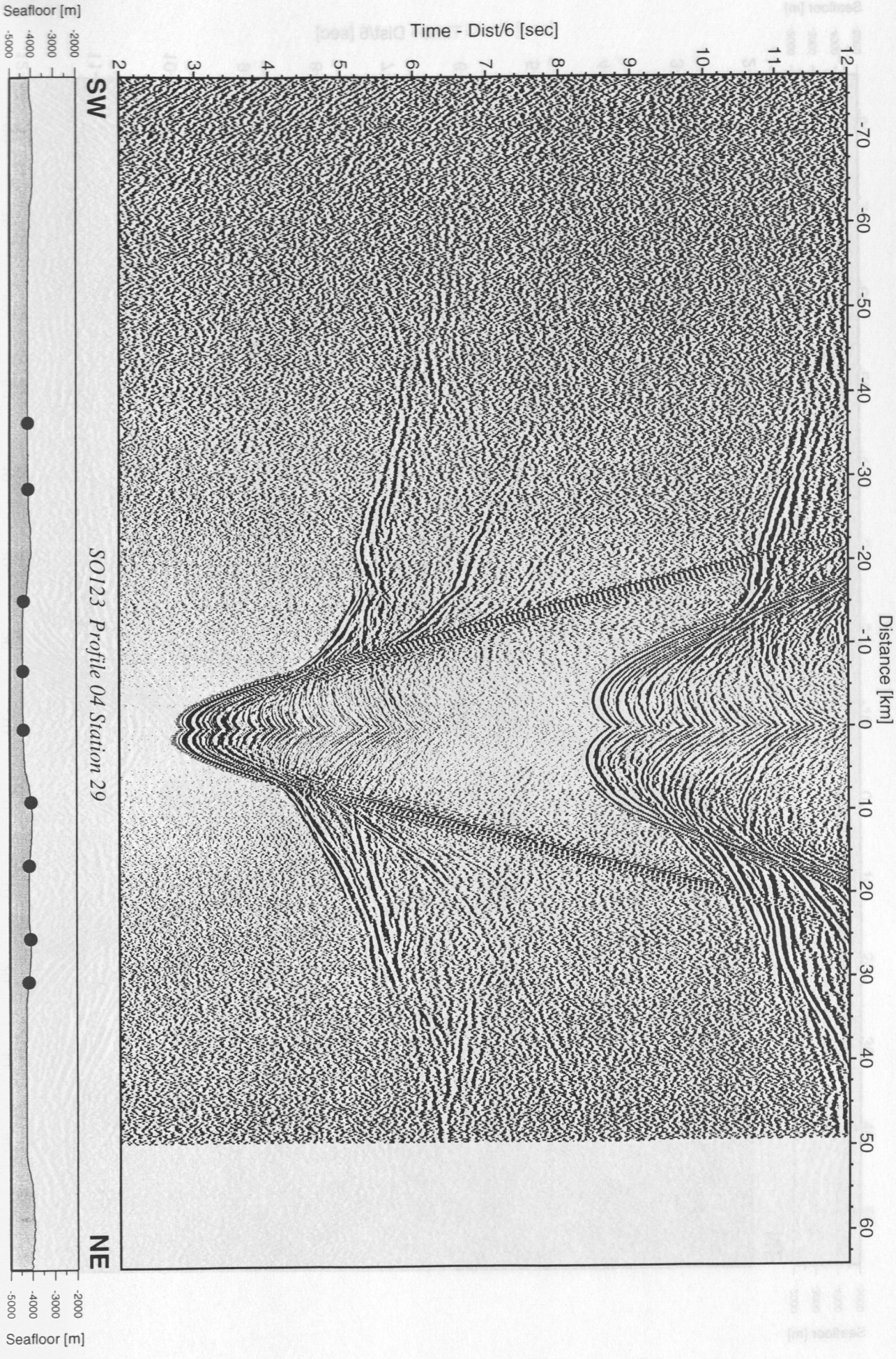

Figure 6.3.4.4.7: Record section from OBH 29, Profile 04.

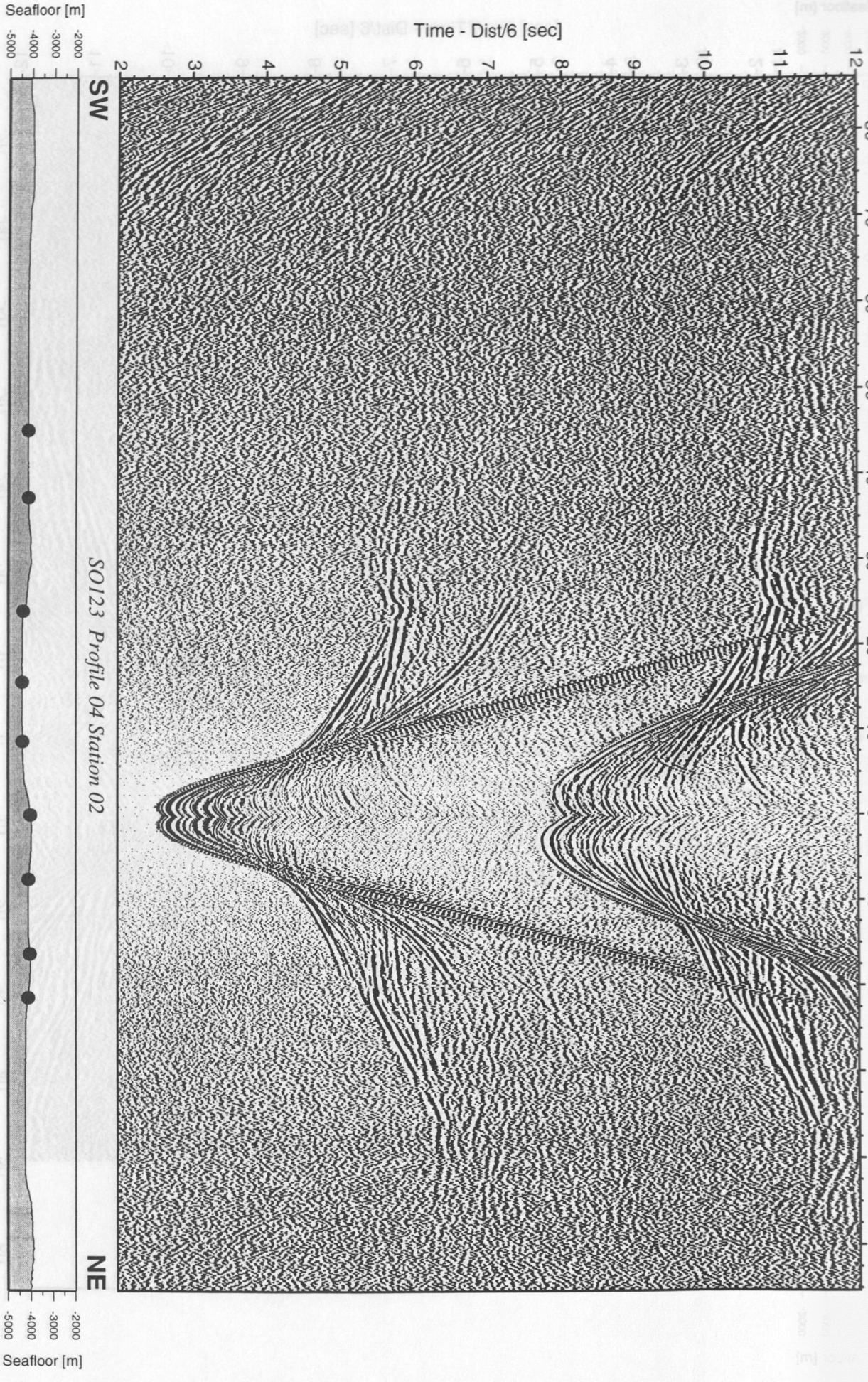

Figure 6.3.4.4.8: Record section from OBS 02, Profile 04, hydrophone.

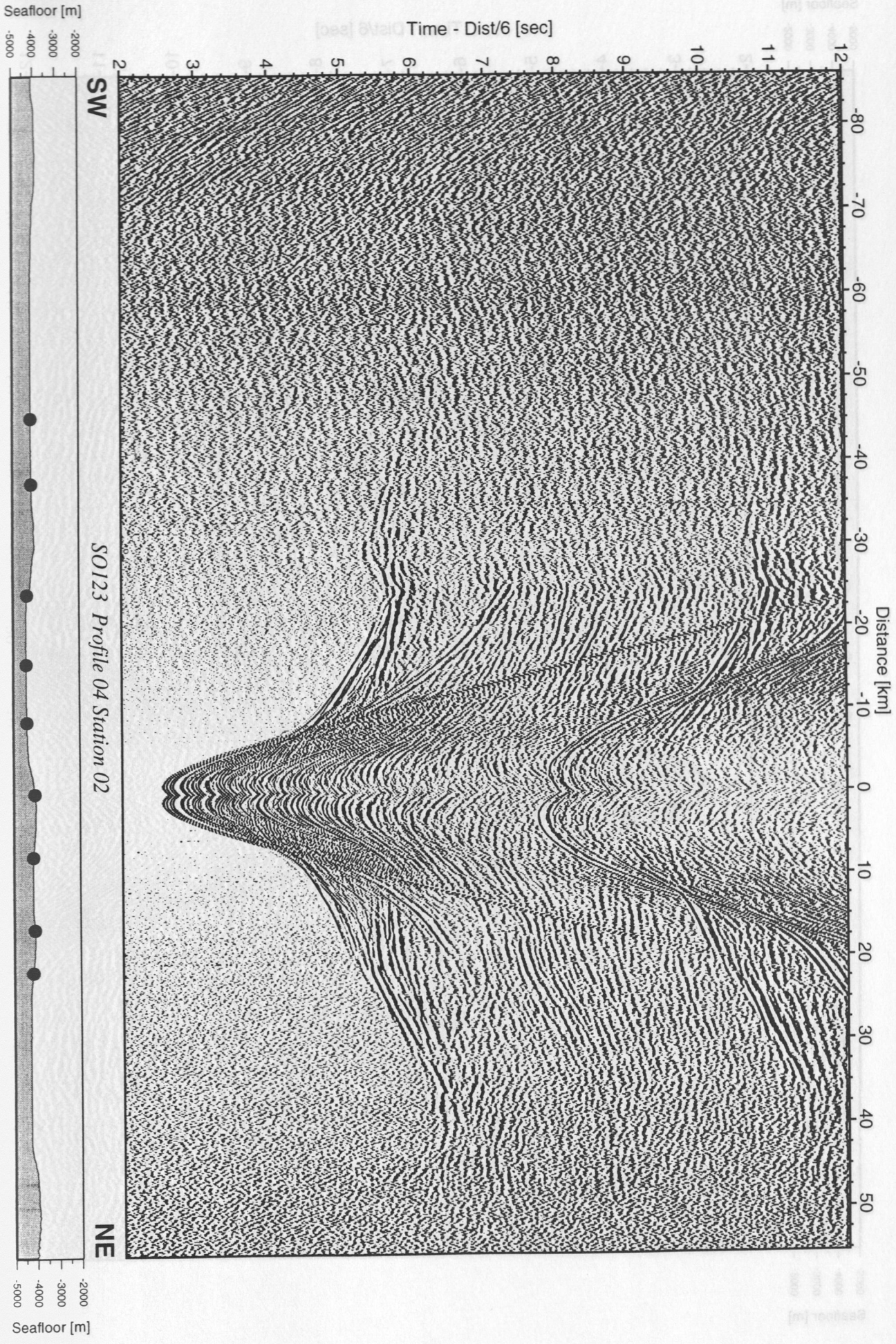

Figure 6.3.4.4.9: Record section from OBS 02, Profile 04, vertical component.

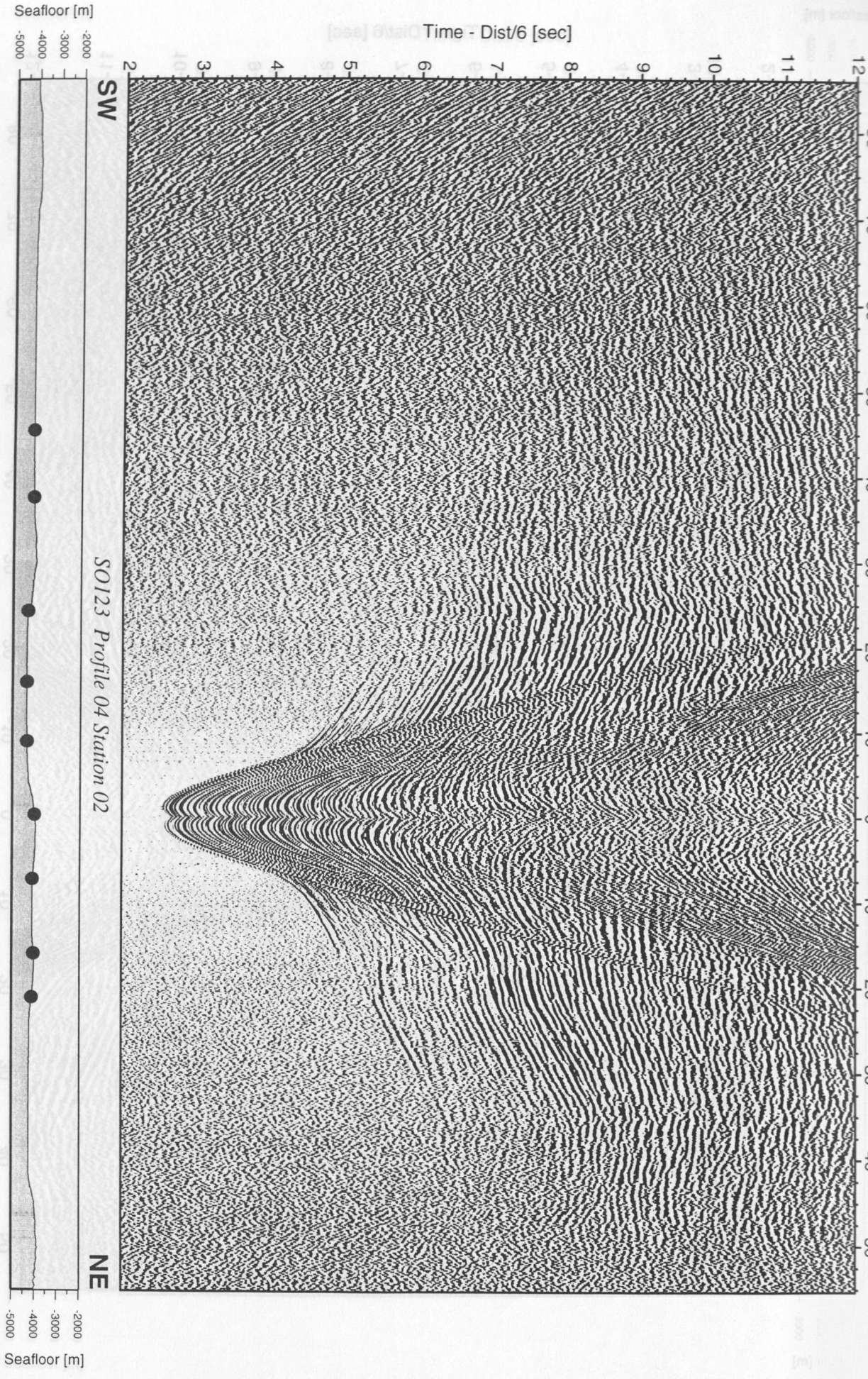

Figure 6.3.4.4.10: Record section from OBS 02, Profile 04, horizontal component.

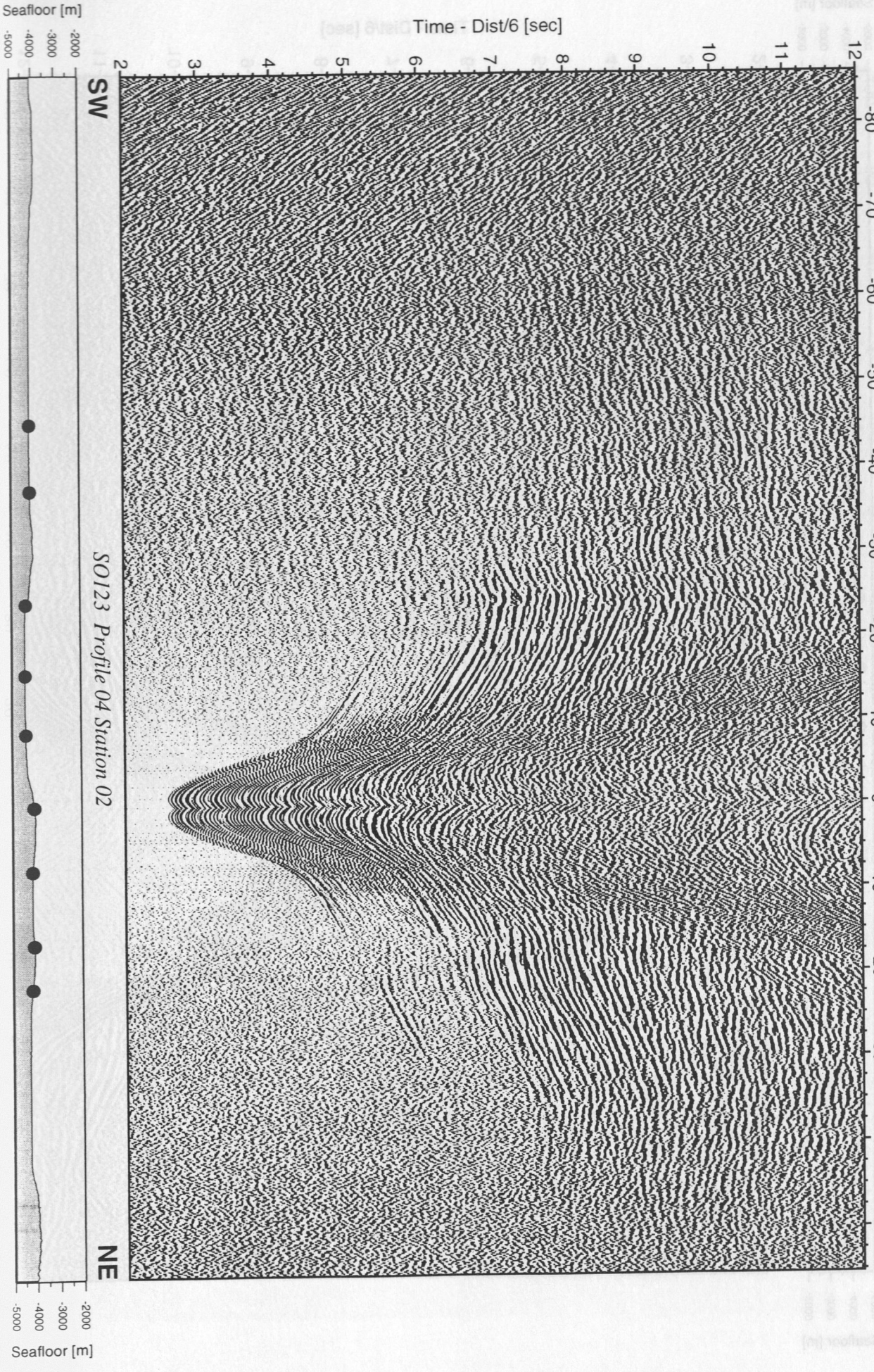

Figure 6.3.4.4.11: Record section from OBS 02, Profile 04, horizontal component.

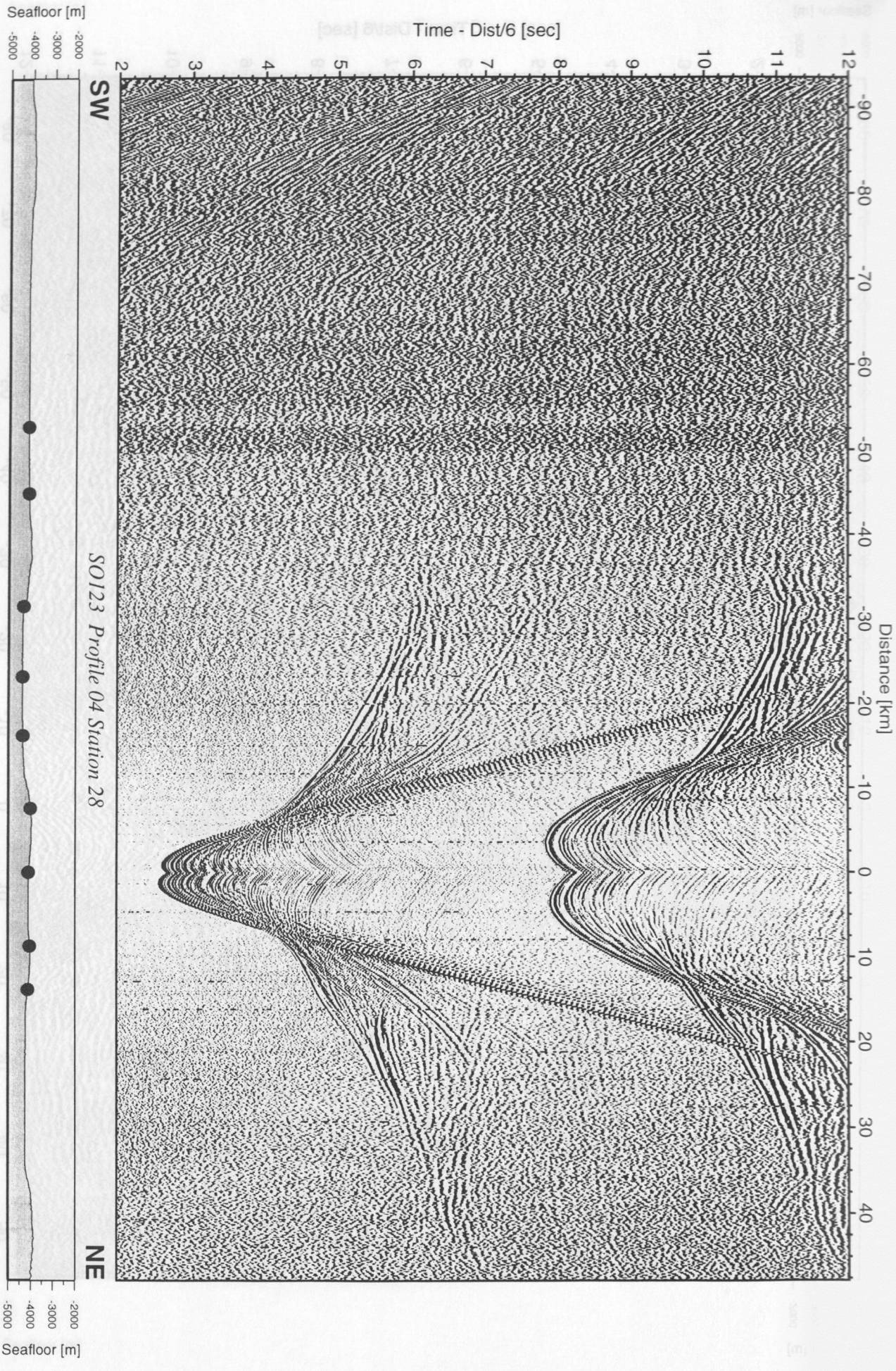

Figure 6.3.4.4.12: Record section from OBH 28, Profile 04.

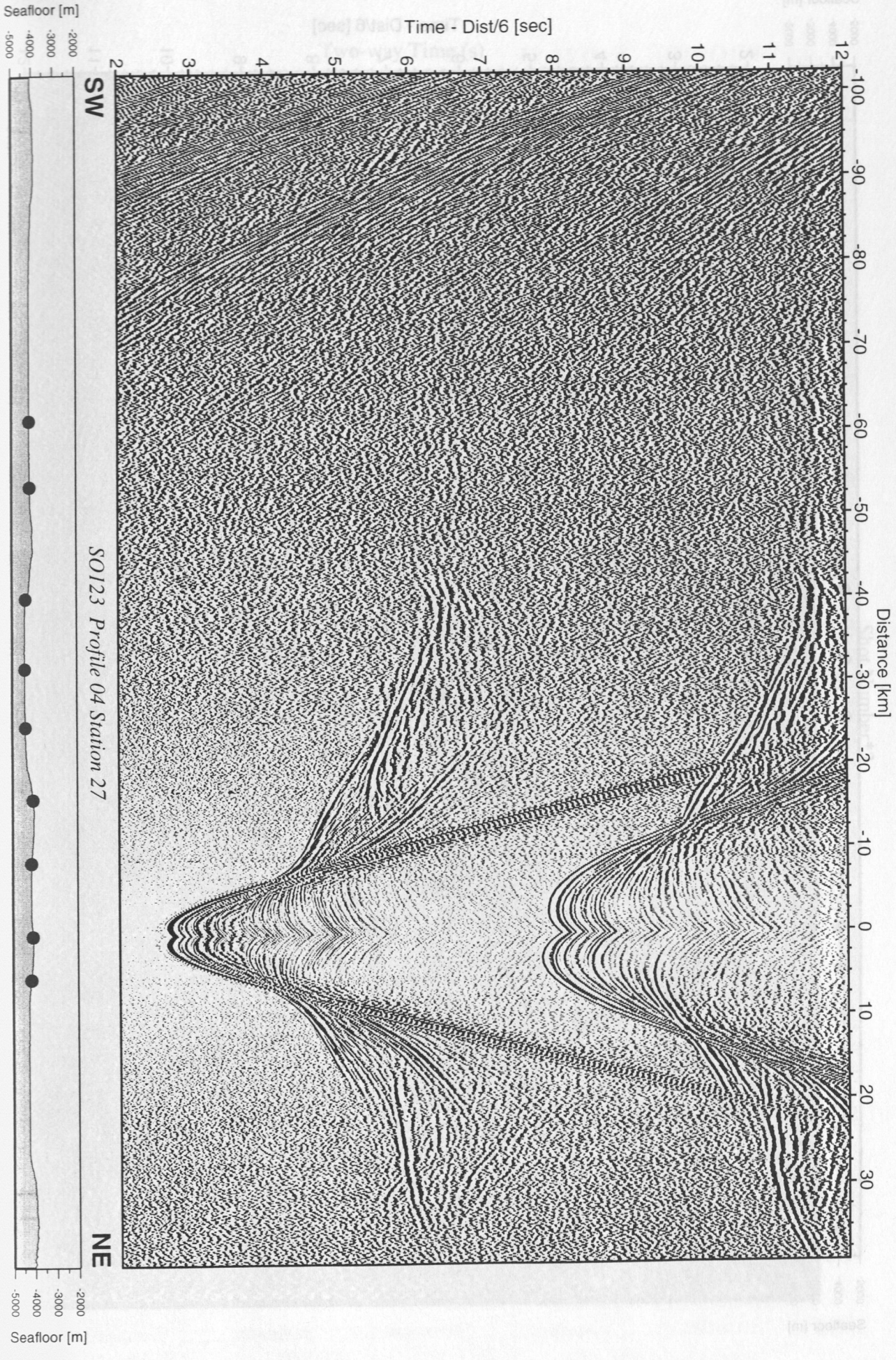

Figure 6.3.4.4.13: Record section from OBH 27, Profile 04.

6.3.4.5 PROFILE SO123-05

(K. Huhn, E. Flueh, C. Kopp, and D. Klaeschen)

Profile SO123-05 is a dip line across Dalrymple Trough and coincident with the multichannel reflection profile CAM29 (Minshull et al., 1992; Edwards et al., in prep., see also Figure 2.3). The northwestern termination is on the south flank of Little Murray Ridge. Nine OBH (27, 34 to 41) and the OBS (03) were deployed between 13:00 and 20:00 17.09. Shooting at 5 knots with 60 s shot intervall along this 75 nm long line was done between 23:30 17.09. and 12:30 18.09. OBH27 and 35 were located at the intersections with profiles SO123-04 and SO123-06 and recorded both lines. Instruments were recovered between 15:00 18.09. and 01:00 19.09., except for OBH35 which was picked up at 12:00 20.09. The location map of the shots and instruments is shown in Figure 6.3.4.5.1. All instruments recorded well and the record sections are shown in Figures 6.3.4.5.3 to 6.3.4.5.13 Further details on instrumentation and locations can be found in Appendix 9.1.5.

1-D velocity models were calculated for OBS03 and several OBH (36, 37, 38) stations along profile 5. The resulting models are shown in Figure 6.3.4.5.14. Minor variations in the record sections indicate only small changes in structure along the profile, and therefore the 1-D approach is valid. Further to the southeast, when approaching Dalrymple Trough, asymetry is apparent between positive and negative offset. The least asymetry is found for OBS03 (Figure 6.3.4.5.4), because it is located in an undisturbed area. To the contrary, 1-D modelling of the southwestern side of OBH38 (Figure 6.3.4.5.10) is not possible because of the morphological differences and also structural inhomogenieties caused by the Dalrymple Trough.

Six phases could be identified on all instruments. At first the direct water-wave, three refraction arrivals from the sediment, and a strong refraction from the basement. Also, in all seismograms the refraction from lower crust is well seen. In the upper 2.5 km sediment layers with velocities from 1.6 km/s to 3.5 km/s can be distinguished. Velocity variation for these sediment between the four stations can be accounted for by local topographic effects, but are of minor importance. The identification of the reflection phases is best done in the multiples, where they are less obscured by the direct water-wave. In all models the basement is marked by a strong refraction and reflections with large amplitudes also at near offset. It can be placed in a depth of approximately 5.3 km and it is connected with a velocity increase from about 3 km/s to more than 4 km/s. Also remarkable in all datasets is the sharp boundary between layer 2 and layer 3. It is characterized by a velocity increase from about 5.0 km/s to 6.0 km/s. Layer 2 and layer 3 are together about 6-7 km thick.

The strong secondary arrivals interpreted as PmP, at offsets of more than 35 km for the southeastern part of OBH36 and the following stations are modeled with a velocity jump from about 7 km/s to 8 km/s at a depth of 12-13 km. Summarizing one can recognize that the crust is build up quite uniformly, though not totally typical for normal oceanic crust, as also noticed in profile SO123-06. A crustal section through OBS03, OHB36, 37, and 38 based on 1-D modelling is shown in Figure 6.3.4.5.14. The record section of OBH37 with calculated traveltimes superimposed is shown in Figure 6.3.4.5.15.

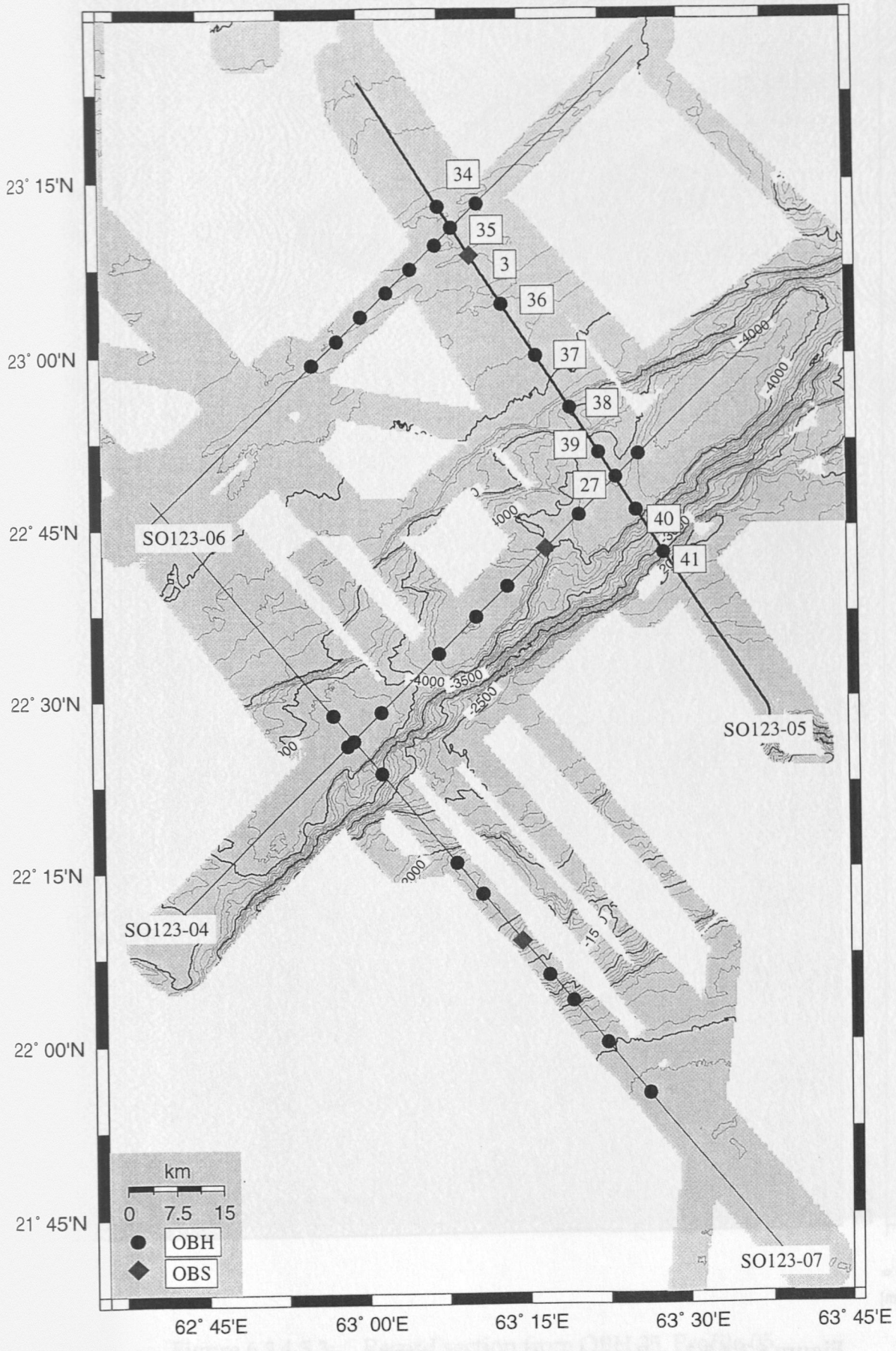

Figure 6.3.4.5.1: Location map of profile SO123-05.

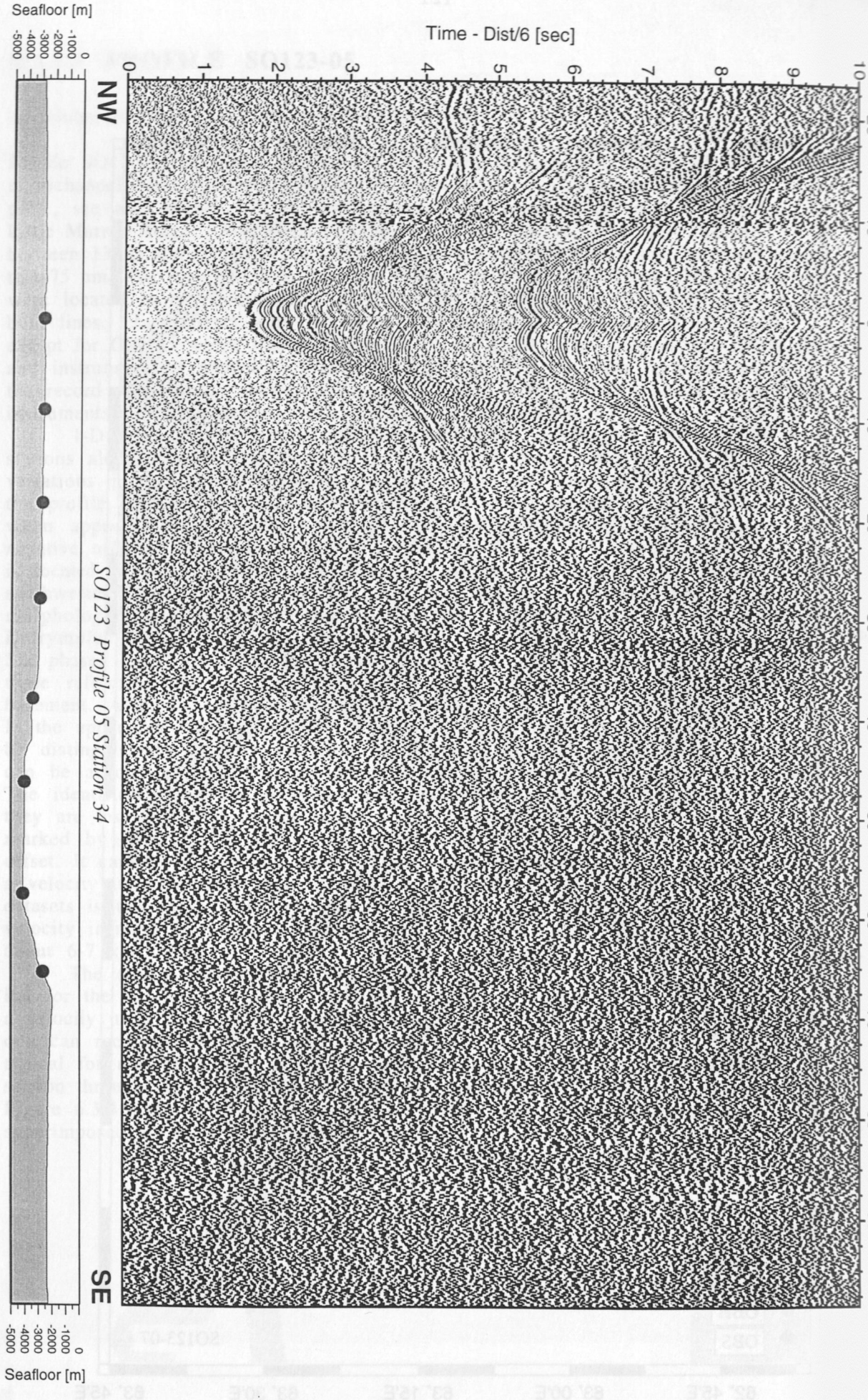

Figure 6.3.4.5.3: Record section from OBH 34, Profile 05.

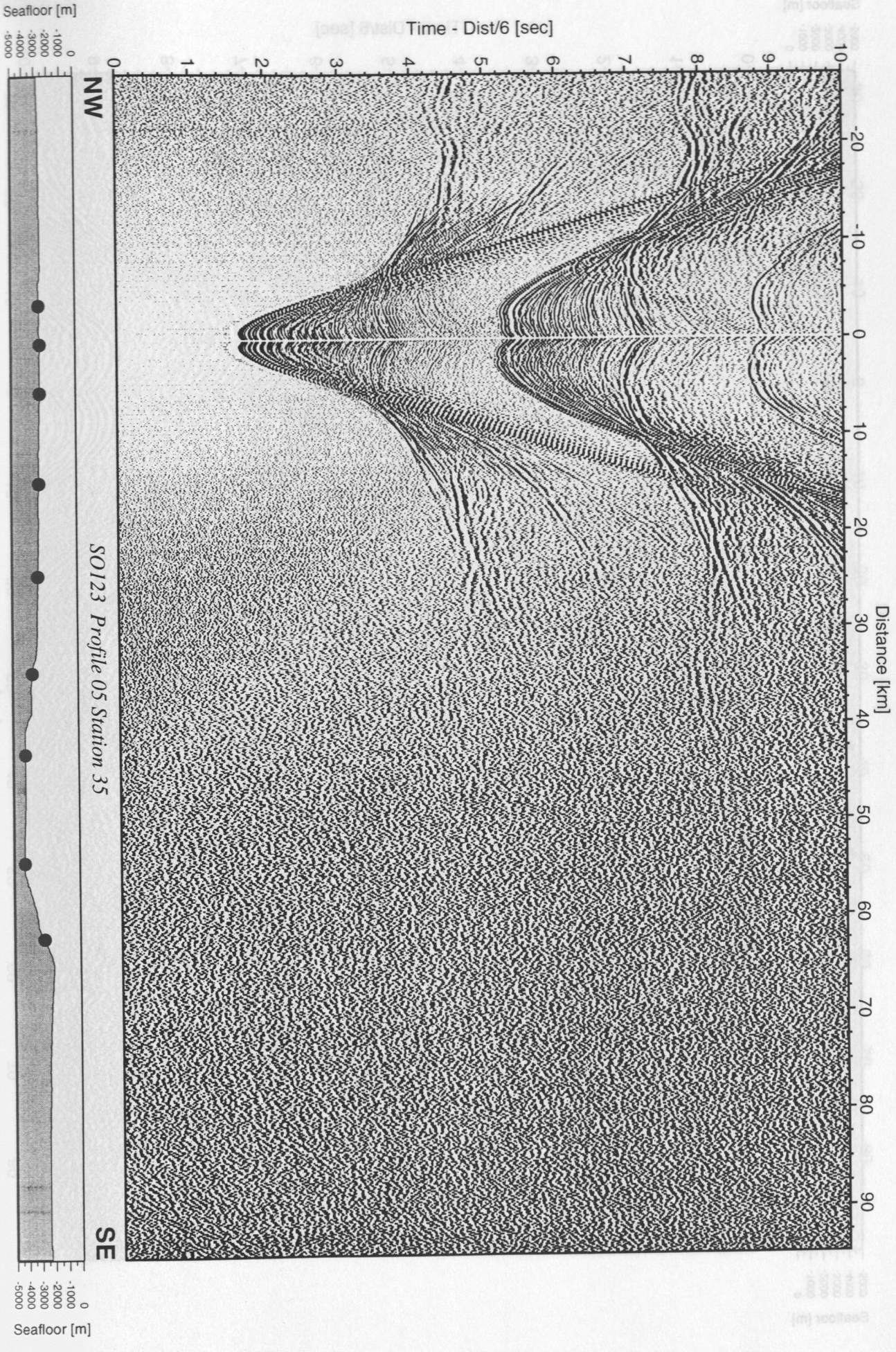

Figure 6.3.4.5.3: Record section from OBH 35, Profile 05.

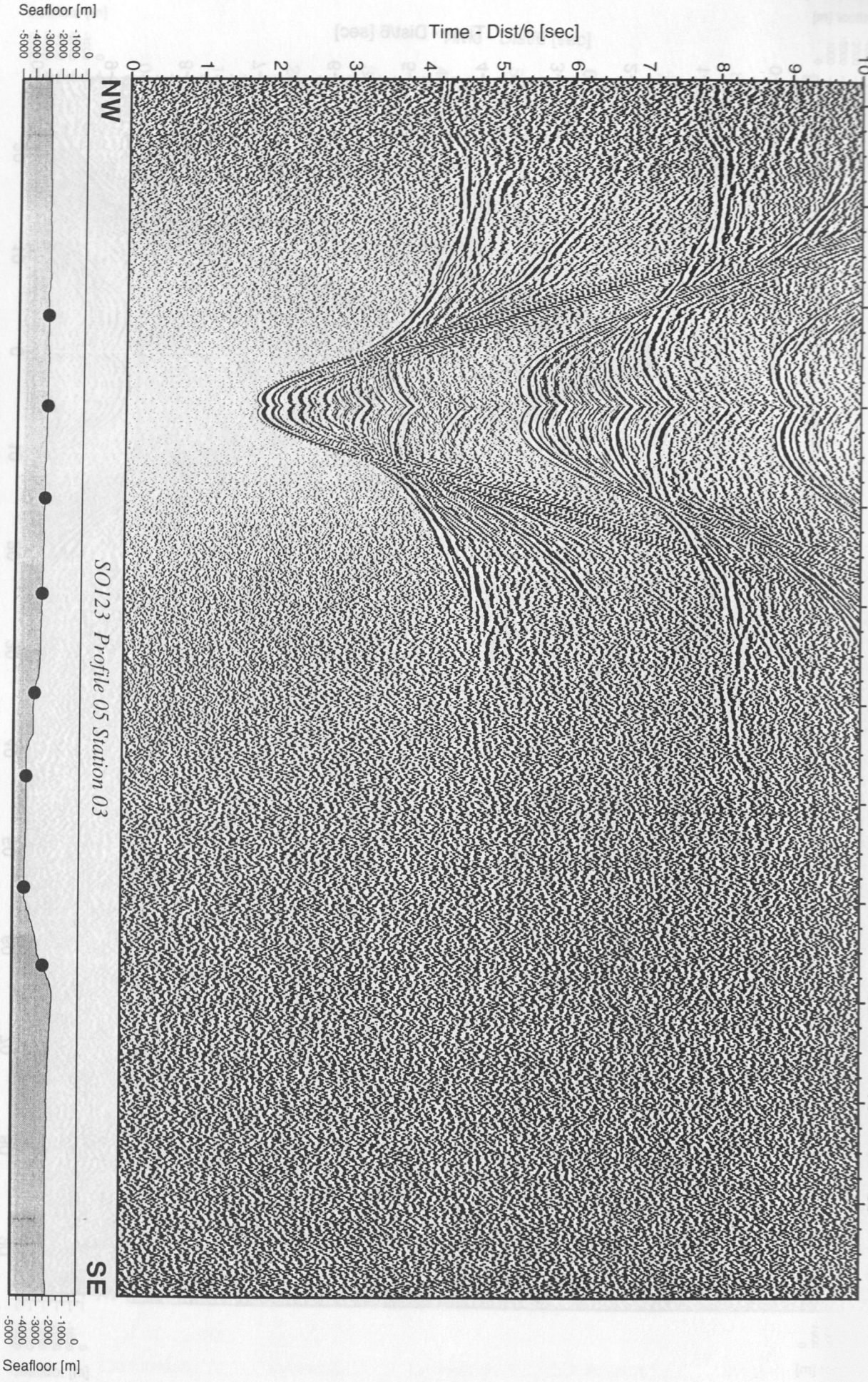

Figure 6.3.4.5.4: Record section from OBS 03, Profile 05, hydrophone.

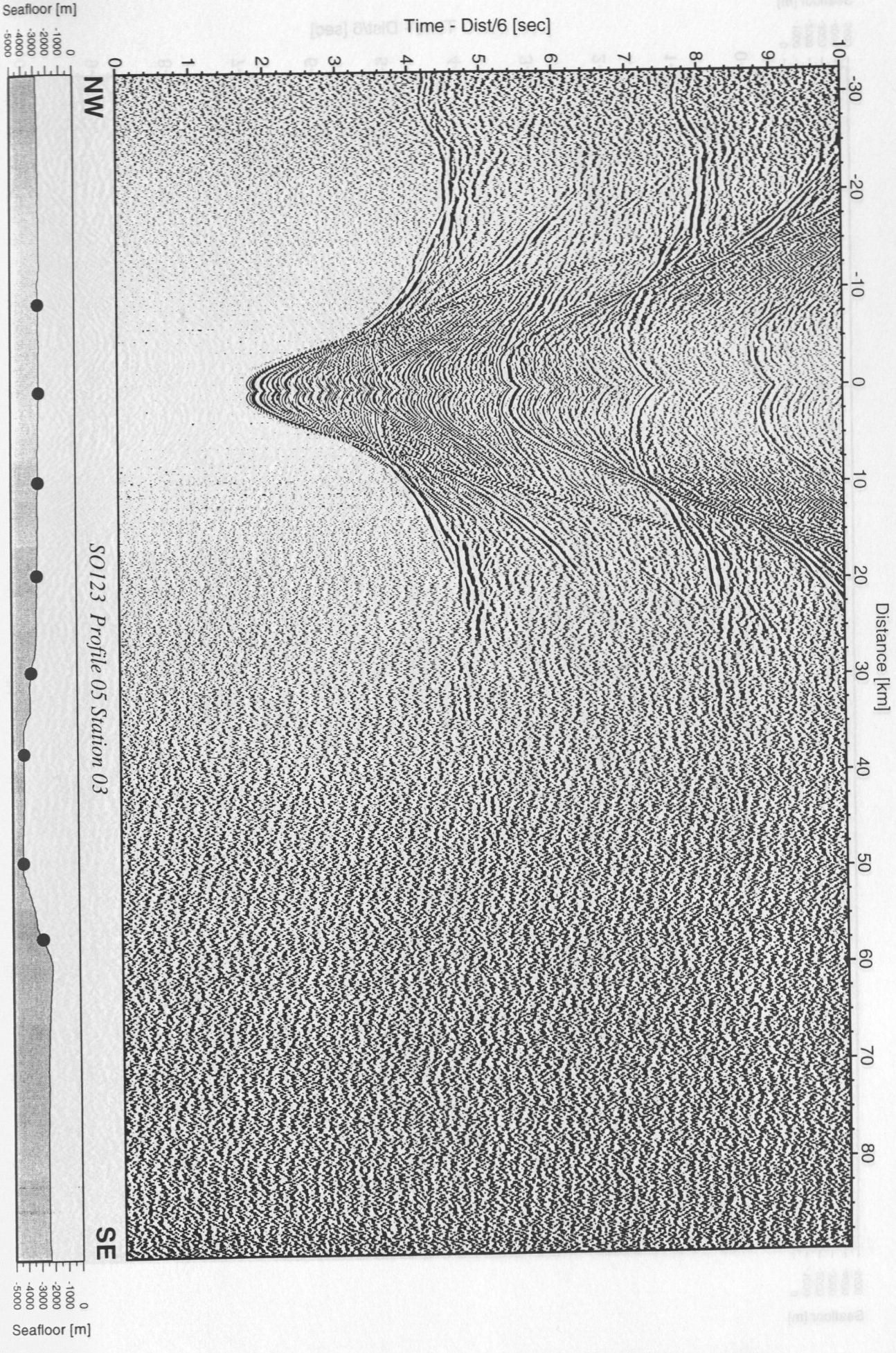

Figure 6.3.4.5.5: Record section from OBS 03, Profile 05, vertical component.

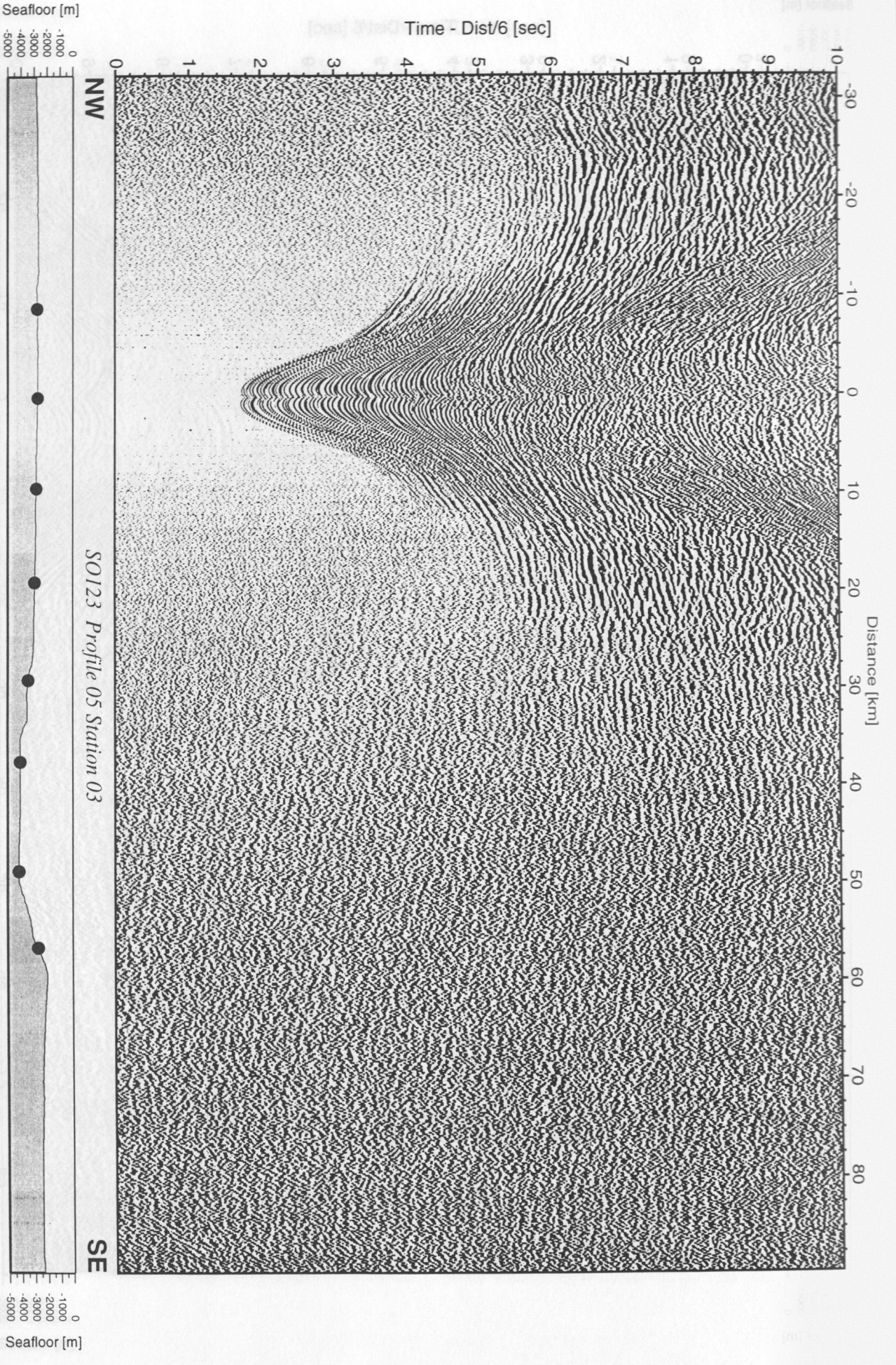

Figure 6.3.4.5.6: Record section from OBS 03, Profile 05, horizontal component.

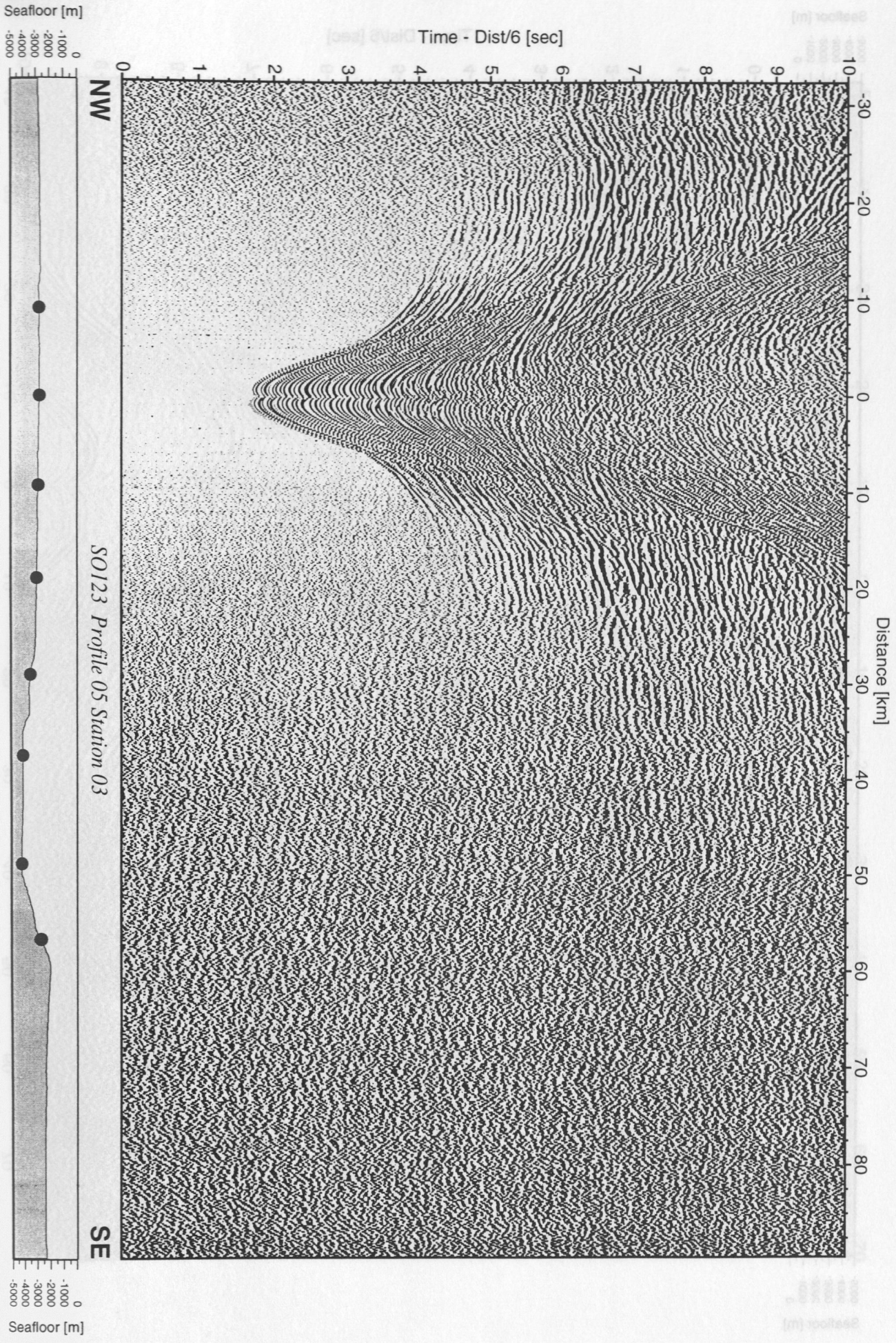

Figure 6.3.4.5.7: Record section from OBS 03, Profile 05, horizontal component.

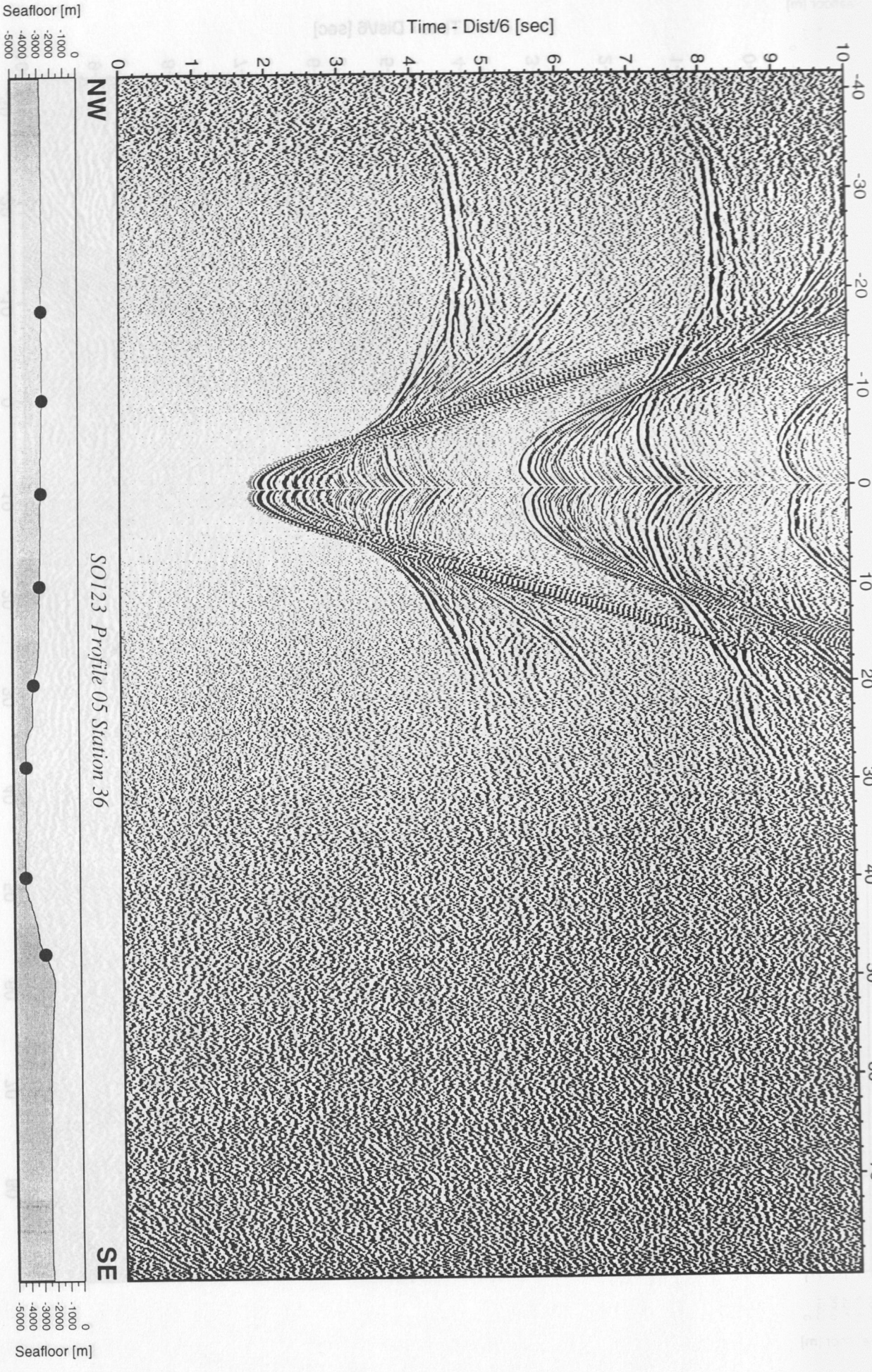

Figure 6.3.4.5.8: Record section from OBH 36, Profile 05.

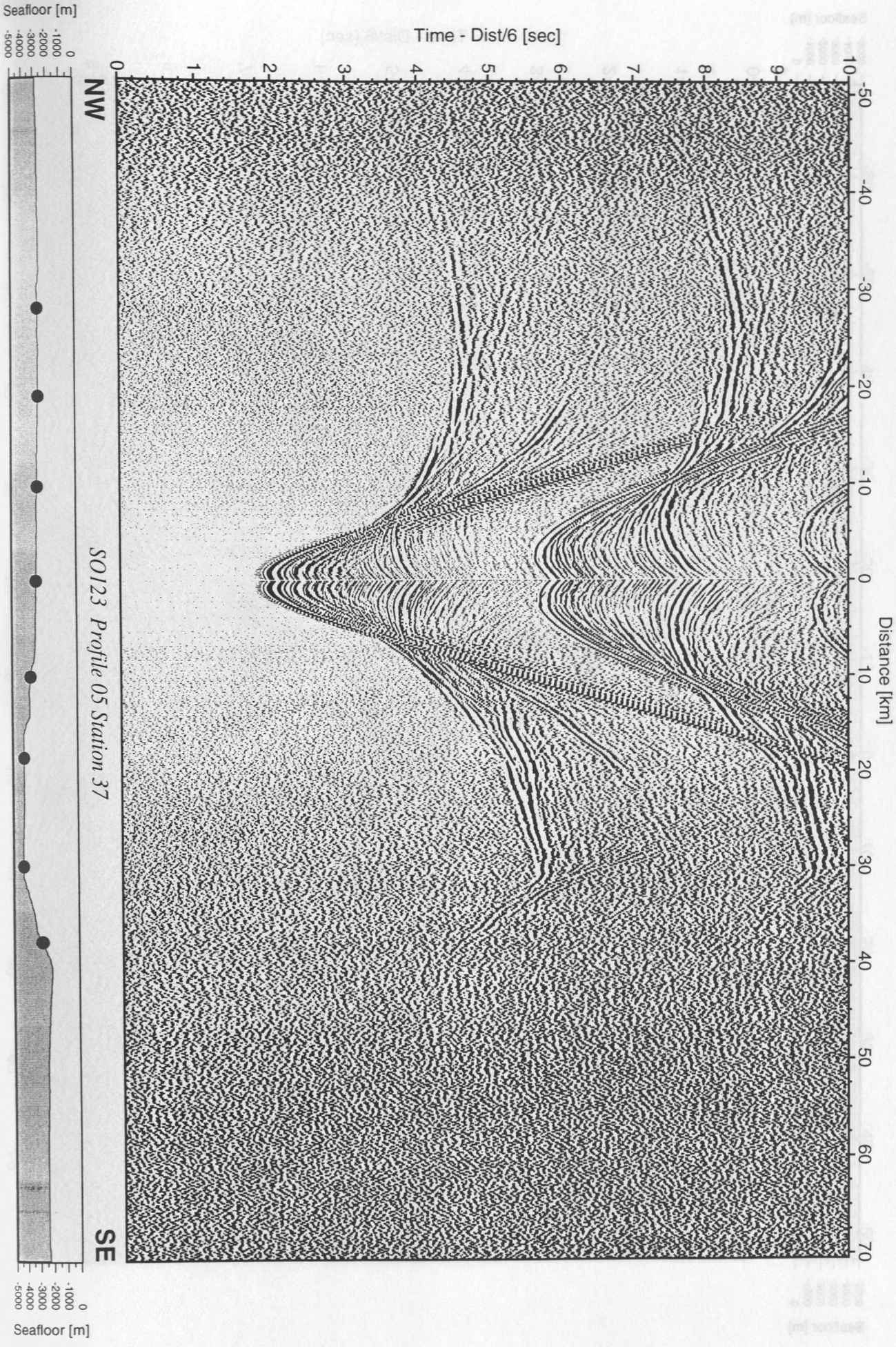

Figure 6.3.4.5.9: Record section from OBH 37, Profile 05.

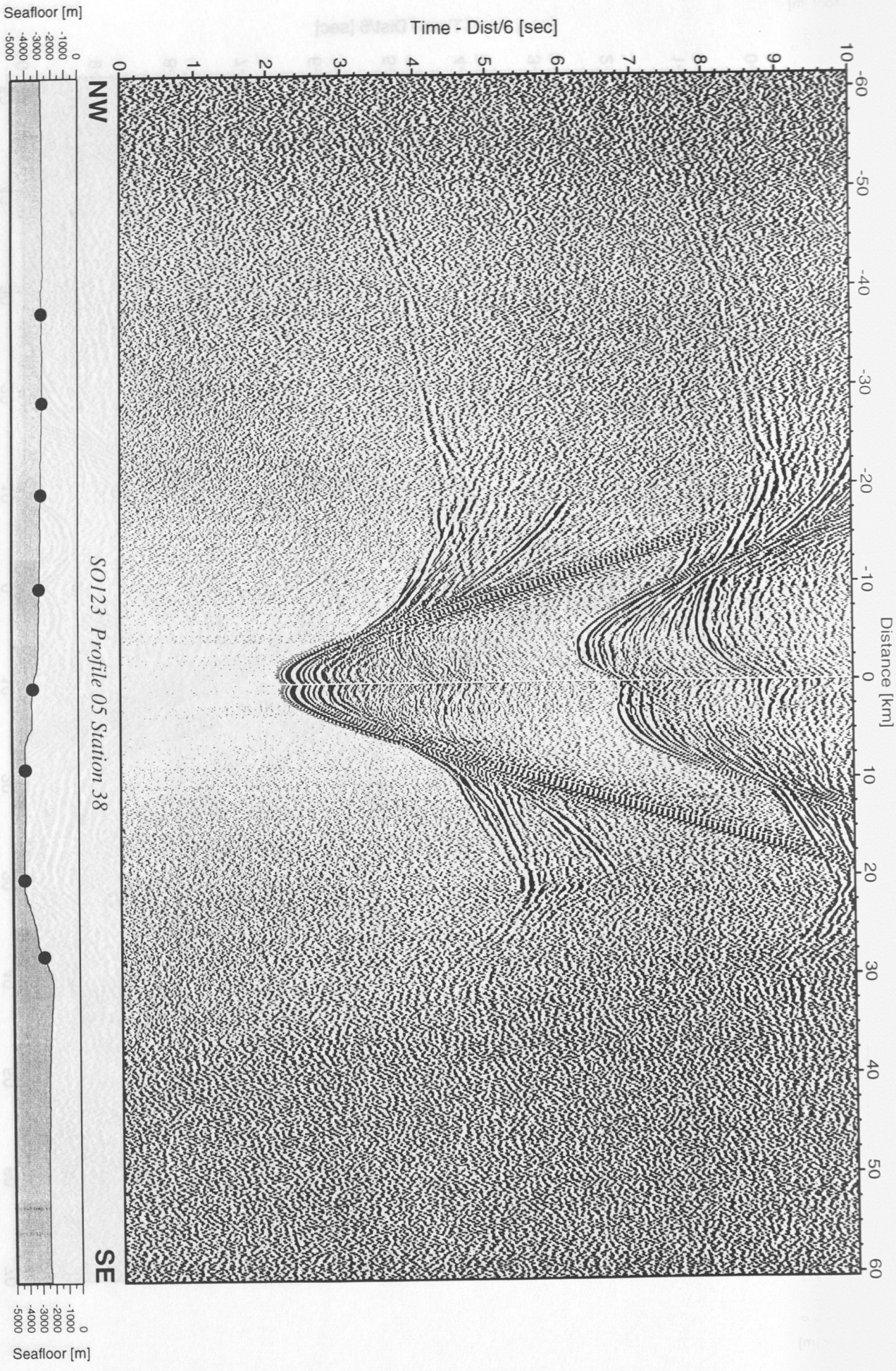

Figure 6.3.4.5.10: Record section from OBH 38, Profile 05.

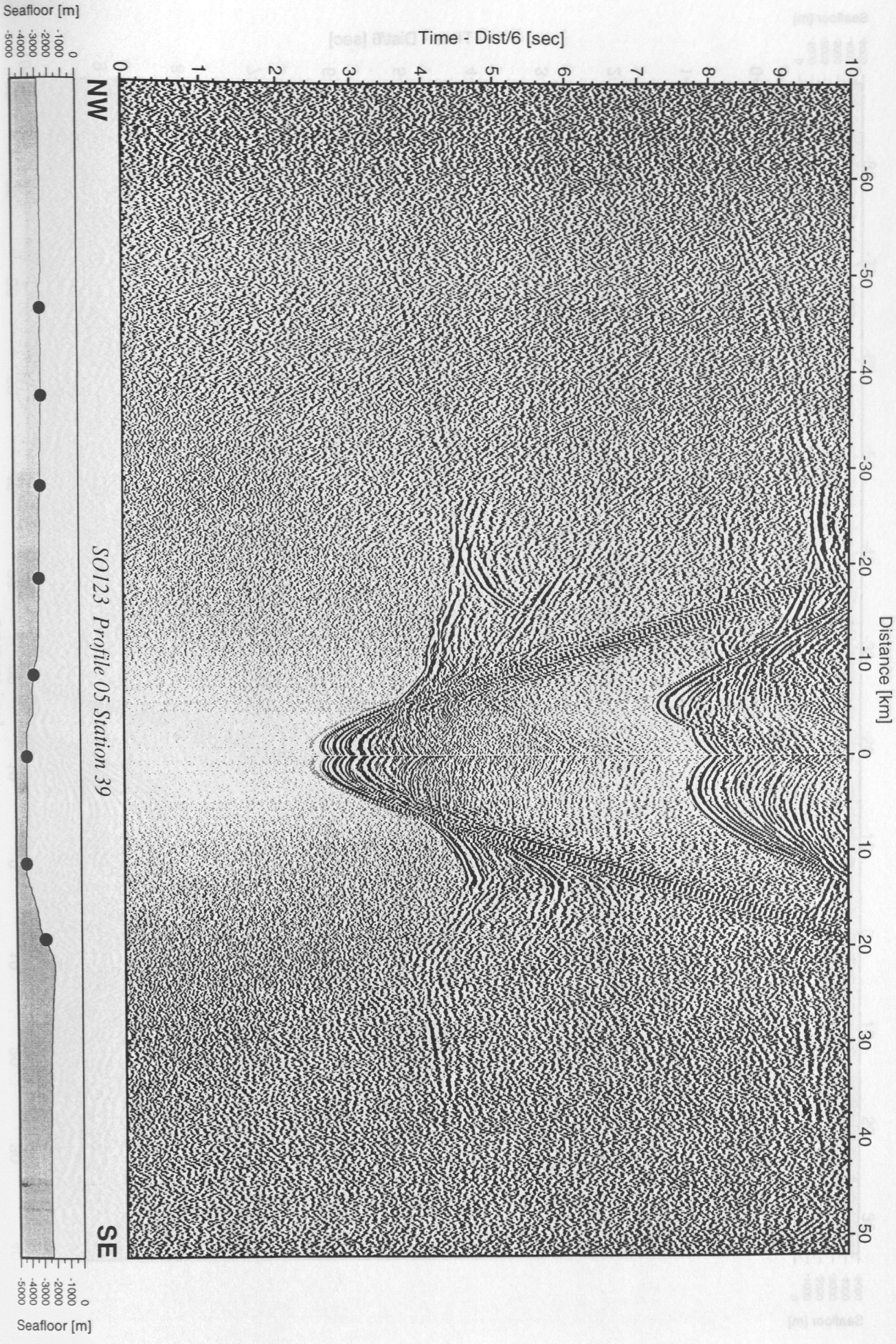

Figure 6.3.4.5.11: Record section from OBH 39, Profile 05.

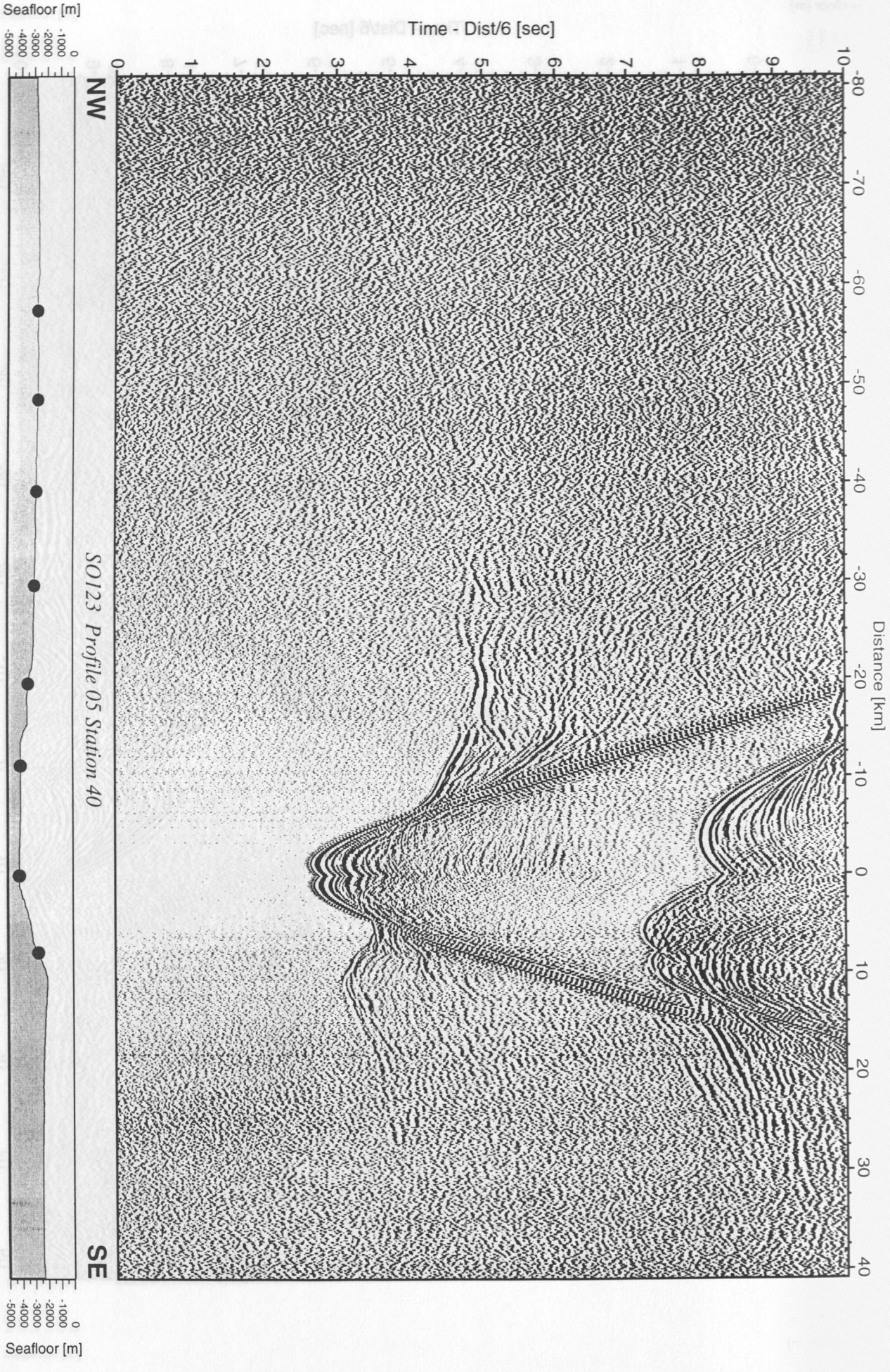

Figure 6.3.4.5.12: Record section from OBH 40, Profile 05.

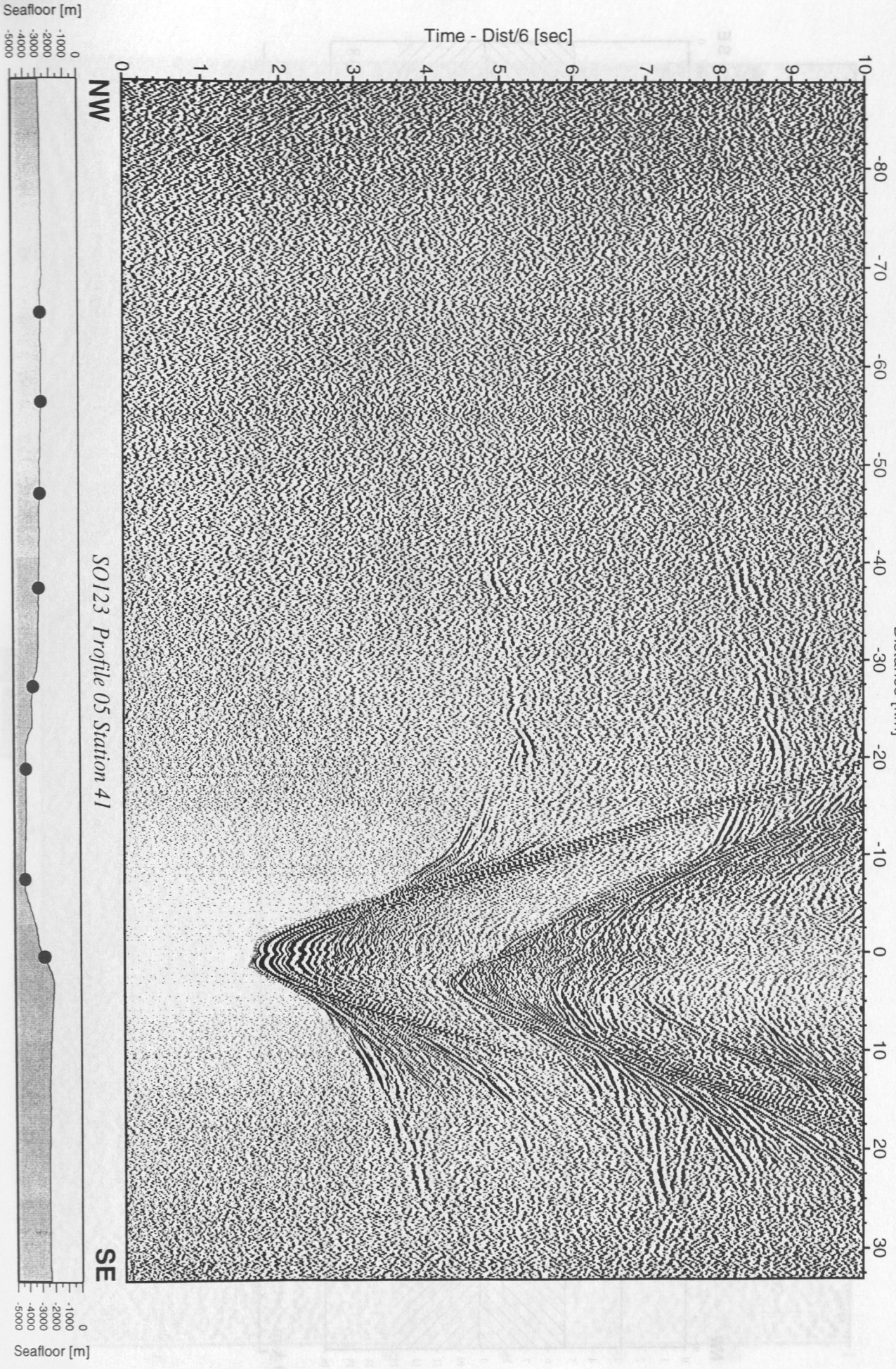

Figure 6.3.4.5.13: Record section from OBH 41, Profile 05.

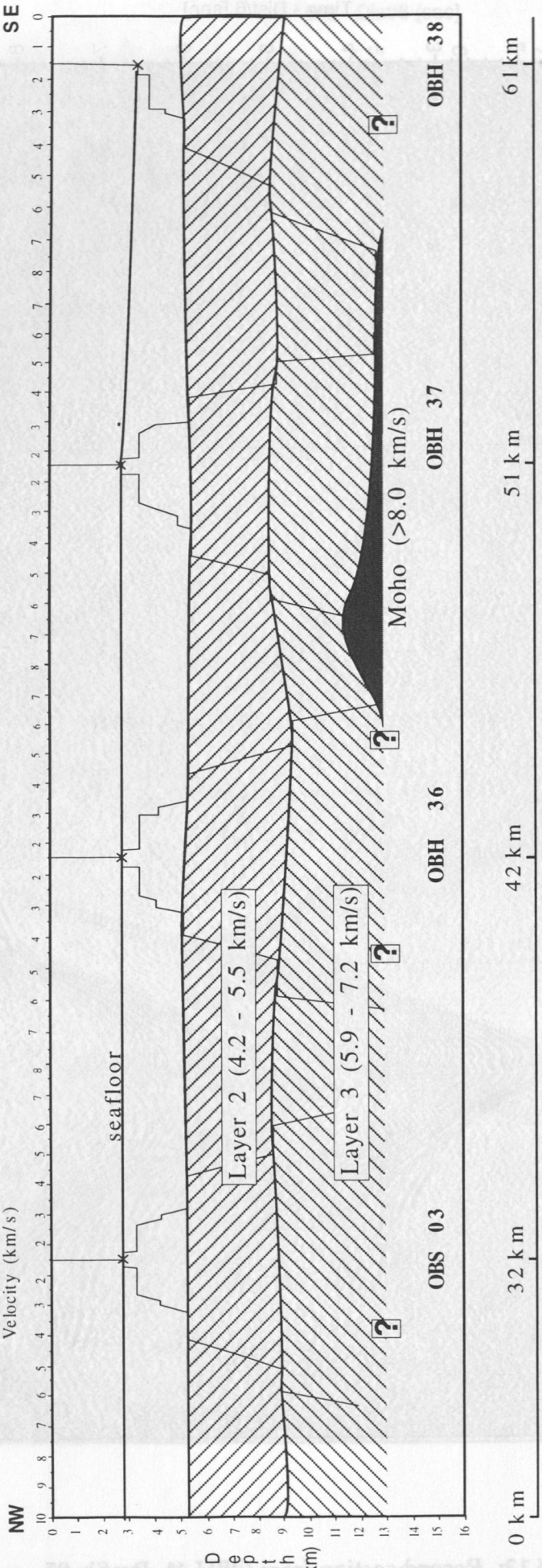

Figure 6.3.4.5.14 : 1D velocity models for OBS03, OBH36, OBH37, and OBH38.

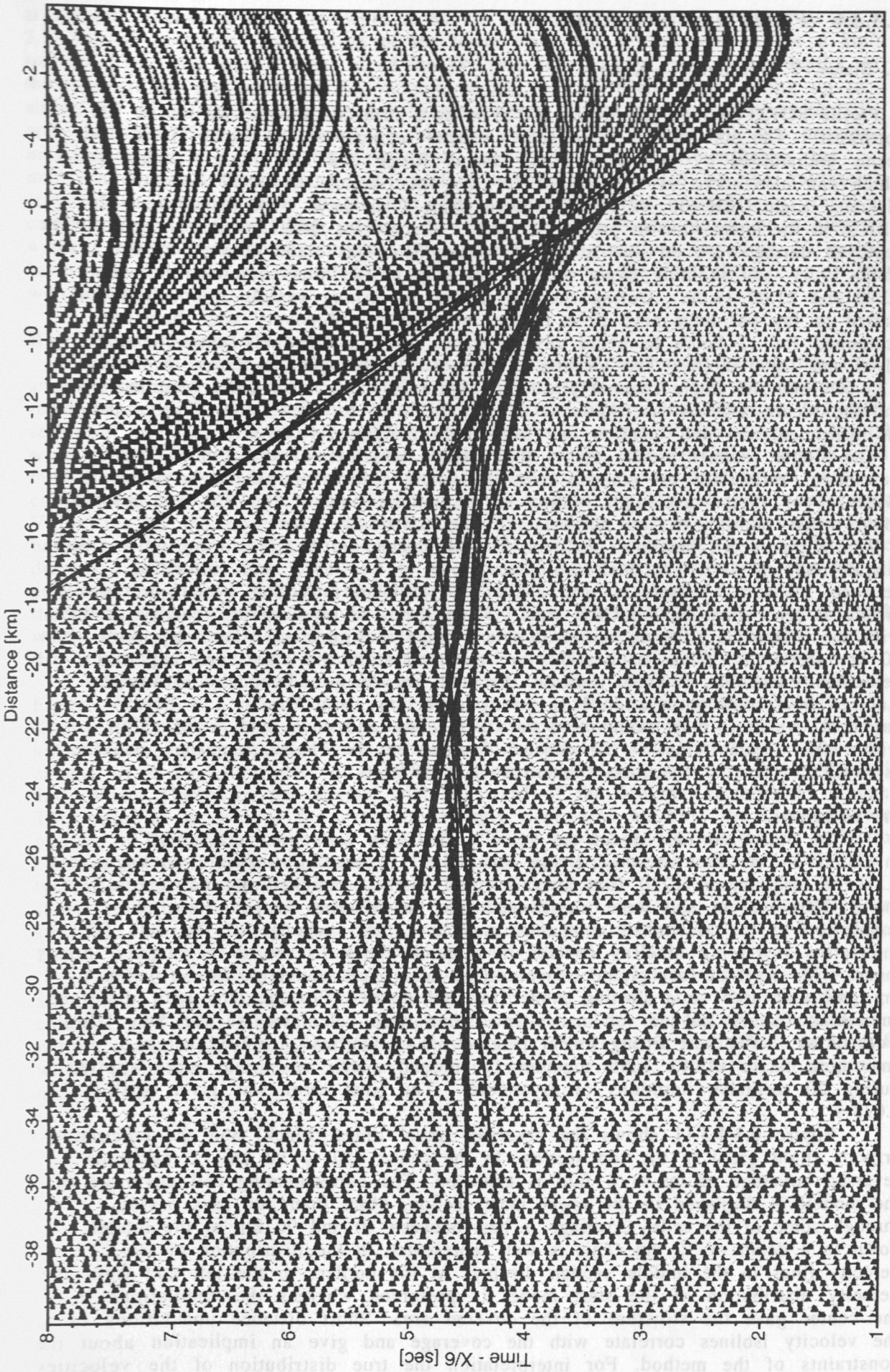

Figure 6.3.4.5.15: Record section from OBH 37 with calculated traveltimes superimposed.

6.3.4.6 PROFILE SO123-06

(J. Bialas, T. Minshull, C. Kopp)

Profile SO123-06 runs parallel to SO123-04 at a distance of about 25 nm to the northwest. The aim was to investigate a crustal segment of the Oman Basin that seems undisturbed by processes along Murray Ridge and Dalrymple Trough and which can also serve as a reference for the crust being subducted beneath Makran. Eight OBH (35, 42 to 48), spaced about 3 nm each, were deployed, with OBH35 at the intersection to profile SO123-05. Except for OBH35 and 42, which were deployed during work on line SO123-05, deployment was made between 03:00 and 06:00 19.09. and shooting along this 60 nm long profile was completed between 10:00 and 21:00 19.09. During shooting a fleet of fishing vessels approached and started to lay out their nets close to the instruments. Recovery was therefore postponed for 12 hours to avoid any problems, but was routinely made between 11:00 and 16:00 20.09. The location of shots and instruments is shown in Figure 6.3.4.6.1. and the single channel profile in Figure 6.3.4.6.2. All OBH recorded well and the record sections are shown in Figures 6.3.4.6.3 to 6.3.4.6.10. Further details on instrumentation and location can be found in Appendix 9.1.6.

The single channel profile shows the shallow structure of the Oman Basin. Continuous reflections are imaged over the whole section and there is some evidence for short wavelength folding in the middle part of the line and possibly some thrust faulting in the northeast (Figure 6.3.4.6.2).

The eight record sections obtained are all rather similar, indicating only small lateral inhomogeniety. A thick sedimentary pile of 2 s TWT with velocities between 1.8 and 3.5 km/s is seen above the basement reflection, which is clearly visible at zero offset on the OBH data. There seems to be a strong velocity gradient with the sedimentary layers, since double bounce multiples at offsets to more than 20 km are seen. Clear triplications are observed from the crust, and apparent velocities exceeding 8 km/s indicate that the crust/mantle boundary is imaged. Another interesting observation is a strong reflection about 0.6 to 1 s below basement, which is most pronounced on OBH35, 44, and 46. Such a reflection within the oceanic crust is an unusual feature, but has been suggested elsewhere as layer 2 - layer 3 transition (Ranero et al., 1997).

Inversion:

To obtain an idea about the velocity field, we first used „raytomorf" inversion on the first arrivals. Using "suxpicker" of the SU software package (see 6.3.3 for description) 2220 first arrivals could easily be picked on the screen for the 8 OBH stations and were transformed into the MacRay format. Network connection to the Macintosh computers enables a fast exchange of the data files. Interactive raytracing MacRay enables in a quick check to set up a rough a priory model with a set of four gradient layers. This model was converted into a 1 km by 1 km grid and used as a starting model for "raytomorf". Several runs with different smoothing factors and no. of matrix inversions were calculated on the Sun Ultra workstation. The best fitting model (Figure 6.3.4.6.11) was achieved using a smoothing factor of 40. All together 10 internal matrix inversions were applied during 20 recursive iterations of raytomorf. The final error was given with 0.078 s.

Figure 6.3.4.3.11 shows the observed travel times (black) and the calculated arrivals (light grey) in the top section. In the center (50 to 80 km) a maximum reversed coverage of up to 6 fold is achieved. The corresponding cell coverage of the modell is displayed in the lower most section. More than 200 rays passed through some of the cells. Coverage is best between 40 and 90 km of the model down to a depth of 12 km. This is well represented in the distribution of iso-velocity lines in the middle section display. At the borders to the left and right the velocity distribution of the start model is preserved whereas the undulations in the center gave the structure of the covered area. Short distance undulations of the velocity isolines correlate with the coverage and give an implication about the constraints of the method. For interpretation the true distribution of the velocities should be understood as an interpolation along the peaks of the short period undulations. With this in mind a velocity of 4.5 km/s is found at about 6 km depth

at 35 km increasing to 7 km depth at 80 km in the SE which is interpreted as up to 2.5 km of sediment. Termination of the lower crust can be followed by the 6 km/s isoline. This leds to two highs at 45 km (8.5 km depth) and 85 km (9 km depth). At these positions the onset of the 7 km/s isoline indicate Moho highs rising up to about 10 km depth. According to the absence of events continuing as secondary arrivals as well as the absence of reflection events this method will not provide more than such a rough estimate about the crust structure. Nevertheless the mentioned details correspond well with the structure revealed by the raytracing "rayinvr" for two stations of the line. The advantage of this method is its rapid computation time. Including picking of the events this model could be achieved within four to five hours working time. A set of 20 iterations including 10 matrix inversions per run are completed within 20 minutes on the Sun Ultra 1 workstation.

Ray tracing and results:

Record sections along line 6 show considerable uniformity along the line, and the same phases can be identified in most of them. Pre- and post-critical reflections, as well as turning rays, give a tightly constrained structure for the sediment column, and crustal arrivals are seen out to about 50 km range. Arrivals were picked from the two instruments at the ends of the line, OBHs 42 and 48, and modelled by raytracing with Rayinvr. Initially a one-dimensional model was constructed for OBH 42, since the record section shows a high degree of symmetry. Velocities in the uppermost sediment layers, for which no picks were made, were based on velocity analyses of multichannel data from Dalrymple Trough. The one-dimensional model was perturbed to account for small asymmetries in the arrivals, and then used as a basis for modelling OBH 48. Lateral variations in layer thicknesses were introduced first, while velocities within layers were varied only when this appeared necessary as well. No inversion steps were attempted, since the model at this stage is overparameterised for number of receivers used.

The resulting velocity models beneath the two receivers are shown in Figure 6.3.4.6.12. Correlation with the crossing multichannel profile CAM29 (Figure 2.3) shows that acoustic basement corresponds to the top of the 5.2-5.5 km/s layer, so there are 4-5 km of sediment. Sediment velocities reach values in excess of 4 km/s, but the variation with depth is similar to that found by Minshull and White (1989) in the abyssal plain seaward of the Makran accretionary wedge. The velocity model for the crust is strongly dependent on how the high-amplitude phases at 20-50 km range are modelled. These have been interpreted as reflections because of their high amplitudes. The crustal velocity structure beneath OBH 42 is typically oceanic, with a 2 km Layer 2 and a 5 km Layer 3. However, the very sharp boundary between these layers is unusual, and indicates a particularly well-stratified crustal section, and the Layer 2 arrivals are unusually weak. Both Layer 2 and Layer 3 are about 1 km thinner beneath OBH48.

Some modelling of the later, slower phases at 10-20 km range was also attempted. These could not be modelled as P wave arrivals from the sediment column, and must therefore be converted S waves. They appear to be turning within oceanic Layer 2 or reflecting at its base. However, it is difficult to identify which boundary generates the mode conversions without synthetic seismogram modelling.

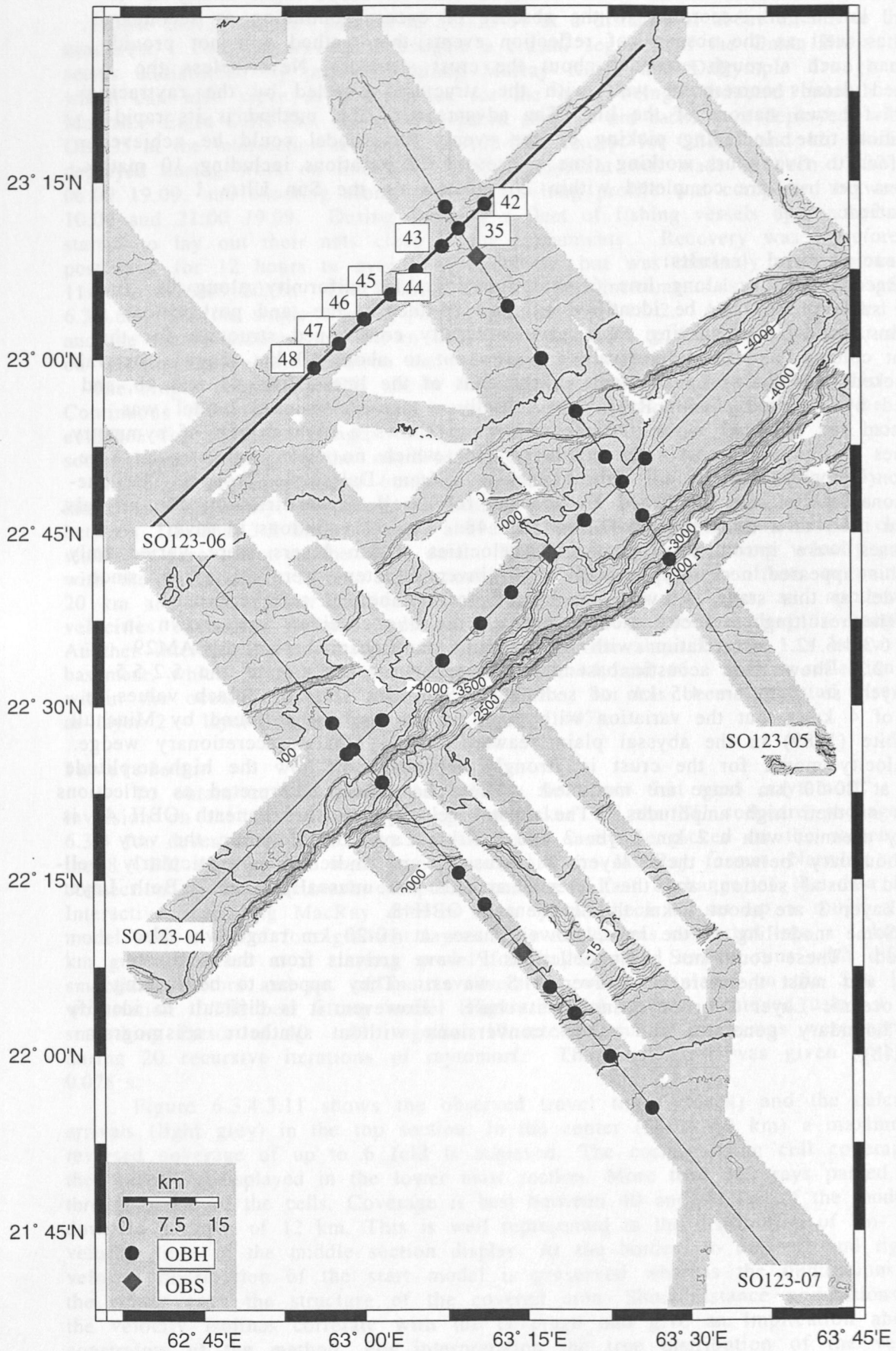

Figure 6.3.4.6.1: Location map of profile SO123-06.

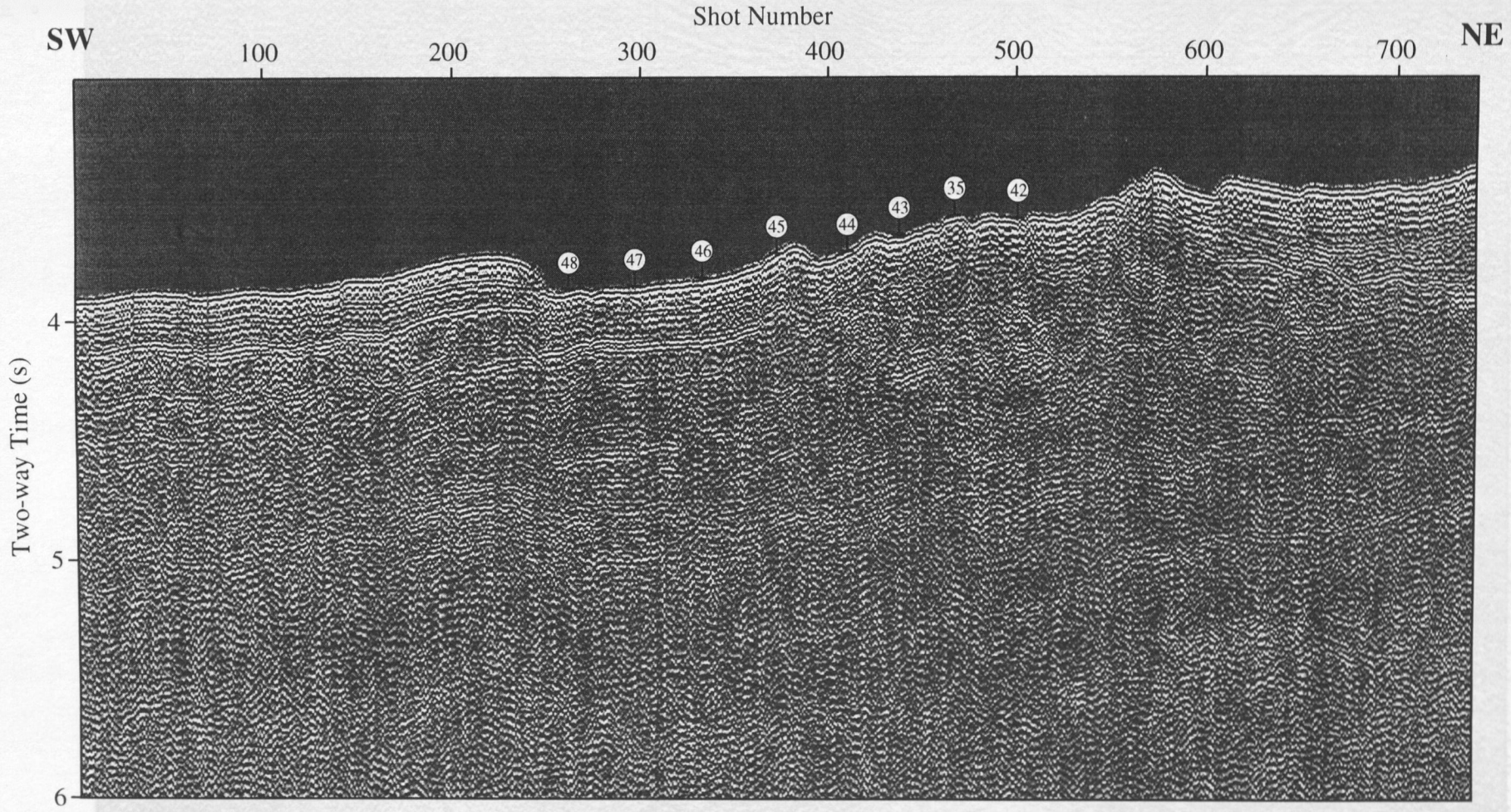

Figure 6.3.4.6.2: Single channel seismic profile SO123-06 (VE=25:1 at the sea-floor). Numbers at the sea-floor mark OBH positions.

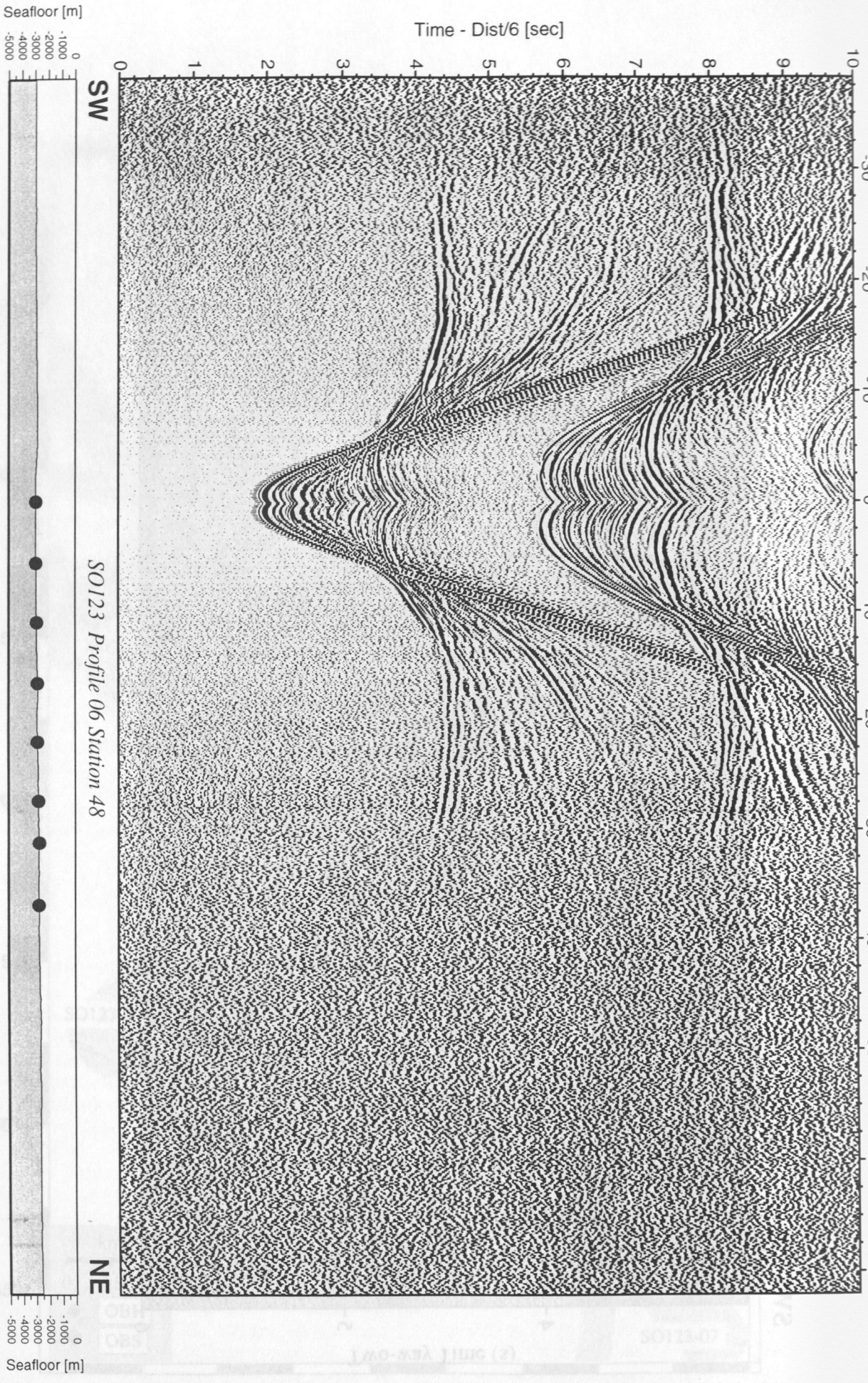

Figure 6.3.4.6.3: Record section from OBH 48, Profile 06.

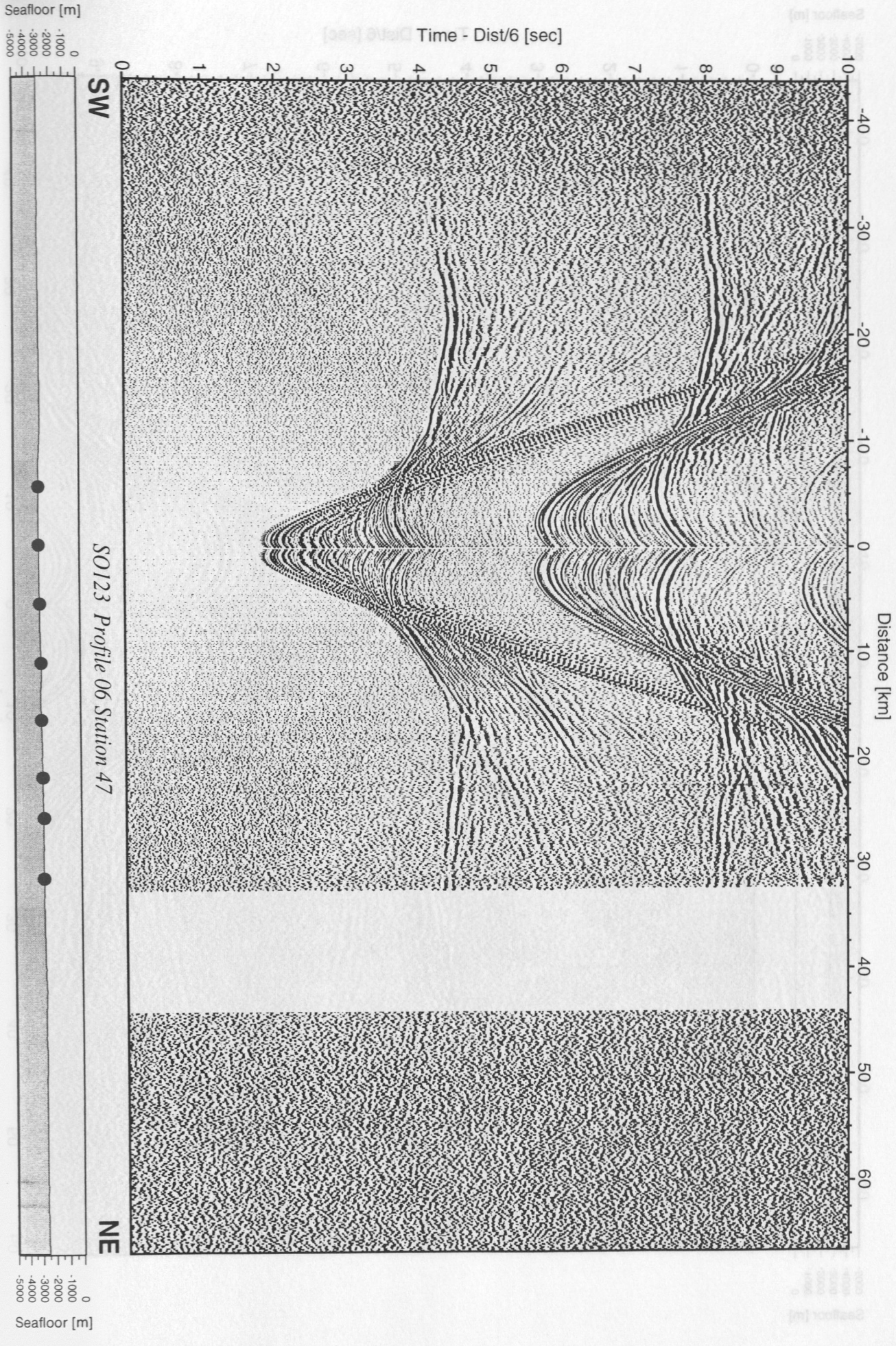

Figure 6.3.4.6.4: Record section from OBH 47, Profile 06.

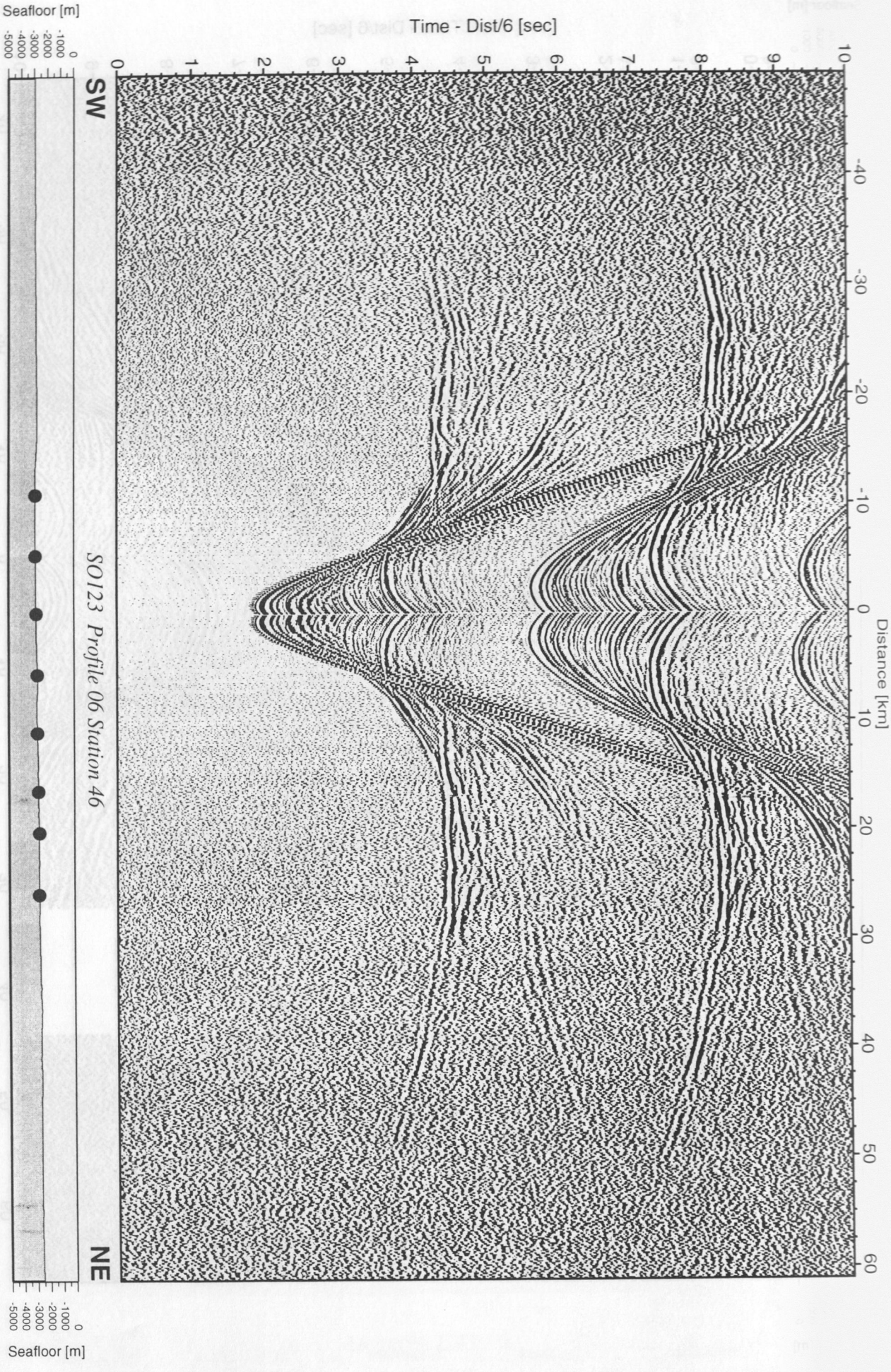

Figure 6.3.4.6.5: Record section from OBH 46, Profile 06.

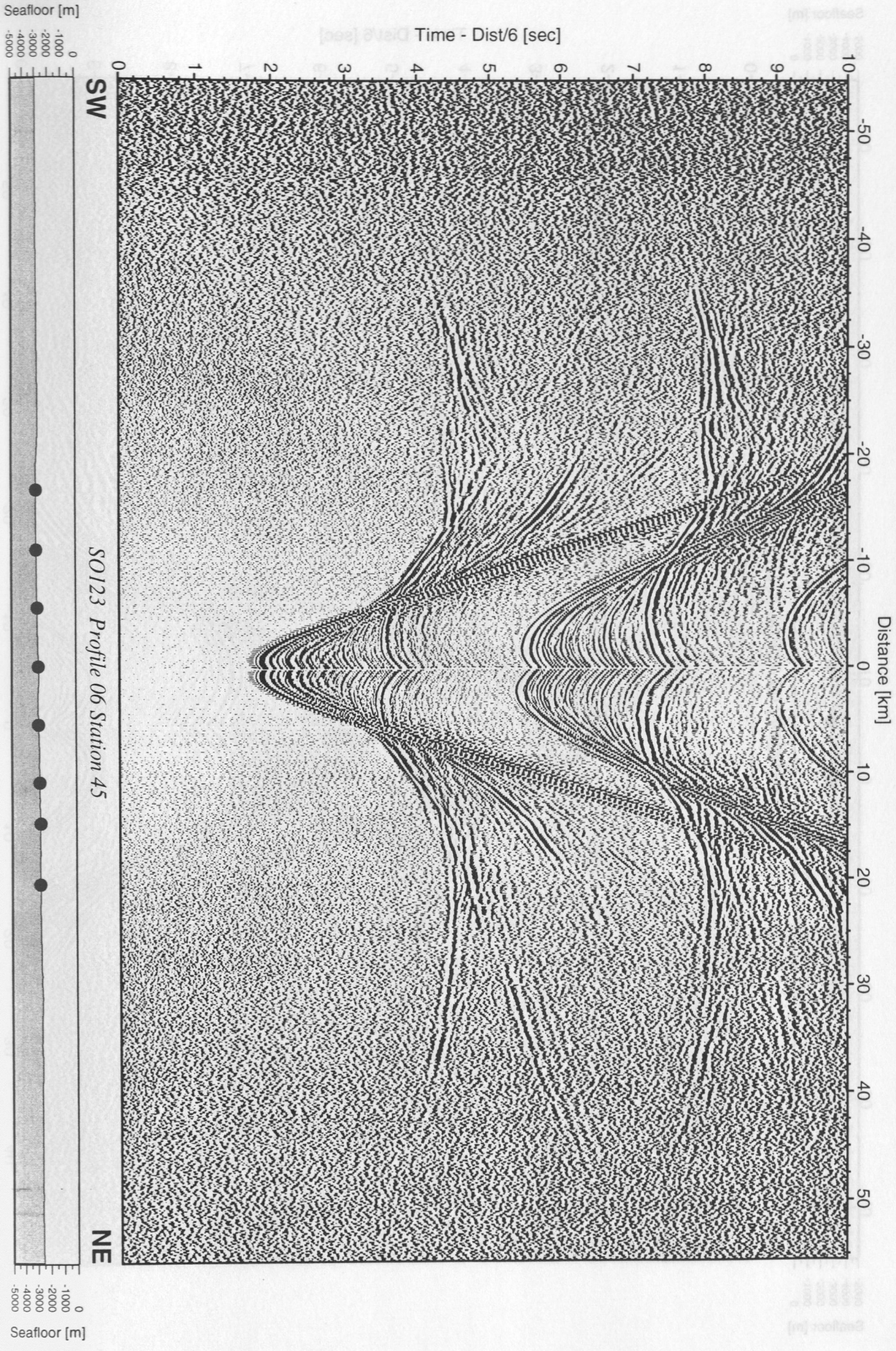

Figure 6.3.4.6.6: Record section from OBH 45, Profile 06.

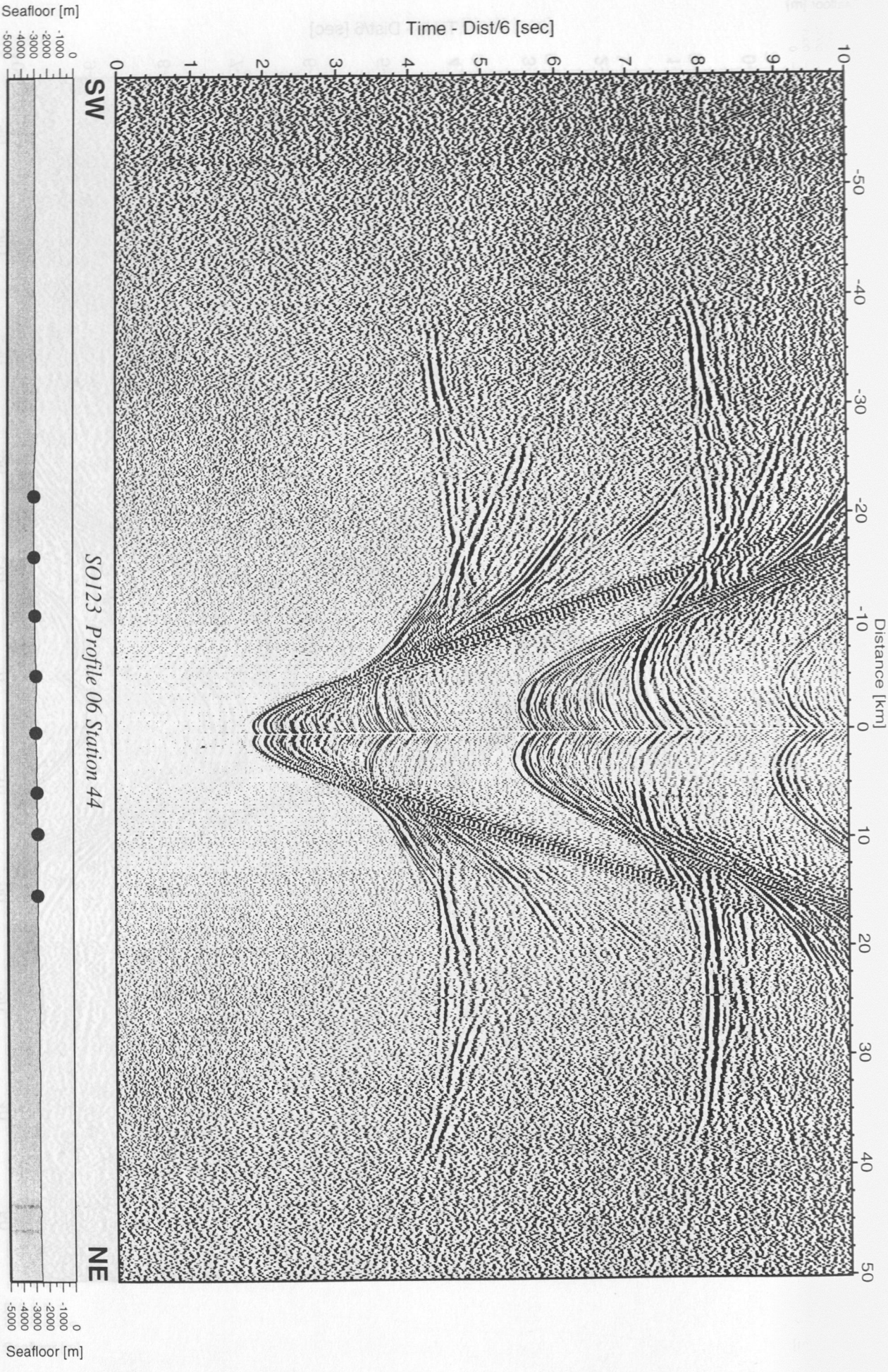

Figure 6.3.4.6.7: Record section from OBH 44, Profile 06.

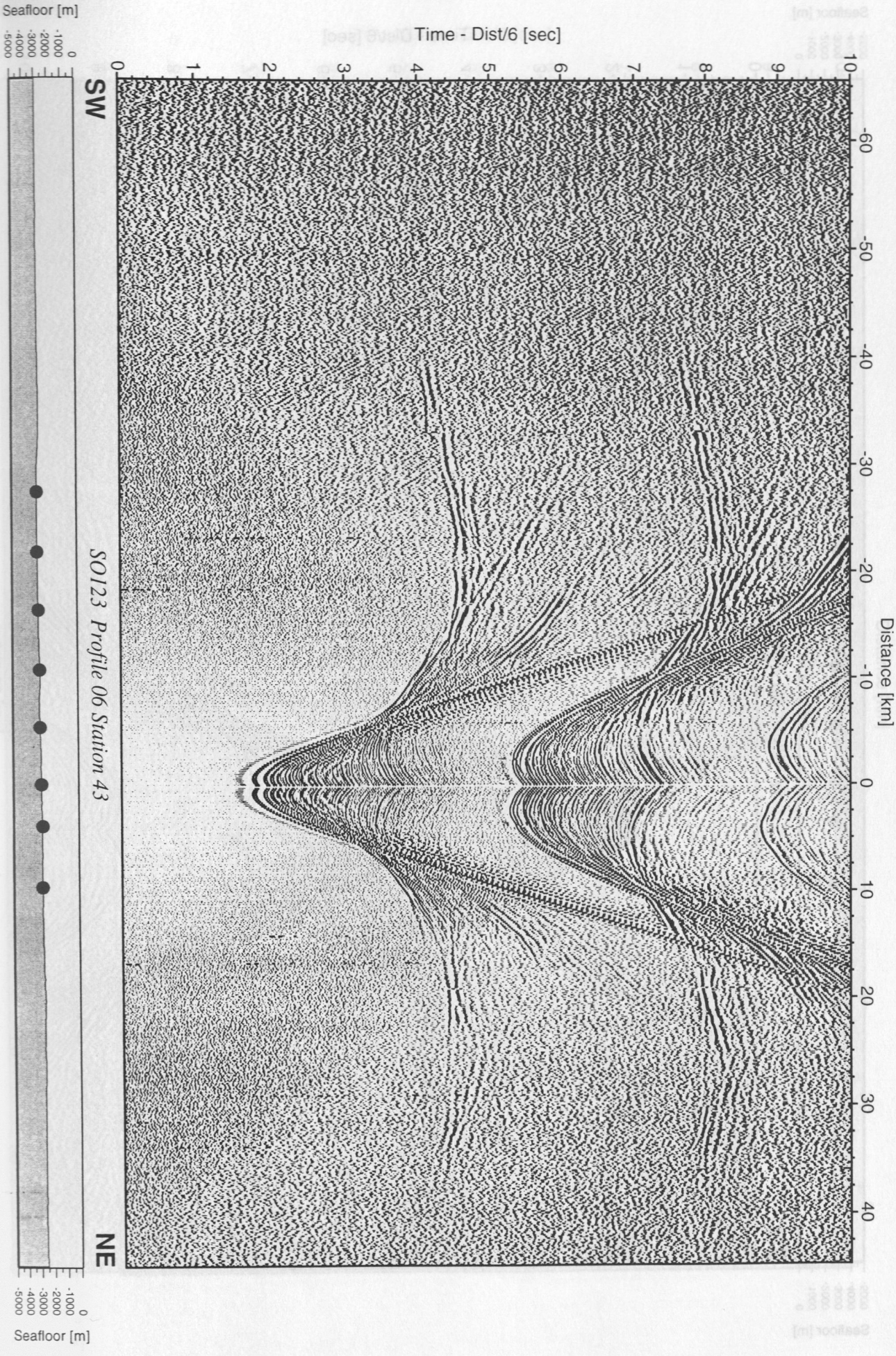

Figure 6.3.4.6.8: Record section from OBH 43, Profile 06.

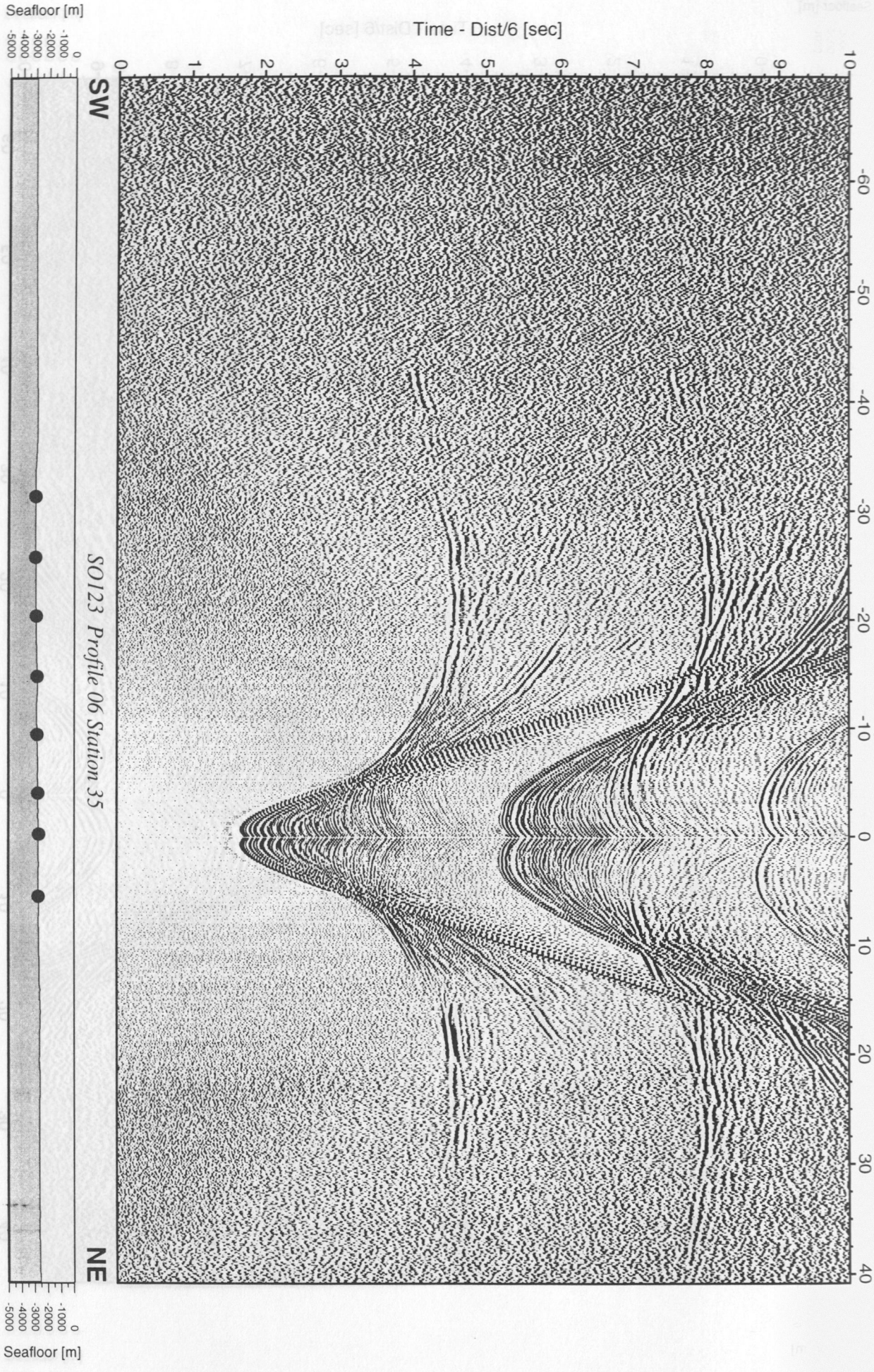

Figure 6.3.4.6.9: Record section from OBH 35, Profile 06.

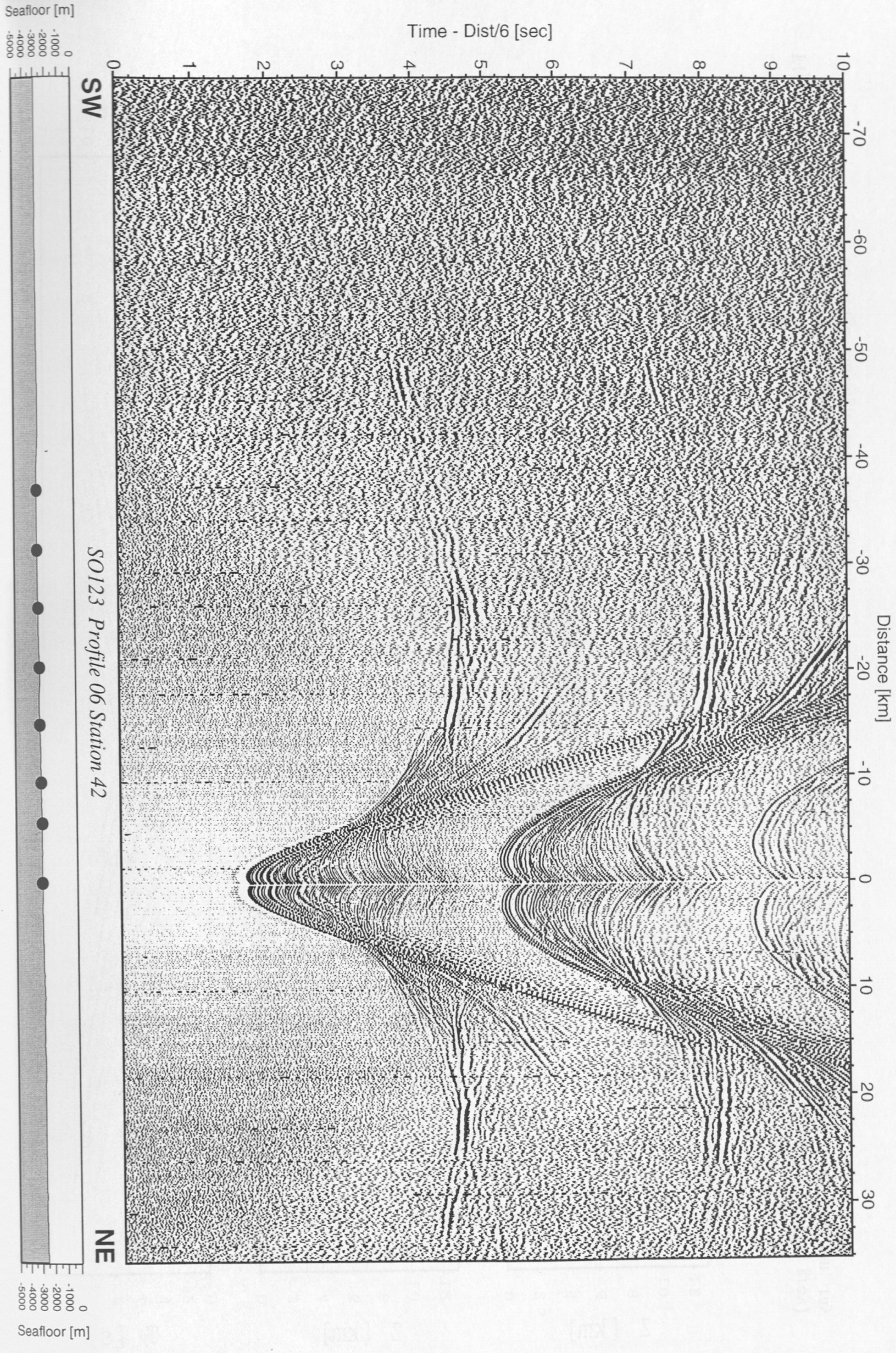

Figure 6.3.4.6.10: Record section from OBH 42, Profile 06.

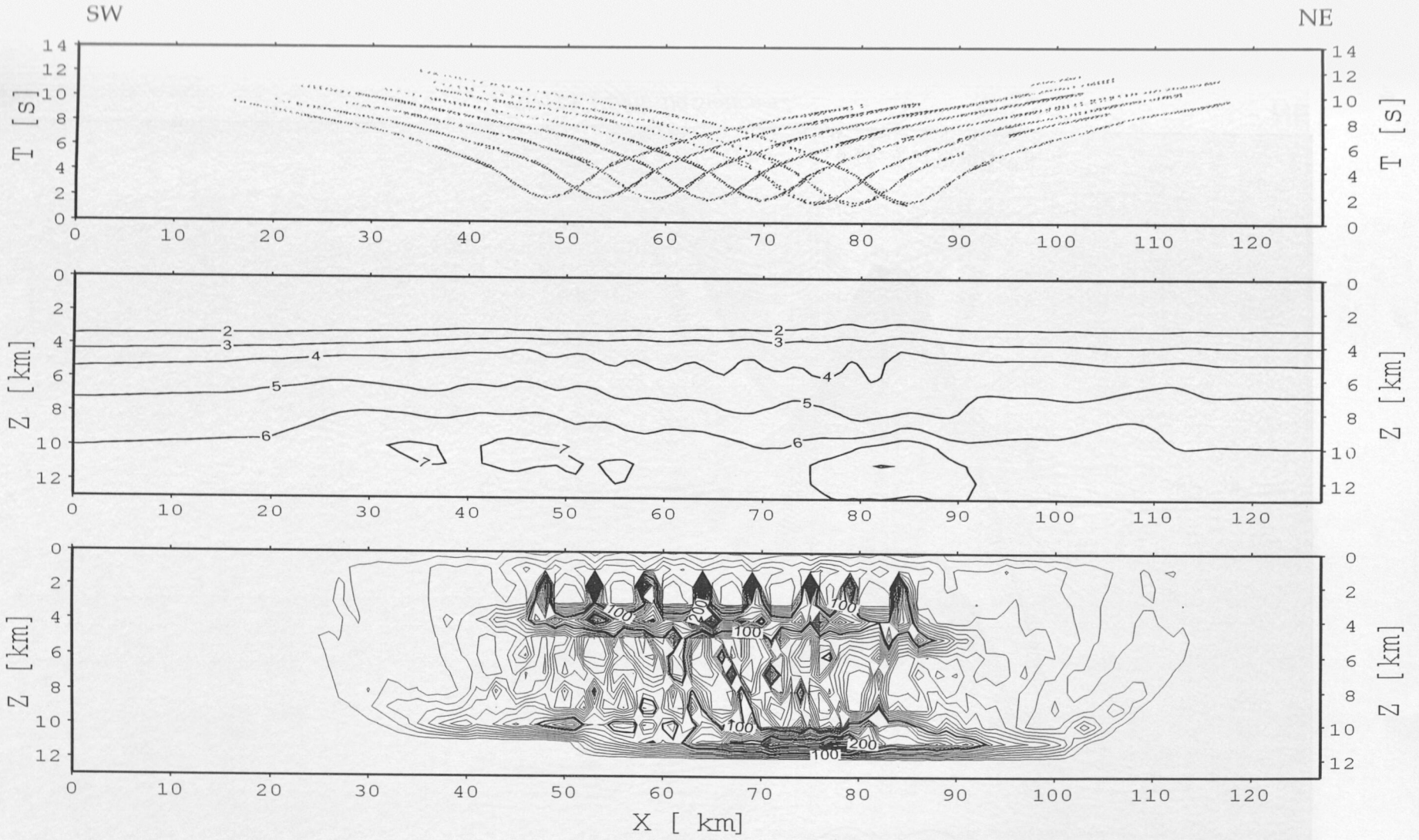

Figure 6.3.4.6.11: Result of the finite-difference inversion with "raytomorf"; top: observed (black) and calculated (light grey) arrival times; middle: velocity model after 20 iterations; final error: 0.078 s grid size: 1 km * 1 km; bottom: ray coverage through the final model.

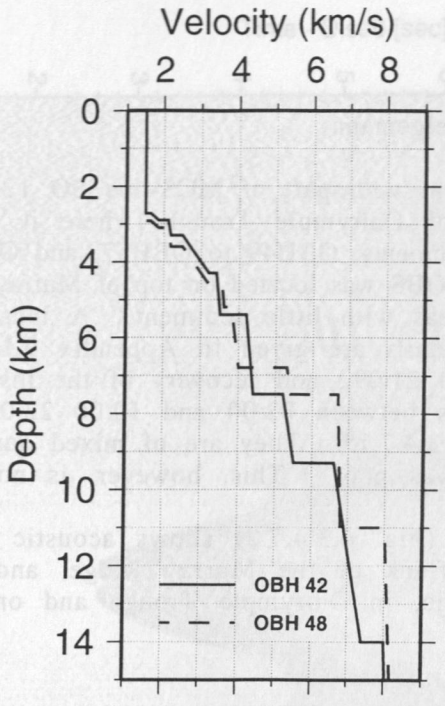

Figure 6.3.4.6.12: Vertical sections through two-dimensional velocity model at the two instrument locations.

6.3.4.7 Profile SO123-07

(T. Minshull, D. Klaeschen, H. Lelgemann)

Profile SO123-07 is coincident with part of MCS-line SO 122-04 and crosses Murray Ridge and the southwestern end of Dalrymple Trough, where it also intersects Profile SO123-04. Deployment of ten instruments, OBH49 to OBH57, and OBS04 was made between 20:00 20.09. and 01:30 21.09. The OBS was located on top of Murray Ridge, also to test coupling of the seismometer in areas with little sediment. A location map is shown in Figure 6.3.4.7.1, and instrument details are given in Appendix 9.1.7. Shooting was done at 5 knots between 5:00 and 22:00 21.09., and recovery of the instruments was accomplished without any problems between 02:00 and 10:00 22.09. All record sections are shown in Figure 6.3.4.7.3 to 6.3.4.7.15. They are of mixed quality, especially on Murray Ridge signal penetration was poor. This, however, is not uncommon for volcanic areas.

The single channel profile (Fig. 6.3.4.7.2) shows acoustic basement dipping steeply beneath the southeastern flank of the Murray Ridge, and layered sediment on the northwestern flank of the ridge, in Dalrymple Trough and on the Arabian plate to the northwest.

Ray tracing and inversion:

The record sections show clear arrivals for shots on the Indus Fan recorded on instruments to the southeast of the Murray Ridge, and also for raypaths down the northeastern flank of Murray Ridge and across Dalrymple Trough. These parts of the velocity structure will be well constrained by the data. Velocities in the upper part of the Murray Ridge are also sampled by OBHs 52-54, but no Moho reflections are observed from this area. Hence the crustal thickness beneath the bathymetric high of the Murray Ridge will not be constrained by these data. Two instruments were selected for traveltime modelling with Rayinvr: OBHs 57 and 52. Shots to the southeast recorded on OBH57, on the Indus Fan, resulted in a relatively simple set of arrivals which could be modelled by an approximately one-dimensional structure (Figure 6.3.4.7.16). Based on comparison with multichannel profiles from SO-122, acoustic basement may be identified as the base of the layer with velocities 4.4-4.7 km/s. Hence there are about 6.5 km of sediment beneath this OBH. The underlying crustal layer is very thin, only about 4 km beneath the OBH, and arrivals turning within this layer indicate relatively high velocities of 6.7-7.5 km/s. A lower velocity upper crustal layer could be present but hidden. The nature of this crust is uncertain; it could be thin oceanic crust, thinned continental crust or serpentinised mantle. The velocity structure resembles that found in some ocean-continent transition zones on non-volcanic rifted margins. The data from OBH 52, where only a thin sediment cover is present, show low velocities of 4.2-4.3 km/s in the upper 2 km of acoustic basement. The deeper structure is not well constrained, but the low apparent velocity of the PmP arrival indicates that the Moho dips steeply toward Dalrymple Trough, and the data are consistent with a thick, low-velocity crust beneath the trough, as observed on Line 4.

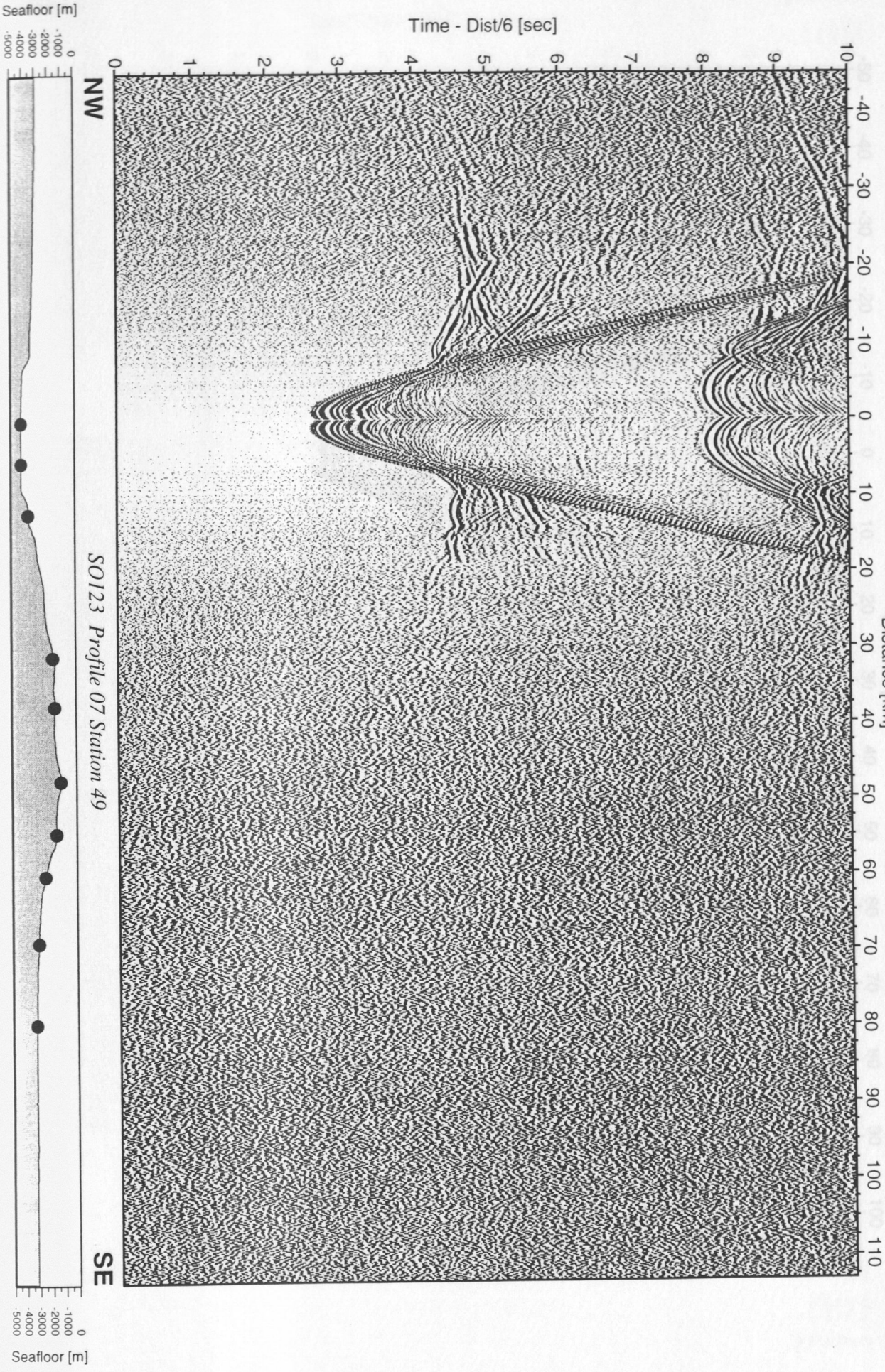

Figure 6.3.4.7.3: Record section from OBH 49, Profile 07.

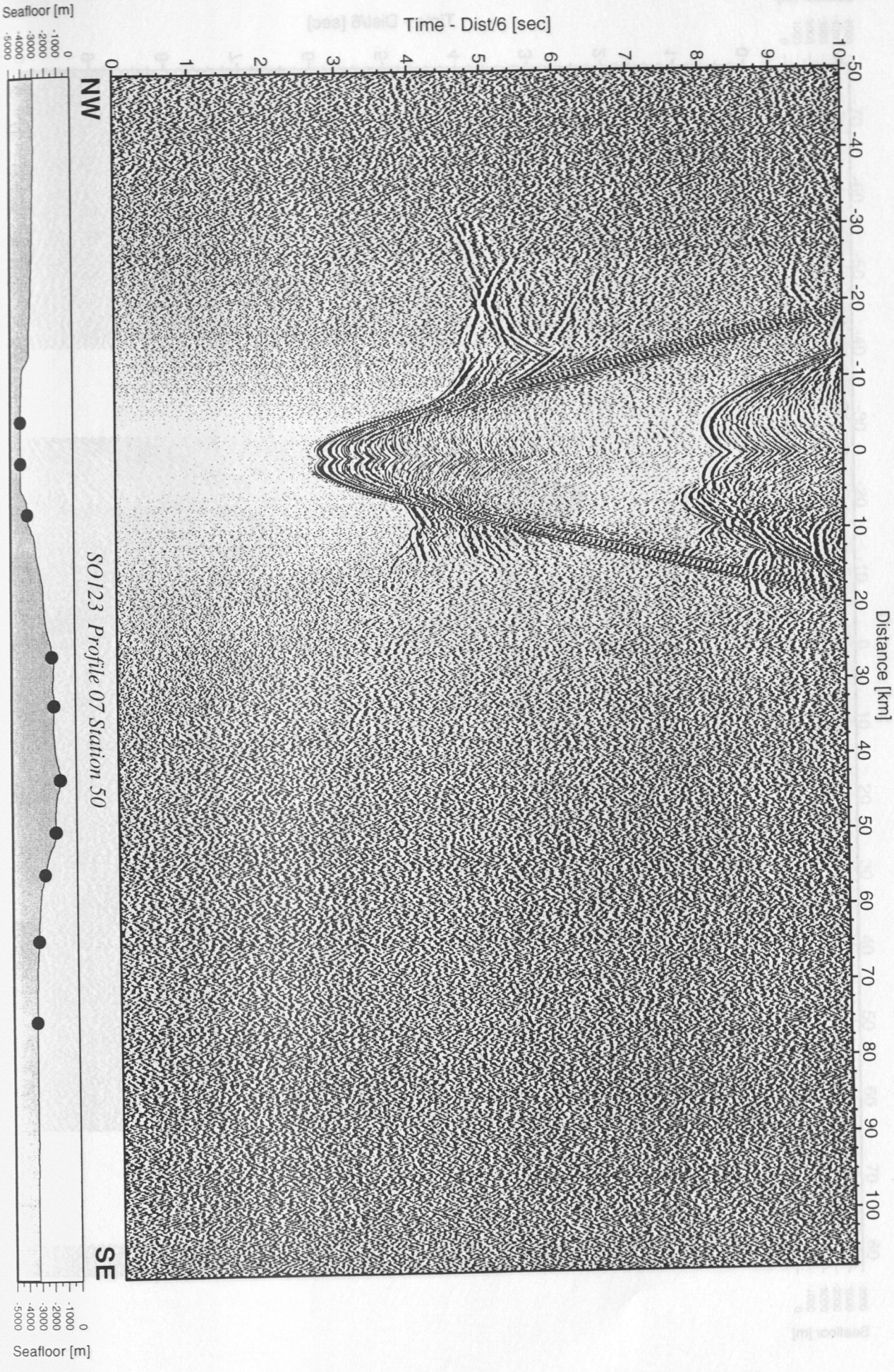

Figure 6.3.4.7.4: Record section from OBH 50, Profile 07.

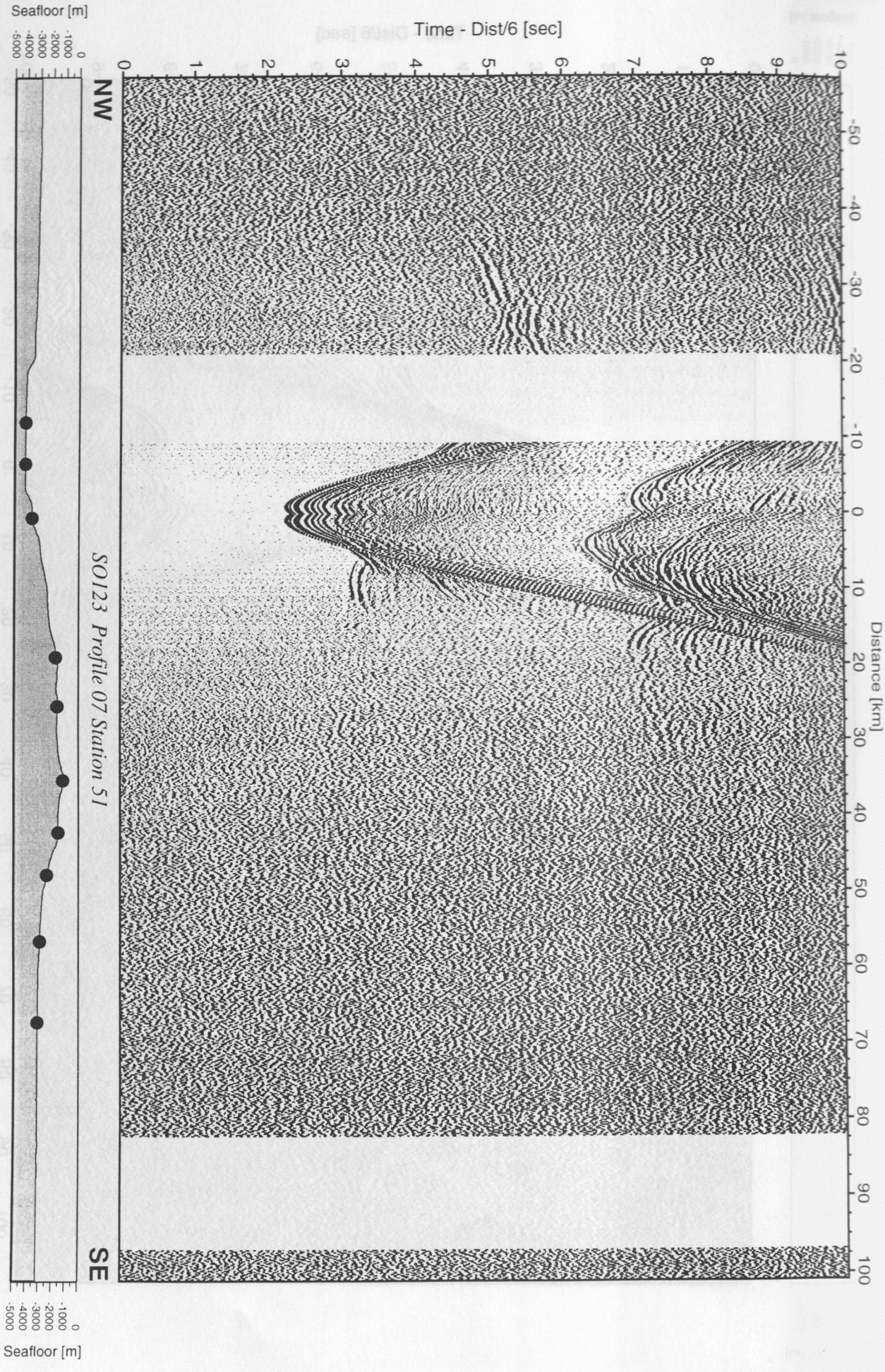

Figure 6.3.4.7.5: Record section from OBH 51, Profile 07.

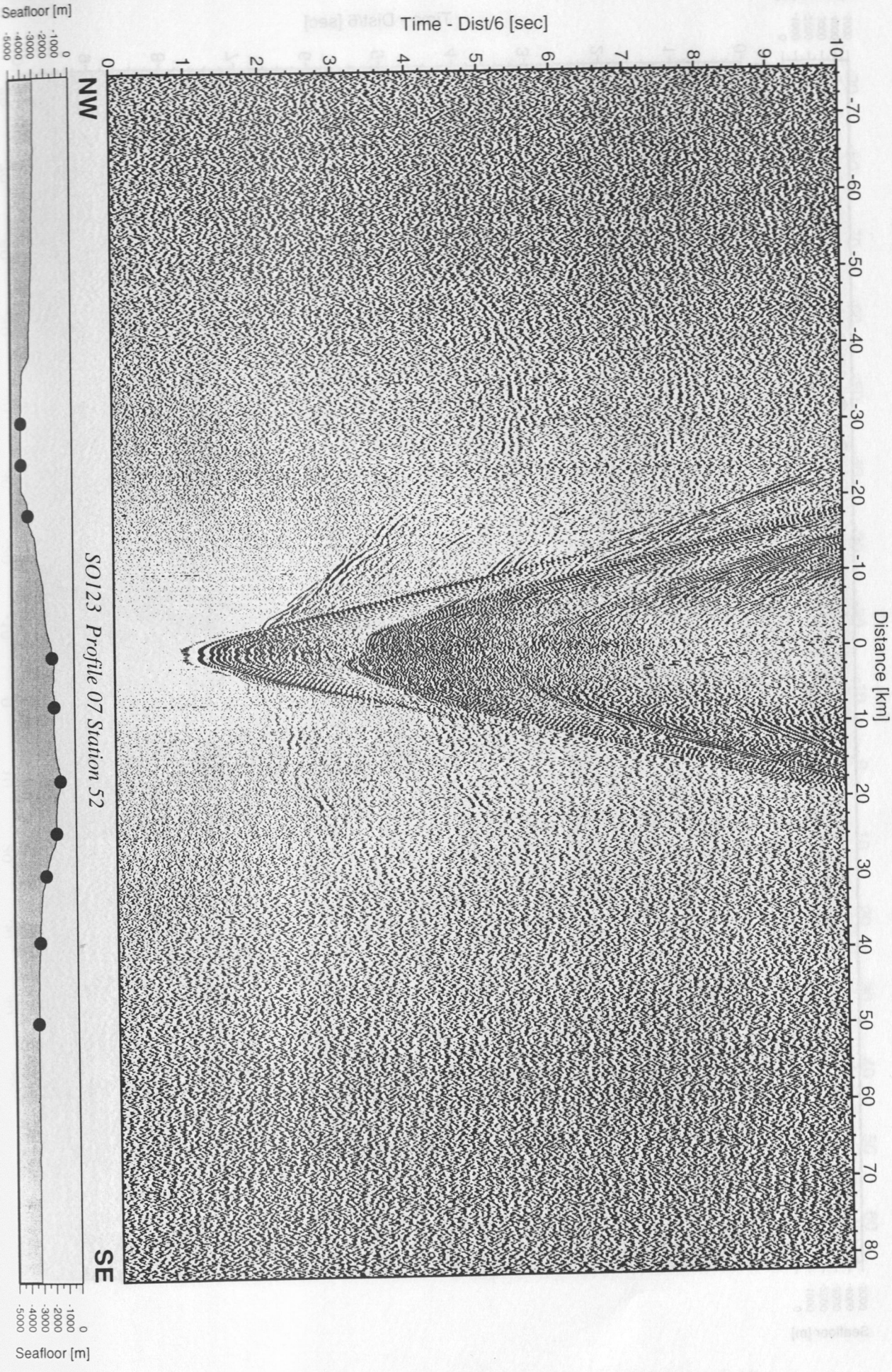

Figure 6.3.4.7.6: Record section from OBH 52, Profile 07.

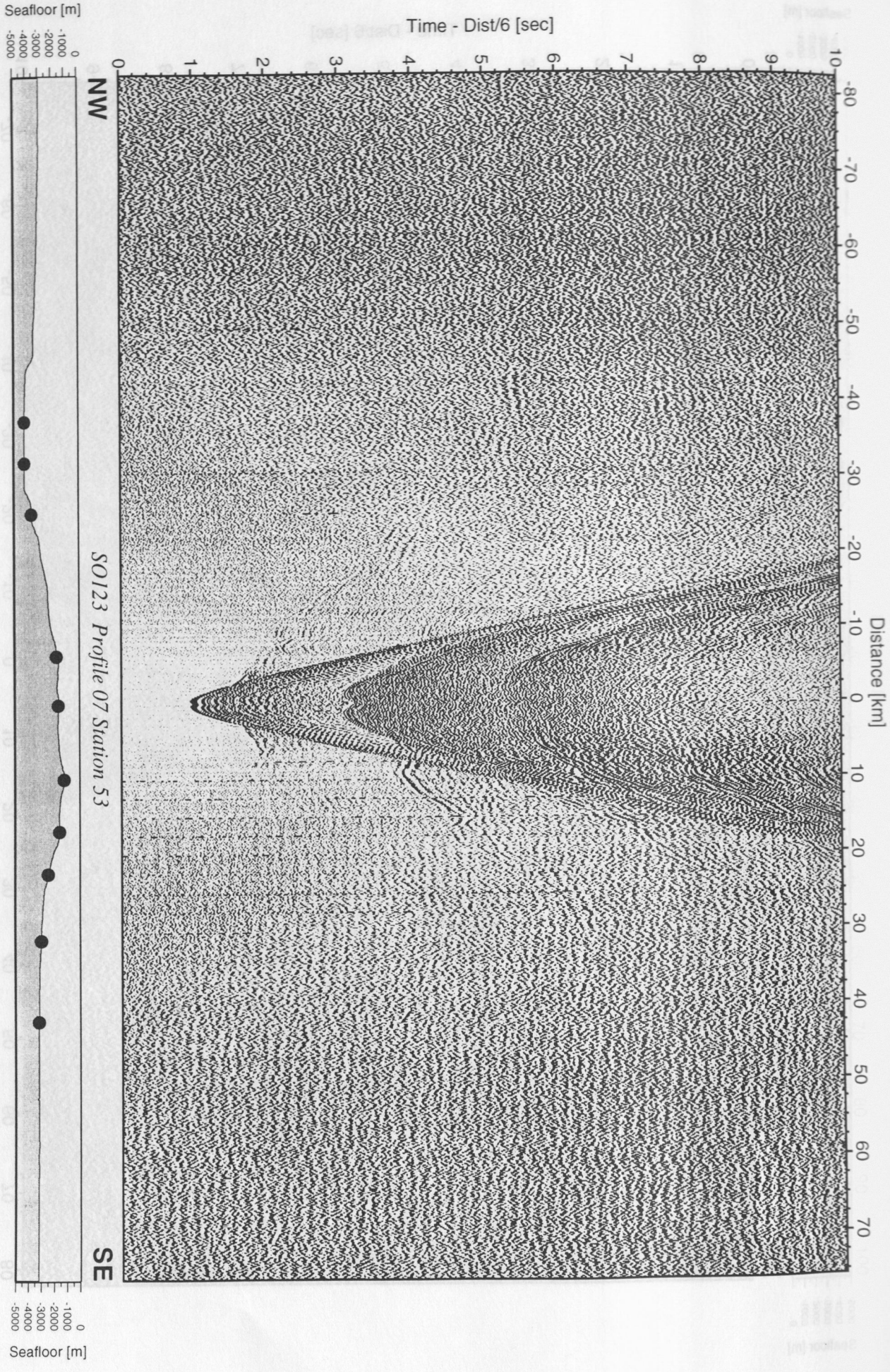

Figure 6.3.4.7.7: Record section from OBH 53, Profile 07.

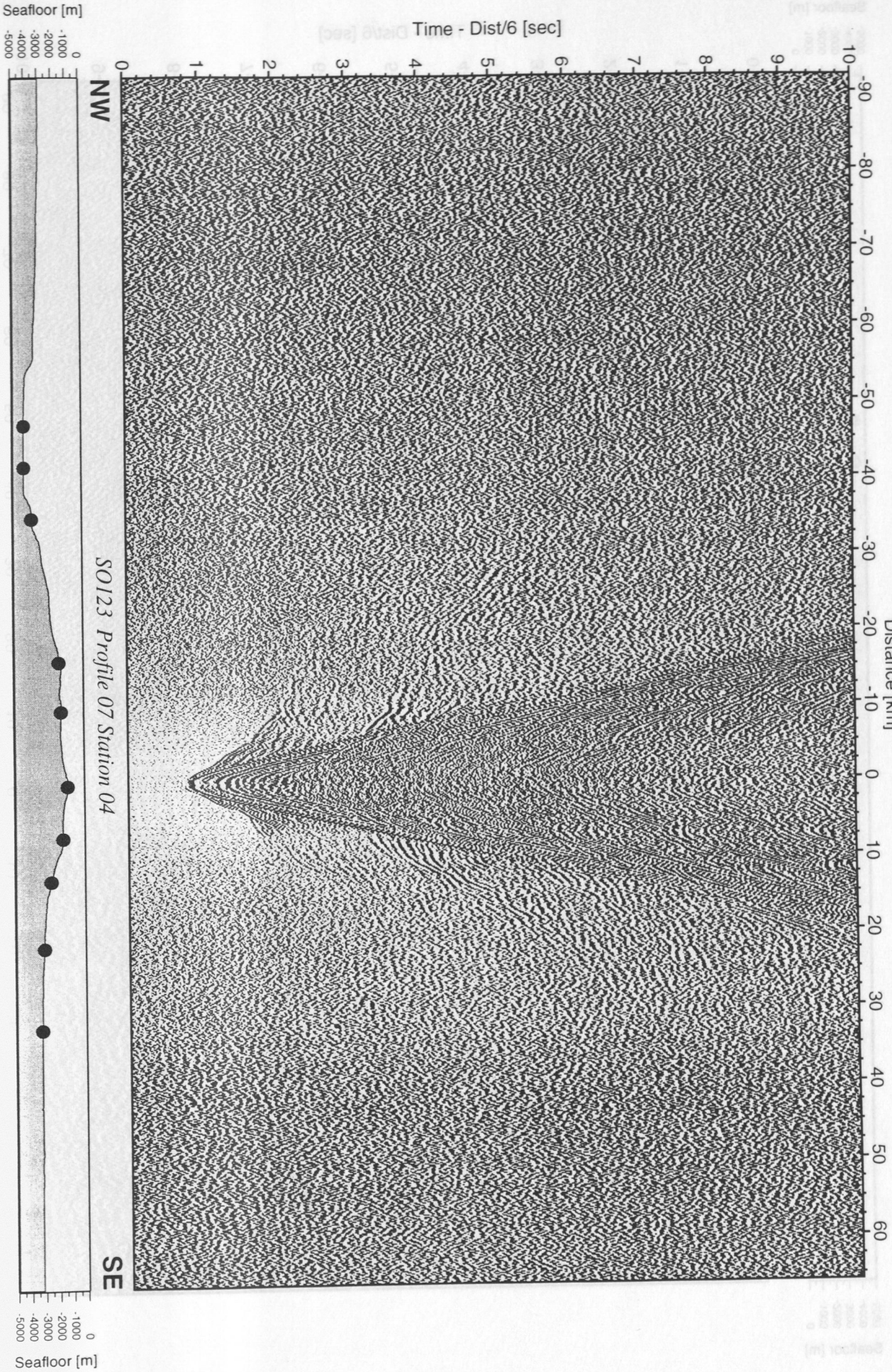

Figure 6.3.4.7.8: Record section from OBS 04, Profile 07, hydrophone.

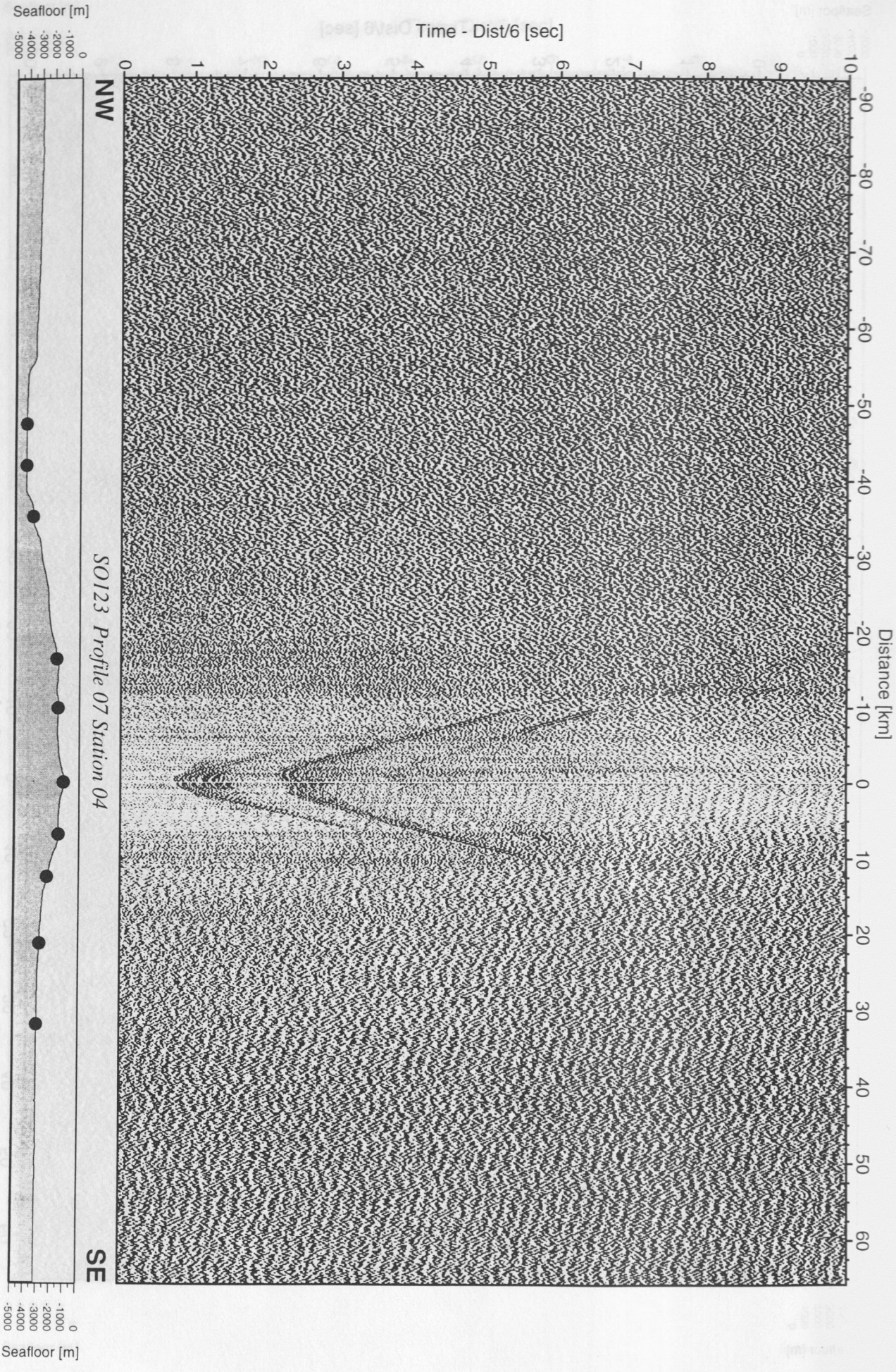

Figure 6.3.4.7.9: Record section from OBS 04, Profile 07, vertical component.

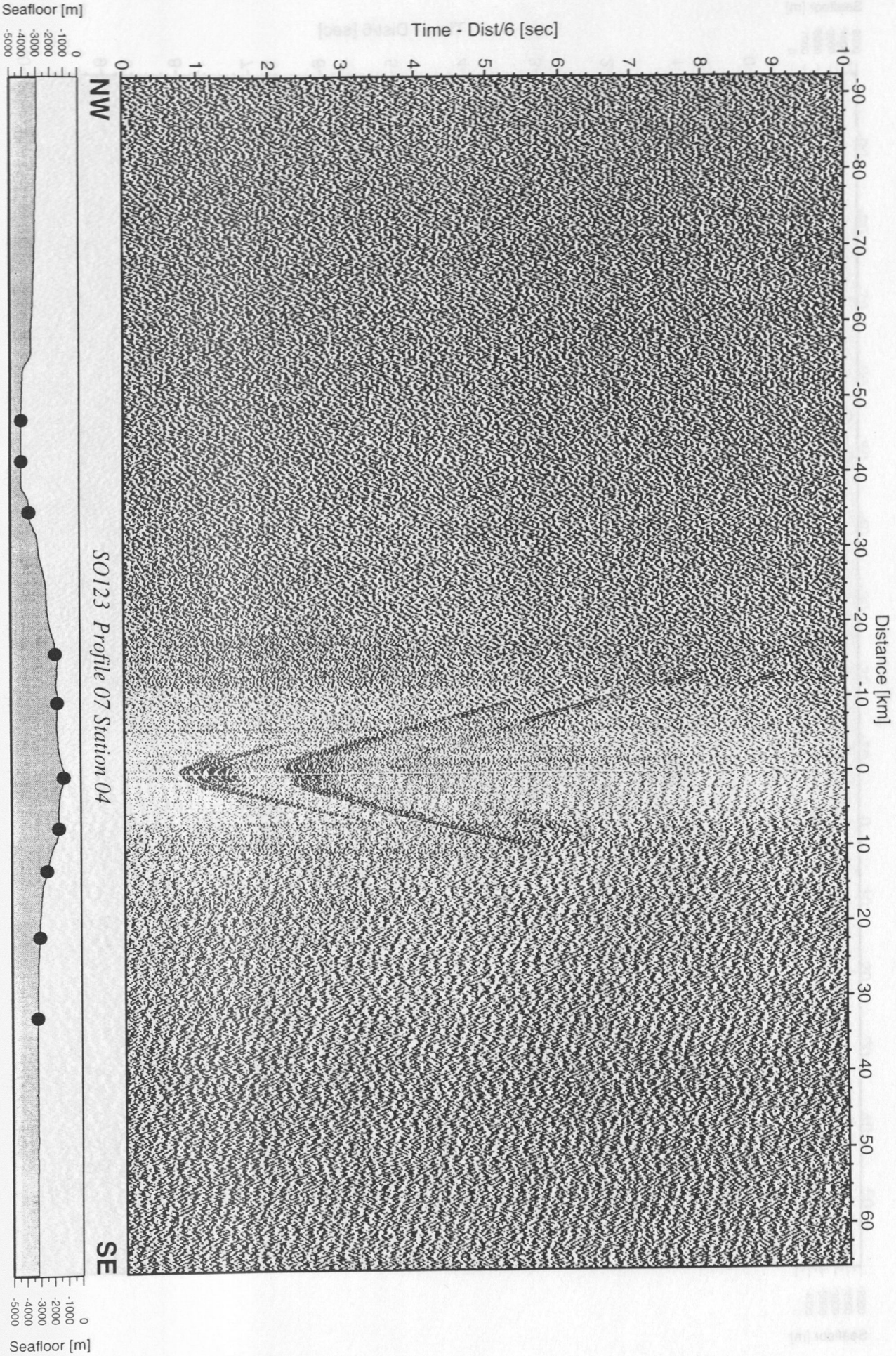

Figure 6.3.4.7.10: Record section from OBS 04, Profile 07, horizontal component.

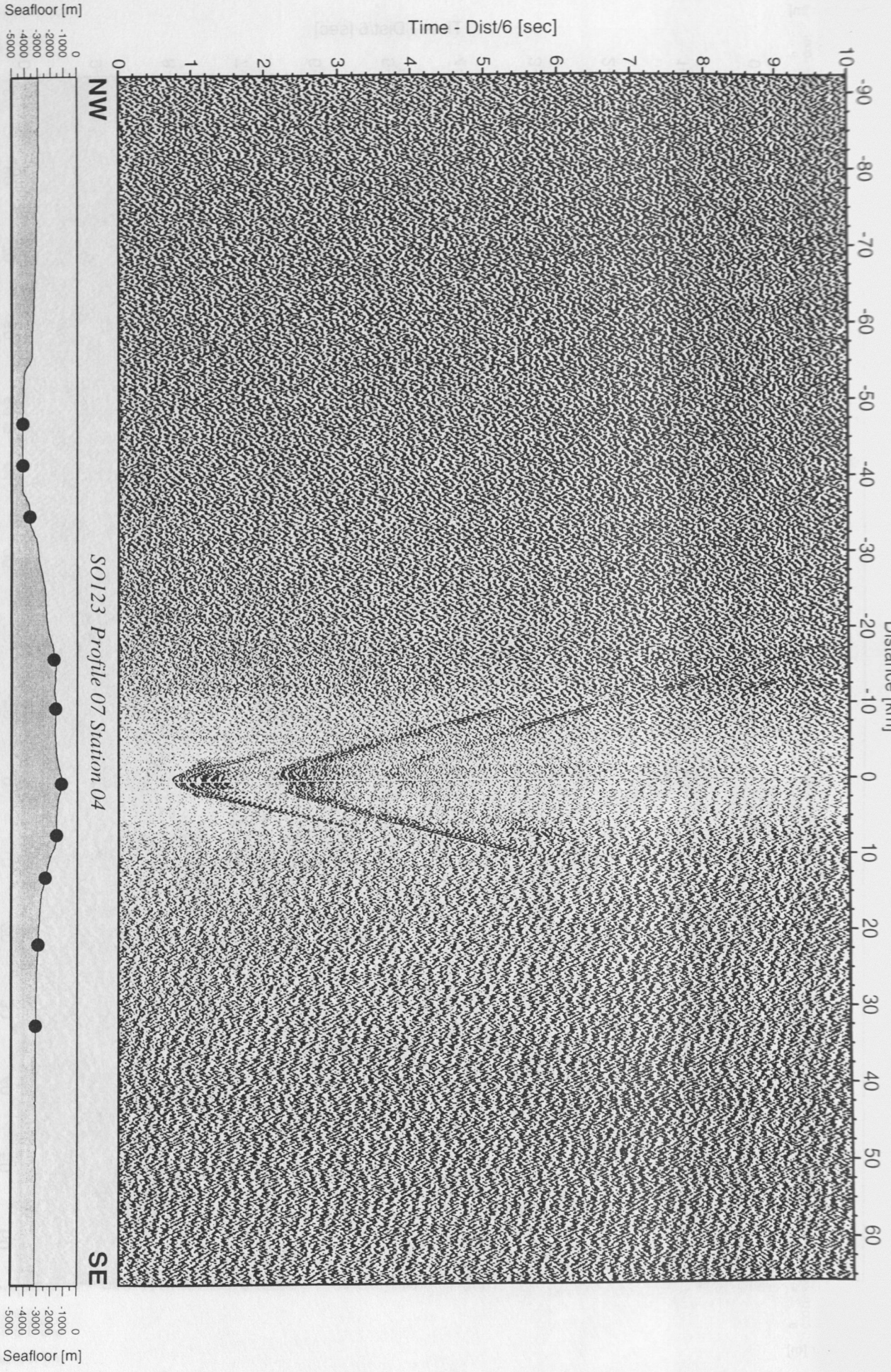

Figure 6.3.4.7.11: Record section from OBS 04, Profile 07, horizontal component.

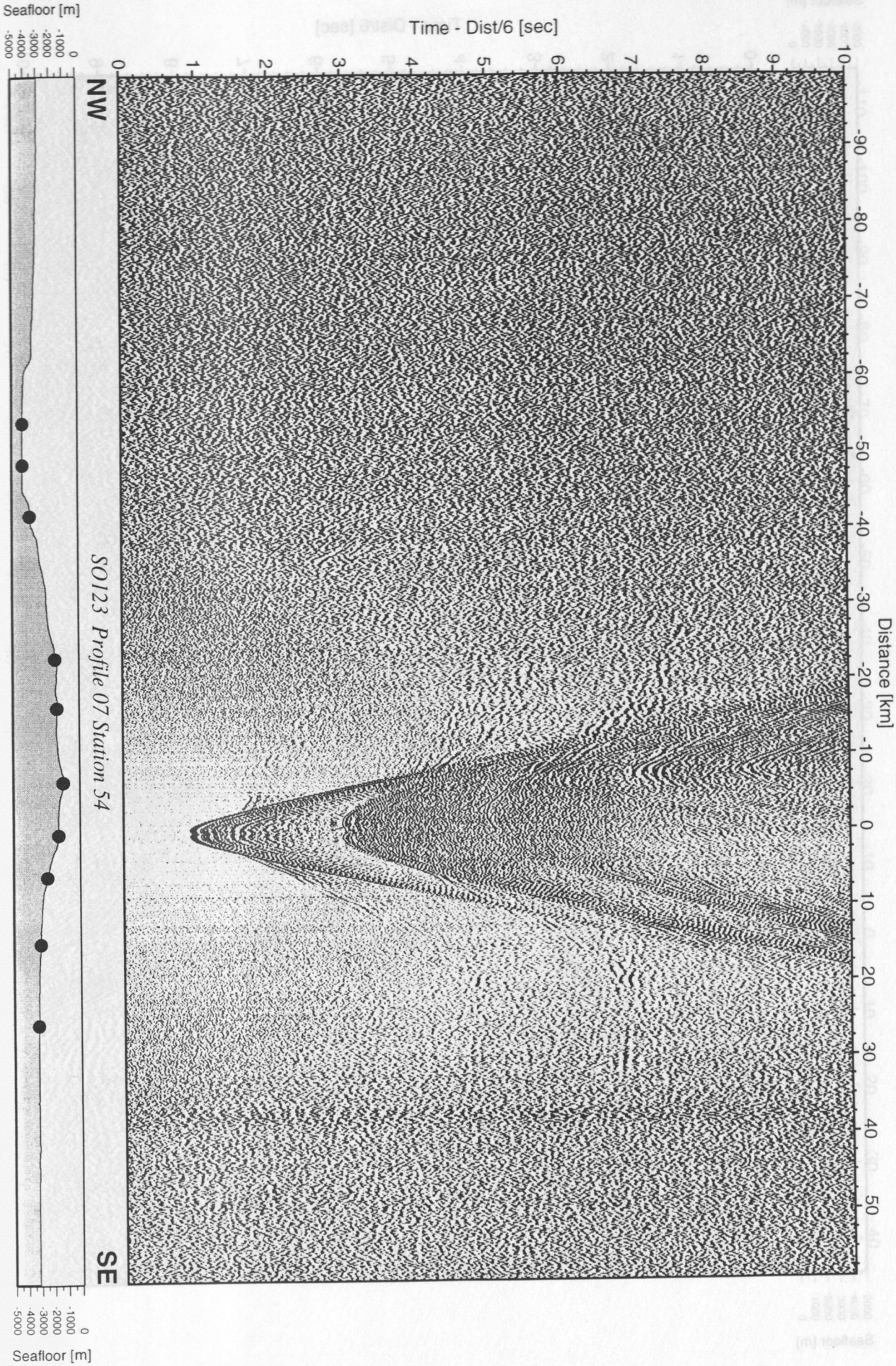

Figure 6.3.4.7.12: Record section from OBH 54, Profile 07.

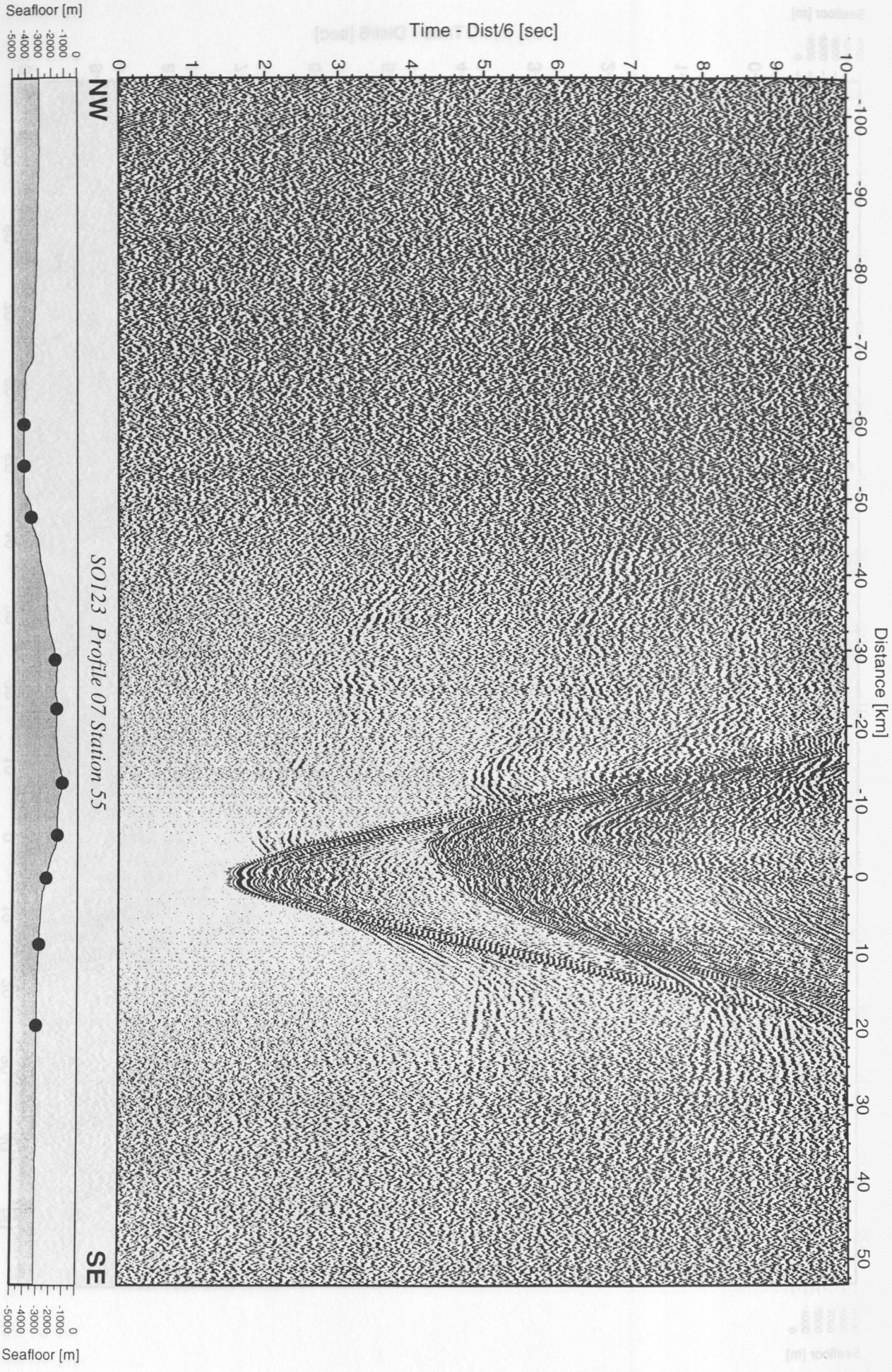

Figure 6.3.4.7.13: Record section from OBH 55, Profile 07.

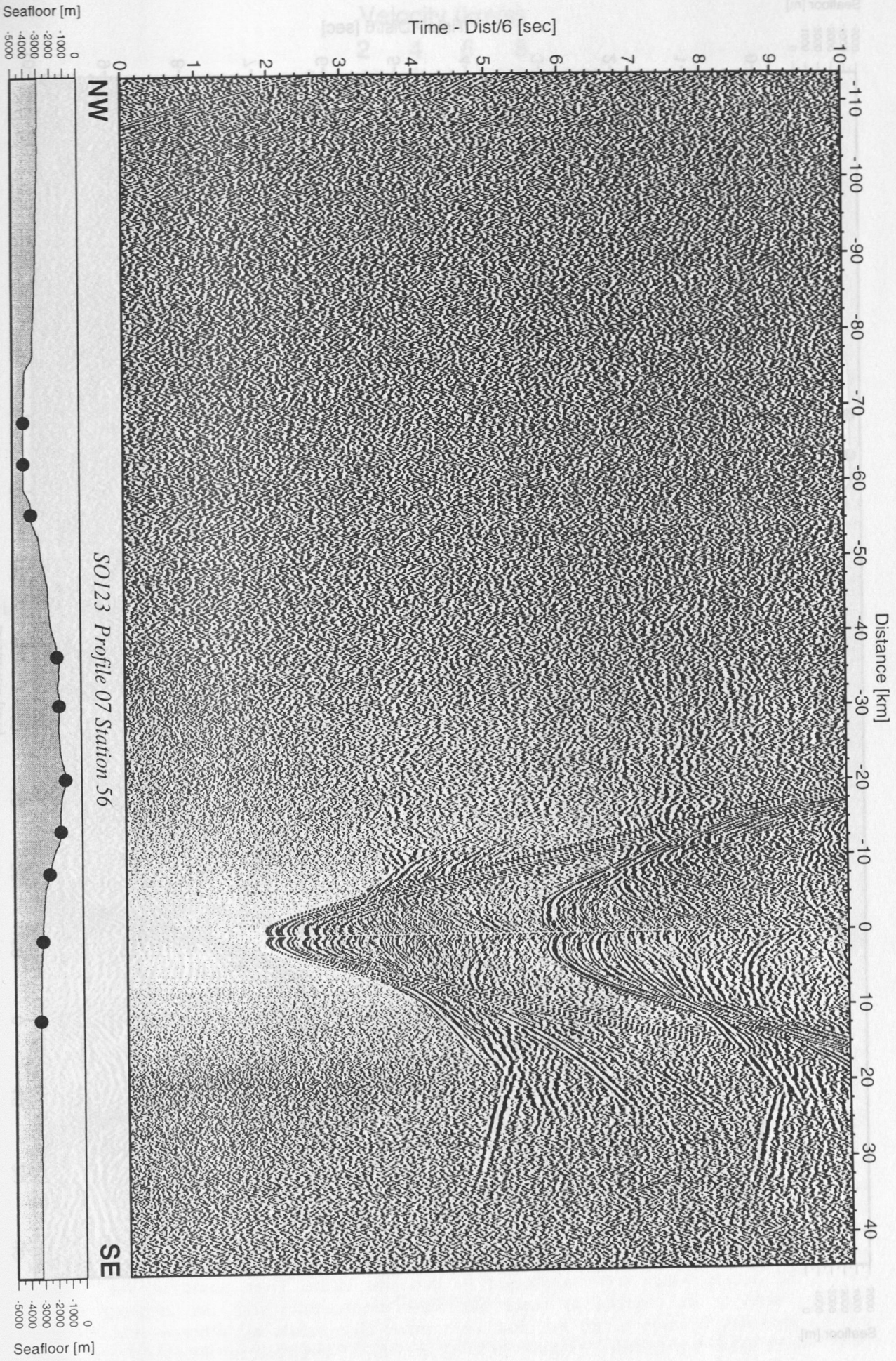

Figure 6.3.4.7.14: Record section from OBH 56, Profile 07.

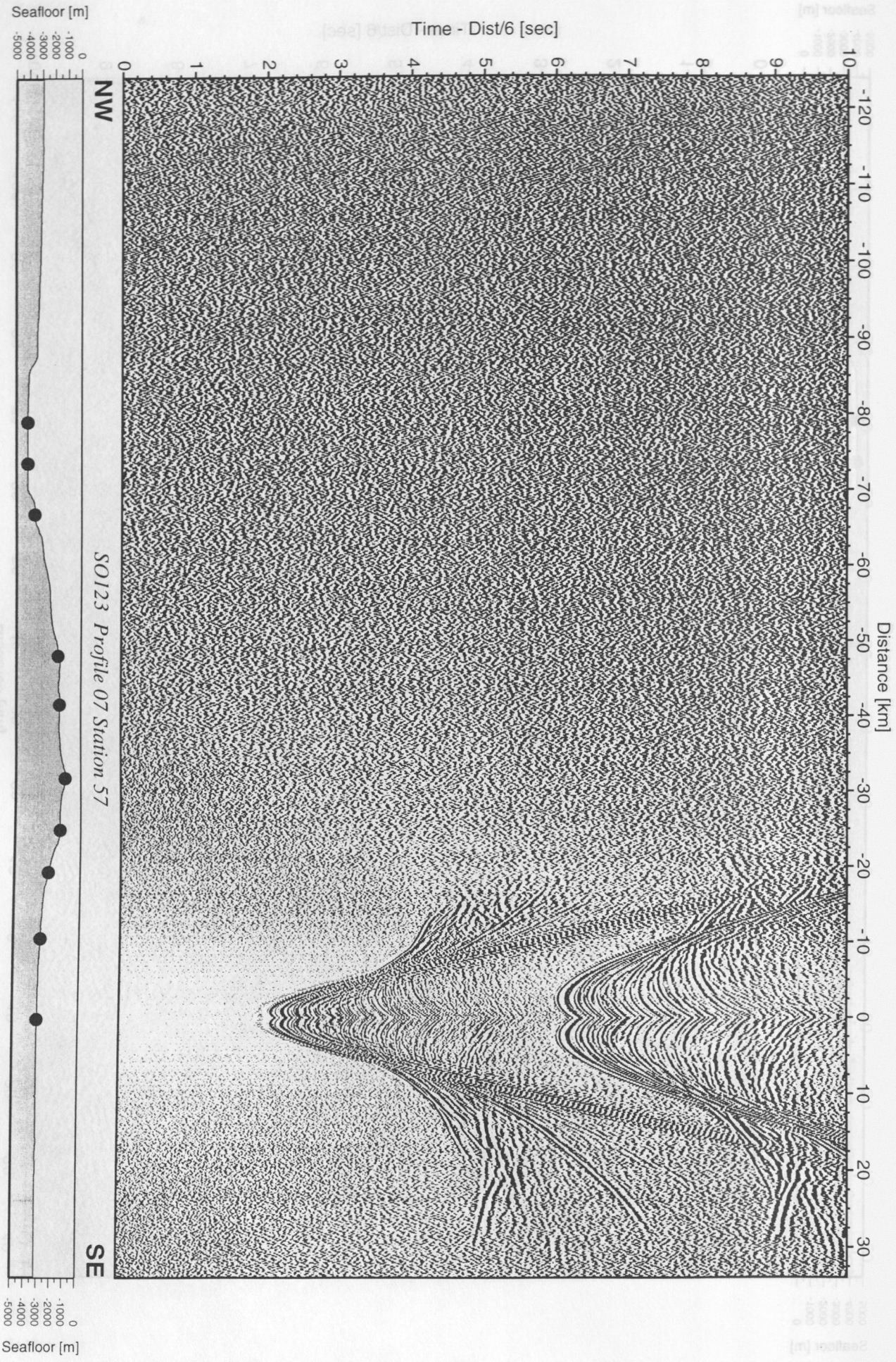

Figure 6.3.4.7.15: Record section from OBH 57, Profile 07.

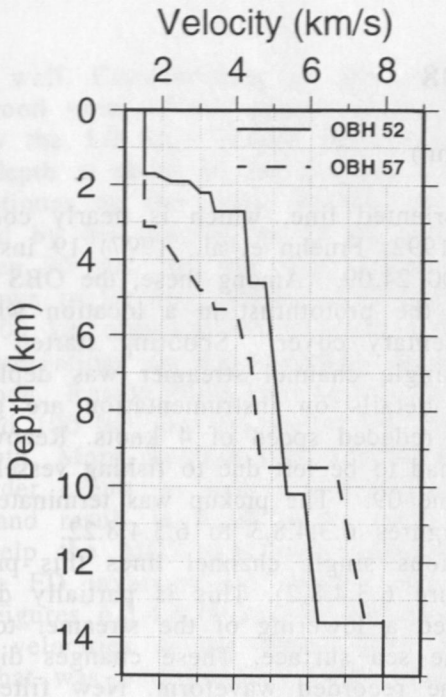

Figure 6.3.4.7.16: Vertical sections through two-dimensional velocity model at the location of OBH52 and 57.

6.3.4.8 Profile SO123-08

(J. Bialas, T. Minshull, J. Fruehn)

Along this nearly N-S oriented line, which is nearly coincident with MCS line CAM 30 (Minshull et al., 1992; Fruehn et al., 1997) 19 instruments were deployed between 05:00 and 17:00 24.09. Among these, the OBS (OBS05) was placed seaward of the first ridge near the protothrust in a location where the MCS line shows brightspots in the sedimentary cover. Shooting started in the south on Little Murray Ridge, and the single channel streamer was deployed also. Locations are shown in Figure 6.3.4.8.1, details on instrumentation are given in Appendix 9.1.8. Shooting was done at a reduced speed of 4 knots. Recovery of instruments started at 18:00 25.09. OBH64 had to be left due to fishing vessels, and OBH69 was left to record also the shots along line 09. The pickup was terminated at 10.00 26.09. All record sections are shown in Figures 6.3.4.8.3 to 6.3.4.8.22.

Compared with the previous single channel lines this profile is of exceptionally good quality (Figure 6.3.4.8.2). This is partially due to the reduced ship speed that must have caused a lowering of the streamer to a depth with considerably less noise from the sea surface. These changes did not only affect the signal-to-noise ratio but also the recorded waveform. New filter tests showed that a zero-phase filter was more appropriate to remove the low frequency noise and not to alter the phase of the signal as much as a minimum phase filter did.

The course of the single channel line deviates from CAM30 (Minshull et al., 1992) in the Oman abyssal plain area. The relatively small deviation of max. 5 km is however large enough to have missed the bright spots imaged in CAM30 at cdp 1100 and 1900 (Figure 2.4). Figure 6.3.4.8.2 shows the line starting at the "Little Murray Ridge" in the south, crossing the Oman abyssal plain and the accretionary wedge over more than 140 km. The abyssal plain segment shows the seismic facies associated with the Makran sands (sub-horizontal reflections) and the Himalayan turbidites (landward dipping reflections) (cf. Fruehn et al., 1997). The Makran sands onlap the Himalayan turbidites along a pronounced unconformity that is well imaged in the area adjacent to the Little Murray Ridge (Figure 6.3.4.8.23). Another conspicuous feature of this segment is the high reflectivity zone beneath the BSR (shot 100 - 250). This is indicative for the occurance of gas and probably trapped fluid. The BSR is disrupted and is getting shallower towards the Little Murray Ridge, which suggests a strong lateral variation in the thermal gradient.

Figure 6.3.4.8.24 shows the deformation front of the accretionary wedge. Distinct reflections of the Makran sands are imaged as well as the top of the Himalayan turbidites (deepest continuous reflection) that is offset along an upwards propagating fault. The BSR is also present with high amplitudes near the fold axis.

In a first approach primary arrivals of line 8 were investigated using the FD inversion code raytomorf. Depth values were taken from the ukooa shot list. Record sections from 16 OBH stations and one OBS were analysed for first arrivals. A total amount of 6526 readings were picked interactivly on the screen. Due to smoothing of the water depth caused by the 1 km grid spacing of the velocity field, depth values for the OBH/OBS positions needed to be recalibrated after gridding. Changes of receiver depth less than one hundred meters were applied to ensure that they were positioned near the seafloor. For a starting model the 2-D velocity field from line 1 (chapter 6.3.4.1) was taken into consideration. The starting model can still be recognized in Figure 6.3.4.8.25 at both ends when no ray coverage exists. Test runs over one iteration showed that a smoothing value of 100 and 5 matrix inversions per run promised best results. 50 iterations were calculated ending up with a remaining rms error of 0.105 s. From the travel time picks and their calculated corresponding values it is obvious that there are still some unsatisfied details which were expressed in this rms value. Even some of the readings need to be checked as there are some uncertainties like the crossing of arrivals that can be seen at 80 km and 16 s travel time while all other events of this branch line up parallel (Figure 6.3.4.8.25 top). Nevertheless the resulting velocity distribution monitors the subduciton complex off the coast of Makran quite well (Figure 6.3.4.8.25 middle). Short wave length undulations of the isolines should not be interpreted as they appear to correlate to the coverage (Figure

6.3.4.8.25 bottom) quite well. Concentrating on the general trend of the velocity distribution provides a good view of the crustal structure. The top of the oceanic crust represented here by the 5.0 km/s isoline can be traced from 4.5 km depth at km 25 down to 10 km depth at about 80 km distance. From here on the isoline rises again as the profile continues up the slope. Further on the downgoing slab of the oceanic crust is indicated by the distribution of the 6.0 km/s isoline. These velocitiy is found between 30 and 100 km only. Again the isoline deepens towards the coast (from 8 km down to 16 km). Velocities larger than 5 km/s are not modeled farther landwards than 100 km although the 5 km/s isoline rises up by 7 km. This is due to the limited observations on the recordings which did not allow to pick arrivals within this branch. Result from this section is the thickening of sediments between 50 and 100 km and tracing of the downgoing slab as far as 100 km down to 16 km depth. More detailed two dimensional modelling including reflection and second order events as well as MCS line interpretations will light up this preliminary model and result in much more detail of the subduction zone which in turn should help the MCS processing sequences.

In addition to the FD inversion ray tracing was performed on 4 instruments across the wedge. The Figures 6.3.4.8.26 and 6.3.4.8.27 show the obtained velocity structure. The sediment velocities at the deformation front were taken from focusing error analysis that was performed in 1996 at GEOMAR (Fruehn et al., 1997). The calculated travel-time curves fitted the observed arrivals within 50 ms. The velocities from the oceanic crust and upper mantle are well constrained on the selected instruments by the corresponding arrivals (reflections and refractions). They match the data within 100 ms. From this very simple model we can already infer some general characteristics of the wedge such as the wedge thickness, the dip of the subducting plate and the thickness of the oceanic crust. The sedimentary cover thickens rapidly landwards from about 7 km at the deformation front to about 15 km beneath OBH64. The oceanic crust is about 7 km thick and dips at an angle of about 2.5°. This is in very good agreement with the results obtained from the first refraction survey in the area (White and Louden, 1982).

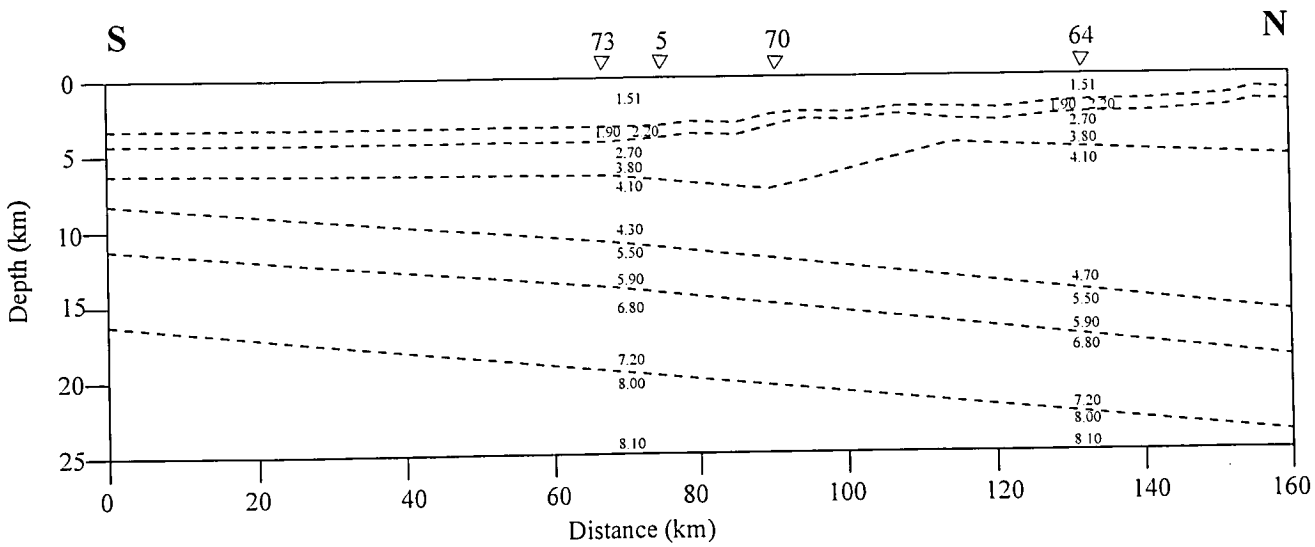

Figure 6.3.4.8.27: Preliminary velocity structure of the Makran accretionary wedge derived from ray tracing at 4 OBH locations. Triangles mark the position of the instruments.

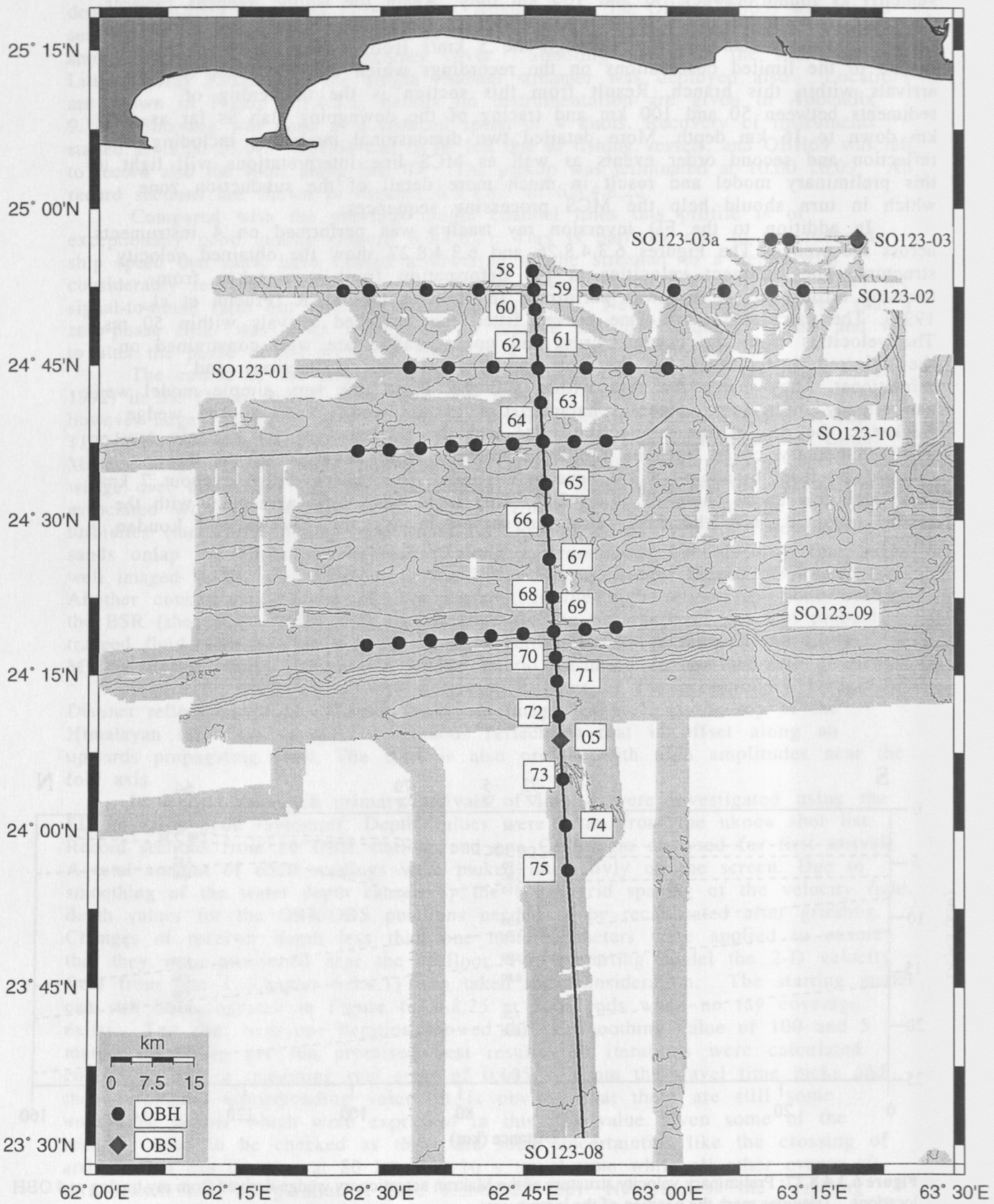

Figure 6.3.4.8.1: Location map of profile SO123-08.

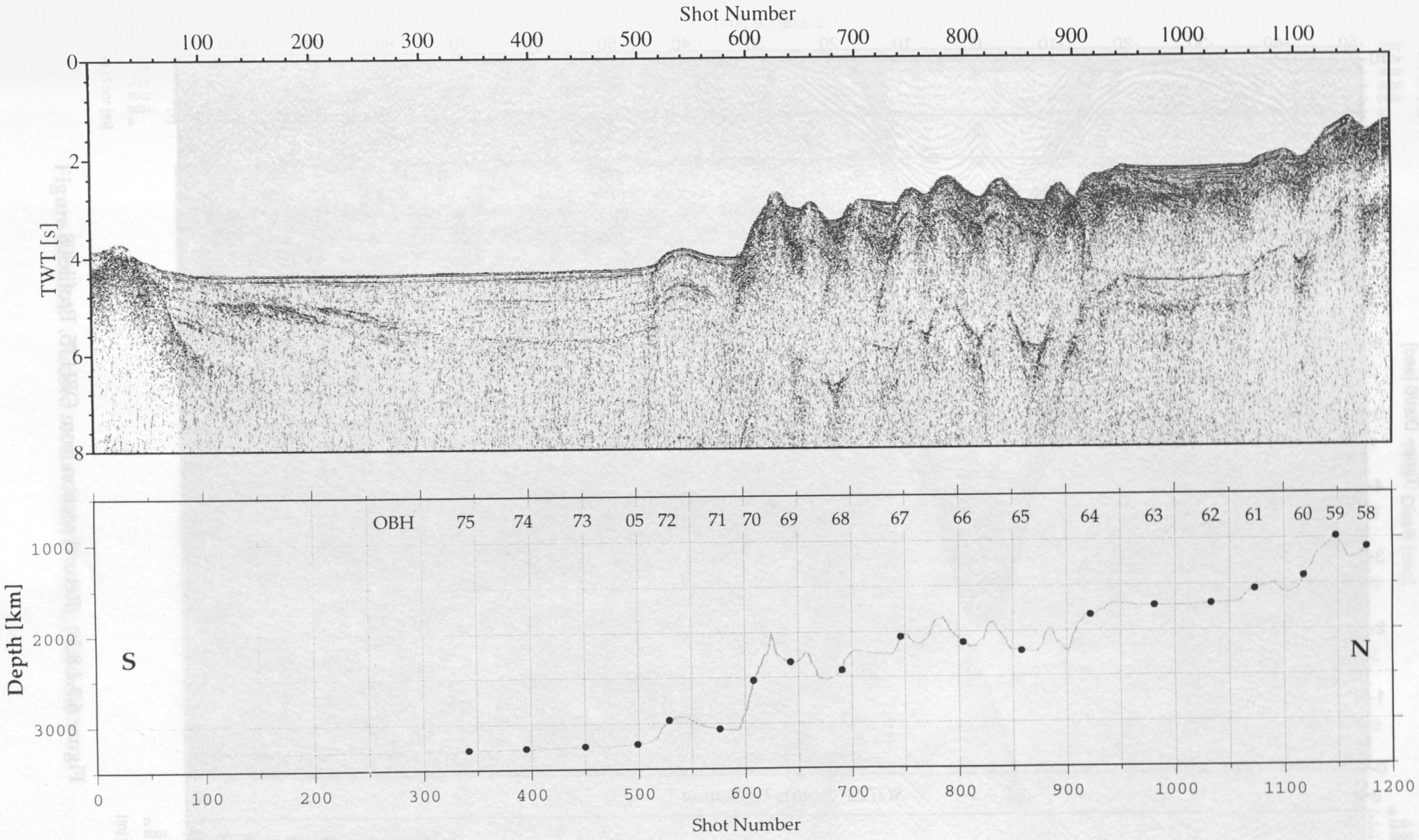

Figure 6.3.4.8.2: Single channel profile SO123-08 (above) and OBH positions.

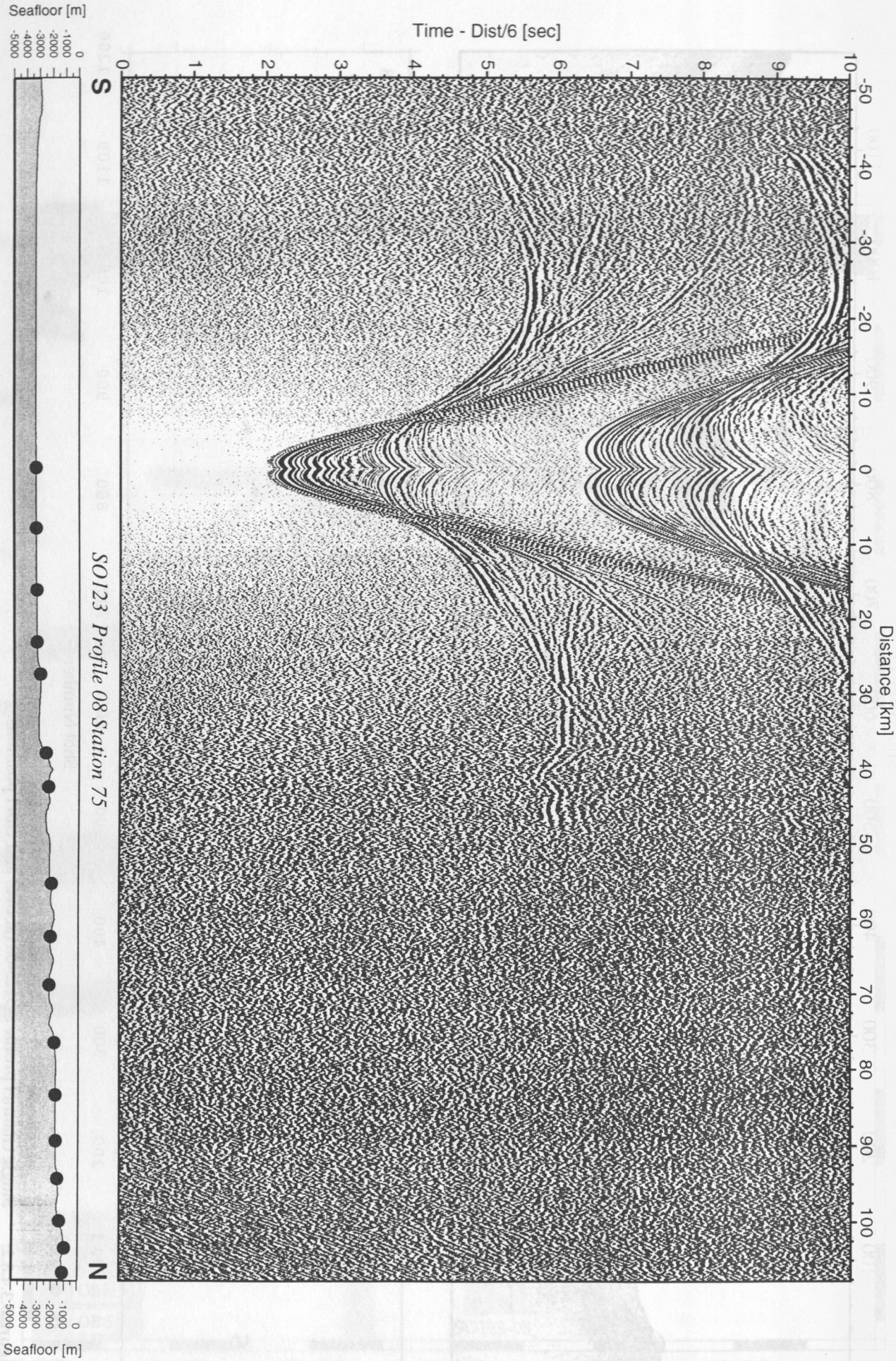

Figure 6.3.4.8.3: Record section from OBH 75, Profile 08.

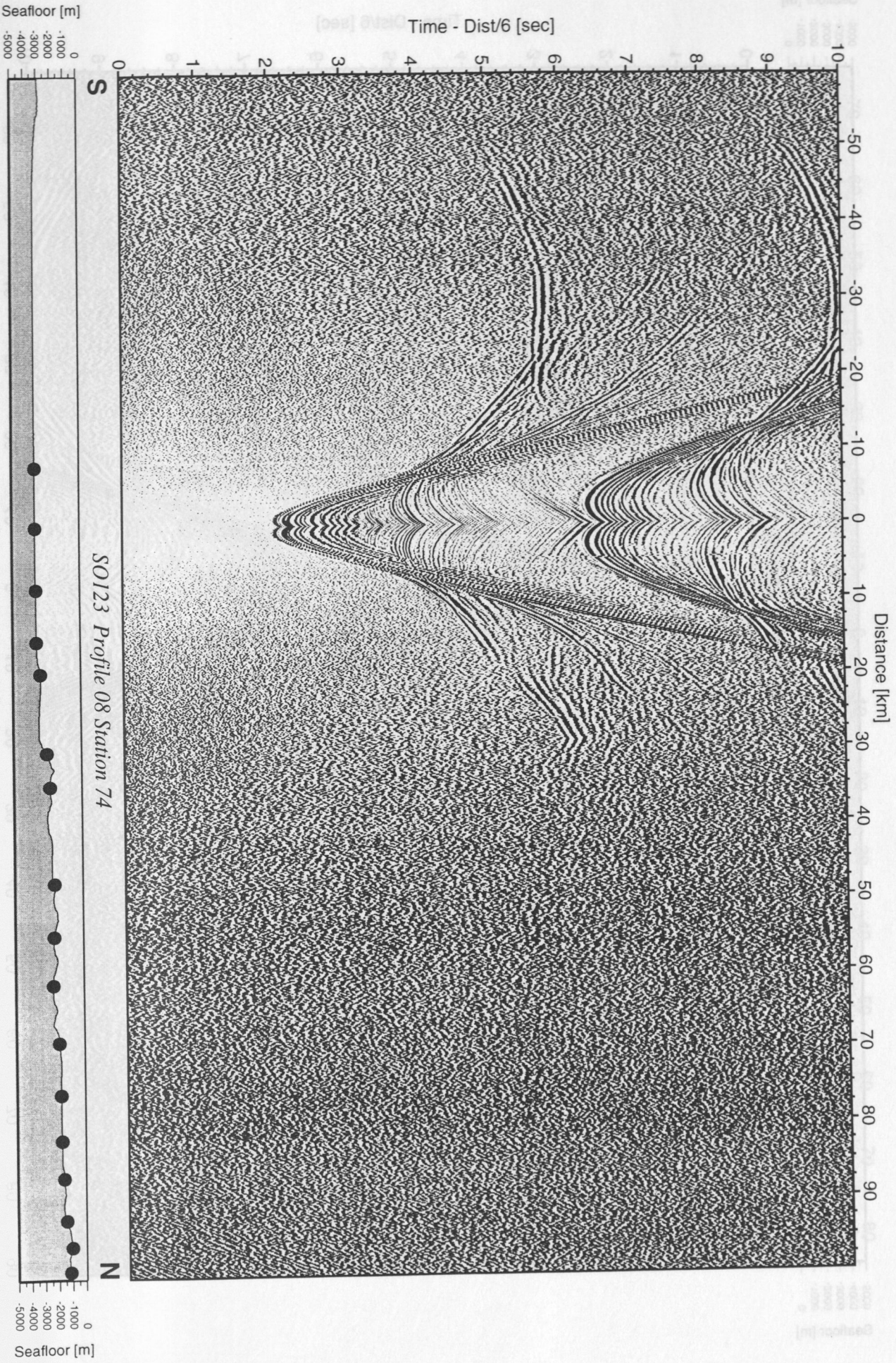

Figure 6.3.4.8.4: Record section from OBH 74, Profile 08.

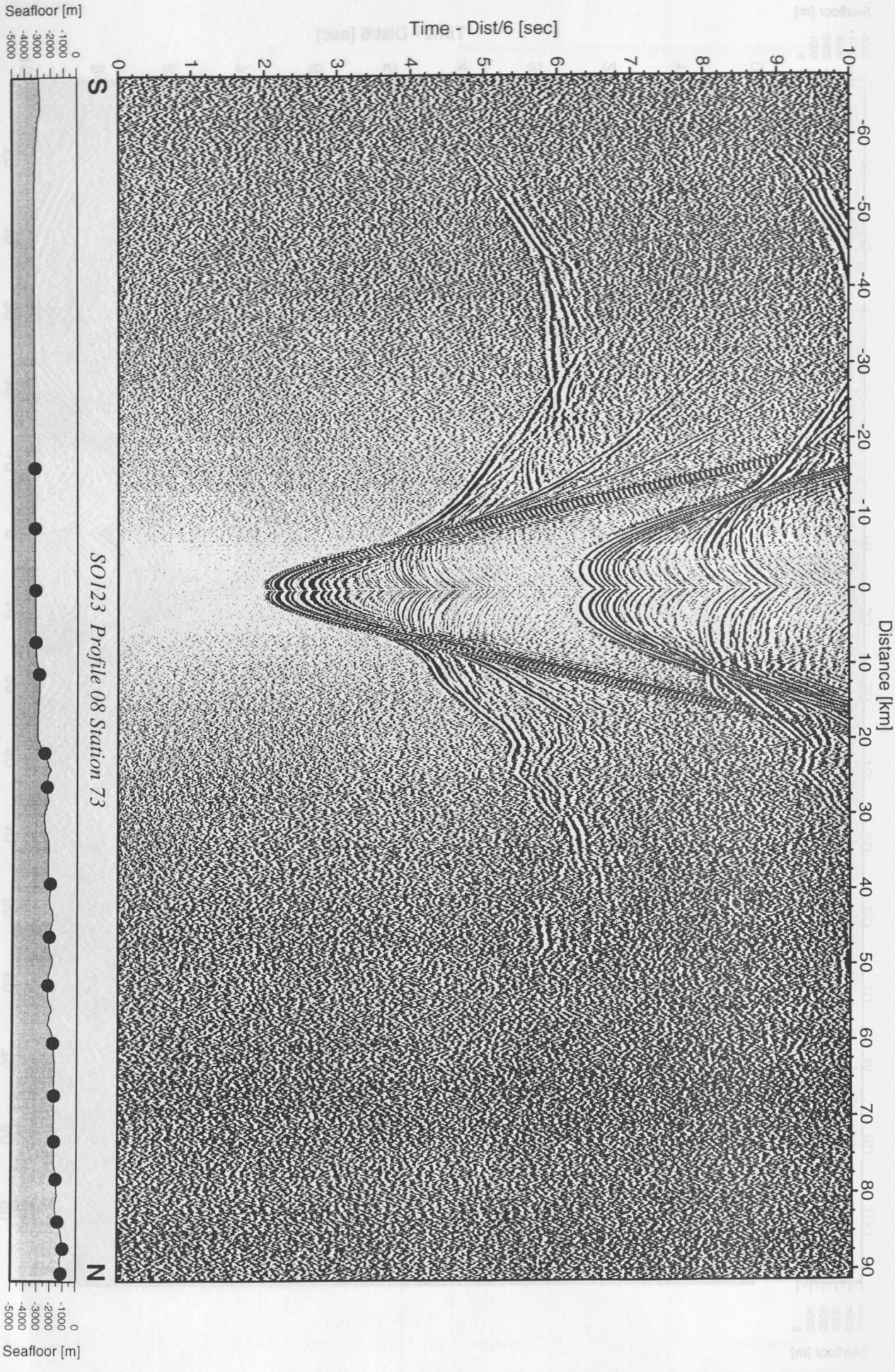

Figure 6.3.4.8.5: Record section from OBH 73, Profile 08.

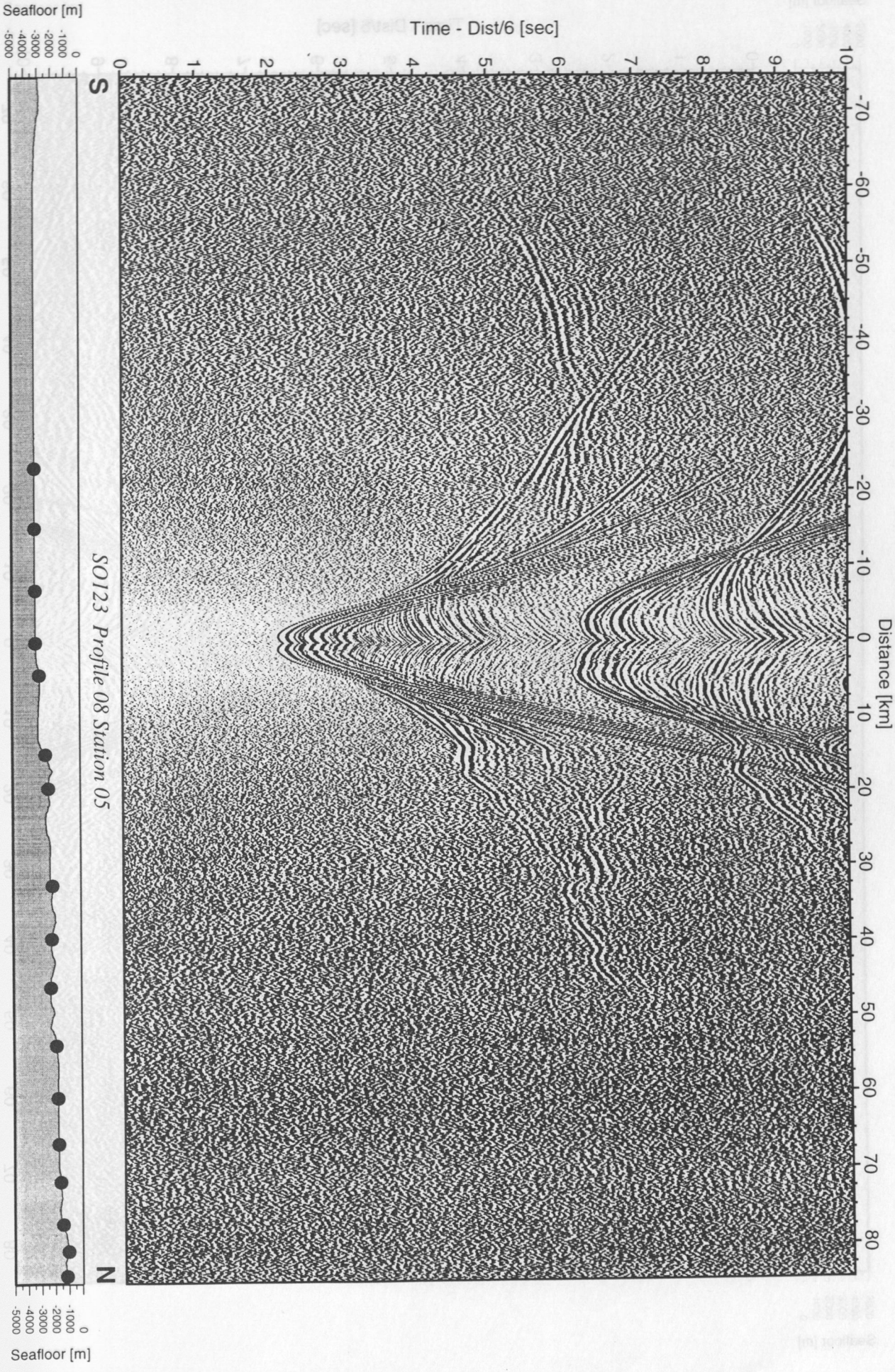

Figure 6.3.4.8.6: Record section from OBS 05, Profile 08, hydrophone.

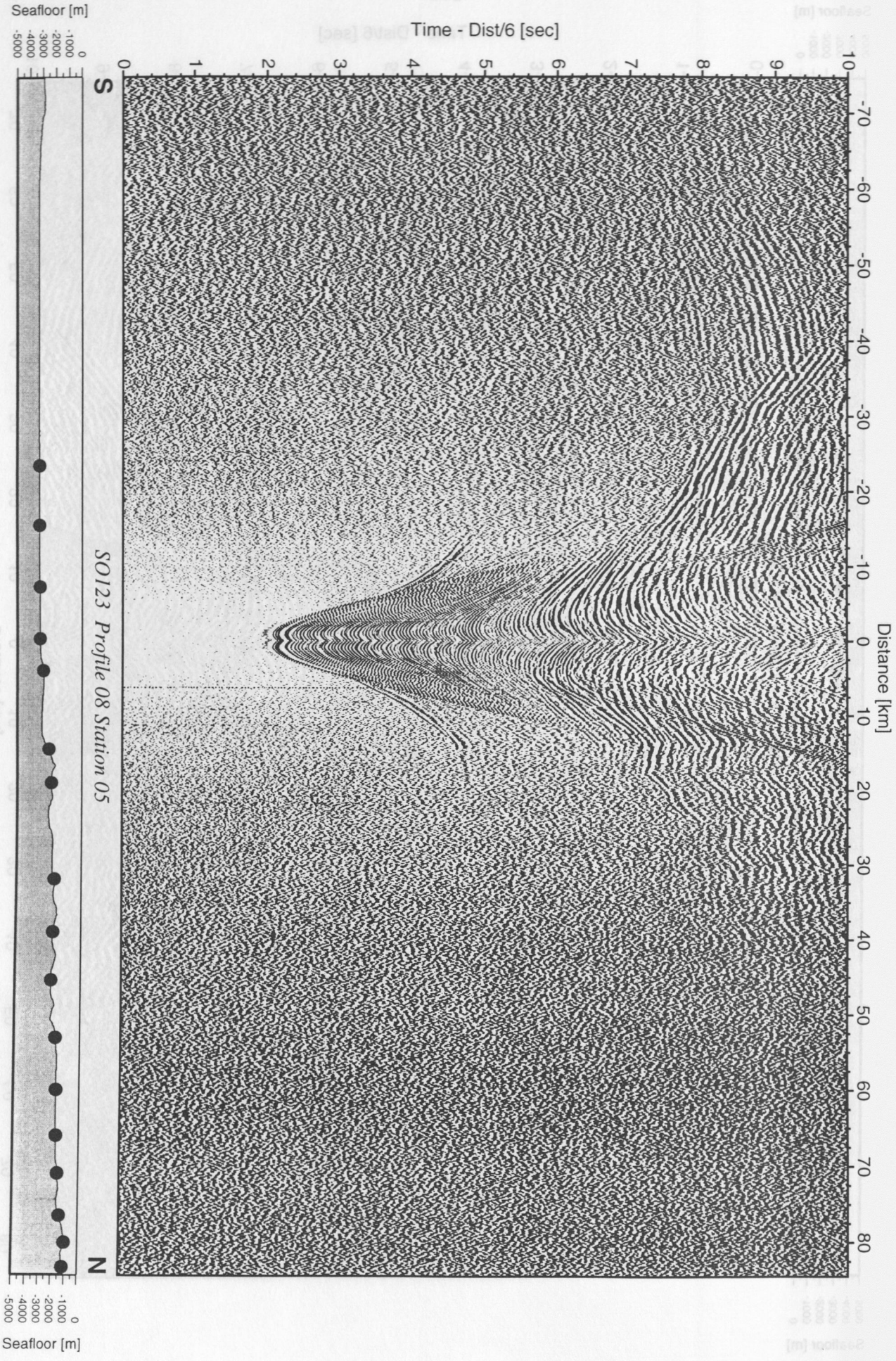

Figure 6.3.4.8.9: Record section from OBS 05, Profile 08, horizontal component.

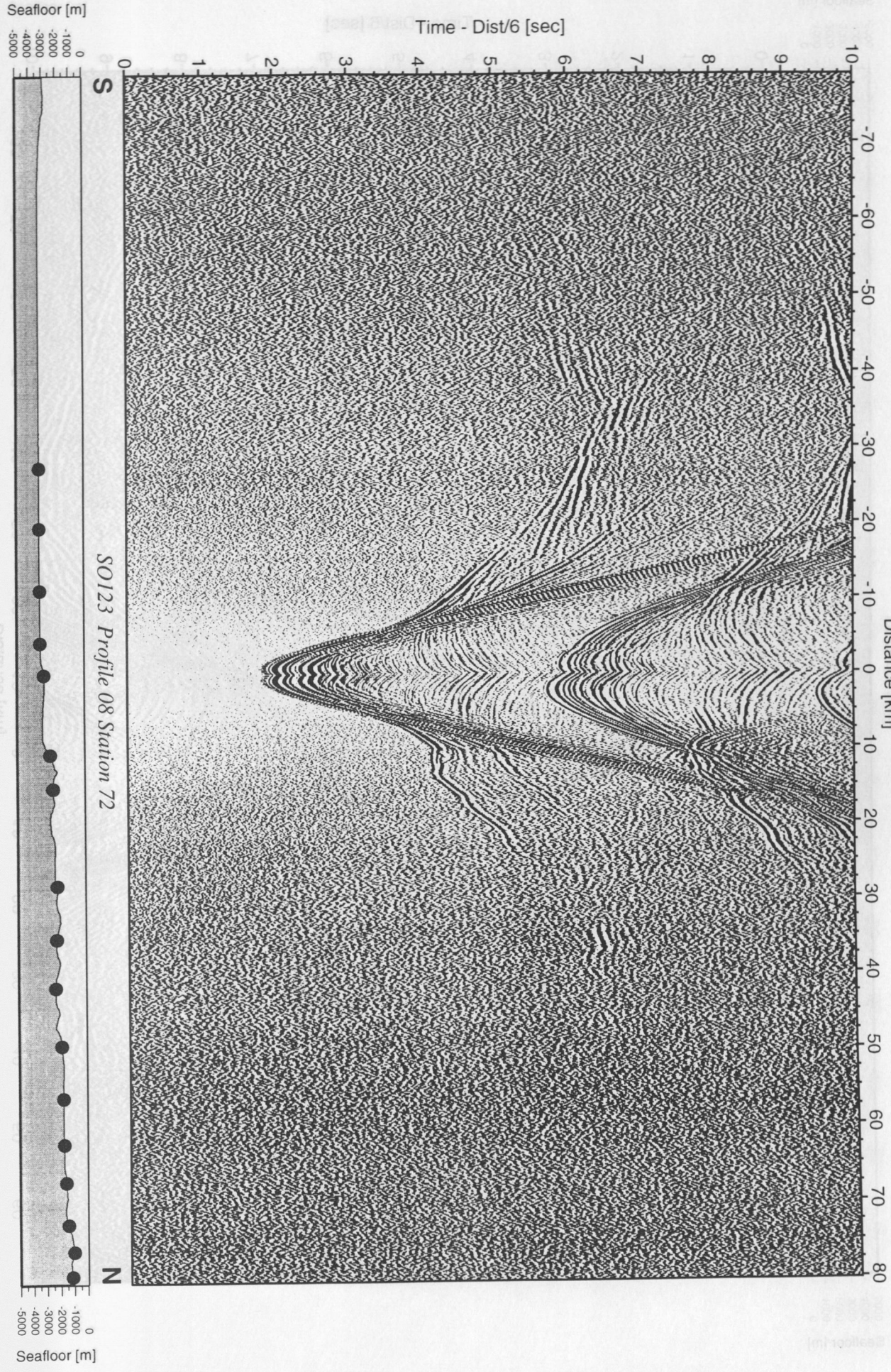

Figure 6.3.4.8.10: Record section from OBH 72, Profile 08.

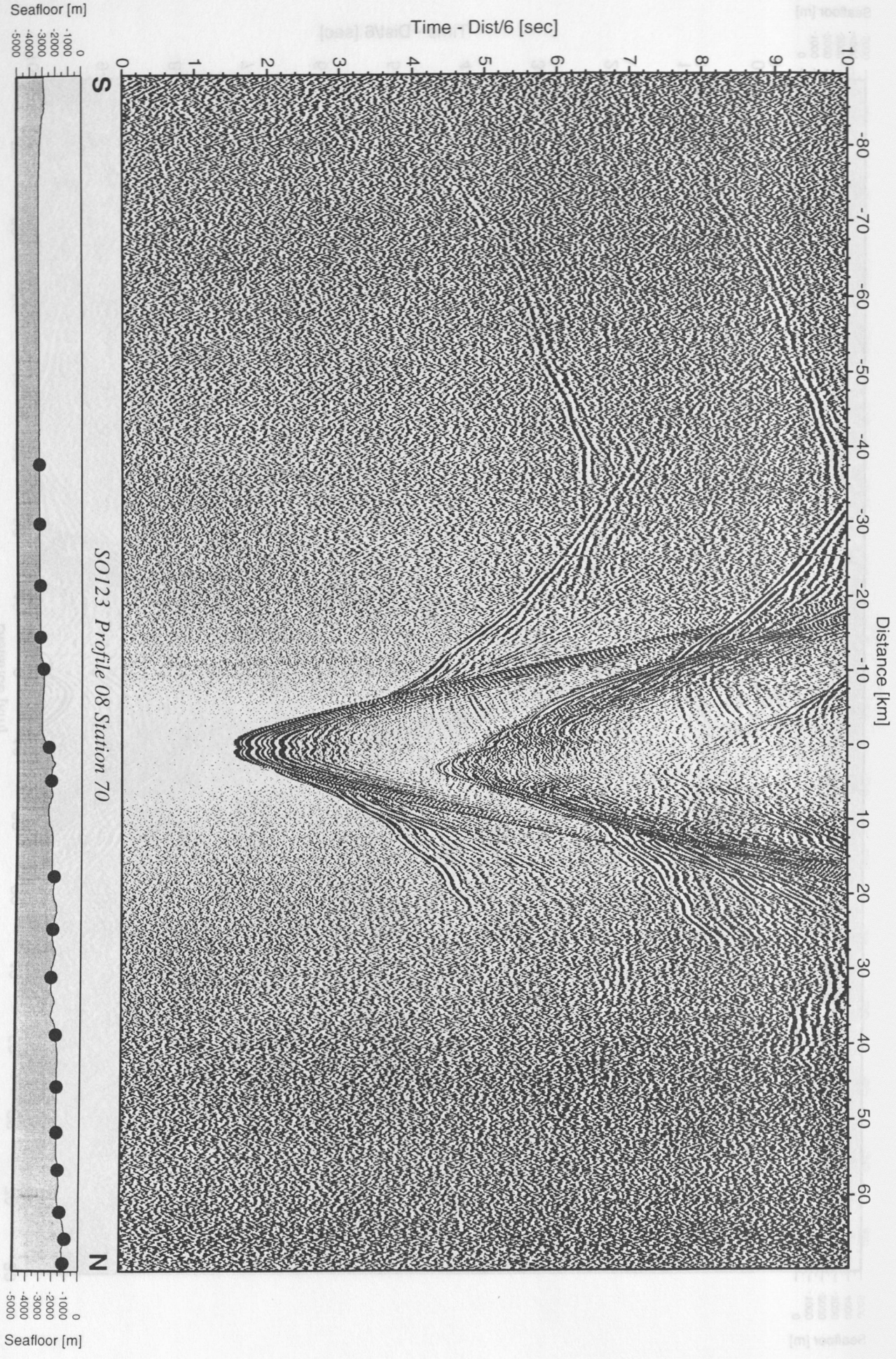

Figure 6.3.4.8.11: Record section from OBH 70, Profile 08.

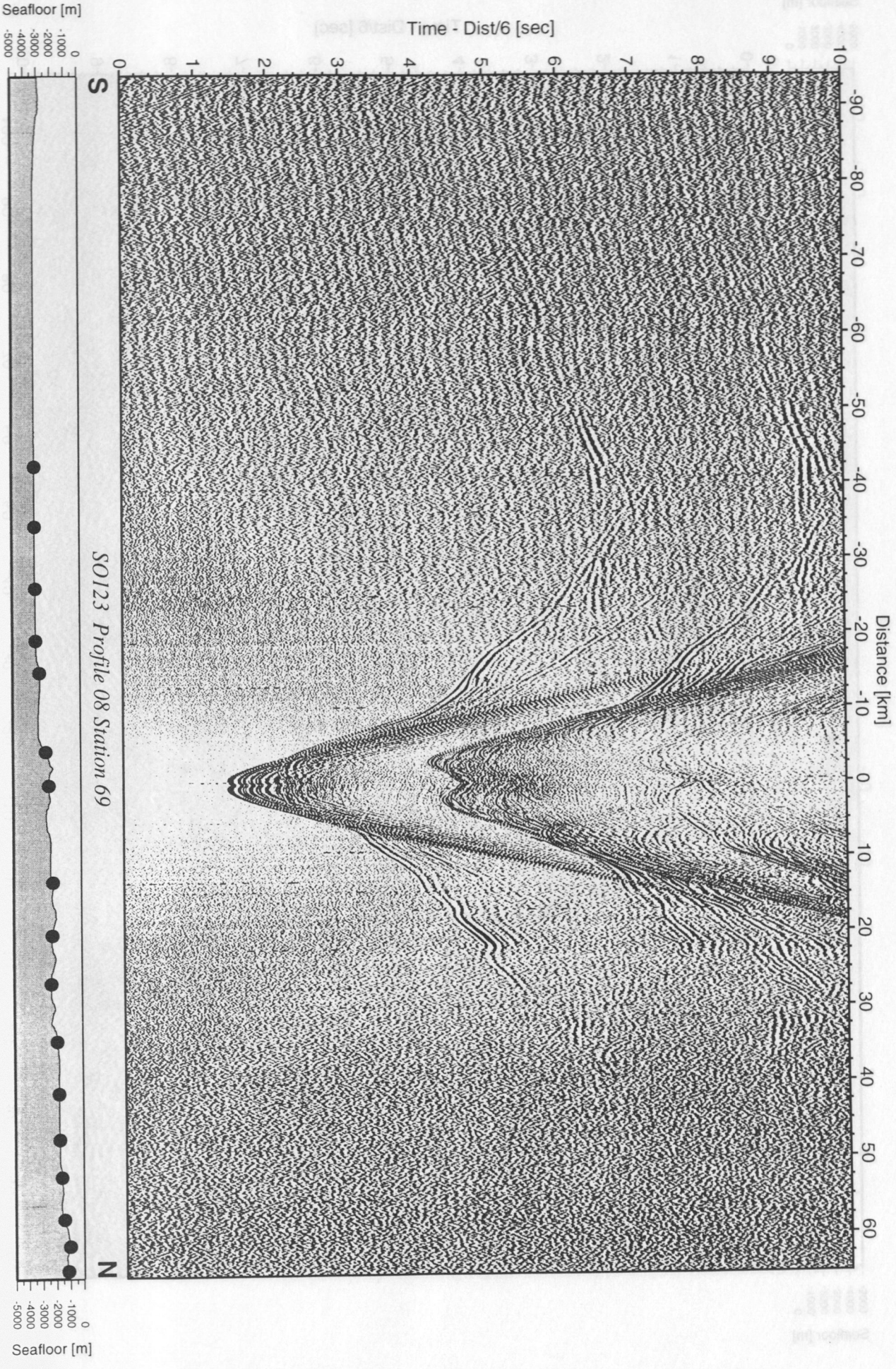

Figure 6.3.4.8.12: Record section from OBH 69, Profile 08.

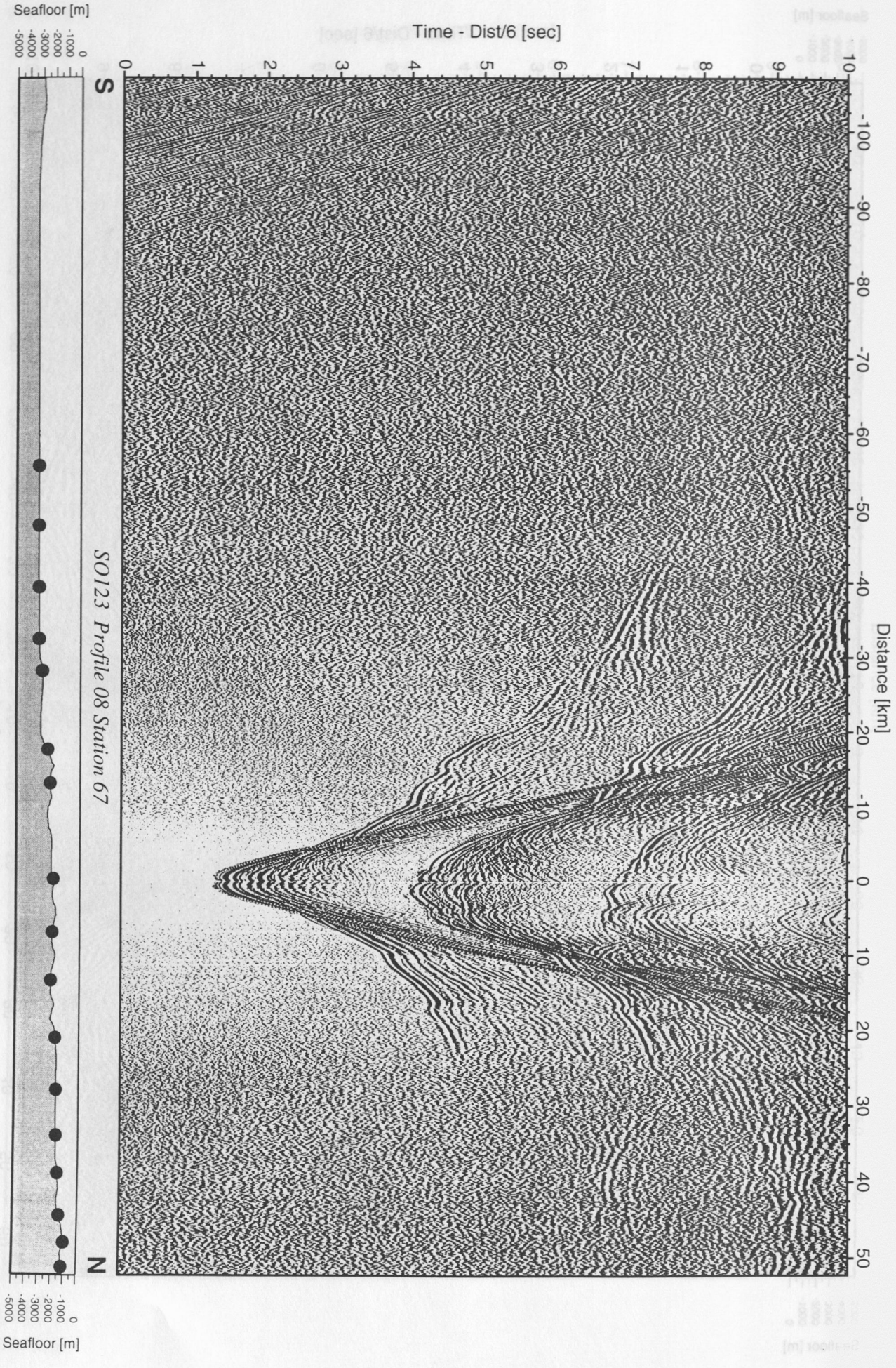

Figure 6.3.4.8.13: Record section from OBH 67, Profile 08.

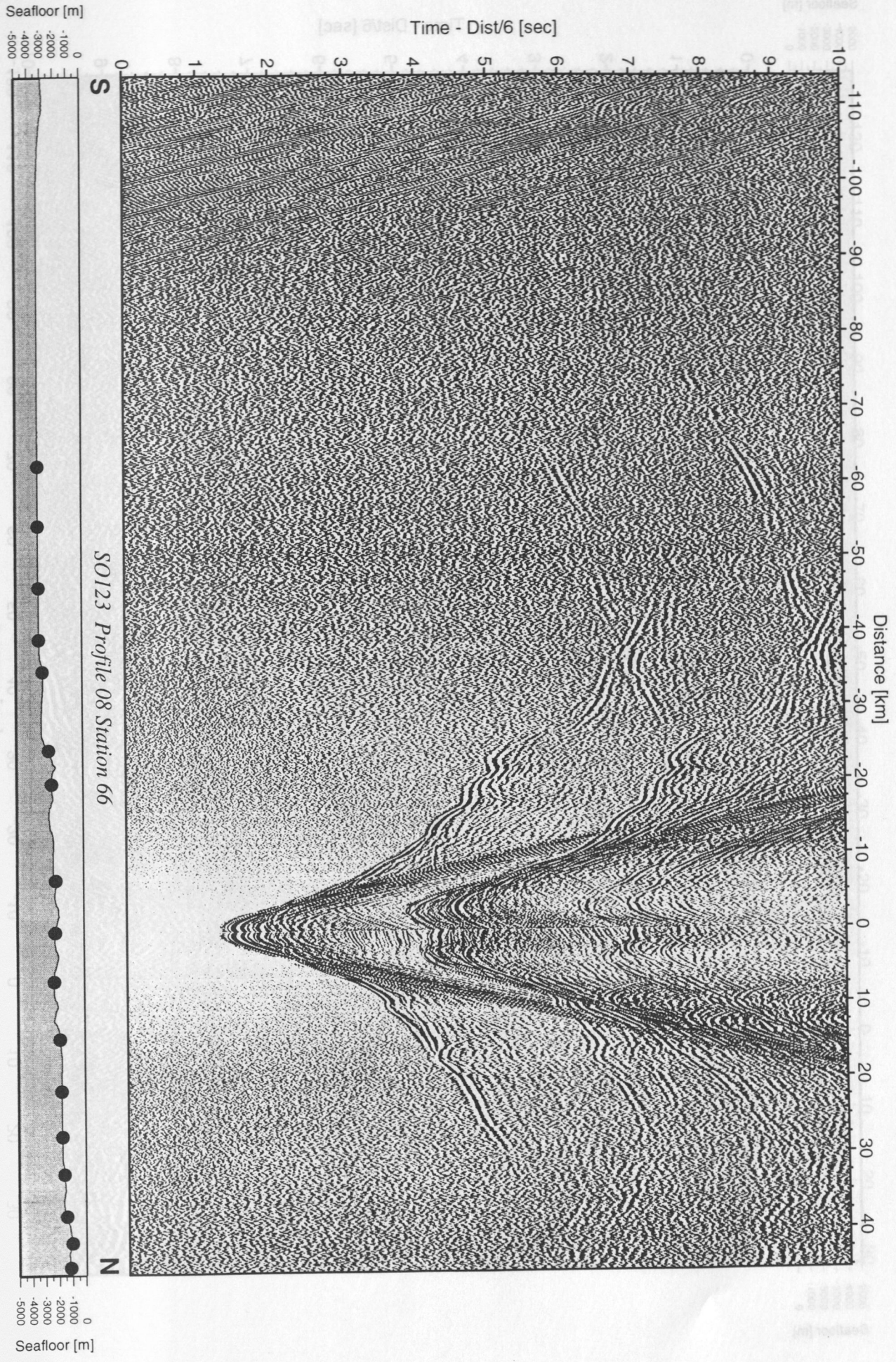

Figure 6.3.4.8.14: Record section from OBH 66, Profile 08.

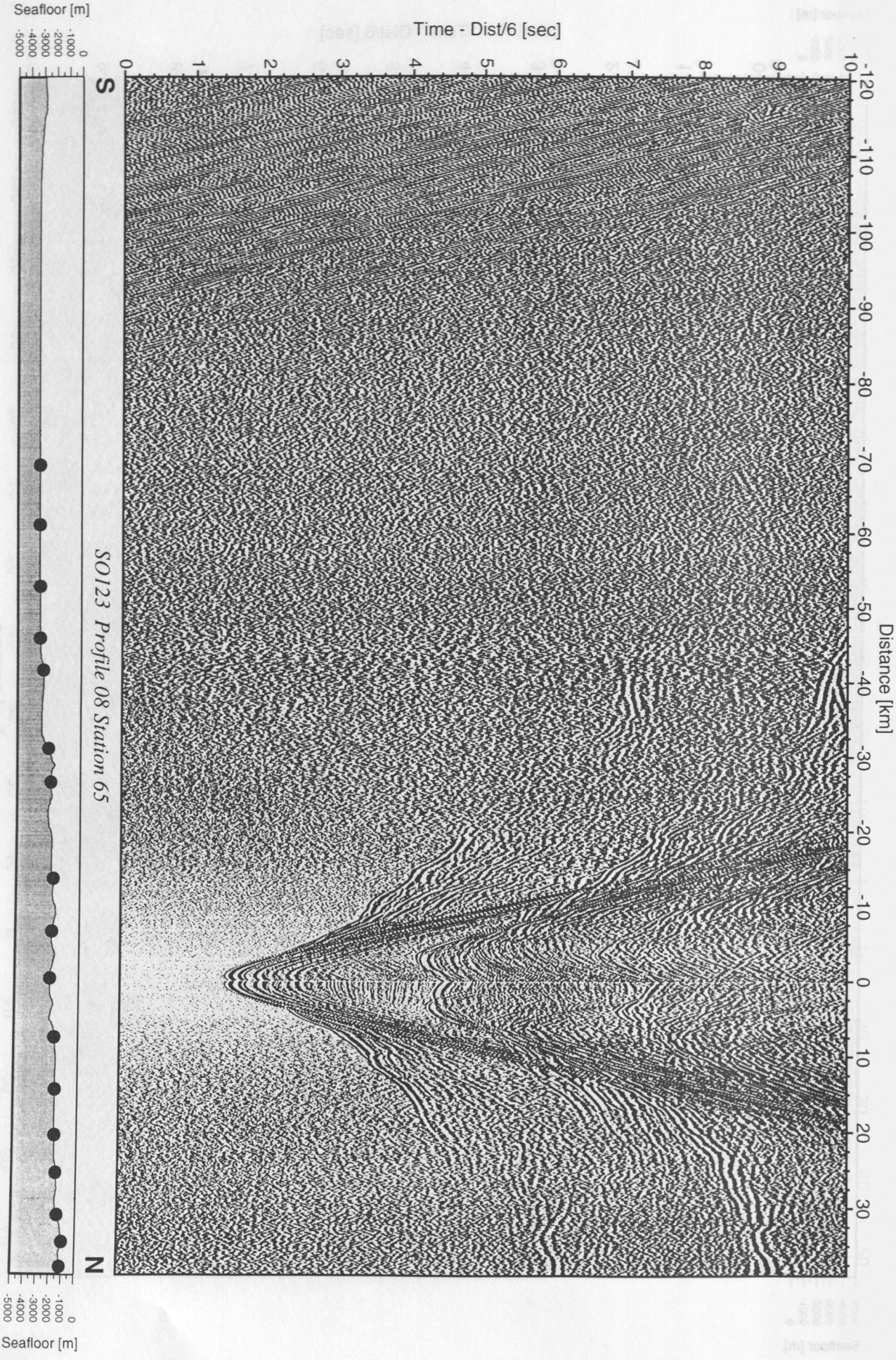

Figure 6.3.4.8.15: Record section from OBH 65, Profile 08.

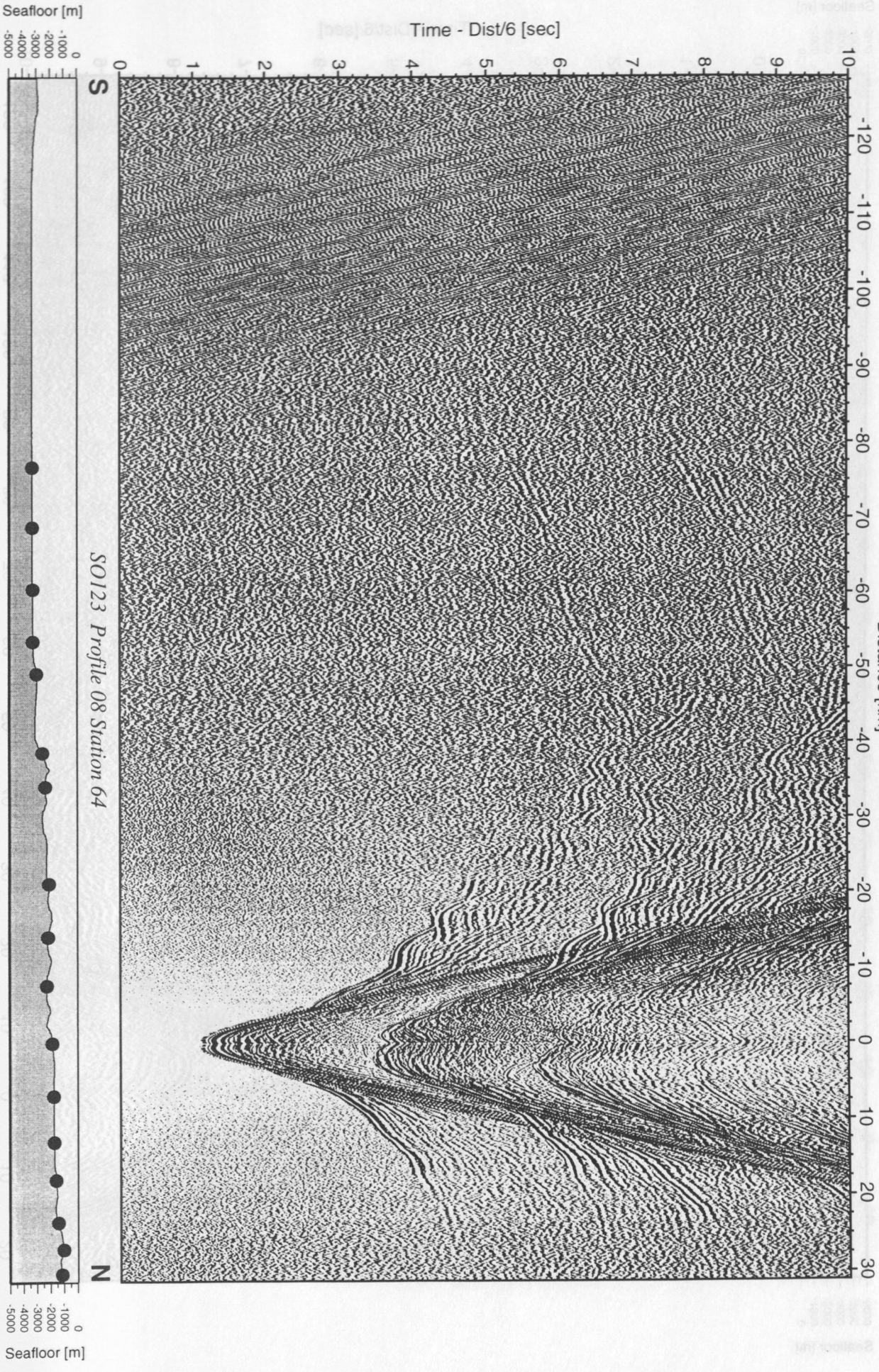

Figure 6.3.4.8.16: Record section from OBH 64, Profile 08.

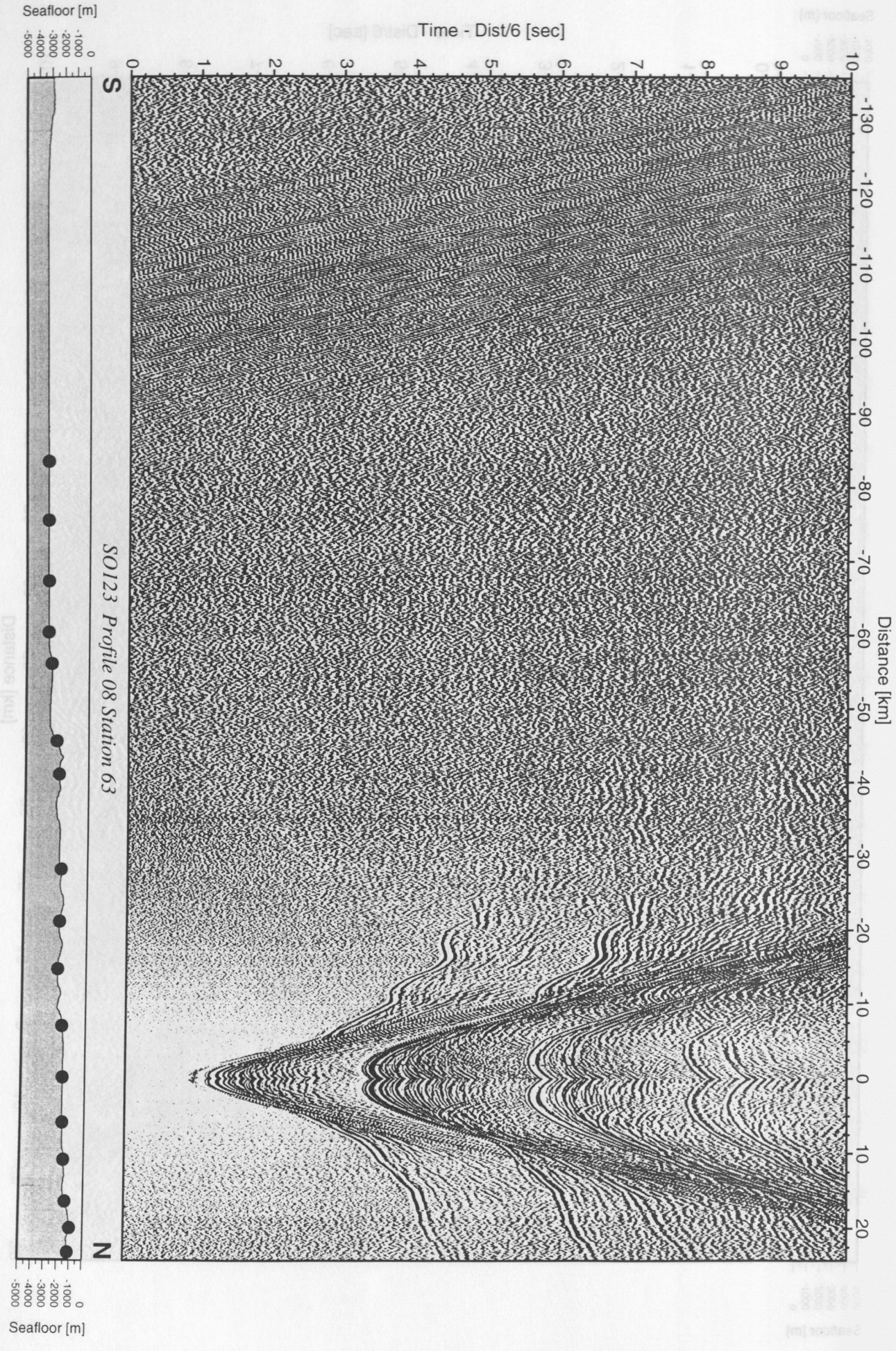

Figure 6.3.4.8.17: Record section from OBH 63, Profile 08.

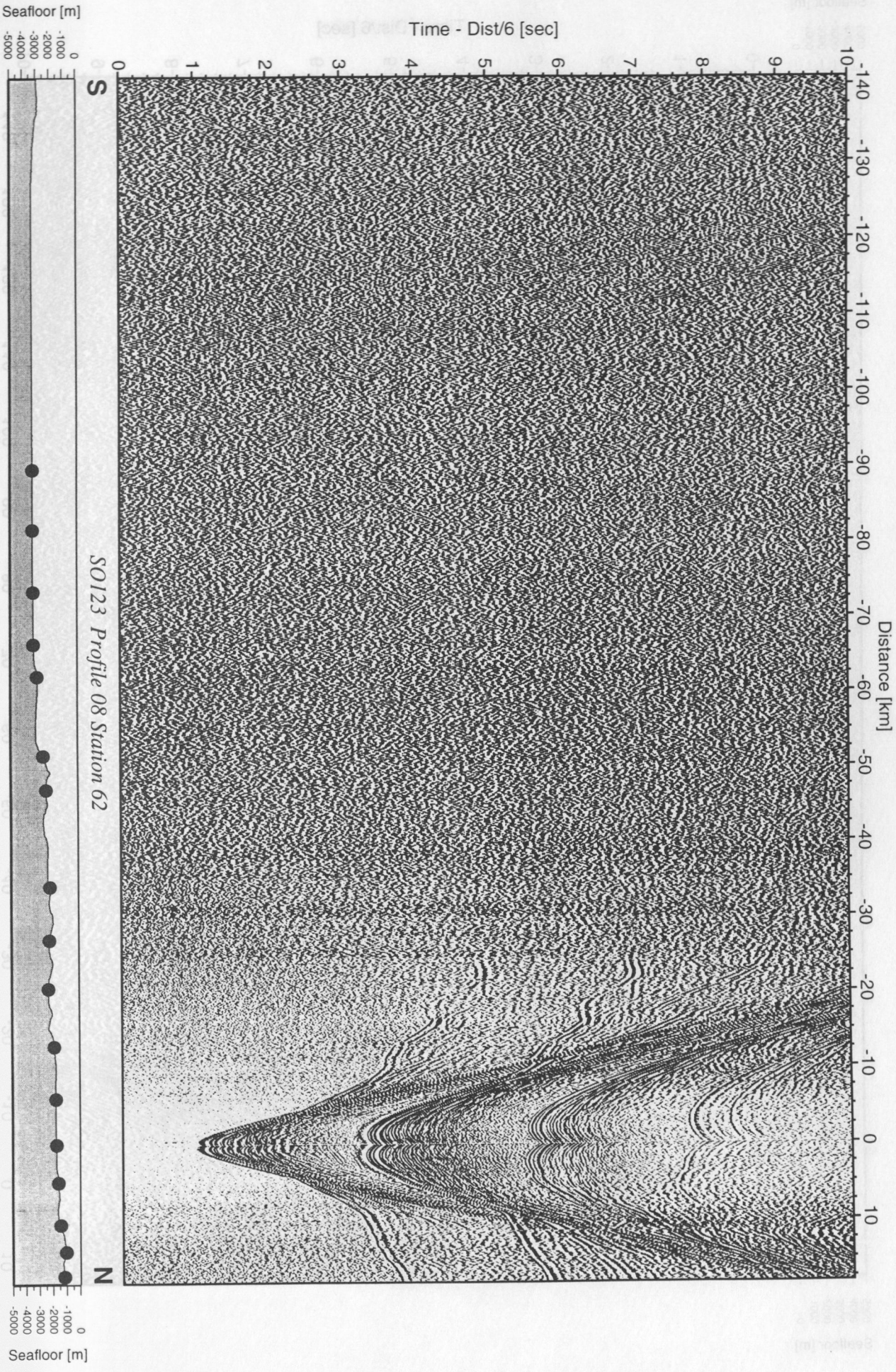

Figure 6.3.4.8.18: Record section from OBH 62, Profile 08.

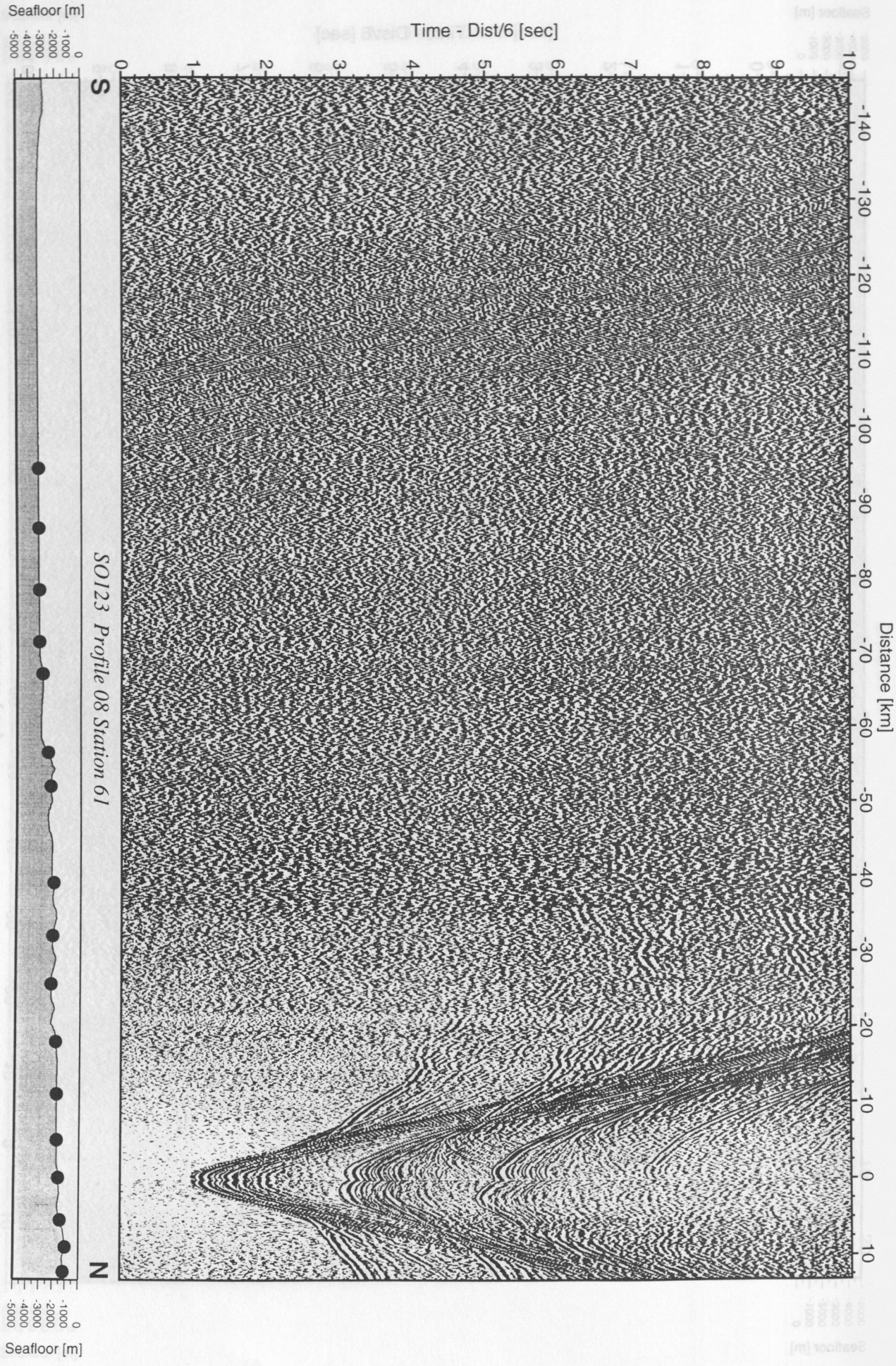

Figure 6.3.4.8.19: Record section from OBH 61, Profile 08.

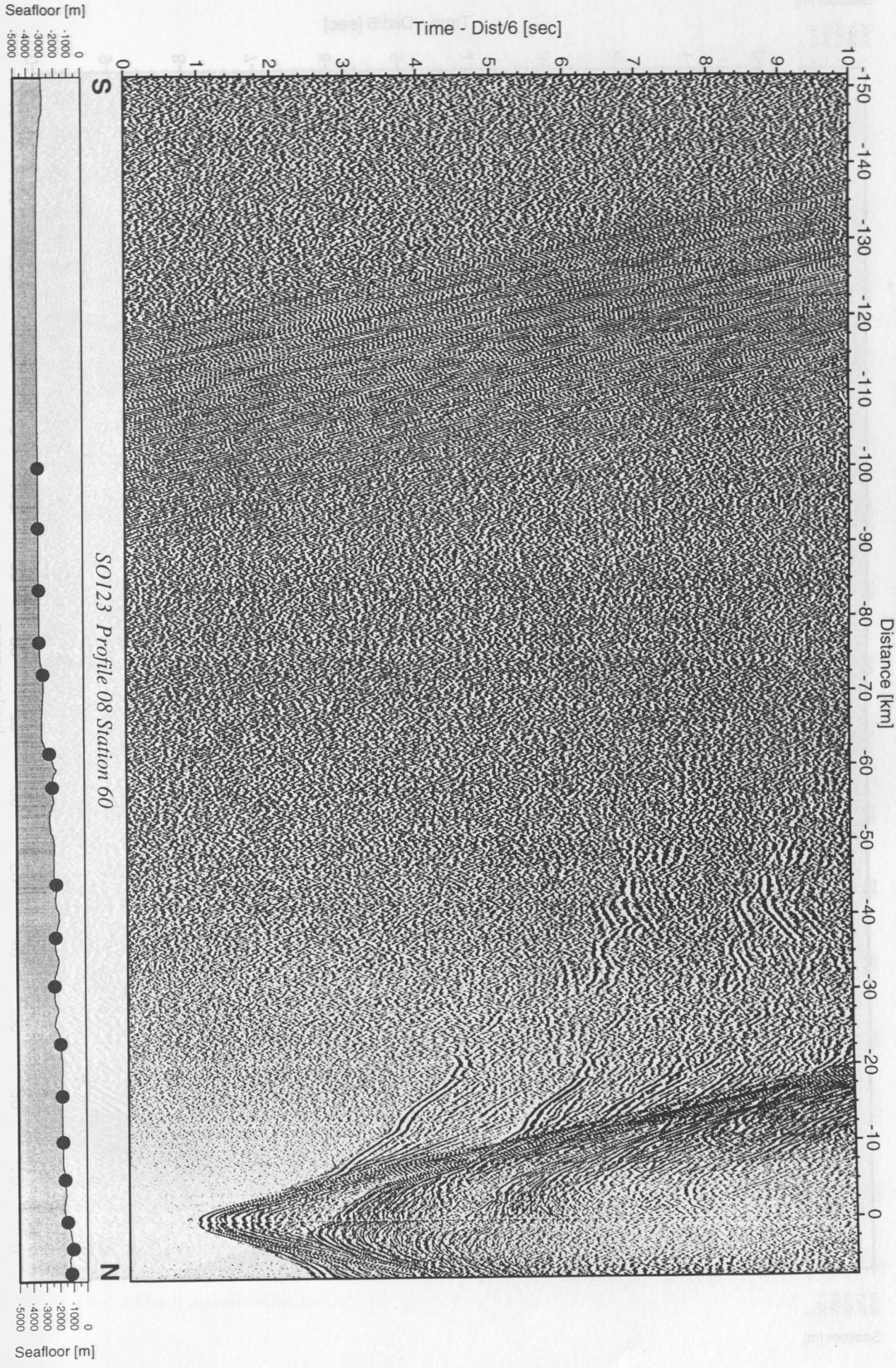

Figure 6.3.4.8.20: Record section from OBH 60, Profile 08.

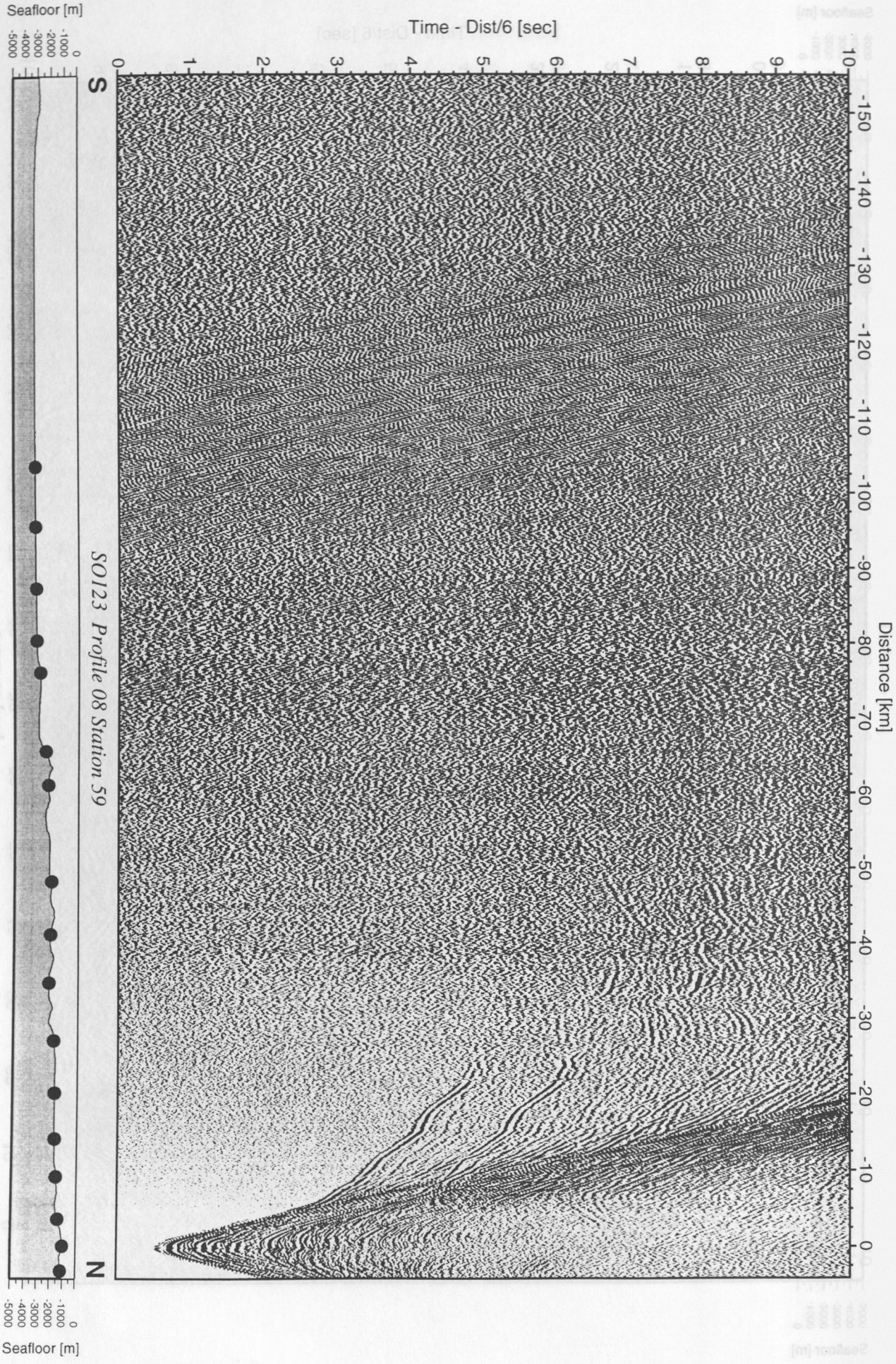

Figure 6.3.4.8.21: Record section from OBH 59, Profile 08.

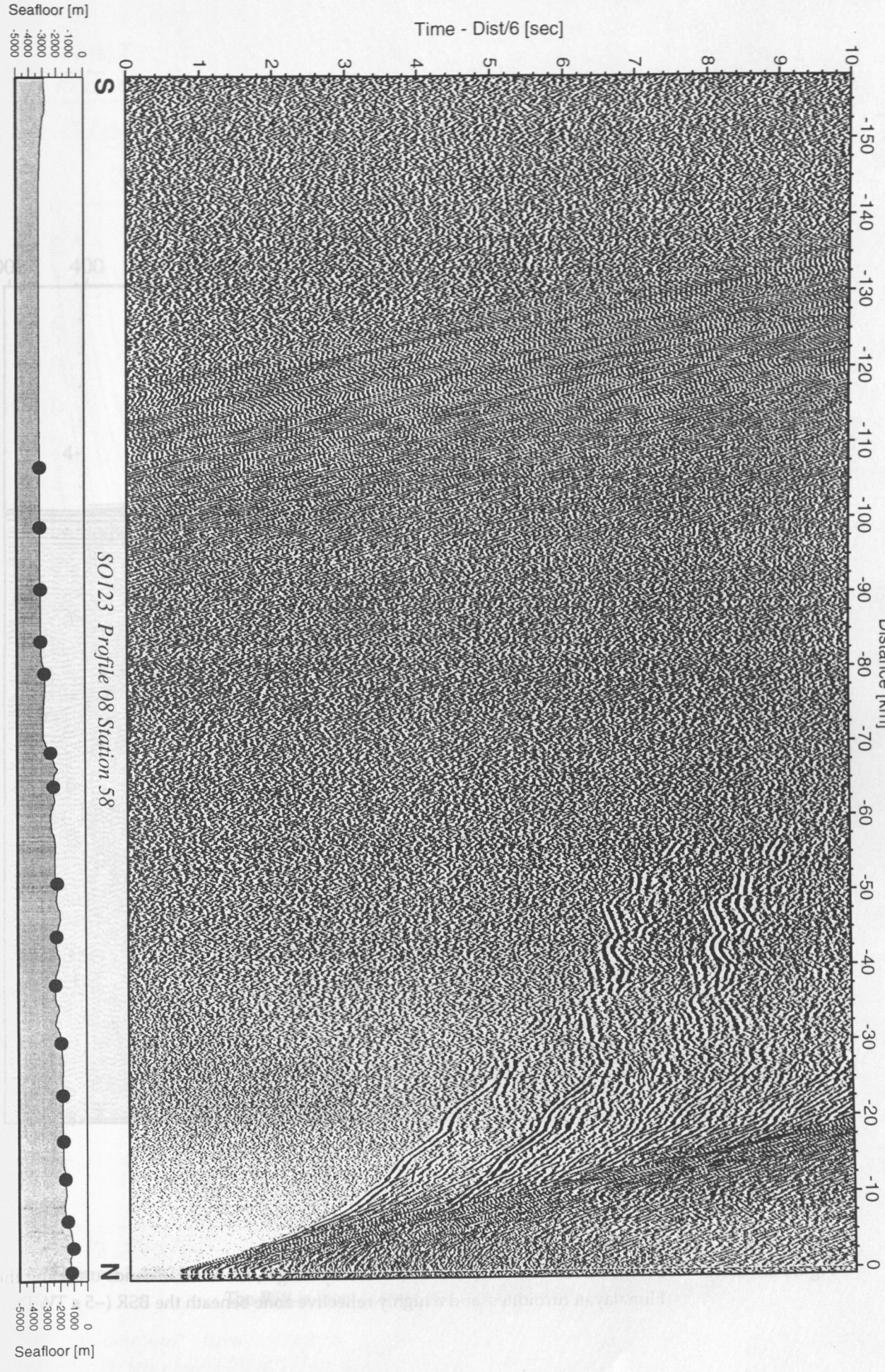

Figure 6.3.4.8.22: Record section from OBH 58, Profile 08.

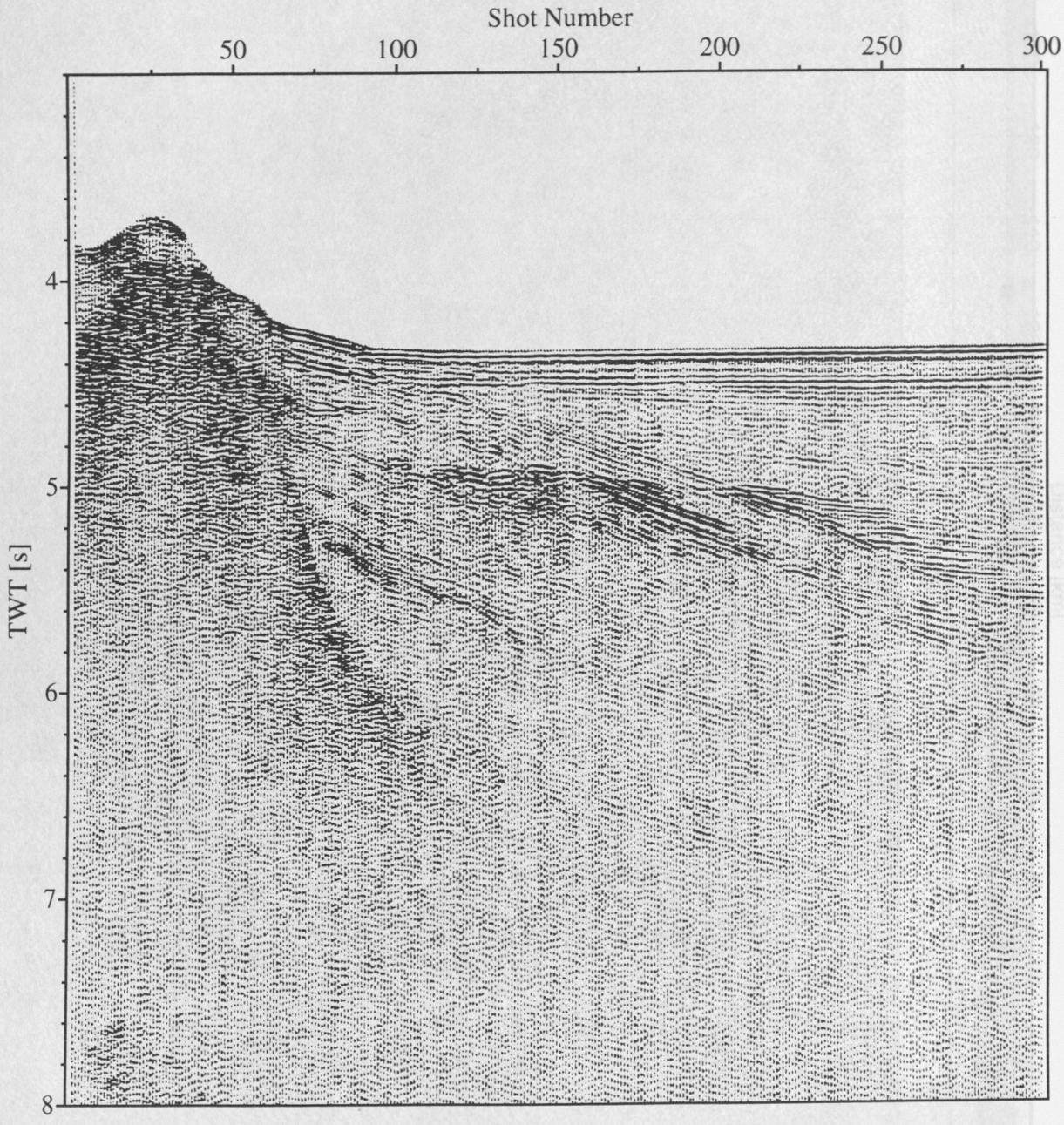

Figure 6.3.4.8.23: Profile SO123-08 shows the "Little Murray Ridge", the Makran sands onlaping the Himalayan turbidites and a highly reflective zone beneath the BSR (~5 s TWT).

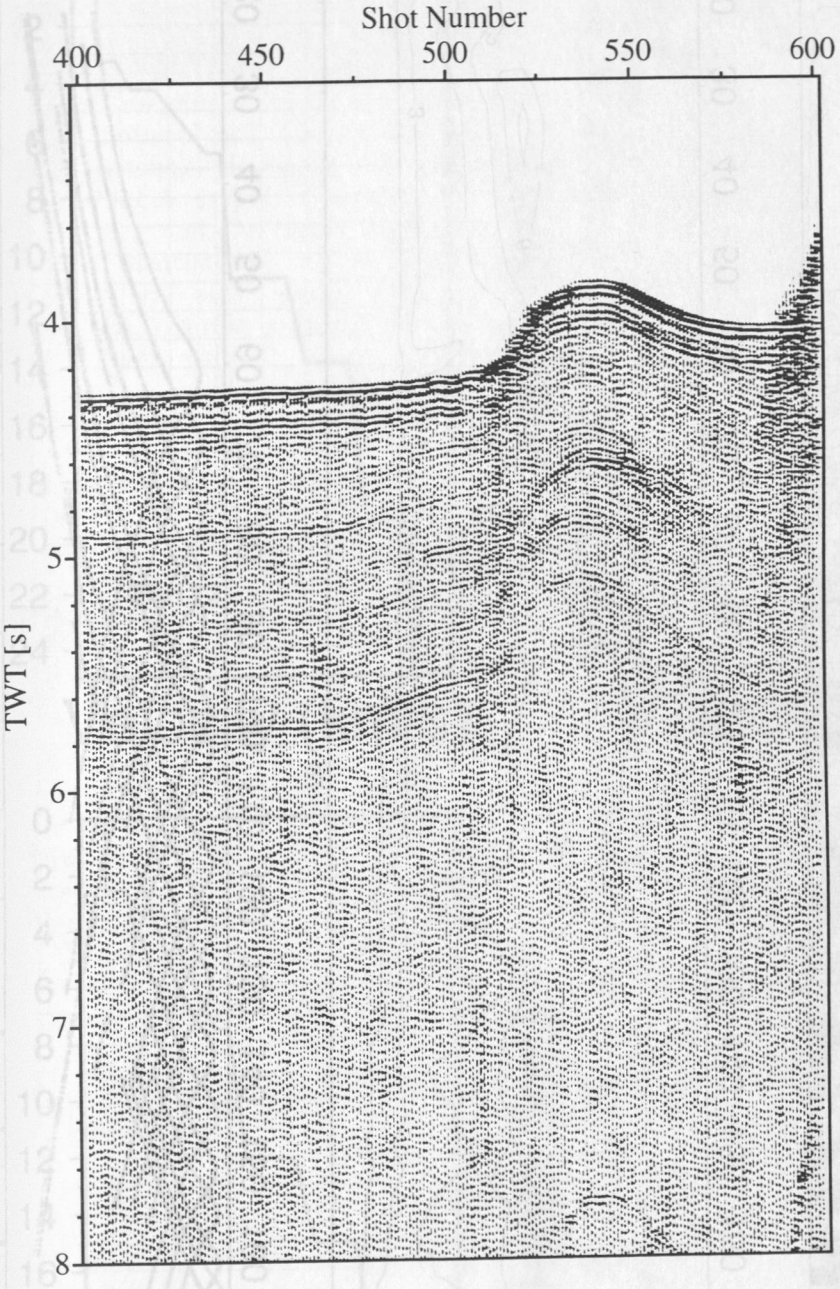

Figure 6.3.4.8.24: The Deformation front is clearly imaged in this segment of profile SO123-08. The BSR is cross-cutting the arched reflections of the first fold.

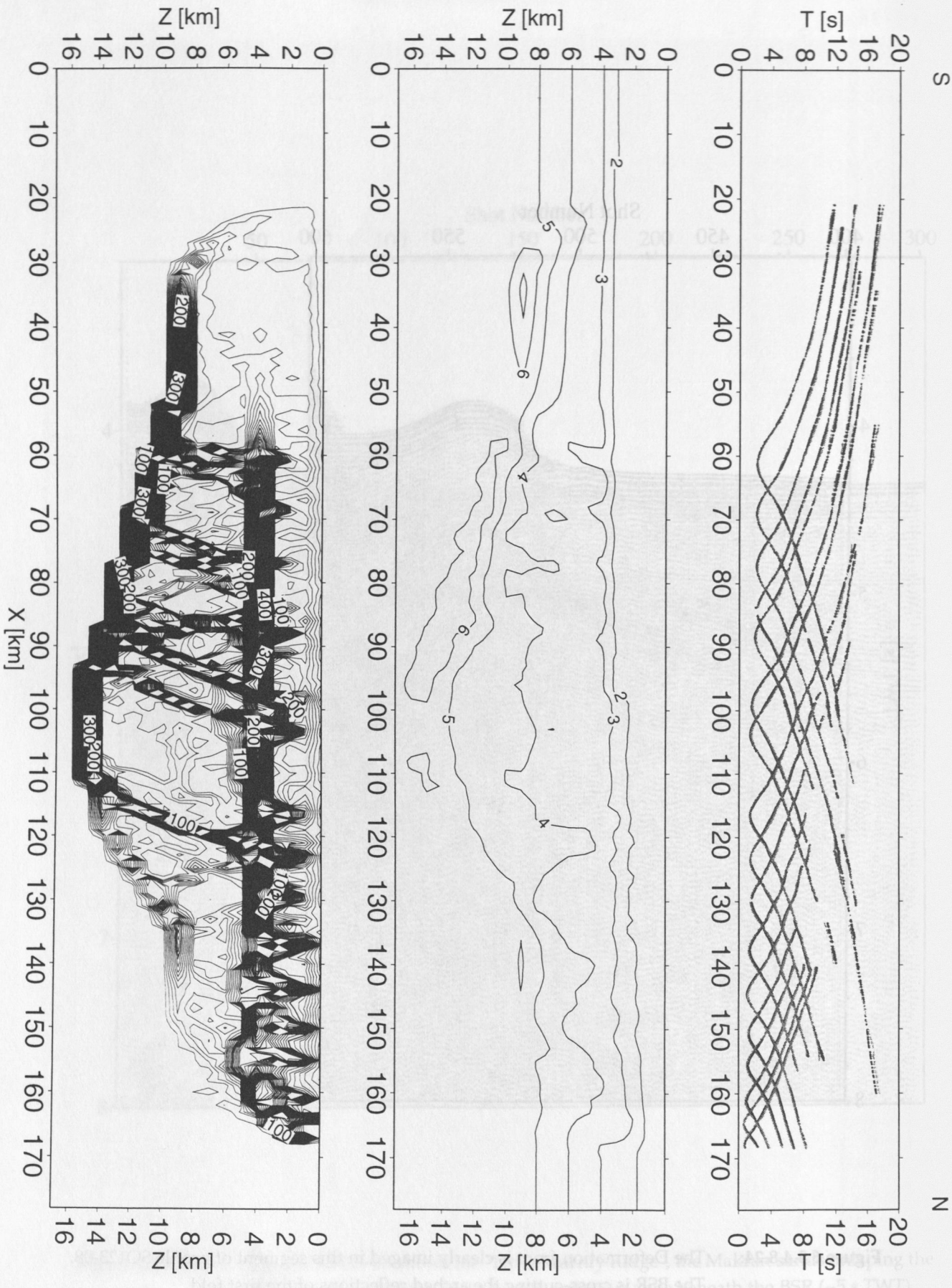

Figure 6.3.4.8.25: Result of the finite-difference inversion with "raytomorf"; top: observed (black) and calculated (light grey) arrival times; middle: velocity model after 50 iterations; final error: 0.105 s grid size: 1 km * 1 km; bottom: ray coverage through the final model.

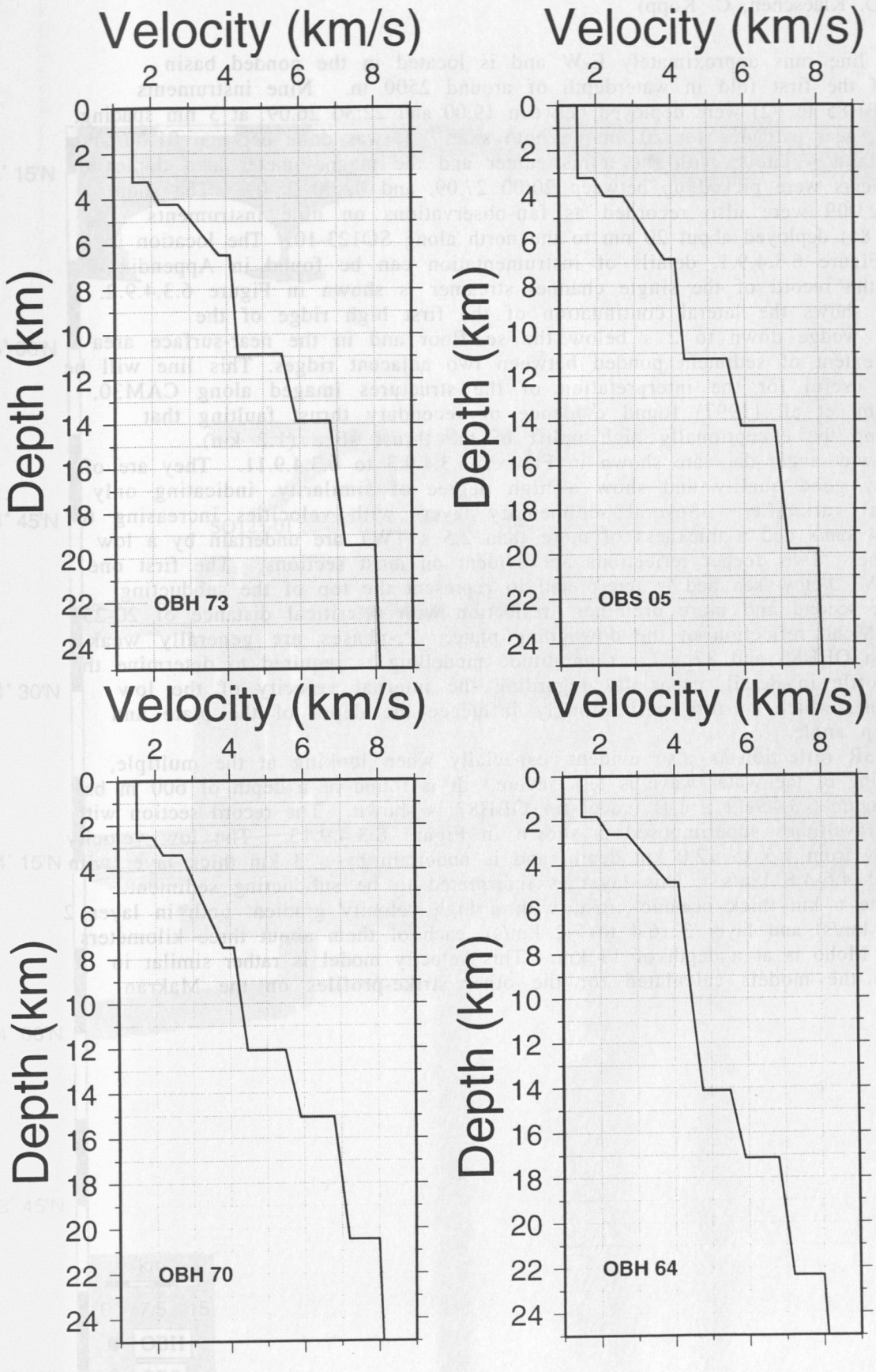

Figure 6.3.4.8.26: Vertical sections through two-dimensional velocity model at the location of OBH73, OBS05, OBH70, and OBH64.

6.3.4.9 Profile SO123-09

(E. Flueh, D. Klaeschen, C. Kopp)

This line runs approximately E-W and is located in the ponded basin landward of the first fold in waterdepth of around 2500 m. Nine instruments (OBH69, OBH85 to 92) were deployed between 19:00 and 22:30 26.09. at 3 nm spacing, and shooting was extended for 20 nm on both sides. It was done between 01:00 and 17:00 27.09. at 4 knots, with the ministreamer and the magnetometer also deployed. The instruments were picked up between 20:00 27.09. and 02:00 28.09. The shots along SO123-09 were also recorded as fan-observations on nine instruments (OBH76 to 84) deployed about 20 nm to the north along SO123-10. The location is shown in Figure 6.3.4.9.1, details of instrumentation can be found in Appendix 9.1.9, and the record of the single channel streamer is shown in Figure 6.3.4.9.2. This figure shows the lateral continuation of the first high ridge of the accretionary wedge down to 2 s below the sea-floor and in the near-surface area the lateral extent of sediment ponded between two adjacent ridges. This line will be particularly useful for the interpretation of the structures imaged along CAM30, where Fruehn et al. (1997) found evidence of secondary thrust faulting that occurs during the exceptionally high uplift of the thrust slice (1.2 km).

The wide-angle data are shown in Figures 6.3.4.9.3 to 6.3.4.9.11. They are of exceptionally good quality and show a high degree of similarity, indicating only small lateral variability. Several sedimentary layers with velocities increasing to more then 4 km/s and a thickness of more than 2.5 s TWT are underlain by a low velocity zone. Two deeper reflections are evident on most sections. The first one at 6.0 s TWT below sea bed is interpreted to represent the top of the subducting plate. The second and more prominent reflection with a critical distance of 20-25 km is the Moho reflection of the downgoing plate. P_n-phases are generally weak but clear on OBH86 and 87. Later amplitude modelling is required to determine the velocity profile in detail, especially regarding the internal velocity of the low velocity zone, which in turn will strongly influence the depth of the plate and thus the dip angle.

A BSR reflection is also evident, especially when looking at the multiple, where clipping of the water wave is less severe. It is found at a depth of 600 m bs.

In Figure 6.3.4.9.12 a 1-D model for OBH87 is shown. The record section with calculated traveltimes superimposed is shown in Figure 6.3.4.9.13. The low velocity zone extends from 7.5 to 12.0 km depth, and is underlain by a 3 km thick layer with velocities of 4.6-4.8 km/s. This layer is interpreted to be subducting sediment. Below is the 6 km thick oceanic crust, with a high velocity gradient both in layer 2 (5.5 to 6.1 km/s) and layer 3 (6.4 to 7.2 km/s), each of them about three kilometers thick. The Moho is at a depth of 19 km. This velocity model is rather similar in structure to the models calculated for the other strike-profiles on the Makran wedge.

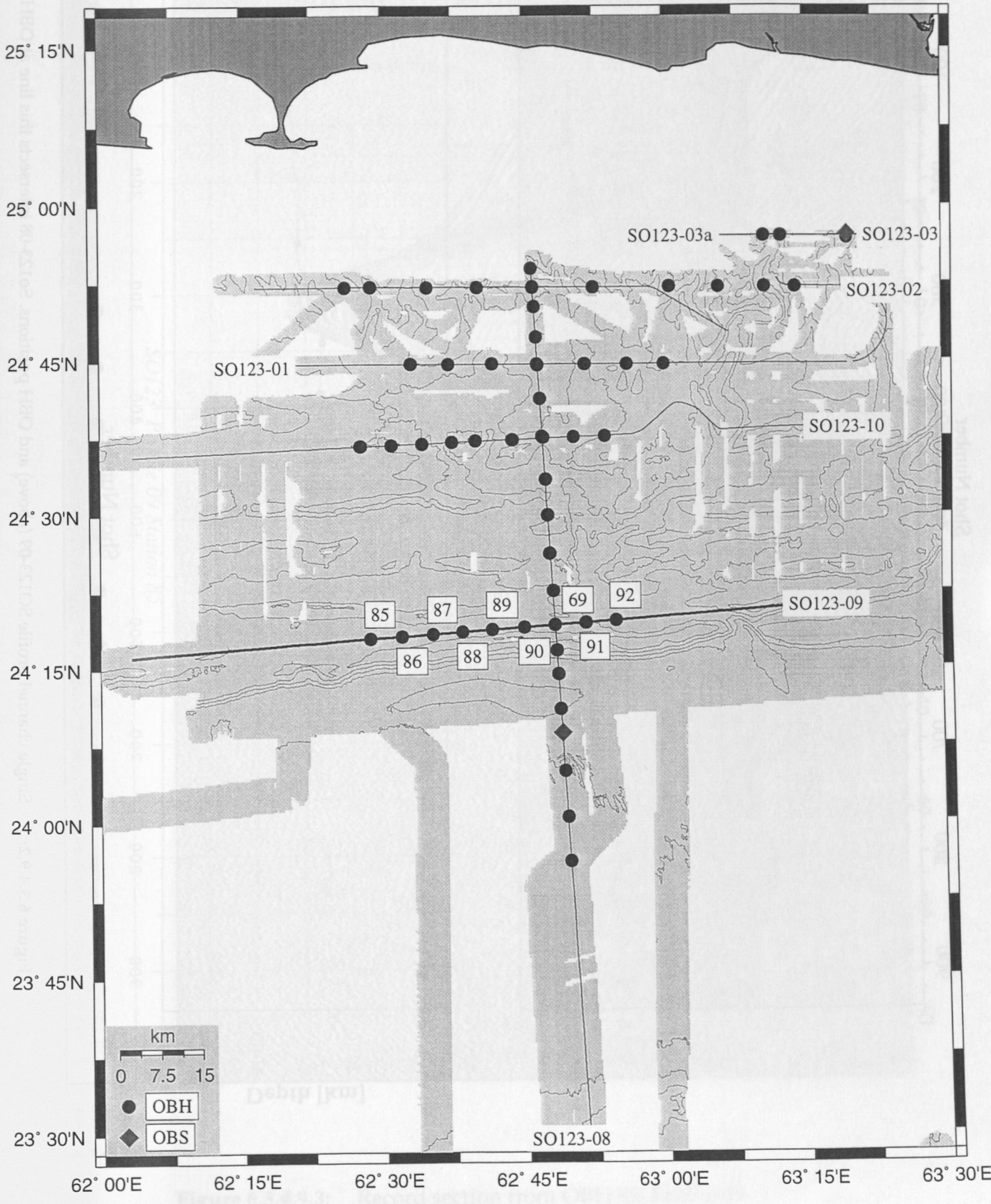

Figure 6.3.4.9.1: Location map of profile SO123-09.

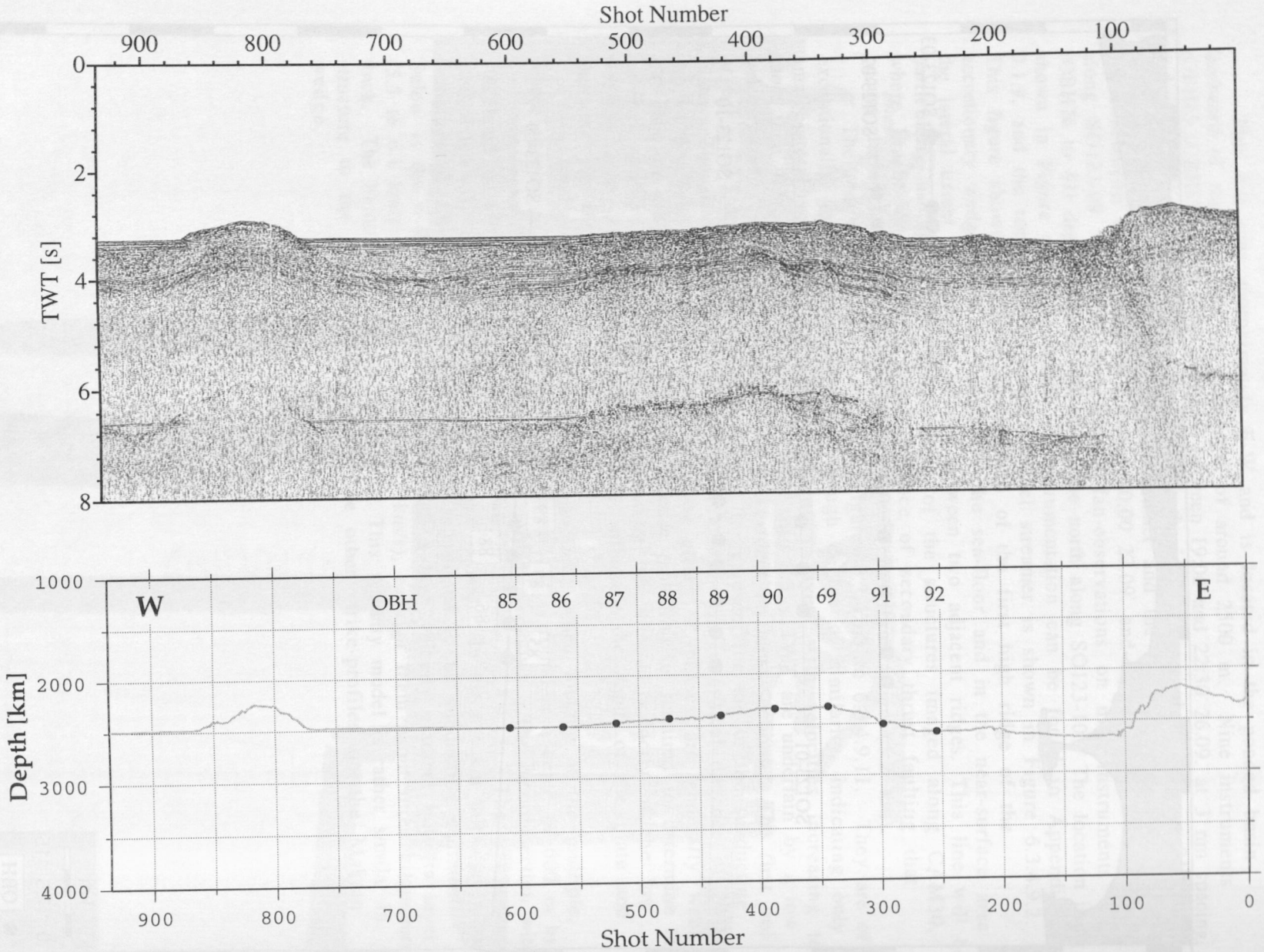

Figure 6.3.4.9.2: Single channel profile SO123-09 (above) and OBH positions. So123-08 intersects this line at OBH 69.

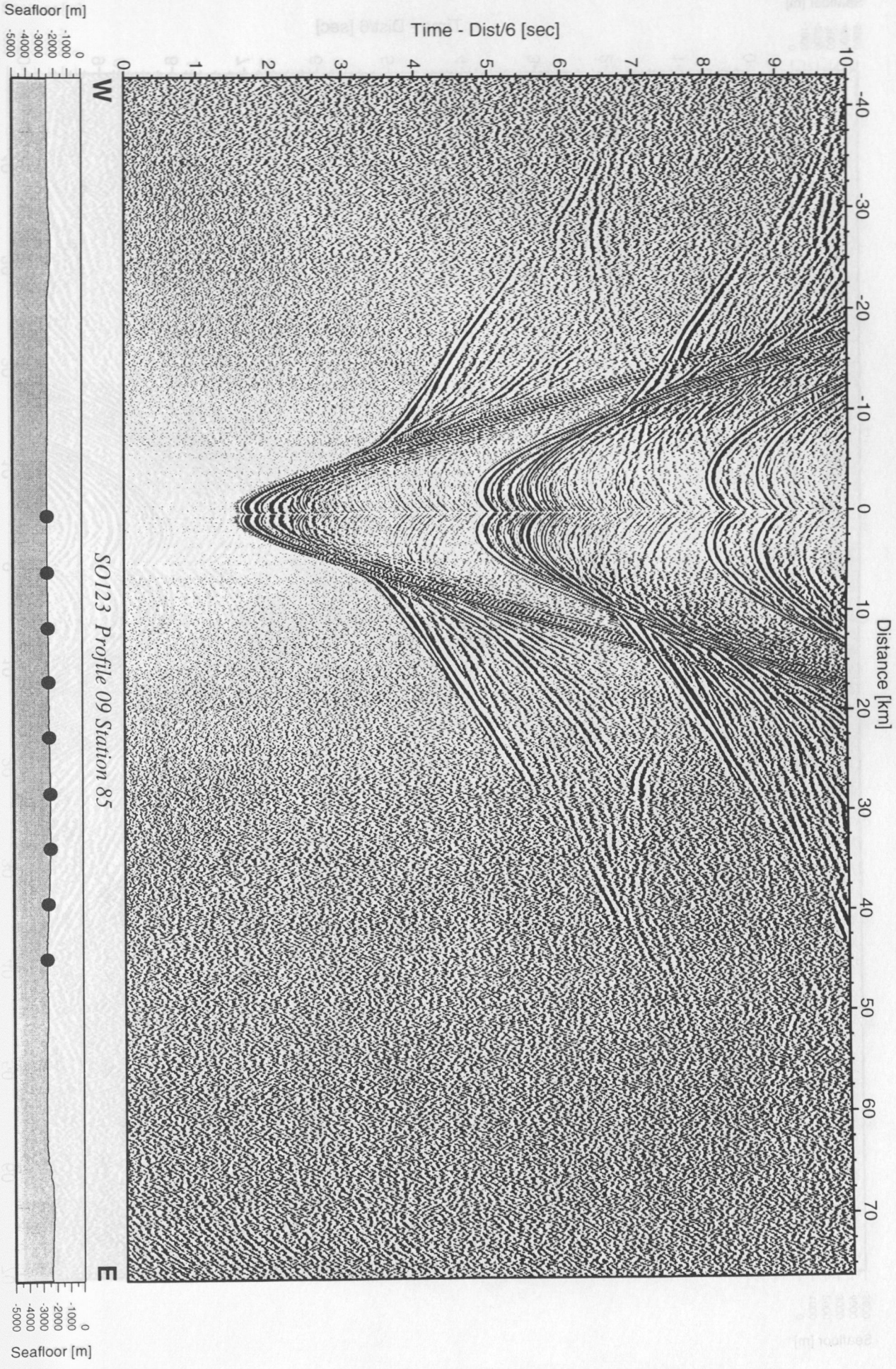

Figure 6.3.4.9.3: Record section from OBH 85, Profile 09.

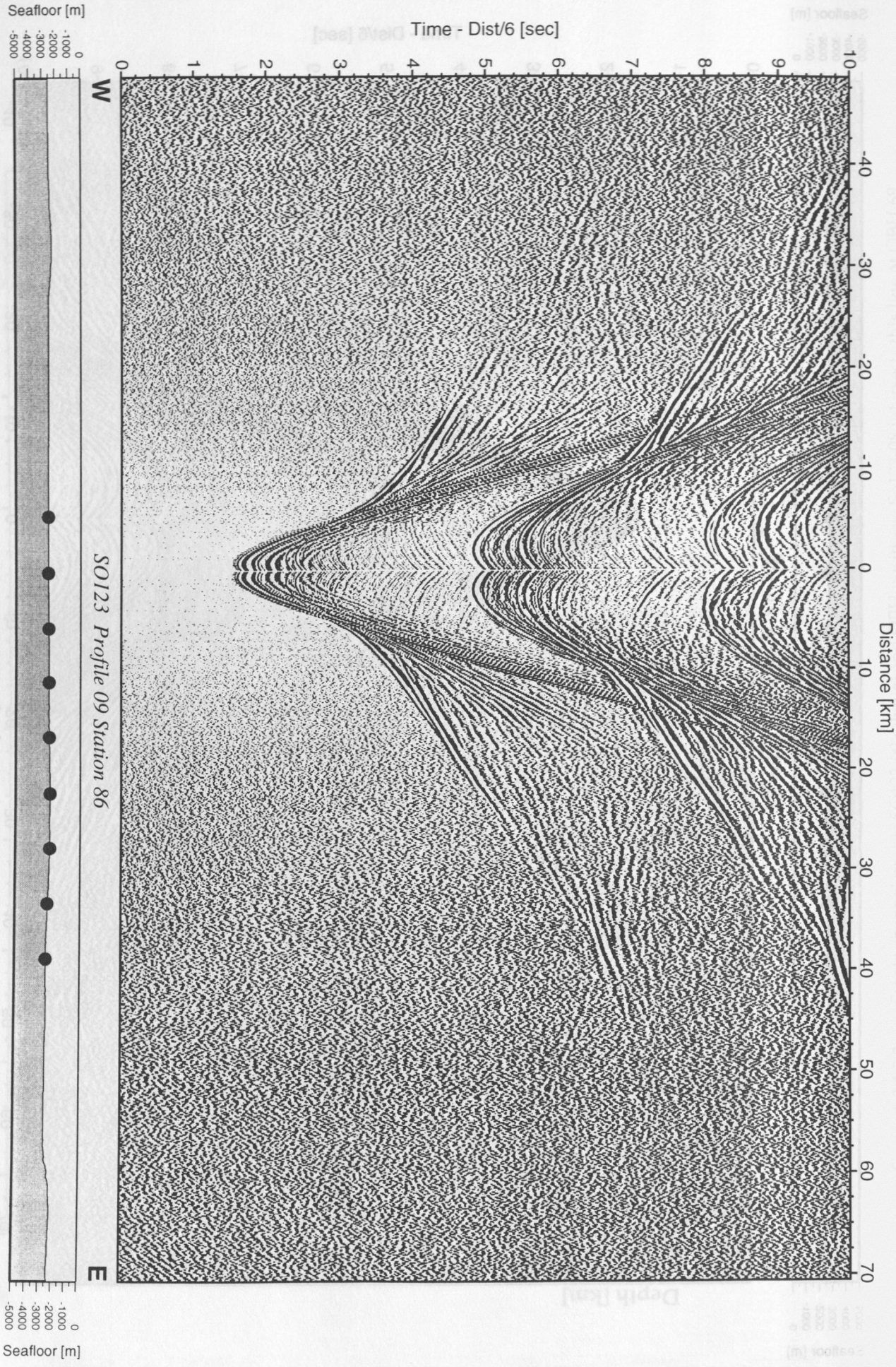

Figure 6.3.4.9.4: Record section from OBH 86, Profile 09.

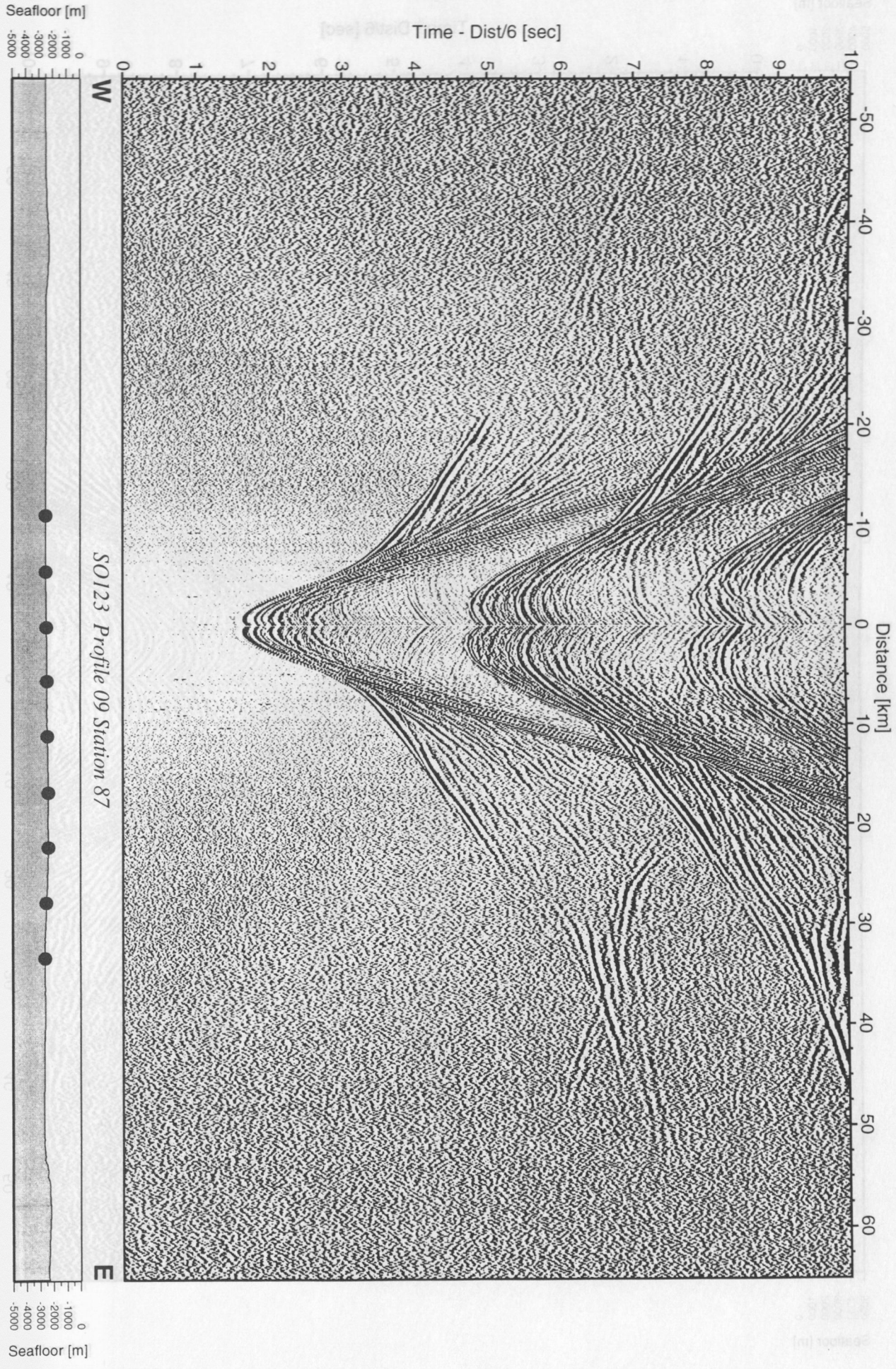

Figure 6.3.4.9.5: Record section from OBH 87, Profile 09.

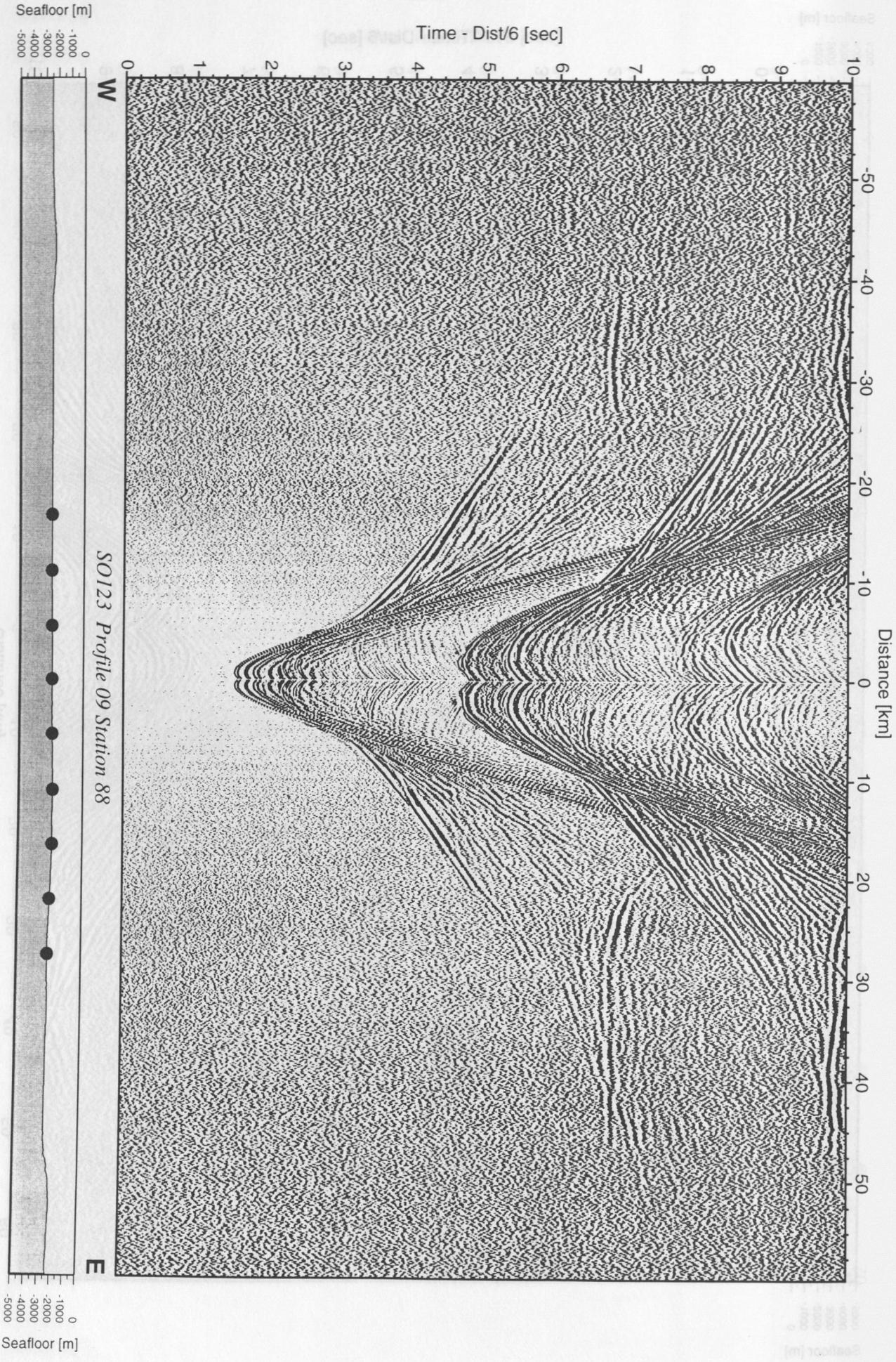

Figure 6.3.4.9.6: Record section from OBH 88, Profile 09.

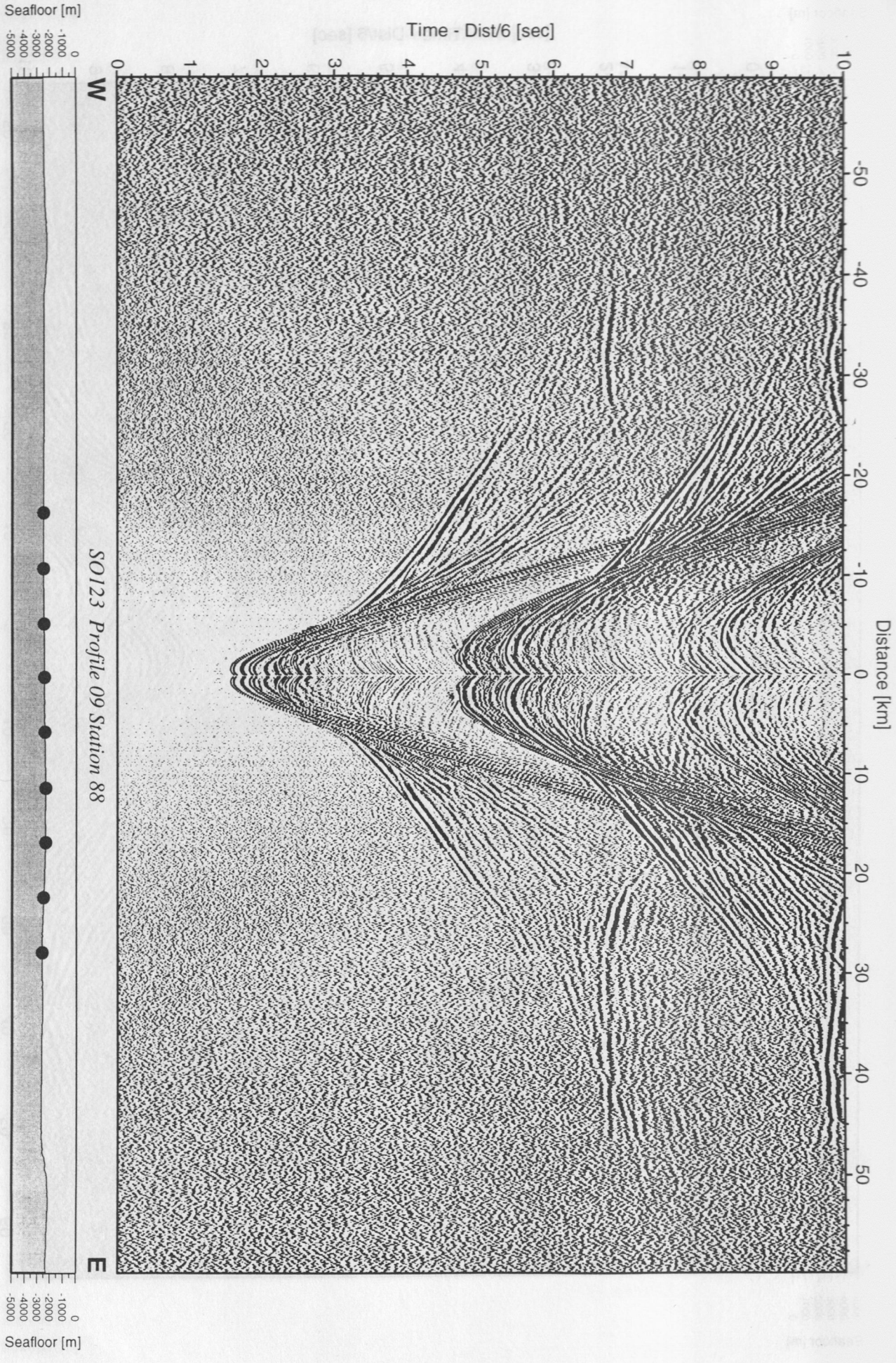

Figure 6.3.4.9.6: Record section from OBH 88, Profile 09.

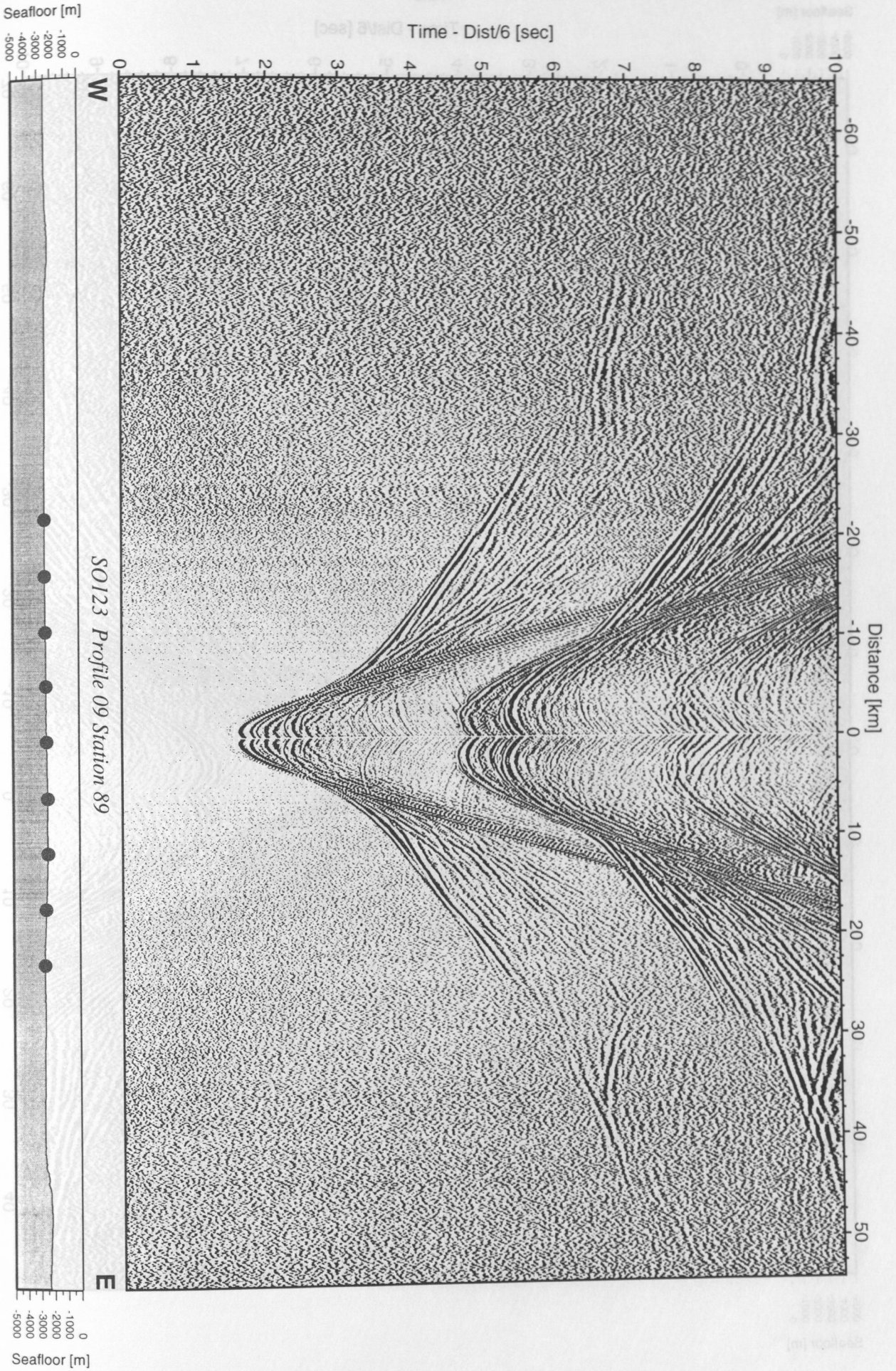

Figure 6.3.4.9.7: Record section from OBH 89, Profile 09.

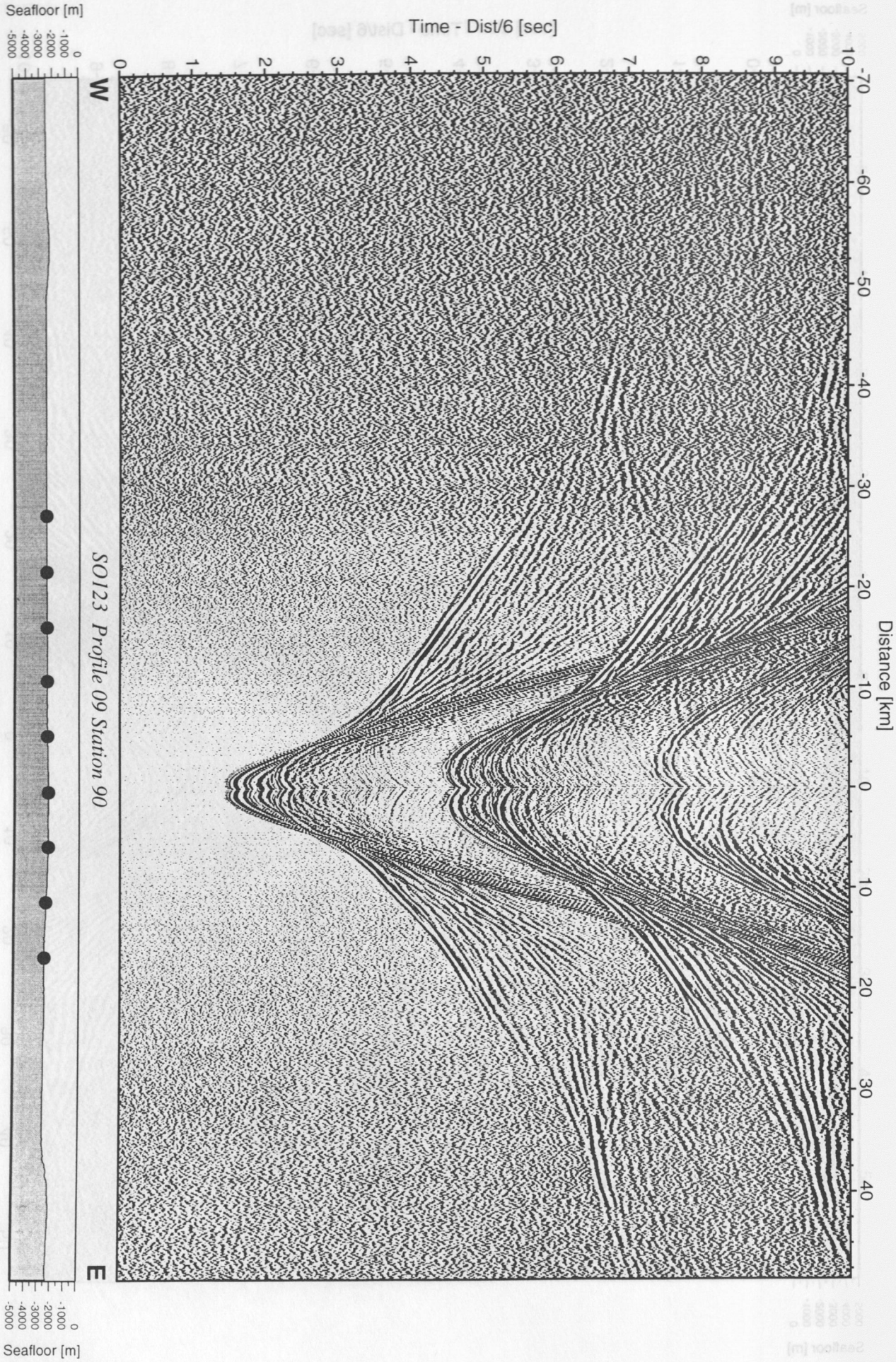

Figure 6.3.4.9.8: Record section from OBH 90, Profile 09.

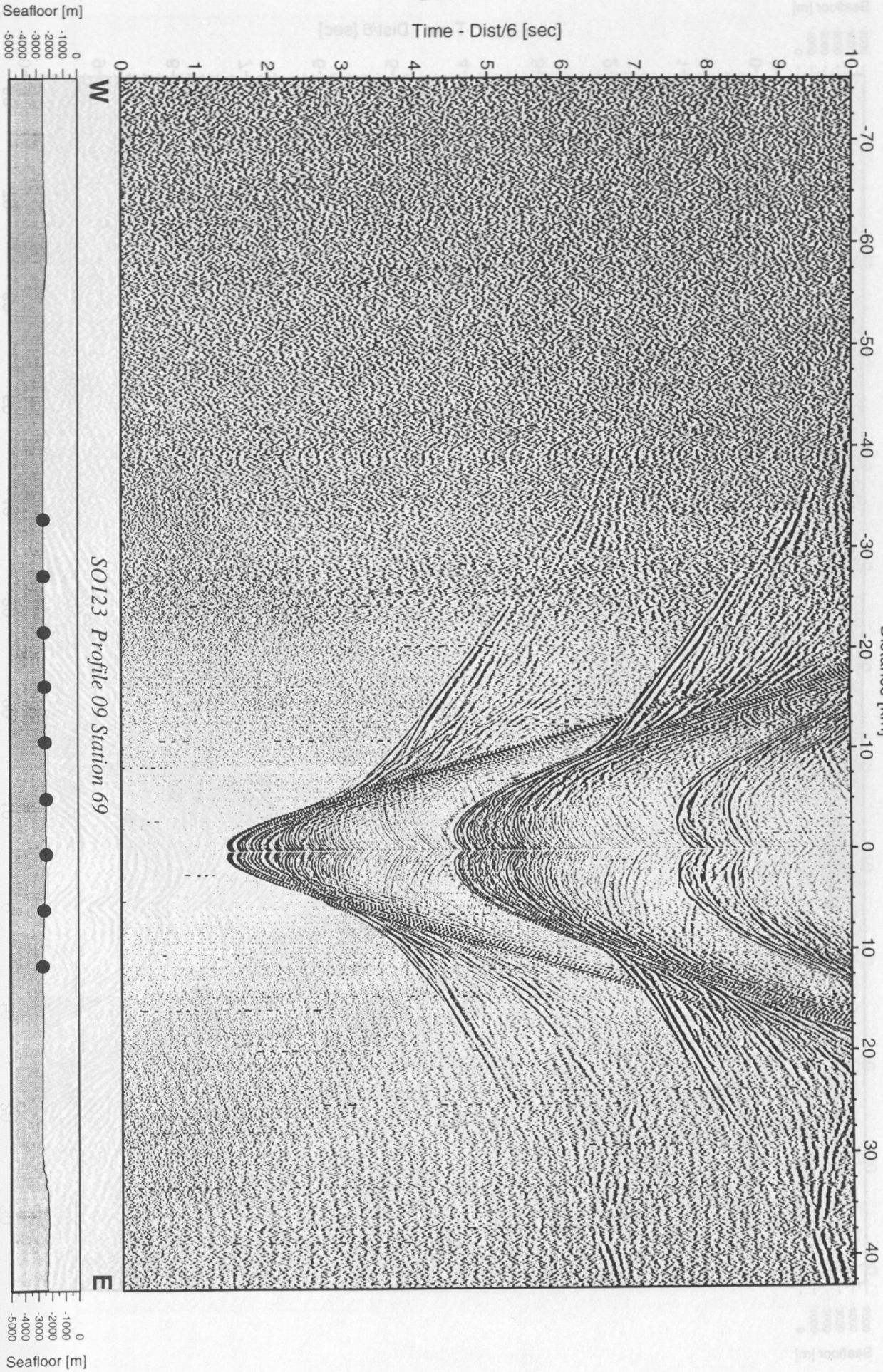

Figure 6.3.4.9.9: Record section from OBH 69, Profile 09.

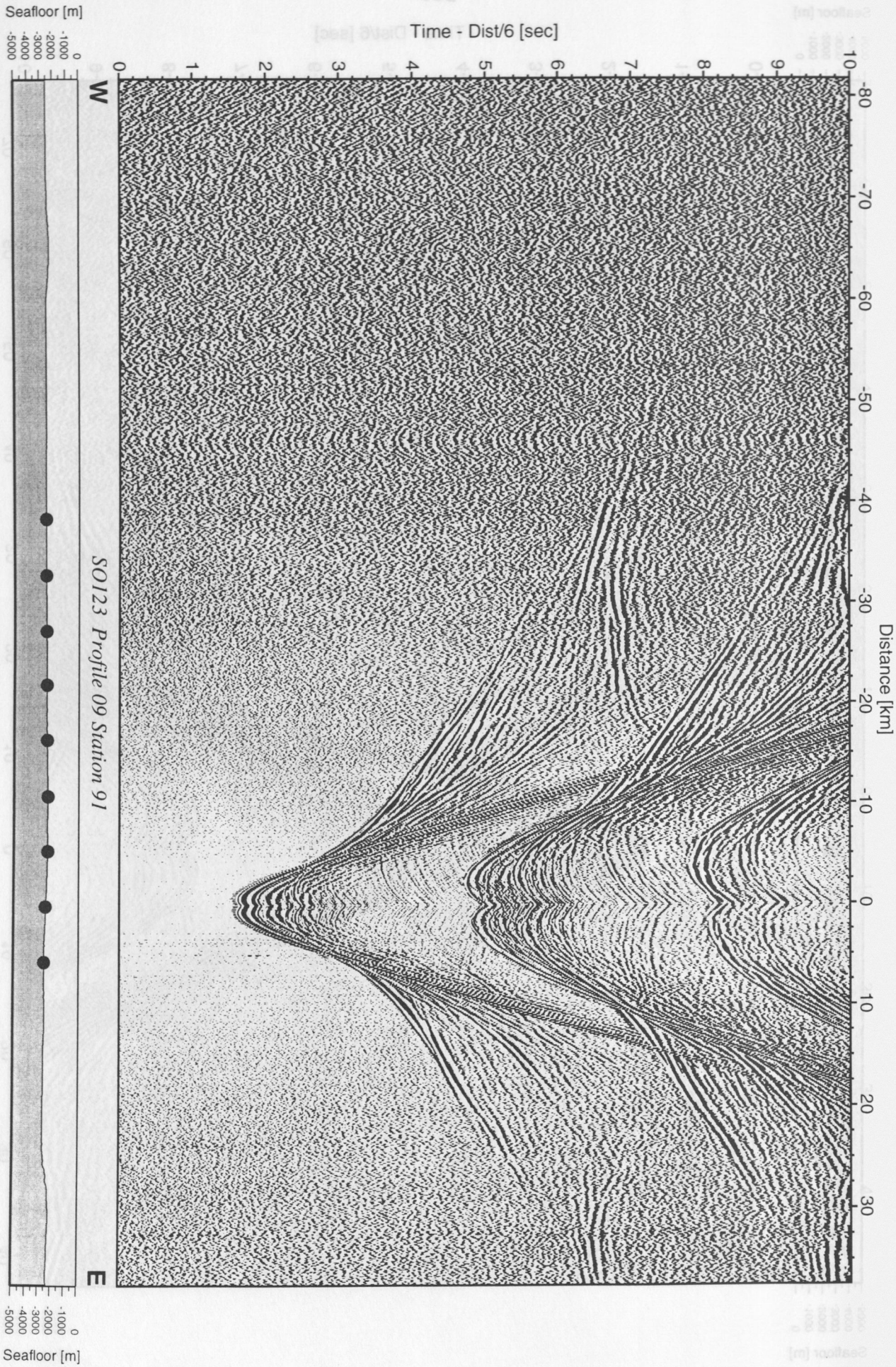

Figure 6.3.4.9.10: Record section from OBH 91, Profile 09.

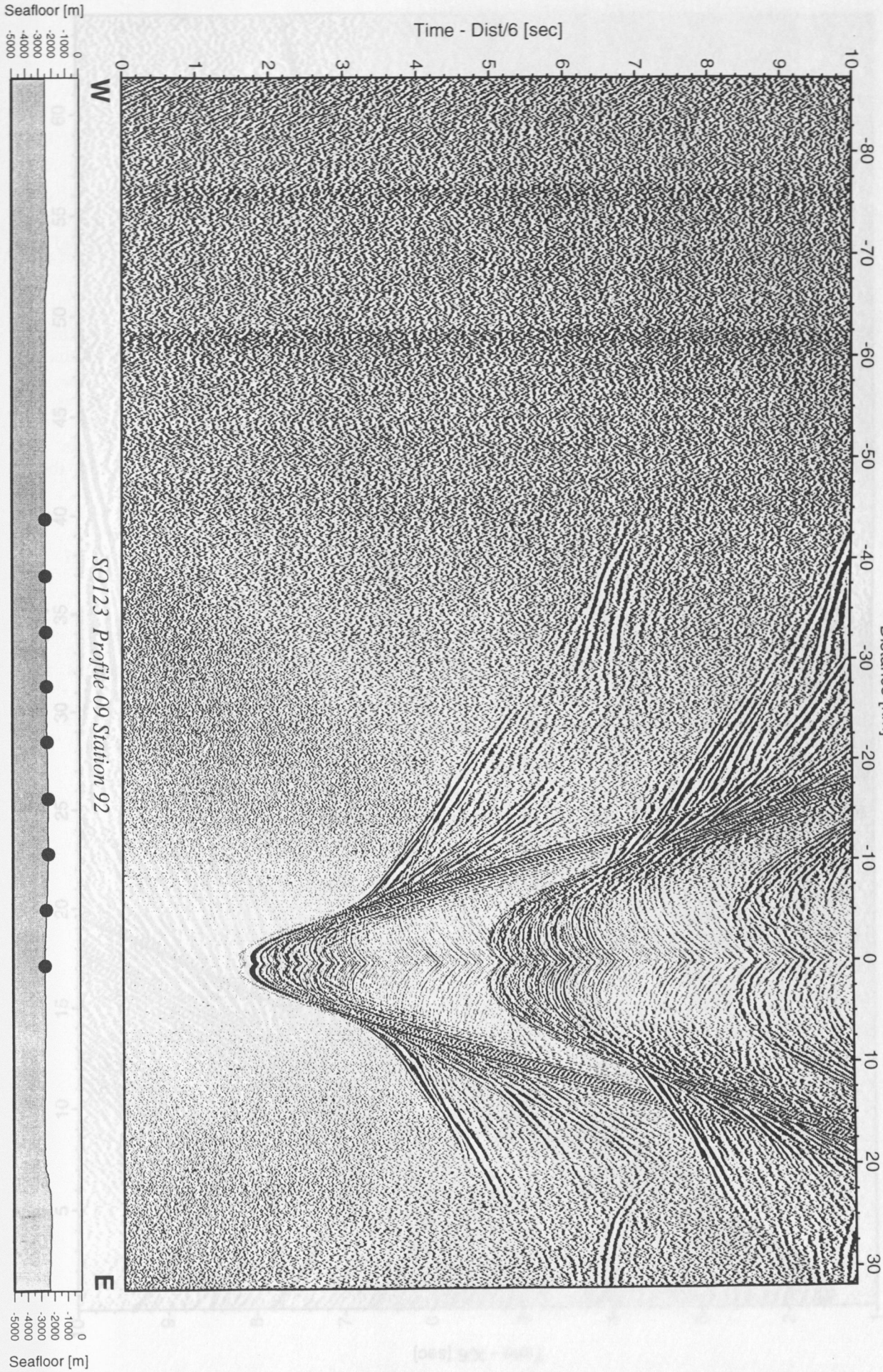

Figure 6.3.4.9.11: Record section from OBH 92, Profile 09.

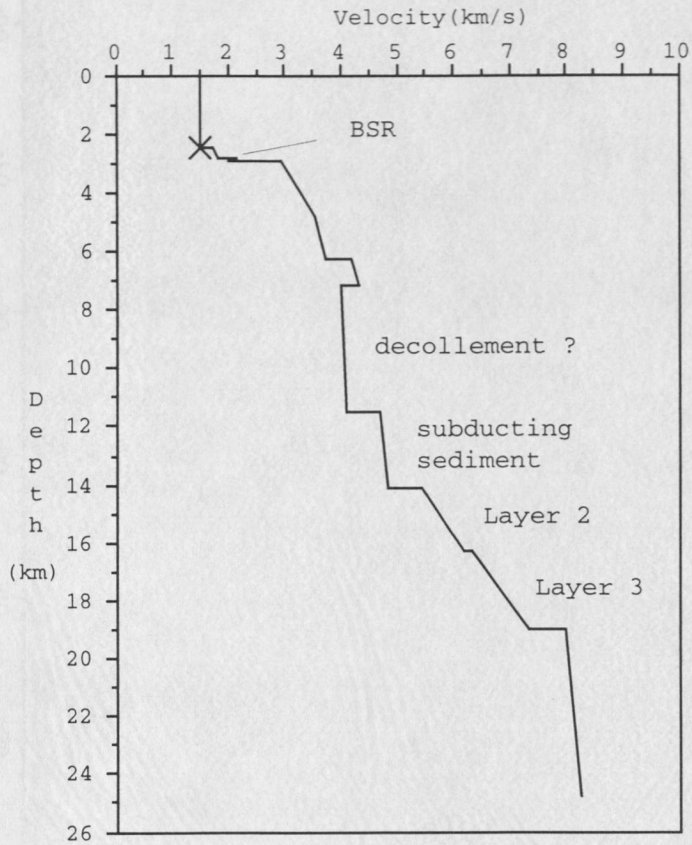

Figure 6.3.4.9.12: 1-D velocity-depth model for OBH87.

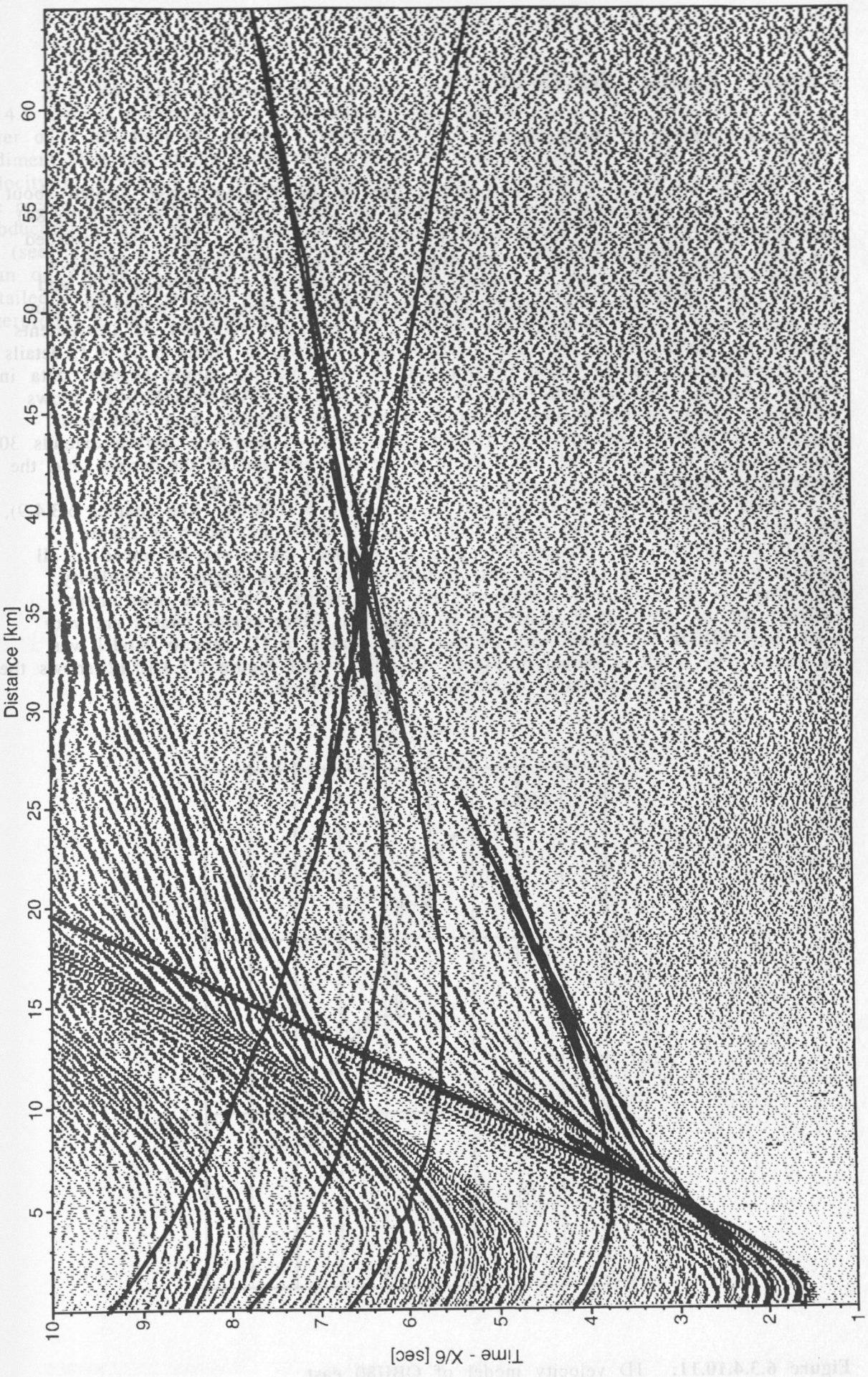

Figure 6.3.4.9.13: Record section of OBH87 east with calculated traveltimes from velocity model of Figure 6.3.4.9.12 superimposed.

6.3.4.10 Profile SO123-10

(S. Husen, E. Flueh, D. Klaeschen)

Profile SO123-10 is the fourth strike line on the Makran wedge located about midslope at waterdepth between 1700 and 1900 m. Nine instruments (OBH76 to 84) were deployed at 3 nm spacing between 14:00 and 17:30 26.09. They also recorded the shots along Profile SO123-09, but these fan observations were not analyzed onboard. Shooting was made at 4 knots with 60 s shot interval between 5:00 and 21:30 28.09. Soon after the beginning of the profile shooting had to deviate from the profile and bypass some fishing vessels. Subsequent recovery of instruments lasted from 1:00 to 6:00 29.09. The location map is shown in Figure 6.3.4.10.1, details of instrumentation can be found in Appendix 9.1.10, and the single channel data in Figure 6.3.4.10.2. This cross-line ("cross" with respect to CAM30/SO123-08) shows the lateral extent of the shallow structure in a highly thrusted area. The line intersects CAM30 around cdp 4000 (Figure 2.4), where a midslope terrace extends 30 km landwards. In line 10 the thrust fault at the seaward end of the terrace and the underthrust sediment can be traced laterally for at least 45 km.

Data quality is not as exceptional as in profile SO123-09 (see chapter 6.3.4.9), but still of good quality. The record sections of the OBH are shown in Figure 6.3.4.10.3 to 6.3.4.10.10 . Phases belonging to sediment layers can be traced in all sections to an offset up to 30 km. All sections show a good degree of similarity, indicating no strong lateral variation along the profile. On some instruments (OBH84, 82, 81, 80) a PmP phase can be identified. Other crustal phases are very weak. For OBH80, the station with the best data quality, a 1D velocity model was calculated. The result is shown in Figure 6.3.4.10.11 and Figure 6.3.4.10.12 shows the record section with calculated traveltimes superimposed.

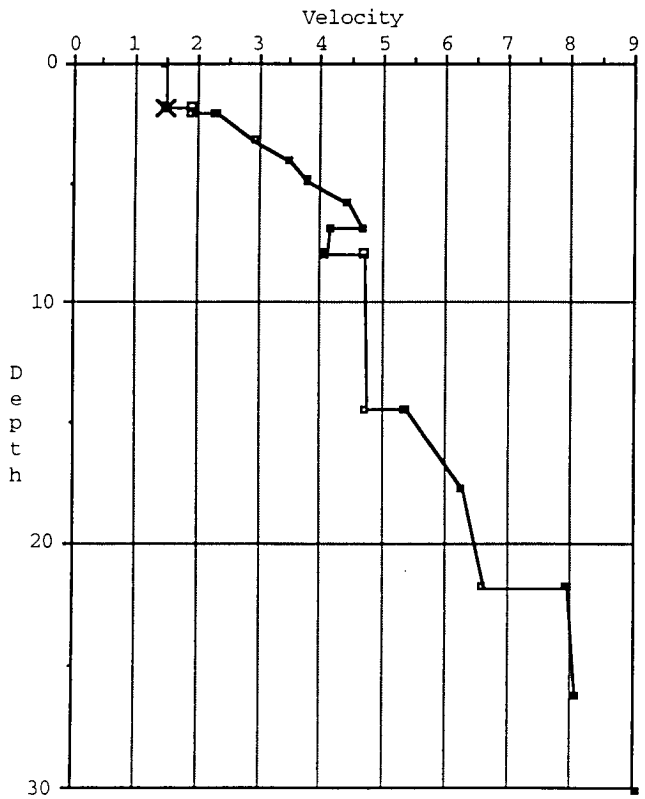

Figure 6.3.4.10.11: 1D velocity model of OBH80 east.

A 7 km thick sequence of sediment with velocities increasing from 1.8 km/s to 4.5 km/s is underlain by a low velocity zone with a thickness of 1 km. Below, a layer of 7 km thickness shows a velocity of 4.5 km, interpreted as subducted sediment. The top of the subducting oceanic crust is modeled at 15 km depth with a velocity of 5.5 km/s. A reflection from the oceanic Moho can clearly identified in the record and is modelled at a depth of 22 km. This gives a thickness of the subducting oceanic plate of 7 km which is slighty more than in the profile SO123-09 (see chapter 6.3.4.9). Also, the velocities in layer 3 seem to be lower (6.7 km/s) than on profile SO123-09, but this cannot be determined with confidence without detailed amplitude studies. As for the other strike lines, the low velocity zone is interpreted as an overpressured zone, that may correspond to the decollement.

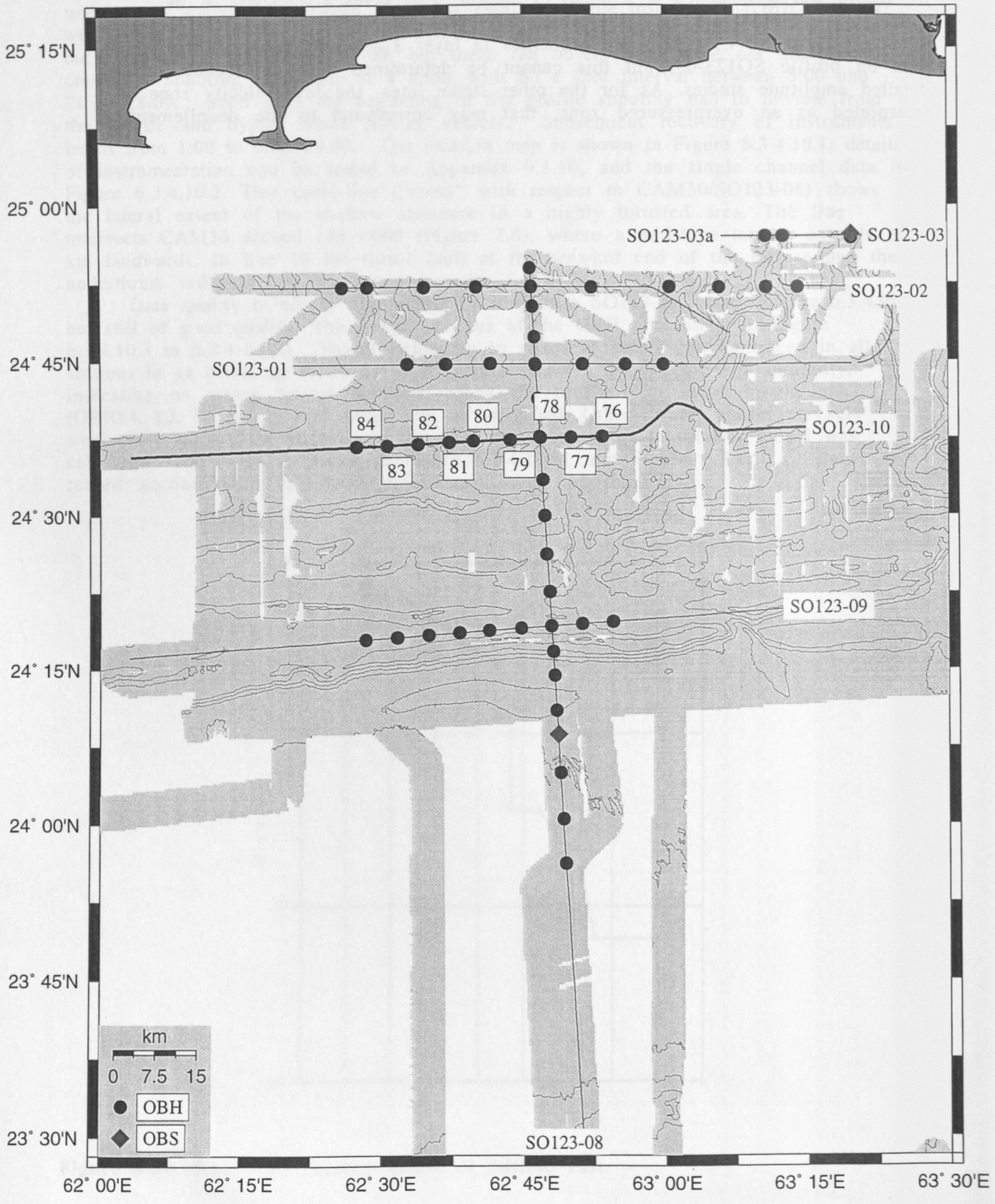

Figure 6.3.4.10.1: Location map of profile SO123-10.

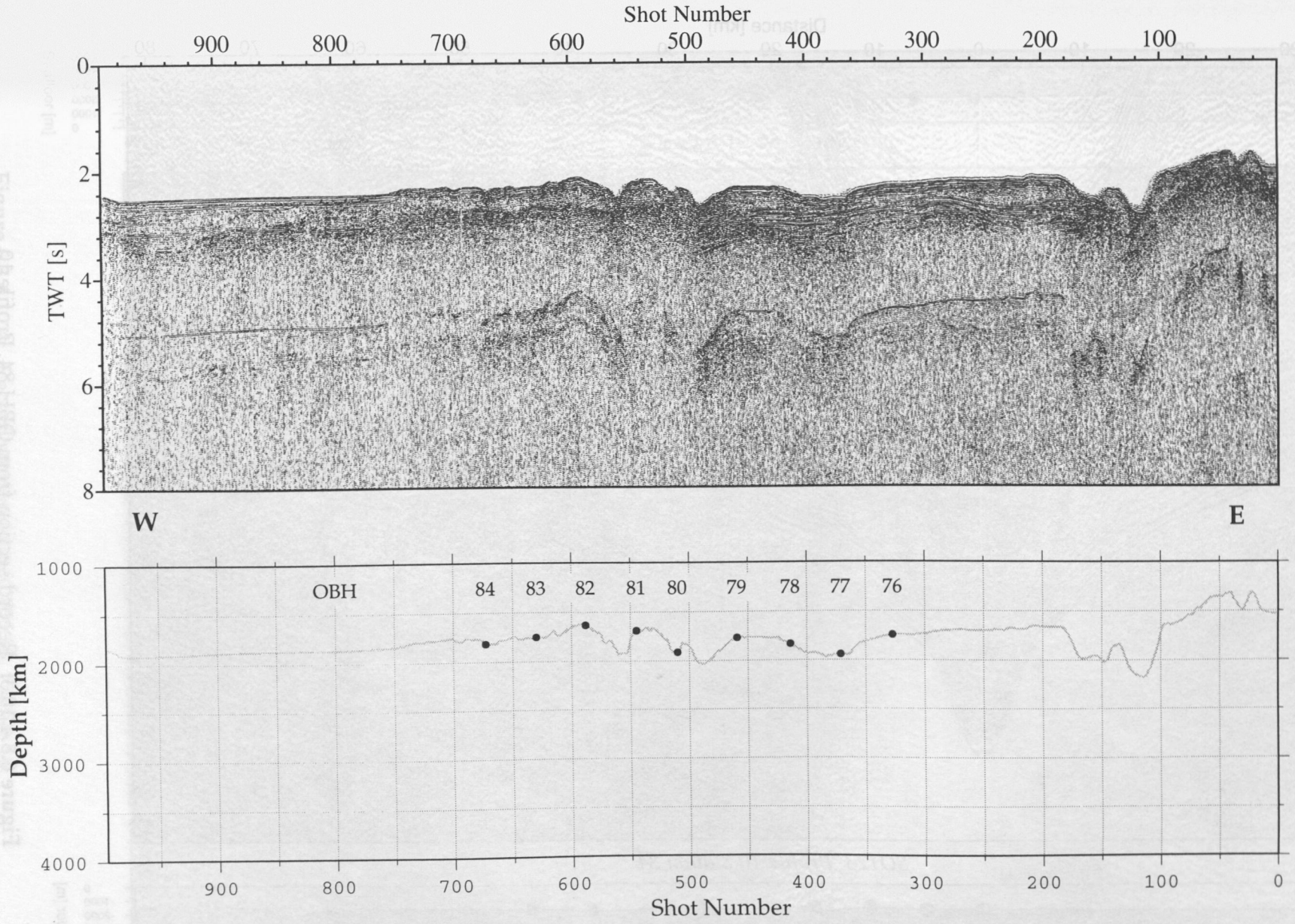

Figure 6.3.4.10.2: Single channel profile SO123-10 (above) and OBH positions. SO123-08 intersects this line at OBH 78.

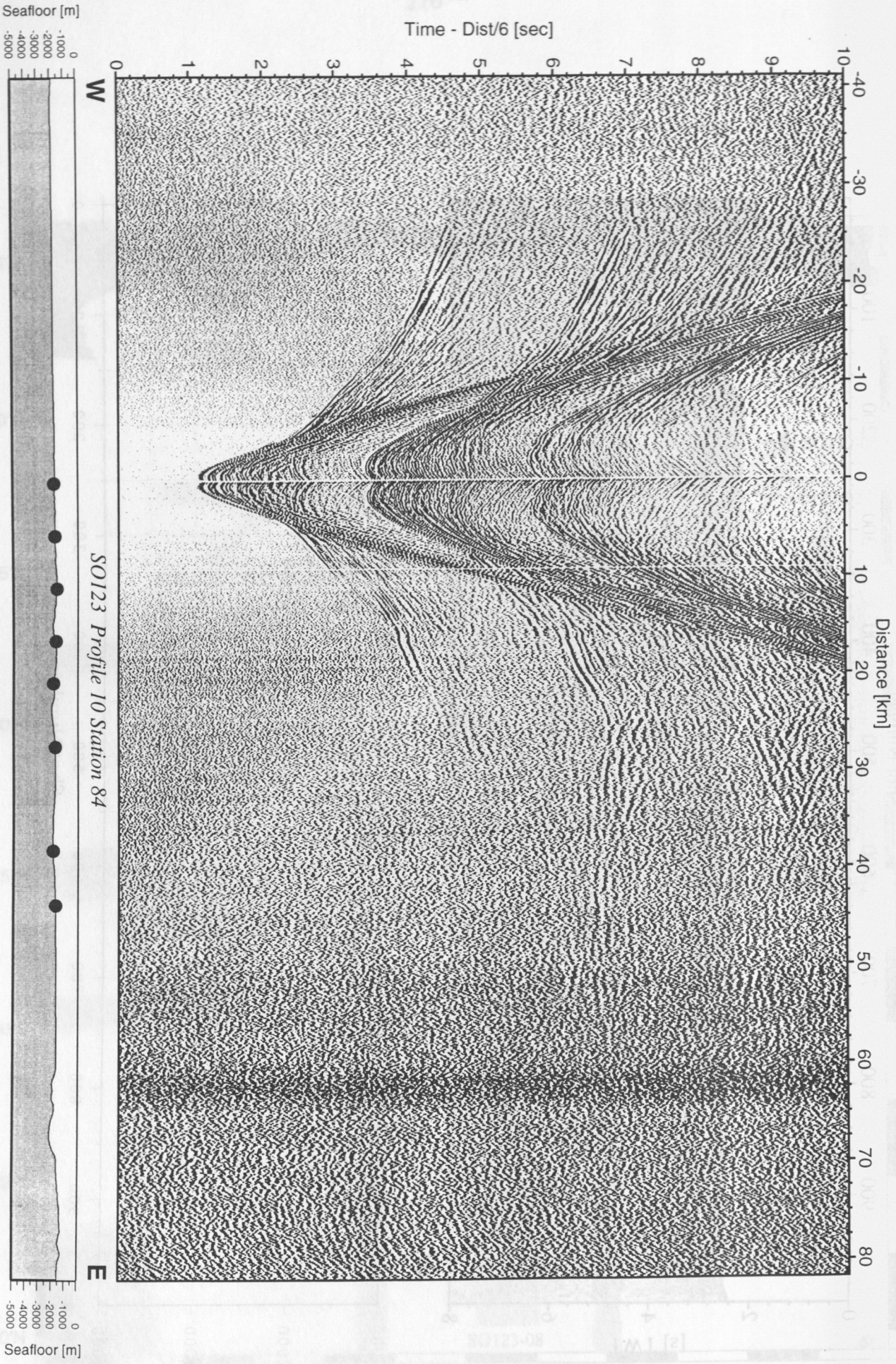

Figure 6.3.4.10.3: Record section from OBH 84, Profile 10.

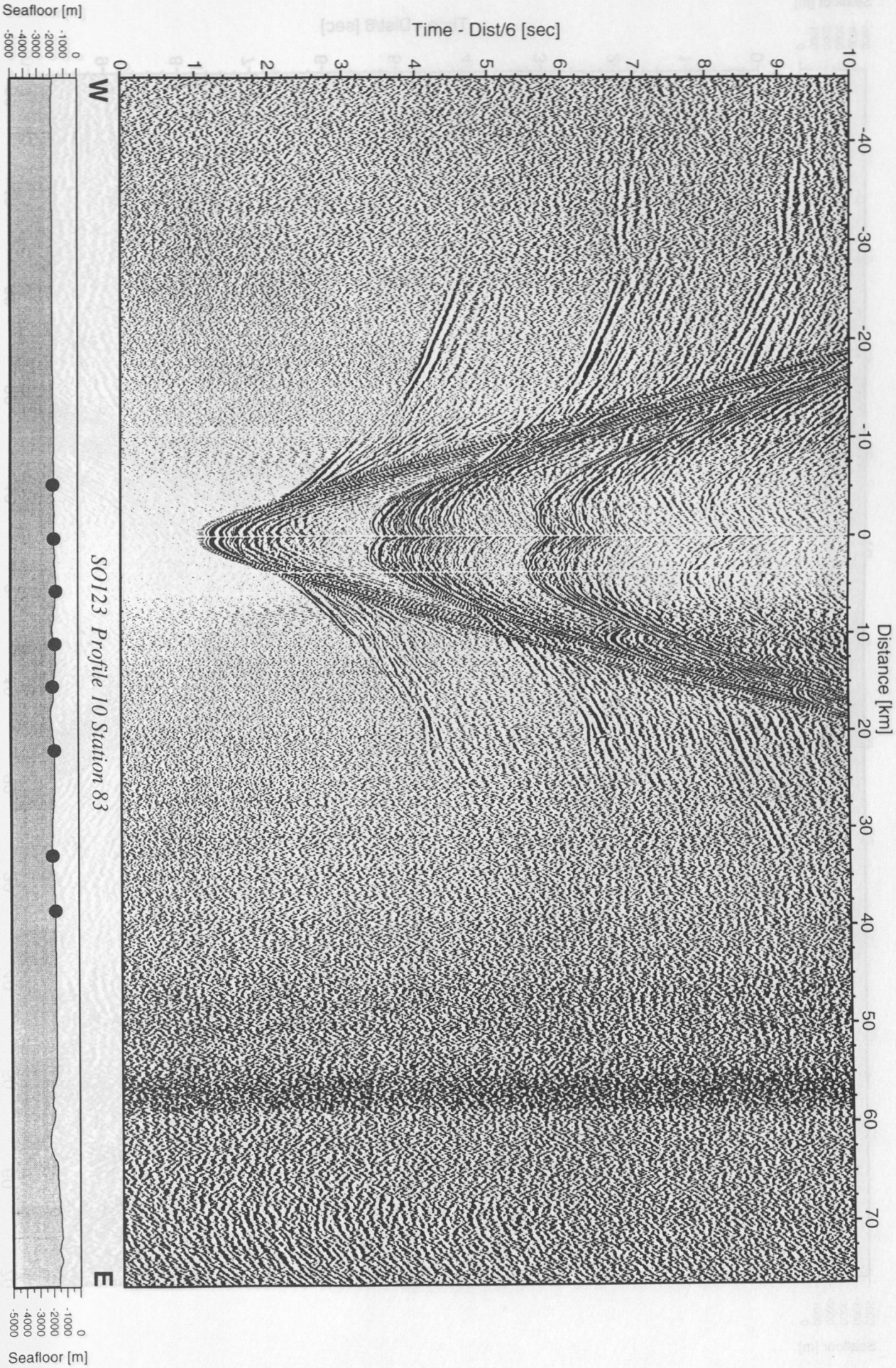

Figure 6.3.4.10.4: Record section from OBH 83, Profile 10.

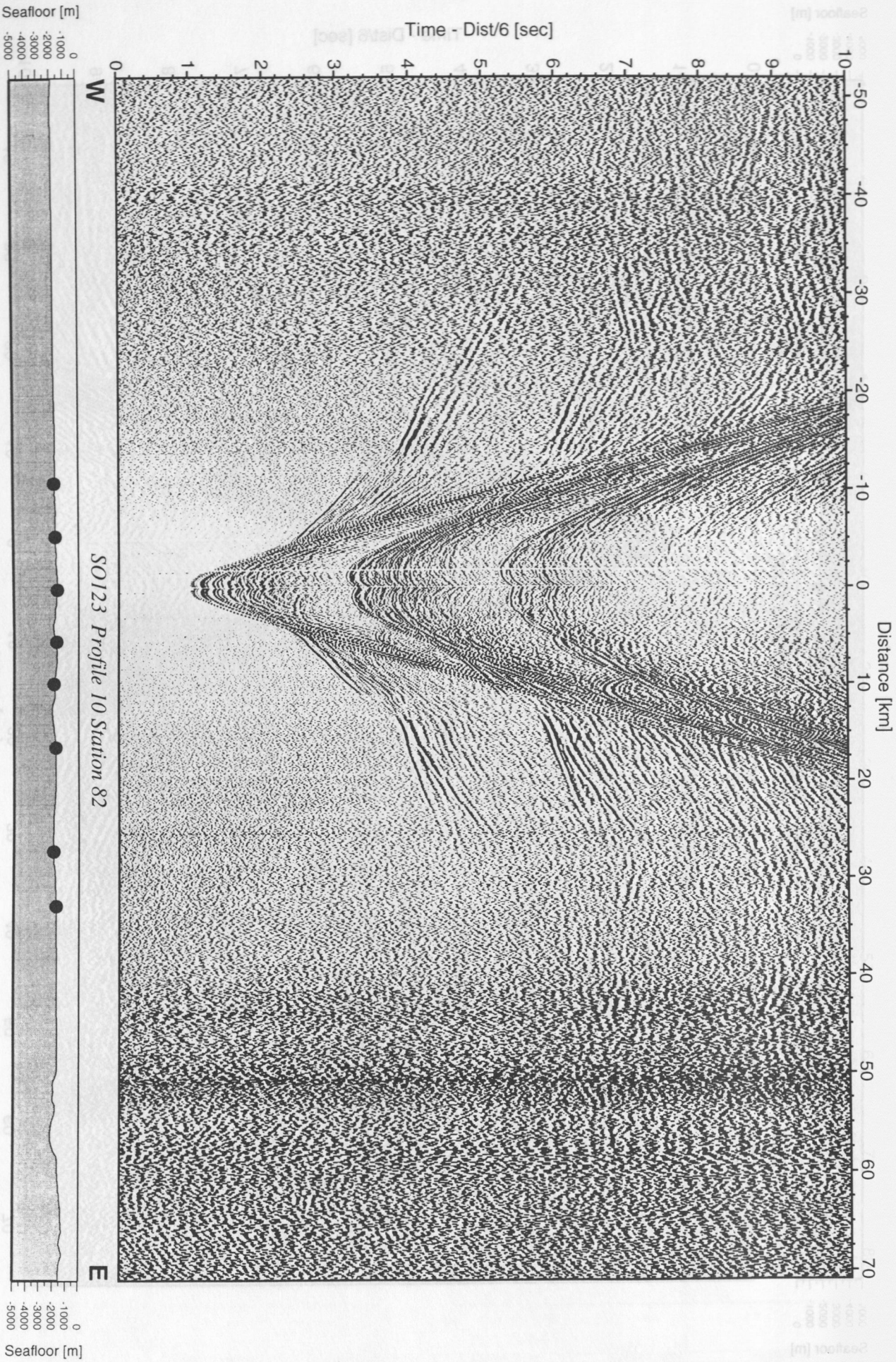

Figure 6.3.4.10.5: Record section from OBH 82, Profile 10.

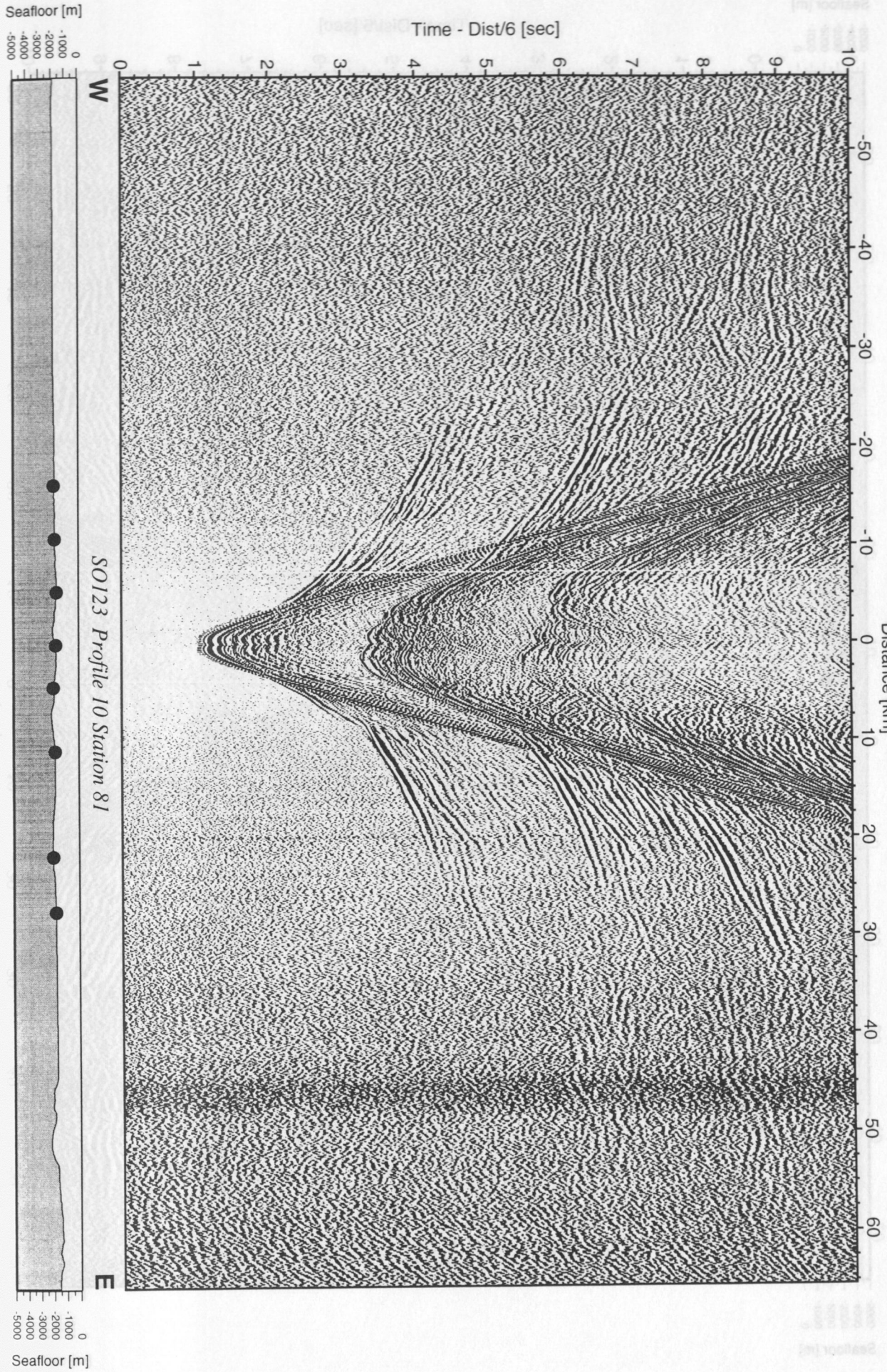

Figure 6.3.4.10.6: Record section from OBH 81, Profile 10.

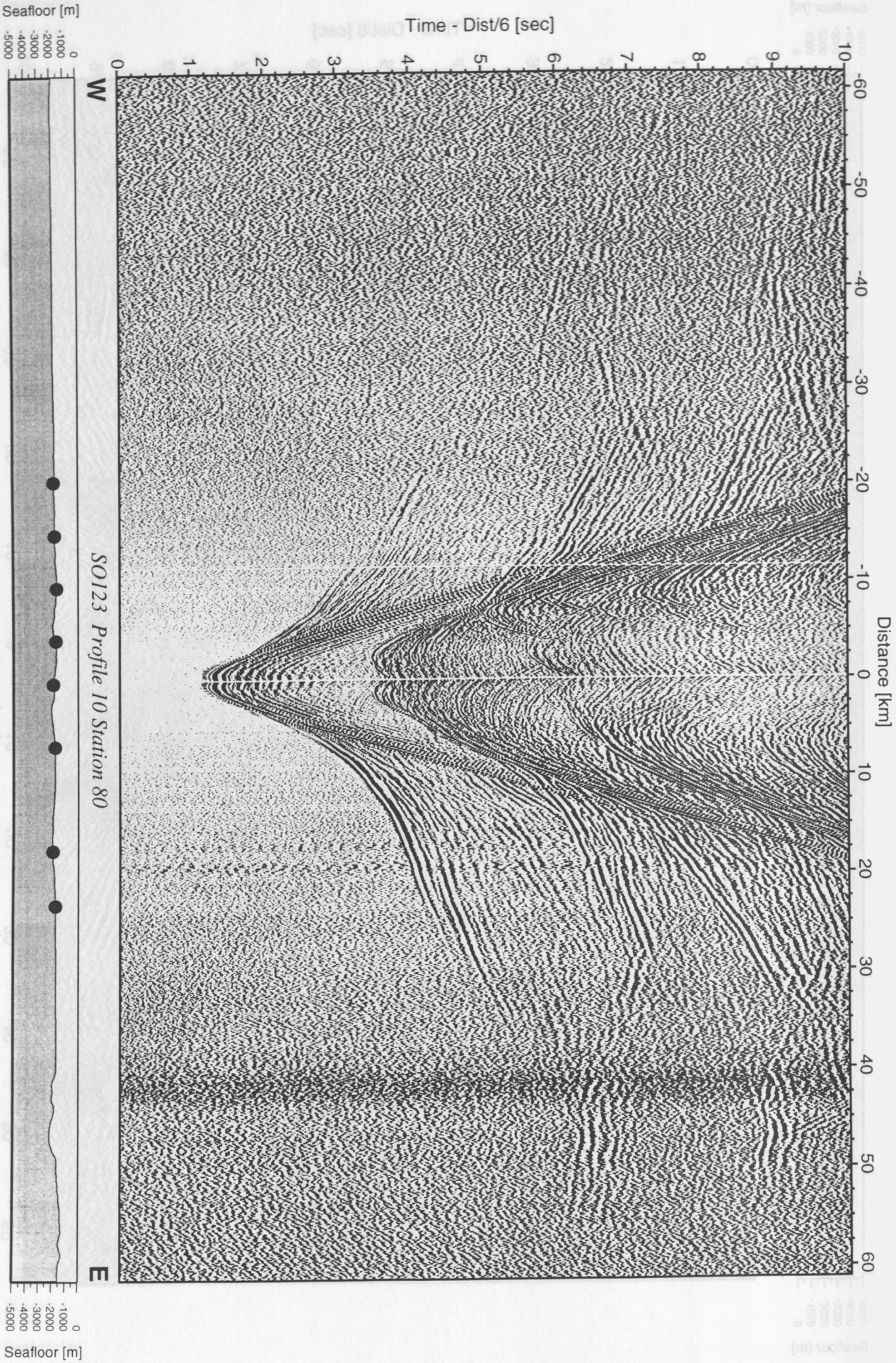

Figure 6.3.4.10.7: Record section from OBH 80, Profile 10.

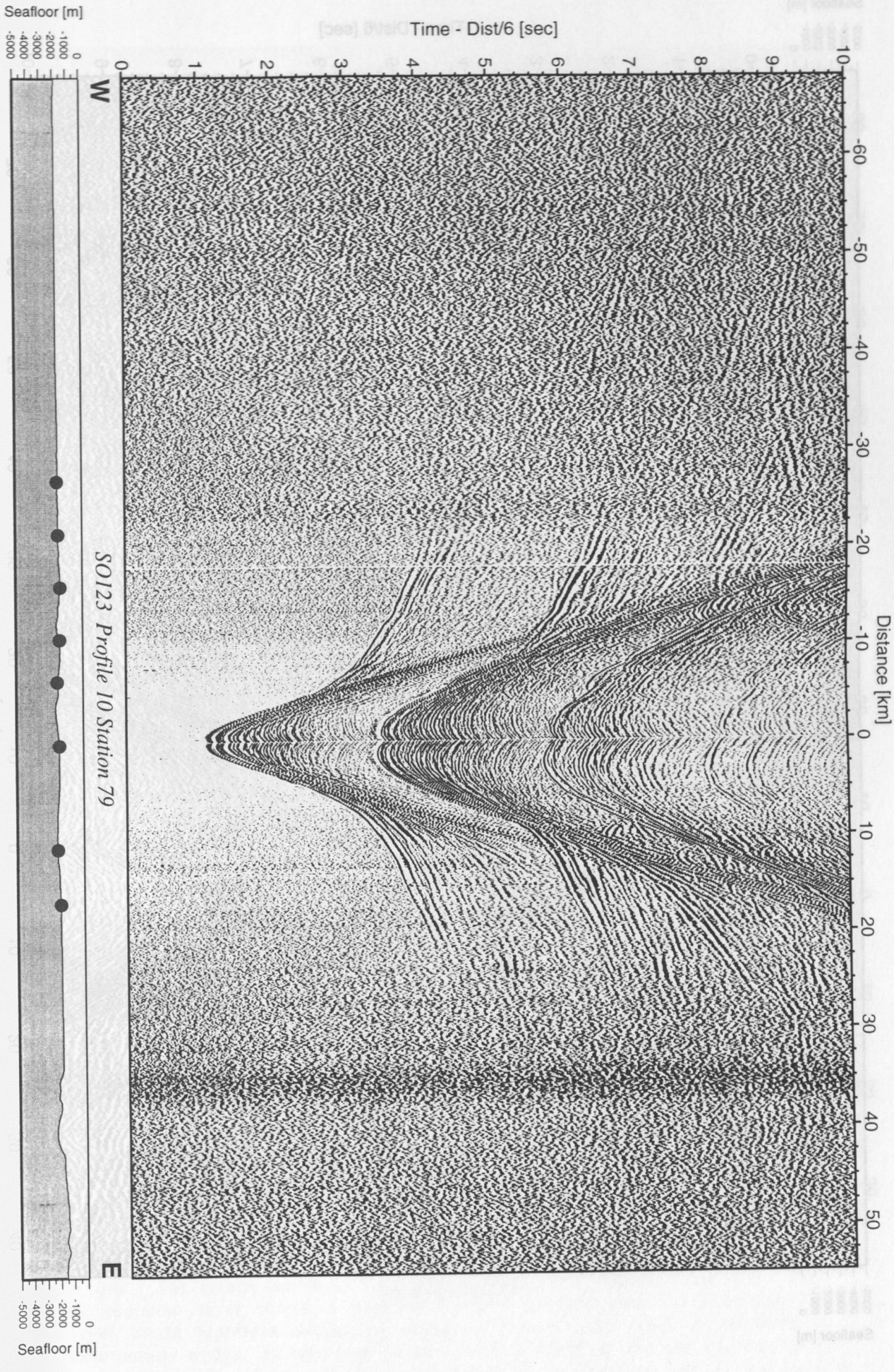

Figure 6.3.4.10.8: Record section from OBH 79, Profile 10.

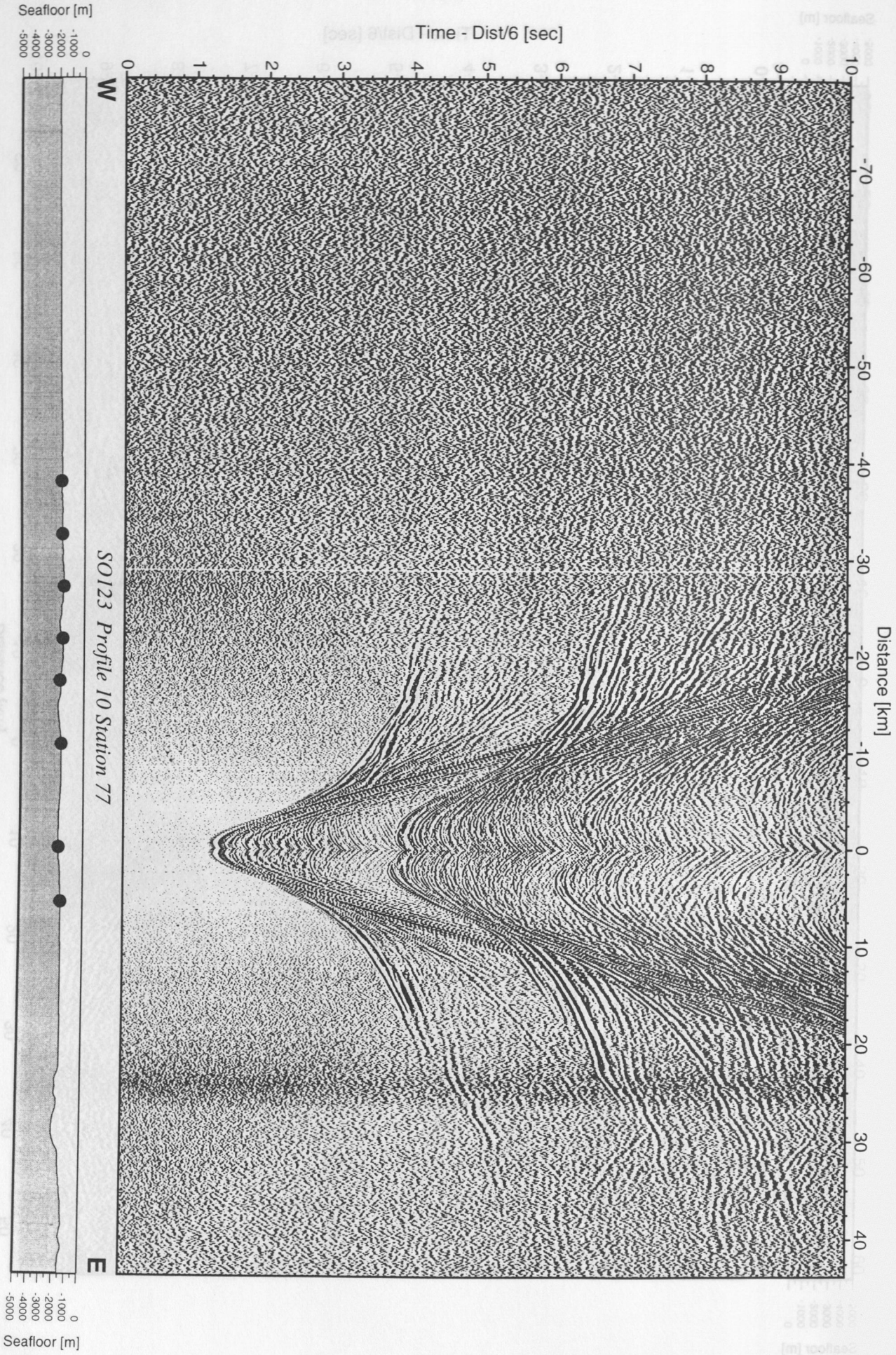

Figure 6.3.4.10.9: Record section from OBH 77, Profile 10.

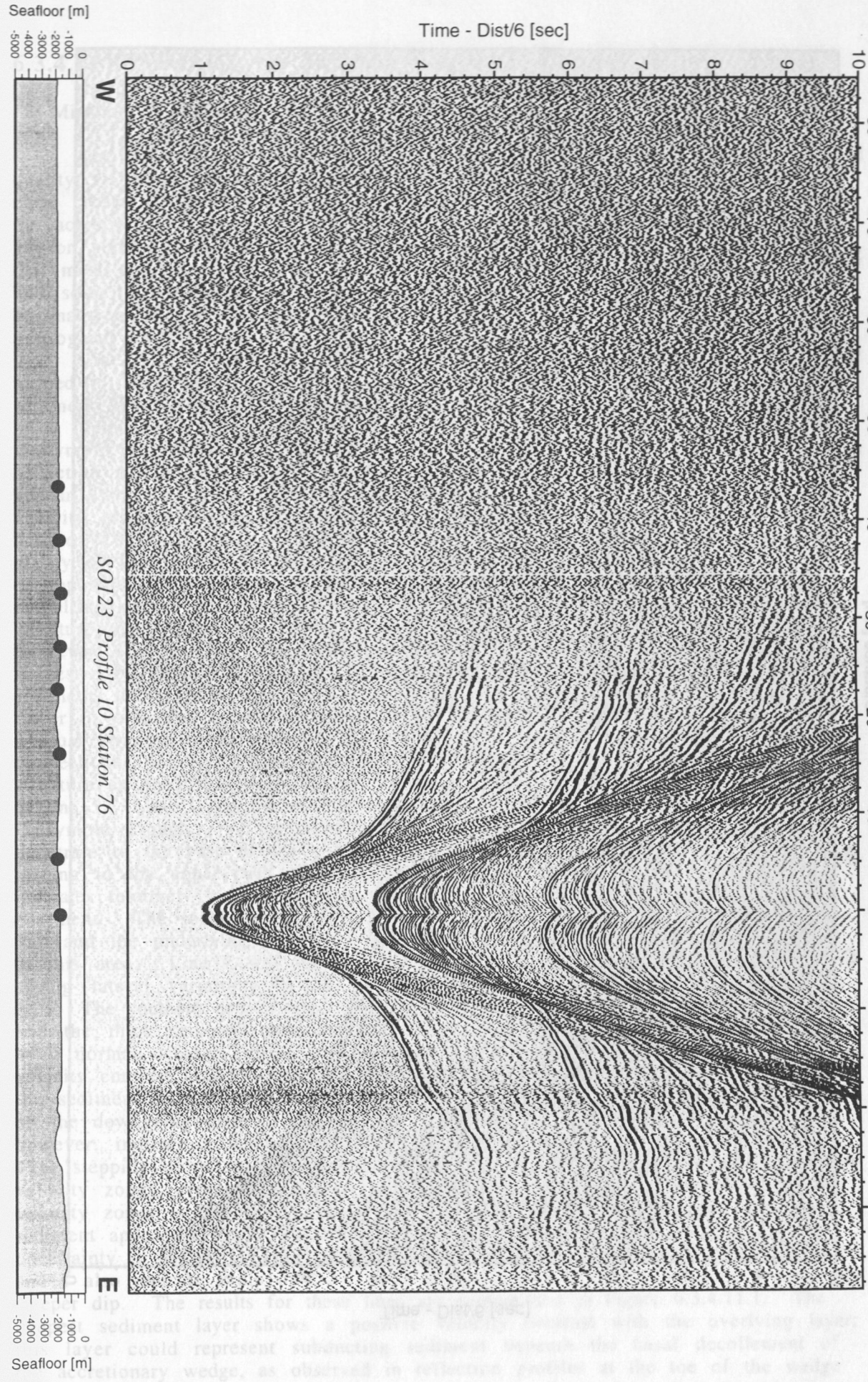

Figure 6.3.4.10.10: Record section from OBH 76, Profile 10.

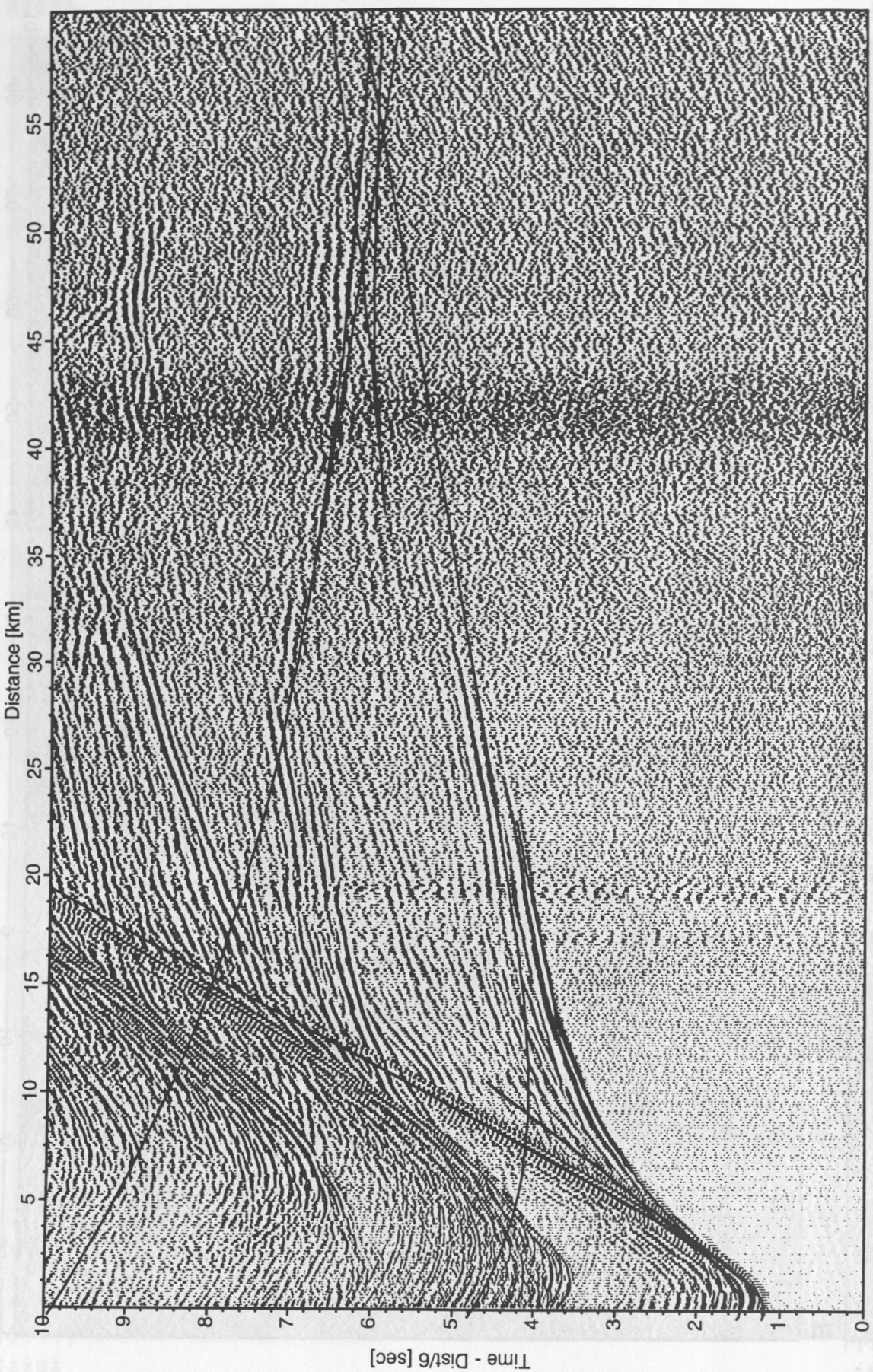

Figure 6.3.4.10.12: Record section of OBH80 east with calculated traveltimes superimposed

6.3.4.11 SUMMARY OF WIDE-ANGLE RESULTS

(T. Minshull, E. Flueh, R. Edwards)

The majority of the OBH and OBS deployments produced data of excellent quality. Despite the moderate total source volume and the thick sediment cover, clear crustal arrivals were observed everywhere except on the thickest parts of the accretionary wedge, and coherent arrivals were observed at ranges of up to 80 km on some instruments. The broadband, impulsive nature of the source means that most phases are sharp and easy to pick, including a variety of second arrivals, and some strong precritical reflections. Converted S-wave arrivals are apparent on many of the record sections and will provide additional constraints on geological interpretations.

Line 6, the oceanic crustal reference line parallel to Dalrymple Trough, proved to have the simplest structure. A series of laterally fairly uniform sediment layers, with velocity increasing monotonically with depth, is underlain by a typical oceanic crustal section 5-7 km thick. Acoustic basement in the Dalrymple Trough area is well imaged on preexisting multichannel seismic reflection profiles, which also facilitate the interpretation. Oceanic Layers 2 and 3 appear with very typical velocities, and the PmP arrival is clear. However, the velocity gradient in Layer 3 appears to be unusually low and the velocity contrast between Layers 2 and 3 is unusually large. The close instrument spacing, the clarity of the various phases, and the relatively flat seabed, should allow a variety of sophisticated modelling and imaging techniques to be applied to this line. The modelling of the northwestern part of line 5 shows that this simple oceanic crustal structure must extend almost to the northwestern wall of the Dalrymple Trough. However, line 4 along the Dalrymple Trough confirms the unusual structure suggested by the old Cambridge OBS data from the trough: beneath 5-6 km of sediment, the crust is about 10 km thick and has unusually low velocities, with Layer 3 velocities apparently absent. The geological interpretation of this unusual structure must await more detailed analysis. The nature of the transition between the relatively normal oceanic crust to the northwest and the unusual structure in the Dalrymple Trough will be clarified by two-dimensional modelling of line 5. Line 7 appears to sample the same unusual crust at its crossing of Dalrymple Trough. Unfortunately the source was not powerful enough to penetrate to the base of the crust beneath the Murray Ridge itself, but energy turning in the upper part of the ridge is clear in several instruments and indicates relatively low velocities of 4.0-4.5 km/s in the upper 2 km of acoustic basement. The southeastern end of line 7 samples the thick sediments of the Indus Fan and the underlying crustal structure. The crust appears to be unusually thin in this area. Line 7 will require considerable further modelling to constrain the strong lateral variations in crustal structure.

The southern end of line 8 shows the same set of phases observed on line 6, and the thick sediment entering the accretionary wedge appear to be underlain by a normal oceanic crustal section about 7 km thick, though again with a sharp velocity contrast between Layers 2 and 3. Data from this part of the line, where the sediment velocities appear to incease monotonically with depth, suggest a dip on the downgoing plate of about 2.5°. The four strike lines further north, however, indicate a much more complicated structure for the sediment column. The "stepping down" of several phases indicates the presence of a number of low velocity zones, presumably caused by overpressuring. The thickness of these low velocity zones is hard to constrain by travel-time modelling alone and the sediment appear to reach velocities in excess of 5 km/s, so there is some uncertainty in the dip of the underlying slab. Comparison of models for lines 9, 10 and 1 also indicate a dip of 2-3°, while comparison with line 2 indicates a somewhat steeper dip. The results for these lines are summarised in Figure 6.3.4.11.1. The deepest sediment layer shows a positive velocity contrast with the overlying layer; this layer could represent subducting sediment beneath the basal decollement of the accretionary wedge, as observed in reflection profiles at the toe of the wedge (Fruehn et al., 1997). PmP arrivals are observed as far north as line 1, and suggest a crustal thickness of about 6 km beneath the wedge. The data from line 2 are of poorer quality, and do not constrain the properties of the crust beneath.

Instruments on the lower part of accretionary wedge in line 8 show clear arrivals to very long ranges and will allow good constraints on the crustal structure and slab dip in this area. Modelling of data from instruments further back in the wedge is more difficult, since there are strong topographic effects. The model shown in Figure 6.3.4.8.27 ignores the low velocity zones detected by the strike lines, since their lateral extent along the line cannot be constrained by modeling a small number of instruments. The model shows a 2-3° dip of the slab throughout, but this must be regarded as a lower limit for the landward part of the wedge. Line 8 will also require considerable further work to properly constrain the strong lateral variations.

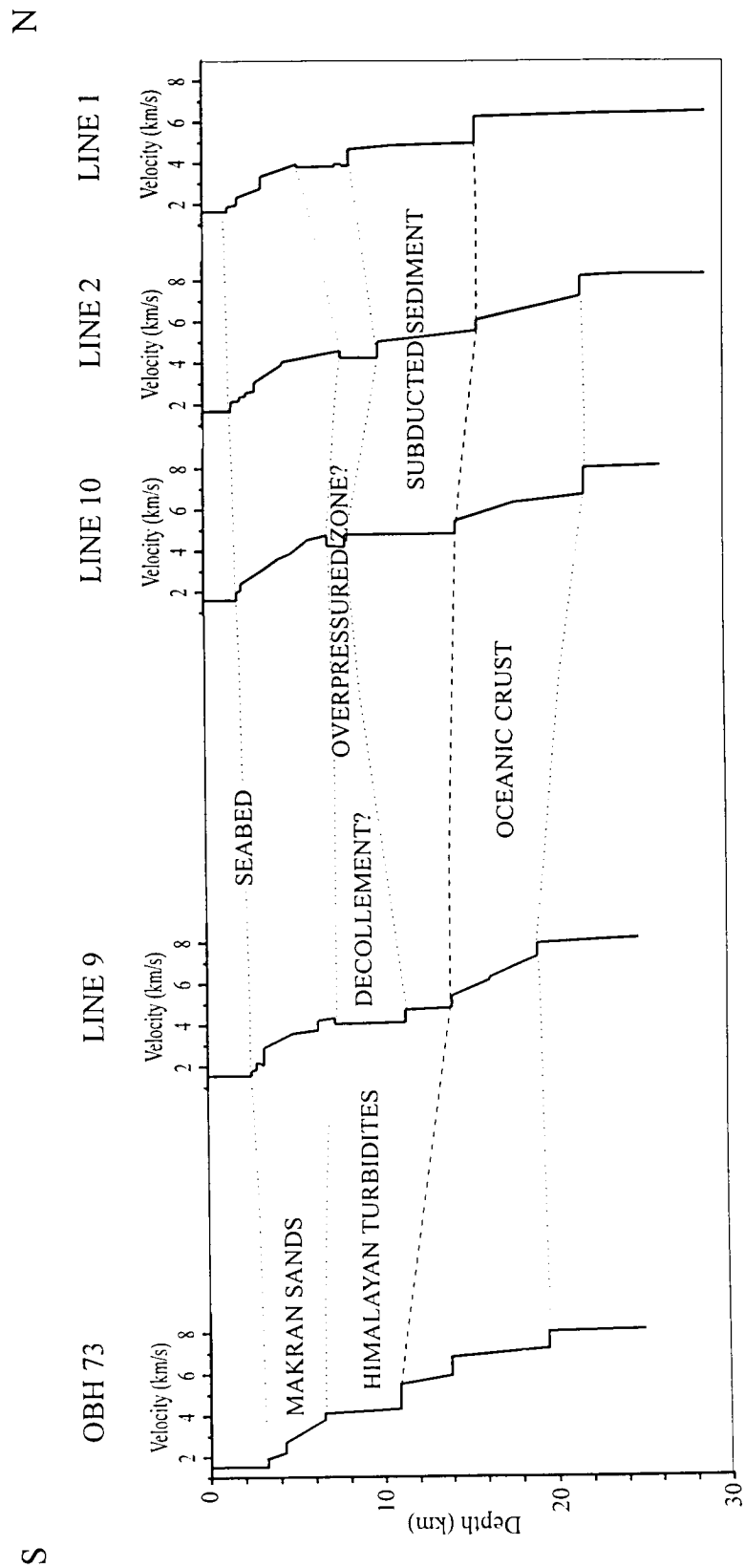

Figure 6.3.4.11.1: Tentative velocity model across the Makran accretionary wedge.

6.4 GRAVITY AND MAGNETICS
6.4.1 GRAVITY MEASUREMENTS AND TIES TO LAND STATIONS

(B. Schreckenberger, P. Kewitsch, and J. Fritsch)

The results of different surveys of gravity at sea are only comparable if the gravity data is related to the International Gravity Standardization Net IGSN71 (Morelli, 1974). Therefore, gravity tie measurements at land have to be carried out to connect the gravity measurements at sea with the world gravity net. The marine geophysical group of BGR uses for the gravity connections a LaCoste-Romberg gravimeter model G, no. 480.

The International Gravity Standardization Net IGSN71 was established in 1971 by the International Union of Geodesy and Geophysics (IUGG) as a set of world-wide distributed locations with known gravity values better than a few tenths of mGal. It replaced the formerly Potsdam System which did not conform any more to the necessities of modern geodesy and geophysics. According to the recommendations of the IUGG, every gravity survey, marine or land, should be related to the datum and to the scale of the IGSN71. The data of the IGSN71 reference stations are provided on request by the Bureau Gravimetrique International (BGI), Toulouse/France.

Although there is no official IGSN71 station in Muscat/Oman, the BGI helped with information about gravity measurements in Oman, well described in a recent report 'Gravity data in Oman' by Patrick M.U. Ravaut and Waris E.K. Warsi (unknown year and place). There are two well surveyed base stations near Muscat/Oman that we could use for our ties with the kind assistance of Dr. W.E.K. Warsi from the Sultan Qaboos University in Oman.

R.V. SONNE moored in the harbour Mina Qaboos in Mutrah/Oman at berth 6 near the third bollard from the south-western end of the pier (Figure 6.4.1.1) in the morning of September, 6. During our two day stay at the pier four series of measurements with our LaCoste-Romberg gravimeter model G, no. 480 have been made (Table 6.4.1.1) about 50 cm from the 3rd bollard to the north-east (station Q6A). Conditions were good for all measurements. Only one single visit to the reference stations SIA and SQU could be made (Table 6.4.1.1) from which we calculated an absolute gravity value of 978974.79 mGal in the IGSN71 system (reduced to the water level 0.0 m). During the last measurement before R.V. SONNE left the pier the water was 2.15 m below the instrument which results in a gravity value for the water level of 978975.36 mGal that corresponds to the reading of -906.90 mV for the KSS31 at that time.

Because this report had to be finished before the end of the cruise, it was not possible to calculate the instrument drift from our second stay in Muscat. Experience shows that normally the drift is in the order of 1-2 mGal/month. So we conclude that the error of the measured gravity anomalies will have the same order of magnitude for a one month cruise. Final processing of the data including drift corrections will be made after the cruise.

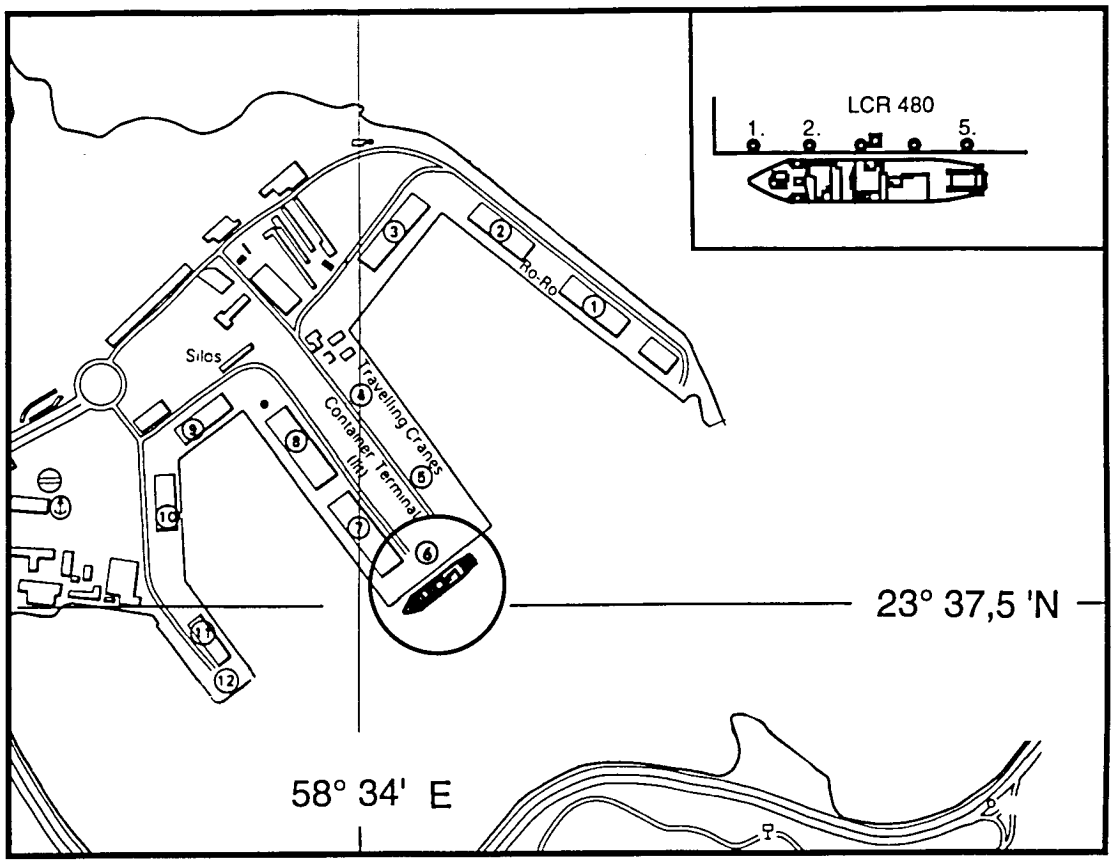

Figure 6.4.1.1: Port of Mutrah/Oman (after Admiralty Chart 3518). Circle shows the mooring site of R.V. SONNE during September 6 to 8, 1997 at berth 6. Inlet shows details of the gravity observation station at bollard 3.

Table 6.4.1.1: Observation report on the gravity tie in Muscat/Oman.

Federal Institute for Geosciences and Natural Resources, Hannover/Germany
Gravity Observations
with LaCoste-Romberg (LCR) Gravimeter G 480

Research cruise: SO-122/SO-123
Reference station (SIA): Seeb International Airport, Oman (SIA), (NSA GPS point 7911001), IGSN71 gravity: 978921.955 mGal
Reference station (SQU): Sultan Qaboos University, Oman (SQU), College of Science building, IGSN71 gravity: 978907.16 mGal
Gravity station (Q6A): Port Mina Qaboos, Mutrah, Oman, RV SONNE site at berth 6 (bollard 3 from East)
Observers: F = Fritsch, K = Kewitsch, S = Schreckenberger, R = Reichert

station	sea level	date	UTC	reading units	tidal corrected	average (-0.0m)	gravity mGal
(Q6A)/S	-1.5m	06.09.97	07:10	2556.18	2556.20		
(Q6A)/K		06.09.97	07:13	2556.17	2556.19	2556.26	2596.46
(Q6A)/F		06.09.97	07:15	2556.18	2556.20		
(Q6A)/K	-1.6m	07.09.97	08:40	2556.15	2556.19	2556.26	2596.46
(SIA)/K		07.09.97	09:30	2504.29	2504.34		
(SIA)/K		07.09.97	09:32	2504.29	2504.34	2504.35	2543.65
(SIA)/S		07.09.97	09:34	2504.30	2504.36		
(SQU)/K		07.09.97	10:53	2489.70	2489.76	2489.76	2528.81
(SQU)/S		07.09.97	10:55	2489.71	2489.77		
(Q6A)/S	-3.0m	07.09.97	13:27	2556.11	2556.12	2556.25	2596.45
(Q6A)/R		07.09.97	13:32	2556.12	2556.13		
(Q6A)/S	-2.15	08.09.97	05:25	2556.18	2556.16	2556.25	2596.45
(Q6A)/S		08.09.97	05:30	2556.19	2556.17		

Gravity in mGal was calculated using LCR scaling table and scale constant BGR85/86 as 1.000447.

Differences between gravity stations: (Q6A) - (SIA) = 52.81 mGal
(Q6A) - (SQU) = 67.64 mGal

(SIA) - (SQU) = 14.84 mGal (own measurement)
(SIA) - (SQU) = 14.79 mGal (from reference station)

Absolute gravity at (Q6A) from difference to SIA: 978974.77 mGal
Absolute gravity at (Q6A) from difference to SQU: 978974.80 mGal
Absolute gravity at (Q6A) (average): 978974.79 (with water level 0.00m)

Absolute gravity for (Q6A) (reduced to water level -2.15m) 978975.36 mGal (IGSN71 system) used for the gravity tie on 08.09.97 (5:30 UTC). Reading of the gravimeter KSS31 at that time: -906.90 mV.

6.4.2 MAGNETIC GRADIENT MEASUREMENTS

(B. Schreckenberger)

GENERAL REMARKS

Magnetic measurements carried out during cruise SO-123 cover about 3550 profile kilometers on 56 lines. We use the line numbering scheme for the seismic lines (SO123-01 to -10) and an additional numbering scheme for magnetic lines that is different from that used for hydroacustics. In this chapter the pre-fix 'M' denotes lines surveyed without seismics (SO123-M01 to -M47). Appendix 9.3 contains a complete list of this profiles. On nearly all of the lines we made gradiometer measurements except of a few lines between some OBH positions that were too short in order to deploy the whole magnetometer array.

From the measurements on cruise SO-122 (Roeser et al., 1997) we knew that one of the sensors (no. 805) causes problems as it showed a high dependency of the gradient on the azimuth. From another sensor (no. 904) we knew that it had also problems suggesting magnetic impurities near the sensor. Because the combination of sensors 841 and 833 worked very well during cruise SO-122 we deployed that configuration on nearly all lines of SO-123.

Table 6.4.2.1 documents the parameters that are relevant for the reconstruction process for all lines up to SO123-09 where we stopped the processing of the gradient data due to time constraints. The mean gradient along each respective line is of special interest because it should be zero if there is no linear trend in the magnetic anomaly field. By visual inspection of the plotted gradient curves it was tried to separate the influence of the instrument from the linear parts of the true gradient in the magnetic anomalies. The result, which reflects errors in the measuring process (Eilers et al., 1994), is given in Table 6.4.2.1 in the column labeled 'false gradient'.

Figure 6.4.2.1 shows the mean false gradient from Table 6.4.2.1 plotted against the course for those lines where 841 was deployed as the master sensor and 833 as the slave sensor. For all profile directions this value ranges between 0.1 and 0.8 nT/150 m. This is very low and provides higher quality compared with the results from cruise SO-122 where we had a variation of the mean gradient with respect to azimuth between +3 and -2 nT/150m when we deployed sensor 805 on most of the lines.

The troubling sensors 805 and 904 were opened and the coil systems were removed and cleaned. No obvious reason for erroneous values could be detected except of a low resistance (a few MΩ) between the coil circuit and its shield in sensor 904. After fixing this problem, both sensors were deployed as slave sensors for a check on lines SO123-M21, -05, -M22, -M23, -06 respectively, along with sensor 841 as the master. It can be seen from Table 6.4.2.1 that the values of the false gradient for these lines are conspicuous high compared with the other lines. Sensor 805 shows a moderate difference between the false gradients for the two different profile directions while sensor 904 causes a false gradient of up to 8 nT/150m which is unacceptable. If function and position of 841 and 833 as master and slave are interchanged (lines SO123-01, -02, -02A) then again higher variation with the course results. From all these experiments we concluded that the combination with 841 as the master sensor and 833 as the slave sensor is the best choice and kept this configuration until the end of the cruise.

RECONSTRUCTION OF THE GRADIENT

The most simple method for the reconstruction of the magnetic field is the integration of the gradient in the space domain along the profile line. Another approach is the formulation of the problem in the frequency and in the wavenumber domain, respectively (Eilers et al., 1994). In this method the integration corresponds to a filter operation on the Fourier transform of the gradient. It provides a better insight into the problems of the reconstruction and can be combined with additional filter methods. However, for a first interpretation on board we used the simple integration/summation method in the space domain.

A constant value must always be removed from the gradient record because an offset of varying magnitude is present on nearly every line (Table 6.4.2.1). In the reconstruction process this would result in a strong linear deviation from the true anomaly. The disadvantage of the procedure is that any constant offset of the gradient (equivalent to a linear slope in the magnetic anomaly field) will be simultaneously removed even if we are dealing with a true feature of the anomaly.

Figure 6.4.2.2 shows an example where the processing of the gradient helped in the detection of very weak anomalies over the accretionary prism off the Makran coast. On line SO123-01 (Figure 6.4.2.3) many low amplitude short-wavelength anomalies can be seen. On lines SO123-M02 and -M04 at 24° 40' N we have anomalies with a similar amplitude and shape. The upper part of Fig 6.4.2.2a shows the reconstruction of the magnetic anomaly (continuous curve) and the anomaly derived from the master sensor (dotted line). It can be seen that the anomaly that was computed from the gradient does not contain the small scale anomalies present in the continuous curve. All of them arise from time dependent variations of the magnetic field. On the contrary, Figs. 6.4.2.2b and 6.4.2.2.c show that even weaker anomalies in the vicinity of profile kilometer 25 on lines SO123-M02 and -M04 survive the reconstruction process. This is also illustrated in the record of the gradients in the lower part of each example. Although the gradient is noisy it shows amplitudes of about 1 nT/150 m on lines SO123-M02 and -M04 (Figs. 6.4.2.2b and 6.4.2.2c), while on line SO123-01 (Figure 6.4.2.2a) the gradient does not contain variations that correspond to the distinct 'anomalies' in the magnetic field measured by the master sensor.

This analysis demonstrates that the use of the gradient measurements enables the distinction between true magnetic anomalies generated by sub-seafloor properties and variations of the earth's magnetic field. Figure 6.4.2.2 and Figure 6.4.2.3 show that small anomalies striking in an E-W direction can be correlated between lines SO123-M02 and -M04. It is inferred that they have their sources within the accretionary prism of the Makran because their wavelength seems to be too short to be caused by the subducting oceanic plate.

Despite of the successful reconstruction shown in Figure 6.4.2.2 the gradient method will always have its limitations with respect to long-wavelength anomalies, and land-based records of the variations will be needed even in the future. For this cruise support from the Space and Upper Atmosphere Research Commission (SUPARCO) of Pakistan will be obtained: the values of the magnetic total intensity from the magnetic observatory in Karachi will be provided to BGR via the NIO after the cruise. Therefore, the final processing of the magnetic data and the reconstruction of the magnetic anomalies from the gradient can only be done after the cruise.

6.4.3 PRELIMINARY INTERPRETATION
6.4.3.1 GRAVIMETRIC AND MAGNETIC MAPS

(B. Schreckenberger and C. Reichert)

Figures 6.4.2.3 and 6.4.2.4 show the magnetic and gravimetric anomalies plotted along the profile line in the northern part of the survey area off the Makran coast over the accretionary wedge. Figures 6.4.2.5 and 6.4.2.6 show the same for the southern working area over the Murray Ridge and the Dalrymple Trough. Data from SO-122 lines that cross the survey area are also plotted. There are a few lines in the northern area where we have measured the gravity but not the magnetic field (SO123-03, -08, and -10).

The magnetic anomalies displayed are the values from the master sensor of the magnetometer array after subtracting the appropriate reference field IGRF95 (IAGA, 1996) and an additional constant value of 80 nT which adjusts the anomalies to a level around zero. This value was determinated in the middle of cruise SO-122 by visual inspection of the anomalies. On this cruise we calculated 77 nT as the mean of the magnetic anomaly and because this is sufficiently near to the shift of 80 nT we maintained this value for cruise SO-123.

Disturbances caused by magnetic variations were small during the whole cruise, partly because we are near the minimum of the sun spot cycle. Short-wavelength variations are clearly visible on line SO123-01 (Figure 6.4.2.3, already discussed in 6.4.2) and on lines SO123-05 and -M26 (Figure 6.4.2.5). The distinct step in the anomaly at 80 km on line SO123-05 (see also Figure 6.4.2.7) was completely removed when the anomaly was reconstructed from the gradient. The same is true for a similar step on line SO123-M26. Presently it is not very useful to show anomalies reconstructed from the gradient because they will change when the data are reprocessed using observatory data from Karachi (see 6.4.2). Visual inspection of the anomalies shows moderate cross-over errors in the magnetic maps. They are due to diurnal variations which can be removed more successfully using the gradient together with observatory data.

The gravity data in Figures 6.4.2.4 and 6.4.2.6 are free-air anomalies obtained after application of the instrumental corrections described in chapter 5.4.1 and subtraction of the normal gravity field. Experience shows that the correction for the instrumental drift will not exceed a few mGal.

6.4.3.2 PECULIARITIES OF SELECTED DATA PRESENTED HERE

Figures 6.4.2.7 to 6.4.2.10 show gravimetric free-air and magnetic anomalies together with the waterdepth for all profiles with single-channel reflection and wide-angle seismic measurements and for selected lines without seismics. The gravimetric record in Figures 6.4.2.10a and 6.4.2.10b shows sinusoidal artifacts of the data processing process at the junction of lines SO123-M17 and -M18 and SO123-M32 and -M31 where the ship changed the course. A similar effect is visible at kilometer 105 on line SO123-M32 and at the beginning of line SO123-M33 (Figure 6.4.2.10c).

6.4.3.3 DISCUSSION
THE OMAN ABYSSAL PLAIN

The free-air gravity anomaly is generally negative over the Oman Abyssal Plain and over the Makran accretionary wedge (Figure 6.4.2.4). A broad minimum over the deepest parts of the Oman Abyssal Plain is followed by a slow ascend up to the Makran shelf where the gravity approaches zero (SO123-08 in Figure 6.4.2.8 and SO123-M17/M18 in Figure 6.4.2.10a).
To the south there is a local gravity high (e.g. on SO123-M17/M18, -M32/M31, and -05, SO122-02 and -04) trending from 23°45'N/62°45'E to the northeast, that probably results from a broad basement high in the strike of line SO123-06 (Figure 6.4.2.6).

North of that high there is another structure concealed by the oceanic sediments that pierces through the seafloor on lines SO123-M32, -08, -M17 as well as on line SO122-04A where its sub-seafloor structure can be seen in the reflection seismic section (Roeser et al., 1997). On lines SO122-05A and -06 there is no bathymetric expression of that basement high nor do we have seismic reflection data. However, the gravity data strongly suggest, that it is also present here. Lines SO123-M32, -08, and -M17 (Figure 6.4.2.8 and 6.4.2.10) show a positive free-air anomaly over the basement outcrop. On line SO122-04A at 23°15'N (Figure 6.4.2.6) as well as on line SO122-05A at 23°45'N and line SO122-06 at 24°05'N (Figure 6.4.2.4) a gravity anomaly is observed that indicates that this structure, the 'Little Murray Ridge', extends far to the northeast. The crest of the ridge seems to be associated with the minimum or the flank to the positive part of the magnetic anomaly. It is not yet clear what causes the anomaly because it is very wide (Figures 2.7 and 6.4.2.3) and the topography of the basement can by no means explain the shape of the anomaly. There must be a considerable change in the thickness of a crustal body that has a typical magnetization of oceanic basalt. Indications are observed on the seismic reflection line SO122-04A (Roeser et al., 1997) that an about 100 km wide volcanic structure partly overlies oceanic crust of same or older age. If the strong magnetic anomaly trending SW to NE can be explained by the volcanic structure then there remain only very weak anomalies in the Oman Abyssal Plain. In particular there would be no indications for magnetic seafloor-spreading lineations.

THE MAKRAN ACCRETIONARY PRISM

From the low values in the Oman Abyssal Plain the free-air gravity increases over the accretionary prism and reaches zero between 24°40'N and 24°50'N (Figure 6.4.2.4). Only on the northernmost lines of the cruise (north of 24°50'N and east of 63°E) a positive gravimetric anomaly is observed that may be due to the general increase of the gravity from the Oman Abyssal Plain to the coast or may represent a local high. There seems to be a correlation with a weak positive magnetic anomaly in the same area but this may only be a variation of the general trend along the coast.

Additionally, as already discussed in 6.4.2 there are small scale low amplitude anomalies (max. 10 nT) superimposed that are correlatable in an E-W direction across lines SO123-M02, -M03, and M04 (Figure 6.4.2.3). They also correlate with small bathymetric ridges parallel to the margin at a waterdepth of nearly 2000 meters. Simple magnetic models show that the ridges could explain the anomalies when the sediments at the seafloor had a magnetization of about 0.1 A/m. This value seems to be a high for sediments but it is definitely too low to indicate igneous basic material.

To the East regularly spaced N-S lines (SO123-M37 to -M47, Figure 6.4.2.3) show an increase of the magnetic field superimposed by correlatable small scale

anomalies that are inferred to have their origin also within the accretionary prism.

THE MURRAY RIDGE AREA

In the southern Murray Ridge area the free-air gravity anomaly reflects partly the sea-floor topography as it shows strong positive values over the Murray Ridge and negative values over the Dalrymple Trough (Figure 6.4.2.6 and 6.4.2.8b). In contrast to the Oman Abyssal Plain, the Arabian Sea south of the Murray Ridge is characterized by a positive free-air anomaly (Roeser et al., 1997). In the view of the high sediment thicknesses of the Indus Fan this requires a smaller thickness of the igneous crust while the crust of the Oman Abyssal Plain should be thicker due to its negative free-air anomaly. First gravimetric modeling for the reflection seismic line SO122-17 (location see Figure 2.7) from cruise SO-122 (Roeser et al., 1997) in the northwest of our survey area suggests an analogue conclusion. Here we have a very similar structural arrangement: a ridge to the southeast, a trough to the northwest, and a broad basement high northwest of the trough that seem to be equivalents or extensions of the structures on the Murray Ridge - Dalrymple Trough transects. Moreover, using common densities for the sediments and the oceanic crust it was necessary to introduce a crustal root below the equivalent of the Murray Ridge and below the adjacent trough into the gravity model. On the Murray Ridge - Dalrymple transects (lines SO122-04 and SO123-07, Figures 6.4.2.6) this is in contrast to a gravity model of Whitmarsh (1979) for a single channel seismic line near to our profiles. Here a continuous sub-horizontal Moho was modeled requiring a narrow and strong decrease in crustal density beneath the Dalrymple Trough. The crustal root model, however, is in good agreement with the increased crustal thickness in the Dalrymple Trough postulated by Edwards (in prep.) and with the initial velocity models calculated for line SO123-04 and 07 (see chapter 6.3.4).

Magnetic anomalies over the Murray Ridge are surprisingly low regarding its inferred volcanic origin (Figure 6.4.2.5). Short-wavelength anomalies over the top of the ridge on line SO123-07 (Figure 6.4.2.8b) correlate with bathymetric features, suggesting that they are of basaltic origin but the ridge as a whole does obviously not cause an anomaly. There seems to be a tendency that to the northeast where the ridge comes nearer to the sea-level a negative anomaly develops (lines SO122-02, SO123-M21 in Figure 6.4.2.5). A possible explanation would be that the ridge consists of two different structures: 1) underlying oceanic crust of normal sea-floor spreading origin that has a constant thickness and magnetic polarity and causes virtually no magnetic anomaly, and 2) a thin volcanic cover of later origin. This may become thicker to the northwest indicated by the bathymetric high at 22°30'N/63°50'E and thus generates stronger magnetic anomalies. The magnetic map of Barker (1966) however shows that nowhere on the Murray Ridge the magnetic anomaly becomes as strong as over the seamount at 23°N.

Line no.	Course [deg]	Length [km]	Mean gradient [nT/150m]	False gradient [nT/150m]	No. master	No. slave
01	90.00	99.00	-0.14	0.00	833	841
02	270.00	13.00	-1.42	-1.40	833	841
02A	270.00	86.00	-1.42	-1.30	833	841
M02	180.00	58.00	0.31	0.50	841	833
M03	0.00	28.00	0.86	0.70	841	833
M04	180.00	74.50	0.47	0.50	841	833
M05	270.00	87.00	0.51	0.40	841	833
M06	90.00	82.00	0.13	0.30	841	833
M07	300.00	44.00	0.75		841	833
M08	128.00	23.00	0.29	0.30	841	833
M09	270.00	63.50	0.53	0.40	841	833
M10	90.00	40.50	0.23		841	833
M11	180.00	40.00	0.39	0.30	841	833
M12	90.00	38.00	0.36	0.40	841	833
M13	180.00	37.50	0.52	0.40	841	833
M14	90.00	39.00	0.45	0.50	841	833
M15	180.00	38.00	0.45	0.50	841	833
M16	90.00	72.00	0.49	0.40	841	833
M17	181.00	151.50	0.48	0.40	841	833
M18	145.00	68.50	0.12	0.30	841	833
M19	225.00	36.50	0.33	0.30	841	833
04	45.00	141.00	0.32	0.20	841	833
M20	225.00	99.00	0.78	0.80	841	833
M21	147.00	40.00	0.42		841	805
05	225.00	122.00	-2.13	-2.10	841	805
M22	145.00	26.00	1.80	1.30	841	805
M23	227.00	37.00	8.20	8.00	841	904
06	46.00	110.00	-1.50	-1.20	841	904
M25	139.00	32.00	0.17	0.10	841	833
07	320.00	159.00	0.50	0.75	841	833
M26	140.00	39.00	0.06	0.10	841	833
M27	317.00	59.00	0.42	0.50	841	833
M28	45.00	87.00	0.33	0.20	841	833
M29	222.00	48.00	-0.99	0.00	841	833
M31	320.00	45.00	0.17	0.20	841	833
M32	0.00	126.00	0.65	0.50	841	833
M34	86.00	30.00	0.10	0.20	841	833
M35	86.00	30.00	0.57	0.50	841	833
09	266.00	120.00	0.19	0.15	841	833

Table 6.4.2.1: Parameters for magnetic lines of cruise SO-123. For each line the course, the length of the profile, the arithmetic mean of the gradient, the 'false gradient', and the serial numbers of the sensors are listed. With the 'false gradient' it was tried to separate the instrumental error from the true gradient of the magnetic anomalies (see text). For some of the lines the mean gradient could not - be determined.

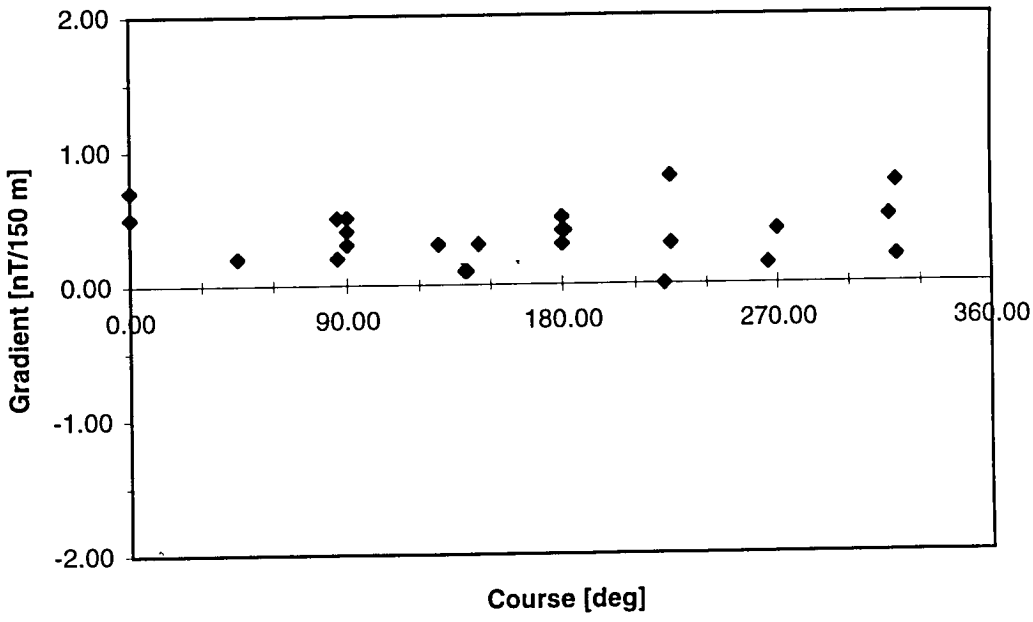

Figure 6.4.2.1: 'False gradient' from Table 6.4.2.1 plotted vs. the course for all SO-123 lines with 841 as the master sensor and 833 as the slave sensor.

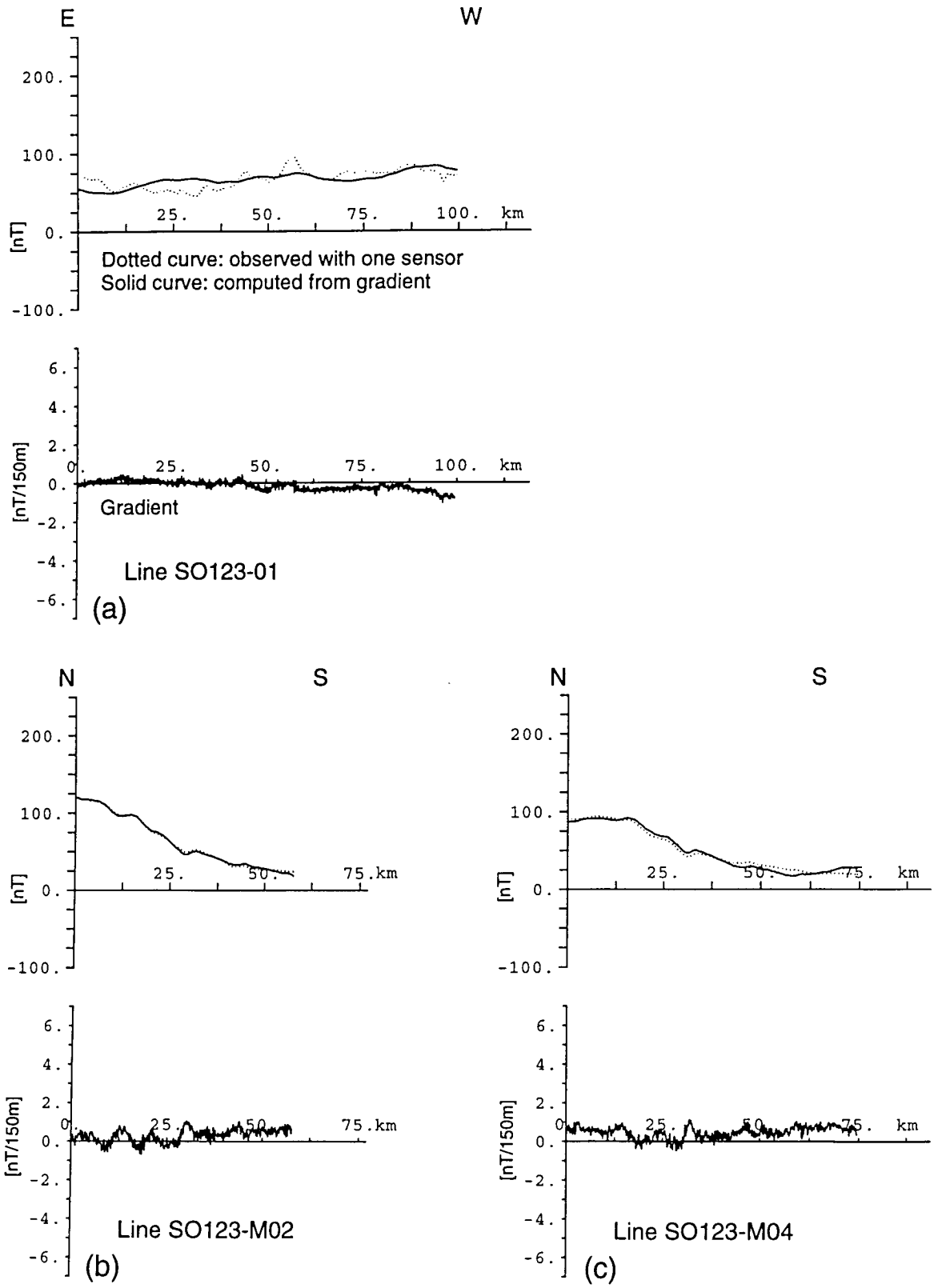

Figure 6.4.2.2: Example for the reconstruction of the magnetic anomaly from the measured gradient (lower part of each example) on (a) line SO123-01, (b) line SO123-M02, and (c) line SO123-M04. The magnetic anomaly from the total intensity values of the master sensor is shown as a dotted line in the upper parts of each example while the continuous curve shows the anomaly calculated from the gradient. In (b) and (c) the dotted line is partly invisible because it coincides with the continuous line.

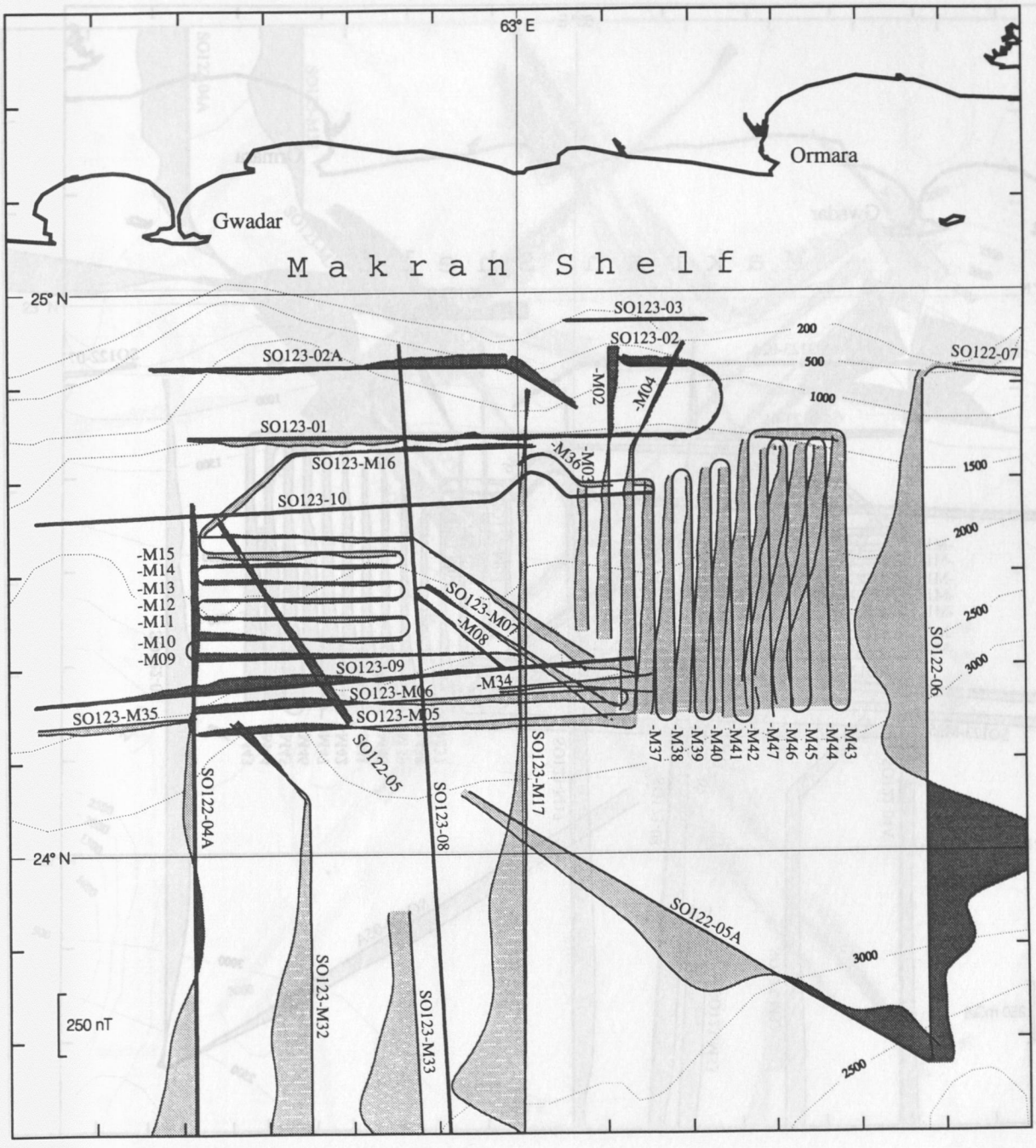

Figure 6.4.2.3: Magnetic anomalies (master sensor) plotted along the ship tracks for the northern part of the survey area of the SO-123 cruise. Positive amplitudes in dark gray, negative amplitudes in light gray. The map also contains some lines from cruise SO-122.

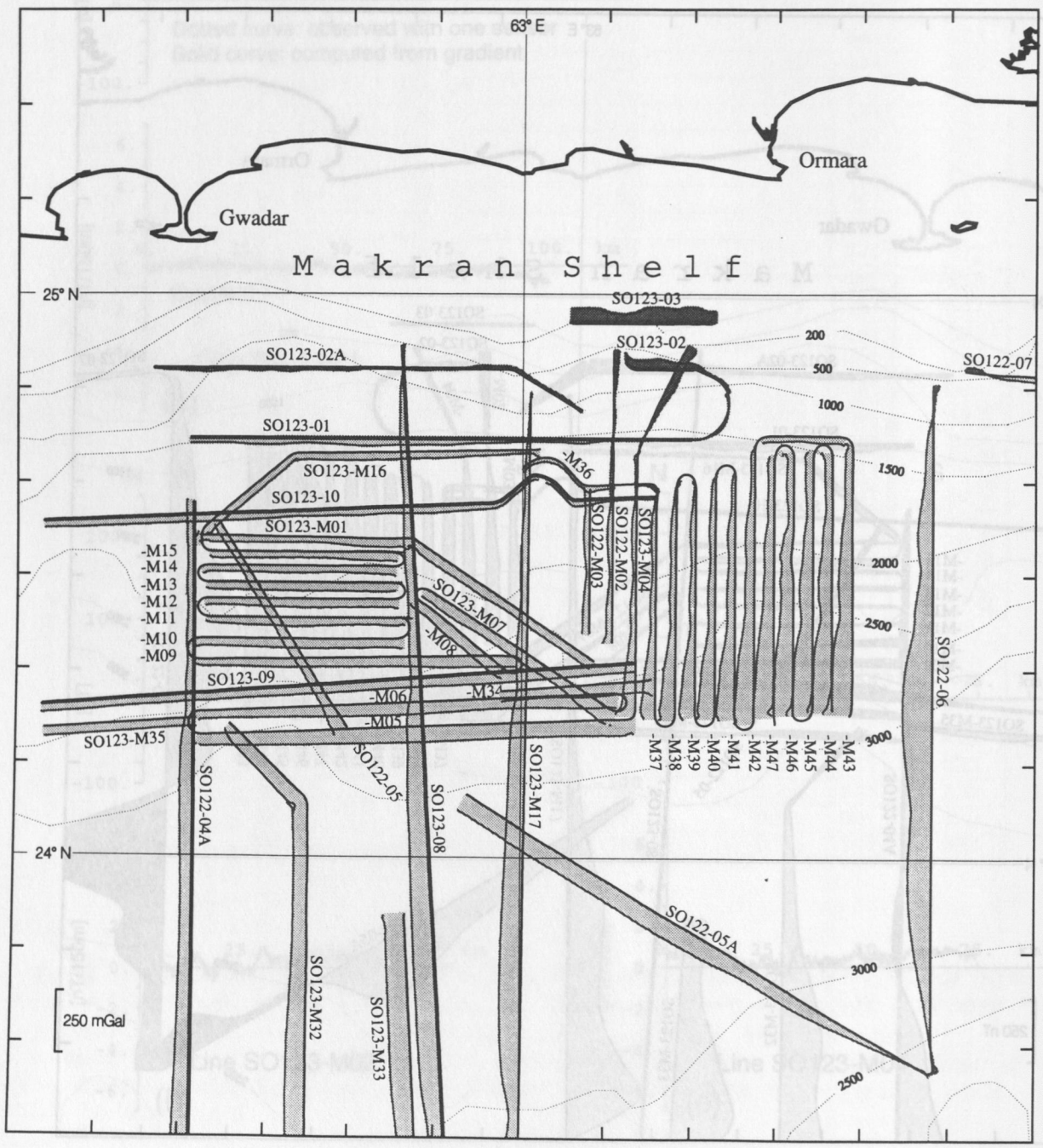

Figure 6.4.2.4: Free-air gravity anomalies plotted along the ship tracks for the northern part of the survey area of the SO-123 cruise. Positive anomalies in dark gray, negative anomalies in light gray. The map also contains some lines from cruise SO-122.

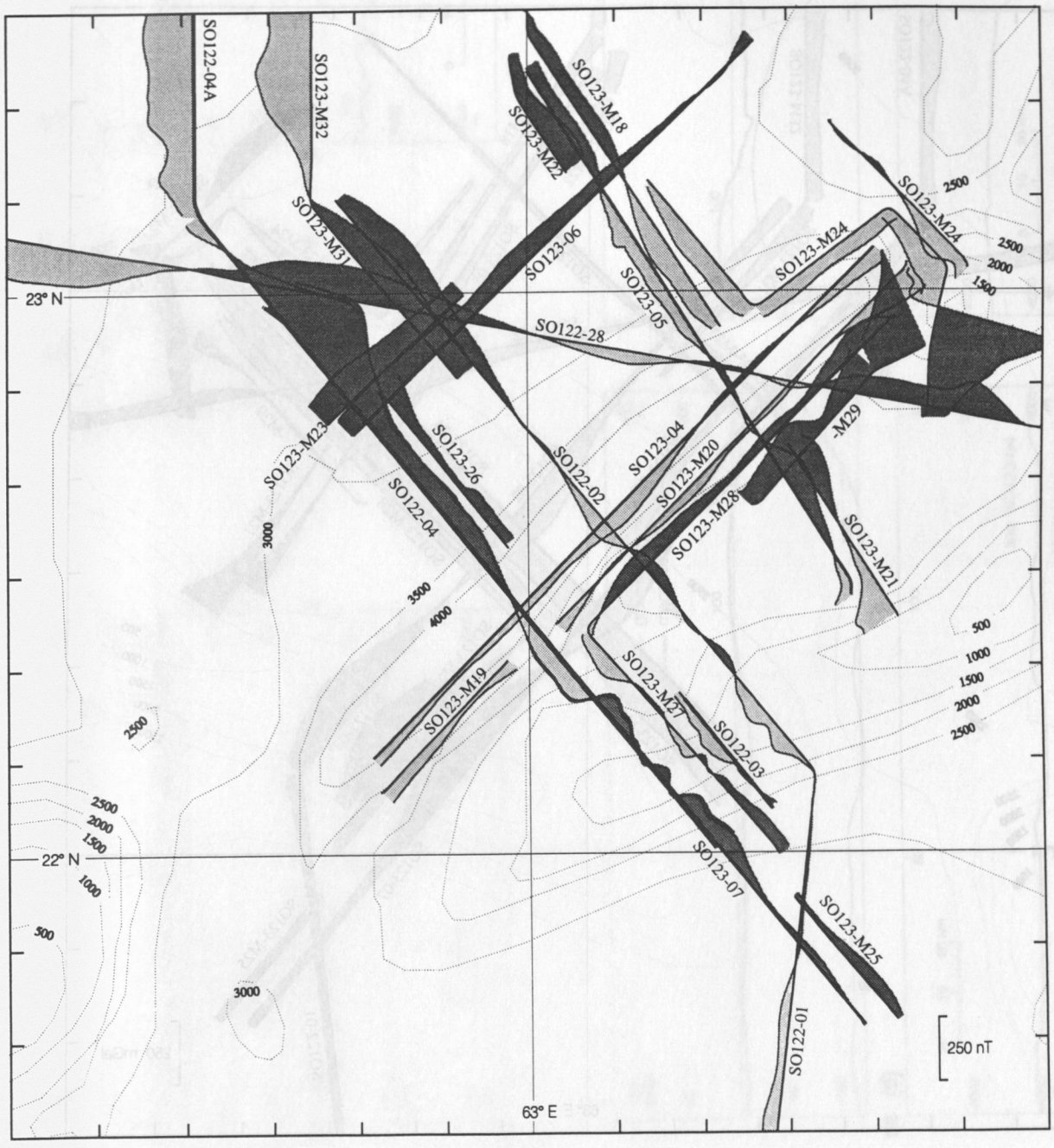

Figure 6.4.2.5: Magnetic anomalies (master sensor) plotted along the ship tracks for the southern part of the survey area of the SO-123 cruise. Positive amplitudes in dark gray, negative amplitudes in light gray. The map also contains some lines from cruise SO-122.

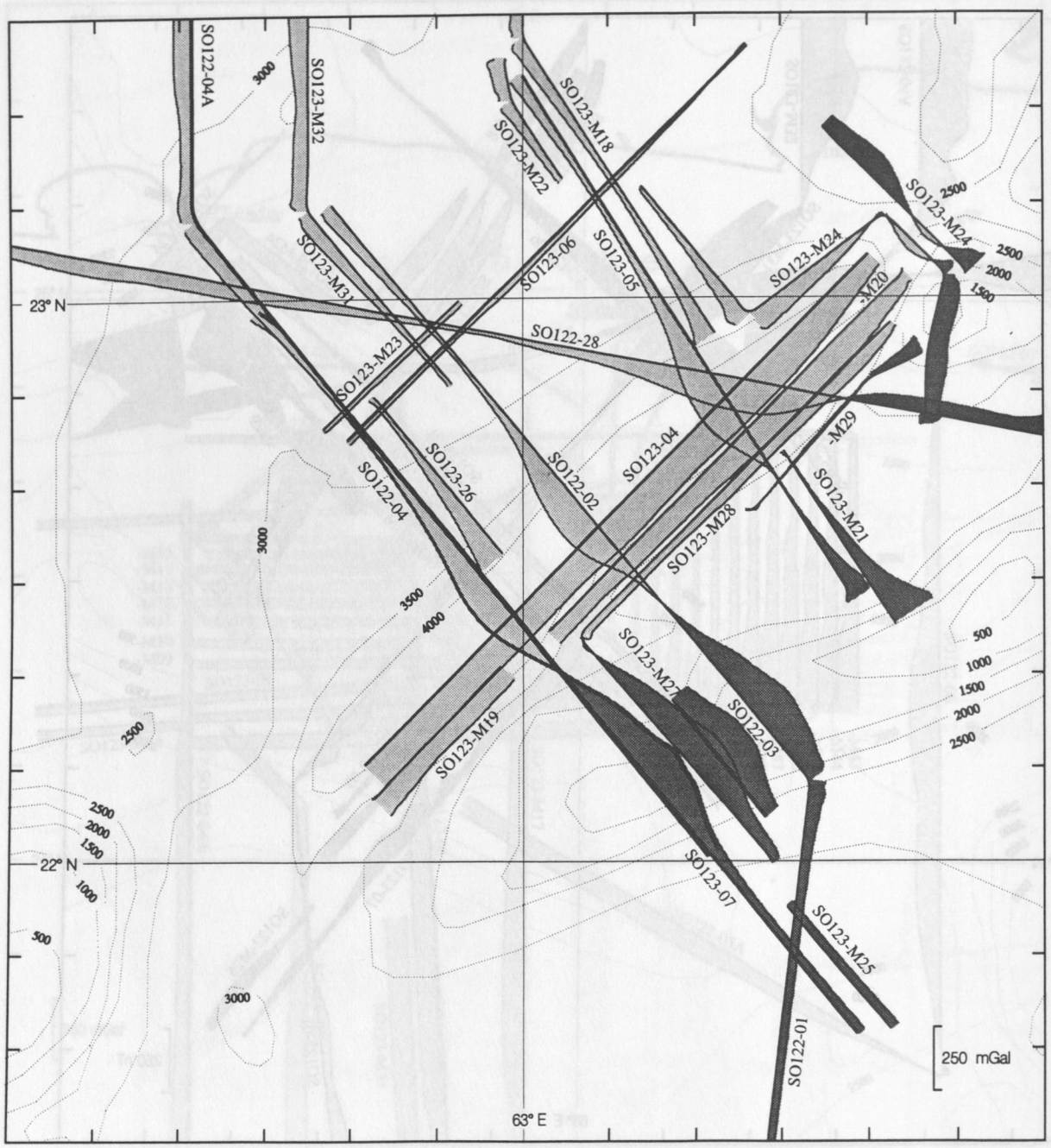

Figure 6.4.2.6: Free-air gravity anomalies plotted along the ship tracks for the southern part of the survey area of the SO-123 cruise. Positive anomalies in dark gray, negative anomalies in light gray. The map also contains some lines from cruise SO-122.

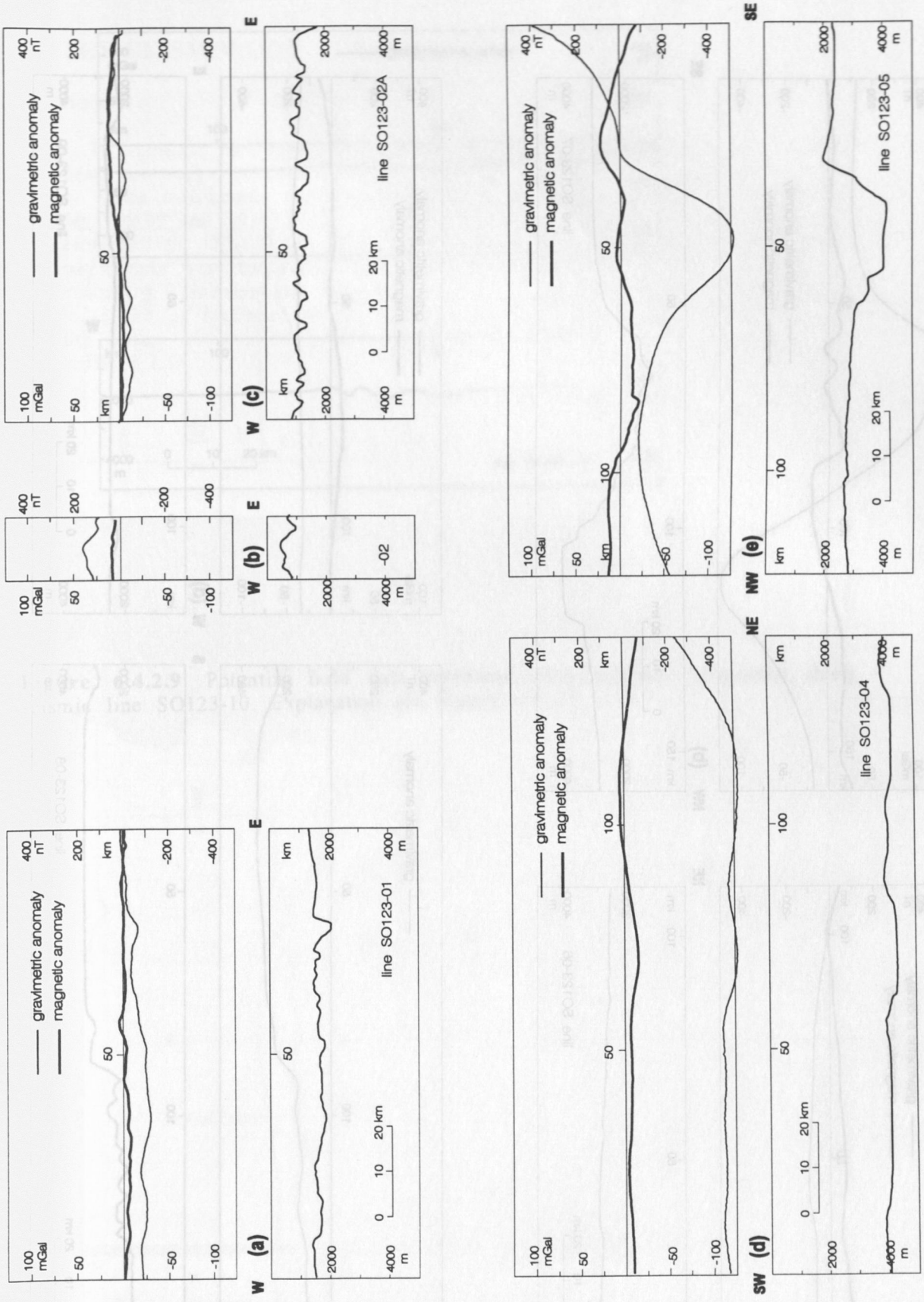

Figure 6.4.2.7: Potential field data combined with seafloor topography along seismic lines: (a) SO123-01, (b) -02, (c) -02A, (d) -04, and (e) -05. Thin lines in the upper parts of the respective figures show the free-air anomaly (scale on the left margin), thick lines the magnetic anomaly from the master sensor (scale at the right margin). The lower part of each figure shows the waterdepth in meters from the central beam of Hydrosweep.

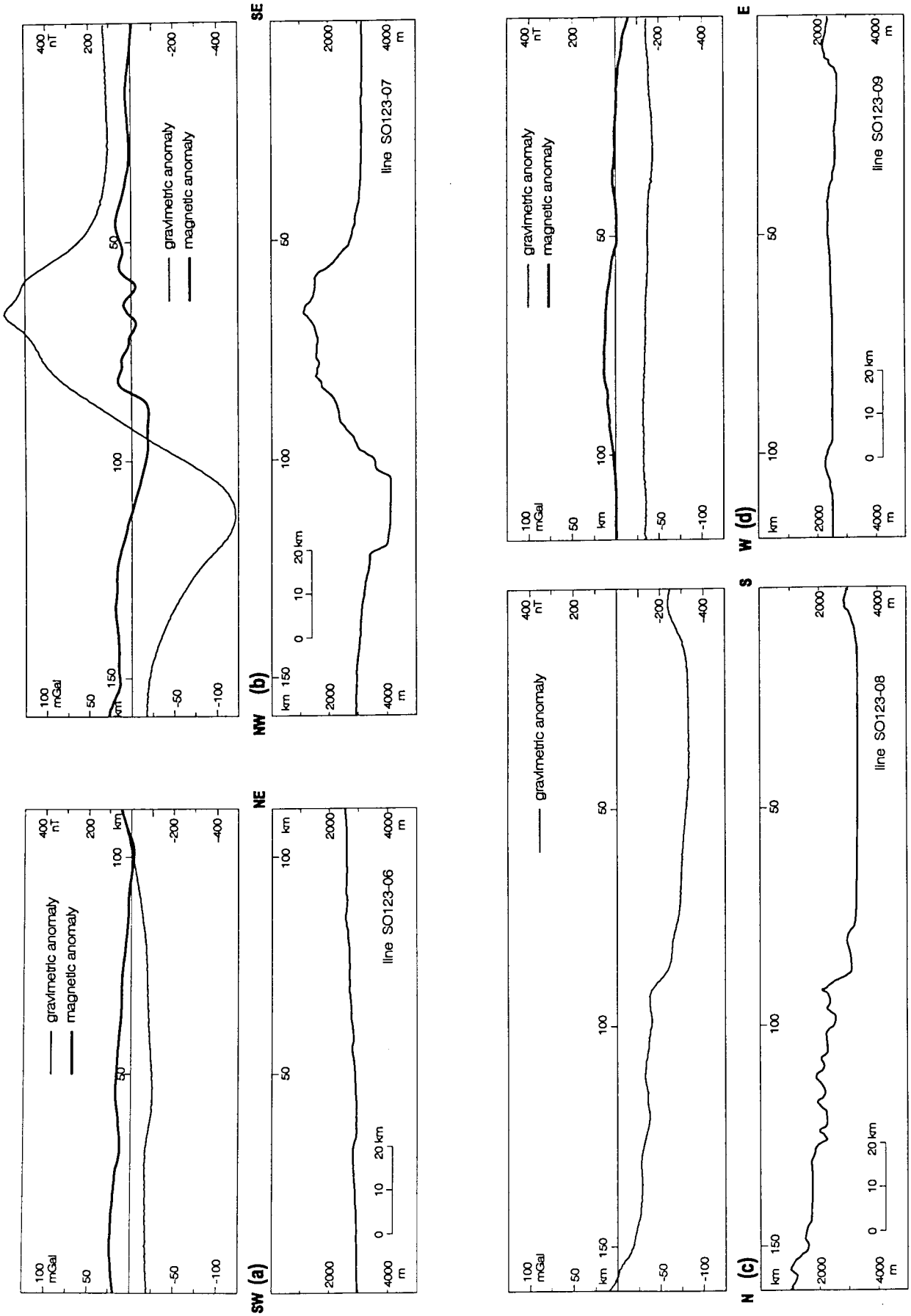

Figure 6.4.2.8: Potential field data combined with seafloor topography along seismic lines: (a) SO123-06, (b) -07, (c) -08, and (e) -09. Explanation see Figure 6.4.2.7.

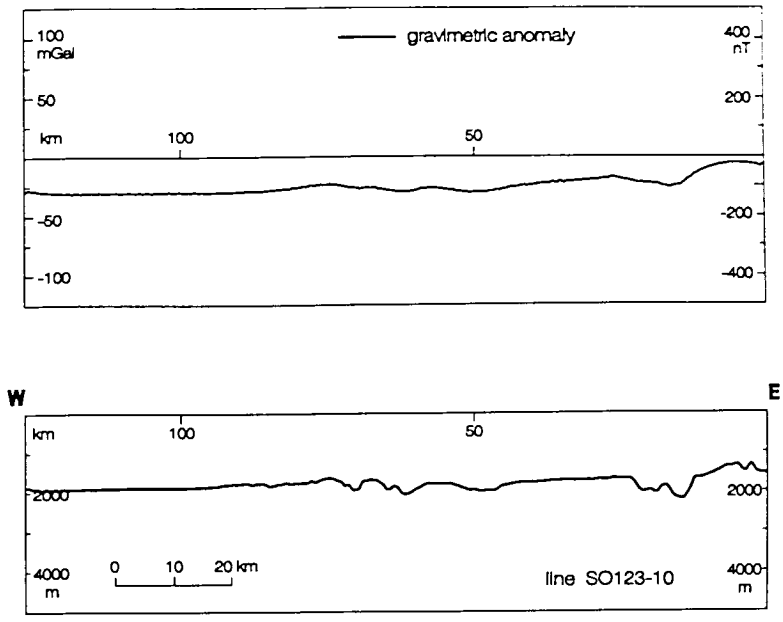

Figure 6.4.2.9: Potential field data combined with seafloor topography along seismic line SO123-10. Explanation see Figure 6.4.2.7.

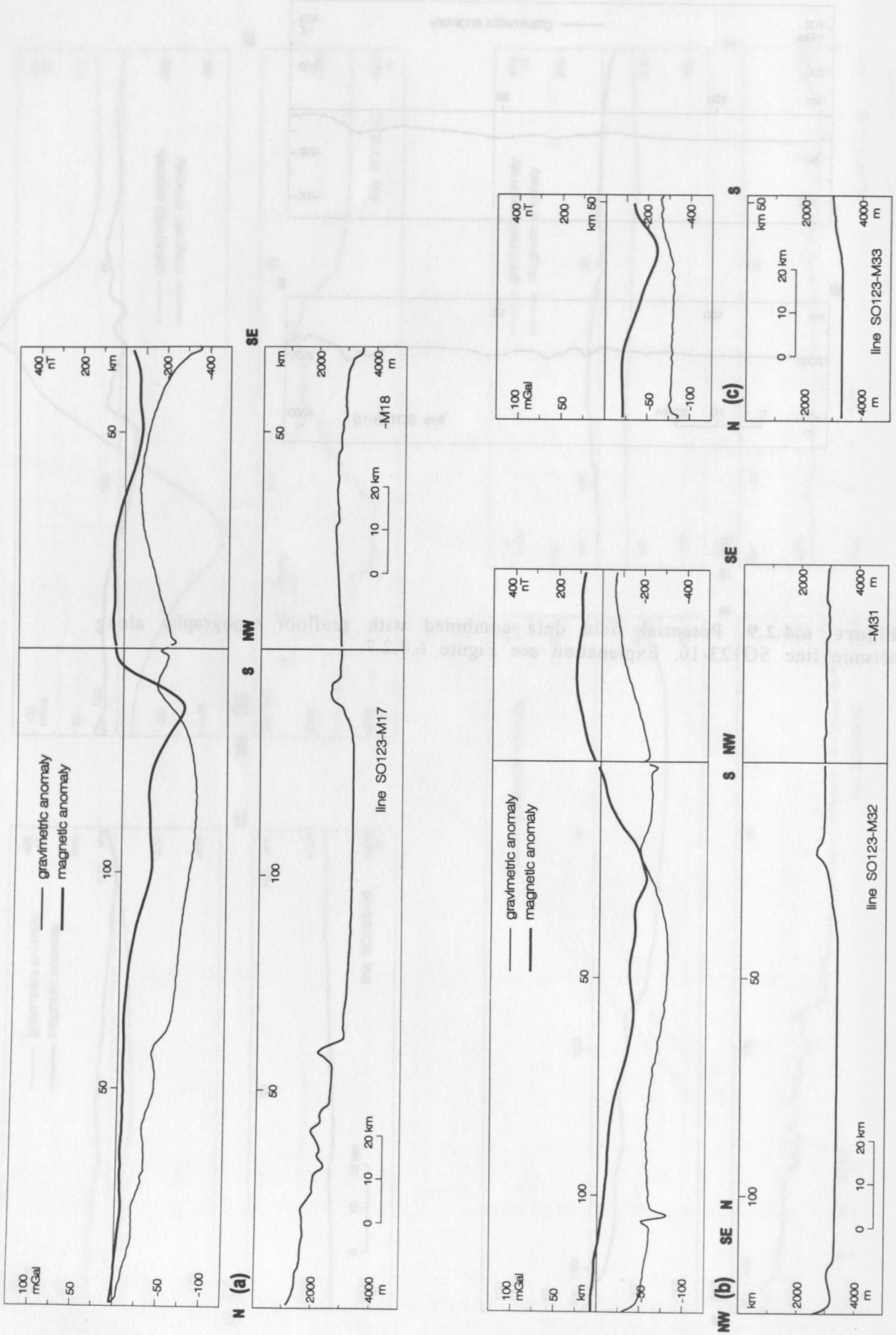

Figure 6.4.2.10: Potential field data combined with seafloor topography along lines without wide-angle seismic measurements. (a) SO123-M17 and -M18, (b) SO123-M32 and -M31, (c) SO123-M33. Explanation see Figure 6.4.2.7.

6.5 THE SEISMOLOGY NETWORK

(S. Husen)

To monitor the local seismicity across the Makran accretionary wedge a temporary network consisting of 12 OBH was installed at the beginning of the cruise. The instruments were deployed at an average spacing of 20 nm during the days 09.09 and 10.09.1997. The design of the network is shown in Figure 6.5.1. Two instruments, OBH09 and OBH16, were recovered after 4 days. The remaining 10 instruments were recovered after 12 days during day 23.09 and 24.09.1997. Unfortunately 3 instruments, OBH04, 06 and 18, had recording problems due to power failure or hardware problems. Therefore only data from 7 OBH were left for the entire observation period. Details on intrumentation are given in Appendix 9.1.11.

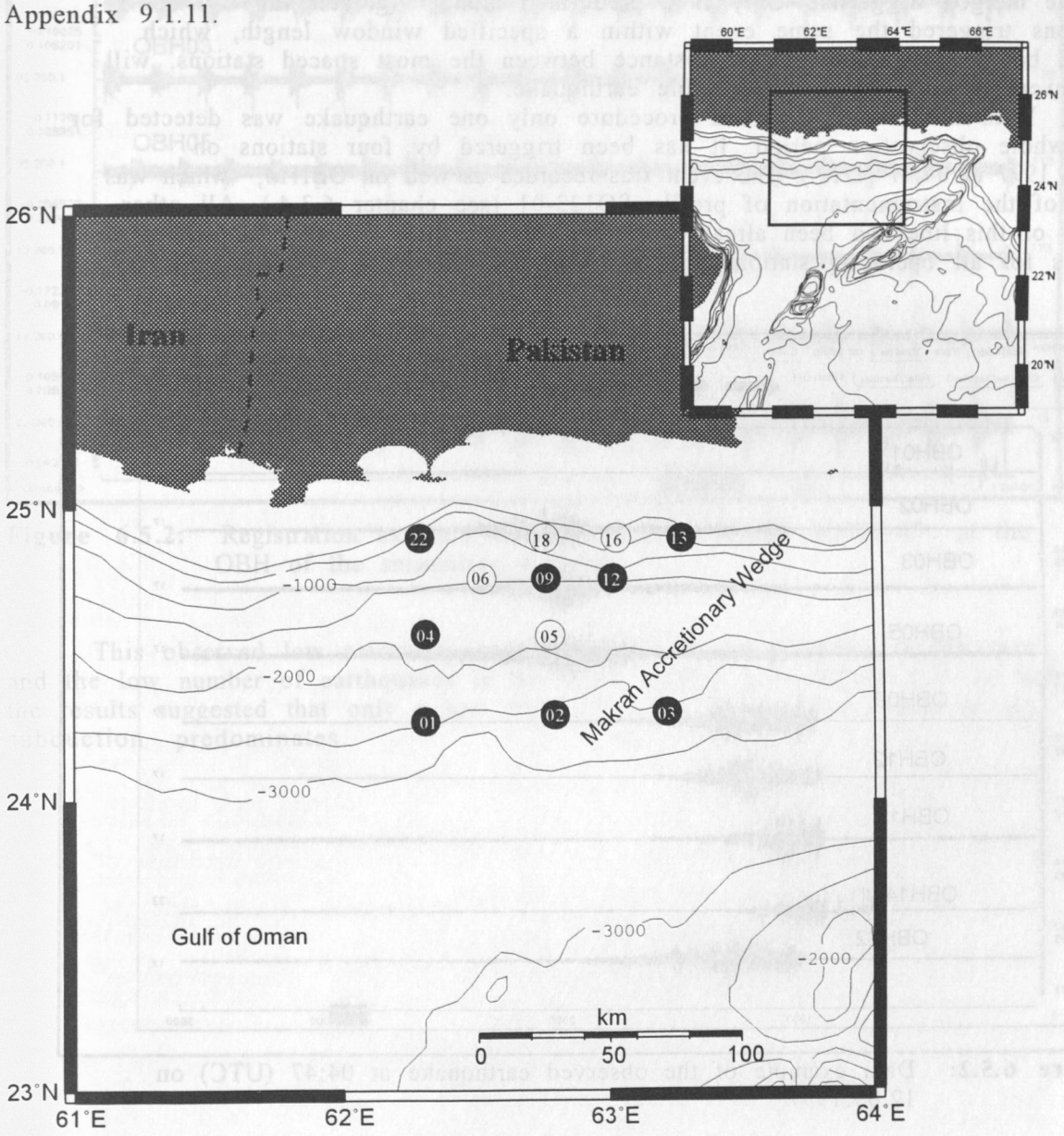

Figure 5.6.1: Design of the seismology network. The open circles mark OBH with data loss due to hardware problems.

All instruments were running at 10 ms sampling rate and in continous mode. The last secures observation throughout the whole period in contrast to trigger based systems, where a badly calibrated trigger can cause data loss.

After downloading the rawdata with the ref2segy software (see chapter 5.2.2) a software trigger was used to search the datastream for possible events. The code is based on the AUTOPICK software in the IASPEI Software Library Supplement #1 (R. Banfill, 1993). It applies a 2nd order bandpass, frequency cutoff at 2 and 10 Hz, to the data before analysing the long term and short term average. The long term average is the average amplitude over a window length of 4 s whereas the short term average is calculated over a window of 0.1s. If the ratio of short term average (STA) and long term average (LTA) is greater than a predefined value and this lasts over a predefinded space of time (event length), the event will be triggered and added to a triggerlist of this station. For this study we use a STA to LTA ratio of 8 and an event length of 0.3s. In a next step all this triggerlists will be merged and sorted by increasing time. To identify a triggered event as a possible earthquake a final coincidence test will be applied to the merged triggerlist. Only if a predefined number (greater than 4) of stations triggered the same event within a specified window length, which could be the traveltime for the distance between the most spaced stations, will the event be accepted as a possible earthquake.

With the above described procedure only one earthquake was detected for the whole observation period. It has been triggered by four stations on 12.09.1997 at 04:47 (UTC). The event was recorded as well on OBH14, which was part of the instrumentation of profile SO123-01 (see chapter 6.3.4.). All other OBH of this line had been already recovered at this time. Figure 6.5.2 shows the traces for all operating stations at this time.

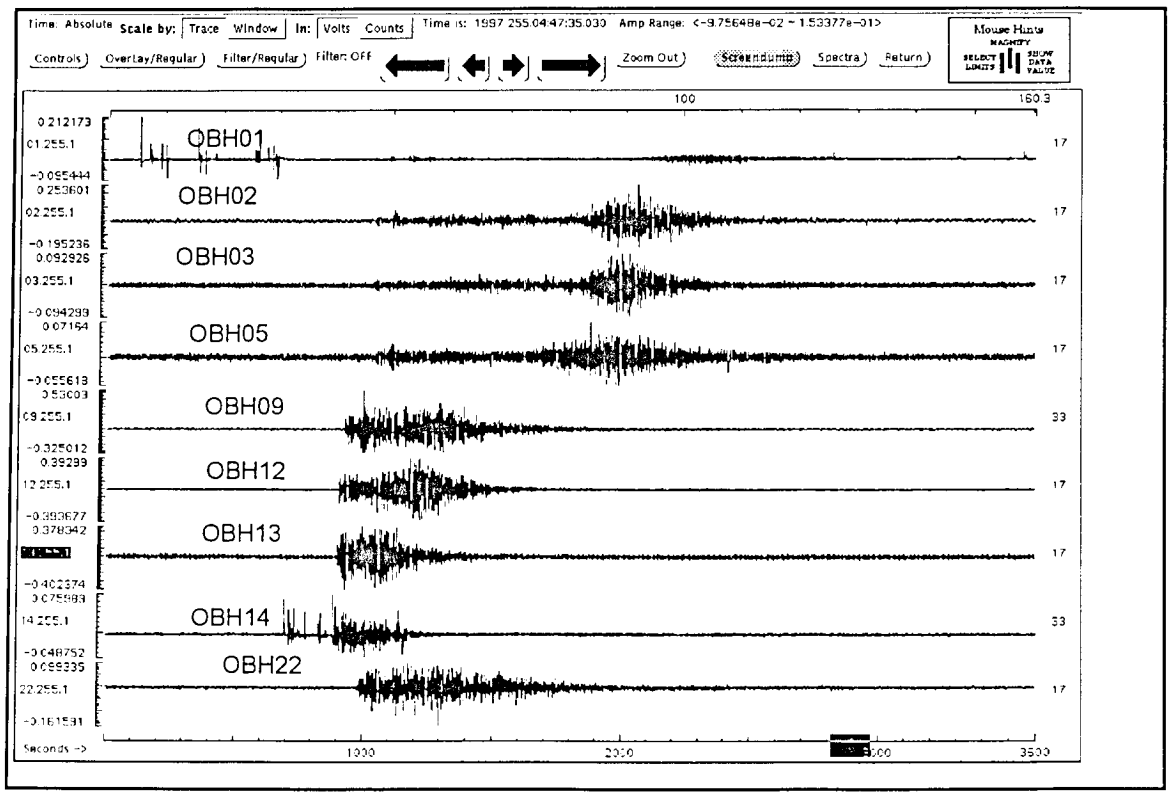

Figure 6.5.2: Data example of the observed earthquake at 04:47 (UTC) on 12.09.1997.

OBH09, 12, 13 and 22 show clear onsets of the first arrival, whereas the other instruments show only noisy and weak signals. This could indicate that the observed event is of small magnitude and is located close to the OBH09,12,13 or OBH22. Beside this event no other earthquakes have been detected. The airgunshots of profiles SO123-04 to 07 across the Murray Ridge (see chapter 6.3.4.4 to 6.3.4.7) could be clearly identified over a distance up to 300 km. Figure

6.5.3 shows an example for the registrations of few shots of profile SO123-05. This clearly demonstrates that the ambient noise level is rather low and earthquakes were not missed because of high noise.

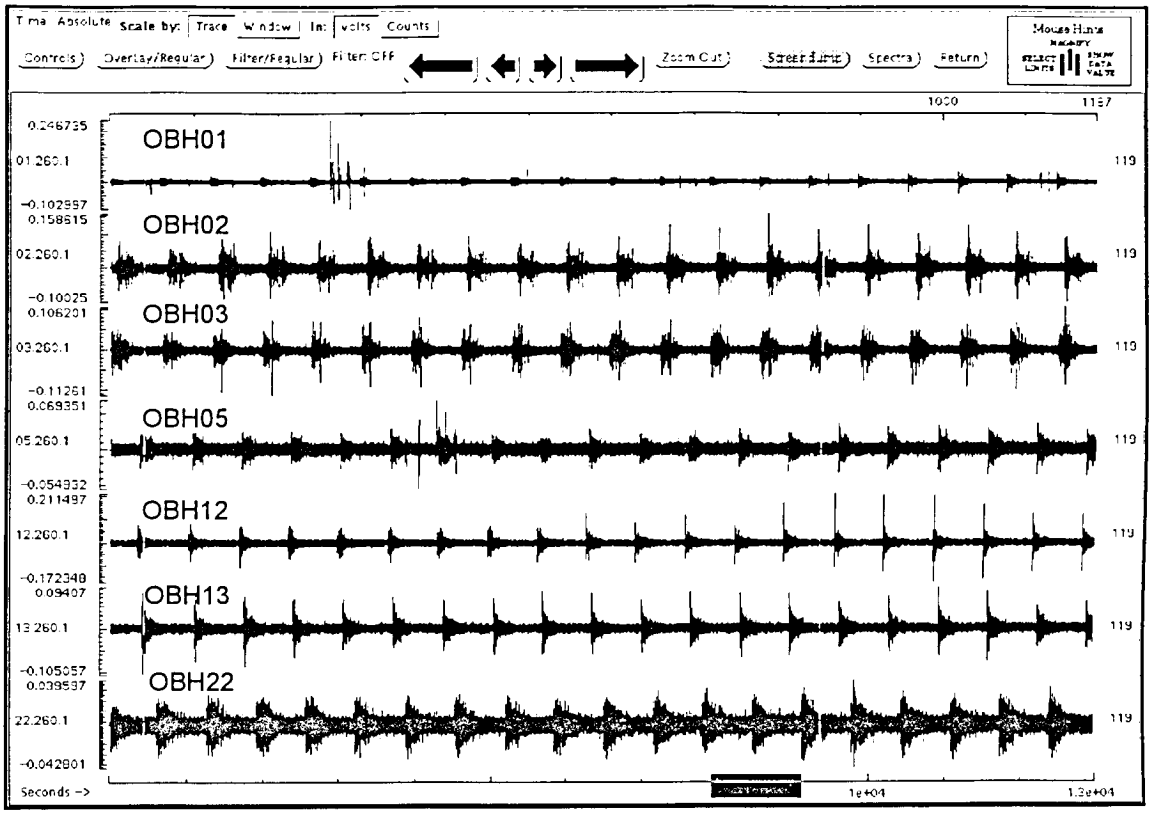

Figure 6.5.2: Registration example of airgunshots of profile SO123-05 at the OBH of the seismology network.

This observed low seismicity is coincident with other studies in the area and the low number of earthquakes in the NEIC catalog (see chapter 2.2), so that the results suggested that only a low level of earthquake activity related to the subduction predominates.

7. ACKNOWLEDGEMENTS

The cruise SO 123 was funded by the German Ministery of Education, Research, Science, and Technologie (BMBF) under project No. 03 G 0123 A within the continued most commendable support for marine sciences with an oustanding research vessel like SONNE. The participation of R. Edwards and T. Minshull from Bullard Laboratories, Cambridge, UK, was made possible through the EU Programme "Training and Mobility of Researchers", Access for Researchers to the Large-Scale Facility called "Research Vessel (SONNE)". The helpful support by Director General Dr. Shahid Amjad (National Institute of Oceanography, Karachi, Pakistan), by Captain C.D. Bhatti (Pakistan Navy), by Director General Hilal A. Raza (Hydrocarbon Development Institute of Pakistan, Islamabad), and by Director Z.M. Khan (Pakistan Space and Upper Atmosphere Research Commission, Karachi) is gratefully acknowledged. We thank Mr. Gilles Balma from the Bureau Gravimetrique International in Toulouse/France for valuable information about gravity stations in Oman and Dr. Waris E.K. Warsi from the Sultan Qaboos University in Oman for help with the gravity ties.

We warmly thank master H. A. Andresen and his crew for the excellent support with all work done and the splendid working atmosphere throughout the whole cruise.

8. REFERENCES

Ammon, C.J. and Vidale, J.E., 1993: Tomography without rays. Bull. Seismol. Soc. Am., 83, 509-528

Bannert, D., 1992: The structural development of the Western Fold Belt, Pakistan. Geol. Jb., B80, 60.

Barker, P.F., 1966a: Bathymetric and magnetic investigations H.M.S. Dalrymple, 1961/2 and 1962/3. London, Hydrographic Department, Ministry of Defence, H.D. 566.

Barker, P. F., 1966b. A reconnaissance survey of the Murray Ridge. Phil. Trans. R. Soc. Lond., A, 259, 187-197.

Closs, H., Bungenstock, H., Hinz, K., 1969: Ergebnisse seismischer Untersuchungen im nördlichen Arabischen Meer: ein Beitrag zur internationalen Indischen Ozean Expedition. METEOR Forschungsergebnisse, Reihe C, 2, 28 pp.

Cohen, J. K. and Jr. J. W. Stockwell, 1997: CWP/SU: Seismic Unix Release 30: a free package for seismic research and processing. Center for Wave Phenomena, Colorado School of Mines.

Collier, J. S. and White, R. S., 1990: Mud diapirism within Indus fan sediments: Murray Ridge, Gulf of Oman. Geophys. J. Int., 101, 345-353.

DeMets, C., Gordon, R. G., Argus, D. F. and Stein, S., 1990: Current plate motions. Geophys. J. Int., 101, 425-478.

Donovan, T.J., Forgey, R. L. and Roberts, A. A., 1979: Aeromagnetic detection of diagenetic magnetite over oil fields. AAPG Bull, 3, 245-248.

Edwards, R. A., Minshull, T. A. and White, R. S.: Extension across the Indian-Arabian plate boundary: the Murray Ridge. In prep. for Geophys. J. Int.

Eilers, G., Roeser, H.A. and Kewitsch, P., 1994: Die Reduktion geomagnetischer Variationen bei seemagnetischen Messungen durch ein Gradientenmagnetometer. BGR-Report, 73 S., Hannover.

Farah, A., Lawrence, R.D. and DeJong, K.A, 1984: An overview of the tectonics of Pakistan. In: B.U. Haq and J. D. Milliman. Marine geology and oceanography of Arabian Sea and coastal Pakistan, New York, 161-171.

Flueh, E. R. and Fisher,M. A., 1996: Cruise report SO108-ORWELL. GEOMAR Report 49, ISSN 0936-5788, 278 pp.

Flueh, E. R., Bialas, J., 1996: A digital, high data capacity ocean bottom recorder for seismic investigations. Int. Underwater Systems Design, 18, 3, 18 - 20..

Fowler, S. R., R. S. White, and K. E. Louden, 1985: Sediment dewatering in the Makran accretionary prism. Earth Plan. Sci. Lett., 75, 427-538.

Fruehn, J., R. S. White and T. A. Minshull, 1997: Internal deformation and compaction of theMakran accretionary wedge. Terra Nova, in press.

Gordon, R. G., DeMets, C., 1989: Present-day motion along the Owen Fracture Zone and Dalrymple Trough in the Arabian Sea. J. Geophys. Res., 94, 5560-5570.

Grant, J. A. and Schreiber, R., 1990: Modern swathe sounding and sub-bottom profiling technology for reserch applications: The Atlas Hydrosweep system. Marine Geophys. Res., 12, 9 - 19.

Gutscher, M.-A., Kukowski, N., Malavieille, J., Lallemand, S., in press: Cyclical behavior of thrust wedges: Insights from high basal friction sandbox experiments. Geology.

Harms, J.C., H.N. Cappel and Francis, D.C., 1982: Geology and petroleum potential of the Makran coast, Pakistan. In: Proceedings of the Offshore Southeast Asia 82 Conference, 9-12 Feb, Singapore. Southeast Asia Petrol. Explor. Soc., 1-9.

Harms, J. C., Cappel, H. N., Francis, D. C., and Shackelford, T. J., 1983: Summary of the geology of the Makran coast. In: : A.W. Bally (ed.), Seismic Expression of Structural Styles, AAPG Stud. Geol., 15, 3.4.2.173-3.4.2.175.

Harms, J.C., Cappel, H.N., Francis, D.C. and Shackelford, T.J., 1985: Summary of the geology of the Makran coast. In: A.W. Bally (ed.), Seismic expression of structural styles. AAPG studies in Geology Series 15, vol.3, 173-177.

Hiller, K., 1994. Pakistan. In: H. Kulke (ed.), Regional petroleum geology of the world - part 1. Borntraeger, Stuttgart, 607-628.

Hutchison, I., Louden, K. E., White, R.S., 1981: Heat flow and age of the Gulf of Oman Earth Planet. Sci. Lett., 56, 252-262.

IAGA Division V, Working Group 8, 1996: International geomagnetic reference field, 1995 revision. Geophys. J. Int., 125, 318-321.

Kukowski, N., Gutscher, M.-A., Malavieille, J. and Lallemand, S.E., 1994a: Structural evolution of convergent margins; Insight from scaled sandbox modelling. EGS, Grenoble.

Kukowski, N. , von Huene, R., Malavieille, J. and Lallemand, S.,1994b: Sediment accretion against a buttress beneath the Peruvian continental margin as simulated with sandbox modeling. Geol. Rdsch, 83, 822-831.

Lehner, P., Doust, H., Bakker, G., Allenbach, P., and Gueneau, J., 1983: Makran fold belt, profile N 1804. In Seismic Expression of Structural Styles, AAPG Stud. Geol., 15.

Miles, P.R. and Roest, W. R. 1993: Earliest sea-floor spreading magnetic anomalies in the North Arabian Sea and the ocean-continent transition. Geophys. J. Int., 115, 1025-1031.

Minshull, T. A., and White, R. S., 1989: Sediment compaction and fluid migration in the Makran accretionary prism. J. Geophys. Res., 94, 7387-7402.

Minshull, T. A., White, R. S., Barton, P. J., and Collier, J. S., 1992: Deformation at plate boundaries around the Gulf of Oman. Mar. Geol., 104, 265-277.

Morelli, C., 1974: The International Standardization Net 1971. International Association of Geodesy Special Publication 4, 194.

Mountain, G. and Prell, W. I. 1990: A multiphase plate tectonic history of the southeast continental margin of Oman. In: A.H.F. Robertson, M.P. Searle and A.C. Ries (Editors), The Geology and Tectonics of the Oman Region. Spec. Publ. Geol. Soc. London, 49, 725-743.

Niazi, M, Shimura, H., Matsu'ura, M., 1980: Microearthquakes and Crustal Structure off the Makran Coast of Iran. Geophys. Res. Let., 7, 5, 297-300.

Page, W. D., Alt, J. N., Cluff, L. S., Plafker, G., 1978: Evidence for the recurrence of large-magnitude earthquakes along the Makran coast of Iran and Pakistan. Tectonophysics, 52, 533-547.

Ranero, C. R., Reston, T. J., Belykh, I., Gnibidenko, H., 1997: Reflective oceanic crust formed at a fast-spreading center in the Pacific. Geology, 25, 499-502.

Raza, H.A. and S. Alam, 1983: Stratigraphic synthesis and its implication on the geology of petroleum in Makran. Geol. Bull., 18, 74-79.

Raza, H.A., Riaz, A. and Manshoor Ali, S., 1990: Pakistan offshore - an attractive frontier. Pak. J. Hydrocarb. Res., 1-42.

Roeser, H.A., Bargeloh, H.-O., and Schreckenberger, B., 1992: Technischer Bericht über ein kleines Navigationssystem für seegeophysikalische Arbeiten. BGR report, 31 pages, Hannover.

Roeser, H.A. and scientific party, 1997. MAKRAN 1: The Makran accretionary wedge off Pakistan - tectonic evolution and fluid migration (part 1). Cruise report, BGR archive no 116 643, Hannover.

Spieß V, 1993: Digitale Sedimentechographie - Neue Wege zu einer hochauflösenden Akustostratigraphie. - Habilitationsschrift, U. Bremen, 199pp.

Stein, C.S. and Cochran, J. R., 1985: The transition between the Sheba Ridge and Owen basin: rifting of old oceanic lithosphere. Geophys. J. Int., 81, 47-74.

Suess, E. (ed.) Fahrtbericht SO-97 Kodiak-Vent, Geomar Report, ISSN 0936-5788, 29, 135 - 156.

Taylor, P.T., 1968: Interpretation of the North Arabian Sea aeromagnetic survey. Earth Planet. Sci. Lett., 43, 232-236.

Vidale, J.E., 1988: Finite-difference calculation of traveltimes. Bull. Seis. Soc. Am., 78, 2062-2076

Von Huene, R.,1994: Fahrtbericht SO-96, KODIAKSEIS, Kiel, unpub.

Von Rad U (ed.), 1993: Fahrtbericht SO-90 PAKOMIN, BGR Achiv No. 111987, Hannover, unpub.

Von Rad, U. and Tahir, M. , 1997: Late Quaternary sedimentation on the outer Indus shelf and slope (Pakistan): evidence from high-resolution seismic data and coring. Mar. Geol., 138, 193-236.

Wefer, G., Hinz, K. and Roeser, H. A., 1993: Ostantlantik 91/92 - Expedition, METEOR-Fahrt M 20/3. Meteor-Berichte, 93-3, pp 145, Kiel.

Wessel, P. and Smith, W.H.F., 1991: Free software helps map and display data, EOS **72**, 445 - 446.

White, R. S., 1977a: Recent fold development in the Gulf of Oman. Earth Plan. Sci. Lett., 36, 85-91.

White, R. S., 1977b: Seismic bright spots in the Gulf of Oman. Earth Plan. Sci. Lett., 37, 29-37.

White, R. S., 1979: Gas hydrate layers trapping free gas in the Gulf of Oman. Earth Plan. Sci. Lett., 42, 114-120.

White, R.S., 1984: Active and passive plate boundaries around the Gulf of Oman, north-west Indian Ocean. Deep Sea Research, 31.

White, R. S., 1982: Deformation of the Makran accretionary sediment prism in the Gulf of Oman (north-west Indian Ocean). In: Trench and Fore-Arc Geology: Sedimentation and Tectonics on Modern and Ancient Active Plate Margins, ed. J. K. Leggett, Blackwell Scientific, Oxford, England, 357-372.

White, R. S., and Klitgord, K. D., 1976: Sediment deformation and plate tectonics in the Gulf of Oman. Earth Plan. Sci. Lett., 32, 199-209.

White, R. S., and Louden, K. E., 1983: The Makran continental margin: Structure of a thickly sedimented convergent plate boundary. In: Studies in Continental Margin Geology, Mem. Am. Assoc. Pet. Geol., 34, 499-518.

White, R. S., and Ross, D. A., 1979: Tectonics of the western Gulf of Oman. J. Geophys. Res., 84, 3479-3489.

Whitmarsh, R. B., 1979: The Owen Basin off the south-east margin of Arabia and the evolution of the Owen Fracture Zone. Geophys. J. R. Astr. Soc., 58, 441-470.

Appendix 9.1.1 MAMUT - SO123 - Profile 01 Makran

INSTRUMENT	LAT (N)	LON (E)	DIST. TO	DEPTH	RELEASER-	FREQUENCY	RECORDER	SKEW	REMARKS
	D:M	D:M	NEXT (nm)	(m)	CODE	(MHz)	NUMBER	(ms)	
OBH06	24:44.67	62:33.01	3.7	1527	B214	160.785	91.10		not sync., 8 resets
OBH07	24:44.66	62:37.04	4.3	1570	D674	160.785	01.97	-13	tape read error
OBH08	24:44.67	62:41.72	4.3	1843	A319	159.480	04.96	-30	
OBH09	24:44.65	62:46.41	4.6	1706	D654	159.480	91.12	18	
OBH10	24.44.65	62:51.50	4.1	1810	C444	154.585	01.95	0	
OBH11	24:44.64	62:56.01	3.6	1662	A634	159.480	02.97	+1	
OBH12	24:44.63	63:00.01		1469	B559	159.480	03.97	-24	
TRIGGER							91.14	-16	

Appendix 9.1.2 MAMUT - SO123 - Profile 02 Makran

INSTRUMENT	LAT (N)	LON (E)	DIST. TO	DEPTH	RELEASER-	FREQUENCY	RECORDER	SKEW	REMARKS
	D:M	D:M	TO NEXT (nm	(m)	CODE	(Hz)	NUMBER	(ms)	
OBH13	24:52.10	63:14.12	3.0	564	A324	160.785	08.94	-121	
OBH14	24:52.10	63:10.87	4.5	1129	D629	154.585	03.96	-20	
OBH15	24:52.08	63:05.92	4.7	1023	B219	160.725	05.96	2	
OBH16	24:52.11	63:00.69	7.6	1050	6A24	160.785	15.93		no data rec.
OBH17	24:52.09	62:52.41	5.8	1337	D649	159.480	06.96	5	
OBH18	24:52.11	62:46.02	5.3	985	B495	160.725	92.01	-13	tape read error
OBH19	24:52.10	62:40.21	5.0	1366	D669	159.480	19.96	-8	no data rec.
OBH20	24:52.07	62:34.74	5.4	1080	B639	160.725	02.96	-28	
OBH21	24:52.11	62:28.82	2.4	1376	D634	160.785	01.96	-7	
OBH22	24:52.10	62:20.14		1000	6A29	160.725	04.94	28	
TRIGGER							91.14	-16	

Appendix 9.1.3 MAMUT - SO123 - Profile 03 Instrument Tests

INSTRUMENT	LAT (N)	LON (E)	DIST. TO	DEPTH	RELEASER-	FREQUENCY	RECORDER	SKEW	REMARKS
	D:M	D:M	NEXT (nm)	(m)	CODE	(MHz)	NUMBER	(ms)	
OBH23	24:56.97	63:10.81	1.6	471	D629	159.480	91.14	-7	BC6
OBH24	24:56.97	63:12.61	6.6	612	B219	160.785	04.96	-10	AQ16
OBH25	24:56.80	63:19.82	0.4	120	6A34	160.785	02.96	-325	1 reset
OBS01	24:57.16	63:19.81		100	A319	159.480	01.95	1	
TRIGGER							01.96	-2	

Appendix 9.1.4 MAMUT - SO123 - Profile 04 Dalrymple Trough

INSTRUMENT	LAT (N)	LON (E)	DIST. TO	DEPTH	RELEASER-	FREQUENCY	RECORDER	SKEW	REMARKS
	D:M	D:M	TO NEXT (nm	(m)	CODE	(Hz)	NUMBER	(ms)	
OBH26	22:51.41	63:25.83	5.5	4123	D654	154.585	02.97	3	
OBH27	22:49.42	63:23.70	4.6	4035	6A34	160.785	03.96	-37	
OBH28	22:46.12	63:20.16	4.1	4096	D629	154.585	02.96	-30	
OBS02	22:43.19	63:17.02	4.7	4016	A319	160.725	01.95	-1	
OBH29	22:39.88	63:13.45	3.8	4359	B219	159.480	04.96	-21	
OBH30	22:37.21	63:10.56	4.6	4386	D674	160.785	91.12	4	
OBH31	22:33.99	63:07.08	7.2	4322	D669	159.480	05.96	-2	
OBH32	22:28.86	63:01.58	4.1	4114	B639	160.725	19.96	-5	
OBH33	22:25.93	62:58.43		4138	D634	159.480	06.96	1	
TRIGGER							91.12	3	

Appendix 9.1.5 MAMUT - SO123 - Profile 05 Murray Ridge

INSTRUMENT	LAT (N)	LON (E)	DIST. TO	DEPTH	RELEASER-	FREQUENCY	RECORDER	SKEW	REMARKS
	D:M	D:M	NEXT (nm)	(m)	CODE	(MHz)	NUMBER	(ms)	
OBH34	23:12.82	63:07.44	2.1	2716	D629	160.785	91.14	-12	
OBH35	23:11.02	63:08.64	2.8	2681	D674	160.785	06.96	1	
OBS03	23:08.62	63:10.30	4.9	2693	A319	159.480	01.95	-2	
OBH36	23:04.41	63:13.21	5.2	2806	B219	159.480	19.96	-4	
OBH37	22:59.98	63:16.29	5.4	2920	C444	160.725	05.96	-1	
OBH38	22:55.45	63:19.41	4.6	3438	D669	159.480	91.12	2	
OBH39	22:51.54	63:22.09	5.9	4040	B639	160.725	04.96	-19	
OBH40	22:46.50	63:25.56	3.4	4147	D654	154.585	01.96	-7	
OBH27	22:49.42	63:23.70	7.8	4035	6A34	160.725	03.96	-37	
OBH41	22:42.78	63:28.09		2610	D634	160.785	02.96	-23	
TRIGGER							02.97	-1	

Appendix 9.1.6 MAMUT - SO123 - Profile 06 Murray Ridge

INSTRUMENT	LAT (N)	LON (E)	DIST. TO	DEPTH	RELEASER-	FREQUENCY	RECORDER	SKEW	REMARKS
	D:M	D:M	NEXT (nm)	(m)	CODE	(MHz)	NUMBER	(ms)	
OBH42	23:13.07	63:11.05	3.0	2710	D629	160.785	02.97	2	
OBH35	23:11.02	63:08.63	2.1	2681	D674	160.785	06.96	1	
OBH43	23:09.48	63:07.09	3.0	2742	C444	160.785	91.14	-15	
OBH44	23:07.43	63:04.74	2.9	2804	6A34	154.585	05.96	0	
OBH45	23:05.42	63:02.47	3.0	2789	D634	160.785	91.12	3	
OBH46	23:03.34	63:00.11	2.9	2880	D654	160.785	19.96	-6	
OBH47	23:01.28	62:57.81	2.9	2921	B639	159.480	04.96	-24	
OBH48	22:59.22	62:55.52		2918	D669	160.785	01.96	-8	
TRIGGER							02.96	-8	

Appendix 9.1.7

MAMUT - SO123 - Profile 07 Murray Ridge

INSTRUMENT	LAT (N)	LON (E)	DIST. TO	DEPTH	RELEASER-	FREQUENCY	RECORDER	SKEW	REMARKS
	D:M	D:M	NEXT (nm)	(m)	CODE	(MHz)	NUMBER	(ms)	
OBH49	22:28.61	62:57.10	2.9	4121	D669	154.585	03.96	-17	
OBH50	22:26.37	62:59.08	3.7	4142	B639	160.785	19.96	-6	
OBH51	22:23.52	63:01.60	10.1	3604	D654	160.725	04.96	-21	two data gaps
OBH52	22:15.67	63:08.54	3.5	1701	C444	159.480	15.93	-12	
OBH53	22:12.96	63:10.95	5.2	1603	D629	160.785	02.97	1	
OBS04	22:08.89	63:14.52	3.8	1169	A319	159.480	01.95	-3	
OBH54	22:05.97	63:17.12	3.0	1524	B219	160.725	01.96	-5	
OBH55	22:03.64	63:19.19	4.7	2436	D634	159.480	91.12	2	
OBH 56	21:59.96	63:22.44	5.7	2923	6A34	160.725	05.96	1	
OBH57	21:55.56	63:26.30		3120	D674	159.480	02.96	-27	
TRIGGER							06.96	5	

Appendix 9.1.8 MAMUT - SO123 - Profile 08 Makran

INSTRUMENT	LAT (N)	LON (E)	DIST. TO	DEPTH	RELEASER-	FREQUENCY	RECORDER	SKEW	REMARKS
	D:M	D:M	NEXT (nm)	(m)	CODE	(MHz)	NUMBER	(ms)	
OBH58	24:53.89	62:45.86	1.8	1103	A324	160.725	02.97	2	
OBH59	24:52.10	62:46.00	1.9	990	A314	160.785	91.14	-14	
OBH60	24:50.22	62:46.14	3.0	1411	C454	159.480	01.96	-6	
OBH61	24:47.25	62:46.32	2.7	1548	B219	154.585	91.13	-55	
OBH62	24:44.57	62:46.49	3.3	1709	B559	160.785	03.97	-5	
OBH63	24:41.28	62:46.70	3.7	1726	6A29	159.480	06.96	3	
OBH64	24:37.59	62:46.90	4.2	1824	D629	160.785	08.94	-19	
OBH65	24:33.44	62:47.22	3.5	2219	C444	154.585	15.93	-32	
OBH66	24:29.94	62:47.42	3.9	2121	B644	160.725	03.94	1	
OBH67	24:26.18	62:47.63	3.7	2056	C459	159.480	92.06	4	
OBH68	24:22.53	62:47.93	3.3	2392	D674	160.785	03.96	-21	data read error
OBH69	24:19.20	62:48.09	2.5	2330	B214	154.585	02.95	-20	
OBH70	24:16.71	62:48.28	2.3	2565	B495	160.785	19.96	-8	
OBH71	24:14.42	62:48.43	3.4	3062	6A34	159.480	04.96	-27	data read error
OBH72	24:11.01	62:48.64	2.3	2960	D634	160.785	91.12	0	
OBS05	24:08.71	62:48.81	3.8	3222	A319	154.585	01.95	-6	
OBH73	24:04.96	62:49.04	4.5	3248	D654	160.725	05.96	0	
OBH74	24:00.49	62:49.31	4.3	3268	B639	159.480	02.96	-32	
OBH75	23:56.23	62:49.59		3280	D669	160.785	91.09		not determined
TRIGGER							92.01	-12	

Appendix 9.1.9

MAMUT - SO123 - Profile 09 Makran

INSTRUMENT	LAT (N)	LON (E)	DIST. TO	DEPTH	RELEASER-	FREQUENCY	RECORDER	SKEW	REMARKS
	D:M	D:M	NEXT (nm)	(m)	CODE	(MHz)	NUMBER	(ms)	
OBH85	24:17.90	62:28.59	3.0	2493	D654	160.725	03.94	-1	
OBH86	24:18.12	62:31.89	3.0	2491	D634	159.480	92.06	0	
OBH87	24:18.34	62:35.20	2.9	2463	A319	154.585	03.96	-15	
OBH88	24:18.56	62:38.36	2.9	2426	B495	160.785	04.96	-20	
OBH89	24:18.77	62:41.54	3.0	2400	D674	159.480	19.96	-6	
OBH90	24:19.00	62:44.88	3.0	2342	C459	160.725	05.96	-1	
OBH69	24:19.20	62:48.09	2.9	2330	B214	154.585	02.95	-20	
OBH91	24:19.43	62:51.36	3.0	2507	B644	159.480	91.12	1	
OBH92	24:19.64	62:54.63		2591	B559	154.585	01.95	-3	
TRIGGER							02.96	-11	

Appendix 9.1.10

MAMUT - SO123 - Profile 10 Makran

INSTRUMENT	LAT (N)	LON (E)	DIST. TO	DEPTH	RELEASER-	FREQUENCY	RECORDER	SKEW	REMARKS
	D:M	D:M	NEXT (nm)	(m)	CODE	(MHz)	NUMBER	(ms)	
OBH76	24:37.65	62:53.55	3.0	1740	C444	160.725	91.13	-95	
OBH77	24:37.55	62:50.22	2.9	1942	B219	154.585	15.93	-56	
OBH78	24:37.51	62:46.99	3.0	1831	D629	160.785	92.01	-63	
OBH79	24:37.29	62:43.76	3.3	1770	C634	159.480	01.96	-9	
OBH80	24:37.22	62:39.91	2.5	1911	C454	160.785	08.94	-23	
OBH81	24:37.08	62:37.40	3.0	1693	A314	159.480	91.14	-21	
OBH82	24:36.89	62:34.12	2.9	1632	A324	160.785	02.97	2	
OBH83	24:36.79	62:30.91	3.0	1753	D669	159.480	91.09	-30	
OBH84	24:36.67	62:27.69		1823	B639	160.785	03.97	-5	
TRIGGER							96.05	1	

INSTRUMENT	LAT (N)	LON (E)	DIST. TO	DEPTH	RELEASER-	FREQUENCY	RECORDER	SKEW	REMARKS
	D:M	D:M	NEXT (nm)	(m)	CODE	(MHz)	NUMBER	(ms)	
OBH01	24:17.97	62:21.27	24.6	2490	C454	160.785	91.13	-366	
OBH02	24:19.17	62:48.09	21.2	2330	C459	154.585	92.06	77	
OBH03	24:19.69	63:10.86	25.9	2779	B644	160.785	03.96	-162	
OBH04	24:33.99	62:47.22	23.7	2229	A314	154.585	91.15		rec. error/no data
OBH05	24:34.21	62:21.25	15.0	1840	C634	159.480	02.95	-88	
OBH06	24:44.67	62:33.01	12.1	1527	B214	160.785	91.10		not synchronized
OBH09	24:44.65	62:46.41	12.4	1706	D654	159.480	91.12	18	
OBH12	24:44.63	63:00.01	14.9	1469	B559	159.480	03.97	-24	
OBH13	24:52.10	63:14.12	12.2	564	A324	160.785	08.94	-121	
OBH16	24:52.11	63:00.69	13.4	1050	6A24	160.785	15.93		late recovery
OBH18	24:52.11	62:46.02	18.2	985	B495	160.725	92.01		not synchronized
OBH22	24:52.10	62:20.14		1000	6A29	160.725	04.94	28	

APPENDIX 9.2

SEISMIC PROFILES

Line number	Shot points	Date	Time [UTC]	Position [dd:mm]		Course	Length Methods
SO123-01	1	10.9.97	11:42	24 44.7 N	62 20.9 E	90°	100.07 km
	656	10.9.97	22:37	24 44.6 N	63 20.2 E		S G M P
SO123-K01	1	10.9.97	22:40	24 44.6 N	63 20.4 E		20.95 km
	144	11.9.97	01:03	24 52.1 N	63 20.1 E		S G M P
SO123-02	1	11.9.97	01:06	24 52.1 N	63 20.0 E	270°	14.09 km
	108	11.9.97	02:53	24 53.2 N	63 12.1 E		S G M P
SO123-02A	1	11.9.97	05:19	24 47.6 N	63 07.0 E	300°/270°	87.50 km
	596	11.9.97	15:14	24 52.1 N	62 16.3 E		S G M P
SO123-03	1	12.9.97	12:05	24 57.0 N	63 22.3 E	270°	28.02 km
	448	12.9.97	15:48	24 57.0 N	63 05.4 E		S G P
SO123-03A	1	12.9.97	16:23	24 57.0 N	63 05.7 E	90°	28.46 km
	159	12.9.97	19:01	24 57.0 N	63 22.7 E		S G M P
SO123-04	1	16.9.97	02:48	22 10.3 N	62 41.7 E	45°	141.76 km
	915	16.9.97	18:02	23 04.6 N	63 40.1 E		S G M P
SO123-05	1	17.9.97	19:24	22 27.5 N	63 37.6 E	225°	122.89 km
	790	18.9.97	08:33	23 23.7 N	62 59.8 E		S G M P
SO123-06	1	19.9.97	04:57	22 44.9 N	62 39.6 E	46°	110.48 km
	738	19.9.97	17:14	23 26.6 N	63 26.2 E		S G M P
SO123-07	1	21.9.97	00:50	21 41.5 N	63 38.7 E	320°	158.77 km
	1016	21.9.97	17:45	22 47.8 N	62 40.1 E		S G M P
SO123-08	1	24.9.97	17:23	23 28.5 N	62 51.4 E	357°	160.08 km
	1185	25.9.97	13:07	24 54.7 N	62 45.8 E		S G P
SO123-09	1	26.9.97	21:12	24 20.9 N	63 13.3 E	266°	119.38 km
	935	27.9.97	12:46	24 16.1 N	62 02.8 E		S G M P
SO 123-10	1	28.9.97	00:49	24 38.5 N	63 16.0 E	266°	126.46 km
	993	28.9.97	17:21	24 35.7 N	62 03.1 E		S G P

Methods used:

G - gravity
M - magnetics
P - Hydrosweep,Parasound
S - refraction seismics

APPENDIX 9.3

MAGNETIC PROFILES

	Date	Time [UTC]	Position [dd:mm]		Course	Methods Length
SO123-M01	09.9.97	16:21	24 21.0 N	63 08.6 E	303°/270°	M G P
	09.9.97	20:35	24 34.3 N	62 21.2 E		80.22 km
SO123-M02	12.9.97	22:20	24 54.1 N	63 10.7 E	180°	G M P
	13.9.97	01:12	24 22.8 N	63 10.7 E		57.83 km
SO123-M03	13.9.97	01:36	24 24.0 N	63 08.0 E	0°	G M P
	13.9.97	02:55	24 39.5 N	63 08.0 E		28.79 km
SO123-M04	13.9.97	06:58	24 54.6 N	63 19.4 E	205°/180°	G M P
	13.9.97	10:38	24 15.2 N	63 13.2 E		74.80 km
SO123-M05	13.9.97	10:38	24 15.1 N	63 13.2 E	270°	G M P
	13.9.97	14:49	24 13.0 N	62 21.9 E		86.89 km
SO123-M06	13.9.97	15:15	24 15.5 N	62 23.2 E	90°	G M P
	13.9.97	19:10	24 17.6 N	63 11.5 E		81.68 km
SO123-M07	13.9.97	19:30	24 15.8 N	63 10.8 E	300°	G M P
	13.9.97	21:32	24 28.6 N	62 49.0 E		44.43 km
SO123-M08	13.9.97	21:43	24 27.7 N	62 47.6 E	128°	G M P
	13.9.97	22:52	23 19.8 N	62 58.5 E		23.59 km
SO123-M09	13.9.97	23:10	24 21.4 N	62 59.3 E	270°	G M P
	14.9.97	02:20	24 21.1 N	62 21.5 E		63.97 km
SO123-M10	14.9.97	02:36	24 23.3 N	62 22.1 E	90°	G M P
	14.9.97	04:32	24 23.3 N	62 45.8 E		40.62 km
SO123-M11	14.9.97	04:46	24 25.3 N	62 46.7 E	270°	G M P
	14.9.97	06:47	24 26.4 N	62 23.9 E		40.00 km
SO123-M12	14.9.97	07:03	24 27.5 N	62 22.1 E	90°	G M P
	14.9.97	08:53	24 28.4 N	62 46.4 E		38.68 km
SO123-M13	14.9.97	09:10	24 29.2 N	62 44.4 E	270°	G M P
	14.9.97	11:03	24 29.2 N	62 23.1 E		37.71 km
SO123-M14	14.9.97	11:16	24 31.0 N	62 23.0 E	90°	G M P
	14.9.97	13:07	24 31.0 N	62 45.6 E		39.26 km
SO123-M15	14.9.97	13:20	24 32.3 N	62 44.2 E	270°	G M P
	14.9.97	15:08	24 32.5 N	62 22.8 E		37.89 km

Methods used:
G - gravity
M - magnetics
P - Hydrosweep,Parasound

Line number	Date	Time [UTC]	Position [dd:mm]		Course	Methods Length
SO123-M16	14.9.97	15:22	24 35.6 N	62 23.2 E	51°/90°	G M P
	14.9.97	18:42	24 43.5 N	63 02.3 E		72.66 km
SO123-M17	15.9.97	06:41	24 50.0 N	63 01.0 E	181°	G M P
	15.9.97	14:10	23 27.0 N	63 01.0 E		151.76 km
SO123-M18	15.9.97	14:10	23 27.0 N	63 01.0 E	145°	G M P
	15.9.97	17:25	22 56.1 N	63 22.4 E		63.36 km
SO123-M19	16.9.97	00:15	22 20.1 N	62 57.4 E	225°	G M P
	16.9.97	02:06	22 06.5 N	62 42.5 E		36.69 km
SO123-M20	16.9.97	18:56	23 02.7 N	63 44.0 E	225°	G M P
	16.9.97	23:53	22 24.2 N	63 02.9 E		102.05 km
SO123-M21	17.9.97	16:28	22 43.6 N	63 30.3 E	147°	G M P
	17.9.97	18:22	22 25.1 N	63 43.1 E		40.69 km
SO123-M22	18.9.97	09:04	23 26.0 N	62 58.5 E	179°/145°	G M P
	18.9.97	10:22	23 12.5 N	63 04.7 E		26.72 km
SO123-M23	19.9.97	02:26	22 59.8 N	62 52.5 E	227°	G M P
	19.9.97	04:10	22 46.0 N	62 36.7 E		37.17 km
SO123-M24	19.9.97	19:13	23 17.9 N	63 34.9 E	Div.	G M P
	20.9.97	06:24	23 11.9 N	63 13.8 E		230.32 km
SO123-M25	20.9.97	22:28	21 55.1 N	63 30.6 E	139°	G M P
	20.9.97	23:58	21 41.9 N	63 42.6 E		31.90 km
SO123-M26	21.9.97	18:40	22 49.0 N	62 42.7 E	140°	G M P
	21.9.97	20:36	22 32.7 N	62 57.7 E		40.47 km
SO123-M27	22.9.97	06:56	22 00.0 N	63 29.0 E	317°	G M P
	22.9.97	09:32	22 23.7 N	63 06.8 E		58.92 km
SO123-M28	22.9.97	09:32	22 23.7 N	63 06.8 E	45°	G M P
	22.9.97	13:16	22 57.3 N	63 43.1 E		87.19 km
SO123-M29	22.9.97	13:50	22 54.0 N	63 46.0 E	245°/222°	G M P
	22.9.97	16:05	22 37.2 N	63 25.8 E		47.46 km
SO123-M30	22.9.97	16:05	22 37.2 N	63 25.8 E	div.	G M P
	22.9.97	19:52	22 46.0 N	62 56.1 E		80.91 km
SO123-M31	22.9.97	19:52	22 46.0 N	62 56.1 E	320°	G M P
	22.9.97	21:52	23 09.0 N	62 34.9 E		44.93 km
SO123-M32	22.9.97	21:52	23 09.0 N	62 34.9 E	0°/315°	G M P
	23.9.97	03:18	24 14.3 N	62 35.5 E		126.38 km

Methods used:

G - gravity
M - magnetics
P - Hydrosweep,Parasound

Line number	Date	Time [UTC]	Position [dd:mm]		Course	Methods Length
SO123-M33	24.9.97	13:50	23 54.0 N	62 46.5 E	177°	G M P
	24.9.97	16:23	23 26.6 N	62 48.2 E		51.44 km
SO123-M34	26.9.97	19:11	24 17.8 N	62 57.5 E	86°	G M P
	26.9.97	20:36	24 20.7 N	63 15.5 E		30.61 km
SO123-M35	27.9.97	13:35	24 13.9 N	62 02.5 E	86°	G M P
	27.9.97	14:57	24 14.8 N	62 21.4 E		29.68 km
SO123-M36	29.9.97	02:59	24 41.6 N	63 00.0 E	86°	G M P
	29.9.97	04:21	24 40.0 N	63 15.6 E		
SO123-M37	29.9.97	04:21	24 40.0 N	63 15.6 E	180°	G M P
	29.9.97	06:38	24 14.7 N	63 15.8 E		45 km
SO123-M38	29.9.97	06:52	24 14.7 N	63 18.1 E	360°	G M P
	29.9.97	09:05	24 40.4 N	63 18.1 E		45 km
SO123-M39	29.9.97	09:20	24 40.4 N	63 20.4 E	180°	G M P
	29.9.97	11:35	24 14.9 N	63 20.4 E		47 km
SO123-M40	29.9.97	11:50	24 14.9 N	63 22.8 E	360°	G M P
	29.9.97	14:02	24 41.2 N	63 22.8 E		47 km
SO123-M41	29.9.97	14:18	24 41.3 N	63 25.1 E	180°	G M P
	29.9.97	16:42	24 14.4 N	63 25.1 E		48 km
SO123-M42	29.9.97	16:57	24 14.4 N	63 27.1 E	360°	G M P
	29.9.97	19:26	24 44.6 N	63 27.1 E		52 km
SO123-M43	29.9.97	20:23	24 44.6 N	63 38.8 E	180°	G M P
	29.9.97	22:59	24 15.5 N	63 38.8 E		52 km
SO123-M44	29.9.97	23:15	24 15.5 N	63 36.6 E	360°	G M P
	30.9.97	01:35	24 43.6 N	63 36.6 E		51 km
SO123-M45	30.9.97	01:50	24 43.6 N	63 33.2 E	180°	G M P
	30.9.97	04:18	24 15.2 N	63 33.2 E		48 km
SO123-M46	30.9.97	04:33	24 15.2 N	63 32.0 E	360°	G M P
	30.9.97	07:12	24 43.5 N	63 32.0 E		50 km
SO123-M47	30.9.97	07:32	24 43.5 N	63 29.5 E	180°	G M P
	30.9.97	10:22	24 14.3 N	63 29.5 E		50 km

Methods used:
G - gravity
M - magnetics
P - Hydrosweep,Parasound

APPENDIX 9.4

STATION PROTOCOLS

R.F. Reedereigemeinschaft
Forschungsschiffahrt GmbH

F.S. "S O N N E"
Kapt.H.Andresen

Stationsprotokoll F.S. "S O N N E" Reise SO 123

Gebrauchte Abkürzungen für die eingesetzten Geräte und Anzahl der Einsätze:

CTD	CTD Sonde (Seabird)
OBH	Ocean Bottom Hydrophon
OBS	Ocean Bottom Seismometer

Eingesetzte Winden:

Winde			RF-Nr.	SO 123 Einsatz	Gesamt Einsatz	SO 123 S`länge	gefierte max.Sl	Gesamt S`länge	Zust
W 1	NSW	18,2	813004	000 h	0438 h	000000 m	5150 m	349216	3
W 2	LWL	18,2	865017	000 h	0540 h	010513 m	2160 m	362995	3
W 4	Roches	11,0	816189	000 h	0721 h	027783 m	2150 m	573307	5
W 5	NSW	11,0	816187	003 h	0058 h	0003250 m	3250 m	063665	2
W 6	Drako	18,2	30518	005 h	0326 h	0006300 m	3200 m	450254	3

Geräteverluste:

Abkürzungen im Stationsprotokoll:

z.W.	zu Wasser
a.D.	an Deck
Boko	Bodenkontakt
Sl	Seillänge
Wt	Wassertiefe
W x	eingesetzte Winde
HS	Hydrosweep
PS	Parasound

09.09.1997 **Zeit : UTC +04h**

0230 – 0505	Releasertest	W6	WT 3342m	23-58,90N	61-39,70E
0836 – 1048	Releasertest	W6	WT 3313m	24-02,99N	62-20,00E

Station 01

1054	Beginn 01			
1056	CTD z/W	W5	24-03,00N	62-20,01E
1200	SL 3250m	WT 3313m	24-02,99N	62-20,00E
1325	CTD a/D	Ende 01		

1336 – 1348 Streamertest, L = 70m

OBH # 01

1517	OBH # 01 z/W	WT 2493m		
1518	OBH geslippt		24-17,97N	62-21,27E

OBH # 02

1742	OBH # 02 z/W	WT 2331m		
1743	OBH geslippt		24-19,16N	62-48,09E

OBH # 03

1958	OBH # 03 z/W	WT 2780m		
2001	OBH geslippt		24-19,69N	63-10,86E

Profil # Man 01 (Magnetometer, Gravimeter)

2014	Beginn Profil 01		24-20,28N	63-09,82E
2209	Ende Profil 01	(24sm)	24-33,10N	62-48,60E

OBH # 04

2226	OBH # 04 z/W	WT 2229m		
2228	OBH geslippt		24-33,99N	62-47,21E

Profil # Man 02 (Magnetometer, Gravimeter)

2239	Beginn Profil 02		24-33,99N	62-46,50E

10.09.1997 **Zeit : UTC + 04h**

0025	Ende Profil 02	(21sm)	24-34,21N	62-23,33E

OBH # 05

0049	OBH # 05 z/W	WT 1844m		
0051	OBH geslippt		24-34,20N	62-21,25E

OBH # 06

0218	OBH # 06 z/W	WT 1529m		
0219	OBH geslippt		24-44,66N	62-33,01E

OBH # 07

0249	OBH # 07 z/W	WT 1576m		
0250	OBH geslippt		24-44,65N	62-37,02E

OBH # 08				
0322	OBH # 08 z/W	WT 1846m		
0324	OBH geslippt		24-44,67N	62-41,71E
OBH # 09				
0357	OBH # 09 z/W	WT 1708m		
0358	OBH geslippt		24-44,65N	62-46,41E
OBH # 10				
0432	OBH # 10 z/W	WT 1814m		
0433	OBH geslippt		24-44,65N	62-51,49E
OBH # 11				
0505	OBH # 11 z/W	WT 1664m		
0506	OBH geslippt		24-44,65N	62-55,98E
OBH # 12				
0553	OBH # 12 z/W	WT 1474m		
0554	OBH geslippt		24-44,65N	63-00,00E
OBH # 13				
0721	OBH # 13 z/W	WT 565m		
0723	OBH geslippt		24-52,10N	63-14,20E
OBH # 14				
0807	OBH # 14 z/W	WT 1128m		
0808	OBH geslippt		24-52,09N	63-10,87E
OBH # 15				
0852	OBH # 15 z/W	WT 1024m		
0853	OBH geslippt		24-52,08N	63-05,91E
OBH # 16				
0935	OBH # 16 z/W	WT 1047m		
0936	OBH geslippt		24-52,10N	63-00,69E
OBH # 17				
1028	OBH # 17 z/W	WT 1333m		
1029	OBH geslippt		24-52,10N	62-52,41E
OBH # 18				
1112	OBH # 18 z/W	WT 985m		
1113	OBH geslippt		24-52,10N	62-48,02E
OBH # 19				
1151	OBH # 19 z/W	WT 1365m		
1153	OBH geslippt		24-52,10N	62-40,20E
OBH # 20				
1229	OBH # 20 z/W	WT 1077m		
1230	OBH geslippt		24-52,08N	62-34,72E
OBH # 21				
1308	OBH # 21 z/W	WT 1376m		
1309	OBH geslippt		24-52,10N	62-28,80E

OBH # 22

1332	OBH # 22 z/W	WT 998m		
1333	OBH geslippt		24-52,11N	62-26,14E
1515	Magnetometer z/W	L = 750m		
1517	Bb Airgun-Array z7W	L = 70m		
1528	Stb Airgun-Array z/W	L = 70m		
1532	Streamer z/W	L = 80m		

Profil SO-123/01 (Magnetometer, Airgun-Array, Streamer, Gravimeter)

1542	Beginn Profil 01	24-44,65N	62-21,05E

11.09.1997 **Zeit : UTC + 04h**

0236	Ende Profil 01 (54sm)	24-44,65N	63-20,00E
0236	Beginn Schleife über Bb	24-52,10N	63-20,00E
0506	Ende Schleife über Bb	24-52,10N	63-20,00E

Profil SO-123/02 (Magnetometer, Airgun-Array, Streamer, Gravimeter)

0506	Beginn Profil 02	24-52,10N	63-20,00E
0653	Ende Profil 02 (8sm)	24-53,10N	63-12,10E

(Abbruch wegen größerer Ansammlung von Fischerbooten; Fischerboote werden umfahren)

0658	Streamer a/D		
0700	Bb Airgun-Array vorgeholt		
0705	Stb Airgun-Array vorgeholt, Magnetometer vorgeholt		
0910	Bb Airgun-Array ausgesteckt L = 70m		
0915	Stb Airgun-Array ausgesteckt L = 70m		
0918	Streamer ausgesteckt L = 80m, Magnetometer ausgesteckt L = 750m		

Profil SO-123/02A (Magnetometer, Airgun-Array, Streamer, Gravimeter)

0919	Beginn Profil 02/A	24-47,66N	63-06,95E
1914	Ende Profil 02/A (38sm)	24-52,10N	62-16,44E
1928	Bb Airgun-Array a/D		
1936	Stb Airgun-Array a/D		
1942	Streamer a/D		
1954	Magnetometer a/D		

OBH # 21

2111	OBH # 21 ausgelöst		
2125	OBH gesichtet und geortet		
2137	OBH a/D	24-52,14N	62-29,03E

0BH # 20

2203	OBH # 20 ausgelöst		
2221	OBH gesichtet und geortet		
2234	OBH a/D	24-54,18N	62-34,87E

OBH # 19

2335	OBH # 19 ausgelöst		
2351	OBH gesichtet und geortet		

Stationsprotokoll F.S. "S O N N E" Reise 123

12.09.1997 **Zeit : UTC + 04h**

0003	OBH a/D	24-52,13N	62-40,41E
OBH # 07			
0049	OBH # 07 ausgelöst		
0106	OBH gesichtet und geortet		
0120	OBH a/D	24-44,66N	62-37,19E
OBH # 08			
0142	OBH # 08 ausgelöst		
0200	OBH gesichtet und geortet		
0220	OBH a/D	24-44,57N	62-41,91E
OBH # 10			
0307	OBH # 10 ausgelöst		
0322	OBH gesichtet und geortet		
0339	OBH a/D	24-44,65N	62-51,62E
OBH # 11			
0400	OBH # 11 ausgelöst		
0427	OBH gesichtet und geortet		
0438	OBH a/D	24-44,63N	62-56,10E
OBH # 17			
0533	OBH # 17 ausgelöst (Keine Antwort)		
0615	OBH erneut ausgelöst		
0638	Hydrofon z/W		
0705	OBH gesichtet		
0719	OBH a/D	24-52,09N	62-52,59E
OBH # 15			
0822	OBH # 15 ausgelöst		
0833	OBH gesichtet und geortet		
0853	OBH a/D	24-51,95N	63-06,12E
OBH # 14			
0914	OBH # 14 ausgelöst		
0926	OBH gesichtet und geortet		
0937	OBH a/D	24-51,99N	63-11,05E
Profil # HS-01 (Hydrosweep, Gravimeter)			
1032	Beginn Profil 01	24-57,00N	63-05,00E
1140	Ende Profil (19sm)	24-57,00N	63-20,00E
Profil # HS-02 (Hydrosweep, Gravimeter)			
1140	Beginn Profil 02	24-57,00N	63-20,00E
1200	Ende Profil (3sm)	24-53,00N	63-20,00E
Profil # HS-03 (Hydrosweep, Gravimeter)			
1200	Beginn Profil 03	24-53,00N	63-20,00E
1255	Ende Profil (19sm)	24-55,62N	63-10,10E

OBH # 23

1311	OBH # 23 z/W	WT 463m		
1313	OBH geslippt		24-56,98N	63-10,80E

OBH # 24

1337	OBH # 24 z/W	WT 600m		
1338	OBH geslippt		24-56,97N	63-12,61E
1418	Beginn Test mit OBS			
1421	Ende Test mit OBS			

OBS # 01

1440	OBS # 01 z/W	WT 101m		
1441	OBS geslippt		24-57,15N	63-19,79E

OBH # 25

1500	OBH # 25 z/W	WT 120m		
1501	OBH geslippt		24-56,80N	63-19,83E
1540	Bb Airgun-Array z/W	L = 70m		
1543	Streamer z/W	L = 70m		
1556	Stb Airgun-Array z/W	L = 70m		

Profil SO-123/03 (Airgun-Array, Streamer, Gravimeter)

1601	Beginn Profil 03	24-57,00N	63-22,52E
1949	Ende Profil (16sm)	24-57,00N	63-05,50E
1949	Streamer a/D		
1955	Beginn Schleife über Stb	24-57,00N	63-05,00E
2015	Ende Schleife über Stb, Streamer z/W	24-57,00N	63-04,80E

Profil SO-123/3A (Airgun-Array, Streamer, Gravimeter)

2023	Beginn Profil 03/A	24-57,00N	63-05,70E
2302	Ende Profil (15sm)	24-57,00N	63-22,60E
2307	Streamer a/D		
2320	Bb Airgun-Array a/D		
2330	Stb Airgun-Array a/D		

13.09.1997 **Zeit : UTC + 04h**

OBH # 24

0052	OBH # 24 ausgelöst		
0059	OBH gesichtet und geortet		
0109	OBH a/D	24-57,00N	63-12,90E

OBH # 23

0109	OBH # 23 ausgelöst (Keine Antwort)		
0125	OBH erneut ausgelöst		
0130	OBH gesichtet und geortet		
0139	OBH a/D	24-57,00N	63-11,02E

Profil # HS-04 (Hydrosweep, Magnetometer, Gravimeter)

0147	Beginn Profil 04	24-57,00N	63-10,70E
0217	Magnetometer z/W L = 750m		

0511	Ende Profil 04 (24sm)	24-23,00N	63-10,70E
	Profil # HS-05 (Hydrosweep, Magnetometer, Gravimeter)		
0537	Beginn Profil 05	24-24,00N	63-08,00E
0721	Magnetometer a/D (Eingeholt wegen Fischerei)		
0816	Ende Profil 05 (36sm)	24-50,00N	63-08,00E
	Profil # HS-06 (Hydrosweep, Gravimeter)		
0816	Beginn Profil 06	24-50,00N	63-08,00E
0837	Ende Profil (4sm)	24-54,00N	63-08,00E
	Profil # HS-07 (Hydrosweep, Gravimeter)		
0837	Beginn Profil 07	24-54,00N	63-08,00E
0907	Ende Profil (7sm)	24-54,00N	63-15,00E
	Profil # HS-08 (Hydrosweep, Gravimeter)		
0907	Beginn Profil 08	24-54,00N	63-15,00E
0931	Ende Profil (5sm)	24-57,00N	63-19,50E
	OBS # 01		
0934	OBS # 01 ausgelöst		
0942	OBS gesichtet		
0955	OBS a/D	24-57,07N	63-20,26E
	OBH # 25		
0955	OBH # 25 ausgelöst		
1004	OBH gesichtet und geortet		
1022	OBH a/D	24-56,70N	63-20,31E
	Profil # HS-09 (Hydrosweep, Magnetometer, Gravimeter)		
1022	Beginn Profil 09	24-56,70N	63-20,31E
1056	Magnetometer z/W L = 600m		
1208	Ende Profil (15sm)	24-43,00N	63-13,50E
	Profil # HS-10 (Hydrosweep, Magnetometer, Gravimeter)		
1208	Beginn Profil 10	24-43,00N	63-13,50E
1436	Ende Profil (28sm)	24-15,39N	63-13,30E
	Profil # HS-11 (Hydrosweep, Magnetometer, Gravimeter)		
1441	Beginn Profil 11	24-14,90N	63-12,85E
1843	Ende Profil (46sm)	24-13,00N	62-23,00E
	Profil # HS-12 (Hydrosweep, Magnetometer, Gravimeter)		
1914	Beginn Profil 12	24-15,50N	62-23,00E
2253	Ende Profil (41sm)	24-17,50N	63-08,00E
	Profil # HS-13 (Hydrosweep, Magnetometer, Gravimeter)		
2345	Beginn Profil 13	24-17,50N	63-08,00E
14.09.1997			**Zeit : UTC + 04h**
0130	Ende Profil (21sm)	24-28,50N	62-49,00E
	Profil # HS-14 (Hydrosweep, Magnetometer, Gravimeter)		
0159	Beginn Profil 14	24-26,00N	62-50,00E

0238	Ende Profil (7sm)	24-21,50N	62-56,00E
	Profil # HS-15 (Hydrosweep, Magnetometer, Gravimeter)		
0326	Beginn Profil 15	24-21,50N	62-56,00E
0616	Ende Profil (31sm)	24-21,00N	62-22,00E
	Profil # HS-16 (Hydrosweep, Magnetometer, Gravimeter)		
0641	Beginn Profil 16	24-23,25N	62-22,50E
0827	Ende Profil (22sm)	24-23,25N	62-45,00E
	Profil # HS-17 (Hydrosweep, Magnetometer, Gravimeter)		
0854	Beginn Profil 17	24-25,00N	62-45,00E
1045	Ende Profil (20sm)	24-25,50N	62-23,00E
	Profil # HS-18 (Hydrosweep, Magnetometer, Gravimeter)		
1104	Beginn Profil 18	24-27,50N	62-23,00E
1250	Ende Profil (20sm)	24-27,50N	62-45,00E
	Profil # HS-19 (Hydrosweep, Magnetometer, Gravimeter)		
1309	Beginn Profil 19	24-29,25N	62-45,00E
1501	Ende Profil (20sm)	24-29,25N	62-23,00E
	Profil # HS-20 (Hydrosweep, Magnetometer, Gravimeter)		
1520	Beginn Profil 20	24-31,00N	62-23,00E
1705	Ende Profil (20sm)	24-31,00N	62-45,00E
	Profil # HS-21 (Hydrosweep, Magnetometer, Gravimeter)		
1722	Beginn Profil 21	24-32,50N	62-45,00E
1907	Ende Profil (20sm)	24-32,50N	62-23,00E
	Profil # HS-22 (Hydrosweep, Magnetometer, Gravimeter)		
1927	Beginn Profil 22	24-35,50N	62-23,00E
2027	Ende Profil (12sm)	24-43,00N	62-33,00E
	Profil # HS-23 (Hydrosweep, Magnetometer, Gravimeter)		
2027	Beginn Profil 23	24-43,00N	62-33,00E
2241	Ende Profil (20sm)	24-43,50N	63-02,00E
2308	Magnetometer a/D		
2335	Div. Versuche Auslösen OBH # 16, Keine Antwort		

15.09.1997 **Zeit : UTC + 04h**

0112	Abbruch Versuche Auslösen OBH # 16		
	OBH # 09		
0251	OBH # 09 ausgelöst		
0303	OBH gesichtet und geortet		
0315	OBH a/D	24-44,63N	62-46,50E
0316	Div. Auslöseversuche für OBH # 16; fahren div. Suchkurse		
1000	Suchkurse abgebrochen		
1033	Magnetometer z/W L = 750m		

Stationsprotokoll F.S. "S O N N E" Reise 123

Profil # HS-24 (Hydrosweep, Magnetometer, Gravimeter)

1033	Beginn Profil 24		24-50,30N	63-01,00E
1809	Ende Profil (83sm)		23-27,50N	63-00,00E

Profil # HS-25 (Hydrosweep, Magnetometer, Gravimeter)

1809	Beginn Profil 25		23-27,50N	63-00,00E
2217	Ende Profil (43sm)		22-51,50N	63-25,70E
2152	Magnetometer a/D			

OBH # 26

2225	OBH # 26 z/W	WT 4121m		
2227	OBH geslippt		22-51,39N	63-25,83E

OBH # 27

2256	OBH # 27 z/W	WT 4034m		
2257	OBH geslippt		22-49,42N	63-23,70E

OBH # 28

2336	OBH # 28 z/W	WT 4098m		
2337	OBH geslippt		22-46,11N	63-20,16E

16.09.1997 **Zeit : UTC + 04h**

OBS # 02

0010	OBS # 02 z/W	WT 4016m		
0011	OBS geslippt		22-43,19N	63-17,02E

OBH # 29

0048	OBH # 29 z/W	WT 4357m		
0049	OBH geslippt		22-39,87N	63-13,45E

OBH # 30

0120	OBH # 30 z/W	WT 4387m		
0121	OBH geslippt		22-37,21N	63-10,57E

OBH # 31

0156	OBH # 31 z/W	WT 4330m		
0157	OBH geslippt		22-33,98N	63-07,10E

OBH # 32

0247	OBH # 32 z/W	WT 4115m		
0248	OBH geslippt		22-28,86N	63-01,60E

OBH # 33

0321	OBH # 33 z/W	WT 4139m		
0322	OBH geslippt		22-25,91N	62-58,42E
0329	Magnetometer ausgesteckt	L = 750m		

Profil # HS-26 (Hydrosweep, Magnetometer, Gravimeter)

0414	Beginn Profil 26		22-20,90N	62-37,55E
0600	Ende Profil (19sm)		22-07,55N	62-43,61E

0638	Bb Airgun-Array z/W L = 70m		
0645	Stb Airgun-Array z/W L = 70m		
0650	Straemer z/W L = 100m		
	Profil # SO-123/04 (Magnetometer, Airgun-Array, Streamer, Gravimeter)		
0648	Beginn Profil 04	22-10,34N	62-41,30E
2202	Ende Profil (76sm)	23-04,50N	63-40,00E
2208	Streamer a/D		
2218	Bb Airgun-Array a/D		
2227	Stb Airgun-Array a/D		
	Profil # HS-27 (Hydrosweep, Magnetometer, Gravimeter)		
2258	Beginn Profil 27	23-02,20N	63-43,70E

17.09.1997 **Zeit : UTC + 04h**

0353	Ende Profil (53sm)	22-24,68N	63-03,26E
0427	Magnetometer a/D		
	OBH # 33		
0427	OBH # 33 ausgelöst		
0450	OBH gesichtet und geortet		
0500	OBH a/D	22-26,03N	62-58,31E
	OBH # 32		
0500	OBH # 32 ausgelöst		
0546	OBH gesichtet und geortet		
0555	OBH a/D	22-29,03N	63-01,52E
	OBH # 31		
0623	OBH # 31 ausgelöst		
0707	OBH gesichtet und geortet		
0717	OBH a/D	22-34,16N	63-07,11E
	OBH # 30		
0717	OBH # 30 ausgelöst		
0758	OBH gesichtet und geortet		
0808	OBH a/D	22-37,36N	63-10,58E
	OBH # 29		
0754	OBH # 29 augelöst		
0907	OBH gesichtet und geortet		
0916	OBH a/D	22-39,99N	63-13,42E
	OBS # 02		
0910	OBS # 02 ausgelöst		
1015	OBS gesichtet und geortet		
1024	OBS a/D	22-43,39N	63-16,95E
	OBH # 28		
1025	OBH # 28 ausgelöst		
1129	OBH gesichtet und geortet		
1144	OBH a/D		

Profil # HS-28 (Hydrosweep, Gravimeter)

1200	Beginn Profil 28		22-48,80N	63-20,70E
1410	Ende Profil (25sm)		23-10,16N	63-06,14E
	OBH # 34			
1435	OBH # 34 z/W	WT 2716m		
1436	OBH geslippt		23-12,83N	63-07,73E
	OBH # 35			
1456	OBH # 35 z/W	WT 2680m		
1457	OBH geslippt		23-11,02N	63-08,63E
	OBS # 03			
1519	OBS # 03 z/W	WT 2693m		
15120	OBS geslippt		23-08,61N	63-10,31E
	OBH # 36			
1555	OBH # 36 z/W	WT 2805m		
1556	OBH geslippt		23-04,41N	63-13,21E
	OBH # 37			
1632	OBH # 37 z/W	WT 2921m		
1633	OBH geslippt		22-59,99N	63-16,29E
	OBH # 38			
1709	OBH # 38 z/W	WT 3430m		
1710	OBH geslippt		22-55,45N	63-19,41E
	OBH # 39			
1741	OBH # 39 z/W	WT 4034m		
1742	OBH geslippt		22-51,54N	63-22,09E
	OBH # 26			
1742	OBH # 26 ausgelöst			
1830	OBH gesichtet und geortet			
1840	OBH a/D		22-51,37N	63-25,88E
	OBH # 40			
1916	OBH # 40 z/W	WT 4138m		
1917	OBH geslippt		22-46,51N	63-25,55E
	OBH # 41			
1952	OBH # 41 z/W	WT 2617m		
1954	OBH geslippt		22-42,78N	63-28,10E
2050	Magnetometer z/W	L = 750m		

Profil # HS-29 (Hydrosweep, Magnetometer, Gravimeter)

2026	Beginn Profil 29		22-44,00N	63-30,00E
2221	Ende Profil (22sm)		22-25,10N	63-43,10E
2308	Bb Airgun-Array z/W	L = 70m		
2316	Stb Airgun-Array z/W	L = 70m		
2321	Streamer z/W	L = 100m		

Stationsprotokoll F.S. "S O N N E" Reise 123

Profil , SO-123/05 (Magnetometer, Airgun-Array, Streamer, Gravimeter)

2324	Beginn Profil SO-123/05	22-27,51N	63-37,59E

18.09.1997 **Zeit : UTC + 04h**

1232	Ende Profil (63sm)	23-23,50N	63-00,00E
1238	Streamer a/D		
1248	Bb Airgun-Array a/D		
1258	Stb Airgun-Array a/D		

Profil # HS-30 (Hydrosweep, Magnetometer, Gravimeter)

1331	Beginn Profil 30	23-20,65N	62-58,81E
1422	Ende Profil (10sm)	23-12,57N	63-04,61E
1446	Magnetometer a/D		

OBH # 34

1431	OBH # 34 ausgelöst		
1502	OBH gesichtet und geortet		
1510	OBH a/D	23-12,87N	63-07,56E

OBH # 42

1541	OBH # 42 z/W WT 2709m		
1545	OBH geslippt	23-13,07N	63-11,05E

OBS # 03

1541	OBS # 03 ausgelöst		
1638	Hydrophon z/W		
1642	Hydrophon a/D		
1657	OBS gesichtet und geortet		
1704	OBS a/D	23-08,77N	63-10,38E

OBH # 36

1700	OBH # 36 ausgelöst		
1752	Hydrophon z/W		
1755	Hydrophon a/D		
1806	OBH gesichtet und geortet		
1813	OBH a/D	23-04,59N	63-13,35E

OBH # 37

1806	OBH # 37 ausgelöst		
1853	Hydrophon z/W		
1857	Hydrophon a/D		
1909	OBH gesichtet und geortet		
1923	OBH a/D	23-00,22N	63-16,52E

OBH # 38

1909	OBH # 38 ausgelöst		
2000	Hydrophon z/W		
2012	Hydrophon a/D		
2022	OBH gesichtet und geortet		
2033	OBH a/D	22-55,56N	63-19,56E

OBH # 39

2022	OBH # 39 ausgelöst		
2050	OBH gesichtet und geortet		
2114	OBH a/D	22-51,79N	63-22,23E

OBH # 40

2105	OBH # 40 ausgelöst		
2141	Hydrophon z/W		
2202	Hydrophon a/D		
2232	Hydrophon z/W		
2245	Hydrophon a/D		
2248	OBH gesichtet und geortet		
2258	OBH a/D	22-46,65N	63-25,60E

OBH # 41

2248	OBH # 41 ausgelöst		
2334	Hydrophon z/W		
2344	Hydrophon a/D		
2348	OBH gesichtet und geortet		
2356	OBH a/D	22-42,93N	63-28,17E

OBH # 27

2348	OBH # 27 ausgelöst		

19.09.1997 **Zeit : UTC + 04h**

0033	OBH gesichtet und geortet		
0100	OBH a/D	22-50,52N	63-24,14E

Profil # HS-31 (Hydroswepp, Gravimeter)

0142	Beginn Profil 31	22-50,50N	63-16,50E
0312	Ende Profil (18sm)	23-05,79N	63-06,26E

OBH # 43

0342	OBH # 43 z/W	WT 2744m	
0343	OBH geslippt	23-09,48N	63-07,09E

OBH # 44

0408	OBH # 44 z/W	WT 2806m	
0409	OBH geslippt	23-07,43N	63-04,74E

OBH # 45

0433	OBH # 45 z/W	WT 2791m	
0434	OBH geslippt	23-05,42N	63-02,77E

OBH # 46

0459	OBH # 46 z/W	WT 2880m	
0500	OBH geslippt	23-03,33N	63-00,11E

OBH # 47

0523	OBH # 47 z/W	WT 2923m	
0524	OBH geslippt	23-01,27N	62-57,83E

OBH # 48

0547	OBH # 48 z/W	WT 2917m		
0548	OBH geslippt		22-59,22S	62-55,53E
0619	Magnetometer z/W	L = 750m		

Profil # HS-32 (Hydrosweep, Magnetometer, Gravimeter)

0624	Beginn Profil 32		23-00,00N	62-52,70E
0810	Ende Profil	(20sm)	22-46,06N	62-36,69E
0843	Bb Airgun-Array z/W	L = 70m		
0850	Stb Airgun-Array z/W	L = 70m		
0854	Streamer z/W	L = 100m		

Profil # SO-123/06 (Hydrosweep, Airgun-Array, Streamer, Magnetometer, Gravimeter)

0857	Beginn Profil 06		22-44,94N	62-39,65E
2114	Ende Profil	(60sm)	23-26,50N	63-26,00E
2125	Streamer a/D			
2133	Bb Airgun-Array a/D			
2142	Stb Airgun-Array a/D			

Profil # HS-33 (Hydrosweep, Magnetometer, Gravimeter)

2215	Beginn Profil 33		23-24,40N	63-27,90E
2255	Magnetometer a/D, Reperatur			
2308	Magnetometer z/W	L = 750m		

20.09.1997 **Zeit : UTC + 04h**

0100	Ende Profil	(31sm)	23-02,50N	63-51,45E

Profil # HS-34 (Hydrosweep, Magnetometer, Gravimeter)

0100	Beginn Profil 34		23-02,50N	63-51,45E
0619	Ende Profil	(59sm)	23-02,60N	63-48,60E

Profil # HS-35 (Hydrosweep, Magnetometer, Gravimeter)

0619	Beginn Profil 35		23-02,60N	63-48,60E
0709	Ende Profil	(9 sm)	23-08,80N	63-41,90E

Profil # HS-36 (Hydrosweep, Magnetometer, Gravimeter)

0709	Beginn Profil 36		23-08,80N	63-41,90E
0843	Ende Profil	(18sm)	22-58,56N	63-27,00E

Profil # HS-37 (Hydrosweep, Magnetometer, Gravimeter)

0852	Beginn Profil 37		22-58,66N	63-25,57E
1024	Ende Profil	(18sm)	23-11,91N	63-13,76E

1048 Magnetometer a/D

OBH # 42

1030	OBH # 42 ausgelöst			
1102	OBH gesichtet und geortet			
1111	OBH a/D		23-13,14N	63-11,14E

Stationsprotokoll F.S. "S O N N E" Reise 123

OBH # 35				
1103	OBH # 35 ausgelöst			
1147	OBH gesichtet und geortet			
1157	OBH a/D		23-11,08N	63-08,65E
OBH # 43				
1148	OBH # 43 ausgelöst			
1215	OBH gesichtet und geortet			
1227	OBH a/D		23-09,61N	63-07,19E
OBH # 44				
1215	OBH # 44 ausgelöst			
1256	Hydrophon z/W			
1258	Hydrophon a/D			
1305	OBH gesichtet und geortet			
1315	OBH a/D		23-07,54N	63-04,80E
OBH # 45				
1300	OBH # 45 ausgelöst			
1333	OBH gesichtet und geortet			
1344	OBH a/D		23-05,52N	63-02,57E
OBH # 46				
1337	OBH # 46 ausgelöst			
1411	Hydrophon z/W			
1415	Hydrophon a/D			
1442	OBH gesichtet und geortet			
1450	OBH a/D		23-03,44N	63-00,13E
OBH # 47				
1435	OBH # 47 ausgelöst			
1510	OBH gesichtet und geortet			
1520	OBH a/D		23-01,41N	62-57,80E
OBH # 48				
1518	OBH # 48 ausgelöst			
1547	OBH gesichtet und geortet			
1555	OBH a/D		22-59,29N	62-55,55E
Profil # HS-38 (Hydrosweep, Gravimeter)				
1631	Beginn Profil 38		22-54,00N	62-56,00E
1807	Ende Profil (18sm)		22-42,00N	62-56,00E
Profil # HS-39 (Hydrosweep, Gravimeter)				
1807	Beginn Profil 39		22-42,00N	62-56,00E
1944	Ende Profil (19sm)		22-26,70N	62-53,80E
OBH # 49				
2013	OBH # 49 z/W	WT 4119m		
2014	OBH geslippt		22-28,60N	62-57,10E
OBH # 50				
2039	OBH # 50 z/W	WT 4138m		
2040	OBH geslippt		22-26,36N	62-59,08E

OBH # 51

2109	OBH # 51 z/W	WT 3606m		
2111	OBH geslippt		22-23,51N	63-01,60E

OBH # 52

2213	OBH # 52 z/W	WT 1704m		
2214	OBH geslippt		22-15,67N	63-08,54E

OBH # 53

2243	OBH # 53 z/W	WT 1600m		
2244	OBH geslippt		22-12,5N	63-10,95E

OBS # 04

2318	OBS # 04 z/W	WT 1169m		
2321	OBS geslippt		22-08,89N	63-14,52E

OBH # 54

2353	OBH # 54 z/W	WT 1523m		
2354	OBH geslippt		22-05,97E	63-17,11E

21.09.1997 **Zeit : UTC + 04h**

OBH # 55

0024	OBH # 55 z/W	WT 2404m		
0025	OBH geslippt		22-03,64N	63-19,18E

OBH # 56

0101	OBH # 56 z/W	WT 2922m		
0102	OBH geslippt		21-59,96N	63-22,42E

OBH # 57

0143	OBH # 57 z/W	WT 3119m		
0144	OBH geslippt		21-55,55N	63-26,31E

Magnetometer z/W L = 750m

Profil # HS-40 (Hydrosweep, Magnetometer, Gravimeter)

0226	Beginn Profil 40	21-55,40N	63-30,37E
0357	Ende Profil (18sm)	21-42,01N	63-42,50E

0436	Bb Airgun-Array z/W	L = 70m
0445	Stb Airgun-Array z/W	L = 70m
0450	Streamer z/W	L = 70m

Profil SO-123/07 (Hydrosweep, Airgun-Array, Streamer, Magnetometer, Gravimeter)

0450	Beginn Profil 07	21-41,34N	63-38,76E
2145	Ende Profil (85sm)	22-47,65N	62-40,21E

2152	Streamer a/D
2200	Bb Airgun-Array a/D
2209	Stb Airgun-Array a/D

Profil # HS-41 (Hydrosweep, Magnetometer, Gravimeter)

2242	Beginn Profil 41	22-49,20N	62-43,10E

22.09.1997 **Zeit : UTC + 04h**

0038	Ende Profil (22sm)	22-32,41N	62-57,97E
0106	Magnetometer a/D		
OBH # 49			
0045	OBH # 49 ausgelöst		
0211	OBH gesichtet und geortet		
0219	OBH a/D	22-28,62N	62-57,09E
OBH # 50			
0122	OBH # 50 ausgelöst		
0240	OBH gesichtet und geortet		
0249	OBH a/D	22-26,52N	62-59,16E
OBH # 51			
0135	OBH # 51 ausgelöst		
0305	OBH gesichtet und geortet		
0324	OBH a/D	22-23,46N	63-01,67E
Profil # HS-42 (Hydrosweep, Gravimeter)			
0324	Beginn Profil 42	22-23,46N	63-01,67E
0444	Ende Profil (15sm)	22-15,87N	63-08,41E
OBH # 52			
0430	OBH # 52 ausgelöst		
0445	OBH gesichtet und geortet		
0455	OBH a/D	22-15,92N	63-08,50E
OBH # 53			
0455	OBH # 53 ausgelöst		
0527	Hydrophon z/W a/D		
0529	OBH gesichtet und geortet		
0537	OBH a/D	22-13,17N	63-10,93E
OBS # 04			
0557	OBS # 04 ausgelöst		
0617	OBS gesichtet und geortet		
0624	OBS a/D	22-09,03N	63-14,51E
OBH # 54			
0625	OBH # 54 ausgelöst		
0657	OBH gesichtet und geortet		
0705	OBH a/D	22-06,10N	63-17,09E
OBH # 55			
0658	OBH # 55 ausgelöst		
0742	Hydrophon z/W		
0749	Hydrophon a/D		
0744	OBH gesichtet und geortet		
0752	OBH a/D	22-03,79N	63-19,16E
OBH # 56			
0744	OBH # 56 ausgelöst		

0832	OBH gesichtet und geortet		
0845	OBH a/D	22-00,00N	63-22,36E
OBH # 57			
0847	OBH # 57 ausgelöst		
0940	OBH gesichtet und geortet		
0955	OBH a/D	21-55,68N	63-26,15E
1030	Magnetometer z/W L = 750m		
Profil # HS-43 (Hydrosweep, Magnetometer, Gravimeter)			
1048	Beginn Profil 43	21-58,30N	63-29,80E
1330	Ende Profil (33sm)	22-24,00N	63-06,50E
Profil # HS-44 (Hydrosweep, Magnetometer, Gravimeter)			
1330	Beginn Profil 44	22-24,00N	63-06,50E
1715	Ende Profil (47sm)	22-57,26N	63-42,53E
	(Abbruch wegen größerer Ansammlung von Fischerbooten)		
Profil # HS-45 (Hydrosweep, Magnetometer, Gravimeter)			
1750	Beginn Profil 45	22-53,98N	63-46,18E
2003	Ende Profil (26sm)	22-36,50N	63-26,00E
Profil # HS-46 (Hydrosweep, Magnetometer, Gravimeter)			
2003	Beginn Profil 46	22-36,50N	63-26,00E
2203	Ende Profil (24sm)	22-51,00N	63-10,00E
Profil # HS-47 (Hydrosweep, Magnetometer, Gravimeter)			
2203	Beginn Profil 47	22-51,00N	63-10,00E
2320	Ende Profil (16sm)	22-46,00N	62-56,30E
Profil # HS-48 (Hydrosweep, Magnetometer, Gravimeter)			
2320	Beginn Profil 48	22-46,00N	62-56,30E
23.09.1997			**Zeit : UTC + 04h**
0151	Ende Profil (31sm)	23-09,31N	62-35,00E
Profil # HS-49 (Hydrosweep, Magnetometer, Gravimeter)			
0151	Beginn Profil 49	23-09,31N	62-35,00E
0620	Ende Profil (57sm)	24-06,00N	62-35,00E
Profil # HS-50 (Hydrosweep, Magnetometer, Gravimeter)			
0620	Beginn Profil 50	24-06,00N	62-35,00E
0754	Ende Profil (16sm)	24-17,30N	62-22,10E
0742	Magnetometer a/D		
OBH # 01			
0724	OBH # 01 ausgelöst		
0756	OBH gesichtet und geortet		
0807	OBH a/D	24-18,14N	62-21,03E
Profil # HS-51 (Hydrosweep, Gravimeter)			
0819	Beginn Profil 51	24-18,72N	62-21,84E

1017	Ende Profil (23sm)		
OBH # 02			
0958	OBH # 02 ausgelöst		
1024	OBH gesichtet und geortet		
1034	OBH a/D	24-19,21N	62-47,89E
Profil # HS-52 (Hydrosweep, Gravimeter)			
1053	Beginn Profil 52	24-19,70N	62-50,50E
1221	Ende Profil (17sm)	24-20,27N	63-09,13E
OBH # 03			
1205	OBH # 03 ausgelöst		
1239	OBH gesichtet und geortet		
1248	OBH a/D	24-19,70N	63-10,81E
Profil # HS-53 (Hydrosweep, Gravimeter)			
1305	Beginn Profil 53	24-21,81N	63-10,88E
1330	Ende Profil (6sm)	24-21,81N	63-05,49E
Profil # HS-54 (Hydroswepp, Gravimeter)			
1330	Beginn Profil 54	24-21,81N	63-05-49E
1457	Ende Profil (18sm)	24-31,24N	62-48,84E
OBH # 04			
1449	OBH # 04 ausgelöst		
1525	Hydrophon z/W a/D		
1533	OBH gesichtet und geortet		
1544	OBH a/D	24-33,90N	62-47,04E
Profil # HS-55 (Hydrosweep, Gravimeter)			
1600	Beginn Profil 55	24-35,05N	62-44,79E
1725	Ende Profil (17sm)	24-35,27N	62-25,67E
OBH # 05			
1725	OBH # 05 ausgelöst		
1809	OBH gesichtet und geortet		
1816	OBH a/D	24-34,46N	62-21,01E
Profil # HS-56 (Hydrosweep, Gravimeter)			
1824	Beginn Profil 56	24-34,20N	62-21,20E
2011	Ende Profil (21sm)	24-50,60N	62-31,30E
Profil # HS-57 (Hydrosweep, Gravimeter)			
2011	Beginn Profil 57	24-50,60N	62-31,30E
2109	Ende Profil (11sm)	24-50,60N	62-43,60E
OBH # 18			
2109	OBH # 18 ausgelöst		
2124	OBH gesichtet und geortet		
2136	OBH a/D	24-52,08N	62-46,03E
Profil # HS-58 (Hydrosweep, Gravimeter)			
2137	Beginn Profil 58	24-52,10N	62-46,00E
2300	Ende Profil (15sm)	24-44,70N	62-59,90E

OBH # 12				
2244	OBH # 12 ausgelöst			
2321	OBH gesichtet und geortet			
2333	OBH a/D		24-44,62N	63-00,03E
Profil # HS 59 (Hydrosweep,, Gravimeter)				
2400	Beginn Profil 59		24-43,10N	63-03,80E
24.09.1997				**Zeit : UTC + 04h**
0041	Ende Profil		24-41,97N	63-12,70E
OBH # 13				
0135	OBH # 13 ausgelöst			
0144	OBH gesichtet und geortet			
0154	OBH a/D		24-52,07N	63-13,90E
Profil # HS-60 (Hydrosweep, Gravimeter)				
0154	Beginn Profil 60		24-52,07N	63-13,90E
0223	Ende Profil (5sm)		24-50,43N	63-08,91E
Profil # HS-61 (Hydrosweep, Gravimeter)				
0223	Beginn Profil 61		24-50,43N	63-08,91E
0246	Ende Profil (5sm)		24-50,43N	63-03,68E
OBH # 16				
0309	Stand by OBH # 16, Hydrophon z/W			
0327	OBH gesichtet und geortet			
0346	OBH a/D		24-52,05N	63-00,65E
OBH # 58				
0508	OBH # 58 z/W	WT 1108m		
0509	OBH geslippt		24-53,88N	62-45,87E
OBH # 59				
0530	OBH # 59 z/W	WT 989m		
0531	OBH geslippt		24-52,10N	62-46,01E
OBH # 60				
0550	OBH # 60 z/W	WT 1407m		
0551	OBH geslippt		24-50,22N	62-46,15E
OBH # 61				
0622	OBH # 61 z/W	WT 1550m		
0625	OBH geslippt		24-47,25N	62-46,32E
OBH # 62				
0650	OBH # 62 z/W	WT 1703m		
0652	OBH geslippt		24-44,58N	62-46,49E
OBH # 06				
0742	OBH # 06 ausgelöst			
0800	OBH gesichtet und geortet			
0814	OBH a/D		24-44,69N	62-32,88E

OBH # 22				
0850	OBH # 22 ausgelöst			
0902	OBH gesichtet und geortet			
0910	OBH a/D		24-52,12N	62-26,12E
OBH # 63				
1110	OBH # 63 z/W	WT 1726m		
1112	OBH geslippt		24-41,29N	62-46,70E
OBH # 64				
1138	OBH # 64 z/W	WT 1825m		
1141	OBH geslippt		24-37,59N	62-46,91E
OBH # 65				
1209	OBH # 65 z/W	WT 2221m		
1210	OBH geslippt		24-33,44N	62-47,22E
OBH # 66				
1237	OBH # 66 z/W	WT 2120m		
1238	OBH geslippt		24-29,94N	62-47,45E
OBH # 67				
1305	OBH # 67 z/W	WT 2094m		
1307	OBH geslippt		24-26,18N	62-47,64E
OBH # 68				
1333	OBH # 68 z/W	WT 2387m		
1334	OBH geslippt		24-22,53N	62-47,93E
OBH # 69				
1359	OBH # 69 z/W	WT 2329m		
1401	OBH geslippt		24-19,19N	62-48,09E
OBH # 70				
1423	OBH # 70 z/W	WT 2557m		
1424	OBH geslippt		24-16,72N	62-48,28E
OBH # 71				
1445	OBH # 71 z/W	WT 3063m		
1446	OBH geslippt		24-14,43N	62-48,43N
OBH # 72				
1511	OBH # 72 z/W	WT 2962m		
1512	OBH geslippt		24-11,00N	62-48,64N
OBS # 05				
1533	OBS # 05 z/W	WT 3222m		
1534	OBS geslippt		24-08,71N	62-48,81E
OBH # 73				
1603	OBH # 73 z/W	WT 3248m		
1605	OBH geslippt		24-04,96N	62-49,04E
OBH # 74				
1637	OBH # 74 z/W	WT 3268m		

1638	OBH geslippt		24-00,49N	62-49,31E
OBH # 75				
1710	OBH # 75 z/W	WT 3281m		
1712	OBH geslippt		23-56,22N	62-49,59E
1736	Magnetometer z/W	L = 750m		
Profil # HS-62 (Magnetometer, Hydrosweep, Gravimeter)				
1750	Beginn Profil 62		23-53,97N	62-46,46E
2020	Ende Profil (27sm)		23-26,70N	62-48,10E
2042	Magnetometer a/D			
2107	Bb Airgun-Array z/W	L = 70m		
2115	Stb Airgun-Array z/W	L = 70m		
2119	Streamer z/W	L = 100m		
Profil # SO-123/08 (Magnetometer, Airgun, Streamer, Hydrosweep)				
2123	Beginn Profil SO-123/08		23-28,50N	62-51,37E

25.09.1997 **Zeit : UTC + 04h**

1707	Ende Profil (84sm)	24-54,46N	62-45,86E
1711	Streamer a/D		
1726	Bb Airgun-Array a/D		
1734	Stb Airgun-Array		
OBH # 58			
1753	OBH # 58 ausgelöst		
1806	OBH gesichtet und geortet		
1830	OBH a/D	24-53,85N	62-45,74E
OBH # 59			
1831	OBH # 59 ausgelöst		
1858	OBH geortet und gesichtet		
1905	OBH a/D	24-52,11N	62-45,88E
OBH # 60			
1910	OBH # 60 ausgelöst		
1930	OBH gesichtet und geortet		
1936	OBH a/D	24-50,21N	62-46,04E
OBH # 61			
1936	OBH # 61 ausgelöst		
2005	OBH gesichtet und geortet		
2014	OBH a/D	24-47,24N	62-46,21E
OBH # 62			
2014	OBH # 62 ausgelöst		
2033	OBH gesichtet und geortet		
2042	OBH a/D	24-44,57N	62-46,43E
OBH # 63			
2042	OBH # 62 ausgelöst		

2110	OBH gesichtet und geortet		
2120	OBH a/D	24-41,20N	62-46,66E

OBH # 65

2228	OBH # 65 ausgelöst		
2254	OBH gesichtet und geortet		
2306	OBH a/D	24-33,33N	62-47,14E

OBH # 66

2307	OBH # 66 ausgelöst		
2353	OBH gesichtet und geortet		

26.09.1997 **Zeit : UTC + 04h**

0006	OBH a/D	24-29,89N	62-47,41E

OBH # 67

0010	OBH # 67 ausgelöst		
0045	OBH gesichtet und geortet		
0056	OBH a/D	24-26,13N	62-47,67E

OBH # 68

0048	OBH # 68 ausgelöst		
0138	Hydrophon z/W		
0140	Hydrophon a/D		
0143	OBH gesichtet und geortet		
0153	OBH a/D	24-22,51N	62-47,97E

OBH # 70

0210	OBH # 70 ausgelöst		
0249	OBH gesichtet und geortet		
0301	OBH a/D	24-16,80N	62-48,31E

OBH # 71

0253	OBH # 71 ausgelöst		
0342	OBH geortet und gesichtet		
0356	OBH a/D	24-14,53N	62-48,50E

OBH # 72

0350	OBH # 72 ausgelöst		
0430	Hydrophon z/W a/D		
0448	OBH gesichtet		
0458	OBH a/D	24-11,01N	62-48,64E

OBS # 05

0438	OBS # 05 ausgelöst		
0527	Hydrophon z/W		
0531	OBS gesichtet und geortet, Hydrophon a/D		
0542	OBS a/D	24-08,82N	62-48,83E

OBH # 73

0535	OBH # 73 ausgelöst		
0630	OBH gesichtet und geortet		
0636	OBH a/D	24-05,03N	62-49,05E

Stationsprotokoll F.S. "S O N N E" Reise 123

OBH # 74				
0630	OBH # 74 ausgelöst			
0729	OBH gesichtet und geortet			
0737	OBH a/D		24-00,52N	62-49,42E
OBH # 75				
0730	OBH # 75 ausgelöst			
0830	Hydrophon z/W			
0831	Hydrophon a/D			
0837	OBH gesichtet und geortet			
0846	OBH a/D		23-56,30N	62-49,68E
Profil # HS-63 (Hydrosweep, Gravimeter)				
0923	Beginn Profil 63		24-00,43N	62-53,86E
1020	Unterbrechen Profil 63 (Bootsmanöver)			
1110	Fortsetzung Profil 63			
1330	Ende Profil (37sm)		24-37,47N	62-53,46E
OBH # 76				
1343	OBH # 76 z/W	WT 1741m		
1344	OBH geslippt		24-37,67N	62-53,49E
OBH # 77				
1412	OBH # 77 z/W	WT 1942		
1413	OBH geslippt		24-37,55N	62-50,22E
OBH # 64				
1413	OBH # 64 ausgelöst			
1441	OBH gesichtet und geortet			
1449	OBH a/D		24-37,58N	62-46,88E
OBH # 78				
1456	OBH # 78 z/W	WT 1829m		
1457	OBH geslippt		24-37,50N	62-46,99E
OBH # 79				
1524	OBH # 79 z/W	WT 1765m		
1525	OBH geslippt		24-37,29N	62-43,76E
OBH # 80				
1557	OBH # 80 z/W	WT 1916m		
1558	OBH geslippt		24-37,20N	62-39,91E
OBH # 81				
1617	OBH # 81 z/W	WT 1693m		
1618	OBH geslippt		24-37,08N	62-37,40E
OBH # 82				
1642	OBH # 82 z/W	WT 1631m		
1643	OBH geslippt		24-36,90N	62-34,12E
OBH # 83				
1706	OBH # 83 z/W	WT 1754m		
1708	OBH geslippt		24-36,79N	62-30,91E

OBH # 84

1731	OBH # 84 z/W	WT 1819m		
1732	OBH geslippt		24-36,67N	62-27,68E

Profil # HS-64 (Hydrosweep, Gravimeter)

1732	Beginn Profil 64		24-36,67N	62-27,68E
1919	Ende Profil (19sm)		24-18,00N	62-28,60E

OBH # 85

1922	OBH # 85 z/W	WT 2491m		
1924	OBH geslippt		24-17,89N	62-28,59E

OBH # 86

1954	OBH # 86 z/W	WT 2491m		
1957	OBH geslippt		24-18,11N	62-31,88E

OBH # 87

2022	OBH # 87 z/W	WT 2461m		
2024	OBH geslippt		24-18,33N	62-35,18E

OBH # 88

2046	OBH # 88 z/W	WT 2425m		
2048	OBH geslippt		24-18,54N	62-38,36E

OBH # 89

2110	OBH # 90 z/W	WT 2397m		
2111	OBH geslippt		24-18,76N	62-41,54E

OBH # 90

2133	OBH # 90 z/W	WT 2337m		
2135	OBH geslippt		24-18,89N	62-44,87E

OBH # 91

2212	OBH # 91 z/W	WT 2508m		
2213	OBH geslippt		24-19,43N	62-51,35E

OBH # 92

2235	OBH # 92 z/W	WT 2586m		
2237	OBH geslippt		24-19,63N	62-54,62E

2303	Magnetometer z/W	L = 750m		

Profil # HS-65 (Magnetometer, Hydrosweep, Gravimeter)

2309	Beginn Profil 65		24-17,70N	62-57,00E

27.09.1997 **Zeit : UTC + 04h**

0033	Ende Profil (16sm)		24-19,02N	63-14,86E

0100	Bb Airgun-Array z/W	L = 70m
0107	Stb Airgun-Array z/W	L = 70m
0111	Streamer z/W	L = 80m

Profil # SO-123/09 (Magnetometer, Airgun, Streamer, Gravimeter, Hydrosweep)

0111	Beginn Profil SO-123/09		24-20,88N	63-13,23E

1646	Ende Profil (64sm)	24-16,18N	62-03,10E
1652	Streamer a/D		
1701	Bb Airgun-Array a/D		
1705	Stb Airgun-Array a/D		

Profil # HS-66 (Magnetometer, Hydrosweep, Gravimeter)

1735	Beginn Profil 66	24-13,62N	62-03,46E
1930	Ende Profil (21sm)	24-15,10N	62-26,70E

OBH # 85

1930	OBH # 85 ausgelöst		
2013	OBH gesichtet und geortet		
2023	OBH a/D	24-17,98N	62-28,54E

OBH # 86

2020	OBH # 86 ausgelöst		
2044	OBH gesichtet und geortet		
2056	OBH a/D	24-18,18N	62-31,83E

OBH # 87

2056	OBH # 87 ausgelöst		
2137	OBH gesichtet und geortet		
2145	OBH a/D	24-18,26N	62-35,14E

OBH # 88

2145	OBH # ausgelöst		
2218	OBH gesichtet und geortet		
2225	OBH a/D	24-18,47N	62-38,31E

OBH # 89

2225	OBH # 89 ausgelöst		
2303	OBH gesichtet und geortet		
2308	OBH a/D	24-18,67N	62-41,56E

OBH # 90

2308	OBH # 90 ausgelöst		
2340	OBH gesichtet und geortet		
2346	OBH a/D	24-18,86N	62-44,92E

OBH # 69

2346	OBH # 69 ausgelöst		

28.09.1997 **Zeit : UTC + 04h**

0005	OBH gesichtet		
0020	OBH a/D	24-19,18N	62-48,16E

OBH # 91

0015	OBH # 91 ausgelöst		
0044	OBH gesichtet und geortet		
0058	OBH a/D	24-19,37N	62-51,46E

OBH # 92

0050	OBH # 92 ausgelöst		

0134	Hydrophon z/W a/D		
0141	OBH gesichtet und geortet		
0150	OBH a/D	24-19,67N	62-54,74E

Profil # HS-67 (Hydrosweep, Gravimetrie)

0150	Beginn Profil 67	24-19,67N	62-54,74E
0422	Ende Profil (28sm)	24-38,40N	63-18,22E

0433	Bb Airgun-Array z/W	L = 70m
0440	Stb Airgun-Array z/W	L = 70m
0448	Streamer z/W	L = 80m

Profill SO-123/10 (Hydrosweep, Streamer, Airgun, Gravimeter)

0449	Beginn Profil SO-123/10	24-38,51N	63-15,90E
2121	Ende Profil (67sm)	24-35,70N	62-03,20E

2127	Streamer a/D
2139	Bb Airgun-Array a/D
2209	Stb Airgun-Array a/D

Profil # HS-68 (Hydroswepp, Gravimetrie

2241	Beginn Profil 68	24-37,10N	62-03,40E

29.09.1997 **Zeit : UTC + 04h**

0035	Ende Profil (22sm)	24-38,15N	62-26,97E

OBH # 84

0025	OBH # 84 ausgelöst		
0044	OBH gesichtet und geortet		
0056	OBH a/D	24-36,77N	62-27,90E

OBH # 83

0048	OBH # 83 ausgelöst		
0129	Hydrophon z/W		
132	Hydrophon a/D		
0138	OBH gesichtet und geortet		
0147	OBH a/D	24-36,81N	62-31,08E

OBH # 82

0138	OBH # 82 ausgelöst		
0215	Hydrophon z/W a/D		
0220	OBH gesichtet und geortet		
0230	OBH a/D	24-36,85N	62-34,25E

OBH # 81

0220	OBH # 81 ausgelöst		
0255	OBH gesichtet und geortet		
0306	OBH a/D	24-36,96N	62-37,48E

OBH # 80

0255	OBH # 80 ausgelöst		
0320	OBH gesichtet und geortet		
0338	OBH a/D	24-37,07N	62-39,98E

OBH # 79

0325	OBH # 79 ausgelöst		
0346	OBH gesichtet und geortet		
0412	OBH a/D	24-37,19N	62-43,79E

OBH # 78

0408	OBH # 78 ausgelöst		
0429	OBH gesichtet und geortet		
0445	OBH a/D	24-37,41N	62-47,02E

OBH # 70

0440	OBH # 70 ausgelöst		
0505	OBH gesichtet und geortet		
0515	OBH a/D	24-37,51N	62-50,18E

OBH # 77

0523	OBH # 77 ausgelöst		
0540	OBH gesichtet und geortet		
0549	OBH a/D	24-37,59N	62-53,49E

Profil # HS-69 (Magnetometer, Hydrosweep, Gravimeter)

0610	Beginn Profil 69	24-39,10N	62-53,40E
0656	Magnetometer z/W L = 750m		
0819	Ende Profil (20sm)	24-40,00N	63-15,80E

Profil # HS-70 (Magnetometer, Hydrosweep, Gravimeter)

0819	Beginn Profil 70	24-40,00N	63-15,80E
10	Ende Profil (25sm)		

Profil # HS-71 (Magnetometer, Hydrosweep, Gravimeter)

1052	Beginn Profil 71	24-15,00N	63-18,10E
1302	Ende Profil (25sm)	24-40,00N	63-18,10E

Profil # HS-72 (Magnetometer, Hydrosweep, Gravimeter)

1319	Beginn Profil 72	24-40,00N	63-20,40E
1534	Ende Profil (25sm)	24-15,00N	63-20,40E

Profil # HS-73 (Magnetometer, Hydrosweep, Gravimeter)

1550	Beginn Profil 73	24-15,00N	63-21,70E
1755	Ende Profil (25sm)	24-40,00N	63-22,70E

Profil # HS-74 (Magnetometer, Hydrosweep, Gravimeter)

1817	Beginn Profil 74	24-41,00N	63-25,00E
2040	Ende Profil (26sm)	24-15,00N	63-25,00E

Profil # HS-75 (Magnetometer, Hydrosweep, Gravimeter)

2059	Beginn Profil 75	24-15,00N	63-27,30E
2325	Ende Profil (29sm)	24-44,00N	63-27,30E

30.09.1997 **Zeit : UTC + 04h**

Profil # HS-76 (Magnetometer, Hydrosweep, Gravimeter)

0025	Beginn Profil 76	24-44,00N	63-38,80E
0257	Ende Profil (28sm)	24-16,00N	63-38,80E
	Profil # HS-77 (Magnetometer, Hydrosweep, Gravimeter)		
0316	Beginn Profil 77	24-16,00N	63-36,50E
0533	Ende Profil (27sm)	24-43,00N	63-36,50E
	Profil # HS-78 (Magnetometer, Hydrosweep, Gravimeter)		
0553	Beginn Profil 78	24-43,00N	63-34,20E
0817	Ende Profil (28sm)	24-16,00N	63-34,20E
	Profil # HS-79 (Magnetometer, Hydrosweep, Gravimeter)		
0837	Beginn Profil 79	24-16,00N	63-31,90E
1109	Ende Profil (27sm)	24-43,00N	63-31,90E
	Profil # HS-80 (Magnetometer, Hydrosweep, Gravimeter)		
1129	Beginn Profil 80	24-43,00N	63-2,60E
1407	Ende Profil (27sm)	24-16,00N	63-29,60E
1414	Magnetometer a/D		
	Profil # HS-81 (Hydrosweep, Gravimeter)		
1422	Beginn Profil 81	24-14,00N	63-29,60E
2059	Ende Profil (70sm)	24-10,00N	62-13,80E
	Profil # HS-82 (Hydrosweep, Gravimeter)		
2059	Beginn Profil 82	24-10,00N	62-13,80E
2245	Ende Profil (23sm)	24-31,10N	62-16,10E
	Profil # HS-83 (Hydrosweep, Gravimeter)		
2245	Beginn Profil 83	24-31,10N	62-16,10E

01.10.1997 **Zeit : UTC + 04h**

0041	Ende Profil (22sm)	24-12,00N	62-19,00E
	Profil # HS-84 (Hydrosweep, Gravimeter)		
0041	Beginn Profil 84	24-12,00N	62-19,00E
0253	Ende Profil (27sm)	24-39,25N	62-18,30E
	Profil # HS-85 (Hydrosweep, Gravimeter)		
0253	Beginn Profil 85	24-39,25N	62-18,30E
0450	Ende Profil (22sm)	24-38,85N	62-42,50E
	Profil # HS-86 (Hydrosweep, Gravimeter)		
0450	Beginn Profil 86	24-38,85N	62-42,50E
0700	Ende Profil (25sm)	24-25,00N	63-05,50E
	Profil # HS-87 (Hydrosweep, Gravimeter)		
0700	Beginn Profil 87	24-25,00N	63-05,50E
1324	Ende Profil (87sm)	24-40,75N	62-40,00E
	Profil # HS-88 (Hydrosweep, Gravimeter)		
1324	Beginn Profil 88	24-40,75N	62-40,00E
1516	Ende Profil (22sm)	24-40,75N	62-16,10E

Profil # HS-89 (Hydrosweep, Gravimeter)			
1516	Beginn Profil 89	24-40,75N	62-16,10E
1611	Ende Profil (10sm)	24-32,50N	62-13,80E
Profil # HS-90 (Hydrosweep, Gravimeter)			
1611	Beginn Profil 90	24-32,50N	62-13,80E
1704	Ende Profil (10sm)	24-41,00N	62-11,50E
Profil # HS-91 (Hydrosweep, Gravimeter)			
1704	Beginn Profil 91	24-41,00N	62-11,50E
1957	Ende Profil (31sm)	24-10,00N	62-11,50E
	Ende der wissenschaftlichen Arbeiten SO-123		

APPENDIX 9.5

PRESS CLIPPINGS

Techno A Fortnightly Feature

A boost to marine geoscience

By Abul Farah

During August-October 1997, a German research vessel, (R/V) Sonne, will cruise in the waters of North Arabian Sea off Makran Coast to mark the launching of a two-year project called "Joint International Marine Geo-scientific Investigations."

The ship will be operated by the German Federal Institute for Geo-Sciences and Natural Resources (BGR) and the Research Center for Marine Geoscience (GEOMAR). The project is entirely funded by the German Federal Ministry for Education, Science, Research and Technology. Participating scientific organisations include: National Institute of Oceanography (NIO) Karachi; Hydrocarbon Development Institute of Pakistan (HDIP), Islamabad; BGR, Hanover, and Bullard Laboratories, Cambridge (U.K.).

The programme and the objectives of the international project were described by Dr Christian Reichert and Dr Ditrich Von Rad of BGR at a seminar organised by NIO on 28th May, 1997. The project will be executed in two parts in Makran Margin and Murray Ridge regions. While 1997 will be devoted to geophysical and bathymetric surveys, sedimentalogical, oceanographic and geochemical studies will be undertaken in 1998.

During August-October 1997, multi-channel seismic reflection surveys will be carried out in order to resolve important issues related to the geodynamic evolution of the complex accretionary wedge in the Makran Subduction Zone. The energy to obtain reflections from the seafloor and underlying interfaces of different acoustic properties will be produced by means of 20 air guns towed at the stern of the ship which will generate pulses of compressed air (130 bars) at every 20 seconds. The reflected energy will be detected by 3,000 pressure sensitive hydrophones (called geophones in land surveys) arranged in a 3 kilometre long 'streamer' and by ocean 'bottom hydrophones' and finally recorded by an appropriate on-board electronic system. Concomitantly, anomalies of the gravimetric and magnetic fields related to variations in densities and magnetic susceptibilities of sub- bottom rocks will be recorded. Combination of seismic, gravity and magnetic data will enable to exercise control and precise constrain in modelling the sub-bottom geology. The ocean bottom hydrophones will also detect energy waves created by earthquakes in the Benioff Zone of subducting plate with hypocentres at depths below the overriding plate which depend upon the angle at which the oceanic plate sinks at the trench.

Additionally, the seafloor topography in Makran margin-Murray ridge region will be imaged in greater detail by a sophisticated on-board multi-beam sonor (sound navigation ranging) system and by special "side-scan sonar" which will be towed in depth close to the sea floor and help in delineating small vents and structures. Also, during 1997 vertical temperature variations will be recorded by special gauges within the upper most layers of the seafloor enabling the assessment of the heat flow from depths in Makran oceanic-continental crust Convergence Zone.

The Second Operation, April-May 1998 will be devoted to geological/geochemical studies. For obtaining samples of the water column and of the seafloor sediments, besides conventional techniques, a variety of T.V. guided bottom samplers and corers (30 meter long) will be deployed. Study of these samples will reveal the complex sedimentation history and the paleoclimate changes in the region. Also, samples from methane-vents of coastal and sub-marine 'mud volcanoes' will be directly taken in order to determine the composition and discharge rates of the fluid. A T.V. guided GEOMAR 'ventspider' and free returnvent sampler will be used.

Later on in the laboratories in Germany, the participating scientists will analyse and interpret all the collected data with the help of the most modern computing techniques.

The geophysical/geological information obtained in the Makran convergent margin will lead to a clearer and better understanding of the formation and the deformation of the subduction-related accretionary wedge emplaced in imbricate thrust sheets on the continental plate-side. Some of the features like disharmony in frontal folding pattern and 'Decollement Zone' at 2 1/2 km depth interpreted by R.S. White (1979) from the seismic reflection data collected on Leg 3 of a cruise of RRS Shackleten in 1975 will be checked. The inferences drawn by K.H. Jacob and R.L. Quittneyer (1979) about the existence of a "weak and sporadic expression of earthquake activity to depths of only 80 kilometre" (Shallow Benioff Zone) will be ascertained.

The understanding of the depositional and deformational processes and pattern and of the associated thermal regime will enable a rational assessment of the petroleum potential of the Makran accretionary wedge. It may be mentioned that a rapidly accredited sedimentary margin like Makran underlain by a mobile oceanic cust is not usually considered a favourable hydrocarbon environment.

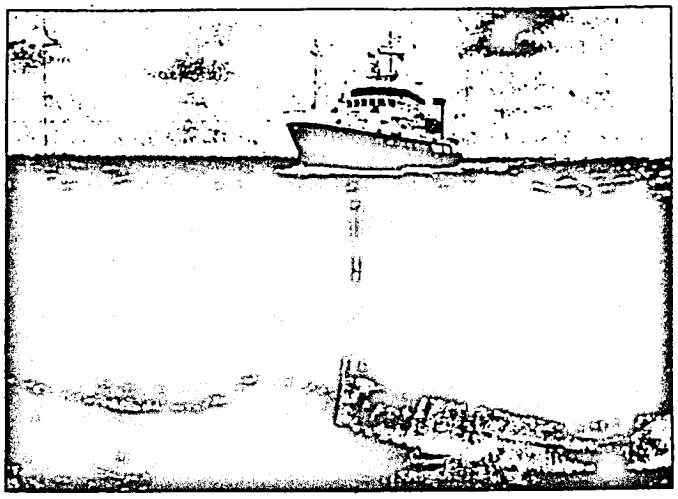

Combination of side scanning and depth contouring

The geophysical/geological data, particularly gravity and magnetic anomalies, will unravel the physiography and geodynamics of Murray ridge which is a feature of global significance. It is a SW-NE trending feature extending from the continental slope SW of Karachi over 750 km and conspicuously separates the active Makran margin in the west from the passive continental margin, including the prominent submarine Indus Fan in the east. It consists of sea monts, scraps and small basins. Besides bathymetry, very little is known about Murray Redge Geology. During October 1961 and March 1963 magnetic data collection (along wide apart profiles) and dredgining of one rock sample were done on board the HMS Darlymple by the Geophysical Department of the Imperial College London. The results were published by Barkar (1966). The data collected during Sonne cruises (1997-1998) will elaborate Barker's work and also provide a check on the geodynamics model proposed by Farah and Lawrence (1988); whether Murray Ridge was formed by sporadically distributed eruptive centres along a leaky transform fault with the Arabian plate moving faster than the Indian plate along a divergent boundary or that it is (obducted) obducted oceanic crust on-to oceanic crust with the Indian plate moving faster along a convergent boundary.

The geological/geochemical study programme on-board RV/Sonne during 1998 will lead to a deciphering of the complex rapid sedimentation history in the Makran margin and of the paleoclimatic history in the past 50,000 to 150,000 years. Due to the unique oceanographic property of oxygen deficiency in water column between 150 and 1,000 meter depth off Pakistani Makran coast no life, except certain microfauna, is possible below the seafloor in the "Oxygen-minimum Zone." Therefore, in this zone a few millimetre think layers of sediment-rich inorganic mater and fossils deposited during the summer and winter monsoon seasons, are not disturbed by burrowing organisms unlike anywhere else and they are optimally preserved in the annually laminated sediments. These layers constitute an extremely valuable and informative archive of climate and changes in oceanographic property during the recent past which may also reflect on future climate change.

The results of geoscientific studies with the help of Sonne cruises will be an original and substantial contribution in the advancement of marine geoscience research in Pakistan. It is suggested that as long as NIO does not have a research vessel it should endeavour to arrange more collaborative projects with friendly countries which possess advanced capabilities and facilities for Maine Science Research. This is an assured way to success. ■

GEOMAR REPORTS

1 GEOMAR FORSCHUNGSZENTRUM FÜR MARINE GEOWISSENSCHAFTEN DER CHRISTIAN-ALBRECHTS-UNIVERSITÄT ZU KIEL
BERICHT FÜR DIE JAHRE 1987 UND 1988. 1989. 71 + 6 pp.
In German

2 GEOMAR FORSCHUNGSZENTRUM FÜR MARINE GEOWISSENSCHAFTEN DER CHRISTIAN-ALBRECHTS-UNIVERSITÄT ZU KIEL
JAHRESBERICHT / ANNUAL REPORT 1989. 1990. 96 pp.
In German and English

3 GEOMAR FORSCHUNGSZENTRUM FÜR MARINE GEOWISSENSCHAFTEN DER CHRISTIAN-ALBRECHTS-UNIVERSITÄT ZU KIEL
JAHRESBERICHT / ANNUAL REPORT 1990. 1991. 212 pp.
In German and English

4 ROBERT F. SPIELHAGEN
DIE EISDRIFT IN DER FRAMSTRASSE WÄHREND DER LETZTEN 200.000 JAHRE. 1991. 133 pp.
In German with English summary

5 THOMAS C. W. WOLF
PALÄO-OZEANOGRAPHISCH-KLIMATISCHE ENTWICKLUNG DES NÖRDLICHEN NORDATLANTIKS SEIT DEM SPÄTEN NEOGEN
(ODP LEGS 105 UND 104, DSDP LEG 81). 1991. 92 pp.
In German with English summary

6 SEISMIC STUDIES OF LATERALLY HETEROGENOUS STRUCTURES - INTERPRETATION AND MODELLING OF SEISMIC DATA.
Edited by ERNST R. FLUEH
Commission on Controlled Source Seismology (CCSS), Proceedings of the 8th Workshop Meeting, held at
Kiel - Fellhorst (Germany), August 27-31, 1990. 1991. 359 pp.
In English

7 JENS MATTHIESSEN
DINOFLAGELLATEN-ZYSTEN IM SPÄTQUARTÄR DES EUROPÄISCHEN NORDMEERES: PALÖKOLOGIE UND PALÄO-OZEANOGRAPHIE. 1991. 104 pp
In German with English summary

8 DIRK NÜRNBERG
HAUPT- UND SPURENELEMENTE IN FORAMINIFERENGEHÄUSEN - HINWEISE AUF KLIMATISCHE UND OZEANOGRAPHISCHE ÄNDERUNGEN
IM NÖRDLICHEN NORDATLANTIK WÄHREND DES SPÄTQUARTÄRS. 1991. 117 pp.
In German with English summary

9 KLAS S. LACKSCHEWITZ
SEDIMENTATIONSPROZESSE AM AKTIVEN MITTELOZEANISCHEN KOLBEINSEY RÜCKEN (NÖRDLICH VON ISLAND). 1991. 133 pp.
In German with English summary

10 UWE PAGELS
SEDIMENTOLOGISCHE UNTERSUCHUNGEN UND BESTIMMUNG DER KARBONATLÖSUNG IN SPÄTQUARTÄREN SEDIMENTEN DES ÖSTLICHEN
ARKTISCHEN OZEANS. 1991. 106 pp.
In German with English summary

11 FS POSEIDON - EXPEDITION 175 (9.10.-1.11.1990)
175/1: OSTGRÖNLÄNDISCHER KONTINENTALRAND (65° N)
175/2: SEDIMENTATION AM KOLBEINSEYRÜCKEN (NÖRDLICH VON ISLAND)
Hrsg. von J. MIENERT und H.-J. WALLRABE-ADAMS. 1992. 56 pp. + app.
In German with some English chapters

12 GEOMAR FORSCHUNGSZENTRUM FÜR MARINE GEOWISSENSCHAFTEN DER CHRISTIAN-ALBRECHTS-UNIVERSITÄT ZU KIEL
JAHRESBERICHT / ANNUAL REPORT 1991. 1992. 152 pp.
In German and English

13 SABINE E. I. KÖHLER
SPÄTQUARTÄRE PALÄO-OZEANOGRAPHISCHE ENTWICKLUNG DES NORDPOLARMEERES UND EUROPÄISCHEN NORDMEERES ANHAND VON
SAUERSTOFF- UND KOHLENSTOFF- ISOTOTPENVERHÄLTNISSEN DER PLANKTISCHEN FORAMINIFERE
Neogloboquadrina pachyderma (sin.). 1992. 104 pp.
In German with English summary

14 FS SONNE - FAHRTBERICHT SO 78 PERUVENT: BALBOA, PANAMA - BALBOA, PANAMA, 28.2.1992-16.4.1992
Hrsg. von ERWIN SUESS. 1992. 120 pp.
In German with some English chapters

15 FOURTH INTERNATIONAL CONFERENCE ON PALEOCEANOGRAPHY (ICP IV): SHORT- AND LONG-TERM GLOBAL CHANGE:
RECORDS AND MODELLING 21-25 SEPTEMBER 1992, KIEL/GERMANY
PROGRAM & ABSTRACTS. 1992. 351 pp.
In English

16 MICHAELA KUBISCH
DIE EISDRIFT IM ARKTISCHEN OZEAN WÄHREND DER LETZTEN 250.000 JAHRE. 1992. 100 pp.
In German with English summary

17 PERSISCHER GOLF: UMWELTGEFÄHRDUNG, SCHADENSERKENNUNG, SCHADENSBEWERTUNG AM BEISPIEL DES MEERESBODENS; ERKENNEN
EINER ÖKOSYSTEMVERÄNDERUNG NACH ÖLEINTRÄGEN. Schlußbericht zu den beiden BMFT-Forschungsvorhaben 03F0055 A + B. 1993. 108 pp.
In German with English summary

18 TEKTONISCHE ENTWÄSSERUNG AN KONVERGENTEN PLATTENRÄNDERN / DEWATERING AT CONTINENTAL MARGINS.
Hrsg. von/ed. by ERWIN SUESS. 1993. 106 + 32 + 68 + 16 + 22 + 38 + 4 + 19 pp.
Some chapters in English, some in German

19 THOMAS DICKMANN
DAS KONZEPT DER POLARISATIONSMETHODE UND SEINE ANWENDUNGEN AUF DAS SEIMISCHE VEKTORWELLENFELD IM WEITWINKELBEREICH. 1993. 121 pp.
In German with English summary

20 GEOMAR FORSCHUNGSZENTRUM FÜR MARINE GEOWISSENSCHAFTEN DER CHRISTIAN-ALBRECHTS-UNIVERSITÄT ZU KIEL
JAHRESBERICHT / ANNUAL REPORT 1992. 1993. 139 pp.
In German and English

21 KAI UWE SCHMIDT
PALYNOMORPHE IM NEOGENEN NORDATLANTIK - HINWEISE ZUR PALÄO-OZEANOGRAPHIE UND PALÄOKLIMATOLOGIE. 1993. 104 + 7 + 41 pp.
In German with English summary

22 UWE JÜRGEN GRÜTZMACHER
DIE VERÄNDERUNGEN DER PALÄOGEOGRAPHISCHEN VERBREITUNG VON *BOLBOFORMA* - EIN BEITRAG ZUR REKONSTRUKTION UND DEFINITION VON WASSERMASSEN IM TERTIÄR. 1993. 104 pp.
In German with English summary

23 RV PROFESSOR LOGACHEV - Research Cruise 09 (August 30 - September 17, 1993): SEDIMENT DISTRIBUTION ON THE REYKJANES RIDGE NEAR 59°N
Edited by H.-J. WALLRABE-ADAMS & K.S. LACKSCHEWITZ. 1993. 66 + 30 pp.
In English

24 ANDREAS DETTMER
DIATOMEEN-TAPHOZÖNOSEN ALS ANZEIGER PALÄO-OZEANOGRAPHISCHER ENTWICKLUNGEN IM PLIOZÄNEN UND QUARTÄREN NORDATLANTIK. 1993. 113 + 10 + 25 pp.
In German with English summary

25 GEOMAR FORSCHUNGSZENTRUM FÜR MARINE GEOWISSENSCHAFTEN DER CHRISTIAN-ALBRECHTS-UNIVERSITÄT ZU KIEL
JAHRESBERICHT / ANNUAL REPORT 1993. 1994. 69 pp.
In German and English

26 JÖRG BIALAS
SEISMISCHE MESSUNGEN UND WEITERE GEOPHYSIKALISCHE UNTERSUCHUNGEN AM SÜD-SHETLAND TRENCH UND IN DER BRANSFIELD STRASSE - ANTARKTISCHE HALBINSEL. 1994. 113 pp.
In German with English summary

27 JANET MARGARET SUMNER
THE TRANSPORT AND DEPOSITIONAL MECHANISM OF HIGH GRADE MIXED-MAGMA IGNIMBRITE TL, GRAN CANARIA: THE MORPHOLOGY OF A LAVA-LIKE FLOW. 1994. 224 pp.
In English with German summary

28 GEOMAR LITHOTHEK. Edited by JÜRGEN MIENERT. 1994. 12 pp + app.
In English

29 FS SONNE - FAHRTBERICHT SO 97 KODIAK-VENT: KODIAK - DUTCH HARBOR - TOKYO - SINGAPUR, 27.7. - 19.9.1994
Hrsg. von ERWIN SUESS. 1994.
Some chapters in German, some in English

30 CRUISE REPORTS:
RV LIVONIA CRUISE 92, KIEL-KIEL, 21.8.-17.9.1992: GLORIA STUDIES OF THE EAST GREENLAND CONTINENTAL MARGIN BETWEEN 70° AND 80°N
RV POSEIDON PO200/10, LISBON-BREST-BREMERHAVEN, 7.-23.8.1993: EUROPEAN NORTH ATLANTIC MARGIN: SEDIMENT PATHWAYS, PROCESSES AND FLUXES
RV AKADEMIK ALEKSANDR KARPINSKIY, KIEL-TROMSØ, 5.-25.7.1994: GAS HYDRATES ON THE NORTHERN EUROPEAN CONTINENTAL MARGIN
Edited by JÜRGEN MIENERT. 1994.
In English; report of RV AKADEMIK ALEKSANDR KARPINSKIY cruise in English and Russian

31 MARTIN WEINELT
BECKENENTWICKLUNG DES NÖRDLICHEN WIKING-GRABENS IM KÄNOZOIKUM - VERSENKUNGSGESCHICHTE, SEQUENZSTRATIGRAPHIE, SEDIMENTZUSAMMENSETZUNG. 1994. 86 pp.
In German with English summary

32 GEORG A. HEISS
CORAL REEFS IN THE RED SEA: GROWTH, PRODUCTION AND STABLE ISOTOPES. 1994. 141 pp.
In English with German summary

33 JENS A. HÖLEMANN
AKKUMULATION VON AUTOCHTHONEM UND ALLOCHTHONEM ORGANISCHEM MATERIAL IN DEN KÄNOZOISCHEN SEDIMENTEN DER NORWEGISCHEN SEE (ODP LEG 104). 1994. 78 pp.
In German with English summary

34 CHRISTIAN HASS
SEDIMENTOLOGISCHE UND MIKROPALÄONTOLOGISCHE UNTERSUCHUNGEN ZUR ENTWICKLUNG DES SKAGERRAKS (NE NORDSEE) IM SPÄTHOLOZÄN. 1994.
In German with English summary

35 BRITTA JÜNGER
TIEFENWASSERERNEUERUNG IN DER GRÖNLANDSEE WÄHREND DER LETZTEN 340.000 JAHRE.
DEEP WATER RENEWAL IN THE GREENLAND SEA DURING THE PAST 340,000 YEARS. 1994. 6 + 109 pp.
In German with English summary

36 JÖRG KUNERT
UNTERSUCHUNGEN ZU MASSEN- UND FLUIDTRANSPORT ANHAND DER BEARBEITUNG REFLEXIONSSEISMISCHER DATEN AUS DER KODIAK-SUBDUKTIONSZONE, ALASKA. 1995. 129 pp.
In German with English summary

37 CHARLOTTE M. KRAWCZYK
DETACHMENT TECTONICS DURING CONTINENTAL RIFTING OFF THE WEST IBERIA MARGIN: SEISMIC REFLECTION AND DRILLING CONSTRAINTS. 1995. 133 pp.
In English with German summary

38 CHRISTINE CAROLINE NÜRNBERG
BARIUMFLUSS UND SEDIMENTATION IM SÜDLICHEN SÜDATLANTIK - HINWEISE AUF PRODUKTIVITÄTSÄNDERUNGEN IM QUARTÄR. 1995. 6 + 108pp.
In German with English summary

39 JÜRGEN FRÜHN
TEKTONIK UND ENTWÄSSERUNG DES AKTIVEN KONTINENTALRANDES SÜDÖSTLICH DER KENAI-HALBINSEL, ALASKA. 1995. 93 pp.
In German with English summary

40 GEOMAR FORSCHUNGSZENTRUM FÜR MARINE GEOWISSENSCHAFTEN DER CHRISTIAN-ALBRECHTS-UNIVERSITÄT ZU KIEL
JAHRESBERICHT / ANNUAL REPORT 1994. 1995.
In German and English

41 FS SONNE - FAHRTBERICHT / CRUISE REPORT SO 103 CONDOR 1 B: VALPARAISO-VALPARAISO, 2.-21.7.1995.
Hrsg. von ERNST R. FLUEH. 1995. 140 pp.
Some chapters in German, some in English

42 R/V PROFESSOR BOGOROV CRUISE 37. CRUISE REPORT "POSETIV": Vladivostok - Vladivostok, September 23 - October 22, 1994.
Edited by CHRISTOPH GAEDICKE, BORIS BARANOV and EVGENIY LELIKOV. 1995. 48 + 33 pp.
In English

43 CHRISTOPH GAEDICKE
DEFORMATION VON SEDIMENTEN IM NANKAI-AKKRETIONSKEIL, JAPAN. BILANZIERUNG TEKTONISCHER VORGÄNGE ANHAND VON SEISMISCHEN PROFILEN UND ERGEBNISSEN DER ODP-BOHRUNG 808. II + 89 pp.
In German with English summary

44 MARTIN ANTONOW
SEDIMENTATIONSMUSTER UM DEN VESTERIS SEAMOUNT (ZENTRALE GRÖNLANDSEE) IN DEN LETZTEN 250.000 JAHREN. 1995.
In German with English summary

45 INTERNATIONAL CONGRESS: CORING FOR GLOBAL CHANGE - ICGC '95. KIEL, 28 - 30 June, 1995.
Edited by JÜRGEN MIENERT and GEROLD WEFER. 1996.
In English

46 JENS GRÜTZNER
ZUR PHYSIKALISCHEN ENTWICKLUNG VON DIAGENETISCHEN HORIZONTEN IN DEN SEDIMENTBECKEN DES ATLANTIKS. 1995. 96 pp.
In German with English summary

47 INGO A. PECHER
SEISMIC STUDIES OF BOTTOM SIMULATING REFLECTORS AT THE CONVERGENT MARGINS OFFSHORE PERU AND COSTA RICA. 1996. 159 pp.
In English with German summary

48 XIN SU
DEVELOPMENT OF LATE TERTIARY AND QUATERNARY COCCOLITH ASSEMBLAGES IN THE NORTHEAST ATLANTIC. 1996. 120 pp. + 7 pl.
In English with German summary

49 FS SONNE - FAHRTBERICHT / CRUISE REPORT SO 108 ORWELL: SAN FRANCISCO - ASTORIA, 14.4. - 23.5.1996
Edited by ERNST R. FLUEH and MICHAEL A. FISHER. 1996.

50 GEOMAR FORSCHUNGSZENTRUM FÜR MARINE GEOWISSENSCHAFTEN DER CHRISTIAN-ALBRECHTS-UNIVERSITÄT ZU KIEL
JAHRESBERICHT / ANNUAL REPORT 1995. 1996. 93 pp.
In German and English

51 THOMAS FUNCK
STRUCTURE OF THE VOLCANIC APRON NORTH OF GRAN CANARIA DEDUCED FROM REFLECTION SEISMIC, BATHYMETRIC AND BOREHOLE DATA. 1996. VI, 144 pp.
In English with German summary

52 PETER BRUNS
GEOCHEMISCHE UND SEDIMENTOLOGISCHE UNTERSUCHUNGEN ÜBER DAS SEDIMENTATIONSVERHALTEN IM BEREICH BIOSTRATIGRAPHISCHER DISKONTINUITÄTEN IM NEOGEN DES NORDATLANTIK, ODP LEG 104, SITES 642B UND 643A. 1993. V, 73 pp.
n German with English summary

53 CHRISTIANE C. WAGNER
COLD SEEPS AN KONVERGENTEN PLATTENRÄNDERN VOR OREGON UND PERU: BIOGEOCHEMISCHE BESTANDSAUFNAHME. 1996. 108, XXXVI pp.
In German with English summary

54 FRAUKE KLINGELHÖFER
MODEL CALCULATIONS ON THE SPREADING OF SUBMARINE LAVA FLOWS. 1996. 98 pp.
In English with German summary

55 HANS-JÜRGEN HOFFMANN
OBJEKTORIENTIERTE ANALYSE UND MIGRATION DIFFRAKTIERTER WELLENFELDER UNTER VERWENDUNG DER STRAHLENMETHODE UND DER EDGE-WAVE-THEORIE. 1996. XX!, 153 pp.
In German with English summary

56 DIRK KLÄSCHEN
STRAHLENSEISMISCHE MODELLIERUNG UNTER BERÜCKSICHTIGUNG VON MEHRFACHDIFFRAKTIONEN MIT HILFE DER EDGE-WAVES: THEORIE UND ANWENDUNGSBEISPIELE. 1996. X, 159 pp.
In German with English summary

57 NICOLE BIEBOW
DINOFLAGELLATENZYSTEN ALS INDIKATOREN DER SPÄT- UND POSTGLAZIALEN ENTWICKLUNG DES AUFTRIEBSGESCHEHENS VOR PERU. 1996. IV, 100, 17, 14 (7 pl.) pp.
In German with English summary

58 RV SONNE - CRUISE REPORT SO109: HYDROTRACE. ASTORIA-VICTORIA-ASTORIA-VICTORIA. MAY 23 - JULY 8, 1996.
Ed. by PETER HERZIG, ERWIN SUESS, and PETER LINKE. 1997.
In English

59 RV SONNE - CRUISE REPORT SO110: SO - RO (SONNE - ROPOS). VICTORIA-KODIAK-VICTORIA. JULY 9 - AUGUST 19, 1996.
Ed. by ERWIN SUESS and GERHARD BOHRMANN. 1997.
In English

60 RV AKADEMIK M. A. LAVRENTYEV CRUISE 27. CRUISE REPORT: GREGORY. VLADIVOSTOK-PUSAN-OKHOTSK SEA-PUSAN-VLADIVOSTOK. SEPTEMBER 7 - OCTOBER 12, 1996. Ed. by DIRK NÜRNBERG, BORIS BARANOV, and BORIS KARP. 1997. 143 pp.
In English

62 FS SONNE - FAHRTBERICHT/CRUISE REPORT SO123: MAMUT (MAKRAN MURRAY TRAVERSE - GEOPHYSIK PLATTENTEKTONISCHER EXTREMFÄLLE). Maskat - Maskat, 07.09 - 03.10.1997Ed. by ERNST R. FLUEH, NINA KUKOWSKI, and CHRISTIAN REICHERT